Development of a ppGpp capture compound to assist mapping the stringent response signalling network in *Staphylococcus aureus*

University of Sheffield

The University of Sheffield
Department of Biosciences

Mark Edward Gainford

A thesis submitted in fulfilment of the requirements for the degree of Doctor of Philosophy

October 2024

Abstract

The alarmones guanosine tetra-phosphate (ppGpp) and guanosine penta-phosphate (pppGpp), collectively termed (p)ppGpp, are universally conserved second messenger nucleotides in prokaryotes. (p)ppGpp control the stringent response, a survival response that occurs in bacteria exposed to external stresses such as nutrient starvation. This response promotes cell survival through a form of quiescence and has been implicated in antimicrobial tolerance and persistent/chronic infections. Despite the discovery of these alarmones in 1969, numerous binding targets remain unidentified, and how these nucleotides facilitate a dormant state is incompletely understood. Here, I describe the synthesis of a (p)ppGpp target-protein capture compound *via* an enzymatic and chemical synthesis. This compound was validated against known ppGpp binding proteins before its use in pulldown assays with lysates of *Staphylococcus aureus*. Subsequent proteomics revealed many putative hits enriched by the compound. These hits were preliminarily screened for binding to [α-^{32}P]-ppGpp to highlight proteins of interest. A number of binding candidates were purified and their binding to ppGpp was established using ^{31}P-NMR. The binding affinity of one protein involved in carbon metabolism, HxlB, was investigated by microscale thermophoresis (MST) and an assay was designed to examine the impact of ppGpp on HxlB enzymatic activity. Similar capture compound approaches have previously been implemented in *Escherichia coli*. However, as the protein pathways utilised by *E. coli* often differ to those of *S. aureus*, applying this method to different species allows for the identification of new protein targets that aid in the understanding of this stress response. In addition to the capture compound, I also describe the synthesis and *in vitro* testing of the fluorescent chemosensor PyDPA, capable of quantifying (p)ppGpp levels in the presence of structurally similar nucleotides. This chemosensor allows us to circumnavigate issues associated with current (p)ppGpp quantification methods, with the eventual aim of probing (p)ppGpp synthesis in response to various stressors.

.

Acknowledgments

This won't be a typical length acknowledgment section, as my PhD experience has been far from "normal." There were a lot of twists and turns, and so many people have made this possible. Firstly, I'd like to thank my supervisors, Dr. Rebecca Corrigan and Dr. David Williams, for their scientific guidance and encouragement of my development as a scientist. This was just one of the contributions they made to my personal growth and PhD. They were also supportive in a more emotional sense, too. Rebecca, I'm sorry for crying so much, and David, I appreciated our chats about LFC and our shared love for the city.

My family and friends were pivotal in this, and it wouldn't have been possible without my parents, mum, and dad; thank you. Your constant support, reassurance, and faith in me made an impact in more ways than you will ever know. I appreciated that you always answered the phone when I had late nights in the labs, where I would over-explain my science and go on tangents. My short weekend visits home to see you both helped me get through this - they usually resulted in all my washing done, being cooked for, and cared for, but I promise they weren't the only reasons I visited. Mainly, I came home because I love you more than words can convey, and any time with you is a blessing, even if it's just our casual short brunch/coffee trips. Even writing this now, you have both brought me a cup of coffee and have no idea what I'm writing about you. You are both relentlessly selfless and have given me everything I could ever need, allowed me to take every opportunity that came my way, told me I can achieve anything I put my mind to, and supported me while I tried - I couldn't ask for more. The same goes for Vanessa, the epitome of what a big sister should be, we would call on weekends in the lab when our times matched, you even bought me a laptop when I couldn’t afford a new one – I’ve now written this thesis on it, you have been supportive when I’ve been ill in hospital from a 14 year old kid to a 27 year old man. Our phone calls and voice notes always leave me smiling and they were always just to make sure I was okay. You are going to do great things for yourself in this world and I can't wait to see you accomplish it all. So, to my family I love you all and none of this would have been achieved without you.

Concerning my friends, some of you I've known for over a decade, and others I've known for only four years, but what a privilege it's been to class myself as your friend. To Dr Reuben Ouanounou, we bonded under some difficult circumstances for both of us; for me, these felt unjust at the time. However, it led to me befriending you, so I would happily go through it all again for that reason alone. I'm so proud of you and can't wait to leather you at pool again. Dr Lucy and Dr Naznin, I would not have gotten through this without you, you are incredible scientists and people, your levels of insanity and OCD made me feel normal. Neil, our shared love for the Reds, Geoguesser, and Darwin Núñez was always the recipe for a good break while waiting for a reaction to progress. To Laura, Jack, and Sam, you are some of my best friends; you taught me how to be myself and more confident. I always looked forward to our late-night drinks, chatting about everything and anything, foraging included; our chaotic trip abroad will

live in my memory for a long time. Jack, Felix, and Dylan, our karaoke trips to bar one, climbing, and our chats next to the E-floor water cooler were always a welcomed break. Adam, thank you for organising football and welcoming me into that group. This was something I hadn't done since my time on the playground, but I always had so much fun.

Noah, Dom James, and El, your generosity did not go unnoticed. You really helped me out in a desperate time, and despite our house trips being few, they were always entertaining. Our walk home in the snow after Noah's first BJJ tournament is one of my favourite memories from my time at Sheffield and our climbing trips always helped push me to another level. Noah, keep it up, lad. You have something with BJJ, and I love hearing you talk about your work; it would be a challenge to find someone as passionate about their work as you. To the Sheffield lot, you are all incredible researchers, and I cannot wait to see what you do and what you go on in the world of science. To the lads and girls back home you carried me through when times were really tough, I'm so lucky to be forever linked with such a good group of caring people, from visiting me in the hospital to the halfway quiz and the occasional night out. The only thing that would have made it better is a holiday... To Tom, Jamie, and Lyd, you do more than anyone could reasonably ask for: you are the first to pick up the phone when I call and to help my family out when I'm ill; the way you deal with setbacks is an inspiration, and you are the definition of what friends should be. Our showdown matches, raids, coffee trips, food, and even tattoos were always stand-out days for me over the past few years. To the Leeds lot, we might not see each other as often as we used to due to travelling apart, but I always felt your support no matter where you were. I love all of you.

The final person I would like to thank is my best friend and girlfriend, Tayla. The last few months of your PhD are usually expected to be the toughest, but having you by my side made them a breeze. Your constant support and ability to work late "alongside" me, regardless of whether it was chemistry or biology, made everything so simple. Our late-night cooking sessions after 12-14 hrs days meant we were both a bit delirious but would always try something new and dance in the kitchen. Runs in the cold when we definitely were not in the state to be exerting ourselves were always rallied by your carefree attitude. Your passion for your research is unparalleled, and it really lit something within me that made me appreciate what I was doing. You were beside me for three years as one of my best friends, and I would never have anticipated where we would end up; home is meant to be a place where you are the most comfortable and can indeed be yourself; it just so happens I feel at home whenever I'm with you. I love you to bits and can't wait to see where your research takes you.

One final thanks to Rebecca and David for providing me with a challenging project with genuine impact, one I am incredibly passionate about. Midway through my PhD, I was hospitalised by chance by the very bacteria we work with, and I was struggling with motivation. Rebecca told me, "Bacteria are insidious; that's why we do what we do." This really shifted my entire mindset. So, I thank you for that.

I entered this PhD as an out-of-practice medicinal chemist and I have left as a biochemist/molecular biologist with a competent synthetic chemistry skill set. That is all thanks to the people mentioned above. Science is not a linear path; it's a mess of ropes all intertwined with knots. You cannot solve complex problems like that alone; you need a network with surplus support and a wide range of expertise. Even then, you might not solve it. I advise anyone undertaking a PhD to be optimistic about your progress; every knot you untangle is a significant achievement and has left you as a more competent scientist. Do not compare yourself to anyone other than yourself a few months prior; appreciate the progress.

Declaration

I, the author, confirm that this Thesis is my own work. I am aware of the University's guidance on the Use of Unfair Means. This work has not been previously presented for an award at this, or any other university.

List of Figures

List of Tables

List of abbreviations

Abbreviation	Definition
(p)ppGpp	Guanosine 3'-bids (diphosphate) and guanosine 3'-diphosphate 5'- triphosphate
°	Degrees
°C	Degrees Celsius
5PRA	5'-phosphoribosylamine
A	Absorbance
AcOH	Acetic acid
ACP	Acyl carrier protein
Adk	Adenylate kinase
Adneosine synthase A	AdsA
ADP	Adenosine diphosphate
agr	accessory gene regulator
AMP	Adenosine monophosphate
ANOVA	Analysis of variance
Ar	Argon
A-site	Aminoacyl site
Atet	Anhydrotetracycline
ATP	Adneosine triphosphate
BCAA	Branched chain amino acids
BSA	Bovine serum albumin
CA	Community acquired
Ca $(BH_4)_2$	Calcium borohydride
Cam	Chloramphenicol
cAMP	cyclic adenosine monophosphate
Carb	Carbenicillin
CBr_4	Carbon tetrabromide
CC	Conserved cysteine
$CDCl_3$	Deuterated chloroform
c-di-AMP	Cyclic di adenosine monophosphate
c-di-GMP	cyclic diguanylate monophosphate

$CHCl_3$	Chloroform
cm	Centimetre
CNS	Coagulase negative staphylococci
CPS	Coagulase positive staphylococci
CryoEM	Cryo electron microscopy
CTD	C-terminal domain
CWA	Cell wall associated proteins
Da	Dalton
D-Ala	D-alanine
DCC	N,N′-Dicyclohexylcarbodiimide
DCM	Dichloromethane
dd	Double distilled
DDM	n-dodecyl-β-D-maltoside
DIBAL	di-isobutyl aluminium
DIPEA	diisopropylethylamine
D-Lac	D-lactate
DMAP	Dimethylaminopyridine
DMAPP	dimethylallyl pyrophosphate
DMF	dimethylformamide
DMSO	Dimethyl sulphoxide
DMT	Dimethoxytrityl
DNA	Deoxyribonucleic acid
DNase	Deoxyriboonuclease
DRaCALA	differential radial capillary action of ligand assay
DTT	Dithiothreitol
ECL	Electrochemiluminescence
EDC	N- (3-Dimethylaminopropyl)-N′-ethylcarbodiimide
EDTA	ethylenediaminetetraacetic acid
EF	Elongation factor
ELISA	Enzyme linked immunosorbent assay
eqv	Equivalent
Erm	Erythromycin
ESI	Electrospray ionisation
E-site	Exit site
Et_2O	Diethyl ether
EtOAc	Ethyl acetate
EtOH	Ethanol
F6P	Fructose-6-phosphate

FB	Fraction bound
FBS	Fetal bovine serum
FDR	False discovery rate
Fmet	N-formylmethionine
FnBPs	Fibronectin binding proteins
g	Gram
GDP	Guanosine diphosphate
GFP	green fluorescent protein
Gmk	guanylate kinase
GMP	Guanosine monophosphate
GTP	Guanosine triphosphate
GTPase	Guanosine triphosphate hydrolase
H_2O_2	Hydrogen peroxide
H_2SO_4	Sulphuric acid
HA	Hospital acquired
HAS	Human serum albumin
HATU	1-[Bis (dimethylamino)methylene]-1*H*-1,2,3-triazolo[4,5-*b*]pyridinium 3-oxid hexafluorophosphate
HBr	Hydrogen bromide
HCl	Hydrochloric acid
HCTU	2- (6-Chloro-1-H-benzotriazole-1-yl)-1,1,3,3-tetramethylaminium hexafluorophosphate
HEPES	4- (2-hydroxyethyl)-1-piperazineethanesulfonic acid
Hex	Hexane
HFIP	Hexafluoroisopropanol
HGT	Horizontal gene transfer
HOCl	Hypochlorous acid
hpf	Hibernation promoting factor
HPLC	High performance liquid chromatography
HprT	hypoxanthine ribosyl transferase
Hr	Hour
HRP	Horse radish peroxidase
HYD	Hydrolase
Hz	Hertz
IF	Initation factor
IgG	Human immunoglobulin
IMAC	Immobilized Metal Affinity Chromatography
IMP	Inosine monophosphate

IP	Photostimulable phosphor imaging plate
IPP	isopentenyl pyrophosphate
IPTG	Isopropyl ß-D-1-thiogalactopyranoside
ITC	Isothermal calorimetry
Kan	Kanamycin
Kb	kilobase
K_d	Dissociation constant
kDa	Kilodalton
KEGG	Kyoto encyclopaedia of genes and genomes
KH_2PO_4	Monopotassium phosphate
KI	Potassium iodide
KOH	Potassium hydroxide
LB	Luria Bertani broth
LCMS	Liquid chromatography mass spectrometry
LFQ	Label free quantification
$LiAlH_4$	Lithium aluminium hydride
L-PG	lysyl-phospholipidphosphatidylglycerol
LPS	Lipopolysaccharide
M	Molar
mA	Milliamps
MBP	Maltose binding protein
MDM	Monocyte derived macrophages
MDR	Multidrug resistant
MeCN	Acetonitrile
MeOH	Methanol
MES	Morpholinoethanesulphonic acid
Met-tRNA	methyl-transfer RNA
mg	Milligram
$MgCl_2$	Magnesium Chloride
MGE	Mobile genetic elements
$MgSO_4$	Magnesium sulphate
Min	Minute
mL	Millilitre
mM	Millimolar
MPO	myeloperoxidases
mRNA	Messenger RNA
MRSA	Methicillin resistant *staphylococcus aureus*
MS	Mass spectrometry

MSCRAMM	microbial surface component recognising adhesive matrix molecules
MSG	Monosodium glutamate
MSSA	Methicillin sensitive staphylococcus aureus
MST	Microscale thermophoresis
MWCO	Molecular weight cut off
Na_2CO_3	Sodium carbonate
Na_2SO_4	Sodium sulphate
NaCl	Sodium chloride
NADPH	Nicotinamide adenine dinucleotide phosphate
NaH	Sodium hydride
$NaHCO_3$	Sodium hydrogen carbonate
NaN	Not a number
NaOH	Sodium hydroxide
NBCS	Newborn calf serum
NC	Nanoclusters
NEAT	near ion transporter
NETs	neutrophil extracellular traps
ng	Nanogram
NH_4Cl	Ammonium chloride
NH_4HCO_3	Ammonium bicarbonate
nM	Nanomolar
NMR	Nuclear magnetic resonance
NTD	N-terminal domain
Nuc	Staphylococcal nuclease
O/N	Overnight
OD	Optical density
ORF	Open reading frame
p (s)pGpp	Thiolated ppGpp analog
PAGE	Polyacrylamide gel electrophoresis
PBP	Penicillin binding protein
PBr_3	Potassium tribromide
PBS	Phosphate buffered saline
PBST	Phosphate buffered saline with TWEEN20
PC	Pyruvate carboxylase
PCA	Principal component analysis
PCR	Polymerase chain reaction
Pd/C	Palladium on carbon

PDB	Protein data bank
$PdCl_2$	Palladium (II) chloride
PEG	Polyethylene glycol
PFP	Pentafluorophenol
PG	Peptidoglycan
pGpp	guanosine 5'-monophosphate-3'-diphosphate
pH	Potential of hydrogen
pI	Isoelectric point
PMSF	phenylmethylsulfonyl
ppApp	Adenosine 5'-diphosphate-3'-diphosphate
ppGpp	Guanosine 5'-diphosphate-3'-diphosphate
PPh_3	Triphenylphosphine
PPi	Inorganic phosphate
ppm	Parts per million
pppGpp	guanosine 5'-triphosphate-3'-diphosphate
PRPP	phosphoribosylpyrophosphate
P-site	Peptidyl site
PSM	Phenol soluble modulin
PurF	amidophosphoribosyltransferase
PVDF	Polyvinyldifluoride
PVL	Panton valentine leucocidin
PyDPA	Pyrenyl dipicolylamine
RF	Release factor
rmf	Ribosome modulation factor
RNA	Ribonucleic acid
RNAP	RNA-polymerase
RNase	Ribonuclease
ROS	Reactive oxygen species
RP	Reverse phase
rpm	Revolutions per minute
RRM	RNA recognition motif
rRNA	Ribosomal RNA
RSH	RelA/SpoT homologue
RT	Room temperature
s	Second
SAH	Small alarmone hydrolases
SAS	Small alarmone synthetases
SASP	*Staphylococcus aureus* surface associated proteins

SCC	Staphylococcal cassette chromosome
SCV	Small colony variant
SDS	Sodium dodecyl sulphate
SILAC	Stable isotope labelled in culture
SiR_3	Silyl ethers
Spa	Staphylococcal protein A
Spec	Spectinomycin
SPIN	staphylococcal peroxidase inhibitor
SR	Stringent response
SYNTH	synthetase
TBAF	Tetra n-butylammonium fluoride
TBS	*t*-butyldimethylsilyl
TCA	Tricarboxylic acid
TCS	Two component system
TEA	Triethylamine
TEAB	Triethylammonium bicarbonate
TEG	Tetraethylne glycol
TEMED	Tetramethylethylenediamine
Tet	Tetracycline
TFA	Trifluoroacetic acid
THF	Tetrahydrofuran
TIPS	triisopropysilyl
TLC	Thin layer chromatography
TMB	3,3',5,5'-tetramethylbenzidine
TMS	trimethylsilyl
Tris	Tris buffered saline
tRNA	Transfer ribonucleic acid
TSA	Tryptic soy agar
TSB	Tryptic soy broth
TsCl	Tosyl chloride
TSST	toxic shock syndrome toxin
UTP	uridine triphosphate
UV	Ultraviolet
V	Volts
v/v	Volume/volume
VraRS	vancomycin resistance associated system
VRE	Vancomycin resistant enterococci
VRSA	Vancomycin resistant *staphylococcus aureus*

w/v	Weight/volume
XMP	Xanthine monophosphate
ZNF	Zinc finger domain
µg	Microgram
µL	Microlitre
µM	Micromolar
Ω	Ohms

Appendices

The following tables list details of proteins that were isolated from various pulldowns across this project and previous studies.

Table 1: Summary of the significantly enriched proteins from the stationary phase pulldown.

Gene locus	Gene name	Protein function	-logP	q-value	KEGG mapping
SAUSA300_1490	*efp*	Translation Elongation Factor P	2.373	0.0240	Ribosome
SAUSA300_0636	*dhaK*	Delta-Aminolevulinic Acid Dehydratase	1.927	0.0266	Metabolism
SAUSA300_1278	*pepF1*	Oligoendopeptidase F	2.459	0.0269	Nucleotide Metabolism
SAUSA300_1617	*hemC*	Mannose-6-Phosphate Isomerase, Class I	2.207	0.0273	Synthesis Of Cofactors
SAUSA300_0573	*mvaD*	Glyceraldehyde 3-Phosphate Dehydrogenase	1.970	0.0275	Metabolism
SAUSA300_1293	*lysA*	Cysteinyl-tRNA Synthetase	3.271	0.0276	Biosynthesis Of Amino Acids
SAUSA300_2327	*YdaG*	Conserved Hypothetical Protein	1.843	0.0280	Hypothetical Protein/Function Unknown
SAUSA300_2186	*rpmD*	Ribosomal Protein L30P/L7E	3.206	0.0281	Ribosome
SAUSA300_2079	*fba*	Porphobilinogen Deaminase	1.952	0.0283	Metabolism
SAUSA300_1713	*ribBA*	UTP-Glucose-1-Phosphate Uridylyltransferase Family Protein	2.104	0.0284	Metabolism
SAUSA300_2631		Nh (3)-Dependent NAD+ Synthetase	2.388	0.0288	Hypothetical Protein/Function Unknown
SAUSA300_0756	*gapC*	Conserved Hypothetical Protein	1.742	0.0288	Biosynthesis Of Amino Acids
SAUSA300_2193	*rplX*	Ribosomal Protein L24	2.198	0.0289	Ribosome

SAUSA300_2241	*ureE*	Urease Accessory Protein Uree	1.864	0.0290	Metabolism
SAUSA300_2460		Acetyltransferase, Gnat Family	1.975	0.0291	Hypothetical Protein/Function Unknown
SAUSA300_0556	*hxlB*	Sis Domain Protein	1.825	0.0292	Biosynthesis Of Amino Acids
SAUSA300_2164		Surface Protein, Putative	2.327	0.0292	Virulence Factor
SAUSA300_0835	*dltA*	Chaperonin, 60 kDa	1.741	0.0296	Virulence Factor
SAUSA300_0786	*Ohr*	Osmc/Ohr Family Protein	1.825	0.0296	Metabolism
SAUSA300_0789	*trxA*	Putative Thioredoxin	2.647	0.0299	Chaperones
SAUSA300_0515	*CysS*	Catalase	2.303	0.0299	Amino-Acyl tRNA Biosynthesis
SAUSA300_1476	*accB*	Acetyl-Coa Carboxylase, Biotin Carboxyl Carrier Protein	1.703	0.0300	Metabolism
SAUSA300_0136		Transcriptional Regulator Cody	1.856	0.0300	Virulence Factor
SAUSA300_2130		Transcriptional Regulator, Putative	2.071	0.0301	Metabolism
SAUSA300_2517		Ornithine Carbamoyltransferase	2.041	0.0304	Hypothetical Protein/Function Unknown
SAUSA300_1514	*fur*	Ferric uptake regulator	1.752	0.0305	Signalling
SAUSA300_1004		Conserved Hypothetical Protein	1.936	0.0305	Hypothetical Protein/Function Unknown
SAUSA300_1624	*MutT*	Heat Shock Protein Grpe	1.867	0.0307	Nucleotide Metabolism
SAUSA300_0727		Diaminopimelate Decarboxylase	2.718	0.0307	Metabolism
SAUSA300_0475	*spoVG*	Spovg Protein	1.957	0.0308	Growth And Division
SAUSA300_2351		Zn-Binding Lipoprotein Adca-Like Protein	2.472	0.0308	Transporter
SAUSA300_1545	*rpsT*	30S Ribosomal Protein S20	1.584	0.0309	Ribosome
SAUSA300_2226	*moaB*	Molybdenum Cofactor Biosynthesis Protein B	1.559	0.0310	Synthesis Of Cofactors
SAUSA300_1102	*gmk*	Guanylate Kinase (Metabolism)	2.421	0.0311	Nucleotide Metabolism
SAUSA300_2447		Uncharacterised Protein	2.296	0.0312	Hypothetical Protein/Function Unknown
SAUSA300_2132		Hypothetical Protein	1.557	0.0313	Hypothetical Protein/Function Unknown

SAUSA300_1094	*pyrC*	Dihydroorotase (Purine Metabolism)	1.490	0.0313	Synthesis Of Cofactors
SAUSA300_2146		Alcohol Dehydrogenase (General Metabolism)	1.742	0.0313	Metabolism
SAUSA300_0883	*map*	Putative Surface Protein	2.283	0.0313	Virulence Factor
SAUSA300_1256	*msrA*	Methionine Sulfoxide Reductase A	1.937	0.0313	Metabolism
SAUSA300_1902		Hypothetical Protein (Carbohydrate Metabolism)	1.637	0.0313	Metabolism
SAUSA300_1725	*TalB*	Putative Transaldolase	1.511	0.0314	Biosynthesis Of Amino Acids
SAUSA300_1460		Peptidase, M20/M25/M40 Family, (Protein Fate And Metabolism	1.528	0.0316	Metabolism
SAUSA300_0758	*tpiA*	Triosephosphate Isomerase (General Metabolism)	1.666	0.0317	Metabolism
SAUSA300_2111	*GlmM*	phosphoglucosamine mutase	1.777	0.0318	Metabolism
SAUSA300_1804		Glucosamine-6-Phosphate Isomerase (Central Intermediary Metabolism)	1.641	0.0318	Metabolism
SAUSA300_1844	*ygaF*	Bacterioferritin Comigratory Protein (Cellular Processes)	1.721	0.0319	Metabolism
SAUSA300_1893	*nadE*	Fructose-Bisphosphate Aldolase, Class Ii	1.810	0.0319	Synthesis Of Cofactors
SAUSA300_0385		General Stress Protein 17M-Like Domain-Containing Protein (Same Family As Yflt?)	2.350	0.0319	Hypothetical Protein/Function Unknown
SAUSA300_2177	*rplQ*	50S Ribosomal Protein L17	2.313	0.0320	Ribosome
SAUSA300_0367	*ssb*	Single Strand DNA Binding Protein	1.665	0.0320	DNAReplication And Repair
SAUSA300_0688		Aldo/Keto Reductase Family Oxidoreductase	1.776	0.0320	Metabolism
SAUSA300_0972	*purF*	Phosphoribosyltransferase (Purine Metabolism)	1.632	0.0320	Nucleotide Metabolism
SAUSA300_1029	*IsdA (frpA, stbA)*	Iron Transport Associated Domain-Containing Protein (Heme Extraction)	1.594	0.0321	Virulence Factor
SAUSA300_1759		Probable Beta Lactamase	1.839	0.0321	Virulence Factor

SAUSA300_1994	*scrB*	Sucrose-6-Phosphate Hydrolase (Metabolism)	2.867	0.0321	Metabolism
SAUSA300_2315		Uncharacterised Lipoprotein	1.697	0.0322	Hypothetical Protein/Function Unknown
SAUSA300_1454	*zwf*	Glucose-6-Phosphate Dehydrogenase (Pentose Phosphate Pathway)	1.657	0.0322	Metabolism
SAUSA300_0759	*pgm*	Phosphoglyceromutase (Glycolysis)	1.804	0.0323	Biosynthesis Of Amino Acids
SAUSA300_1148	*codY*	N-Acetyltransferase Family Protein	2.004	0.0324	Signalling
SAUSA300_1362	*hup*	Dna-Binding Protein Hu	2.155	0.0324	Dna Replication And Repair
SAUSA300_1869	*map*	Methionine Aminopeptidase (Protein Metabolism)	1.617	0.0326	Biosynthesis Of Amino Acids
SAUSA300_1355	*aroA*	3-Phosphoshikimate 1-Carboxyvinyltransferase (Amino Acid Biosynthesis)	2.869	0.0327	Biosynthesis Of Amino Acids
SAUSA300_1615	*hemB*	Mevalonate Diphosphate Decarboxylase	2.230	0.0327	Synthesis Of Cofactors
SAUSA300_2529		Phnb-Like Domain-Containing Protein (Putative Dna Binding)	1.939	0.0328	Hypothetical Protein/Function Unknown
SAUSA300_1541	*grpE*	DNA-Binding Response Regulator Vrar	1.971	0.0328	Chaperones
SAUSA300_0427	*mpsC*	Na^+-Translocating Membrane Potential-Generating System Mpsc Domain-Containing Protein	2.524	0.0331	Transporter
SAUSA300_2082	*rpoE*	Dna-Directed Rna Polymerase, Delta Subunit	1.862	0.0333	Transcription
SAUSA300_1370	*ebpS*	Cell Surface Elastin Binding Protein	1.647	0.0333	Virulence Factor
SAUSA300_0655	*Regulator*	Cell Wall Surface Anchor Family Protein	2.026	0.0336	Hypothetical Protein/Function Unknown
SAUSA300_2096	*manA*	Transcriptional Regulator, Putative	2.160	0.0338	Synthesis Of Cofactors
SAUSA300_1152	*frr*	Ribosome Recycling Factor	2.029	0.0344	Ribosome
SAUSA300_0293		Membrane Transport	1.704	0.0345	Transporter
SAUSA300_1044	*trxA*	Thioredoxin	1.873	0.0347	Chaperones

SAUSA300_1860	*pepS*	Aminopeptidase	1.664	0.0354	Biosynthesis Of Amino Acids
SAUSA300_0525	*rplI*	50S Ribosomal Protein L7/L12	2.088	0.0357	Ribosome
SAUSA300_1582	*CsbD*	Sigmab-Controlled Gene Product	2.100	0.0362	Signalling
SAUSA300_0902	*pepF*	Dnak Protein	2.289	0.0369	Hypothetical Protein/Function Unknown
SAUSA300_1434		Phislt Orf104A-Like Protein, Repressor	1.672	0.0371	Hypothetical Protein/Function Unknown
SAUSA300_0253	*scdA*	Cell Wall Biosynthesis Protein Scda	1.578	0.0373	Virulence Factor
SAUSA300_0008	*hutH*	Histidine Ammonia-Lyase	1.460	0.0373	Biosynthesis Of Amino Acids
SAUSA300_2569	*arcB*	Flavohemoprotein, Putative	1.742	0.0375	Biosynthesis Of Amino Acids
SAUSA300_2362	*gpmA*	Phosphoglyceromutase	1.624	0.0377	Biosynthesis Of Amino Acids
SAUSA300_1261	*ysdC*	Putative Glutamyl Aminopeptidase	1.540	0.0378	Biosynthesis Of Amino Acids
SAUSA300_1517	*nfo*	Endonuclease	1.562	0.0378	DNAReplication And Repair
SAUSA300_1540	*dnaK*	Leucyl-tRNA Synthetase	1.840	0.0380	Chaperones
SAUSA300_0990	*rnpZA*	Conserved Hypothetical Protein	1.775	0.0384	Hypothetical Protein/Function Unknown
SAUSA300_0593		Hypothetical Protein	1.686	0.0387	Hypothetical Protein/Function Unknown
SAUSA300_0686	*nagA*	N-Acetylglucosamine-6-Phosphate Deacetylase	1.611	0.0387	Metabolism
SAUSA300_1476	*accB*	Acetyl-Coa Carboxylase, Biotin Carboxyl Carrier Protein	2.927	0.0391	Metabolism
SAUSA300_0226	*fadb*	3-Hydroxyacyl-Coa Dehydrogenase	2.418	0.0391	Metabolism
SAUSA300_1527	*era*	Gtp-Binding Protein Era	1.664	0.0395	Ribosome
SAUSA300_2102	*ywpJ_1 PE*	Haloacid Dehalogenase-Like Hydrolase	1.664	0.0396	Metabolism

SAUSA300_1653		Metal-Dependent Hydrolase	1.472	0.0397	Hypothetical Protein/Function Unknown
SAUSA300_0025	*adsA*	5'-Nucleotidase Family Protein	1.485	0.0409	Nucleotide Metabolism
SAUSA300_1368	*ansA*	L-Asparaginase	1.911	0.0411	Biosynthesis Of Amino Acids
SAUSA300_2225	*moaC*	Molybdenum Cofactor Biosynthesis Protein Moac	1.784	0.0413	Transporter
SAUSA300_0491	*cysK*	Cysteine Synthase A	1.661	0.0414	Biosynthesis Of Amino Acids
SAUSA300_1150	*tsf*	Elongation Factor Ts	1.637	0.0416	Ribosome
SAUSA300_1654	*pepQ*	Proline Dipeptidase	1.690	0.0416	Biosynthesis Of Amino Acids
SAUSA300_1900	*ppaC*	Putative Manganese-Dependent Inorganic Pyrophosphatase	1.525	0.0416	Metabolism
SAUSA300_1728		Aldo/Keto Reductase Family Oxidoreductase	1.613	0.0417	Metabolism
SAUSA300_1232	*katA*	D-Alanine-Activating Enzyme/ D-Alanine-D-Alanyl Carrier Protein Ligase	2.085	0.0419	Metabolism
SAUSA300_1659	*tpx*	Thiol Peroxidase (Adaptions To Atypical Conditions)	1.716	0.0420	Metabolism
SAUSA300_1790	*prsA*	Dihydroxyacetone Kinase	1.870	0.0420	Chaperones
SAUSA300_0372		Hypothetical Protein (Peptidase Family Pepsy	2.152	0.0423	Hypothetical Protein/Function Unknown
SAUSA300_1884	*CamS*	Cams Sex Pheromone Cam373 (Sporulation And Germination)	1.497	0.0424	Hypothetical Protein/Function Unknown
SAUSA300_1865	*vraR*	Adenylate Kinase	1.847	0.0425	Signalling
SAUSA300_1697		Peptidase Pepv	1.552	0.0425	Biosynthesis Of Amino Acids
SAUSA300_0856	*kapB*	Kinase Associated Protein B	2.148	0.0426	Signalling
SAUSA300_0547	*sdrD*	Gram-Positive Signal Peptide	1.505	0.0428	Virulence Factor
SAUSA300_0772	*clfA*	Fibrinogen-Binding Protein	3.810	0.0429	Virulence Factor
SAUSA300_2432	*nudG*	Mutt/Nudix Family Protein	2.291	0.0429	Dna Replication And Repair
SAUSA300_0141	*drm*	3,4-Dihydroxy-2 -Butanone-4-	1.913	0.0430	Nucleotide Metabolism

		Phosphate Synthase /GTP Cyclohydrolase Ii			
SAUSA300_0916		Hypothetical Protein (Rna Processing)	2.447	0.0431	Synthesis Of Cofactors
SAUSA300_0833	*nagD*	Acid Sugar Phosphatase	1.551	0.0431	Metabolism
SAUSA300_0569	*chdC*	Coproheme Decarboxylase	1.665	0.0432	Synthesis Of Cofactors
SAUSA300_0791	*gcvH*	Glycine Cleavage System Protein H	2.280	0.0433	Metabolism
SAUSA300_0790		Hypothetical Protein (Arsenate Reductase)	1.943	0.0433	Metabolism
SAUSA300_1982	*GroEL*	Conserved Hypothetical Protein	1.891	0.0433	Chaperones
SAUSA300_1492		Hypothetical Protein (Putative Lipoprotein)	1.649	0.0434	Hypothetical Protein/Function Unknown
SAUSA300_1691	*pepA*	Glutamyl-Aminopeptidase	2.321	0.0435	Biosynthesis Of Amino Acids
SAUSA300_1664	*ezrA*	Oligoendopeptidase F	1.996	0.0436	Growth And Division
SAUSA300_2230	*modA*	Molybdenum Abc Transporter Molybdenum-Binding Protein Moda	1.548	0.0436	Transporter
SAUSA300_2259	*Regulator*	Peptidylprolyl Isomerase	2.035	0.0436	Signalling
SAUSA300_2400		Glutamyl-Aminopeptidase	1.505	0.0436	Biosynthesis Of Amino Acids
SAUSA300_1842	*PerR*	Transcriptional Regulator, Fur Family	1.764	0.0437	Signalling
SAUSA300_0816		Csbd-Like Superfamily Protein	1.975	0.0437	Hypothetical Protein/Function Unknown
SAUSA300_0693	*saeP*	Hypothetical Protein (Putative Lipoprotein)	1.701	0.0439	Hypothetical Protein/Function Unknown
SAUSA300_1037	*pheS*	Phenylalanyl-Trna Synthetase Subunit Alpha	2.118	0.0439	Amino-Acyl tRNA Biosynthesis
SAUSA300_1611	*ValS*	Valyl tRNA synthetase	2.045	0.0439	Amino-Acyl tRNA Biosynthesis
SAUSA300_1856	*yhbO*	Hypothetical Protein	2.477	0.0440	Hypothetical Protein/Function Unknown
SAUSA300_1511		50S Ribosomal Protein L33	2.667	0.0440	Ribosome
SAUSA300_1197	*bsaA*	Glutathione Peroxidase	1.632	0.0441	Biosynthesis Of Amino Acids

SAUSA300_2396	*pnbA*	Para-Nitrobenzyl Esterase	1.563	0.0441	Metabolism
SAUSA300_2090	*deoC*	Purine Nucleoside Phosphorylase	2.096	0.0442	Metabolism
SAUSA300_0419	*lpl9*	Tandem Lipoprotein	1.685	0.0444	Hypothetical Protein/Function Unknown
SAUSA300_1453	*rnz*	Ribonuclease Z (Trna Processing)	2.497	0.0445	Ribosome
SAUSA300_1321		Hypothetical Protein (Putative Bacilliredoxin)	2.286	0.0445	Hypothetical Protein/Function Unknown
SAUSA300_1014	*cfiB (pyc)*	Pyruvate Carboxylase	2.429	0.0448	Biosynthesis Of Amino Acids
SAUSA300_0078	*copB*	Atpase Copper Transport	1.600	0.0450	Transporter
SAUSA300_2183	*adk*	Deoxyribose-Phosphate Aldolase	2.342	0.0453	Nucleotide Metabolism
SAUSA300_2621	*drp35*	Hypothetical Protein (Lactonase Drp35)	1.535	0.0457	Metabolism
SAUSA300_1690	*ytpP*	Putative Thioredoxin	1.744	0.0460	Metabolism
SAUSA300_1082		Hypothetical Protein (Pyridoxal Phosphate)	1.603	0.0463	Metabolism
SAUSA300_2091	*deoD*	Conserved Hypothetical Protein Tigr01033	1.804	0.0466	Nucleotide Metabolism
SAUSA300_0173	*srpF*	Hypothetical Protein (3-Methyl-2-Oxobutanoate Hydroxymethyltransferase)	1.659	0.0467	Hypothetical Protein/Function Unknown
SAUSA300_0234	*hmp*	Phosphopentomutase	1.836	0.0469	Metabolism
SAUSA300_0958	*Regulator*	Peptidase T	1.941	0.0470	Signalling
SAUSA300_1704	*leuS*	Leucyl tRNA synthetase	1.893	0.0471	Amino-Acyl tRNA Biosynthesis
SAUSA300_2534	*panB*	3-Methyl-2-Oxobutanoate Hydroxymethyltransferase	1.588	0.0472	Synthesis Of Cofactors
SAUSA300_0969	*purS*	Phosphoribosylformylglycinamidine Synthase, Purs Protein	1.907	0.0474	Nucleotide Metabolism
SAUSA300_1459	*gndA*	6-Phosphogluconate Dehydrogenase	1.690	0.0475	Metabolism
SAUSA300_1909		Hypothetical Protein (Thioredoxin Family Protein)	2.556	0.0476	Hypothetical Protein/Function Unknown
SAUSA300_2418	*ahpD*	Carboxymuconolactone Decarboxylase-Like Domain-Containing Protein	2.183	0.0477	Metabolism

SAUSA300_1011		Uncharacterized Protein (Ylal)	1.711	0.0480	Hypothetical Protein/Function Unknown
SAUSA300_0605	*sarA*	Staphylococcal Accessory Regulator A	1.915	0.0491	Signalling
SAUSA300_1969		Phi77 Orf011-Like Protein, Phage Transcriptional Repressor	1.564	0.0492	Hypothetical Protein/Function Unknown
SAUSA300_1983	*groS*	Chaperonin, 10 Kda	1.819	0.0495	Chaperones
SAUSA300_2136	*yhfQ (htsA)*	Iron Compound Abc Transporter Iron Compound-Binding Protein	1.776	0.0498	Transporter
SAUSA300_1050	*rdgB*	Mutt/Nudix Family Protein	1.702	0.0541	Nucleotide Metabolism
SAUSA300_1874	*ftnA*	Bacterial Non-Heme Ferritin	2.616	0.0544	Metabolism

The threshold for significant enrichment of these proteins was set to a q-value of 0.05.

Table 2: Overlapping proteins identified between the pulldown experiments of Haas *et al* and Wang *et al*

Protein	Function	*E. coli*		S. typhimurium (Soluble)
		Soluble	*Membrane*	
FtsY	Signal recognition particle receptor	X		
GlmM	Phosphoglucosamine mutase	X		X
Gpt	Xanthine phosphoribosyltransferase	X	X	
NfsA	Oxygen-insensitive NADPH nitroreductase	X		
PcnB	Poly (A) polymerase I		X	
PfkA	ATP-dependent 6-phosphofructokinase isozyme 1	X		
PfkB	ATP-dependent 6-phosphofructokinase isozyme 2	X		X
Rng	Ribonuclease G	X		
SelB	Selenocysteine-specific elongation factor	X		
YjiA	P-loop guanosine triphosphatase	X		

These experiments investigated the proteins isolated from both the soluble and membrane fractions of cell lysates.

Table 3: Overlapping proteins between this study and Wang *et al*

Protein	Function	q- value (this study)	Wang *et al* log2 (heavy/light)
GlmM	Phosphoglucosamine mutase	0.0318	1.63
PurF	Amidophosphoribosyltransferase	0.0320	
GpmA	Phosphoglycero mutase	0.0377	2.19
Era	GTP-binding protein	0.0395	3.27
Tsf	Elongation factor Ts	0.0416	2.06
Gnd	6-phosphogluconate dehydrogenase	0.0475	2.76

A ratio of heavy/light atoms was used in the Wang *et al.* study to determine significant enrichment with a threshold of >2.5. Whereas, this study utilises q-value as a determinant of significance.

Table 4: Overlapping proteins between this study and Haas *et al*

Protein	Function	q-value *S. aureus* (this study)	q-value *E. coli*		q-value S. typhimurium (soluble)
			soluble	membrane	
EF-P	Elongation Factor P	0.024	0.02	-	0.00
FadB	3-hydroxyacyl-CoA dehydrogenase	0.0391	0.00	-	-
GlmM	Phosphoglucosamine mutase	0.0318	0.01	-	0.00
GpmA	Phosphoglycero mutase	0.0377	0.00	0.00	-
GroS	Heat Shock protein	0.0495	0.00	-	-
GrpE	Heat shock protein	0.0307	0.00	-	-
Hup	DNA-binding protein HU	0.0304	0.01-0.00	-	-
MoaB	Molybdenum cofactor biosynthesis protein B	0.0310	0.01-0.00	-	-
NagD	Hypothetical protein	0.0431	0.00	-	-
PepQ	Dipeptidase	0.0416	0.01-0.00	-	-
RdgB	Nucleoside 5-triphosphatase	0.0541	0.01-0.00	-	-
Ssb	Single-strand binding protein	0.0320	0.02-0.00	-	0.00
TalB	Transaldolase	0.0314	0.01-0.00	-	-
Tpx	Thiol peroxidase	0.0420	0.00	0.00	-
ValS	Valyl-tRNA synthetase	0.0439	0.02-0.01	-	-
Zwf	Glucose-6-phosphate 1-dehydrogenase	0.0322	0.00	-	-

q-value comparisons between this study and Haas *et al* utilise a q-value significance threshold of 0.05.

Table 5: All proteins identified by the DRacALA methodology employed by Zhang *et al* 2018

Protein	Species
YgdH	*E. coli*
Gpt	*E. coli*
Hpt	*E. coli, B. subtilis, S. aureus*
GuaB	*E. coli, B. subtilis*
PurA	*E. coli*
Apt	*E. coli*
LepA	*E. coli*
Era	*E. coli, S. aureus*
HflX	*E. coli, S. aureus*
RsgA	*E. coli, S. aureus*
Der	*E. coli, S. aureus*
PrfC	*E. coli, D. vulgaris*
ObgE	*E. coli, B. subtilis*
Ef-Tu	*E. coli*
Ef-G	*E. coli*
InfB	*E. coli*
BipA	*E. coli*
DnaG	*E. coli, B. subtilis*
DksA	*E. coli*
MutT	*E. coli, T. thermophilus*
NudG	*E. coli*
TrmE	*E. coli*
NadR	*E. coli*
PhoA	*E. coli*
UshA	*E. coli*
RelA	*E. coli*
SpoT	*E. coli*
GppA	*E. coli*
HypB	*E. coli*
IdcI	*E. coli*
IdcC	*E. coli*
Ppx	*E. coli*
SpeC	*E. coli*
SpeF	*E. coli*

Table 6: All proteins identified by the capture compound approach employed Wang *et al* in *E. coli* 2019

Gene name		
gpt	*gnd*	*glmM*
hpt	*purA*	*pfkA*
speC	*nfsA*	*pcnB*
rsgA	*gsk*	*obgE*
znuC	*dksA*	
EF-G	*mpl*	
engB	*pyrI*	
ffh	*pgk*	
nudC	*selB*	
gdhA	*RF-3/prfC*	
mnmE	*gpmA*	
IF-2/infB	*pfkB*	
upp	*purC*	
bipA	*EF-Ts/tsf*	
der/engA	*ettA*	
ftsY	*ppx*	
EF-Tu	*tatD*	
EF-4/lepA	*purF*	
era	*guaB*	
yjiA	*cmk*	
folC	*purB*	
rnG	*pykF*	
ryrH	*ndh*	
rfbB	*entC*	
spoT	*dapB*	
YhhX	*Icd*	

Table 7: All proteins identified by the capture compound approach employed Haas *et al*

Gene name in *E. coli*					Gene name in *S. aureus*
aroK	*dbpA*	*cspE*	*aceA*	*cspC*	*asnS*
gcvP	*grxA*	*moaE*	*manY*	*rfaF*	*aspA*
sbcD	*fabH*	*zwf*	*degP*	*fadJ*	*cbiC*
ssb	*purC*	*efp*	*gapA*	*dtpA*	*dkgA*
yciK	*moaE*	*rlmD*	*tpx*	*tnaB*	*fabB*
yjiA	*pepN*	*dps*	*sodB*	*ybbO*	*fdhE*
galF	*nfsB*	*topB*	*yeeX*	*mdoH*	*gltA*
ydcF	*grxB*	*obgE*	*pssA*	*damX*	*himD*
yheS	*nanE*	*engB*	*nuoF*	*murF*	*hutG*
gstA	*glmM*	*ribF*	*yrbL*	*wecG*	*icdA*
ftsY	*fldA*	*uvrY*	*ghrA*	*yhfK*	*lysS*
hisB	*yjgM*	*yajO*	*ycgR*	*nirB*	*mdh*
fbp	*modF*	*elaA*	*grpE*	*mglA*	*mgsA*
sspA	*apaH*	*aceE*	*lpxB*	*rluB*	*pgm*
cmoM	*cmoM*	*pykA*	*narJ*	*yciE*	*rdgC*
deoB	*yjbJ*	*queF*	*nagD*	*pinE*	*rfbG*
aroH	*rdgB*	*groS*	*clpX*	*fadB*	SL1344_0397
moeA	*talB*	*cmoB*	*tdcD*	*nuoE*	SL1344_1220
ppnN	*metE*	*hsdR*	*fadD*	*araC*	SL1344_1223
yaeH	*moaB*	*rnb*	*dksA*	*htpG*	SL1344_1259
glnS	*thrC*	*argG*	*iscS*	*fklB*	SL1344_4176
pfkB	*sucD*	*frr*	*hcr*	*upp*	SL1344_4508
nagC	*valS*	*anmK*	*ackA*	*ppc*	*tktA*
gnd	*glcB*	*topA*	*pcnB*		*trxA*
pka	*rfbA*	*yhhA*	*artP*		*yaaA*
hslV	*galK*	*yeaG*	*focA*		*ygcX*
typA	*yeiP*	*prs*	*rpsA*		*asnS*
hisS	*pgk*	*hupB*	*msrA*		*aspA*
gpt	*bglA*	*ydfG*	*mtfA*		*cbiC*
mglB	*ydcH*	*ynfE*	*modC*		*dkgA*
selB	*rng*	*def*	*ybhF*		*fabB*
araD	*eno*	*yebE*	*rpoD*		*fdhE*
tig	*aceB*	*tldD*	*atpA*		*gltA*
galU	*pyrG*	*hupA*	*mlaD*		
folE	*apt*	*yjgA*	*icd*		

fusA	*purA*	*pdxH*	*ygiW*
pepQ	*purB*	*hemH*	*mlaF*
pfkA	*amn*	*cobB*	*rbbA*
proB	*ydjA*	*glf*	*bcp*
nfsA	*gpmA*	*pnp*	*lpxD*
pcm	*yjdC*	*ybjS*	*intF*
moeA	*uxuB*	*maeA*	*mrcA*
btsR	*trpB*	*aphA*	*fadI*

Where gene names are absent the proteins have been described by gene loci

Table of Contents

Chapter 1:

Introduction

1.1. Staphylococcus aureus

Staphylococcus aureus is a facultative anaerobic gram positive bacterium of the phylum bacillota, that was first identified as an infectious agent after isolation from a surgical abscess of a knee joint by Ogston in 1880, where close inspection of the bacteria revealed spherical clusters of cells (Ogston, 1984, Lowy, 1998). These clusters resembled grape bunches and led to the genus being named Staphylococcus, staphyle from Greek for “bunch of grapes” and kokkus “berry”. The bacterium was then further classified by Rosenbach in 1884 who isolated pure culture, and suggested the name Staphylococcus aureus due to the characteristic yellow/golden colour (aureus) (Rosenbach, 1884). The pigment responsible for this – staphyloxanthin, has been shown to be involved in virulence and viability of S. aureus in the presence of reactive oxygen species and neutrophils, with mutants preventing the formation of the carotenoid having impaired survival (Clauditz et al., 2006, Liu et al., 2005). The unique pigmentation of the colonies makes S. aureus easily identifiable from other species in the staphylococcal genus, of which there are 45 species and 24 subspecies (Lowy, 1998, Gherardi et al., 2018). The staphylococcal genus was initially divided into two major groups, coagulase positive staphylococci (CPS) and coagulase negative staphylococci (CNS) of which S. aureus is part of the former. Coagulases are polypeptides that form clots in blood plasma by activating prothrombin, an enzyme that converts fibrinogen to fibrin. The ability of S. aureus to bind to the mesh-like networks formed by fibrinogen and fibrin allows dissemination throughout the host bloodstream as thromboembolic lesions makes these polypeptides important in disease pathogenesis (Foster and Höök, 1998, McAdow et al., 2012). Therefore, the absence of coagulases was initially associated with a lack of pathogenicity in the CNS which account for around 30 of the species. However, this taxonomic approach is no longer viable, with commensal strains such as Staphylococcus epidermidis demonstrating themselves as true pathogens particularly in hospitalised patients (Toltzis, 2023, Becker et al., 2014). In 2018 the use of comparative genomics by Coates-Brown et al led to the introduction of three new categories: group A, which consists of species capable of causing human infection, including S. aureus, while groups B and C are known to cause infections in animals.

The genomes of staphylococcal strains are approximately 2.8 Mbp in size with relatively low G + C content of around 32.7% (Wang et al., 2012a). Despite the majority of the genome being ubiquitous, around 20% is subject to change as large sections display high variability (Ml·ynarczyk et al., 1998). These large sections, commonly referred to as genomic islands, were likely obtained through horizontal gene transfer (HGT)(Baba et al., 2008). Additionally, virulence and antibiotic resistant genes that contribute to persistent staphylococcal diseases can be attributed to these variable genome sections, which consist of mobile genetic elements (MGEs) such as: plasmids, pathogenicity islands, staphylococcal cassette chromosomes (SCC) and transposons (Baba et al., 2002, Ml·ynarczyk et al., 1998). These MGEs are largely involved in maintaining the plasticity of the genome, allowing bacteria to adapt to selective pressures such as antibiotics by enriching specific genes that promote fitness and survival.

1.1.1. Epidemiology

S. aureus is commonly found throughout the human population colonising flora such as the skin and mucosal membranes (5%) but is predominantly found around the anterior nares (20-30%) (Tong et al., 2015). It is a commensal and opportunistic organism that does not typically cause infection on healthy skin, with around 30% of the population unknowingly acting as permanent carriers (Gorwitz et al., 2008). However, due to a lack of symptoms, colonisation is not detected leaving the bacterium with a significant presence. This is best demonstrated by a study in 2004, involving the screening for *S. aureus* of 14,008 adults *via* nasal swab before admission to a non-surgical department, with 3420 testing positive (1 in 4). (Sakr et al., 2018, Wertheim et al., 2004). In addition throughout 2017 there were around 119,247 cases of *S. aureus* bloodstream infections resulting in around 19,382 deaths in the USA and around 12,073 deaths between 2018-2019 in the UK, a 37.7% increase from 2011-2012 (8767 deaths) (Kourtis et al., 2019, Thelwall et al., 2019). Following this percentage increase, in 2020 the USA was not on track for its goal of reducing 50% of in hospital-onset methicillin resistant *S. aureus* (MRSA) bloodstream infections from the 2015 baseline set by the Healthcare-Associated Infection National Plan (Kourtis et al., 2019). *S. aureus* was responsible for the most deaths globally at 1.1 million, while also being the leading cause of bacterial death in 135 countries (Vos et al., 2020, Murray et al., 2022). Unsurprisingly colonisation rates of *S. aureus* are higher in at-risk populations, such as individuals with open wounds or who regularly use hypodermics, patients with diabetes, immunocompromised patients and hospitalised patients (Tracey A. Taylor, 2020, Miller et al., 2015). The recurrence of *S. aureus* within these groups is also heightened perhaps due to the persistent colonisation that they experience. While *S. aureus* does not typically present a danger to healthy individuals, it is opportunistic and if given access to the circulatory system or internal tissues it can be a versatile and dangerous pathogen responsible for various clinical infections (Lowy, 1998). Several strains cause invasive infections such as: infective endocarditis in which it is the most common cause in the industrialised world (responsible for >25% of cases) along with; meningitis; septic arthritis; skin and soft tissue infections (impetigo); or toxin-mediated diseases such as toxic shock syndrome by the release of superantigens into the blood stream(Foster, 1996, Tong et al., 2015). Mortality rates associated with these infections remain high at around 15-50%(Turner et al., 2019, Lam and Stokes, 2023). MRSA infections that arise in a clinical environment are termed hospital-acquired (HA-MRSA) and these were predominant from the 1960s onwards, however, in the late 1990s and early 2000s MRSA infections became more common occurrences within the community and thus are termed community-acquired MRSA (CA-MRSA) (Wang et al., 2019b). It is therefore imperative that decolonisation of patients occurs before surgical intervention in order to reduce incidence rates. To assist this, preoperative techniques have been introduced, including the use of topical chlorhexidine and nasally administered mupirocin to decolonise the dermis and nares (Rao et al., 2008), significantly reducing the number of recurrent community-acquired and nosocomial MRSA infections while remaining cost effective (Miller et al., 2012, Wassenberg et al., 2011, Rao et al., 2008). Although preventative methods remain cost effective, the extensive pressures *S. aureus* places on the community and healthcare systems cannot be overstated.

In 2003 up to 400,000 inpatients in the US had *S. aureus*-related infections with the inpatients alone resulting in an economic burden of around $14.5 billion and an additional $12.5 billion for those requiring surgical intervention (Noskin et al., 2007). The prevalence of MRSA in health care was also noted to have risen in 2008 due to newly discovered virulence factors and was responsible for necrotising, frequently lethal, pneumonia along with a variety of other potentially fatal infections in otherwise healthy individuals, making it responsible for more deaths than HIV infection in that year (Noskin et al., 2007, Boucher and Corey, 2008, Rasigade and Vandenesch, 2014).

1.1.2. The evolution of antibiotic resistance and MRSA

When preventative methods are not enough, the treatment of active *S. aureus* infections can be difficult, due to the wide range of antibiotic resistances that can arise. One of the hallmark resistances developed by *S. aureus* was to penicillin, which occurred in the early 1940s. The full extent of how penicillin functions is unknown besides it interfering directly with cell wall assembly. Here, it binds to the penicillin binding proteins (PBPs), these proteins are responsible for integrating peptidoglycan into the nascent bacterial cell wall by cross linking due to their transpeptidase activity (Fisher and Mobashery, 2020). Penicillin functions as it shares high structural similarity to the D-alanyl-D-alanine residues of the peptidoglycan pre-cursor UDP-MurNAc-pentapeptide (Tipper and Strominger, 1965). This similarity allows for competitive inhibition of the native substrate and the formation of stable and long lasting acyl-complexes rendering the PBPs useless (Tipper and Strominger, 1965). While the production/maintenance of cell walls during growth is inhibited, the deconstruction of the cell wall by autolysins continues, meaning the cell is made susceptible to internal osmotic pressure and as a result, bursts and dies (Tomasz, 1979, Fisher and Mobashery, 2020). However, the structural feature that allowed penicillin to function would eventually become its downfall. Penicillin contains a characteristic β-lactam ring that is readily hydrolysed by penicillinases. Due to the selective pressure *S. aureus* experienced, it began to produce a penicillinase termed β-lactamase, this enzyme readily degrades the β-lactam ring acting as the pharmacophore, allowing the bacteria to cause persistent infections (Kirby, 1944). These penicillin resistant strains were subsequently responsible for large outbreaks of *S. aureus* in communities, as well as in clinical settings, by the 1950-1960s all over the world (Rountree and Freeman, 1955). As a result, the first semi-synthetic penicillin was introduced to clinical settings in 1961. Methicillin was an effective form of treatment as the steric hindrance associated with its ortho-dimethoxyphenyl group prevented staphylococcal β-lactamase from binding. However, only two years after its introduction MRSA was reported in the UK, marking the second wave of resistance (Jevons, 1961).

The genetic determinant for resistance in these strains was the presence of the staphylococcal cassette chromosome (SCC*mec*). This mobile genetic element is around 21-60 kb and contains the *mecA* gene, and was likely acquired by horizontal gene transfer from coagulase negative staphylococcal strains such as *Staphylococcus fleurettii* (Tsubakishita et al., 2010, Hashemizadeh et al., 2019). The *mecA*

gene encodes penicillin binding protein 2a (PBP2a), this protein benefits from poor affinity towards most β-lactam antibiotics, meaning it confers resistance to methicillin and its variants like oxacillin along with conjunction therapies that inhibit β-lactamases, such as clavulanic acid alongside amoxicillin (Vestergaard et al., 2019, Severin et al., 2005, Katayama et al., 2000, Prieto et al., 1998). As a result, the trans-peptidase enzymes (PBPs) can continue to cross link peptidoglycan polymers of the bacterial cell wall, maintaining the structural integrity of the cell (Malachowa and Deleo, 2010, Chambers and Deleo, 2009). Furthermore, MRSA has a resistance profile capable of spanning penicillin, cephalosporins and carbapenems, making treatment considerably more difficult (Papp-Wallace et al., 2011, Rayner and Munckhof, 2005). At the time, this newly found resistance caused significant problems, and by 1970-1980s these strains were endemic in the United States (US) and were ultimately responsible for a global pandemic of MRSA in hospitals that still persists to the present day. The *mec* gene complex also contains two other regulatory genes, the repressor *mecI* and the transmembrane β-lactam sensing signal transducer *mecR1*. In the presence of a β-lactam antibiotic, de-repression of both *mecA and mecR1* occurs allowing for the cleavage and activation of the metalloprotease domain of MecR1, which subsequently cleaves MecI and allows binding of the *mecA* operon, promoting transcription and synthesis of PBP2a (Berger-Bächi and Rohrer, 2002, Deurenberg and Stobberingh, 2008). SCC*mec* also contains the *ccr* gene complex that encodes two site-specific cassette chromosome recombinases CcrA and CcrB. As SCC*mec* is not a transposon or a phage, it requires these enzymes to successfully excise and insert itself into a specific site on the chromosome (Ito et al., 2014, Ito et al., 1999). There are around 13 variants of SCC*mec,* with the commonality being the presence of both *mec and ccr* complexes, however, allotypes of these genes are what define the variants. Interestingly both HA-MRSA and CA-MRSA can be associated with these allotypes, type I-III being HA-MRSA and CA-MRSA carrying IV and V (Uehara, 2022, Yamaguchi et al., 2020).

Due to the sheer number of MRSA infections, a last resort antibiotic, vancomycin was increasingly prescribed. This glycopeptide was the chosen method for clearance of MRSA, however, due its wide usage it acted as an intense selective pressure and around 20 years after its introduction, enterococcal species began to display resistance and were termed vancomycin-resistant enterococci (VRE)(Uttley et al., 1988). Shortly after this, vancomycin resistance emerged in MRSA supposedly due to the uptake of a vancomycin gene cluster containing the *vanA* gene obtained from VRE (McGuinness et al., 2017). As mentioned previously, the main function of many β-lactam antibiotics is to target cell wall production which eventually leads to cell death. Vancomycin works in a markedly similar way, targeting the terminal D-Ala-D-Ala of peptidoglycan preventing trans-glycosylation to the peptidoglycan chain which prevents further cross linking by trans-peptidation (Courvalin, 2006). The *vanA* gene encodes for a ligase that forms D-Ala-D-Lac in place of D-Ala-D-Ala altering the target of vancomycin and encouraging a third wave of resistance, in which vancomycin-resistant MRSA strains emerged termed VRSA (Courvalin, 2006). However, this might not be the only mechanism of resistance. One case study involving a chemotherapy patient undergoing treatment for *S. aureus*, allowed for the sequencing of vancomycin

susceptible isolates throughout treatment. Upon the treatment failing, vancomycin non-susceptible isolates were also obtained. Upon sequencing these isolates, 35 point mutations were identified across 31 loci with the most interesting being in the *vraR* operon, with 6 isolates displaying this mutation (Mwangi et al., 2007). With resistance to β-lactams, cephalosporins, carbapenems and even glycopeptides, MRSA is often classified as causing a multidrug resistant infection and as such constant efforts to find effective treatments continue. One of these drugs, daptomycin, was also trialled in the aforementioned case study. When comparing vancomycin-susceptible and -resistant isolates a 100-fold decrease in susceptibility towards daptomycin was observed (Mwangi et al., 2007).

Daptomycin is a lipopeptide antibiotic that has an unknown mechanism of action, however there are two proposed processes. Firstly upon binding Ca^{2+} it inhibits production of lipoteichoic acid – a polymer that is essential for normal growth in *S. aureus* (Boaretti et al., 1993). With the former mechanism being disputed the following was suggested. Upon binding to Ca^{2+}, daptomycin adopts a new conformation, allowing it to insert itself into the cell membrane bound, depolarizing it and disrupting membrane stability while also allowing vital ions and molecules such as K^{+}, Mg^{2+} and ATP to be lost (Heidary et al., 2017, Jung et al., 2004, Silverman Jared et al., 2003). Daptomycin has a few pharmacological advantages over vancomycin, namely it does not initiate nephrotoxicity and is often used as a substitute when this has progressed too far in the patient (Gaudard et al., 2019). In a comparative study, patients suffering from an MRSA blood stream infection were found to have decreased rates of all-cause mortality, 55% and 45% when switching from vancomycin to daptomycin within 3 or 5 days respectively, highlighting the benefit of having daptomycin as an available treatment. Despite daptomycin being used as a last resort against multidrug resistant strains of MRSA, instances of resistance have begun to arise. Although the resistance mechanism is unknown, these instances were more prevalent in cases where low doses were administered over a prolonged period or prior treatment with vancomycin had occurred (Julian et al., 2007, van Hal et al., 2011, Camargo et al., 2008). Interestingly, the VraRS two-component regulatory system (TCS) seemed to be upregulated in some of these cases, while the *dlt* operon has also been over expressed in others (Yang et al., 2009). *dlt* is associated with alanylation of cell wall teichoic acids meaning over expression could lead to over alanylation and a net increase in the charge of the cell surface, potentially affecting the insertion of daptomycin and as a result its effectiveness. This also validates the resistance pathway associated with the multiple peptide resistance factor MprF. Normally this virulence factor transports the lysyl-phospholipidphosphatidylglycerol (L-PG) to the outer region of the cytoplasmic membrane, a process that is essential for maintaining a net-negative charge (Ernst and Peschel, 2019, Ernst et al., 2009). Increased survival often occurs in *mprF* mutants, as the net charge becomes more positive due to decreased transport of L-PG to the outer region of the cell membrane. As with most antimicrobial peptides, daptomycin struggles to embed itself into the membrane as a result of this and its efficiency decreases (Thitiananpakorn et al., 2020). Although not widespread, daptomycin resistance is a bleak prospect when considering the lack of options clinicians currently have available.

Antibiotics can be considered the most intense selective pressure ever placed upon *S. aureus* and despite it being naturally susceptible to virtually every antibiotic, resistance has been and will continue to be acquired through phage events, horizontal gene transfer, mobile genetic elements or random mutants. The emergence of these strains is a testament to the organism's ability to adapt to selective pressures and survive irrespective of their cause (Chambers and Deleo, 2009). Resistance events have significantly marked the pharmaceutical industry with a 90% reduction in the approval of new antibiotics by the United States Food and Drug Administration over the last 30 years, meaning it is imperative that alternative strategies are explored for the treatment of such a clinically relevant pathogen (Shlaes et al., 2013).

1.1.2.1. Alternatives strategies for the treatment of staphylococcal infections

Vaccines are typically modelled on surface antigens or toxins as these are both readily recognised by the immune system, however, in the case of *S. aureus* the genome plasticity complicates the process with a large number of strains requiring assessment for suitability to ensure the vaccines have a broad range of protection (Proctor, 2012). Attempts have been made to develop a staphylococcal vaccine and initial results seemed promising in animal studies. One study found that using *S. aureus* surface associated proteins (SASP) in a vaccine led to a significant reduction in the cases of bovine mastitis (Vidlund et al., 2024). The use of the virulence factor staphylococcal protein A (SpA), allowed mice to prevent dissemination of *S. aureus* throughout the blood stream despite not preventing infection. This is attributed to anti-SpA antibodies that encouraged phagocytosis, potentially preventing *S. aureus* transitioning from the skin to the blood (Mandelli et al., 2024). Despite this success, staphylococcal vaccines have not yet proven effective in human trials. There are several explanations for this, *S. aureus* is commensal and exposure throughout life may reduce the effectiveness of vaccines due to "original antigenic sin" (Francis, 1960, Proctor, 2012). This can be explained as the immune system encountering a similar pathogen to one that was responsible for a previous infection and using its recall responses that were effective against the original strain but less effective against the current pathogen (Francis, 1960). Additionally, animal studies used for *S. aureus* often translate to human models poorly e.g. *S. aureus* is not part of mice skin flora.

There is a plethora of possible targets for developing human therapies. Surface antigens are able to stimulate opsonophagocytosis and as a result impact virulence, while antibodies against toxins are capable of blocking toxicity (Clegg et al., 2021). Other attempts to generate an effective vaccine have employed capsular polysaccharide antigens and surface proteins in the form of ClfA (previously mentioned in section 1.1.). Despite antigens and surface proteins being logical targets there is an abundance of pathogenic *S. aureus* strains that do not express capsular polysaccharides rendering these vaccine targets useless (Boyle-Vavra et al., 2015, Shinefield et al., 2002). This was seen in the failure of of StaphVax®, and SA4Ag which led to the development of the also underwhelming PentaStaph®, which utilised the same formula as StaphVax® with the inclusion of teichoic acid, the

pore forming α-toxin and panton valentine leukocidin (PVL), both important virulence factors (Jahantigh et al., 2022, Genestier et al., 2005). More recently a protein conjugating polysaccharide by GlycoVaxyn® was also trialled that involved glycosylating conserved staphylococcal antigens to *S. aureus* capsular polysaccharides, with the aim of reducing the number of vaccine components (Wacker et al., 2014). Previous bacterial vaccines, such as the ones targeting *Haemophilus influenzae* B and *Streptococcus pneumoniae*, use these protein glycoconjugate along with opsonisation and have been implemented globally (Trotter et al., 2008). Perhaps the lack of success associated with staphylococcal vaccines could be due to their reliance on opsonisation, which has led to more recent studies focusing on T-cell mediated immunity (O'Brien and McLoughlin, 2019).

Bacteriophages are lytic viruses that have been used to selectively kill bacteria for over a century, however, the advent of antibiotics led to a huge decrease in their use. Several studies investigating staphylococcal specific phage therapy are underway, however, they are associated with many complications. Evolution of resistance is a problem that still rears its head even in a context void of antibiotics, although this issue could be minimised using combination phage therapy (Plumet et al., 2022). Evasion of the hosts immune system is also required in order for the phage to perform its role effectively - some murine models have reported phage present in the bloodstream 21-25 days after their introduction with no impact on the killing of *S. aureus*, even in the presence of anti-phage antibodies (Capparelli et al., 2007). Despite their promise as therapeutic agents for treating *S. aureus* infection, phage therapies are still plagued with issues. There is no one phage extraction or purification method and a lack of research into the safety of using these viruses is abundantly clear. In addition, their dynamics with the host immune response, along with pharmacokinetics and pharmacodynamic properties remain to be established. Addressing these concerns would allow for phage therapies to be considered as a suitable treatment in the future (Plumet et al., 2022, Luong et al., 2020).

1.3. Staphylococcal Virulence Factors

The ability of *S. aureus* to act as such a capable pathogen stems from its virulence factors, some of which have been mentioned previously. These factors aid host invasion, immune evasion, use of host resources, antimicrobial resistance, damage to the host tissue by release of toxins that allow the pathogen to cause a multitude of infections spanning dermatitis to more invasive infections such as infective endocarditis or pneumonia.

1.3.1. Adhesion and invasion

The most important step in establishing an infection is to successfully adhere to host cells. This is typically done through cell wall associated (CWA) proteins, of which *S. aureus* can produce a wide variety. Fibronectin binding proteins (FnBPs) are proteins that aid host-cell adhesion, and rely on the formation of fibronectin bridges from these FnBPs towards a5β1 integrin on the cells surface (Sinha et al., 1999, Fowler et al., 2000). There are four different categories of which FnBPs fall under the microbial

surface component recognising adhesive matrix molecules (MSCRAMMs). The aforementioned ClfA also works alongside ClfB with both being essential for establishing bloodstream infections by binding to fibrinogen. Throughout 2012 there was an outbreak of an exceptionally virulent MRSA strain in Asia,due to the CWA protein SasX, that increased adhesion, with the origin of this protein being traced back to a lysogenic bacteriophage (Li et al., 2012, Lacey et al., 2016). Collagen is one of the most abundant proteins in the human body and during wound healing production of type-1 collagen can increase by around 100-fold (Stefanovic et al., 1997). *S. aureus* is capable of producing Cna, an adhesin that is able to tightly bind type-1 collagen with a binding affinity (K_d) of 54 nM (Arora et al., 2021, Xu et al., 2004). Cna was also found to be linked with arthritis, with a murine model showing ~70% of mice exposed to a Cna+ strain developed clinical signs of arthritis, while those exposed to a Cna- strain had a considerably lower incidence rate of 27% (Mohamed et al., 1999, Patti et al., 1994). Other mechanisms for adhesion include the serine aspartate repeat-containing protein SdrD, autolysin Atl and serine rich adhesin for platelets SraPv(Hirschhausen et al., 2010, Corrigan et al., 2009, Yang et al., 2014, Josse et al., 2017). SdrD binds to the cell surface of keratinocytes, Atl mediates internalisation by binding to the chaperone protein Hsc70, while SraP aids adhesion to epithelial cells in the lung by binding to A549 cells (Yang et al., 2014, Hirschhausen et al., 2010, Corrigan et al., 2009, Josse et al., 2017). Atl is also known to be involved in the secretion of *S. aureus* proteins including SdrD, which is also upregulated by neutrophils, implicating Atl with a role in internalisation (Pasztor et al., 2010). Alternative mechanisms of adhesion in the absence of other proteins also occur such as the binding to fibroblasts mediated by the staphylococcal extracellular adherence protein, Eap (Josse et al., 2017). *S. aureus* implements a variety of adhesion mechanisms in order to effectively establish infection, as not all binding targets will be readily available within the host.

1.3.2. Immune evasion and toxin production

Once *S. aureus* has successfully invaded a host, it is targeted immediately by the immune system and as such strategies for survival are a necessity, mainly evasion. Upon internalisation by a macrophage, the bacteria are exposed to a variety of stressors such as reactive oxygen species and neutrophil serine proteases (NSPs) that directly kill bacteria or cleave host immune proteins to produce antimicrobial peptides (Stapels et al., 2014, Stapels et al., 2015). These NSPs can be non-covalently inhibited at low nano-molar concentrations by Eap mentioned in section 1.3.1. preventing bacterial killing and degradation of the phenol soluble modulins (PSMs) (Kretschmer et al., 2021). PSMs are amphipathic α-helical cytolytic peptide toxins that damage the membrane and are an essential part of *S. aureus* immune evasion in serum causing neutrophil lysis by interacting with the neutrophil formyl-peptide receptor 2 (FPR2) (Periasamy et al., 2012, Wang et al., 2007b). This activates phagocytosis and oxidative bursts along with the lysis of leukocytes when in high enough concentrations (Kretschmer et al., 2021, Kretschmer et al., 2010, Weiß et al., 2020). *S. aureus* experiences a variety of environments within a host, yet the secretion of PSMs can occur whether in serum or a phagosome where these toxins assist escape before maturation into a phagolysosome. This occurs in a PSM-α dependent

process, with Δ*psmα* mutants failing to escape, while Δ*psmβ* mutants have no impact (Grosz et al., 2014). A similar trend was seen in the killing of neutrophils in a murine sepsis model, with Δpsmα strains exhibiting reduced virulence and Δ*psmβ* strains being comparative to wildtype (Wang et al., 2007b). Overall there is a clear trend in bacterial survival in neutrophils and the expression of PSMs (Geiger et al., 2012).

PSMs are not the only toxin utilised by *S. aureus*, panton-valentine leukocidin (PVL) is one of several two-component pore forming toxins and is heavily implicated as a virulence factor in necrotising strains of MRSA. These pore forming toxins, including LukAB, LukED, HlgAB and HlgCB, function through membrane destabilisation by binding to the membrane bound ADAM10 metalloprotease and forming heptameric β-barrel pores which ultimately lead to cell death (Spaan et al., 2017, Wilke and Bubeck Wardenburg, 2010). While not present in the majority of *S. aureus* isolates, some studies report PVL genes to be more prevalent in *S. aureus* strains responsible for infecting immunocompromised patients and around 85% of patients with necrotising pneumonia, highlighting its importance in disease progression (Gillet et al., 2002, Lina et al., 1999, Löffler et al., 2010). *S. aureus* is also capable of secreting superantigens (sAg), these are extracellular mitogenic toxins that ultimately lead to an exaggerated immune response (Vrieling et al., 2020). While this seems unhelpful at first, the purpose of these toxins is perceived to involve the debilitation of the host to allow the disease to permeate (Baker and Acharya, 2004). Staphylococcal superantigens such as (SElW), staphylococcal enterotoxin like toxin X (SElX) and the toxic shock syndrome toxin (TSST) bind to the variable β-chains in T-cell receptors leading to cell proliferation and unregulated cytokine release (Wilson et al., 2011, Vrieling et al., 2020, Fleischer and Schrezenmeier, 1988), causing serious immune dysregulation and subsequently rendering the body susceptible to toxic shock syndrome, where hypotension and multiple organ failure occur (Tuffs et al., 2022).

Staphylococcal protein A (Spa) is a virulence factor that attenuates the host's immune response by binding to human immunoglobulin (IgG) at the fragment crystallisable region, the tumour necrosis receptor factor 1 (TNRF1) and the glycoprotein- von Willebrand factor (Foster et al., 2014). Upon Spa binding to IgG, the immunoglobulin can no longer undergo hexamerisation and the bacterial cell becomes covered by IgG adopting an incorrect conformation. In this state it is unable to bind to neutrophil receptors to trigger opsonisation rendering it useless (Cruz et al., 2021). This, taken alongside studies with Spa deficient bacteria showing reduced virulence and lower mortality rates in murine models, heavily implicates Spa as a virulence factor in *S.* aureus (Palmqvist et al., 2002, Patel et al., 1987). Use of the host's nutrition is also essential for survival upon infection, as such, members of the near ion transporter (NEAT) motif family, such as the CWA Isd proteins are involved in capturing haem from haemoglobin. Once acquired, these molecules are transported to the cytoplasm where haemoxygenases liberate iron to aid survival, where iron is a restricted resource (Hammer and Skaar, 2011). Neutrophils have a variety of weapons available to them in the fight against pathogens, including

the distribution of neutrophil extracellular traps (NETs). These consist of intertwining fibrous strands predominantly of DNA associated with antimicrobial proteins that bind and trap pathogens allowing for their termination (Papayannopoulos, 2018, Rada, 2019). These NETs can be trivialised by *S. aureus* due to the release and activation of staphylococcal nuclease (Nuc) and adenosine synthase A (AdsA), that generate deoxyadenosine, leading to macrophage apoptosis.

1.3.3. *S. aureus* and its response to oxidative stress

Once inside the phagosome, bacteria are exposed to reactive oxygen species (ROS) such as $OH^{\cdot}$, O_2^{-} and HOCl generated by myeloperoxidases (MPOs) that use H_2O_2 as a substrate (Foster et al., 2014). Hydroxyl radicals can also be formed by the Fenton reaction where Fe (II) reduces H_2O_2 (Touati, 2000). The damage/toxicity associated with hydroxyl radicals is due to the oxidative damage of biomolecules inside the bacteria through lipid peroxidation, deamination, oxidation of methionine residues and DNA base oxidation as Fe (II) readily associates with nucleic acids causing damage localisation (O'Rourke et al., 2003, Praticò, 2001, Imlay, 2003). In order to resist this, *S. aureus* implements the staphylococcal peroxidase inhibitor (SPIN) that prevents the catalytic cleavage of peroxides by MPOs by directly blocking the active site (de Jong et al., 2017). Concentrations of ROS within the phagosome are estimated to be around 25 μM for $O_2^{\cdot-}$ and H_2O_2 at 1-10 μM, however, in the absence of MPO they rise to 100 μM and 30 μM respectively (Winterbourn et al., 2006, Fang, 2011). Therefore, one would assume that the inhibition of MPO by SPIN would lead to a similar but less extreme increase. Following this, upregulation of SPIN occurs during phagocytosis, while a decrease in survival has been observed in SPIN deficient *S. aureus,* suggesting it has a role as a virulence factor (de Jong et al., 2017).

The ability of *S. aureus* to counteract or prevent oxidative stress is important for host colonisation and survival and the peroxide sensor PerR is intrinsically linked with both colonisation and survival. High concentrations of iron induce the *perR* regulon, which contains KatA, the sole catalase of *S. aureus*, allowing for the reduction of H_2O_2 into O_2 and H_2O (Horsburgh et al., 2001). Despite its importance in detoxifying H_2O_2, KatA has been deemed unmportant for virulence but important for colonisation of the anterior nares, while PeR is required for virulence in murine models of infection (Cosgrove et al., 2007a, Ji et al., 2015). The organic hydroperoxide (Ohr) protein allows for increased resistance to ROS as Δ*ohr* strains of *Pseudomonas aeruginosa* in the presence of organic peroxides such as fatty acid hydroperoxides displayed increased sensitivity (Alegria et al., 2017). These three proteins will be discussed further in section 5.2.1.4.

1.3.4. Regulation of virulence factors using VraR and Agr as examples

TCS are universal protein pathways that convey information about the external cellular environment alongside changes within the cell (Lazar and Tabor, 2021). Signals are sensed by histidine kinases, which undergo a conformational change that leads to phosphorylation of a histidine residue of the intracellular domain (Tiwari et al., 2017, Bleul et al., 2022). The phosphorylated-histidine is now able to donate a phosphoryl group to an aspartate residue on the cytoplasmic-bound response regulator that

then allows DNA binding and transcriptional upregulation or downregulation (Bleul et al., 2022). The most characterised TCS in *S. aureus* is the accessory gene regulator (*agr*) involved in the quorum sensing system. The quorum sensing network in which agr is involved allows cell-cell communication and ultimately leads to gene regulation, with the upregulation of genes involved in toxin secretion and downregulation of genes involved in the synthesis of cell wall-associated proteins, implicating it in virulence (Rutherford and Bassler, 2012, Bleul et al., 2022). In addition, a very interesting member of the TCS group is the vancomycin resistance associated system (VraRS), consisting of the kinase (VraS) and the response regulator (VraR) (Yin et al., 2006). The VraRS TCS is responsible for sensing and transducing cell wall stress, while also facilitating resistance to cell wall targeting antibiotics such as vancomycin by upregulation of the cell wall stimulon. The cell wall stimulon is a group of ~46 unlinked genes that are involved in cell wall synthesis, and upon upregulation lead to a thicker cell wall and increased resistance towards vancomycin, heavily involving it in resistance mechanisms and pathogenicity (Dai et al., 2017, Howden et al., 2008, McCallum et al., 2011). Both the *agr* and VRaRS TCS were recently discovered to be linked, as DNase I footprinting assays during vancomycin induced stress have shown VraR is upregulated and binds to a 15 nucleotide sequence between the *agr* P2 and P3 promoters inhibiting the function of the quorum sensing system and reducing virulence (Dai et al., 2017). VraR will be discussed further in section 5.2.1.4

1.4. The stringent response

S. aureus has an extended reach across the globe due to its ability to colonise the skin and mucosal membranes of a large portion of the population, while its virulence factors aid infection and survival in more challenging conditions. Survival is also aided by a stress response termed the stringent response (SR), an almost ubiquitous response in bacteria with only 35 species incapable of producing it (Atkinson et al., 2011). The SR is responsible for inducing a slow growth phenotype when bacteria are exposed to external stresses, such as alkali shock, fatty acid starvation, and most importantly amino acid starvation. It decreases transcription rates of genes involved in replication and the biosynthesis of macromolecules. The resulting slow growth state allows the bacteria to effectively adapt to their environment forming dormant cells, promoting survival and virulence (Anderson et al., 2010, Pathania et al., 2021, Crosse et al., 2000). The response is predominantly mediated by two alarmones; guanosine pentaphosphate (pppGpp) and guanosine tetraphosphate (ppGpp), collectively termed (p)ppGpp (*Fig. 1.4*). Recently a third signalling molecule - guanosine 5'-monophosphate-3'-diphosphate (pGpp) was identified in *Bacillus subtilis*, although its function is largely unknown and so will not be the main focus of this section (Yang et al., 2020b).

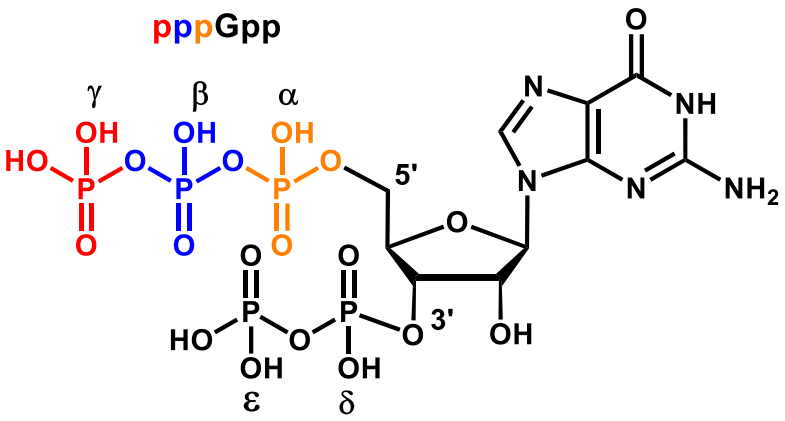

Figure 1.4. Structure of (pp)pGpp: The chemical structures of the stringent response alarmones. Represented by colour. pppGpp = red, ppGpp = blue, pGpp – orange. The nomenclature of the 5´-phosphates (α, β, γ) and 3´-phosphates (δ, ε) are also included.

First discovered in 1967 by Michael Cashel and Jonathan Gallant when starving *Escherichia coli* of amino acids, these hyper-phosphorylated nucleotides were termed the “magic spot” alarmones. High levels of (p)ppGpp result in the down-regulation of genes that play roles in biosynthesis processes, such as ribosomal assembly, translation and nucleotide transport/synthesis, while upregulating genes involved in stress and the starvation response, promoting a slow growth phenotype that allows survival in usually inhospitable conditions (Corrigan et al., 2016, Cashel and Gallant, 1969). Upon the alleviation of stressful conditions, the bacteria revert back to an active growth phenotype with low (p)ppGpp levels, ultimately implicating the stringent response in persistent and chronic infections (Geiger et al., 2014, Gao et al., 2010).

1.4.1. Synthesis and Hydrolysis of (p)ppGpp

These alarmones are intrinsically linked with RelA/SpoT Homologue (RSH) enzymes; named after the two (p)ppGpp synthesis enzymes found in *E. coli,* RelA and SpoT (Bennison et al., 2019, Atkinson et al., 2011). The RelA enzyme was named as shorthand for relaxed, with *relA* mutants exhibiting a relaxed phenotype in comparison to the stringent wildtype (Stent and Brenner, 1961). RSH enzymes catalyse the reaction of guanosine tri/diphosphate (GTP/GDP) with adenosine triphosphate (ATP). Here the 3´-OH group from GTP/GDP initiates an S_N2 (nucleophilic attack) on the β-phosphate of ATP producing (p)ppGpp and adenosine monophosphate (AMP) as a by-product (Fig. 1.4.1) (Sy and Lipmann, 1973). SpoT is also capable of removing inorganic pyrophosphate groups (PPi - the δ and ε phosphates), to produce either GDP or GTP (Beljantseva et al., 2017).

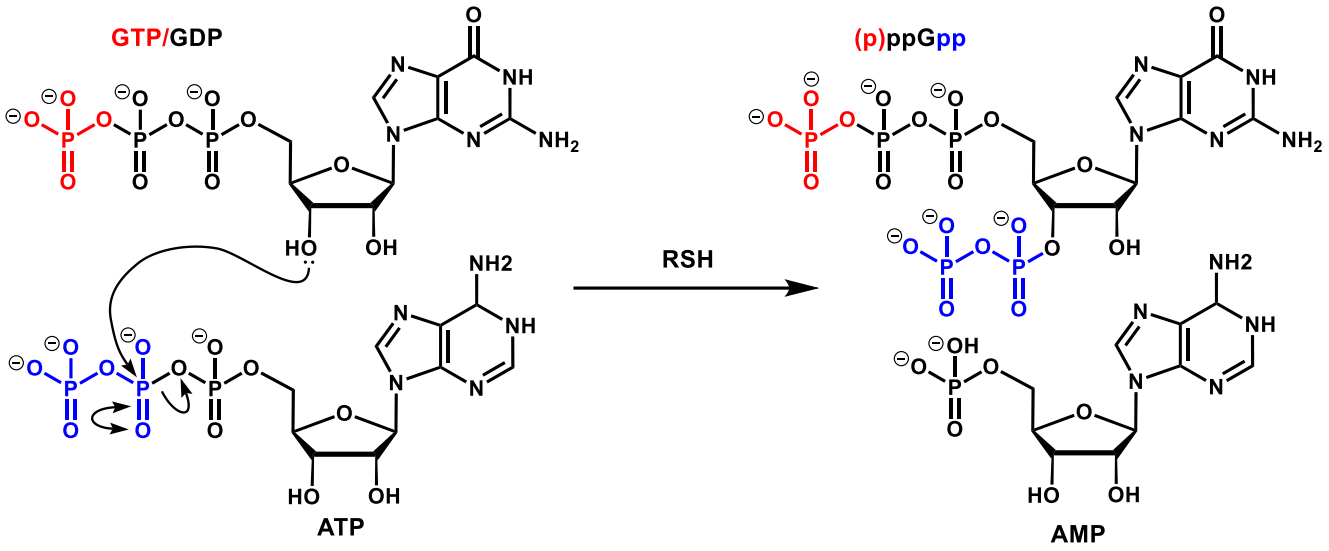

Figure 1.4.1: Mechanism of (p)ppGpp production from ATP and GTP/GDP. Synthesis of (p)ppGpp catalysed by an RSH enzyme. The 3´-OH lone pair of electrons from GTP/GDP initiates an S_N2 (nucleophilic attack) on the β-phosphate of ATP producing (p)ppGpp and adenosine monophosphate (AMP) as a by-product. The hydrolysis step reforms GTP/GDP and PPi. Under physiological conditions (pH ~7.4) the phosphates of the nucleotides would be carrying negative charges as the pH would be higher than the pK_as of the phosphoryl groups.

1.4.2. The stringent response enzymes (RSH)

1.4.2.1. Long RSH enzymes

The RSH enzyme superfamily is conserved throughout the bacterial kingdom and can be separated into three main groups: long-RSH enzymes; small alarmone synthetases (SAS) and the small alarmone hydrolases (SAH), all of which are responsible for the turnover of (p)ppGpp (Figure 1.5.2). Gram-positive bacteria such as *B. subtilis* and *S. aureus* classically have one long-RSH termed Rel and two SAS known as RelP and RelQ. These homologues are ubiquitous, and when comparing between species a high degree of structural similarity is visible (Steinchen et al., 2018, Steinchen et al., 2015b, Pausch et al., 2020). In *S. aureus*, Rel_{Sau} is bi-functional meaning it is able to synthesise and hydrolyse (p)ppGpp (Geiger et al., 2014). In contrast, *E. coli* utilises the aforementioned SpoT, a bifunctional long-RSH, for degradation and synthesis, while RelA is only a synthetase. Long-RSH enzymes have two significant regions - an N-terminal domain (NTD) comprising synthetase (SYNTH) and hydrolase (HD) domains responsible for (p)ppGpp production and degradation respectively. In addition, they have a regulatory C-terminal domain (CTD) consisting of: a threonyl-tRNA synthetase, GTPase and SpoT (TGS) motif; α-helical; a Zinc-Finger/conserved cysteine (ZNF/CC) domain; and an aspartate kinase, Chorismate mutase and a TyrA/RNA Recognition (ACT/RRM) motif (Brown et al., 2016, Steinchen and Bange, 2016). During steady state growth basal levels of (p)ppGpp are typically 10-40 μM, while in late-exponential/early stationary phase they can reach as high as 800 μM. However, upon induction of the stringent response, (p)ppGpp accumulates rapidly and within seconds can exceed cellular GTP pools at around 1-2 mM. This rise from basal levels is drastic, meaning that regulation of (p)ppGpp production is critical (Varik et al., 2017, Zborníková et al., 2019, Cashel, 1975). Typically, the SYNTH and HD

domains from the various enzymes work in conjunction to keep cellular (p)ppGpp levels at an optimum in relation to the bacteria's current stress conditions. One study investigating the role of the CTD in *Acinetobacter baumannii* found that truncating the RRM and ZFD regions of the CTD in SpoT lead to a 5-fold decease in (p)ppGpp hydrolase activity, while further truncations past the TGS regions reduced activity by 70-fold. The HD in $RelA_{Ec}$ is inactive due to the absence of a conserved motif (HDXXED) in the active site, making it monofunctional (Irving and Corrigan, 2018, Aravind and Koonin, 1998, Tamman et al., 2023). The hydrolysis of (p)ppGpp is vital as unmediated production leads to toxic accumulation, making SpoT of gram negatives such as *E. coli* essential (Gratani et al., 2018, Takada et al., 2020, Atkinson et al., 2011, Geiger et al., 2014, Steinchen et al., 2020). A similar trend was seen in *Streptococcus dysgalactiae* equisimilis, where truncation of the Rel CTD led to a 12-fold increase in synthetase activity and a 150-fold decrease in hydrolase activity (Irving and Corrigan, 2018, Geiger et al., 2010, Brown et al., 2016, Mechold et al., 2002), meaning this essentiality is also true of Rel in Bacillota (Au - Fernández-Coll and Au - Cashel, 2019, Gratani et al., 2018). Despite the absence of hydrolase activity in $RelA_{Ec}$, it is compensated for by SpoT, however, the HD of $RelA_{Ec}$ still possesses an important function. It contains a 17-residue loop that, when altered by mutations, leads to an abolition of synthetase activity (Sinha and Winther, 2021). Contrasting this, a reoccurring catalytic loop with a conserved RxKD motif occurs in both gram positive Rel and SpoT from gram negatives. This motif leads to regioselective binding with the γ-phosphate of GTP in both enzymes and the production of pppGpp by SpoT in gram negatives under fatty acid starvation (Sajish et al., 2007). Interestingly in *S. aureus,* amino acid starvation plays a role in the synthesis of both pppGpp and ppGpp, indicating that these secondary messengers ultimately may have different downstream binding partners and, depending on the stress, the molecules can be differentially synthesised (Sajish et al., 2007).

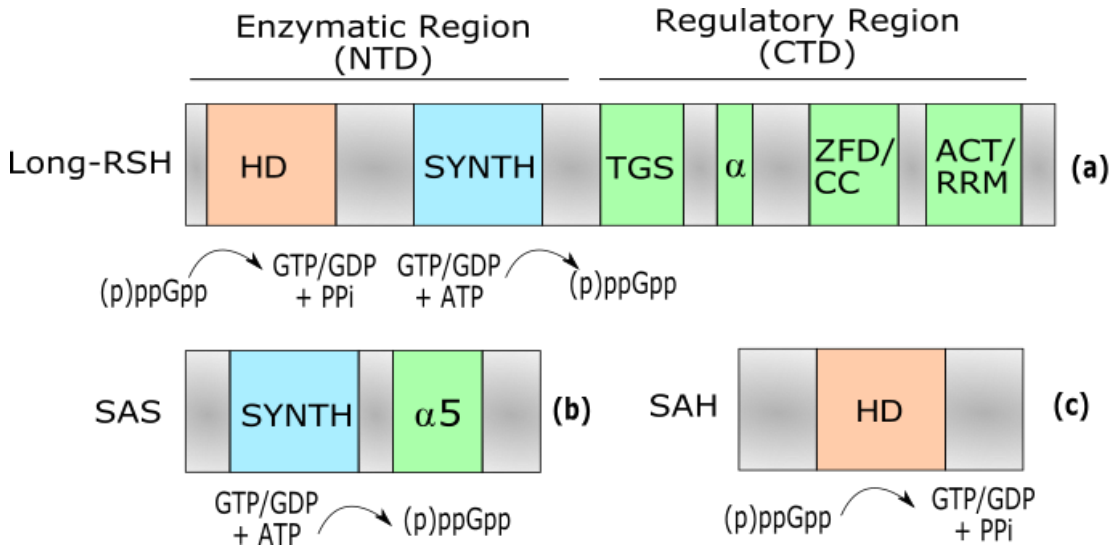

Figure 1.5.2: A summary of the constituent domains of the three classes of RSH enzymes. **a)** A bi-functional long-RSH protein showing the constituent domains of its NTD; HD (orange), SYNTH (blue) followed by Its CTD domains; ThrRS, GTPase, SpoT (TGS), α-helical, Zinc-Finger/conserved cysteine (ZNF/CC) and Aspartate kinase, Chorismate and TyrA/RNA Recognition (ACT/RRM) (green). (**b)** SAS protein showing its SYNTH (blue) and α-helical domain (green). (**c)** SAH protein and its sole HD.

1.4.2.2. Small alarmone synthetases

The SAS enzymes consist of a SYNTH and α-helical domain, of which there are two in most species of the Bacillota (Figure 1.5.2) (Irving and Corrigan, 2018, Geiger et al., 2010). They were first identified in *Streptococcus mutans* as RelQ (YjbM) and RelP (YwaC), with exposure to cell wall stress-inducing antibiotics such as vancomycin causing their expression and subsequent rise in (p)ppGpp levels (Lemos et al., 2007, Nanamiya et al., 2008, Steinchen et al., 2015a). The HD of Rel_{Sau} is responsible for degrading (p)ppGpp produced by the SAS enzymes $RelP_{Sau}$ and $RelQ_{Sau}$ in *S. aureus*, which have high structural homology to SAS enzymes across different species (Figure 1.5.2.2). These enzymes share a relatively high sequence homology of around 50% to each other and deletion of either *relP* or *relQ* in a strain lacking the Rel_{Sau} HD domain allows the bacteria to rescue growth, as both SAS functioning in a HD absent background is toxic (Geiger et al., 2014, Steinchen et al., 2018). Despite Rel_{Sau} being the major (p)ppGpp synthetase upon the induction of amino acid starvation, it is postulated that RelP and RelQ allow for the fine tuning of the stringent response by amplifying the signal, as they are unable to sense stress in the same manner as Rel due to the lack of an accessory domain (Cao et al., 2002, Atkinson et al., 2011, Irving et al., 2020). Because of this, they are both transcriptionally regulated by the aforementioned VraRS TCS, which induces their expression upon the detection of external stresses such as cell wall targeting antibiotics (Geiger et al., 2014). The investigation into why some bacterial species contain multiple (p)ppGpp producing enzymes has also led to the identification of SAS possessing more functional roles. Around five subfamilies of SAS enzymes have been found to act as toxins, with their genes encoded in operons that share high similarities with toxin-antitoxin operons. A prime example is *Cellulomonas marina*, which uses its SAS to produce both ppGpp and another hyperphosphorylated nucleotide adenosine 3'-5'-bis-diphosphate (ppApp) in signalling to other cells, causing depletion in both cellular GTP and ATP pools and eventually death (Jimmy et al., 2020).

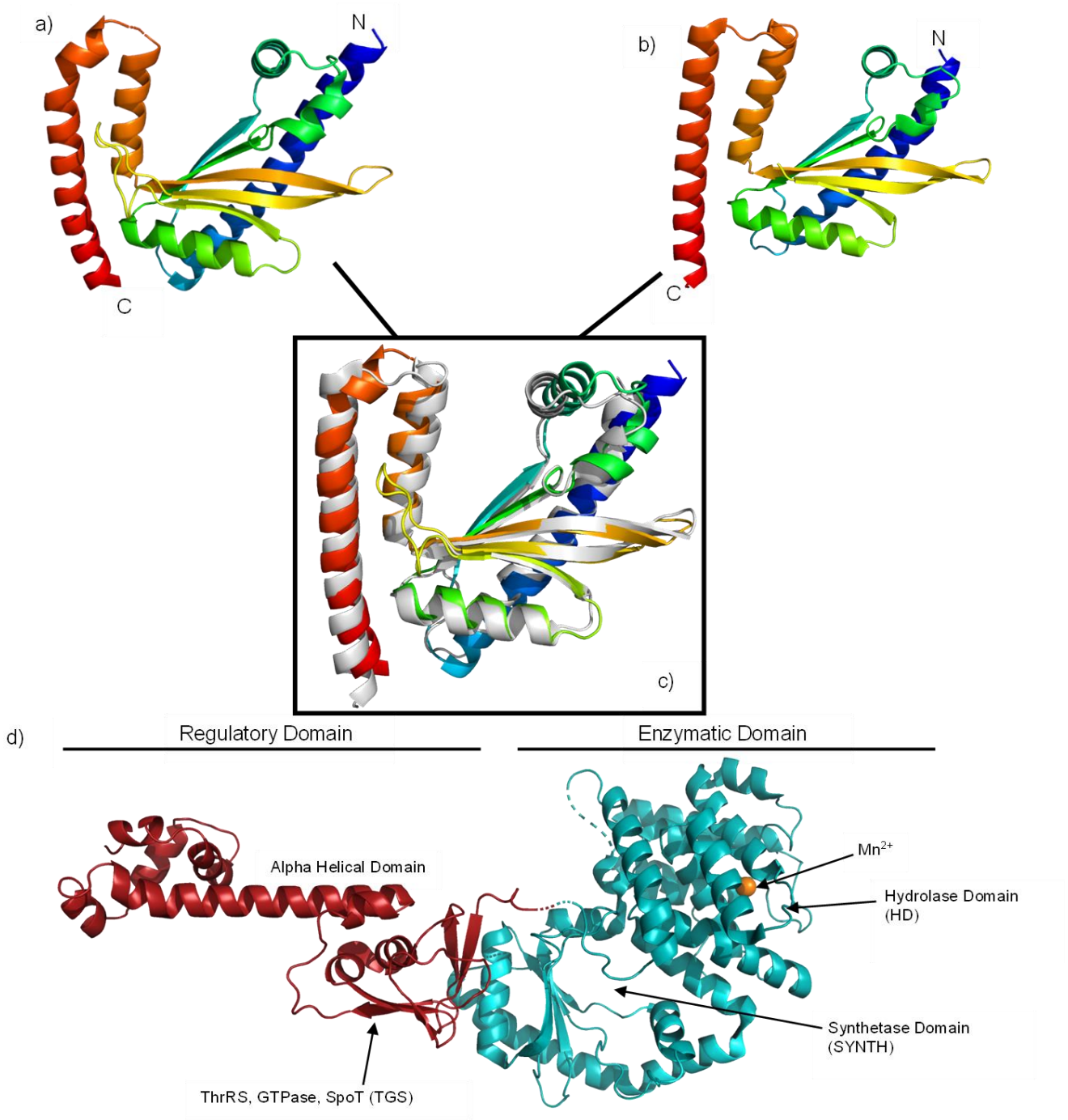

Figure 1.5.2.3: Structures of RelP RelQ and Rel: (**a)** $RelP_{Sau}$ with C and N terminus labelled, PDB: 6FGJ. (**b)** $RelQ_{Bs}$ with C and N terminus labelled, PDB: 5DEC. (**c)** Superimposition of $RelP_{Sau}$ and $RelQ_{Bs}$ to demonstrate the structural similarity in different species (RelQ in grey RelP in colour). (d) Structure of Rel_{Bs} a long bifunctional RSH enzyme in cartoon form, displaying the Regulatory domain (CTD: Red) and the enzymatic domain (NTD: teal) along with a manganese cation PDB: 6YXA. Images (Adapted from (Steinchen et al., 2018, Steinchen et al., 2015b, Pausch et al., 2020)

1.4.2.3. Short RSH – SAH

The previously mentioned SAH enzymes consist of a sole hydrolase domain and were confirmed as active in bacteria as recently as 2018, when the SAH RelH, a Metazoan SpoT Homologue 1 L (MESH1-L), was identified in *Corynebacterium glutamicum*. The confirmation of this homologue could mean that the SAH enzymes are present in some members of Bacillota, although their activity as working hydrolases has only been noted *in vitro* in certain conditions (Irving et al., 2020, Ruwe et al., 2018). SAH enzymes have also been identified in humans and common fruit flies (*Drosophila Melanogaster*), in the form of the SAH, MESH1. Their purpose between these two organisms varies, as in MESH-1 deficient *D. melanogaster*, slowed growth was observed, implicating a role for SAH in starvation responses within this organism (Sun et al., 2010). In contrast, in humans the SAH acts as a NADPH phosphatase, converting NADPH to NADH mediating ferroptosis, a process responsible for mediating programmed cell death (Ding et al., 2020). However, no specific role regarding (p)ppGpp hydrolase activity has been identified in humans, and there are no known (p)ppGpp synthetase enzymes in eukaryotes (Zhu and Dai, 2019, Sun et al., 2010).

1.4.2.4. regulation of (p)ppGpp levels

Bifunctional long-RSH enzymes are responsible for both the synthesis and hydrolysis of (p)ppGpp, therefore they must be tightly regulated in order to prevent hydrolysis of recently synthesised (p)ppGpp, with one enzymatic state often dominating another (Potrykus and Cashel, 2008). An insight into how this facet of the SR is controlled was obtained from the Rel enzyme from *S. equisimilis*, with truncation of the CTD leading to a 12-fold increase in (p)ppGpp synthesis, along with a 150-fold decrease in hydrolase activity (Mechold et al., 2002). During amino acid starvation there is an increase in the number of uncharged tRNA molecules, meaning during translation ribosomes stall more frequently. When this happens, the C-terminal domain of Rel_{Sau} binds to the stalled ribosome *via* the TGS and ZFD of its CTD inducing a conformational change (Gratani et al., 2018, Takada et al., 2020). Rel_{sau} shifts from its closed conformation (HD_{on}/Syn_{off}) where TGS/α-helical domains on the NTD stimulate the HD and ZFD/ACT/RRM domains preventing binding of the required starting materials ATP/GDP, to its open conformation (HD_{off}/Syn_{on}), activating (p)ppGpp synthesis (Chen et al., 2023, Haseltine and Block, 1973, Gratani et al., 2018, Tamman et al., 2023, Arenz et al., 2016, Loveland et al., 2016). Although not exclusive to nutrient starved conditions, the production of (p)ppGpp due to Rel binding to ribosomes occurs in *S. aureus*, while (p)ppGpp synthesis is further included in the absence of the branched amino acids (BCAAs): isoleucine, leucine and valine which are detected by Rel (Geiger et al., 2010, Loveland et al., 2016). Increased (p)ppGpp production can also arise due to a positive feedback loop, with (p)ppGpp allosterically binding to $Rel_{Sau}/RelA_{Ec}$, promoting production of ppGpp (Shyp et al., 2012). ppGpp production occurs more in gram negatives as the long-RSH Rel enzymes favour the synthesis of ppGpp. In contrast, gram positive bacteria such as *S. aureus* opt for the preferential synthesis of pppGpp – the exact reasons for this are yet to be determined (Mechold et al., 2013). The HD of $RelA_{Ec}$, despite being inactive, also plays a role in regulating (p)ppGpp binding, with an extended loop between

α6 and α7 regions sterically hindering the interaction (Tamman et al., 2023, Sinha and Winther, 2021). There is an interesting dichotomy between gram negatives and positives as SpoT is essential for inducing the stringent response during fatty acid starvation along with several other stresses including carbon and iron starvation but not amino acid starvation like Rel_{Sau}/$RelA_{Ec}$. However, this is all mediated by binding of the acyl-carrier protein (ACP) to SpoT (Xiao et al., 1991, Vinella et al., 2005, Battesti and Bouveret, 2006). Under normal conditions ACP is charged i.e it is linked to a fatty acid, however, under starvation conditions the ACP is uncharged (Battesti and Bouveret, 2006, Butland et al., 2005). This allows for an interaction between ACP and the TGS/RRM domain of SpoT. This interaction, however, does not occur with the long-RSH of bacteria only possessing one RSH such as Rel in *S. aureus* despite the conserved motifs. It is common knowledge that ACP relies on electrostatic complementarity between negative and positive surfaces and this may explain the phenomenon (Battesti and Bouveret, 2009). Due to the lower isoelectric point (pI) of ACP ~6.3, it is likely to bind to more basic partners (Battesti and Bouveret, 2009). When comparing this to the pI of both SpoT and Rel/RelA which are 8.9 and 6.3-7.6 respectively, it is clear to see why there is no interaction with the Rel/RelA enzymes (Battesti and Bouveret, 2009, Zhang et al., 2003). Although fatty acid shortage is still a relevant stress in gram positive species such as *B. subtilis*, the mechanism by which it is regulated differs, with regulation by other intracellular nucleotides such as GTP and ATP being likely as there is no real detectable increase in (p)ppGpp levels (Pulschen et al., 2017, Boutte and Crosson, 2011).

Regulation of the SAS enzymes also occurs in order to introduce intricacies and finer control over the stringent response. Cryo electron microscopy (CryoEM) of $RelQ_{Bs}$ resolved the structure in complex with ATP and pppGpp, revealing the protein forms a homo-tetramer with four active sites along with two allosteric nucleotide binding sites. $RelP_{Sau}$ was also investigated and shares the formation of a homo-tetramer, however, differences were present. $RelP_{Sau}$ had its activity downregulated by (p)ppGpp binding, with complete inhibition at 1 mM of either nucleotide, while binding of pppGpp to the allosteric sites of $RelQ_{Bs}$ increased its catalytic activity by 10-fold (Manav et al., 2018, Steinchen et al., 2015a).

Other regulatory mechanisms of the stringent response also exist, for example cross-talk with other secondary messengers such as c-di-AMP occurs. Corrigan *et al* identified that there is a significant overlap in the transcriptional profile of cells with high c-di-AMP concentrations and an induced SR in an *S. aureus* background. Upon examining the intracellular nucleotide pools, it was found that increased c-di-AMP levels led to induction of the SR with increased (p)ppGpp levels. Although this mechanism acts in a Rel-dependent fashion, c-di-AMP does not bind directly to Rel. Similarly, ppGpp also plays an indirect role in the inhibition of the phosphodiesterase GdpP, which is responsible for the degradation of c-di-AMP, leading to c-di-AMP levels remaining high (Corrigan et al., 2015, Holland et al., 2008, Rao et al., 2010). In addition, Rel of *B. subtilis* has been identified as a key interaction partner of the enzyme DarB during potassium starvation. When in its apo-state, DarB binds to Rel stimulating pppGpp production, while in its c-di-AMP bound state it is unable to engage in this interaction with Rel,

highlighting the intertwining roles of c-di-AMP and (p)ppGpp nucleotide signalling systems have on one another (Krüger et al., 2021).

Despite (p)ppGpp being essential for adapting to environmental cues and the regulation of global gene expression, the roles of pppGpp and ppGpp differ across species. Gram-negatives favour the production of ppGpp during amino acid starvation, while gram-positives prioritise production of pppGpp under the same stress (Cashel, 1996, Corrigan et al., 2015, Samarrai et al., 2011). This can be explained by ppGpp having a more regulatory affect than pppGpp, meaning it is important that a certain ratio is maintained to maximise survival (Mechold et al., 2013, Song et al., 2020). This is further supported by the presence of the pyrophosphatase GppA in *E. coli,* which is responsible for the cleavage of a phosphate from pppGpp producing ppGpp allowing for tighter control over the SR (Song et al., 2020). Overall, production of (p)ppGpp by the RSH-enzymes under stress leads to drastic changes in global transcription and translation ultimately affecting the proteome. However, once the removal of stressors has taken place, (p)ppGpp levels return to basal levels and the SR ramps down. Yet this poses the question: how is (p)ppGpp capable of regulating so many targets?

1.5. (p)ppGpp and its targets

1.5.1. Conformational flexibility and (p)ppGpp binding modes

An increase in the cellular (p)ppGpp pool caused by RSH enzymes leads to the interaction of (p)ppGpp with various targets involved in cell proliferation, such as *de novo* nucleotide synthesis, salvage pathways of nucleotide precursors, transcription, ribosomal assembly, translation and even regulation of other nucleotide pools. The range of functionality of these alarmones allows for the instigation of an appropriate stress response subject to the environmental factors *i.e* amino acid starvation. These responses are initiated *via* interactions with targets from numerous families with no distinct/conserved binding site. Structural analysis attributes this abundance of targets to the conformational flexibility exhibited by the 3′- and 5′- phosphate moieties of (p)ppGpp. This structural freedom allows for the molecules to adopt an enclosed “ring-like” or elongated conformation, making modulation of target proteins at various concentrations possible (Steinchen and Bange, 2016).

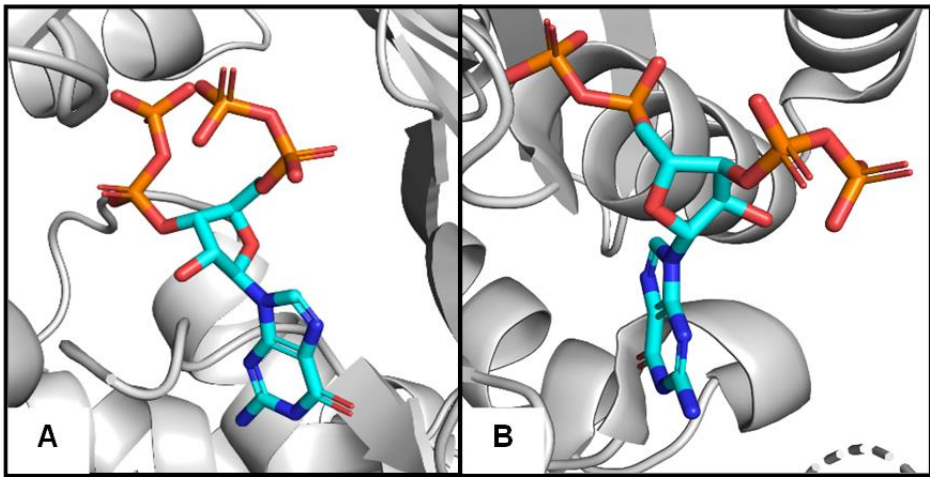

Figure 1.5.1: Molecular modelling of ppGpp in both its enclosed and elongated conformations. **a)** ppGpp docked in NatA acetyltransferase of *Saccharomyces cerevisiae* showing its enclosed conformation with the phosphates (orange) folding inwards this is typically mediated by magnesium or manganese (2+ ions) PDB: 4HNX(Neubauer, 2012). **b)** ppGpp docked in Release Factor 3 of *Nitratidesulfovibrio vulgaris* shown in its elongated formation., PDB: 3VR1(Kihira et al., 2012).

This is further explained by a considerable difference in binding affinity between the two conformations of ~10 fold (Steinchen et al., 2015b, Jores and Wagner, 2003). The ring-like conformation can be adopted with assistance from a Mg^{2+} ion or without assistance. In contrast, the elongated conformation has the 3′- and 5′- phosphates positioned a considerable distance from each other, stabilised by Mn^{2+}/Mg^{2+} metal ions located between the two moieties (Steinchen and Bange, 2016). This was further proven by Zhang *et al* (2019), where a complete loss of alarmone binding was observed in a $PpnN^{RRK}$ triple mutant that lacked all 5′-phosphate interacting residues, implying that the 3′-phosphate interactions are not enough to sustain binding (Irving et al., 2020, Steinchen and Bange, 2016, Zhang et al., 2019). Despite being chemically simple, the ability of (p)ppGpp to adopt two structurally opposing conformations allows for the mediation of its pleiotropic effects by interactions with numerous binding partners.

When examining the conservation of binding modes across (p)ppGpp targets – one study used crystal structures of proteins in complex with (p)ppGpp that were accessible by the protein data bank and categorised interactions into the following; Van der waals; hydrogen bond; weak hydrogen bond; ionic; metal complex; aromatic; polar and weak polar. They first investigated the (p)ppGpp synthetases $SAS1_{Bs}$, $SAS2_{Sau}$ and Rel from *Thermus thermophiles* and found the binding sites consist of mainly polar residues that form hydrogen bonds with (p)ppGpp, while also maintaining π-π stacking through the guanine base and the aromatic side chain of tyrosine. Ionic interactions were also noted between the phosphate groups and guanidinium of arginine residues, while cofactors such as Mg^{2+} played an important role in stabilising the phosphate groups (Steinchen et al., 2015a, Manav et al., 2018, Tamman et al., 2020, Kushwaha et al., 2020).

They also investigated targets of (p)ppGpp involved in metabolism, of which there are six structures in complex with (p)ppGpp available, including well characterised targets such as hypoxanthine ribosyl transferase (HprT), guanylate kinase (Gmk) and amidophosphoribosyltransferase (PurF) whose roles will be discussed later (Anderson et al., 2019, Liu et al., 2015b, Wang et al., 2019a). In terms of a conserved binding site across these proteins, (p)ppGpp seemed to facilitate oligomerisation by binding at the oligomeric interface where there is a plethora of residues involved for π-π stacking with the guanine base such as phenylalanine 152 in HprT and tyrosine 83 in Gmk, while this stacking was absent in PurF(Kushwaha et al., 2020). Phosphate groups were again stabilised by arginine guanidine moieties and Mg^{2+} ions, while the N1, N2, N7 and O6 atoms of the guanine ring were responsible for hydrogen

bonds, along with the ribose ring which interacts with the protein through water mediated hydrogen bonds (Kushwaha et al., 2020)

GTPases were also examined, including RbgA, Obg and BipA. These proteins shared a shallower binding site than metabolic proteins and the synthetases, along with a different binding mode (Pausch et al., 2018, Buglino et al., 2002, Kumar et al., 2015). They predominantly interacted *via* Van Der Waals forces and hydrogen bonds due to the absence of ionic interactions with arginine residues and π-π stacking (Kushwaha et al., 2020).

The ability of (p)ppGpp to regulate transcription is well established and it is able to do this in *E. coli* by directly binding two distinct sites on the RNA-polymerase (RNAP) (Potrykus and Cashel, 2008). The RNAP consists of 5 subunits; α1, α2, β, β' and ω. The first binding site (site 1) is situated between the β' and ω subunits and contains a methionine, alanine, arginine (MAR)-motif at the end of the ω-subunit that is a useful determinant of p)ppGpp binding to RNAP in other species (Hauryliuk and Atkinson, 2017, Sutherland and Murakami, 2018, Hauryliuk et al., 2015, Ross et al., 2013). This shallow opening allows for interactions between the guanine base and a number of residues including arginine, isoleucine, histidine and aspartic acid. The second site (site 2) is only available upon binding of RNAP and (p)ppGpp to the transcriptional regulator DksA, which mediates binding with the residues of the β' rim. This again provides stabilisation through aromatic interactions with tyrosine, while ionic interactions with lysine and arginine stabilise the phosphates (Kushwaha et al., 2020, Ross et al., 2016b).

It is clear to see that (p)ppGpp does not have one conserved binding mode across all of its targets and instead binds through a plethora of interactions. Although these types of studies provide a useful insight into (p)ppGpp binding modes across each cellular process, they require the resolution of protein crystal structures in complex with (p)ppGpp of which there are a select few, therefore no assumptions should be made without further investigation.

1.5.2. Transcription and DNA replication

(p)ppGpp is known to inhibit both DNA replication and transcription, with the former being targeted by binding to the DNA primase DnaG in both *B. subtilis* and *E. coli*. Despite the two species preferring different nucleotides for this role, pppGpp in *B. subtilis* and ppGpp in *E. coli*, both nucleotides bind directly to the active site in their respective background during DNA replication (Wang et al., 2007a, Maciag et al., 2010). (p)ppGpp accumulation during the stringent response also reduces the transcription of the replication initiation ATPase DnaA, leading to a reduction in replication rates (Schreiber et al., 1995). As mentioned previously in section 1.6.1, (p)ppGpp directly binds to $RNAP_{Ec}$. A consequence of this is a decrease in cellular transcription and negative supercoils. These supercoils would typically accumulate near the *oriC* origin and promote replication initiation mediated by DnaA binding, however, with decreased levels of negative supercoils this slows (Kraemer et al., 2019).

Together the effect of (p)ppGpp on DnaG along with both DnaA and *oriC*, leads to regulation over DNA replication.

The effect of (p)ppGpp on the global transcriptional profile is an essential facet of the SR. Altered expression profiles of 1,200 genes were noted within 10 minutes of inducing the SR, highlighting its role in this process and demonstrating that understanding this process is therefore essential for examining how the slow growth phenotype is induced (Sanchez-Vazquez et al., 2019). The first complex found to be regulated by (p)ppGpp was the RNAP in *E. coli.* Upon binding to the site 1 of RNAP, (p)ppGpp is capable of reducing transcription rate by 2-fold, while simultaneous binding to site 2 at the DksA interface leads to a more dramatic decrease in transcription at around 20-fold (Figure 1.5.2) (Ross et al., 2016a, Paul et al., 2005, Paul et al., 2004, Potrykus and Cashel, 2008).

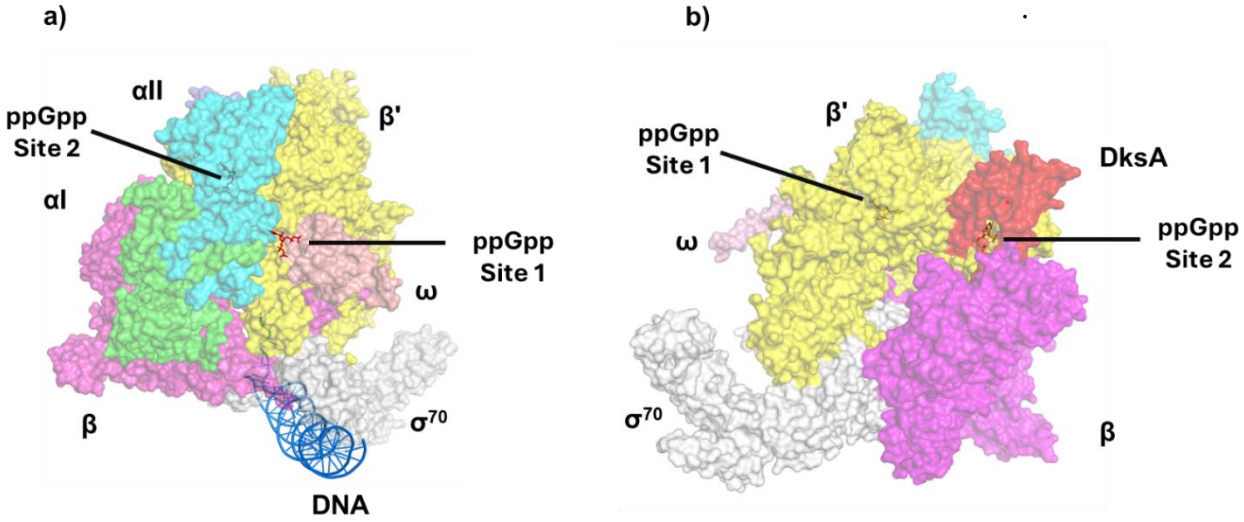

Figure 1.5.2: RNAP of *E. coli* bound to ppGpp in the presence of DksA. a) RNAP complex bound to σ_{70} (grey), *rrnBP1* promoter DNA (blue) and two molecules of ppGpp (orange). Site 1 is present at the front of the complex between the β' (yellow) and ω (pale pink) subunits (PDB: 6WRD now replaced by 7KHI)(Shin et al., 2021). **b)** RNAP in complex with DksA (red) with ppGpp binding site 2 previously hidden at the rear now being visible at the interface of DksA and the β (magenta), β' (yellow) subunits (PDB: 5VSW). The remaining subunits are coloured accordingly, α1 (green) and α2 (cyan). (Shin et al., 2021)

(p)ppGpp further inhibits transcription by interfering with the binding of RNAP to sigma factor σ_{70} (Dalebroux and Swanson, 2012, Kazmierczak et al., 2005). Under normal growth conditions this binding would lead to cell growth, proliferation and virulence, however, the binding of RNAP with σ_{70} is prevented by (p)ppGpp and DksA working in a synergistic manner, leading to downregulation of amino acid biosynthesis genes and reduction of ribosomal RNA (rRNA) through modulation of *rrn* promoters (Bennison et al., 2019, Parshin et al., 2015, Geiger et al., 2010, Paul et al., 2004, Kazmierczak et al., 2005). The reduction in rRNA leads to a decrease in translation due to the decrease in functional ribosome products. However, in Bacillota such as *S. aureus*, (p)ppGpp does not directly bind to the RNAP, instead a different regulatory mechanism involving nucleotide levels affects transcription (Geiger et al., 2010).

1.5.3. Regulation of GTP levels

Under stringent conditions, (p)ppGpp accumulates rapidly with concentrations reaching as high as 1 mM during maximum stress. This in turn rapidly depletes the nucleotide pools of GDP/GTP and ATP, the substrates required for (p)ppGpp synthesis (Bittner et al., 2014). The almost positive feedback-like mechanism that (p)ppGpp engages in by stimulating its own production, along with the inhibition of GTP synthesis enzymes such as HprT and Gmk in *S. aureus* (Fig. 1.5.3), ensure that these levels remain low throughout the duration of the stress (Shyp et al., 2012, Corrigan et al., 2016, Liu et al., 2015b). Gmk is directly involved in *de novo* synthesis of purine nucleotides, mainly GDP, a precursor to GTP, while HprT acts in the salvage pathway where it is responsible for the conversion of hypoxanthine to inosine monophosphate (IMP) and guanine to guanosine monophosphate (GMP). It also weakly inhibits the IMP dehydrogenase (GuaB) with a large portion of its activity remaining even at high concentrations. Inhibition of PurF also leads to a decrease in concentration of early purine nucleotide building blocks as it is responsible for the formation of 5'-phosphoribosylamine (5PRA) from (PRPP) (Kriel et al., 2012, Liu et al., 2015b).

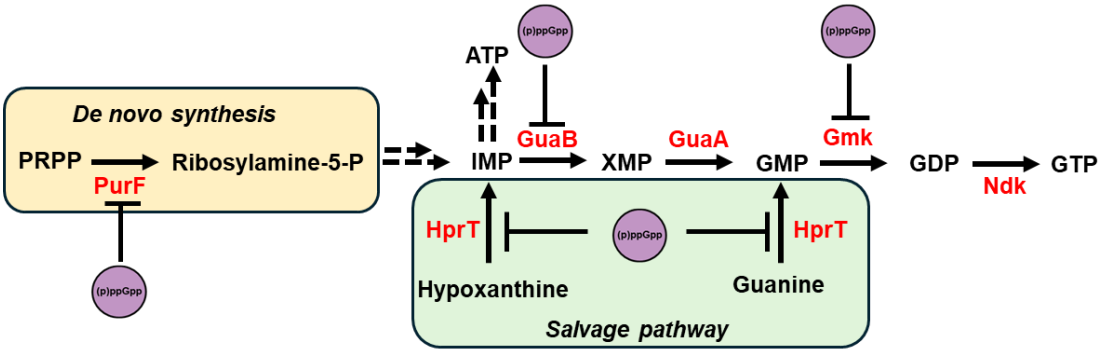

Figure 1.5.3: (p)ppGpp regulates GTP levels by inhibiting multiple targets across *de novo* and purine salvage pathways. (p)ppGpp inhibits multiple enzymes (red) spread across the *de novo* synthesis (yellow) and purine salvage pathways (green). The purine nucleotide synthesis pathway begins with the conversion of PRPP into 5PRA catalysed by PurF. A few steps occur including formylglycinamide ribonucleotide (FGAR) and formylgycinamidine ribonucleotide (FGAM) before the formation of inosine monophosphate (IMP). The IMP dehydrogenase (GuaB) and the guanine synthase (GuaA) catalyse the formation of Xanthine monophosphate and Guanosine monophosphate respectively from IMP. GMP then undergoes the addition of phosphates by the guanylate kinase (Gmk) and nucleoside diphosphate kinase (Ndk) to form GTP. While in the salvage pathway hypoxanthine and guanine due to their structural similarity are salvaged by HprT to form IMP and GMP respectively.

This regulation allows (p)ppGpp to control GTP biosynthesis *via* both *de novo* synthesis and salvage pathways, making it essential for survival in Bacillota such as *S. aureus* but not *E. coli* despite sharing binding partners across species. Without the presence of (p)ppGpp in *B. subtilis*, GTP dysregulation occurs followed by cell death (Kriel et al., 2012, Kriel et al., 2014). Although decreasing GTP levels lead to the downregulation of genes that initiate with a G nucleotide, genes that are initiated by an A nucleotide are still transcribed, including BCAA genes (Wolz et al., 2010, Sherlock et al., 2018). At standard GTP levels in Bacillota, the global transcriptional regulator CodY competes with the RNAP for binding to DNA and represses transcription. However, at low GTP levels induced by amino acid

starvation or entry into stationary phase, CodY derepresses from DNA enabling transcription, with upregulation of around 143 genes implicated in the adaptation to nutrient starvation and virulence, including the aforementioned *agr* promoter (Figure 1.5.3.1) (Corrigan et al., 2016, Geiger et al., 2010, Belitsky and Sonenshein, 2011, Irving et al., 2020, Kaiser et al., 2018, Handke et al., 2008, Majerczyk et al., 2008). This is because GTP along with BCAAs act as co-factors for CodY, repressing its function when these are in short supply de-repression and transcription occurs (Kaiser et al., 2018). In *E. coli* the RNAP-DksA complex binds to *rrn* promoters stimulating production of rRNA but is inhibited by (p)ppGpp leading to a decrease in rRNA, while in *S. aureus* DksA is absent so this depletion of cellular GTP pools leads to the same reduction but *via* a different mechanism as many *rrn* operons require GTP as an initiating nucleotide (Kästle et al., 2015).

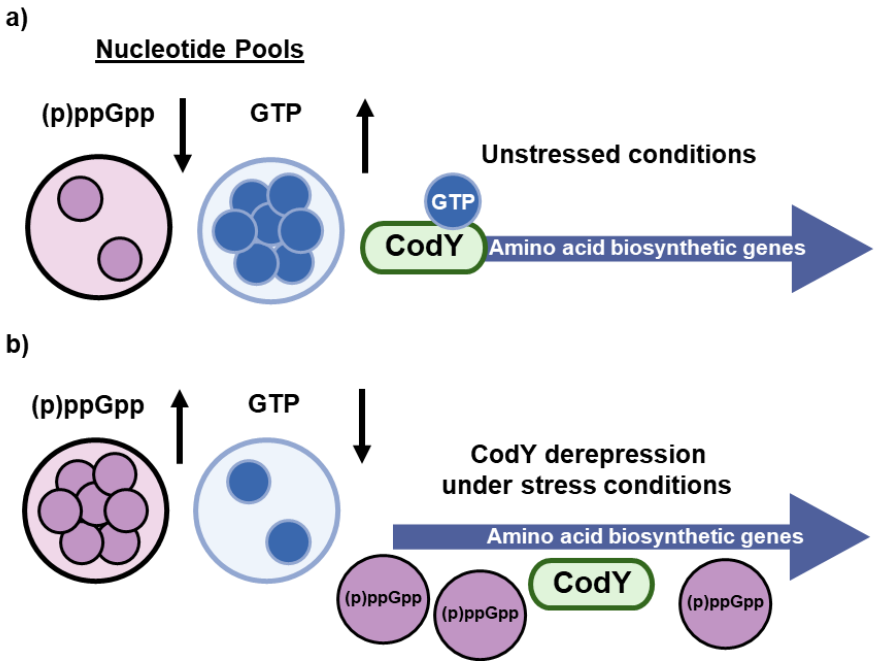

Figure 1.5.3.1: (p)ppGpp exerts control over GTP nucleotide pools and CodY regulation. a) In the presence of sufficient nutrition GTP levels are high and so CodY associates to DNA with assistance from its cofactors GTP and BCAA to repress genes involved in the CodY regulon. **b)** Upon the transition to starvation conditions (p)ppGpp synthesis increased and the GTP nucleotide pools are depleted. The lack of GTP as a cofactor leads to CodY derepression and the transcription of around 143 genes involved in stress adaptation, virulence and amino acid biosynthesis.

The interaction of (p)ppGpp with riboswitches provides an alternative route to the regulation of gene transcription. Riboswitches are defined as non-coding regions of RNA that exert their regulatory control over the transcript by binding a small molecule/ligand (Garst et al., 2011, Mironov et al., 2002). The *ykkC* riboswitches are found within bacteria and can be divided into to subtypes, *ykkCS1* that are capable of binding guanidine and *ykkCS2* that are incapable of making this interaction due to mutations in their binding site (Reiss et al., 2017). ppGpp is able to bind to the *ykkCS2* group, which is unsurprising when considering this riboswitches links to genes involved in BCAA synthesis, ATP binding cassettes

and glutamate synthesis - which is elevated under stringent conditions (Sherlock et al., 2018, Imaizumi et al., 2006). Overall, the ability of (p)ppGpp to regulate a plethora of cellular processes including transcription both directly and through the mediation of GTP levels is impressive, however, it also has effects at a post-transcriptional level.

1.5.4. Translation and the ribosome

In addition to derepressing CodY, (p)ppGpp was shown to further inhibit cell proliferation and slow growth at a post-transcriptional level in *S. aureus* by Corrigan et al who implemented a genome wide nucleotide-protein interaction screen to identify additional (p)ppGpp targets (Corrigan et al., 2016). This led to the identification of several GTPases, a superfamily of ubiquitous enzymes responsible for the hydrolysis of GTP to GDP, as binding targets. The identified targets were: RsgA; RbgA; Era; HflX and ObgE, which were shown to bind with high affinity and specificity to (p)ppGpp. These GTPases are all involved in the biogenesis of the functional 70S ribosome responsible for translation. Prokaryotic ribosomes consist of two main subunits, the 30S subunit and 50S subunit that associate to form 70S ribosomes (Biology, 2020, Belousoff et al., 2017). It was discovered by cryo electron microscopy that both RsgA and Era complex to the 30S ribosomal subunit (Jomaa et al., 2011, Davis et al., 2016). In *S. aureus,* escalated levels of 50S and 30S subunits, along with significantly lower levels of 70S ribosomes and an accumulation of 17S RNA (precursor to 16S RNA), occur in mutants of RsgA and Era when compared to the wildtype (Himeno, 2004, Wood et al., 2019, Corrigan et al., 2016, Sayed et al., 1999). RsgA and Era have been proposed to act as chaperones for the 30S subunit by binding to the 16S rRNA preventing association with the 50S subunit until maturation is complete, while also chaperoning the 3'-end of rRNA (Sharma et al., 2005).

Additionally, RbgA, ObgE and HflX bind to the 50S subunit to perform a checkpoint role *i.e.* they encourage protein-protein interactions to assist RNA folding and are perceived as necessary for ribosomal biogenesis (Jain et al., 2009, Uicker et al., 2006). This was displayed by 70S ribosome levels decreasing and immature 50S subunits levels increasing when RbgA is depleted and is attributed to incorrect incorporation of ribosomal proteins such as L6 before other late assembly proteins (Corrigan et al., 2016, Jain et al., 2009, Uicker et al., 2006). HflX has also been shown to act as a ribosome splitting factor that is responsible for salvaging stalled ribosomes and inactive 100S ribosomes formed by two 70S ribosomes coming together (Coatham et al., 2016, Zhang et al., 2015). This implicates HflX in virulence due to its ability to resuscitate persister cells that contain increased amounts of 100S dimers (Song and Wood, 2020). In *E. coli*, (p)ppGpp does not only inhibit the formation of active ribosomes or dissociation of inactive complexes, it also activates hibernation factors such as ribosome modulation factor (*rmf)* and hibernation promoting factor (*hpf),* which control the rate at which inactive dimers form (Song and Wood, 2020). Recently a new hibernation factor was discovered in *Psychrobacter urativorans* called Balon that may promote the SR (Helena-Bueno et al., 2024). *B. subtilis* contains these proteins - *yyyD* encodes a hibernation factor and shares around 51% gene sequence homology

with *E. coli hpf*, which it is necessary for 100S formation (Tagami et al., 2012). (p)ppGpp binding to these proteins ultimately decreases translation rates by inhibiting their roles in ribosomal assembly and in dissociation of inactive dimers without stopping translation completely.

Assembly of the 70S ribosome for translation is incredibly well controlled in order to maintain translational accuracy. Therefore, it stands to reason that translation is modulated by various proteins to maintain this accuracy, including initiation factors (IF1, IF2, IF3), elongation factors (EF-Tu and EF-G) and release factors (RFs) (Bennison et al., 2019). (p)ppGpp displays binding to several of these proteins. When (p)ppGpp interacts with IF2, association of the methyl-transfer RNA (Met-tRNA) to the ribosomal pre-initiation complex (pre-IC) is negatively affected, with initial dipeptide bond formation decreasing (Milon et al., 2006, Bennison et al., 2019, Irving et al., 2020, Legault et al., 1972). In *E. coli*, IF2 has also been shown to play a role in regulating certain mRNAs for translation when in complex with the 30S subunit (Vinogradova et al., 2020).

(p)ppGpp binding to the essential elongation factors EF-Tu and EF-G prevents the binding of aminoacyl tRNAs to the A site of the ribosome and translocation of the polypeptide chain through the ribosome (Rojas et al., 1984a, Zhang et al., 2018). EF-Tu can be inhibited by direct competitive binding or by binding of ppGpp to a complex of EF-Tu and the cognate guanosine exchange factor, halting the EF-Tu cycle through kinetic trapping of GTPase in an inactive complex (Rojas et al., 1984b, Bennison et al., 2019). *In vitro,* EF-G has been shown to be competitively inhibited by ppGpp, as there was a significant reduction in elongation rate in the presence of excess ppGpp (Bennison et al., 2019, Rojas et al., 1984b). RF3 exists within the cytoplasm in a GDP bound state, however, when bound to GTP it shows increased ribosomal affinity. RF3 can bind to ppGpp as well as GDP/GTP and in its ppGpp-bound state has decreased activity, leading to a reduction in recycling of the other RFs. This was further demonstrated in a reconstituted assay performed by Kihira *et al* where a decrease in the recycling ability of RF1 was exhibited when ppGpp was introduced into the system (Kihira et al., 2012). The characterisation of these aforementioned GTPases has also revealed that their GTPase activity is increased in the presence of ribosomes meaning ribosomal assembly can occur at a rate of 100,000 ribosomes/hr (Chen et al., 2012, Davis et al., 2016). Despite this, the ability of (p)ppGpp to interfere with the GTPases involved in: transcription; ribosome assembly; translation; and recycling of ribosomal constituents, has an almost immediate effect. This emphasises the efficiency of these signalling molecules for introducing a slow growth state, and a greater tolerance to nutrient starvation ultimately promoting survival.

1.5.5. ppGpp Regulates carbon and lipid metabolism

(p)ppGpp has a wider role in cell metabolism than just affecting transcription and translation. For example, during fatty acid starvation (p)ppGpp production is triggered and it begins the inhibition of various metabolic pathways to promote survival (Sinha and Winther, 2021). (p)ppGpp is involved in an

“outside in” model where fatty acid levels define the cell envelope capacity and as a result cell size. In the absence of (p)ppGpp cell lysis occurs due to cell volume exceeding the newly defined threshold, implicating it in the maintenance of the cell’s structural integrity (Vadia et al., 2017).

Despite ACP being responsible for mediating the stress response by binding to SpoT during fatty acid starvation, RelA also plays a role and is responsible for the production of a greater concentration of (p)ppGpp (Sinha et al., 2019). During fatty acid starvation acetyl-coenzyme A (Acetyl-CoA) levels decrease rapidly as this is the main precursor for fatty acid biosynthesis, its own precursor pyruvate is used to replenish these depleted Acetyl-CoA levels (Furukawa et al., 1993, Heath and Rock, 1995). However, pyruvate is required as the substrate for the enzyme DapA to synthesise lysine, meaning these levels are not replenished and a build up of uncharged lysine-tRNAs occurs. These uncharged tRNAs are subsequently detected by RelA and the SR is induced. It is likely that this mechanism of inducing the SR is conserved in Bacillota, as pyruvate is necessary for the production of several amino acids. In *B. subtilis* the pyruvate carboxylase (PC) is responsible for producing oxaloacetate from pyruvate. This is an essential compound for the production of C4 intermediates involved in gluconeogenesis, amino acid biosynthesis and general metabolism. This protein is encoded by the *pycA* gene which is under stringent control, with expression increasing during amino acid starvation due to a build of (p)ppGpp (Krüger et al., 2021, Tojo et al., 2010).

(p)ppGpp also regulates proteins involved in maintaining the structural integrity of the cell wall such as lptA and lpxA, which in *E. coli* are responsible for translating lipopolysaccharides from the inner membrane to the outer membrane and anchoring LPS to the outer membrane respectively, evidenced by (p)ppGpp^0 mutants undergoing cell lysis due to overgrowth (Roghanian et al., 2019). Phospholipid metabolism is also affected by (p)ppGpp with PlsB and PgsA being targeted (Heath et al., 1994, Merlie and Pizer, 1973, Irving et al., 2021).

In *E. coli*, AccA and AccD, key subunits in the formation of acetyl-CoA carboxytransferase, are inhibited by ppGpp, this ultimately leads to a build-up in acetyl-CoA as the attachment of a carboxy group to form malonyl-CoA no longer occurs. Perhaps this provides a resource pool for fatty acid biosynthesis to promote survival (Merlie and Pizer, 1973, Polakis et al., 1973, Stein Jr and Bloch, 1976). However, the inhibition of FabA and FabZ by (p)ppGpp brings this into question, as these proteins are involved in fatty acid elongation (Stein Jr and Bloch, 1976).

The leucine responsive regulatory protein (Lrp), which acts as a transcriptional regulator, is responsible for co-ordinating cellular metabolism with the environment, with control of over 400 *E. coli* genes. Normally the regulator promotes amino acid synthesis and inhibits breakdown of complex molecules that are a good source of nutrients and is regulated by (p)ppGpp (Landgraf et al., 1996). So, it is no surprise that during carbon starvation-induced stationary phase, the increased (p)ppGpp levels promote

addition to internal nutrient reserves (Tani et al., 2002, Zinser and Kolter, 2000). The transition into this stationary phase is controlled by the sigma factor RpoS that detects increased (p)ppGpp levels and is responsible for the transcription of around 10% of all *E. coli* genes, where it changes the expression profile of a multitude of genes in order to increase tolerance to stress (Potrykus and Cashel, 2008, Navarro Llorens et al., 2010, Link et al., 2015, Weber et al., 2005).

The identification of PurF by Wang *et al* exhibits the role of (p)ppGpp in nucleotide metabolism as this is a key enzyme involved at the beginning of the purine nucleotide synthesis pathway (Wang et al., 2019a). PurF is responsible for the conversion of PRPP to 5PRA (Fig 1.5.3), so its inhibition leads to an increase in PRPP levels that would direct the use of this pool for the synthesis of other metabolites (Wang et al., 2020). PRPP is produced from ribose-5-phosphate catalysed by the ribose-phosphate diphosphokinase (PrsA), a key linker between purine nucleotide synthesis and the pentose phosphate pathway. Wang *et al* incubated a Gsk mutant incapable of binding ppGpp in the presence of inosine and guanosine during stringent conditions and observed both a decrease in PRPP and an increase in ADP/ATP levels. As PrsA is readily inhibited by ADP, this is unsurprising however, the synthesis of uridine triphosphate (UTP) was also decreased due to a lack of PRPP. Following this, cultures were supplemented with uridine to bypass the need for PRPP in producing UTP, which rescued the cells, demonstrating the role (p)ppGpp has in balancing both purine and pyrimidine nucleotide synthesis (Wang et al., 2020).

Despite the amount of (p)ppGpp target proteins identified across transcription, translation, ribosomal assembly and nucleotide regulation, there is a staggering degree of complexity associated with metabolism, with a lot of intricacies across all of these pathways remaining to be established. The ability of these alarmones to target these cellular processes, while also having an impact on pathogenicity and antibiotic tolerance, mark (p)ppGpp as incredibly important secondary messenger molecules essential for survival.

1.6. Methods used for (p)ppGpp target elucidation

The first known definitive (p)ppGpp binding protein was the RNAP of *E. coli*. Binding was initially shown by designing a radioactive azido-derivative of (p)ppGpp. This was synthesised with [γ-^{32}P]ATP and an azido UV cross-linker attached to the C8 position of the guanine base (Figure 1.6). This compound was subsequently photo-crosslinked to the RNAP and shown to bind to the β subunit by trypsin digestion and 2D chromatography (Chatterji et al., 1998). A later study using a photo-cross linkable thio-ppGpp and ^{32}P suggested binding to the RNAP β' subunit (Figure 1.6.) (Toulokhonov et al., 2001). The binding site was eventually determined to be between the ω and β' subunits using the same probe along with protease mapping and using mutant RNAP enzymes that do not bind to ppGpp (Ross et al., 2013).

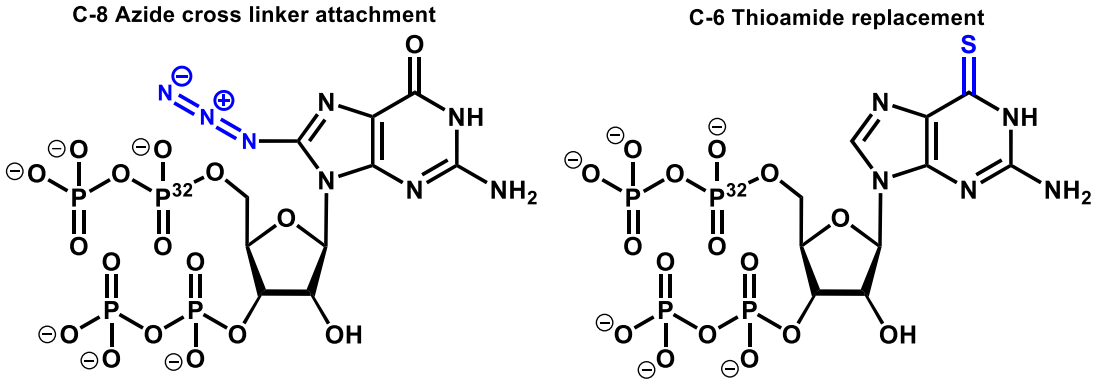

Figure 1.6. Chemical structures of the alternative ^{32}P probes. The photo-crosslinkable azide tag attached to the C8 position of the guanine base, stands to sense as guanine is important for binding, however, it may also interfere with binding. The replacement of the carbonyl with a thio-group removes the likelihood of steric hindrance by introducing a linker or significantly larger group.. Despite both of these drawbacks the probes were capable of estimating the ppGpp binding site.

1.6.1. DRaCALA

With this insight into ppGpp binding targets, more high throughput methodologies were employed to identify novel binding proteins instead of investigating individual targets, as it was known that (p)ppGpp is capable of mediating a variety of cellular processes. One of these methods was differential radial capillary action of ligand assay (DRaCALA) (Roelofs et al., 2011). This assay is used to identify protein binding partners of a specific ligand and can be used with cell lysates containing over-expressed protein in a 96-well format or directly with purified recombinant protein(Orr and Lee, 2017). DRaCALA has yielded numerous novel (p)ppGpp interaction partners across several species, such as *Bacillus anthracis*, *E. coli,* and *S. aureus*, with the aforementioned tightly binding translational GTPases: RsgA (K_d= 2.2 μM); RbgA (K_d= 2.9 μM); HflX (K_d= 3.4 μM); Era (K_d= 4.2 μM) being examples of proteins identified by this methodology (a full list of ppGpp binding proteins identified by DRaCALA is available in Table 6, appendix) (Corrigan et al., 2016, Bennison et al., 2021, Zhang et al., 2018). The methodology relies on the immobilisation of a protein on a nitrocellulose membrane, binding of the ligand (in this case ppGpp) to the protein, annulation of any free ligand and computational densitometry to determine binding affinities (Figure 1.6.1.) However, this methodology has a key drawback - its inefficiency for identifying weak ppGpp interactors due to the low concentrations of radiolabelled ppGpp that can be used in the assay – in these cases there is simply not enough ligand available to differentiate binding from the background signal.

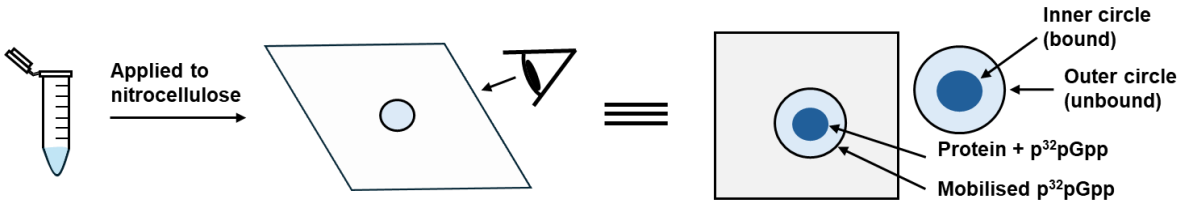

Figure 1.6.1: A cartoon representation of the DRaCALA methodology: In this methodology [α-^{32}P]-ppGpp is mixed with purified recombinant protein or lysate obtained from an overexpression strain that was induced with IPTG (1 mM) and grown overnight at 30 °C. The mixture is dotted onto a nitrocellulose membrane, and any amino acids comprising the protein containing hydrophobic moieties such as phenylalanine, isoleucine, tryptophan and valine, form interactions with the hydrophobic membrane. As a result they stay fixed at the spot in which they were dotted, while the charged [α-^{32}P]-ppGpp molecules do not form these interactions, annulating outwards forming two distinct circles. The fraction bound of [α-^{32}P]-ppGpp is calculated by determining the intensities of both the tightly bound inner circle consisting of [α-^{32}P]-ppGpp bound to protein and the outer circle consisting solely of [α-^{32}P]-ppGpp.

1.6.2. Capture compound approaches

In order to identify weak ppGpp binders and improve mapping of the stringent response signalling network, new methods were developed using nucleotide-probes. These small trifunctional molecules commonly referred to as capture compounds allow for the isolation of nucleotide-protein interactors by specific interactions and subsequent identification *via* mass spec (Köster et al., 2007). The compounds typically consist of three main components; a chosen nucleotide mimic, a photoreactive group that is capable of forming covalent bonds and an affinity handle to allow for isolation.

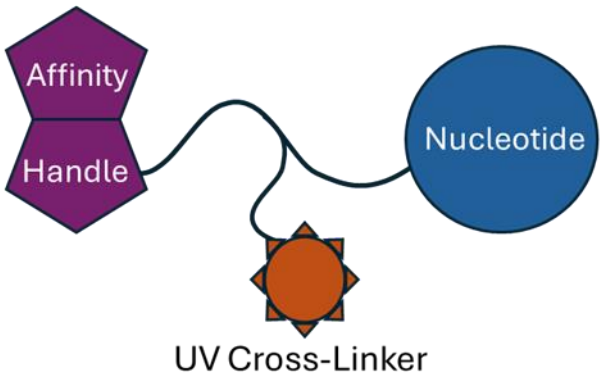

Figure 1.6.2: A cartoon representation of the three main components of a general capture compound: Nucleotide mimic (Blue), Affinity handle (Purple), UV cross linker (Orange).

Biotin is often utilised as the affinity handle for capture compounds as its interaction with streptavidin is the strongest known non-covalent interaction in biochemistry (K_d = 10 fM), with incredibly high tolerance for wide ranges of temperatures and pH (Green, 1963a, Green, 1963b, Scientific, 2024). There are wide range of photoreactive linkers available ranging from azides and psoralens that are structural

analogs of coumarin and diazirines. The first paper to employ this capture compound methodology for (pp)pGpp utilised a diazirine cross linker as their photoreactive group (Wang et al., 2019a). The authors made several compounds with varying length linkers (Table 1.6.2) attached to both 3' and 5'-phosphates (Figure 1.6.2a). The compounds were then combined and used in a pulldown experiment to compare the number of hits isolated. Each compound was incubated with stationary phase lysates of *E. coli* to allow protein-binding before activation with ultraviolet light ($\lambda_{Absorbance}$ = 345 nm) to enable the formation of covalent bonds to ppGpp-binding proteins.

Table 1.6.2: Structural composition of spacer X

Spacer X
-CH_2-
- $(CH_2CH_2O)_2CH_2$-
- $(CH_2CH_2O)_4CH_2$-
- $(CH_2CH_2O)_2CH_2$-CH_2-

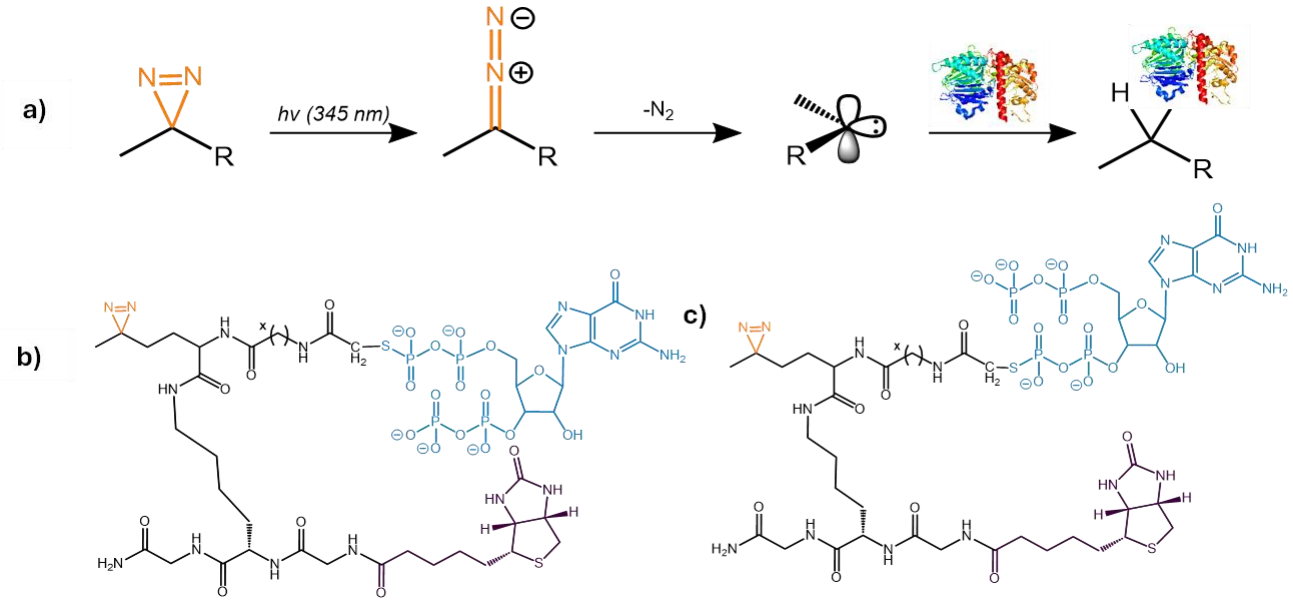

Figure 1.6.2a: Diazarine cross linkers covalently attach affinity handles to protein targets. a) Summary of UV cross linking including: the UV (*hv* = 345 nm) activation of a diazirine cross linker; formation of a highly reactive Sp2 hybridised carbene intermediate; generation of N_2 (g) as a driving force and attachment to a monomer of PurF from Escherichia coli(Wang et al., 2019a). Adapted from:(Musolino et al., 2021). **1b-c**: Capture compounds synthesised by Laub with the diazarine crosslinker and affinity handles attached to the 5' and 3'-phosphates respectively (Wang et al., 2019a).

1.6.2.1. Wang *et al* capture compound approach for the isolation of ppGpp binders

Wang *et al* employed what is termed a stable isotope labelling in culture (SILAC) technique (1.7.2.1), where proteins are metabolically labelled when culturing cells in media containing labelled essential amino acids such as lysine[8] and arginine[10]. After five cell divisions most proteins show ~97% incorporation of the label (Ong et al., 2002). SILAC was first developed in 2002 and it functions on the principle that "heavy" labelled atoms can be distinguished from unlabelled "light" atoms by mass spectrometry when lysates obtained from labelled and unlabelled cultures are mixed (Figure 1.6.2.1) (Ong et al., 2002, Zhang et al., 2014). SILAC was shortly subject to a rise in popularity in the field of quantitative proteomics, as protein quantification can be accurately determined when analysing the intensities of the labelled peptides and their unlabelled counterparts, while sequence information can still be obtained to help determine protein identity (Spellman et al., 2008, Deng et al., 2019). In this capture compound approach, the pulldowns take inspiration from previous work on a c-di-GMP capture compound (Laventie et al., 2017). For (pp)pGpp, Wang et al identified 290 proteins, with 20 of 28 previously identified as ppGpp binding proteins boasting a heavy-to-light ratio of > 2.8. This value was then used as a threshold, generating a list of 56 hits: 32 that were involved in metabolism and 17 that were involved in translation, including the GTPases identified by Corrigan *et al* (Corrigan et al., 2016). Seven of these proteins were purified recombinantly , and their binding to ppGpp assessed further with isothermal calorimetry (ITC) including the aforementioned PurF. (

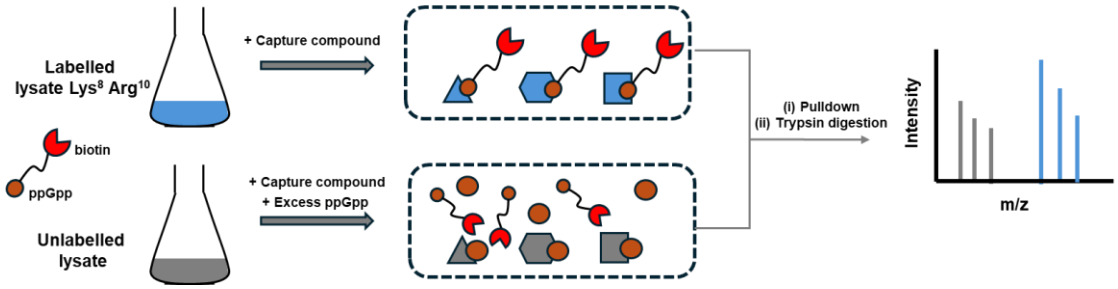

Figure 1.6.2.1: Summary of the SILAC procedure implemented by Wang *et al*: Cultures are grown in media containing unmodified amino acids termed "unlabelled" and media containing radiolabelled amino acids termed "labelled". These cultures are then lysed and capture compound is added to both along with an excess of (p)ppGpp to the unlabelled lysate ensuring the capture compound is in competition. The pulldowns are then performed with streptavidin beads before trypsin digestion and subsequent mass spectrometry. If a protein appears in both the labelled and unlabelled media, the likelihood of it being a false positive is lowered due the competitive (p)ppGpp.

1.6.2.2. Haas *et al* capture compound approach

Following on from the success of this affinity based capture compound approach, another large set of proteins were identified as (pp)pGpp-binding targets across two species: *E. coli* (soluble and membrane fractions) and *Salmonella enterica* serovar Typhimurium (soluble fraction)(Haas et al., 2022). This approach synthesised a catalog of ppGpp structural analogs for use as unique capture compounds (Figure 1.6.2.2). The effects of the affinity handles on both the 3' and 5'-phosphates of ppGpp and its nucleotide relatives pGpp, pppGpp and ppApp, were investigated along with incorporation of the handle and cross-linker directly onto the guanine base of ppGpp.

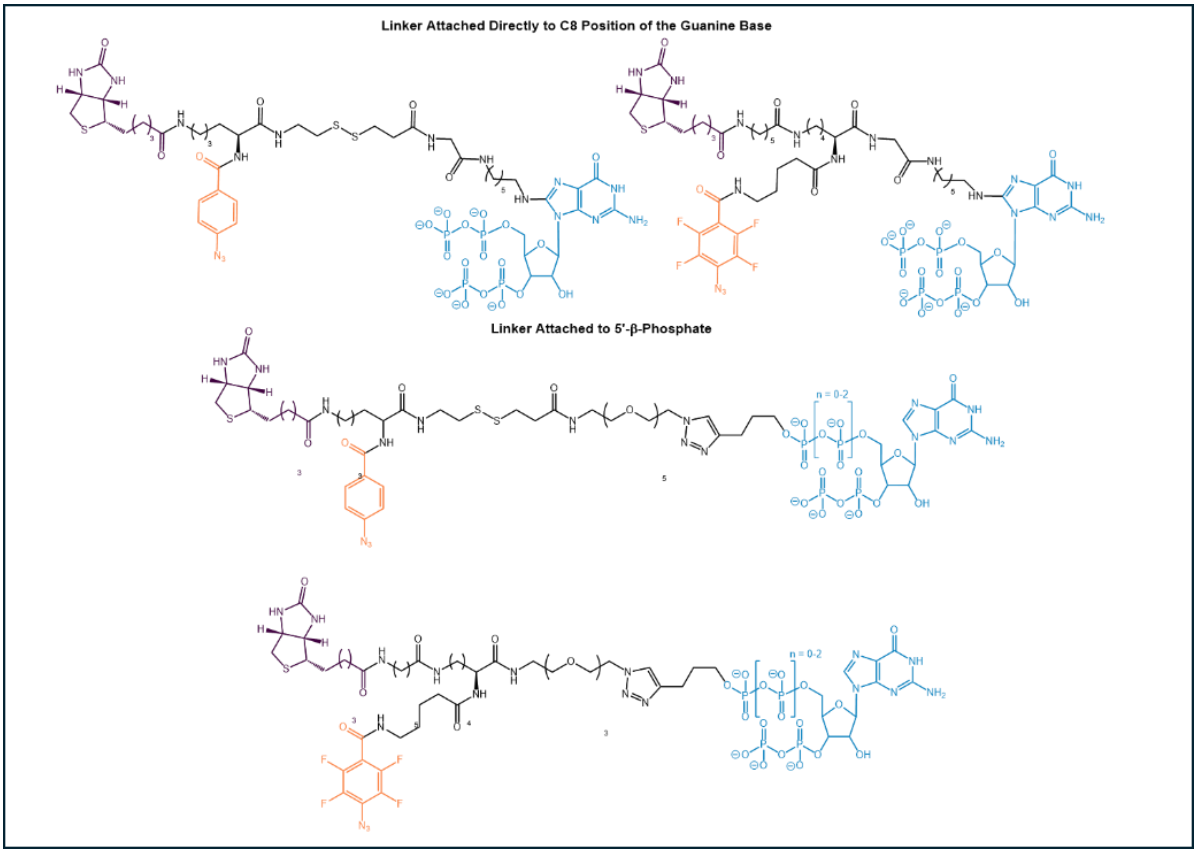

Figure 1.6.2.2: Capture compounds designed by (Haas et al., 2022): Designed compounds with varying attachment of the affinity handle (purple) to the C8 position of the guanine base and to the 5'-phosphates. While also varying the cross-linker between phenylazide or tetrafluoro phenylazide (orange) the nucleotide moiety (blue) does not vary in this instance.

Here, Haas *et* al incubated their (p)ppGpp capture with cell lysates from *E. coli and S.* Typhimurium that had been fractionated into cytoplasmic and membrane fractions and compared their efficiency at capturing ppGpp-binding proteins. Results convincingly suggested that attachment to the 5'-phosphate was more efficient, with other variations isolating few to no hits. Capture compounds that furnish a UV cross-linker can potentially enrich non ppGpp-binding proteins if UV activation occurs when in close proximity to a given protein in solution. In order to minimise the risk of false positives due to this side reaction, a competition control containing a 1000-fold competitive nucleotide in the form of unlabelled (p)ppGpp was included. As this is the native nucleotide, it should preferentially bind to protein targets

inhibiting the capture compound from performing effectively. While at the same time, it does not prevent any unspecific interactions taking place which helps reduce the number of false positives. The thresholds set by Haas *et al* for mass spectrometry were a log2 (enrichment) >2 and a q-value of < 0.05. Using these thresholds, they identified ~185 proteins and further characterised the hydrolase ApaH (Haas et al., 2022). This array of capture compounds was capable of isolating a large number of putative (pp)pGpp binding proteins (Table 1.6.2.2), including previously identified binding partners in both *E. coli* and *S.* Typhimurium suggesting this capture compound approach is a reliable way to map the (pp)pGpp interactome.

Table 1.6.2.2: Summary of both DRaCALA and affinity-based capture methodologies

Author	Methodology	Nucleotide	Organism	Targets Identified
(Corrigan et al., 2016)	DRaCALA	(p)ppGpp	*S. aureus*	7
(Zhang et al., 2018)	DRaCALA	ppGpp, pppGpp	*E. coli*	12
(Wang et al., 2019a)	Capture Compound	ppGpp	*E. coli*	50+
(Yang et al., 2020a)	DRaCALA	pGpp, ppGpp, pppGpp	*B. anthracis*	*30+*
(Haas et al., 2022)	Capture compound	pGpp, ppGpp, pppGpp	*E. coli,* *S.* Typhimurium	*40+*

Overall, capture compound approaches allow for the mapping of the (p)ppGpp interactome including weak interaction partners, while also not requiring overexpression strains of the proteins of interest, advantages which are held over DRaCALA. However, as established previously the preference between ppGpp and pppGpp differs between species, meaning the synthesis of probes mimicking both nucleotides is required to gain a full understanding of their unique targets.

1.7. Chemo-sensors and their roles in ppGpp quantification

The range of activity of (p)ppGpp is astounding, with potentially hundreds of binding partners remaining to be discovered. However, the specific effect (p)ppGpp concentrations have upon the bacterial cell still remains to be elucidated as a result of this. It stands to reason that at low levels of stress, the concentration of (p)ppGpp in the cell will only result in binding to the proteins with the highest affinity, such as nucleotide metabolism and ribosome biogenesis related proteins, suggesting (p)ppGpp is important for regulating these processes under almost all conditions. During stress, other processes such as fatty acid synthesis and carbon metabolism will also be modulated to ensure survival. It is therefore imperative that a method for accurately measuring (p)ppGpp levels is developed to provide insight into the concentration dynamics and how these fluctuations effect regulatory processes.

There are a numerous methods available for the quantification of (p)ppGpp, however, they are often convoluted, unreliable or require specialist training. Initially, the addition of radiolabelled nucleotides

containing ^{32}P to growing cultures allowed for the detection of (p)ppGpp. Upon lysing, the nucleotides were separated by their anionic charge using thin layer chromatography and detected using film (Cashel and Gallant, 1969). A few years later, a radioimmunoassay was developed, this involved using human serum albumin (HAS) linked to both nucleotides radiolabelled with tritium (^{3}H) and native nucleotides obtained from cell-lysates using the coupling agent 1-ethyl-3-[3-dimethylaminopropyl]carbodiimide (EDC). The radiolabelled nucleotides would then be incubated with a specifically designed antibody and the native nucleotide introduced with the displacement of the ^{3}H labelled ppGpp being used to determine native ppGpp concentrations (Hamagishi et al., 1981).

The advancement in HPLC methodologies has allowed for the detection of many analytes of interest including (p)ppGpp, these methods often relied on UV detection and as a result involved separating bacterial cells from growth medium and any other compounds that may cause background noise. The cells were then lysed and their lysates injected, while the areas of the peaks were calculated to provide information on ppGpp levels (Zborníková et al., 2019, Oursel et al., 2007, Varik et al., 2017, Fischer et al., 1982). HPLC methodologies have greatly improved with buffer systems that provide both high resolution between structurally similar nucleotides and reduce signal suppression, while the incorporation of mass spectrometry has aided accurate abundance measurements and real-time confirmation of peaks (Zborníková et al., 2019, Ihara et al., 2015), however this method can be laborious and still requires access to a HPLC.

Alternatives to HPLC focus on chemical methods such as the development of quantum dots. These often consist of lanthanide metals complexes, such as europium molybdate, which naturally fluoresce blue but upon binding ppGpp fluoresce red due to rare earth metal antennae affects (Rong et al., 2020, Chen et al., 2018). Nanoclusters have also been employed, these clusters of hundreds of metal atoms have molecule-like properties such as fluorescence. Silver nanoclusters (Ag-NCs) were first synthesised using DNA as a template. These DNA-Ag-NCs autofluorescence ($\lambda_{Excitation}$ = 585 nm) and are readily quenched by electron transfer when copper (II) ions are introduced into solution due to the high affinity between Cu^{2+} with DNA. However, Cu^{2+} also displays high affinity towards phosphates, including ppGpp. Upon addition, ppGpp chelates to Cu^{2+} ions in DNA-Ag-NC-Cu complexes disrupting any interaction with the DNA-Ag-NCs and restoring fluorescence. This on/off method allows for the detection of ppGpp by relative fluorescence intensities in the presence (F) and absence of ppGpp (F_0), as F/F_0 is proportional to the concentration of ppGpp within a sensitivity range of 2 - 200 μM (Zhang et al., 2013). Despite all of these methods, a simple, inexpensive and safe methodology for the quantification of (p)ppGpp remains elusive.

1.8. Aims and objectives

The SR is a bacterial stress response that promotes survival under a multitude of stress conditions, while being implicated in antibacterial resistance, virulence and metabolism. With current treatment options for MRSA looking bleak, the ability of the SR to mediate adaptations to potential stressors is worrying. It is therefore imperative that the mapping of the (p)ppGpp interactome continues in order to further our understanding of this complicated response. Through continued probing of these interactions, it is possible that novel therapeutic targets that specifically target SR effectors may be identified, ultimately improving current treatment opportunities against various strains of bacteria not only MRSA.

In this study, we aimed to assist the mapping of the (p)ppGpp interactome by the synthesis of our own ppGpp capture compound through basic chemical coupling procedures and enzymatic synthesis of a thiolated-ppGpp structural analog. The initial compound design consisted of a flexible PEG linker, a biotin affinity handle and p(s)pGpp similar to the compound designed by Wang *et al* in section 1.6.2. Our compound aimed to avoid the issues associated with false-positives when using traditional chemical probes such as Wang *et al* by operating in a non-covalent manner with no photo-active cross-linker (Chapter 3). Upon synthesis of the capture compound, we aimed to demonstrate its selectivity towards known ppGpp binders identified by Corrigan *et al*. The capture compound was then be implemented in pulldown assays that utilise traditional streptavidin-biotin interactions and proteomic techniques toenablee the identification of new (p)ppGpp binding proteins (Chapter 4). Following this, our aim was to confirm binding of (p)ppGpp to newly identified proteins through the assessment of binding in both lysates and recombinant protein by various biophysical characterisation methods such as microscale thermophoresis. Finally *in vitro* reactions were replicated to understandthe impact (p)ppGpp has on the respective protein function (Chapter 5).

The final aim of this project was to establish an efficient method for the quantification of (p)ppGpp in the absence of radiolabelling and more convoluted methods that require specialist training and expensive equipment such as HPLC (Chapter 6).

Chapter 2

Materials and Methods

2.1. General Chemical Procedures

Commercially available starting materials, solvents and other reagents were analytical grade and obtained from renowned suppliers Fluorochem, Fischer scientific , Jena Bioscience and Merck (Sigma-Aldrich). As a result, they were used without the need for purification (unless otherwise stated). All reactions were performed in oven dried glassware, agitated with a magnetic stirrer bar, carried out at ambient temperature, pressure and under an inert N2 atmosphere unless stated otherwise. All anhydrous solvents were obtained from the University of Sheffield dry solvent system using N_2 using standard Schlenk techniques, with the exception of methanol, which was freshly distilled when required. All other solvents used were either analytical or chromatography grade. Solvents were evaporated under reduced pressure using a Büchi Rotary Evaporator R100 and solids were dried using a high-vacuum line when required both with an Edwards Direct-drive rotary vane vacuum pump, dual mode, 2.3 cfm, 115/220 VAC.

2.1.1. TLC

Analytical thin layer chromatography (TLC) analyses were performed using pre-coated silica gel plates (silica 2 8 8 0 Kieselgel 60 F_{254}) acquired from Merck and were visualized with ultra-violet radiation (UV: 254-365nm). Several stains were used to identify compounds, including: ceric ammonium molybdate (hydroxyl groups); Potassium permanganate stain (oxidizable species); ninhydrin (primary, secondary amines); Propargyl alcohol (azides); Cinnamaldehyde stain (biotin moieties).

2.1.2. Column chromatography

Flash column chromatography was performed using prepacked Teledyne Isco RediSep silica flash columns (20 mg-80 g) and ran on a Combiflash NEXTGEN 300+ flash purification system or manually with silica gel 60 (30 – 70 µm) purchased from Merck.

2.1.3. General RP-HPLC Procedure

Reverse phase high performance liquid chromatography (RP-HPLC) was perfumed using both analytical GEMINI® 5 µm C18 110 Å LC column (250 × 4.6 mm) and Semi preparative GEMINI® 5 µm C18 110 Å LC column (250 x 10 mm). Mobile Phase A: triethylammonium bicarbonate (TEAB, 100 mM), Acetonitrile (MeCN, 0.1% v/v). Mobile phase B: TEAB (100 mM), MeCN (50% v/v), 3-50% B, 21 minutes (1.6-25.05%), UV detection at 260 nm.

2.1.4. Anion-Exchange HPLC

Both analytical traces and purifications were obtained using a Nucleopac PA-100 (4 × 250 mm column). Mobile phase: Solvent A: NH_4HCO_3 (50 mM) Solvent B: NH_4HCO_3 (500 mM), 9-91% B, 90.5-455 mM 21 minutes.

2.1.5. IR

Infra-red spectroscopy (IR) was performed on a Perkin Elmer 100 FT instrument to obtain the respective spectra.

2.1.6. Mass spectrometry

All mass spectrometry was kindly performed by the University of Sheffield Mass Spectroscopy service using: LC instrument – Agilent 1260 Infinity, Column: Agilent Zorbax Extend-C18 (2.1 mm × 50 mm, 1.8 micron), mobile phase A: formic acid (0.1% v/v), mobile phase B: formic acid (0.1% v/v in MeCN), 5%-95% B,15 mins, Flowrate: 0.4 ml min^{-1}. MS instrument – Agilent 6530 Q-ToF, Mode: ESI +ve ion. Mass spectrometry of the capture compounds was performed by the School of Chemical Biology and Engineering (CBE) LC instrument: Vanquish UHPLC, Column: DNAPacRP column (2.1 mm × 100 mm) Mobile phase A: Triethylamine (TEA, 10 mM); Hexafluoroisopropanol (HFIP, 50 mM), MeCN (0.1% v/v), Mobile phase B: TEA (10 mM); HFIP (50 mM), MeCN (50% v/v), Flowrate 0.25 ml/min.

2.1.7. NMR

Proton (^{1}H), Carbon (^{13}C) and Phosphorus (^{31}P) Nuclear Magnetic Resonance (NMR) spectra for analysis were acquired from a Bruker AV III 400MHz or 500MHz spectrometer using an internal deuterium lock. Chemical shifts (δ) are reported in parts per million (ppm) relative to the internal standard with the respective deuterated solvent stated. Coupling constants (J Values) are reported in Hertz (Hz). And the following abbreviations are used; broad singlet, broad triplet =bt, s = singlet, bs = d = doublet, t = triplet, dd = doublet of doublets, q = quartet, p = pentet, m = multiplet. All ^{1}H.N.M.R were recorded at 400 MHz, ^{13}C.N.M.R were recorded at 101 MHz, ^{31}P NMR were recorded at 162 MHz and ^{19}F NMR were recorded at 377 MHz. Spectra were assigned with the use of COSY, HSQC, NOESY and HMBC analytical techniques when appropriate, in the format: ppm (integral, splitting pattern, coupling constant (Hz), assignment.

2.2. Synthetic methods for the production of a non-covalent capture compound

2.2.1. Synthesis of 1,1-bis (4-methoxyphenyl)-1-phenyl-2,5,8,11-tetraoxatridecan-13-ol (**2**)

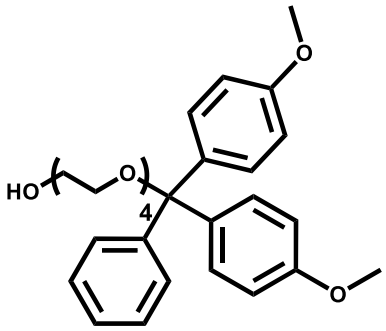

Tetraethylene glycol (44 mL, 256.65 mmol, 8.7 eqv) was co-evaporated with toluene (3 × 50 mL) and placed under high vacuum overnight. To a solution of tetraethylene glycol (44 mL, 256.65 mmol, 8.7 eqv) in DCM (12 mL), DMAP (0.18 g, 1.48 mmol, 0.05 eqv), TEA (6.56 mL, 47.2 mmol, 1.6 eqv) were added followed by dropwise treatment with a solution of DMT-Cl (10 g, 29.5 mmol, 1.0 eqv) in anhydrous DCM (30 mL) and left stirring. After 23 h 5% (w/v) Na_2CO_3 (100 mL) was added and the organic layer washed with water (2 × 140 mL) and saturated brine (2 × 20 mL). The organic layer was dried (Na_2SO_4) and concentrated under reduced pressure to yield the crude product as a yellow oil. The crude product was then purified by column chromatography (Hexane:EtOAc, 70:30 → 0:100, 1% TEA) to yield the product as a pale yellow oil (0.98 g, 1.97 mmol, 6.7%). **^{1}H NMR $^{\delta}$H/ppm (400 MHz, $CDCl_3$)**: δ 7.55-7.53 (2H, m, *m*-phenyl), 7.39-7.19 (12H, m, *o*-methoxy phenyl, *o*-phenyl, *p*-phenyl), 6.88-6.81 (6H, m, *m*-methoxy phenyl), 3.84-3.61 (20H, m; CH_3-O-Ph, Tetra-ethylene glycol CH_2-O), 3.27-3.23 (2H, m, CH_2-OH); **^{13}C NMR $^{\delta}$C/ppm (101 MHz, $CDCl_3$)**: δ 158.43, 145.17, 136.41, 130.12, 128.26, 127.88, 127.80, 126.70, 113.0, 85.98, 70.86, 70.80, 70.8, 70.48 63.2, 61.82 55.22; **MS Expected:** $C_{29}H_{36}O_7$ [M + Na^+]: 519.2 m/z **Found:** 519.2 m/z; **TLC**: Rf = 0.30 (Hexane : EtOAc, 70:30, 1% TEA). When referring to the literature characterisation by (Ries et al., 2017) it was clear excess TEG was present in the sample. This is indicated by the integrations of the peaks in the ^{1}H NMR being higher than expected.

2.2.2. Synthesis of 1,1'- (1,4-Phenylene)bis (2,5,8,11-tetraoxatridecan-13-ol) (**3**)

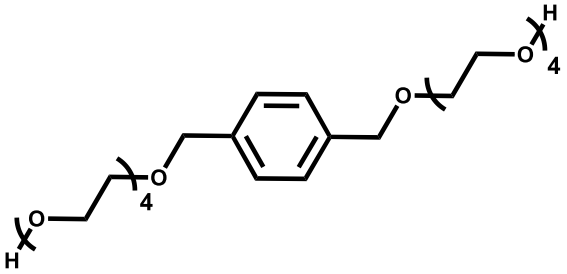

To a stirred solution of tetraethylene glycol (11.7 mL, 67.6 mmol, 2.2 eqv and silver (I) oxide (18.8 g, 81.1 mmol, 2.64 eqv) in anhydrous DCM (50 mL), dibromo-p-xylene (8.1 g, 30.7 mmol, 1 eqv) was added in one portion. The reaction mixture was left stirring (20 h), followed by addition of DCM (100 mL) before filtering *in vacuo*. The filtrate was concentrated under reduced pressure to yield the crude product as a brown oil. The product was purified by column chromatography (DCM : EtOAc, 40:60 → DCM : MeOH, 90:10) to yield the product as a pale yellow oil (10.22 g, 20.83 mmol, 67.9%).**^{1}H NMR δH/ppm (400 MHz, $CDCl_3$)**: δ 7.36-7.30 (4H, m, phenyl), 4.54 (4H, s, CH_2-Phenyl), 3.71-3.57 (34H m, -CH_2-O- tetra-ethylene glycol); **^{13}C NMR δC/ppm (101 MHz, $CDCl_3$)**: δ 137.60, 127.90, 72.95, 72.87, 70.53, 70.30, 69.98, 61.58; **MS Expected:** $C_{24}H_{42}O_{10}$ [M + Na^+]: 513.3 m/z **Found:** 513.3 m/z ; **TLC**: Rf = 0.52 (DCM : MeOH, 90:10). The higher than expected integration of the CH_2-O- peak is due to excess TEG present in the sample meaning purification was unsuccessful.

2.2.3. Synthesis of 2-[2-[2-[2-(4-methylphenyl)sulfonyloxyethoxy]ethoxy]ethoxy]ethyl 4-methylbenzenesulfonate (**11**)

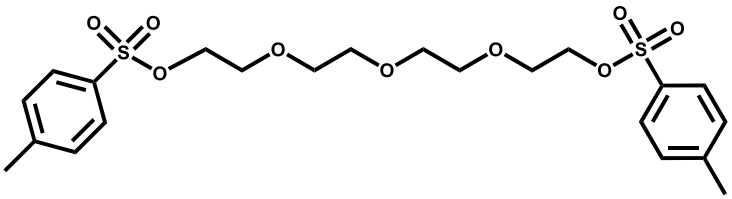

Tosyl chloride (TsCl) was freshly prepared through recrystallisation.

Triethylamine (41.63 mL, 298 mmol, 3 eqv.) was added to a stirred solution of tetraethylene glycol (19.14 g, 99 mmol, 1 eqv.) in anhydrous DCM (100 mL). The reaction was cooled to 0 °C and freshly recrystalised 4-tolenesulfonyl chloride (56.94 g, 298 mmol, 3 eqv) was added and the reaction was stirred overnight before being concentrated under reduced pressure. The crude oil was redissolved in DCM (100 mL) and washed with water (3 × 50 mL). The aqueous layers were combined and extracted with DCM (3 × 80 mL). The organic layers were then combined, washed with acetic acid (0.1 M, 100 mL), sat.$NaHCO_3$ (100 mL), water (2 × 50 mL), dried (Na_2SO_4) and concentrated under reduced pressure to give a crude orange oil. The crude material was purified by column chromatography EtOAc (0→100%) in hexane to give a colourless oil (34.74 g, 69.12 mmol, 69.44%).**^{1}H NMR δH/ppm (400 MHz, $CDCl_3$)**: δ 7.80 (4H, d, J = 8.3 Hz, *o*-Ar); 7.35 (4H, d, J = 7.7 Hz, *m*-Ar), 4.16 (4H, t, J = 4 Hz, CH_2-OTs), 3.69 (4H, t, J = 4 Hz, -$\underline{CH_2}$-CH_2-OTs), 3.62-3.52 (8H, m, -O-CH_2-), 2.45 (6H, s, CH_3-Ar); **^{13}C NMR δC/ppm (101 MHz, $CDCl_3$)**: δ 144.84, 132.98, 129.85, 127.97, 70.55, 69.28, 68.68, 21.64; **MS Expected:** $C_{22}H_{30}O_9S_2$ [M + Na]: 525.1223 m/z **Found:** 525.1236 m/z; **TLC**: Rf = 0.34 (Hexane : EtOAc, 40:60).

2.2.4. Synthesis of 1,11-diazido -3,6,9-trioxaundecane (**12**)

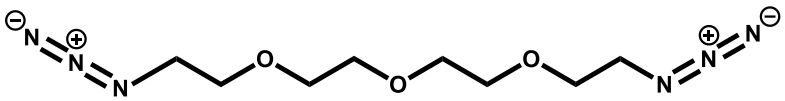

2-[2-[2-[2-(4-methylphenyl)sulfonyloxyethoxy]ethoxy]ethoxy]ethyl 4-methylbenzenesulfonate (8.0 g, 15.92 mmol, 1 eqv) was suspended in EtOH (100 mL) and DMF (50 mL) followed by portion-wise addition of NaN_3 (3.1 g, 47.75 mmol, 3 eqv). The suspension was heated to 70 °C overnight before being concentrated under reduced pressure. The white oil suspension was taken up in EtOAc (300 mL), washed with H_2O (500 mL), the aqueous layers were extracted with EtOAc (2 × 100 mL) and the organic extracts were washed with 10% LiCl solution (100 mL) before being dried (Na_2SO_4) and concentrated under reduced pressure to yield the product as a yellow oil (3.35 g, 13.71 mmol, 86.1%). **^{1}H NMR δH/ppm (400 MHz, $CDCl_3$)**: δ 3.68 (12H, t, J = 4Hz, CH_2-O); 3.40 (4H, t, J = 5.1 Hz, CH_2-N_3); **^{13}C NMR δC/ppm (101 MHz, $CDCl_3$)**: δ 70.71, 70.04, 50.69; **MS Expected:** $C_8H_{16}O_3N_6$ [M + Na]: 267.1176

Found: 267.1188 m/z; **IR (cm^{-1}):** 2100 - N_3 (stretch); **TLC**: Rf = 0.79 (Hexane : EtOAc 30:70). Spectral data in accordance with those seen in the literature (D'Aléo et al., 2015, Gu et al., 2014).

2.2.5. Synthesis of 1-azido-3,6,9-trioxaundecan-11-amine hydrochloride (**13**)

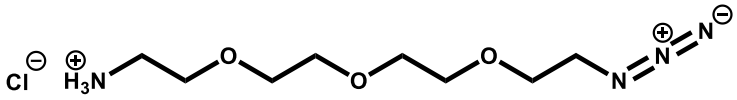

1,11-diazide-3,6,9-trioxaundecane (1.69 g, 6.92 mmol, 1 eqv) was dissolved in diethyl ether (20 mL) followed by addition of 1 M HCl (20 mL). The biphasic mixture was stirred vigorously before addition of PPh_3 (1.82 g, 6.92 mmol, 1 eqv) over 30 min. After 24 h the ether layer was removed and the aqueous layer washed with diethyl ether (3 × 50 mL). The aqueous layer was then evaporated to yield the product as a yellow oil (1.6 g). Purification by silica column chromatography (0 → 100% MeOH in DCM) yielded the pure product as a yellow oil (0.89 g, 3.49 mmol, 51%). **^{1}H NMR $^\delta$H/ppm (400 MHz, MeOD)**: δ 3.74 (2H, bt, J = 4.6 Hz, -O-$\underline{CH_2}$-CH_2-NH_2), 3.70 (10H, t, J = 4.7 Hz, CH_2-O), 3.42 (2H, bt, J= 4.6 Hz, CH_2-N_3), 3.15 (2H, bt, J = 4.6 Hz, CH_2-NH_2); **^{13}C NMR $^\delta$C/ppm (101 MHz, MeOD)**: δ 70.24, 66.49, 50.42, 39.37; **MS Expected:** $C_8H_{19}O_3N_4$ [M + H]: 219.14517 m/z **Found**: 219.1458 m/z; **IR (cm^{-1}):** 3400 – Primary NH_2 (stretch); 2100 - N_3 (stretch), **TLC**: Rf = 0.3 (10% MeOH in DCM). Spectral data in accordance with those seen in the literature (Risseeuw et al., 2013).

2.2.6. Synthesis of Pentafluorophenyl 5-[(3aS,4S,6aR)-2-oxohexahydro-1H-thieno[3,4-d]imidazol-4-yl]pentanoate (**14**)

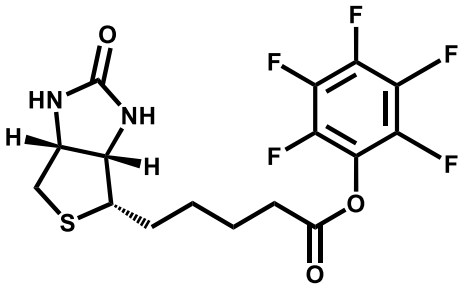

d-Biotin (2.50 g, 10.23 mmol, 1eqv) was dissolved in DMF (44 mL) at 70 ºC, before cooling to 0 ºC. Pentafluorophenol (2.45 g, 13.30 mmol, 1.3 eqv) was added followed by DCC (3.17 g, 15.35 mmol, 1.5 eqv). The reaction was brought to room temperature and stirred overnight before filtering through a celite bed and concentrating the filtrate under reduced pressure to yield a white solid that was recrystallised from methanol to give white crystals of PFP-biotin (1.13 g, 2.75 mmol, 26%).**^{1}H NMR $^\delta$H/ppm (400 MHz, DMSO)**: δ 6.45 (1H, s, N1-ureido, N2-ureido), 6.37 (1H, s, N2-ureido) 4.32 (1H, ddt, *J* = 7.6, 5.2, 1.1 Hz, H-2), 4.16 (1H, ddd, *J* = 7.8, 4.4, 1.9 Hz, H-3), 3.13 (1H, ddd, *J* = 8.3, 6.2, 4.3 Hz, 1H, H-4), 2.84 (1H, dd, J = 12.4, 5.1 Hz, H-1), 2.80 (2H, t, J = 7.3 Hz, H-8), 2.59 (1H, d, J= 12.4 Hz, H-1'), 1.77-1.37 (6H, m, H7, H6, H5). **^{19}F NMR $^\delta$F/ppm (377 MHz, DMSO)**: δ −153.60 (2F, m, *ortho*), −158.10 (1F, t, J = 23.2 Hz, *para*), −162.61 (2F, m, *meta*); **^{13}C NMR $^\delta$C/ppm (101 MHz, DMSO)**: δ170.0

(1), 163.2 (2), 163.0 (3), 142.2 (4), 140.6 (5), 139.9 (6), 139.3 (7), 61.5 (8), 59.75 (9), 55.2 (10), 40.36 (11), 32.77 (12), 28.3 (13), 28.15 (14), 24.8 (15); **MS Expected:** $C_{16}H_{15}F_5N_2O_3S$ [M + H]: 411.079 m/z; **Found**: 411.079 m/z; **TLC**: Rf = 0.63 (10% MeOH in DCM). Spectral data in accordance with those seen in the literature (Vallinayagam et al., 2008).

2.2.7. Synthesis of N-[2-[2-[2-(2-Azidoethoxy)ethoxy]ethoxy]ethyl]hexahydro-2-oxo-(3aS,4S,6aR)- 1H-thieno[3,4-d]imidazole-4-pentanamide (**15**)

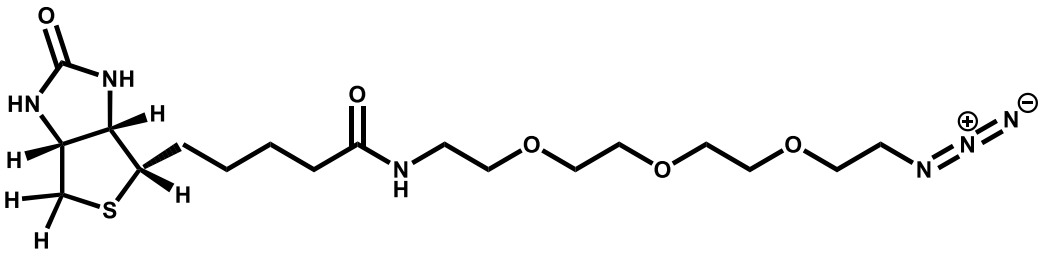

11-Azido-3,6,9-trioxaundecan-1-amine (530 mg, 2.44 mmol, 1 eqv) and DIPEA (946 mg, 7.32 mmol, 3 eqv) were dissolved in anhydrous DMF (5 mL) and stirred for 20 min. PFP-Biotin (1 g, 2.44 mmol, 1 eqv) was added and the reaction stirred under argon for 20 h. The reaction mixture was concentrated under reduced pressure and purified by silica column chromatography (0→100% MeOH in DCM) to yield the product as a white solid (550 mg, 1.24 mmol, 51%).**^{1}H NMR δH/ppm (400 MHz, $CDCl_3$)**: δ 6.68 (1H, bt, J = 5.6 Hz, NH-amide), 6.43 (1H, s, N1-ureido), 5.49 (1H, s, N2-ureido), 4.52 (1H, dd, J = 7.8, 4.8 Hz, H-2), 4.34 (1H, dd, J = 7.8, 1.4 Hz, H-3), 3.72 - 3.38 (16H, m, CH_2-O-; CH_2-NH; CH_2-CH_2-N_3), 3.16 (1H, td, J^1 = 7.4, 4.6 Hz, H-4), 2.98-2.86 (1H, m, H-1), 2.77 (1H, d J= 12.8 Hz, H-1'), 2.25 (2H, t, J = 7.5, 1.6 Hz, H-8), 1.81 -1.6 (3H, m, H-5, H-7), 1.47 (2H, p, J = 7.2 Hz, H-6); **^{13}C NMR δC/ppm (101 MHz, $CDCl_3$)**: δ 173.24, 164.24, 70.65, 70.47, 70.08, 70.02, 61.78, 60.24, 55.72, 50.68, 40.54, 39.14, 36.01, 28.29, 28.11, 25.6; **MS Expected:** $C_{18}H_{32}N_6O_5S$ [M + Na] 467.2047 m/z; **Found:** 467.2047 m/z; **TLC**: Rf = 0.58 (10% MeOH in DCM). Spectral data in accordance with those seen in the literature (Zhou et al., 2017).

2.2.8. Synthesis of 1H-Thieno[3,4-d]imidazole-4-pentanamide, N-[2-[2-[2-(2-aminoethoxy)ethoxy] ethoxy]ethyl] hexahydro-2-oxo-,(3aS,4S,6aR) (**16**)

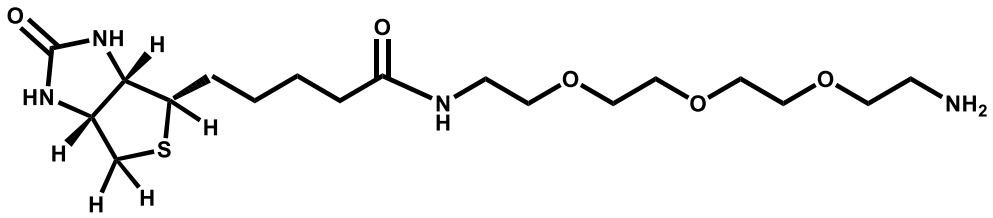

At 0 °C biotin-PEG_3-azide (446 mg, 1 mmol, 1 eqv) was dissolved in THF (20 mL) followed by dropwise addition of PPh_3 (315 mg, 1.2 mmol, 1.2 eqv) and H_2O (8 mL). The mixture was warmed to RT overnight, the layers were separated and the organic layer was concentrated under reduced pressure. The residue was treated with 1 M HCl (20 mL) and then treated with KOH (pH 11) before dissolving the crude product with DCM. The crude material was then purified by silica column chromatography (0-100% MeOH in 1% TEA with DCM) and concentrated under reduced pressure to give the product as a white residue (150 mg, 0.36 mmol, 36%).**^{1}H NMR δH/ppm (400 MHz, $CDCl_3$)**: δ 7.46 (1H, t, J = 5.2 Hz, NH-amide), 6.72 (1H, s, N1-ureido), 5.95 (1H, s, N2-ureido), 4.48 (1H, dd, J = 7.7, 4.8 Hz, H-2), 4.29 (1H, dd, J = 7.6, 4.6 Hz, H-3), 3.63-3.60 (8H, m, CH_2-O), 3.55-3.54 (4H, m, CH_2-NH), 3.42-3.40 (4H, m, CH_2-CH_2-NH), 3.12 (1H, m, H-4), 2.88 (1H, dd, J = 7.9 Hz, 12.8 Hz, H-1), 2.72 (1H, d, J = 12.8 Hz, H-1'), 2.22 (2H, t, J = 7.6 Hz, H-8), 1.74-1.63 (4H, m, H-5, H-7), 1.41 (2H, p, J = 7.1 Hz, 7.4 Hz, H-6); **^{13}C NMR δC/ppm (101 MHz, $CDCl_3$)**: δ 173.71, 164.26, 70.43, 70.41, 70.07, 70.0, 61.81, 60.2, 55.74, 50.29, 40.53, 39.11, 35.83, 28.31, 28.08, 25.69; **MS Expected:** $C_{18}H_{34}N_4O_5S$ [M + H]: 419.2 m/z, **Found:** 419.2 m/z; **IR (cm^{-1}):** 3241.10 (N-H Stretch, aliphatic amine), 2926.22-2863.47 (C-H stretch, alkane), 1697 (C=O stretch, amide) 1644.12 (C=O stretch, urea), 1100 (C-O stretch, aliphatic ether); **TLC**: Rf = 0.20 (20% MeOH in 1% TEA and DCM). Spectral data in accordance with those seen in the literature (Fusz et al., 2008).

2.2.9. Synthesis of H-Thieno[3,4-d]imidazole-4-pentanamide, N-(14-bromo-13-oxo-3,6,9-trioxa-12-azatetradec-1-yl)hexahydro-2-oxo-,(3aS,4S,6aR) (**17**)

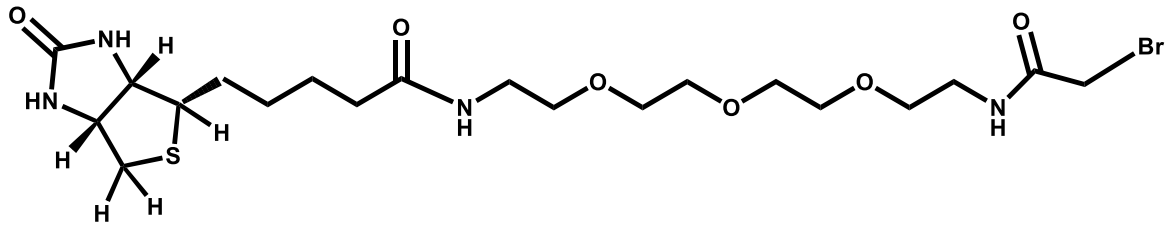

Biotin-PEG_3-amine (150 mg, 0.36 mmol, 1 eqv) was dissolved in anhydrous DCM (6 mL) with anhydrous DIPEA (69 µL, 0.396 mmol, 1.1 eqv) and treated with bromoacetic anhydride (103 mg, 0.396 mmol, 1.1 eqv) at -20 °C. After 2 h the solvent was removed and the residue was washed with EtOAc (20 mL) to remove impurities. DCM (8 mL) and sonication were used to dissolve the crude material before purification by column chromatography (0 → 100% MeOH in DCM) to give a clear oil (2.8 mg, 38.55 µmol, 11%). **^{1}H NMR $^\delta$H/ppm (400 MHz, $CDCl_3$)**: δ 7.44 – 7.36 (1H, m, NH-amide), 6.95-6.87 (1H, bs, N1-ureido), 6.30 (1H, s, N2-ureido), 4.52 (1H, dd *J* = 7.8, 4.9 Hz, H-2), 4.32 (1H, dd, *J* = 7.0, 5.2 Hz. H-3), 3.88 (2H, s, CH_2-Br), 3.72-3.35 (16H, m, HN-CH_2-CH_2-O), 3.16 (1H, td, *J* = 7.3, 4.4 Hz, H-4), 2.92 (1H, dd, *J* = 12.8, 4.9 Hz, H-1), 2.74 (1H, d, *J* = 12.8 Hz, H-1'), 2.24 (2H, t, *J* = 7.4 Hz, H-8), 1.80 – 1.53 (4H, m, H-5, H-7), 1.48-1.40 (2H, m H-6); **MS Expected:** $C_{20}H_{35}BrN_4O_6S$ **Br 79** [M + H]: 539.1533 m/z; **Found**: 539.158 m/z**; Br 81** [M + H]: **Expected:** 541.151 m/z **Found:** 541.156 m/z**; TLC**: Rf = 0.10 (10% MeOH in DCM).

2.2.10. Synthesis of p(s)pGpp ([(2R,3S,4R,5R)-5- (2-amino-6-oxo-1H-purin-9-yl)-4-hydroxy-2-[[hydroxy(phosphonooxy)phosphoryl]oxymethyl]oxolan-3-yl] phosphono thiophosphate) (**18**)

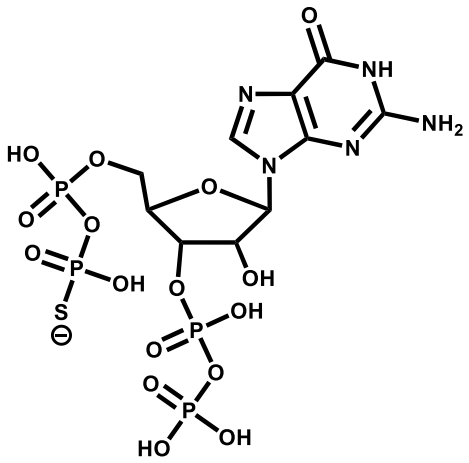

1X buffer (250 µL) consisting of: triethylammonium bicarbonate (TEAB, pH 8.5, 25 mM); Sodium chloride (NaCl, 100 mM); magnesium chloride ($MgCl_2$, 15 mM) was mixed thoroughly with ATP (7 mM), GDPβs (5 mM), YjbM (2 µM) in a final volume of 500 µL. The reaction was incubated at 37 °C overnight. Following this, a 3 kDa cut-off spin column was washed with: sodium hydroxide (NaOH, 200 uL, 0.1 M); x2, ddH_2O (200 uL) and 1X buffer (200 µL). The reaction was added to the column and centrifuged (16,000 xG, 10 min). The lower reservoir now containing the p(s)pGpp was lyophilized overnight and resuspended in ddH_2O (100 L). The impure nucleotide was purified by anion exchange chromatography on a Nucleopac column PA-100 4 mm × 250 mm (4.6 mL column), 9-90% B (B = 500 mM NH_4HCO_3 and 0.5% MeCN) before being concentrated under reduced pressure and re-suspended in ddH_2O (1.15 mL, 1.15 umol). **HPLC:** Mobile phase A: NH_4HCO_3 (50 mM); MeCN (0.5% v/v), Mobile phase B: NH_4HCO_3 (500 mM); MeCN (0.5% v/v), 9-90% B, eluting at 18.8 minutes which is equal to 392.63 mM NH_4HCO_3. **^{31}P NMR δP/ppm (162 MHz, D_2O)**: δ -11.60 (d, J = 20.5, α-3'), -11.37 (d, J= 20 Hz, α-5'), -9.74 (d, J = 19.8, β-3'), 16.08 (d, J = 16.69 Hz, *R*-PSβ-5'), 19.77 (d, J = 5.59 Hz, *S*-PSβ-5'); **Absorption spectra:** Indicative of guanosine; **MS Expected:** $C_{10}H_{17}N_5O_{16}P_4S$ [M - H]: 617.92687 m/z, **Found**: 617.9269 m/z. Phosphorothioate peaks are often diastereotopic, thus the appearance of an extra peak.

2.2.11. Synthesis of Guanosine 3'-diphosphate-5'-phosphoryl-phosphorylthio-11-amido-3,6,9-trioxaundecan-1-biotin (**19**)

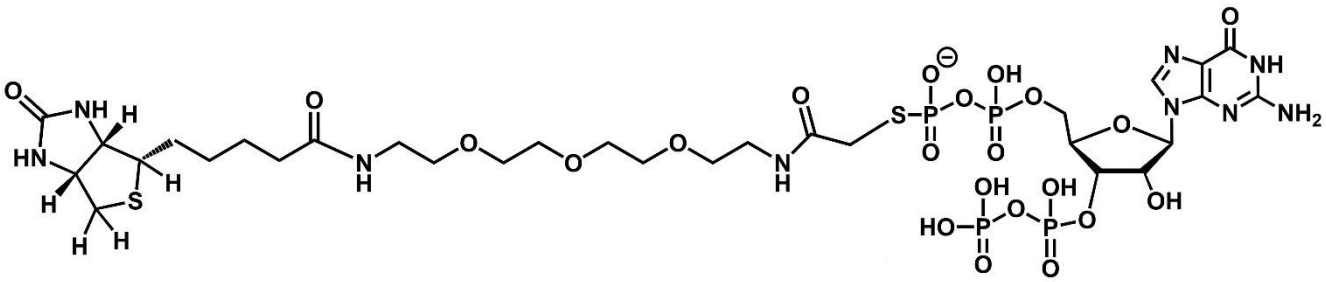

p(s)pGpp (2 µmol, 1 eqv) was dissolved in ddH_2O (120 µL) and sodium borate buffer (pH 9, 500 mM, 30 µL). To this solution, biotin-PEG3-acetyl-bromide (8 µmol, 4 eqv) in DMSO (150 µL) was added and the reaction was left stirring overnight. The reaction mixture was purified by RP-HPLC: 20 min gradient 3→50% B (A =200 mL 2 M TEAB, 4 mL MeCN, 3796 mL H_2O), mobile phase B = (50% MeCN, TEAB pH 8.21) MeCN (1 L), H_2O (900 mL), TEAB (100 mL). The compound was freeze-dried and dissolved in ddH_2O to yield the product in solution (295 nmol, 14.75%). **HPLC:** Mobile phase A: Triethyl ammonium bicarbonate (TEAB, pH 8.2, 20 mM); MeCN (0.5% v/v)**,** Mobile phase B: TEAB (pH 8.2, 20 mM); MeCN (50% v/v), 3-50% B over 20 min compound eluted at 15.96 min which corresponds to MeCN (17.5%)**; Absorption spectra:** Indicative of guanosine; **MS Expected:** $C_{30}H_{51}N_9O_{22}P_4S_2$ [M]:1077.154 m/z, **Found**: 1077.155 m/z.

2.3. Synthetic methods for the production of the fluorescent chemosensor PyDPA

All compounds were synthesised in accordance with the literature with spectral data matching (Conti et al., 2019, Rhee et al., 2008).

2.3.1. Synthesis of 3-Pyren-1-yl-prop-2-yn-1-ol (**21**)

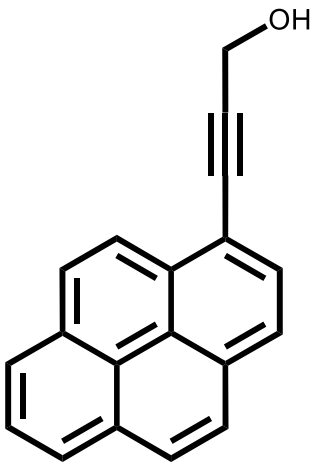

Bromopyrene (1 g, 3.56 mmol, 1eqv) was dissolved with [$Pd(PPh_3)_4$] (127 mg, 0.11 mmol, 0.03 eqv) in n-$BuNH_2$ (20 mL) degassed with Ar. Propargyl alcohol (102 µL, 1.78 mmol, 5.1 eqv) was added to the mixture and the reaction was left to stir at reflux 78 °C for 6 h. The solvent was evaporated under reduced pressure and the crude material purified by automated flash chromatography (hexane/EtOAc 92:8 → 40:60). Product was obtained as a slightly yellow solid (600 mg, 2.34 mmol, 66%). **^{1}H NMR $^\delta$H/ppm (400 MHz, $CDCl_3$)**: δ 8.57 (1H, d, *J* = 9.1 Hz; H_{3Ar}), 8.25 – 8.20 (2H, m; H_{6Ar}, H_{8Ar}), 8.19 – 8.03 (6H, m; $H_{2Ar,}$ H_{4Ar} H_{5Ar}, H_{7Ar}, $H_{9Ar,}$ H_{10Ar}), 4.77 (2H, s; CH_2OH), 1.95 (1H, s, OH). **^{13}C NMR $^\delta$C/ppm (101 MHz, $CDCl_3$)**: δ 132.07, 131.42, 131.21, 131.01, 129.77, 128.42, 128.30, 127.20, 126.27, 125.68, 125.65, 125.36, 124.44, 116.96, 92.75, 84.83, 52.08; **MS Expected:** $C_{19}H_{12}O$ [M + H] 257.096 m/z; **Found**: 257.096 m/z, **Expected**: [M + Na] 279.08 m/z, **Found**: 279.078 m/z; **IR (cm^{-1}):** 3219.5 (OH stretch), 3036.9 (C-H alkene), 1601-1583 (C=C aromatic); **TLC**: Rf = 0.54 (Hex:EtOAc, 2:1)

2.3.2. Synthesis of 3-(pyren-1-yl)propan-1-ol (**22**)

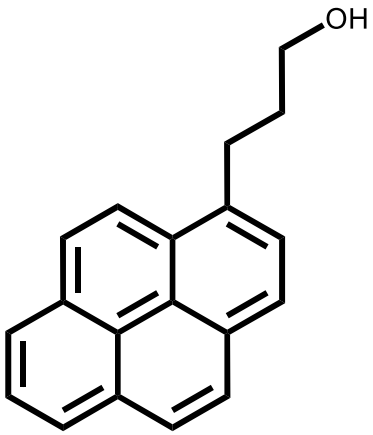

3-Pyren-1-yl-prop-2-yn-1-ol (1.5 g, 5.85 mmol, 1 eqv) was dissolved in freshly distilled MeOH (20 mL). 10% Pd/C (315 mg, 0.29 mmol, 0.05 eqv) was added and the reaction mixture was stirred under hydrogen and argon (1 atm) for 2 h. (TLC: hexane/EtOAc 60:40). The catalyst was removed by filtration through celite and the solvent was evaporated under reduced pressure to give a yellow powder (1.51 g, 5.8 mmol, 99.8%). **^{1}H NMR $^{\delta}$H/ppm (400 MHz, $CDCl_3$)**: δ 8.32 (1H, d, *J* = 9.2 Hz; H_{3Ar}), 8.19 (2H, d, *J* = 7.6 Hz; $H_{6Ar,}$ H_{8Ar}), 8.13 (2H, dd, *J* = 8.5, 3.4 Hz; $H_{2Ar,}$ H_{9Ar}), 8.07 – 7.97 (3H, m; $H_{4Ar,}$ $H_{5Ar,}$ H_{7Ar}), 7.91 (1H, d, *J* = 7.8 Hz; H_{10Ar}), 3.80 (2H, t, *J* = 6.3 Hz; CH_2OH), 3.47 (2H, t, *J* = 7.7 Hz; CH_2Ar), 2.21 – 2.09 (2H, m; CH_2CH_2OH). **^{13}C NMR $^{\delta}$C/ppm (101 MHz, $CDCl_3$)**: δ 136.28, 131.54, 131.01, 129.98, 128.78, 127.61, 127.41, 127.36, 126.75,125.94 125.21, 125.11, 125.00, 124.95, 124.85, 123.45, 62.49, 34.65, 29.75; **MS Expected:** $C_{19}H_{16}O$ [M + H] m/z; 261.1279, **Found:** 261.1291 m/z; **IR (cm^{-1}):** 3295.85 (OH stretch), 3037.61 (C-H alkene), 2945.39-2851.49 (C-H aliphatic), 1603.09-1586.49 (C=C aromatic); **TLC**: Rf = 0.44 (60:40, Hex : EtOAc)

2.3.3. Synthesis of 1- (3-bromopropyl)pyrene (**3**)

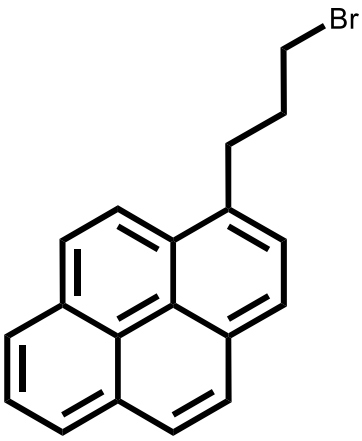

33 % HBr in AcOH (10 mL) was added to 3-(pyren-1-yl)propan-1-ol (1.5 g, 5.8 mmol 1 eqv) in a microwave vial. The reaction was stirred under microwave irradiation at 100 °C for 90 min and diluted with EtOAc (50 mL). The organic layer is washed with 50 % $NaHCO_3$ until basic, water (1 × 25 mL) and dried (Na_2SO_4). **^{1}H NMR $^\delta$H/ppm (400 MHz, $CDCl_3$):** δ 8.26 (1H, d, *J* = 9.3 Hz; H_{3Ar}), 8.21 (2H, d, *J* = 8.3 Hz: H_{6Ar}, H_{8Ar}), 8.11 (2H, d, *J* = 9.2 Hz; H_{2Ar}, H_{9Ar}), 8.08 – 8.03 (3H, m; H_{4Ar}, $H_{5Ar,}$ H_{7Ar}), 7.86 (1H, d, *J* = 7.7 Hz; H_{10Ar}), 3.57 – 3.42 (4H, m; CH_2Br, CH_2Ar), 2.40 (1H, p, *J* = 6.7 Hz; -CH_2CH_2Br); **^{13}C NMR $^\delta$C/ppm (101 MHz, $CDCl_3$):** δ 134.77, 131.48, 130.93, 130.14, 128.72, 127.56, 127.39, 126.89,125.99 125.15, 125.11, 125.00, 124.96, 124.91, 123.15, 34.44, 33.73, 31.66; **MS Expected:** $C_{19}H_{15}Br$ [M] 322.0357 m/z, **Found**: 322.0362 m/z; **IR (cm^{-1}):** 3039.36 (C-H alkene), 2937.23 (C-H aliphatic), 1603.09-1586.49 (C=C aromatic), 680.57 (C-Br stretch); **TLC**: Rf = 0.76 (70: 30, Hex : EtOAc).

2.3.4. Synthesis of 3,5-Bis (hydroxymethyl)phenol (**25**)

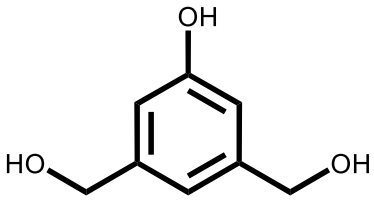

Dimethyl 5-hydroxyisophthalate (3 g, 14 mmol, 1 eqv) in dry THF (30 mL) was added to 2 M $LiAlH_4$ in THF (18 mL, 36 mmol, 2.57 eqv) that was cooled to 0 °C before stirring O/N at room temperature. Ice cooled 10 % H_2SO_4 (30 mL) was added and then removed under reduced pressure. The white residue was resuspended in water and extracted with EtOAc (5 × 50 mL) before drying ($MgSO_4$) and concentrating under reduced pressure. The crude oil was purified by silica column chromatography (0-100% Hex: EtOAc) to yield pure product as a slightly yellow oil (1.56 g, 10.11 mmol, 74%). **^{1}H NMR $^\delta$H/ppm (400 MHz, Acetone^{d6}):** δ 8.24 (1H, bs, Ar-OH), 6.82 (1H, s, H_{4Ar}), 6.75 (2H, s, H_{2Ar}, H_{6Ar}), 4.56 (4H, s, Ar-CH_2), 4.22 (2H, bs, CH_2-OH); **^{13}C NMR $^\delta$C/ppm (101 MHz, Acetone^{d6})**: δ 157.40, 143.85, 115.84, 111.91, 63.82; **MS Expected:** $C_8H_{10}O_3$ [M - H]: 153.0557 m/z, **Found:**153.056 m/z; **TLC**: Rf = 0.13 (10% MeOH in DCM)

2.3.5. Synthesis of (5-[3-(pyren-1-yl)propoxy]-1,3-phenylene)dimethanol (**26**)

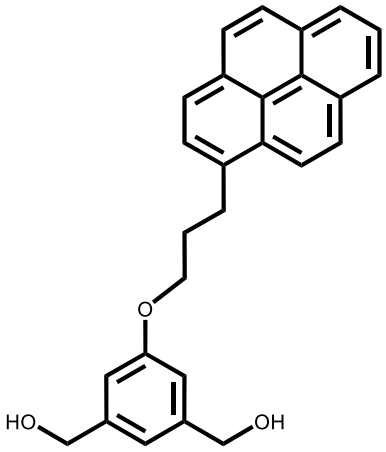

3- (pyren-1-yl)-1-bromo-propane (1.2 g, 3.7 mmol, 1eqv), 3,5-Bis (hydroxymethyl)phenol (680 mg, 4.44 mmol, 1.2 eqv), ground, oven-dried K_2CO_3 (1.5 g, 11.1 mmol, 3eqv) and KI (614 mg, 3.7 mmol, 1 eqv) were dissolved in dry MeCN (20 mL). The reaction mixture was stirred at reflux under MW irradiation for 24 h. The solvent was evaporated under reduced pressure and the crude product was extracted from the resulting brown solid with EtOAc (40 mL). The solution was washed with water (3 × 20 mL) and saturated brine (1 × 15 mL). The organic phase was dried ($MgSO_4$) and the solvent was evaporated under reduced pressure. The crude material was purified by silica column chromatography using

(95:4:1 DCM : MeOH: TEA) to yield a colourless oil (190 mg, 0.479 mmol, 13%).**^{1}H NMR $^{\delta}$H/ppm (400 MHz, $CDCl_3$):** δ 8.32 (1H, d, *J* = 9.2 Hz; H_{8Ar}), 8.18 (2H, d, *J* = 7.5 Hz; H_{4Ar}, H_{6Ar}) ,8.11 (2H, dd, *J* = 9.3, 6.5 Hz; H_{2Ar}, H_{11Ar}), 8.04 (2H, s; H_{1Ar}, H_{12Ar}), 8.01 (1H, dd, *J* = 7.3 Hz; H_{5Ar}) 7.90 (1H, d, *J* = 7.8 Hz; H_{9Ar}), , 6.95 (1H, s; H_{4Ph}) , 6.88 (2H, s; H_{2Ph}), 4.66 (4H, s; CH_2-OH), 4.07 (2H, t, *J* = 6.0 Hz; CH_2-O), 3.56 (2H, t, *J* = 7.7 Hz; Ar-CH_2), 2.35 (2H, p, *J* = 4.0 Hz; Ar$CH_2$$\underline{CH_2}$); **^{13}C NMR $^{\delta}$C/ppm (101 MHz, $CDCl_3$):** δ 159.54, 142.83, 135.76, 131.42, 130.90, 129.95, 128.77, 127.51,127.42 127.39, 126.72, 125.87, 124.94, 124.87, 123.32, 117.53, 112.22, 67.11, 65.12, 31.15, 29.74; **MS Expected:** $C_{27}H_{24}O_3$ [M + Na] 419.16 m/z, **Found**: 419.162 m/z; **TLC**: Rf = 0.42 (5% MeOH in DCM).

2.3.6. Synthesis of (5-[3-(pyren-1-yl)propoxy]-1,3-phenylene)dibromide (**27**)

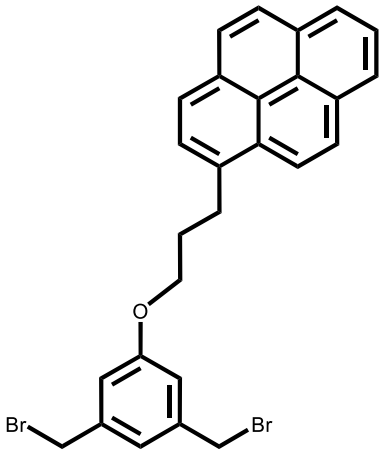

To a stirred solution of (5-[3- (pyren-1-yl)propoxy]-1,3-phenylene)dimethanol (190 mg, 0.479 mmol, 1 eqv) in anhydrous DCM (50 mL) at 0 °C, PBr_3 (580 mg, 204 µL, 2.2 mmol, 4 eq) was slowly added. After stirring at room temperature O/N the reaction was quenched with MeOH (10 mL), the solvents were evaporated and the residue was partitioned between H_2O (30 mL) and DCM (50 mL). The organic layer was washed with saturated brine (40 mL) before drying ($MgSO_4$). The crude product was purified by silica-column chromatography (hexane: DCM= 1:2) to yield a white powder of pure product (160 mg, 0.31 mmol 64%). **^{1}H NMR $^{\delta}$H/ppm (400 MHz, Acetone^{d6})** δ 8.32 (1H, d, J = 9.2 Hz; H_{8Ar}), 8.20 (2H, d, J = 7.6 Hz; H_{4Ar}, H_{6Ar}), 8.13 (2H, t, J -9.3 Hz; H_{2Ar}, H_{11Ar}), 8.09-7.98 (3H, m; H_{1Ar}, $H_{5Ar,}$ $H_{12Ar,}$), 7.91 (1H, d, J = 7.7 Hz; H_{9Ar}), 7.0 (1H, s; H_{4Ph}), 6.90 (2H, s; H_{2Ph}), 4.44 (4H, s; CH_2-Br), 4.05 (2H, t, J = 6 Hz; CH_2-O), 3.56 (2H, t, J = 6.8 Hz; Ar-CH_2), 2.35 (2H, p, J = 8.5 Hz; Ar$CH_2$$\underline{CH_2}$);**^{13}C NMR $^{\delta}$C/ppm (101 MHz, Acetone^{d6})** δ 159.45, 139.63, 135.62, 131.45, 130.93, 130.01, 128.79, 127.54, 127.49, 127.41, 126.79, 125.92, 125.14, 125.00, 124.92, 124.86, 123.27, 121.86, 115.61, 67.15, 32.99, 31.07, 29.71; **MS Expected:** $C_{27}H_{24}Br_2O$ [M + H]: 521.011, **Found**: 520.905 m/z; **TLC**: Rf = 0.8 (10% DCM in Hexane).

2.3.7. 5-[3- (1-Pyrenyl)propoxy]-*N*^{1},*N*^{1},*N*^{3},*N*^{3}-tetrakis (2-pyridinylmethyl)-1,3-benzenedimethanamine (**28**)

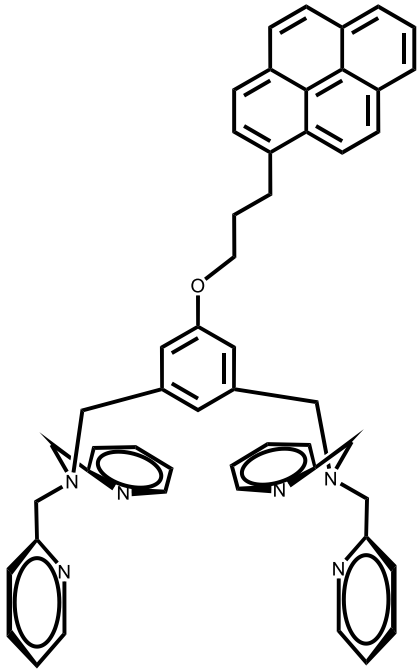

To a stirred solution of 5-[3- (1-Pyrenyl)propoxy]-1,3-dimethylbromo-benzene (160 mg. 0.31 mmol, 1 eqv) in anhydrous DMF (20 mL) at room temperature, dipicolylamine (130 mg, 0.65 mmol 2.1 eq), KI (108 mg 0.65 mmol, 2.1 eq), and K_2CO_3 (129 mg, 0.93 mmol, 3.0 eq) were slowly added. After stirring at room temperature O/N , the solvent was evaporated, and the crude mixture was partitioned between water/EtOAc. The organic layer was dried (Na_2SO_4) and the crude product was then purified by silica-column chromatography (DCM : MeOH : TEA, 90:9:1 → 60:39:1) to give the product as a slightly yellow oil (140 mg, 184 mmol, 61%). **^{1}H NMR $^{\delta}$H/ppm (400 MHz, Acetone^{d6}):** δ 8.48 (4H, d, J = 4.5 Hz; H_{6Py}), 8.31 (1H, d, J = 7.6 Hz; H_{8Ar}), 8.16 (1H, d, J = 8 Hz), 8.09 (2H, dd, J = 7.7 Hz, 11.51 Hz; H_{4Ar}, H_{6Ar}), 8.06-8.0 (3H, m; H_{1Ar}, $H_{5Ar,}$ $H_{12Ar,}$), 7.98 (1H, t, J = 7.9 Hz; H_{2Ar}, H_{11Ar}), 7.90 (1H, d, J = 7.8 Hz; H_{9Ar}), 7.59-7.54 (8H, m; $H_{4Py,}$ H_{5Py}), 7.13-7.09 (4H, m; H_{3Py}), 7.07 (1H, s; H_{4Ph}), 6.90 (2H, s; H_{2Ph}), 4.06 (2H, t, J = 6.0 Hz; CH_2-O), 3.81 (8H, s; Ar-CH_2-NR_2), 3.66 (4H, s; CH_2-NR_2), 3.57 (2H, t, J = 7.5 Hz; Ar-CH_2), 2.36 (2H, p, J = 8 Hz; Ar-$CH_2\underline{CH_2}$);**^{13}C NMR $^{\delta}$C/ppm (101 MHz, Acetone^{d6}):** δ 159.49, 159.22, 148.84, 140.49, 136.64, 135.79, 131.40, 130.85, 129.92, 128.78, 127.48, 127.41, 127.33, 127.71, 125.86, 125.07, 124.95, 124.92, 124.82, 124.77, 123.29, 122.83, 122.09, 121.53, 113.70, 66.86, 59.94, 58.65, 31.17, 29.68; **MS:** $C_{51}H_{46}N_6O$ **Expected**: [M + Na] 781.363 m/z, **Found:** 781.364 m/z; **TLC**: Rf = 0.1 (DCM: MeOH: TEA, 90:9:1)

2.3.8. Synthesis of Chemosensor PyDPA (**29**)

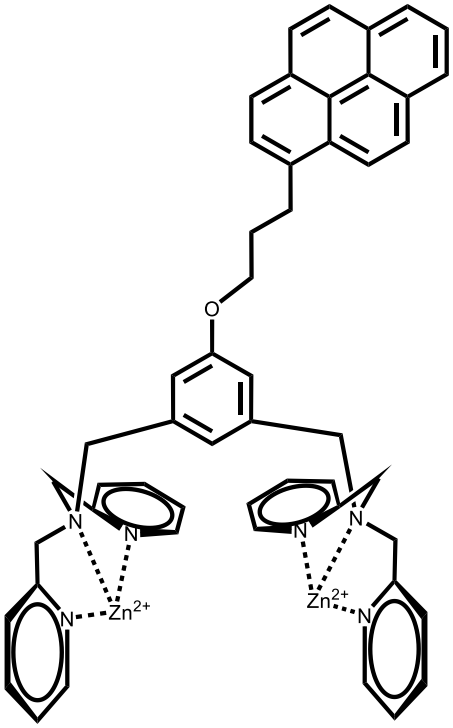

To 5-[3- (1-Pyrenyl)propoxy]-*N*^{1},*N*^{1},*N*^{3},*N*^{3}-tetrakis (2-pyridinylmethyl)-1,3-benzenedimethanamine (140mg, 0.184 mmol, 1 eqv) in MeCN (10 mL), $ZnClO_4$-$6H_2O$ (140 mg, 0.38 mmol, 2.05 eqv) was added slowly and left stirring at RT for 2 h. The solvent was then removed under reduced pressure to yield PyDPA as an off white solid (218 mg, 0.184 mmol, 100%). **^{1}H NMR δH/ppm (400 MHz, CD_3CN):** δ 8.78, (4H, d, J = 4.6 Hz; H_{6Py}), 8.43 (1H, d, J = 9.3 Hz; H_{8Ar}), 8.28-8.16 (3H, m; H_{1Ar}, H_{4Ar} H_{6Ar},) 8.12-8.04 (8H, m; H_{2Ar}, $H_{5Ar,}$ $H_{9Ar,}$ H_{12Ar} H_{4Py}), 7.98 (1H, t; H_{11Ar}) 7.73 (4H, t, J = 7.1 Hz; H_{5Py}), 7.38 (4H, d, J = 7.8 Hz; H_{3Py}), 6.79 (2H, s, *o*-Ph), 6.75 (1H, s, *p*-Ph), 4.21 (d, 4H, J = 16 Hz; Py-CH_2-NR_2), 4.07 (2H, t, J = 5.9 Hz; Ar$CH_2CH_2\underline{CH_2}$O), 3.85 (4H, s; NR_2-CH_2-Ph), 3.69 (4H, d, J = 14.5 Hz), 3.67 (2H, t, J = 6.6 Hz; ArCH $_2CH_2CH_2$O), 2.43 (2H, p, J = 6.4 Hz; Ar-$CH_2\underline{CH_2}$);**^{13}C NMR δC/ppm (101 MHz, Acetone^{d6})**: δ 159.45, 154.39, 148.10, 142.03, 136.33, 133.32, 131.37, 130.87, 129.91, 128.86, 127.91, 127.53, 127.20, 126.72, 126.47, 126.24, 125.48, 125.15, 125.06, 125.01, 124.83, 123.67, 124.67, 118.06, 117.27, 66.94, 55.87, 54.78, 30.92, 28.76; **MS:** $C_{51}H_{46}N_6O$ **Expected**: [M + H] 759.380 m/z, **Found:** 759.381 m/z.

2.4. Biological procedures

2.4.1. Bacterial and DNA work

2.4.1.1 Bacterial strains and growth conditions

S. aureus strains (*Table 1*) were grown on tryptic soy agar (TSA, 37 °C, 18 h) before inoculating tryptic soy broth (TSB) and shaking (37 °C, 200 rpm, 18 h). *Escherichia coli* (Table 2.4.1.1*)* were grown on agar (37 °C, 18 h) before inoculating in Luria Bertani broth (LB) and shaking (37 °C, 18 h, 200 rpm). All bacterial strains were stored by freezing at −80 °C after mixing 1:1 with freezer media: bovine serum albumin (BSA, 10% w/v); monosodium glutamate (MSG, 10% w/v) in water. The following strains were used with appropriate antibiotics included:

Table 2.4.1.1: List of *bacterial* strains used:

Strain	Relevant features	Reference
	***Escherichia coli* strains**	
BL21 DE3	Protein expression strain containing the gene for T7 RNAP	Novagen
XL1 Blue	Cloning strain: TetR	Stratagene
T7IQ pVL791	Protease deficient protein expression strain, lacIq tightly control expression: CamR	New England Biolabs
RMC0162	*XL1 blue* pVL 847: TetR (pvL 847 contains a His and MBP tag)	Laboratory strain collection
RMC0534	*T7IQ* pVL847: CarbR, CamR	Laboratory strain collection
RMC1745	MG1655 *ΔrelA ΔspoT*: CamR	(Magnusson et al., 2007)
RMC2037	*T7IQ* pVL791–*rpoY*: CarbR, CamR	(Corrigan et al., 2016)
RMC2037	*T7IQ* pVL791 – *perR*: CarbR, CamR	(Corrigan et al., 2016)
RMC2038	*T7IQ* pVL791 – *rpoE*: CarbR, CamR	(Corrigan et al., 2016)
RMC2039	*T7IQ* pVL791 – *vraR*: CarbR, CamR	(Corrigan et al., 2016)
RMC2040	*T7IQ* pVL791 – *katA*: CarbR, CamR	(Corrigan et al., 2016)
RMC2041	*T7IQ* pVL791 – *prsA*: CarbR, CamR	(Corrigan et al., 2016)
RMC2042	*MG1655 ΔrelA ΔspoT* pTARA::kan pVL791 – *rpoY*: KanR, CarbR, CamR	This study
RMC2043	*MG1655 ΔrelA ΔspoT* pTARA::kan pVL791 – *rpoE*: KanR, CarbR, CamR	This study
RMC2044	*MG1655 ΔrelA ΔspoT* pTARA::kan pVL791 – *vraR*: KanR, CarbR, CamR	This study
RMC2045	*MG1655 ΔrelA ΔspoT* pTARA::kan pVL791 – *katA*: KanR, CarbR, CamR	This study
RMC2046	*MG1655 ΔrelA ΔspoT* pTARA::kan pVL791 – *prsA*: KanR, CarbR, CamR	This study
RMC2047	*MG1655 ΔrelA ΔspoT* pTARA::kan pVL791 – *perR*: KanR, CarbR, CamR	This study
RMC2056	*T7IQ* pVL791 – *sigB*: CarbR, CamR	(Corrigan et al., 2016)
RMC2057	*T7IQ* pVL791 – *sarA*: CarbR, CamR	(Corrigan et al., 2016)
RMC2058	*T7IQ* pVL791 – *fur*: CarbR, CamR	(Corrigan et al., 2016)
RMC2080	*XL1-blue* pVL847-*rpoY*: CarbR,	This study
RMC2081	*BL21* pVL847 – *rpoY*: CarbR,	This study
RMC2107	*T7IQ* pVL791 – *ohr*: CarbR, CamR	(Corrigan et al., 2016)
RMC2108	*T7IQ* pVL791 –*Ac2460*: CarbR, CamR	(Corrigan et al., 2016)
RMC2109	*T7IQ* pVL791 –*mvaD*: CarbR, CamR	(Corrigan et al., 2016)
RMC2110	*T7IQ* pVL791 –*ureE*: CarbR, CamR	(Corrigan et al., 2016)
RMC2111	*T7IQ* pVL791 –*adk:* CarbR, CamR	(Corrigan et al., 2016)
RMC2112	*T7IQ* pVL791 –*lysA*: CarbR, CamR	(Corrigan et al., 2016)
RMC2113	*T7IQ* pVL791 –*hxlB*: CarbR, CamR	(Corrigan et al., 2016)
	***Staphylococcus aureus* strains**	
RMC1847	*JE2 Δera* pCN55itet-*era*-His: TetR, SpecR	(Bennison et al., 2021)
RMC0905	*JE2 ΔrelQ ΔrelP Δrel* (p)ppGpp^0)	(Carrilero et al., 2023)
RMC0813	*LAC* Δera* pCN55itet	(Boles et al., 2010, Bennison et al., 2021)
RMC0187	*JE2* Wildtype CA-MRSA USA300 strain *LAC* derivative, lacking plasmids p01 and p03, Erm sensitive	(Hammer and Skaar, 2013)

2.4.1.2. Isolation of plasmid DNA

In order to isolate plasmid DNA from *E. coli* a GeneJet Plasmind Miniprep Kit (Thermoscientific) was used. The protocol provided was followed, however, column bound-DNA was eluted with ddH_2O in place of the elution buffer provided by the manufacturer.

2.4.1.3. Restriction digests of DNA

Reactions were incubated (37 °C, overnight (O/N)) and consisted of: DNA/plasmid (2 µg); CutSmart buffer (1X Final Concentration, NEB) and 10 units of the required restriction enzyme (NEB). The digested DNA was then purified using a GeneJet plasmid miniprep kit (ThermoScientific) as described in the protocol provided before visualising *via* agarose gel electrophoresis.

2.4.1.4. Ligation of DNA fragments

Ligation reactions (20 µL) consisted of insert: vector (5:1); digested insert (250 ng), plasmid vector (50 ng), T4 DNA ligase (400 Unit, NEB) and 1X T4 ligase buffer (NEB). The reactions were incubated (25 °C, 4 h) and immediately used for transformation without heat inactivation.

2.4.1.5. Transformation into chemically-competent E. coli cells

In order to transform ligation products into chemically competent *E. coli* cells, the cells (100 µL) are incubated (on ice, 5 min) with ligation product (10 µL). The cells are heat shocked (42 °C, 1 min) and immediately placed on ice for 2 min followed by addition of SOC media (900 uL): yeast extract (0.5% w/v); tryptone (2% w/v); NaCl (0.025% w/v); glucose (20 mM); KCl (pH 7.5, 2.5 mM). The cells were then incubated (37 °C, 1 h) with shaking, before plating onto LB agar with the antibiotics required to select for positive transformations. The plates were left to incubate (37 °C, O/N) and single colonies were screened using colony polymerase chain reaction (PCR).

2.4.1.6. Transformation into electrocompetent *E. coli* cells

A dialysis filter was added to a petridish with sterile ddH_2O, plasmid (15 µL) was added on top of the filter and left to dialyse (20 min). The dialysed plasmid was added to the electrocompetent cells (100 µL) and mixed, before adding to an electroporation cuvette (GeneFlow). Current was passed through the cuvette (1.8 kV, 5 µF, 200 Ω, 1 mm) and the cells were immediately added to SOC recovery media (900 µL) before incubating (37 °C, 1 h) with shaking before plating onto LB agar with the antibiotics required to select for positive transformations. The plates were left to incubate at 37 °C overnight and single colonies were then screened using colony PCR.

2.4.1.7. Polymerase Chain Reaction

The design of primers (Table 2.4.1.7) was carried out using SnapGene software (GSL Biotech LLC) before synthesis by Eurofins. Polymerase chain reactions (PCR) were performed in one of two ways depending on the required fidelity (a high fidelity polymerase ensures the correct insertion of base and as a result, high accuracy in DNA replication, these polymerases are typically referred to as having a low error rate). For high fidelity reactions **Method 1:** Used Phusion master mix with high-fidelity buffer (Thermoscientific). For low fidelity reactions such as colony-PCR **Method 2:** Used Taq polymerase master mix (NEB).

A typical reaction had a total volume (50 µL) and contained: plasmid DNA (~10 ng), forward primer (0.5 µM), reverse primer (0.5 µM) and 1X final concentration of either taq or phusion master mix.

Phusion reactions were placed in a T100 thermocycler (BioRad) and programmed for a general procedure of: denaturation (98 °C, 2 min); 5 cycles of denaturation (98 °C, 2 min); primer annealing (45 °C, 30 min) this overall temperature may vary as it relies on the specific melting temperature of the primers used; elongation (72 °C, x min) where x = 30 seconds per kb of DNA + 1 minute when using phusion or 1 minute per kb when using Taq. This was repeated for 25 cycles with the annealing temperature at 53 °C and an increased final extension time (72 °C, 5 min) to ensure full amplification occurs.

The products of PCR reactions were purified using the GeneJet Gel extraction kit (Thermoscientific) as with the isolation of plasmid DNA according to the manufacturer's protocol with the exception of elution buffer being replaced with ddH_2O to elute column-bound DNA. Colony PCRs were performed with *E. coli* by the direct addition of an individual colony to a reaction mix with Taq. The products from these PCR reactions were then visualised using agarose gel electrophoresis.

Table 2.4.1.7: List of primers used throughout this study with relevant restriction sites included

Number	Name	Sequences	Restriction Sites
RMC062	T7 Promoter	TAATACGACTCACTATAGGG	
RMC063	T7 Terminator	GCTAGTTATTGCTCAGCGG	
RMC1013	F-NdeI-RpoY	GGGCATATGGCAGTATTTAAAGTTTTTTATCAACATAACAGAGACG	NdeI
RMC1014	R-BamHI-RpoY	GGGGGATCCTTTAGCAATCTCCACATTAAAGTGTTCTGAG	BamHI
RMC1015	F-NdeI-PrsA	GGGCATATGAAGATGATAAACAAATTAATCGTTCCGGTAACAG	NdeI
RMC1016	R-BamHI-PrsA	GGGGGATCCTTGGCTCATGCCGGATTGTC	BamHI
RMC1017	F-NheI-katA	GGGGCTAGCACTATGTCACAACAAGACAAAAAGTTAACTG	NheI
RMC1018	R-BamHI-katA	GGGGGATCCTTTTTCAAAGTTTTCGTATGTTTCATCATTTTCAGT	BamHI

2.4.1.8. Agarose Gel electrophoresis

Agarose 1% (w/v) was dissolved in TAE buffer: Tris Acetate (pH 8, 40 mM); ethylenediaminetetraacetic acid (EDTA, 1 mM) with microwave heating before being added to the correct sized casket with Sybrsafe (0.0001% v/v, Invitrogen). After gel setting, DNA was mixed with 6X DNA loading dye (ThermoScientific). The gel was submerged in TAE buffer and the dyed DNA was loaded before electrophoresis was performed (120 V, 400 mA, 27 min) gels were imaged with a ChemiDoc MP imager (BioRad) and band sizes were referenced with a DirectLoad Plus 1 Kb DNA ladder (Merck).

2.4.2. Protein handling and purification

2.4.2.1. Sodium dodecyl-sulfate polyacrylamide gel electrophoresis (SDS-PAGE)

SDS-PAGE was used for analysis and separation of cell lysates along with proteins. The gels consist of two layers: the upper stacking gel and the lower resolving gel. The stacking gels consist of acrylamide (5.6%), stacking buffer comprising: (25% v/v, Tris (pH 8.8, 500 mM)**;** NaCl (120 mM); EDTA; (8 mM); SDS (0.4% w/v); ammonium persulphate (APS, 0.1% v/v); tetramethylethylenediamine (TEMED, 0.1% v/v). Depending on protein size and the resolution required the resolving gels were made up of: acrylamide (7.5 - 15%); resolving buffer comprising (25% v/v, Tris (pH 6.8, 500 mM)**;** NaCl (120 mM); EDTA (8 mM); SDS (0.4% w/v); APS (0.1% v/v); TEMED (0.1% v/v). The proteins and lysates were mixed in a 1:1 ratio with 2X sample buffer: Tris-HCl (pH 6.8, 62.5 mM); SDS (2% w/v); β-mercaptoethanol (5% v/v); glycerol (10% v/v); bromophenol blue (0.010 % w/v) before boiling (95 °C, 10 min) to denature proteins and centrifugation (13,000 rpm, 1 minute) to remove any aggregates. The gels were submerged in SDS-PAGE running buffer: tris-HCl (pH 8.6, 25 mM); glycine (192 mM); SDS (0.1% v/v) before loading the samples and NEB#P7718S Blue Prestained Protein Standard, Broad Range (11-250 kDa) as a ladder and commencing electrophoresis (200 V, 400 mA) until the dye front reached the bottom of the gel. The gels were developed with quick Coomassie stain (AGX104-GENQC1L) for 18 h and washed with ddH_2O or were stained using coomassie brilliant blue stain: methanol (45% v/v); acetic acid (10% v/v); Coomassie brilliant blue R250 (0.25% w/v) before removing excess stain with destaining solution: methanol (45% v/v); acetic acid (10% v/v).

2.4.2.2. Expression of recombinant proteins in *E. coli* strains

Overnight cultures of either *E. coli* MG1655, T7IQ or BL21 containing the appropriate expression vectors were diluted to an OD_{600} of 0.05 into fresh LBM9 media: sodium phosphate dibasic (Na_2HPO_4, 50 mM); potassium phosphate monobasic (KH_2PO_4, 15 mM); NaCl (8.5 mM); ammonium chloride (NH_4Cl, 18.6 mM); glucose (11.1 mM); sodium succinate hexahydrate (3.7 mM); tryptone (139 mM); yeast extract (1% w/v) pH 7.2. The medium was supplemented with the required antibiotics before inoculating and incubating (37 °C, 3 h) until an OD_{600} of 0.3-0.5 was reached. Cultures were induced with anhydrotetracycline (Atet, 100 ng/mL) or Isopropyl ß-D-1-thiogalactopyranoside (IPTG, 1 mM) before incubating (30 °C, O/N) to facilitate protein expression. Cells were pelleted via centrifugation

(6000 × G, 4 °C, 10 min), washed with protein storage buffer: Tris-HCl (pH 7.5 50 mM); NaCl (200 mM); glycerol (5% v/v), and flash frozen with liquid nitrogen before storing at -80 °C.

2.4.2.3. Purification of His-tagged proteins using nickel affinity chromatography

Pellets containing expressed protein were resuspended in 30 ml buffer A: Tris (pH 7.5 50 mM); NaCl (200 mM); glycerol (5% v/v); imidazole (10 mM) along with the addition of one cOmplete, Mini, EDTA-free Protease Cocktail tablet (Merck). The resuspended cells were lysed with the addition of lysozyme (20 µg/mL) and sonication for 10 min (30 seconds ON, 30 seconds OFF) using a 20 kHz ultrasonic liquid processor (Fisher) at 40% amplitude. Cell debris was removed via centrifugation (18,000 × g, 40 mins, 4 °C) and the resulting supernatant was filtered using a 0.45 µm membrane (Millipore). The filtered lysate was injected into a AKTA-prime purification system where it was loaded on to a HisTrap HP Ni^{2+} column (1 mL column volume, GE Healthcare) before gradient elution with increasing concentrations of buffer B: Tris (pH 7.5 50 mM); NaCl (200 mM); glycerol (5% v/v); imidazole (500 mM). The fractions containing the desired protein were determined using 10-15% SDS-PAGE before dialysing into storage buffer: Tris (pH 7.5 50 mM); NaCl (200 mM); glycerol (5% v/v). The proteins were concentrated to the desired volume and concentration using the appropriate molecular weight cut off (MWCO) centrifugal filter (ThermoScientific) before flash freezing with liquid nitrogen and storing at -80 °C.

2.4.2.4. Nickel resin chromatography

Ni-NTA Resin was used in place of a HisTrap column to provide a larger surface area for purification than the pre-packed columns (GE Healthcare) allowing for a higher throughput. All centrifuging steps were performed at 700 × g for 2 mins. The resin was packed into a 20 mL column and the supernatant was removed by spinning before washing with equilibration buffer: sodium phosphate (20 mM); NaCl (300 mM); imidazole (10 mM) and spinning (x2). The protein extract was then mixed with equilibration buffer (1:1) on a rotating wheel for 30 min before spinning down and saving the fractions. The resin was cleaned with wash buffer: sodium phosphate (20 mM); NaCl (300 mM); imidazole (25 mM) and spun down before saving the supernatant for downstream analysis (x3). The his-tagged proteins were eluted using elution buffer: sodium phosphate (20 mM); NaCl (300 mM); imidazole (250 mM) and spinning before collecting the supernatant. The fractions containing the desired protein were determined using 10 - 15% SDS-PAGE Protein were dialysed into storage buffer: Tris (pH 7.5 50 mM); NaCl (200 mM); glycerol (5% v/v). The proteins were then concentrated to the desired volume and concentration using the appropriate molecular weight cut off (MWCO) centrifugal filter, before the pellets were snap frozen with liquid nitrogen and stored at -80 °C.

2.4.2.5. MonoQ column chromatography

This method of purification works *via* anion exchange and a gradually increasing salt gradient to displace proteins by interfering *via* ionic interactions. The same procedure seen in section 2.1 was used with the exception of the column which was replaced with a MonoQ column (1 mL CV, Cytiva) and the buffers. Buffer A: Tris-base (pH 8, 50 mM), buffer B: Tris-base (pH 8, 50 mM); NaCl (1M). The fractions containing the desired protein were determined using 10 - 15% SDS-PAGE before loading into dialysis membrane and dialysing into protein storage buffer: Tris-base (pH 7.5, 50 mM); NaCl (200 mM); glycerol (5% v/v). The proteins were concentrated to the desired volume and concentration using the appropriate molecular weight cut off (MWCO) centrifugal filter (ThermoScientific) before flash freezing with liquid nitrogen and storing at −80 °C.

2.4.2.6. Determination of Protein concentrations using nanodrop

Protein concentrations were calculated using a nanodrop and the relevant extinction co-efficient determined by taking the protein sequence from (UniProt) and calculating using Expasy – Protparam. With this information the Beer-Lambert law (*Equation 2.4.2.6*) could be used to determine the protein concentration (c) upon rearranging (*Equation 2.4.2.6.1*), with the absorbance (A), extinction cofefficient (ε) and path length (l)(Swinehart, 1962).

Equation 2.4.2.6: $A = \varepsilon c l$

Equation 2.4.2.6.1: $\frac{A}{\varepsilon l} = c$

2.4.2.7. Determination of Protein concentrations using a Bicinchoninic acid assay (BCA)

To determine the accurate concentration of proteins, a modified Bradford assay that is also colorimetric known as a BCA (BioRad) assay was used(Bradford, 1976, Kielkopf et al., 2020). A standardisation plot was generated by loading 10 µL of 0, 0.2, 0.4, 0.6, 0.8 and 1 mg/mL BSA into a 96 well plate. The concentration of the sample of interest was determined by nanodrop before diluting the sample into the range of BSA above. The dye reagent (BioRad) was diluted 4:1 in ddH_2O before mixing thoroughly with the standards/samples and leaving to incubate (5 min). The absorbance (595 nm) was then recorded using a Sense 425-301 microplate reader (Hidex) and the concentration determined by calculating the slope (×) (*Equation 2.4.2.7*), with the OD- the blank (y), gradient (m) and y intercept (c).

Equation 2.4.2.7: $y = mx + c$

$\frac{y-c}{m} =$ x

2.4.2.8. Dot blotting procedure

To a nitrocellulose sheet, the negative control, positive control and sample of interest (10 μM, 2.5 μL) are spotted and left to dry before submerging in Tris buffered saline and TWEEN-20 (TBST) consisting of (Tris pH 7.4, 200 mM); NaCl (1.4M); TWEEN-20 (1% v/v) before adding BSA (5% w/v) and shaking for 1 h. The solution is then removed before resubmerging the nitrocellulose in a solution of capture compound (10 nM) in 1X TBST w/ BSA (5% w/v) and shaking for a further hour. The solution is then removed and the nitrocellulose washed with 1X TBST (3 × 10 min). The streptavidin-HRP conjugate (1:1000) was dissolved in 1X TBST w/ BSA (5% w/v) and added to the nitrocellulose sheet and left shaking for 1 h. The membrane is washed again with 1X TBST (3 ×10 min) and ECL reagent (H_2O_2 0.001% v/v) added to coat the membrane (2 min) before imaging with a ChemiDoc MP Imager (BioRad).

2.4.2.9. Silver staining

SDS-PAGE gels were run as described previously. A silver stain Pierce kit (Thermofisher, Cat-24612) was used to visualise proteins. In each step the gel was coated (25 mL) and left gently shaking. The gel is washed with ddH_2O (2 × 5 min) and coated with fixing solution: Ethanol (30% v/v); acetic acid (10% v/v) before incubating (2 × 15 min). The fixing solution was replaced with ethanol (10% v/v) and the gel washed (2 × 5 min) before washing with ddH_2O (2 × 5 min). The water was replaced with sensitizer solution: sensitizer (0.2% v/v) and the gel incubated (1 min) before washing with ddH_2O (2 × 1 min). Staining solution (2% v/v) is added and the gel incubated (30 min) before washing with ddH_2O (2 × 20 seconds). Developer solution (2% v/v) was added and the gel incubated (1-3 min) until bands began to appear, at the desired intensity the development is inhibited by adding acetic acid (5% v/v) to the gel and incubating for 10 min.

2.4.2.10. Western blotting

Proteins were separated as normal with SDS-PAGE before transferring to a polyvinyldifluoride (PVDF) membrane that was soaked with methanol to neutralise hydrophobicity. The membrane was then washed with ddH_2O before soaking in 1X Transfer buffer: methanol (20% v/v); glycine (7.25% w/v); Tris (pH 7.2, 1.5% w/v). The polyacrylamide gel was also washed with ddH_2O and equilibrated in transfer buffer. After equilibrating both membrane and gel, the latter was positioned on the side of the anode before compressing against the membrane. Both gel and membrane were confined by three sheets of Whatmann paper soaked in transfer buffer. The transfer was performed in cold transfer buffer (200 V, 400 mA, 1 hour) to prevent overheating. The membrane is then washed with TBST: Tris-HCl (pH 7.6, 20 mM); NaCl (140 μM); Tween-20 (0.1% v/v) before blocking with milk solution (5% w/v in TBST); human IgG (hIgG: 0.2% v/v); α-His-HRP (0.1% v/v) for 1 hat room temperature with gentle shaking. The addition of hIgG was to prevent the binding of the primary α-His-HRP to protein A which would otherwise cause a background signal. The membrane was then washed with TBST (3 × 10 min), and

ECL reagent: Luminol (2.5 mM); P-coumaric acid (400 µM); Tris-HCl (pH 8.5, 100 mM); H_2O_2 (0.001% v/v) is used to coat the membrane surface before imaging with a ChemiDoc MP imager (BioRad).

2.4.3. Pulldown experiments

2.4.3.1. Preparation of lysates for pulldown assays

Overnight cultures of JE2 (5 mL) were diluted to an OD_{600} of 0.05. When preparing stationary phase, lysates the cultures were left shaking overnight (37 °C). When preparing exponential phase lysates the cultures were grown to an OD_{600} of 0.5, if required amino acid starvation was induced with mupirocin (0.05 ug/mL). The stationary phase cultures were centrifuged (2000 × G, 10 min) and the exponential/mupirocin cultures were centrifuged (2000 × G, 10 min). In both cases the supernatant was removed and the pellets were frozen with liquid nitrogen and stored at -80 °C. Bacterial pellets were resuspended in 1 mL of lysis buffer: HEPES (pH 7.5, 6.5 mM); MES (6.5 mM); KAc (6.5 mM); NaCl (200 mM); DTT (1 mM); DNase1 (10 µg/ mL), lysostaphin (50 µg /mL) and one cOmplete, Mini, EDTA-free Protease Cocktail tablet (Merck) before lysing in a water bath (37 °C, 30 mins). The cells were centrifuged (17,000 x g, 4 °C, 5 mins), transferred to a clean Eppendorf and the pellets discarded. DDM (1% w/v) was added to solubilise the membrane proteins and incubated on a rotating wheel (4 °C, O/N). A PD10 desalting column (Cytiva) was washed with cold lysis buffer (4 × 2.5 mL). The supernatant was then loaded and eluted with cold lysis buffer in 8 fractions (500 µL). The concentrations of each fraction were determined using a BCA assay.

2.4.3.2. Pulldown procedure

Pulldown assays were set up in the following manner: protein extract (300 µg); glycerol (10% v/v); 10X binding buffer (10% v/v): $MgCl_2$ (10 mM); Tris pH 7.5 (50 mM); BSA (500 µg/ml); NaCl (2.30 M); DTT (5 mM)) and incubated (4 °C, 2 h) on a rotating wheel. Capture compound (10 µM final concentration) was added to both the capture experiment pulldown assay and the positive control with ppGpp (1 mM final concentration) also being added to the latter before incubating (4 °C, O/N). Streptavidin dynabeads M280 Magnetic (50 µL, Invitrogen) were placed on a magnet and the supernatant was removed. The beads were washed by adding 1 mL of Buffer B1: NaCl (1 M); Tris (pH 7.5, 5 mM); EDTA (pH 8, 5 mM) and the supernatant was removed by placing on a dynabead magnetic rack (Invitrogen) (2 min, × 2). The reaction mixtures were added to the beads and homogenised before incubating (4 °C, 2 h) on a rotating wheel. Beads were washed with 1 mL of buffer B2: Tris-HCl (pH 7.5, 10 mM); NaCl (230 mM) supplemented with a cOmplete, Mini, EDTA-free Protease Cocktail tablet (Merck) on a dynabead rack (2 min × 4). The beads were resuspended in 40 µL of elution buffer: Tris (HCl pH 7.5, 10 mM); NaCl (230 mM); EDTA (1 mM); Biotin (5 mM); SDS (5% w/v) and heated (95 °C, 5 min) before incubating with gentle shaking (15 min). The samples were centrifuged (2000 × G, 1 min), and the supernatant submitted to the chemical biology mass spectrometry service see section 2.4.3.3.

2.4.3.3. Mass Spectrometry (MS)

Proteins isolated from pulldown assays were precipitated in methanol and trapped on a silica framework. The trapped proteins were digested by addition of trypsin (cleaves on the c-terminal side of lysine and arginine), and the resulting peptide fragments were eluted from the silica framework. MS-based proteomics analyses were performed at the Faculty of Science Mass Spectrometry Centre at the University of Sheffield. For each sample, 2 µL was injected and the MS analysis was performed on an Orbitrap Exploris E480 mass spectrometer (Thermofisher) equipped with a nanospray source, coupled to a Vanquish LC System (Thermofisher). Peptides were desalted online using a nano trap column 75 µm I.D. × 20 mm, Thermofisher) and then separated using an EASY-Spray column 50 cm × 50 µm ID, PepMap C18, 2 µm particles, 10 Å pore size (Thermofisher), Buffer A: Formic acid (0.5% v/v); MeCN (0.5% v/v), Buffer B: Formic acid (0.5% v/v); MeCN (80% v/v). The gradient gradually increased from 3%-20% over 68 min before increasing sequentially to 35% buffer B for 23 min, up to 99% buffer B over 1 min before maintaining at 99% buffer B for a further 9 min.

The Orbitrap Exploris was operated in positive mode with a cycle of 1 MS acquired at a resolution of 120,000 at m/z 400, with the top 20 most abundant multiple charged (2+ and higher) ions in a given chromatographic window subjected to MS/MS fragmentation in the linear ion trap with scan range (m/z) 375–1,200; normalised AGC target 300%; microscan 1. An FTMS target value of 1e4 and resolution of 15,000.

Label-Free Quantification and Bioinformatic Analysis were performed using raw data with MaxQuant version 1.6.10.43. Data were searched against the protein Staphylococcus aureus database consisting of 3,029 proteins (www.uniprot.org) using the following search parameters for standard protein identification: enzyme set to Trypsin/P (2 miss-cleavages), methionine oxidation and N-terminal protein acetylation as variable modifications, cysteine carbamidomethylation was set as a fixed modification for peptide mass identification. A protein FDR of 0.01 and a peptide FDR of 0.01 were used for identification level cut-offs based on a decoy database searching strategy. The MaxQuant output was loaded into Persus (v1.5.6.0), and all label-free quantification (LFQ) intensities were set as main columns. The matrix was filtered to remove all proteins that were potential contaminants and reverse sequences. LFQ intensities were then transformed using log2 (x) function. To group selection lines, rows were categorically annotated with either H or L. Proteins were filtered to identify those present in at least 3 out of 4 replicates (75%) in at least one of the selection lines. Consistency of the replicates were determined and visualised using Pearson's correlation analysis. Proteins' (log2) intensity in each sample was then normalised to median value and missing values were filled using normal distribution imputation. Median values of the 4 biological replicates were calculated for each selection line and log2 fold-changes were calculated to describe differences between selection lines centred around 0. Proteomic differences between selection lines were evaluated for statistical significance ($P < 0.05$)

using two-sided Student's t-tests with permutation-based correction. The P value was performed in -log10 form and corrected for volcano plot scaling.

2.4.3.4. Preparation of bacterial pellets from Monocyte derived macrophages

The following was performed in RPMI medium (Thermofisher) along with: newborn calf serum (NBCS, 10% v/v) thermofisher); L-lutamine (1% w/v); penicillin (1% w/v); streptomycin (1% w/v) and amphotericinB (ampB, 1% w/v). Aperipheral blood mononuclear cells (PBMCs) were isolated from human blood and seeded into tissue culture (TC)-treated dishes at 2×10^6 cells/mL, yielding around 20 million cells per TC dish. This was estimated to provide a final cell density of 2×10^5 cells/mL. Media was replaced with RPMI medium along with: Fetal bovine serum (FBS, (10% v/v) Thermofisher); L-glutamine (1% w/v); penicillin (1% w/v); streptomycin (1% w/v); ampB (1% w/v) every 3-4 days. From day 12 onwards RPMI that did not contain: penicillin (1% w/v); streptomycin (1% w/v); ampB (1% w/v) was used. The MDMs were infected with JE2 at a multiplicity of infection of 100, old media was removed and cells were washed with hanks balanced salt solution (HBSS, 100 mL). The frozen mid-stationary phase stocks were thawed on ice before spinning (16,000 × G, 3 min) and removing the supernatant. The pellet was resuspended in PBS (1 mL) before spinning (16,000 x g, 3 mins) and removing the supernatant. The pellet was then resuspended in RPMI medium, FBS (10% v/v) and L-glutamine (1% w/v) (1 mL). The inoculum was prepared (40 mL, MOI 100) and added to each TC dish. The CFU of frozen stocks were confirmed by plating serial dilutions onto TSA (Neat to 10^{-7}) . The TC dishes were incubated (37 °C, 1 h) before removing the inoculum and washing the cells with ice-cold PBS (80 mL, x2) to prevent further bacterial internalisation. The extracellular bacteria were killed by adding 80 mL of RPMI medium, FBS (10% v/v) and L-glutamine (1% w/v); gentamicin (100 µg/mL) and incubating (37 °C, 30 min). The concentrated gentamicin solution was removed and 100 mL of RPMI medium, FBS (10% v/v) and L-glutamine (1% w/v); gentamicin (4 µg/mL); lysostaphin (0.8 µg/mL) was added to each TC dish before incubating (37 °C) until 4.5 h post-infection. The media was removed and cells washed with PBS (100 mL, x2). Saponin (2% v/v, 40 mL) was added to each TC dish and incubated (37 °C, 20 min) to lyse the MDMS. PBS (40 mL) was added to the TC dish and a scraper used to detach any remaining intact cells. The lysates were transferred to Falcon tubes (50 mL, Fisher) and mixed thoroughly before centrifuging (2000 × G, 5 min, 4 °C). The supernatant was removed before resuspending the pellets, centrifuging (16,000 × G, 5 min), freezing with liquid nitrogen and storing at -80 °C.

2.4.4. Radiolabelling and binding experiments

2.4.4.1. Synthesis of ^{32}P labelled nucleotides

For the formation of [α-^{32}P]-pppGpp, [α-^{32}P]-labelled GTP (Perkin Elmer) was diluted to (18.3 nM) in water. With reaction buffer: Bis-Tris propane (pH 9, 50 mM); NaCl (200 mM); $MgCl_2$ (30 mM) the following reaction was prepared: Rel_{Seq} (2 µM); 2X reaction buffer (50% v/v); ATP (8 mM); [α-^{32}P]-labelled GTP (101 pM) and incubated (37 °C, 18 h). Upon completion, the reaction was passed through

a 3 kDa spin column (16,000 × G, 10 min). To obtain the desired [α-^{32}P]-ppGpp, a cleavage reaction was prepared taking the crude [α-^{32}P]-pppGpp and mixing directly with GppA (1 μM) and incubating (37 °C, 1 h), then the reaction was passed through a 3 kDa spin column (16,000 × G, 10 min). To monitor reactions and confirm the yields a sample of each reaction (1 μL) was spotted onto PEI cellulose TLC, with a mobile phase of KH_2PO_4 (pH 3.6, 1.5 M). The cellulose TLC was exposed to a photostimulable phosphor imaging plate (IP) (FujiFilm) and visualised using a Typhoon FLA7000 Phosphorimager (GE Healthcare) before using pixel densitometry to establish the intensity of each spot. A successful reaction was deemed to have 85%< conversion and the nucleotides stored at -20 °C.

2.4.4.2. Analysis of p(s)pGpp synthesis by TLC

A PEI cellulose F thin TLC plate, GDPβs (1 μL, 0.5 mM) and crude p(s)pGpp (1 μL, 0.5 mM) were spotted and the plate run in KH_2PO_4 (1.5 M). Compounds were visualised in their respective lanes by UV light (254 nm) and determination of sulphur containing compounds was performed with a selective sulphur stain: palladium (II) chloride ($PdCl_2$, 0.5% v/v), HCl (2.6 M).

2.4.4.3. DRaCALA of whole cell lysates

Differential Radial Capillary Action of Ligand Assays (DRaCALA) functions through the binding mode of ligand-protein and densitometry(Roelofs et al., 2011). LBM9 medium was supplemented with chloramphenicol (10 μg/mL); carbenicillin (50 μg/mL) and $MgSO_4$ (2 mM) before adding 1.5 mL to a 96 well deep-dish plate. Each well was inoculated with a specific colony of a strain to be tested and incubated shaking (30 °C, O/N, 150 rpm). Protein expression was induced with IPTG (1 mM) and incubated (30 °C, 6 h) before centrifuging the cultures (2000 × G, 10 min) and supernatant removed. The pellets were resuspended in lysis buffer: Tris (pH 7.5, 40 mM); NaCl (100 mM); $MgCl_2$ (10 mM); DNase (2 mg/mL, 1% v/v); lysozyme (50 mg/mL, 1% v/v); phenylmethylsulfonyl fluoride (PMSF, 1 mM) and subjected to a freeze/thaw cycle × 3. The lysates (10 μL) were transferred to a v bottomed 96 well plate. A master mix: p^{32}pGpp (50 μL); TWEEN-20 (0.025% v/v); 10X binding buffer (10% v/v) was added to each well and the plate was gently shaken before incubating (RT, 5 min). The mixture of lysate and [α-^{32}P]-ppGpp (2.5 μL) was spotted onto nitrocellulose membrane, spots were dried and the membranes exposed to an IP plate (Fujifilm) before visualising using a Typhoon FLA7000 Phosphorimager (GE Healthcare). For recombinant proteins the master mix of [α-^{32}P]-ppGpp (1 uL) was added to each well and the protein (10 μM) in 10X binding buffer (10% v/v) was added with thorough mixing before transferring the reaction to nitrocellulose membrane (2.5 μL) the spots were dried and imaged with the same procedure described above. The fraction bound (Equation 2.4.4.3) was calculated with the fraction of nucleotide bound (FB), area of the spot (A) and the intensity of the spot (I). To determine the total intensity, the intensity of both the inner and outer spot along with the area were measured using pixel densitometry on the ImageQuant software (GE healthcare)(Roelofs et al., 2011).

Equation 2.4.4.3:

$$F_B = \frac{I_{inner} - \left(A_{inner} \times \frac{(I_{total} - I_{inner})}{(A_{total} - A_{inner})}\right)}{I_{total}}$$

2.4.4.4. Phosphorus NMR

ppGpp standards were prepared In the following manner: NaCl (180 mM); Tris (pH 7.5 45 mM); glycerol (4.5% v/v); ppGpp (167 μM); $MgCl_2$ (10 mM); D_2O (10% v/v), protein binding was assessed in the aforementioned buffer system in a 1:1 or 2:1 ppGpp ratio. The ^{31}P experiments were performed on a on a 500 MHz Bruker Avance II equipped with a 5 mm broadband-observed probe at 298 K, 45-120 min and 4000 scans. ^{31}P experiments were run at 202 MHz. Number of points = 8192 (TD in acqupars). Spectral width = 50 ppm (SW) centered at 0 ppm. Referencing was achieved by using an external reference of acetone in D_2O with a ^{1}H chemical shift of 2.22 ppm and calculated from gamma ratios, which altered ^{31}P peak shifts by -0.22 ppm.

2.4.5. *In vitro* assays

2.4.5.1. PyDPA general procedure

A solution of ppGpp (4 mM) in HEPES (pH 7.5, 1 mM) was serially diluted to 0.96 nM in a 96 well black plate followed by a blank of HEPES (pH 7.5, 1 mM). As per the literature, PyDPA (25 mM) in DMSO was dissolved in HEPES (pH 7.5, 1 mM) to give a working stock of PyDPA (40 μM). The working stock was added to each well containing ppGpp and the relative fluorescence was then measured ($\lambda_{Excited}$: 355nm, $\lambda_{Measured}$: 485 nm). For selectivity testing, the nucleotides of interest (14 μM) were mixed with PyDPA (40 μM) in a 1:1 ratio and the relative fluorescence was measured ($\lambda_{Excited}$= 355nm/ $\lambda_{Measured}$= 485 nm) by a Sense 425-301 microplate reader (Hidex)

2.4.5.2. Fructose assay

Using the procedure provided with a high sensitivity fructose assay kit (Merck), a standardisation plot was obtained by measuring fluorescence intensity ($\lambda_{excitation}$ = 535/ $\lambda_{emission}$ = 587 nm). From the standard plot a ratio of 10:1 was chosen for fructose-6-phosphate to enzyme. Fructose-6-phosphate (6 μM) was incubated (37 °C, 10 min) with HxlB (0.6 μM) and the change in fluorescence intensity was recorded by a Sense 425-301 microplate reader (Hidex) and compared to a negative control.

2.4.5.3. Microscale thermophoresis dye binding assessment

MST was performed by labelling the 10X-His-tags of expressed proteins using a His-Tag Labeling Kit RED-Tris-NTA 2nd Generation (NanoTemper). Dye solution (5 μM) was prepared as a stock by dissolving the provided dye in 25 μL of 1X PBST: PBS (pH 7.2); TWEEN-20 (0.1% v/v). The dye solution (5 μM, 2 μL) was then added to PBST (198 μL) to give 200 nM solution. The protein of interest (4 μM, 20 μL) was added to tube 1 of 16 and PBST (10 μL) was added to the remaining tubes. The protein (10 μL) was transferred to tube 2 and a serial dilution was performed, which was completed by discarding 10 μL from tube 16. To every tube (1-16) dye solution (200 nM, 10 μL) was added with mixing before incubating away from light (RT, 3 h). Premium capillaries (Nanotemper) were loaded with a small

amount of solution (3 µL) from each tube and thermophoresis was measured with medium MST power and 40% excitation power on a Monolith NT.115 (Nanotemper).

2.4.5.4. MST Labelling procedure.

The protein of interest (200 nM) was mixed (1:1) with dye solution (100 nM) and incubated (RT, 3 hrs). Samples were centrifuged (4 °C, 10 mins) to remove aggregates and the now labelled protein was transferred to a new tube.

2.4.5.5. MST Binding assay

A solution of 2X ppGpp in PBST was prepared and 20 µL added to tube 1 with PBST (10 µL) being added to the remaining tubes (2-16). 10 µL of the 2X ppGpp solution was transferred to tube 2 and a serial dilution was performed, completed by the removal of 10 µL from tube 16. The labelled protein (10 µL) was then added to each tube (1-16) and left to incubate (RT, 5 min). Premium capillaries (Nanotemper) were loaded with a small amount of solution (3 µL) and thermophoresis of the samples was measured with medium MST power and 40% excitation power on a Monolith NT.115 (Nanotemper).

2.4.5.6. Enzyme linked immunosorbent assay (ELISA)

To a Nunc-Immuno™ MicroWell 96 well plate (Merck), HprT (10 µg/mL) or BSA (10 µg/mL) in coating buffer: Na_2CO_3 (50 mM); $NaHCO_3$ (50 mM); NaOH (pH 9, 50 mM) were added and incubated (4 °C, O/N). Coating buffer was removed and the plate washed with PBST (×3). PBS-BSA blocking solution (pH 7.4, BSA 1% w/v) was added to the plate and incubated (RT, 1 h). The blocking solution was removed and the plate washed with PBST (×3). A solution of capture compound in Tris HCl (pH 8, 50 mM) was serially diluted in the plate starting at 250 nM and finishing at 0.12 nM before incubating (RT, 2 h). The plate was then washed with PBST (×3) and incubated (RT, 1 h) with Horse Radish Peroxidase-streptavidin conjugate (1:1000) in PBS (pH 7.4). After washing with PBST (×3), the colorimetric reagent 3,3',5,5'-tetramethylbenzidine (TMB) was added to each well before incubating (RT, 30 min). The colorimetric reaction was terminated by the addition of H_2SO_4 (2 M) and the UV absorbance measured ($\lambda_{Absorbance}$= 450 nm) using a Sense 425-301 microplate reader (Hidex). This procedure was repeated for the competition assay with HprT replaced for HflX and the capture compound replaced with ppGpp and other structurally similar nucleotides.

2.4.6. Statistics

Graphpad Prism 9.0 and Perseus software were used for determining statistical differences across biological experiments and mass spectrometry experiments, respectively. Student t-tests, Principal Component Analysis (PCA) and one way mixed-effect analysis of variance (ANOVA) were all used with p values reported in figure legends or indicated by: *, $p < 0.05$; **, $p < 0.01$; ***, $p < 0.001$; ****, $p < 0.0001$.

Chapter 3

Chemical synthesis of a non-covalent ppGpp capture compound

3.1. Introduction

Bacteria are often required to respond and adapt to key changes in their environment. In order to survive, these responses are typically facilitated in part by nucleotide signalling networks(Zarrella and Bai, 2020). Notable nucleotides involved in these signalling networks include cyclic adenosine monophosphate (cAMP), which is responsible for the management of carbon catabolite repression. When glucose is present cAMP levels are low, low cAMP levels prevents activation of the *lac* operon that encodes proteins responsible for metabolising lactose. Reduced activity in the *lac* operon essentially allows bacteria to fine tune their carbon source when there are more preferable substrates (McDonough and Rodriguez, 2011, Görke and Stülke, 2008). Another nucleotide, cyclic diguanylate monophosphate (c-di-GMP), has levels often associated with motility: while low levels affect the movement of individual cells, high levels often promote attachment and subsequent biofilm formation(Karaolis et al., 2005). However, this process is inherently complicated and involves multiple steps; expression of flagellar genes along with motor assembly and function. Meaning c-di-GMP has an effect on multiple proteins (Jenal et al., 2017). It is clear to see that nucleotide signalling networks have an important role in cell survival and pathogenicity.

When exposed to stress conditions it is essential that bacteria act quickly, because when a change is too slow the stress could be detrimental to the cell. (p)ppGpp are universally conserved secondary messengers in prokaryotes that promote cell survival under stress conditions such as nutrient starvation and antibiotic exposure (Zhu and Dai, 2019, Zhu and Dai, 2023, Greenway and England, 1999, Jordan et al., 2008, Irving et al., 2020). Due to its conformational flexibility, (p)ppGpp has the ability to adopt both enclosed and elongated conformations and complex with various metal ions. Hence it has a plethora of binding targets involved in multiple cellular processes such as transcription and translation while avoiding a distinct binding motif (Steinchen and Bange, 2016, Anderson et al., 2022, Steinchen et al., 2020, Corrigan et al., 2016, Bennison et al., 2019). This conformational flexibility makes mapping the stringent response signalling network a difficult task.

In order to identify ppGpp binders and improve mapping of the stringent response signalling network, several methods have been employed. DRaCALA is an approach that functions on densitometry calculations and the affinity of (p)ppGpp to its target was widely used after its conception by Roelof *et al* (Roelofs et al., 2011). More recently, a new method was developed using nucleotide-probes. These small trifunctional molecules commonly referred to as capture compounds allow for the isolation of nucleotide-protein interactors by specific interactions and subsequent identification *via* mass spec (Köster et al., 2007). The compounds typically consist of three main components; a chosen nucleotide mimic, a photoreactive group that is capable of forming covalent bonds and an affinity handle to allow for isolation. Both of these methodologies have been utilised with great success with identification of numerous (p)ppGpp interacting proteins occurring in each investigation

Despite the success of affinity based (p)ppGpp capture compound methodologies in *E. coli,* they have not yet been implemented in an *S. aureus* background. This leaves a huge gap in our understanding of the stringent response signalling network. For example, there is a fundamental difference in the operation of the stringent response when comparing Bacillota to Proteobacteria. In *E. coli,* (p)ppGpp binds directly to the RNA-polymerase (RNAP) allosterically inhibiting nucleic acid binding, this reduces the rate of transcription as a result (Zuo et al., 2013, Shin et al., 2021). In Bacillota such as *S. aureus,* transcription is regulated by the production of (p)ppGpp, leading to a decrease in the cellular GTP pool (Geiger et al., 2010, Geiger et al., 2014). GTP is a cofactor of the transcriptional regulator CodY that depresses at low GTP concentrations. This leads to a decrease in the transcription of genes whose products are involved in translation, while genes involved in amino acid biosynthesis and transport are upregulated (Geiger et al., 2010). These two distinct pathways operate *via* a plethora of proteins that may potentially bind to (p)ppGpp, however, due to the lack of research in *S. aureus* they remain undiscovered.

This chapter describes the synthesis of a new class of capture compound, that despite maintaining the aforementioned trifecta of: affinity handle; linker and mimic; functions in a non-covalent manner. The compound will be utilised with *S. aureus* lysates in future chapters to isolate novel ppGpp-binding proteins across numerous pathways, furthering our understanding of the staphylococcal stringent response.

3.2. Results

3.2.1. Design Rationale

With the previous information available, it was our aim to synthesise a novel capture compound, with the unique attribute being a non-covalent mode of action. This compound does not contain a photoreactive cross-linking moiety. It is designed to function purely using specific interactions between the ppGpp mimic and potential binding partners, lowering the risk of false positives. The capture compound was expected to adopt the general structure of previously seen capture compounds utilising a biotin-affinity handle, a variable length linker core comprised of polyethylene glycol (PEG) and xylene, along with a more nucleophilic structural analog of ppGpp referred to as p(s)pGpp (Figure 3.2.1).

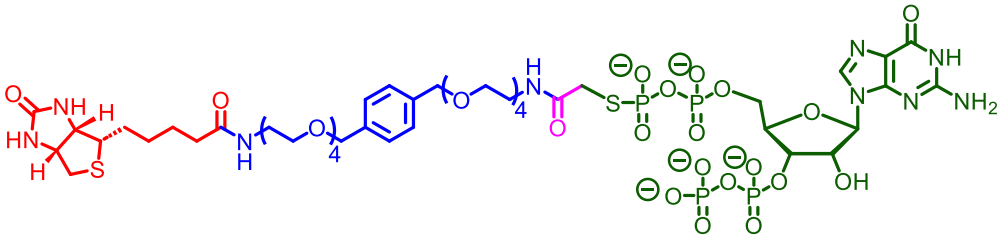

Figure 3.2.1: Structure of the non-covalent ppGpp-protein capture compound: The design consists of: a biotin affinity handle (red); variable length linker (blue); functionalised cap (pink) and a p(s)pGpp analog (green).

Two synthetic routes towards the non-covalent capture compound were attempted. The initial route required significant optimisation and was abandoned with details listed below (Scheme 1).

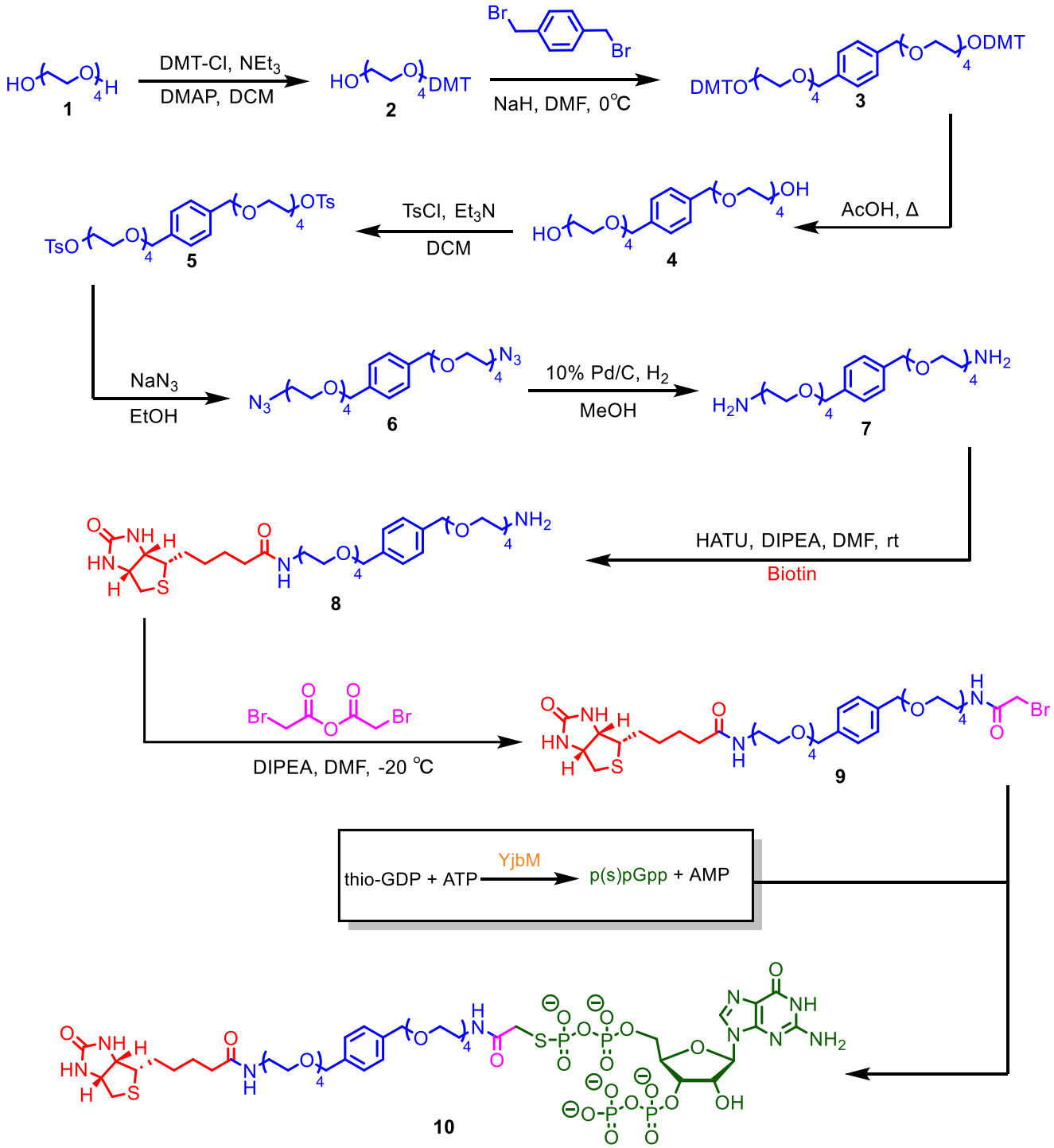

Scheme 1: Planned synthetic route to reach the described capture compound. The route uses basic amide coupling chemistry along with simple protection/deprotection steps. The route is split into three distinct parts, formation of the activated linker (blue); attachment of the biotin affinity handle (red); functionalisation of the linker (pink); and attachment of the more nucleophilic ppGpp structural analog p(s)pGpp (green).

3.2.2. Synthesis of ppGpp capture compound (10)

3.2.2.1. Step 1: Dimethoxytrityl (DMT) Protection of Tetra-ethylene glycol (TEG) to yield (**2)**

The first step of the abovesynthesis was the DMT protection of one side of TEG (**1**) (*Figure* 3.2.2.1). DMT-protecting groups are widely use for the protection of primary alcohols due to their acid labile properties. Protecting only one side of the starting material ensures that the xylene core attached in the following step can only react with one side preventing the formation of side products.

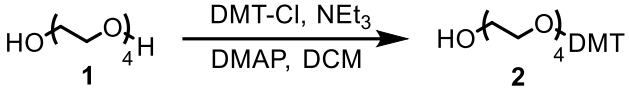

Figure 3.2.2.1: TEG (1) is tritylated in the presence of a catalytic base to give alcohol (2). Statistical approach towards mono-DMT protection of a symmetrical diol. DMT-Cl was used as the tritylating agent; dimethylaminopyridine (DMAP) as a catalytic base; and triethylamine as a proton scavenger.

The initial procedure (method 1) utilised a large excess of TEG (20:1) in comparison to the DMT-Cl to favour mono-protection. Attachment of the highly hydrophobic DMT group was hoped to make separation from unreacted TEG simple by silica column chromatography (Debacker et al., 2019). However, the excess TEG streaked on both TLC plates and silica columns making separation difficult despite the differences in polarity. To combat this problem fewer, equivalents of TEG (4:1) were trialled in the reaction (method 2), allowing the product to be isolated in poor yield (Ries et al., 2017). When repeating the reaction, poor yields continued irrespective of the TEG ratio or the base used, implying degradation of the product during purification. Silica is commonly terminated with Si-OH groups making the gel slightly acidic which can cause deprotection of the aforementioned acid labile DMT group. To avoid product degradation the silica columns were equilibrated with 1% TEA to neutralise the silica before purification (method 3). Low yields still persisted, however, the small quantity of product (**2**) that was obtained was taken forward for the next reaction (Table 3.2.2.1).

Table 3.2.2.1: Summary of the modifications and yield of each reaction attempt

Method	TEG Equivalents	Catalytic Base	Gradient (Hex : EtOAc)	Yield (%)
1	20	Pyridine	50% → 100%	N/A
2	4	DMAP	0% → 100%	6.5
3	4	DMAP	0% → 100%	6.7

3.2.2.2. Step 2a: Williamson ether synthesis with dibromo-p-xylene to produced di-tritylate (**3)**

The next step in the production of the capture compound was a Williamson ether synthesis. This reaction involved the formation of an alkoxide from alcohol (**2)** using sodium hydride (NaH). The oxygen with its increased nucleophilicity attacks and displaces the bromide ions from the dibromo-*p*-xylene *via* S_N2 chemistry to give product **3** (Figure 3.2.2.2.) (Yasukawa et al., 2017).

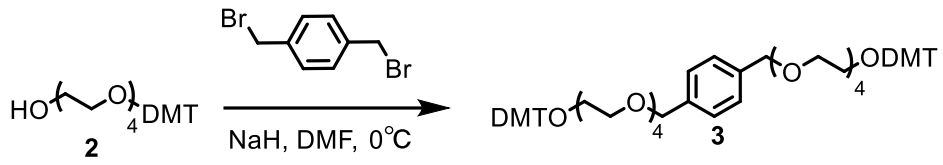

Figure 3.2.2.2: Alcohol (2) was alkylated by dibromo-*p*-xylene and sodium hydride to give di-tritylated product (3). Williamson ether synthesis using NaH to assist alkoxide formation and dimethylformamide (DMF) as a solvent to favour S_n2 conditions with di-bromo-p-xylene.

Reaction progression was slow and after 24 h, alcohol (**2)** was still detected, thus another equivalent of NaH was added to assist alkoxide formation and the reaction was left for a further 24 h. Upon completion the reaction was quenched with ice/water slurry and purified by silica gel-chromatography (Hexane:TEA (1%) in EtOAc:, 1:99). The collected material was analysed by ^{1}H NMR, however, the product's diagnostic benzylic protons (~5 ppm) were not present and the expected m/z value was absent from mass spectrometry, suggesting the product (**3**) was not formed. An alternative methodology was required, as all of alcohol (**2)** had been used attempting this reaction. This alternative Williamson ether synthesis was trialled with the aim of shortening the whole synthetic route while bypassing the low yields and difficult purifications.

3.2.2.3. Step 2b: Alternative Williamson ether synthesis with silver oxide allows direct synthesis of (**4)**

In the following reaction silver (I) oxide was used as an alternative to NaH, deprotonating TEG (**1**) and forming the required intermediary alkoxide (Figure 3.2.2.3) The purification issues associated with the degrading DMT product (**2**) were avoided and the route length was reduced without drastic alterations. (Cao et al., 2018).

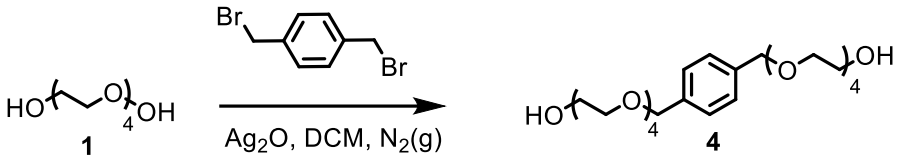

Figure 3.2.2.3: TEG (1) is alkylated with dibromo-*p*-xylene and silver oxide to produce diol (4). Alternative Williamson ether synthesis used to reach **4** made use of AgO to form the alkoxide of TEG while also increasing yield.

The desired product (**4**) was isolated in good yield (68%) and observed by ^{1}H NMR (Figure 3.2.2.3.1) with the diagnostic singlets at 4.55 ppm and 7.31 ppm being indicative of the benzyl and aromatic protons respectively. However, the integral of the glycolic ether protons (CH_2-O-) peak was slightly higher than expected indicating that not all of the excess TEG was not removed.

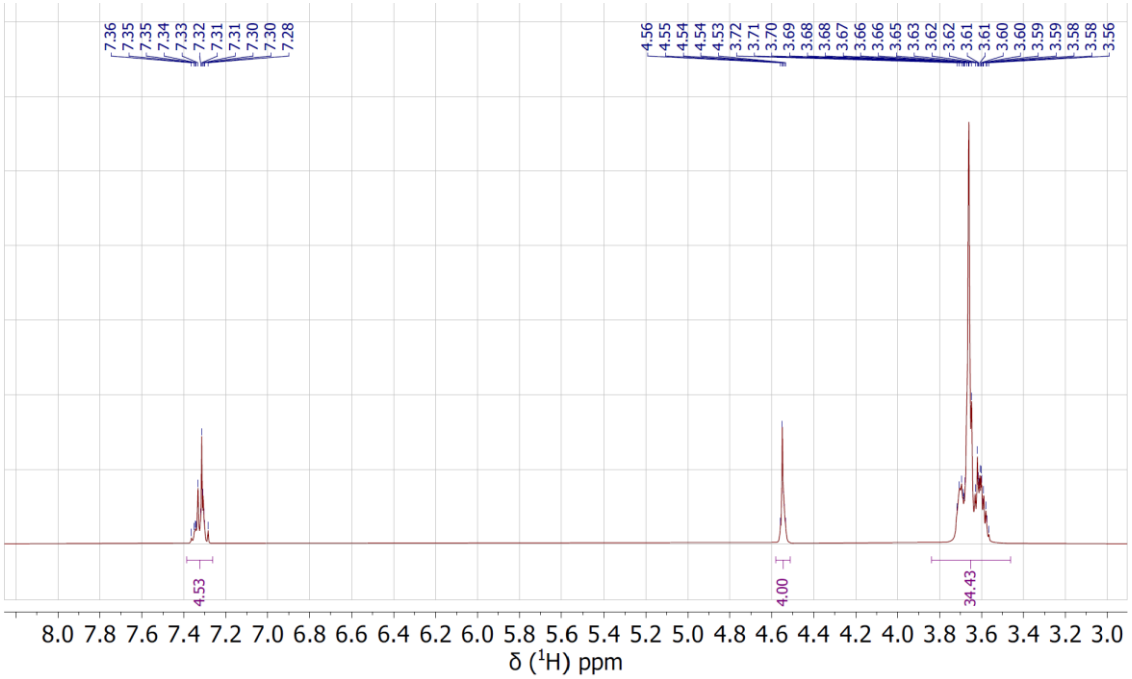

Figure 3.2.2.3.1: ^{1}H NMR spectrum of product (4). The ^{1}H NMR shows both the diagnostic peaks from xylene: Aromatic (7.31 ppm, 4H, singlet); benzylic protons (4.55 ppm, 4H, singlet). The glycolic ether peaks (3.71-3.60 ppm) are visible as a multiplet with a higher integration (H34.4) than the expected (H32).

Although the product was impure and contained excess TEG (9%), the synthetic route (Scheme 1) involved activating alcohols by tosylation. This tosylation drastically changed the polarity of the compound by attaching two large hydrophobic sulfonated groups, increasing hydrophobicity, allowing the product to be easily separated from the hydrophilic TEG impurity. Another benefit of introducing a tosylate group was the incorporation of a chromophore.. This chromophore would aid in the removal of excess TEG, as the aromatic ring would introduce absorption in the UV range (265-280 nm), allowing for visualisation and removal from the desired product, therefore, diol (**4**) was taken forward regardless of the excess TEG.

3.2.2.4. Step 3: Tosylation of the diol

Despite compound (**4**) containing excess TEG (9%), it was used in the following tosylation reaction. (Figure 3.2.2.4). The unreacted TEG from the etherification step would become UV active once tosylated allowing for visualisation and hence removal from the desired product (**5**) by silica column chromatography. As predicted the product and TEG side product were formed, however, isolation of the wrong product occurred due to their polarities being almost identical. After repeating the procedure, the correct product was eventually isolated inincredibly low yield (0.42%). This extremely low yield can be attributed to the excess TEG making isolation of the side product particularly difficult, as a result the synthetic route making use of xylene (Scheme 1) was abandoned.

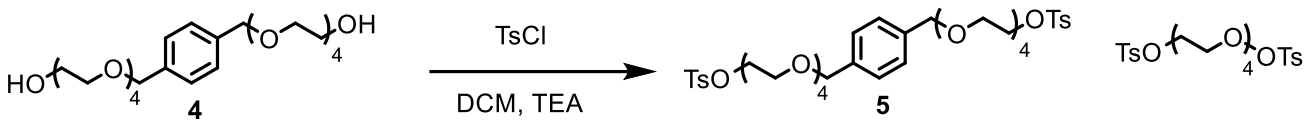

Figure 3.2.2.4: Diol (4) is tosylated to give the di-tosylate (5). Diol (**4**) was reacted with tosyl-chloride to give di-tosylate (**5**), however, due to the starting material being contaminated with unreacted TEG the reaction was unsuccessful and the TEG side product was isolated instead of di-tosylate (**5**).

3.2.3. Synthesis of ppGpp-CC *via* an alternative synthetic route (Scheme 2)

3.2.3.1. Alternative synthetic route to a capture compound

The previous synthetic route (Scheme 1) was associated with numerous problems, including excess TEG, degradation of products during purification and low yields. As a result, a new synthetic route was developed (Scheme 2). Unlike the previously designed synthesis, the intermediates along this routelack a chromophore, making reaction monitoring more challenging. However, the identification of several selective TLC stains provided an alternative solution. In addition, total conversion of TEG in the first step, along with the absence of a DMT group, solved the previously described issues with excess TEG being difficult to remove (section 3.2.2.3) while also shortening the synthesis.

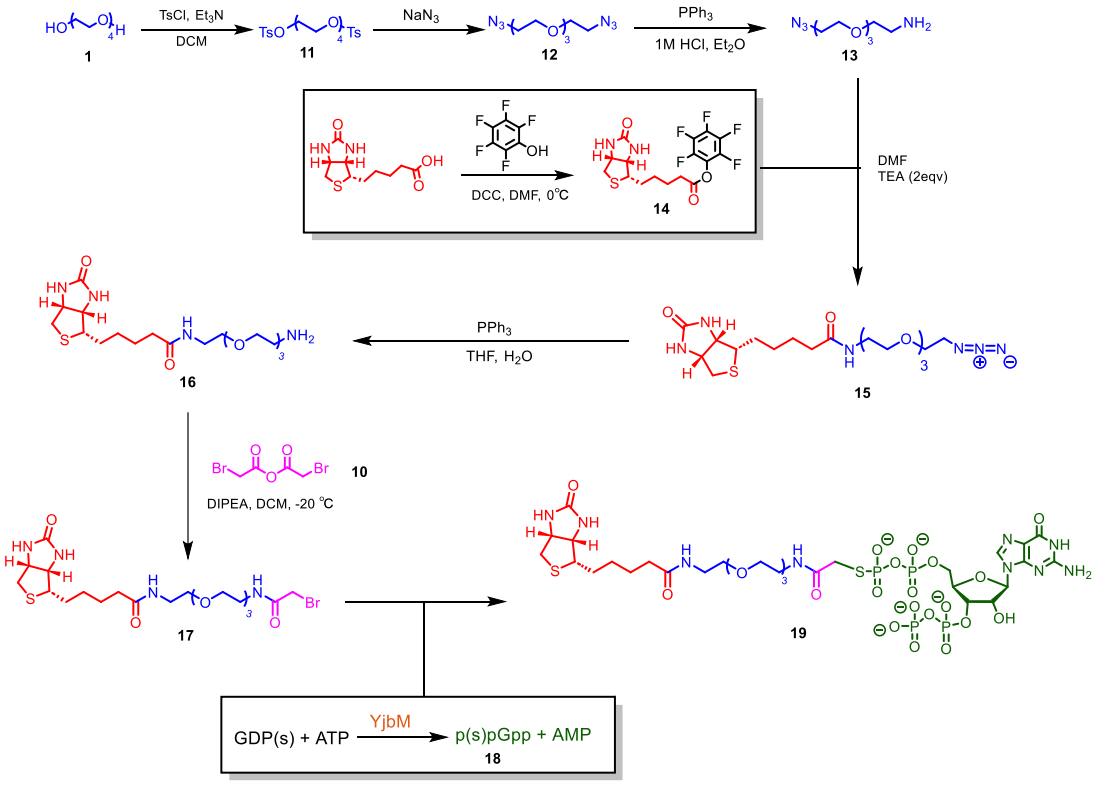

Scheme 2: **A new synthetic route was designed to reach an alternative non-covalent capture compound (19).** In comparison to the initial route (*Scheme 1*), this route is shortened by one step by converting all of the TEG in the initial reaction. However, due to the lack of the xylene moiety many of the intermediate products lack chromophores. Despite this, there is no significant change between the routes.

3.2.3.2. Step 1: Di-tosylation of tetraethylene glycol (**1**)

Previously excess TEG led to issues with purification and yield due to formation of side products. Therefore to prevent TEG from causing any further issues, it was utilised as the limiting reagent in the first step of the new synthesis with tosyl-chloride in excess allowing for full conversion to di-tosylate (**11**) (Figure 3.2.3.2).

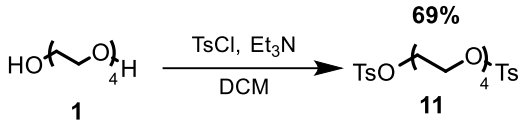

Figure 3.2.3.2: Preparation of di-tosylate (11) from TEG (1) in the presence of TsCl. By increasing the ratio of tosyl-chloride to TEG (**1)**, the formation of side products is significantly reduced allowing for the desired product (**11**) to be isolated.

To prevent any impurities propagating throughout the synthesis it was vital that product (**11**) was obtained in high purity. Tosyl-chloride was recrystallised from petroleum ether 40-60 °C beforehand to remove impurities. The reaction was monitored using TLC and cerium-ammonium-molybdate stain, where this stain allowed for TEG to be visualised, which was previously very difficult due to the lack of a chromophore and specific functional groups. Once the absence of TEG was visually confirmed, the reaction mixture was subjected to an acid-base work up, before silica column chromatography to remove excess tosyl-chloride, yielding the product (**11)** as a colourless oil in high yield (69%).

3.2.3.3. Step 2: Azide substitution of the ditosylate (**11**)

With the terminal alcohols activated *via* tosylation, the α-carbon was subjected to attack by azide ion to yield the di-azide (**12**) (Figure 3.2.3.3).

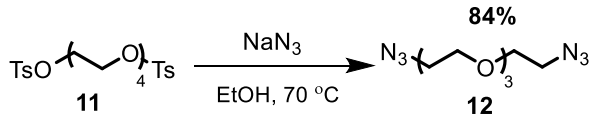

Figure 3.2.3.3: Di-tosylate (11) reacts sodium azide to give diazide (12). Sodium azide produces the strong nucleophile N_3^- which displaces the tosyl groups which form a salt with the dissociated Na^+**.**

Despite product (**12**) not having a chromophore the reaction was monitored using a stain that forms coloured 1,2,3-triazoles from azides in a click reaction with propargylic alcohol and a copper (I) bromide catalyst (Figure 3.2.3.3.1) (Schröder et al., 2007). The reaction was monitored using this triazole stain and occurred as expected yielding a yellow oil of the desired product in a high yield (86%) without the need for further purification.

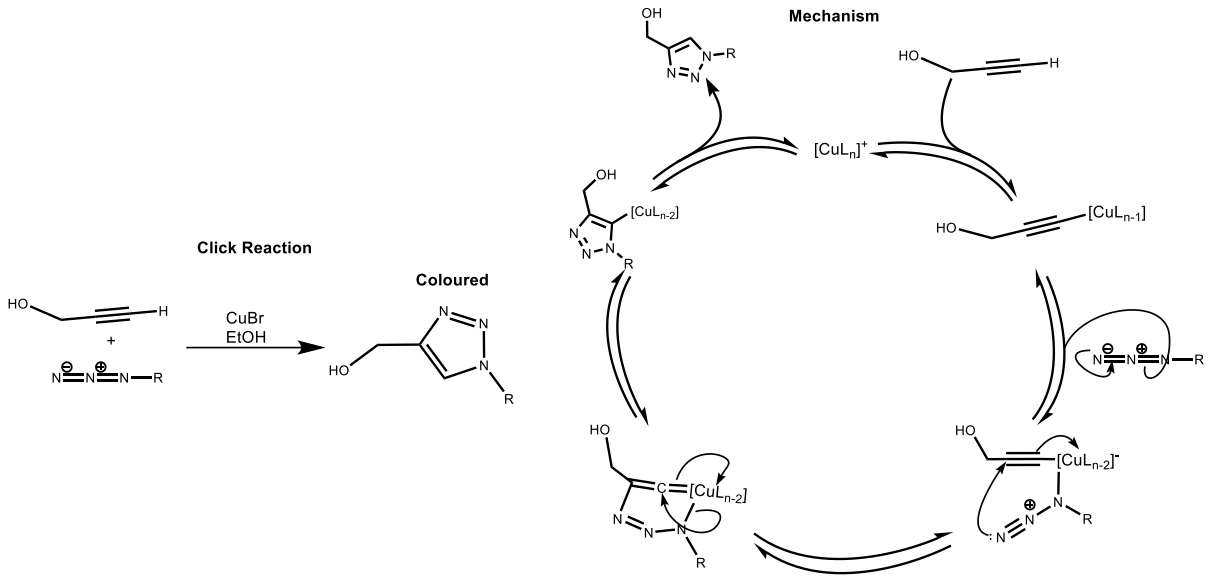

Figure 3.2.3.3.1: Propargyl alcohol forms coloured 1,2,3-triazoles in the presence of copper (I) bromide. Mechanism of action for the formation of 1,2,3-triazoles via cycloaddition of a given azide (N_3R) and propargyl alcohol in the presence of a copper (I) bromide catalyst (Moiola et al., 2019).

3.2.3.4. Step 3: Selective Staudinger reduction of 1,11-diazido -3,6,9-trioxaundecane

Staudinger reductions are incredibly convenient ways to form iminophosphoranes which are then hydrolysed to give the respective amine(Staudinger and Meyer, 1919). Triphenylphosphine (PPh_3) was used as the reducing agent and, in order to favour the reduction of only one azide in compound **12**, it was used as the limiting reagent (Figure 3.2.3.4). Regardless of the ratio of reducing agent to starting material there was the possibility of reducing both azide groups in diazide (**12**) and forming the diamine. This diamine impurity would be a problematic impurity to remove due to its similar polarity to the desired product and streaking on silica.

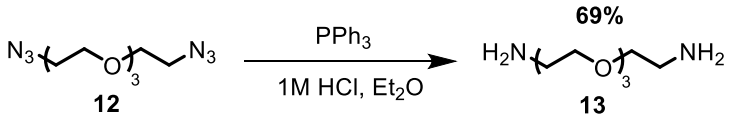

Figure 3.2.3.4: Di-azide (12) is selectively reduced in the presence of HCl to form amine (13). Formation of amine (**13**) from di-azide (**12**) via a biphasic "selective" staudinger reduction using: PPh_3, HCl (1M) and diethyl ether.

To circumvent this issue, the solubility of the compounds was exploited. Typically the amine would share similar solubility to the starting material. However, by performing the reaction in a biphasic solvent mixture such as hydrochloric acid (HCl) and diethyl ether (Et_2O) along with vigorous mixing, the amine is immediately protonated by the HCl and partitions into this aqueous layer (Figure 3.2.3.4.1).

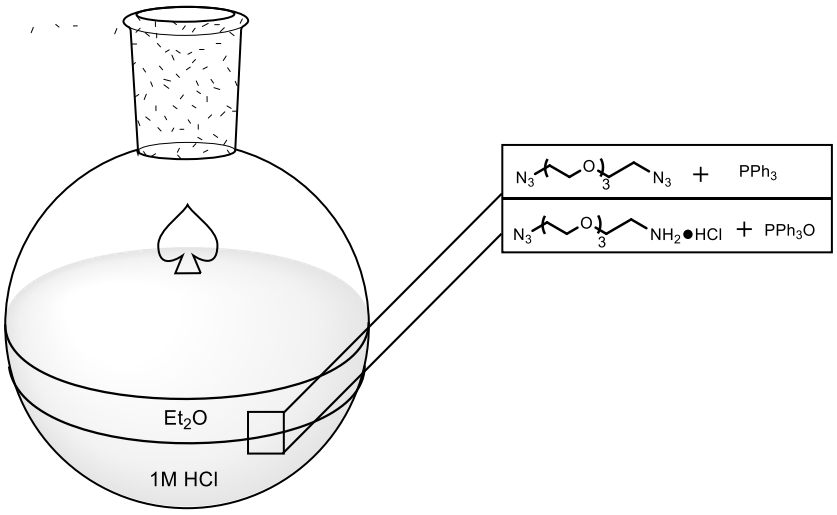

Figure 3.2.3.4.1: Staudinger reductions performed in biphasic reactions improve regioselectivity Diagram illustrating the solubility effects associated with the biphasic reaction mixture. The di-azide remains in the ether layer while the newly generated amine (**13**) immediately forms a hydrochloride salt and partitions into the acidic aqueous layer.

By making use of the compound's solubilities, the regioselectivity of the reaction can be controlled by preventing the reduction of both azides, while also driving the reaction forward, due to a decrease ofproduct concentration in the ether layer (Okoth and Basu, 2013, Martinek et al., 1981). Upon reaction completion the aqueous layer was basified with potassium hydroxide (KOH) to improve the solubility of amine (**13**) in organic solvents with subsequent extraction by dichloromethane (DCM) to give the product in good yield (69%).

3.2.3.5. Step 4: Activation of d-biotin by the addition of a pentafluorophenol moiety

The incorporation of d-biotin into the capture compound (**19**) is essential, however, biotin is a relatively weak carboxylic acid (pKa= 9.7)(Said, 2009). In order for it to be effective coupling to the amine its electrophilicty needed to be increased. In order to activate biotin towards coupling, the biotin was converted to a pentafluorophenol (PFP) ester (**14**) in the presence of N,N′-Dicyclohexylcarbodiimide (DCC) (Figure 3.2.3.5)(Vallinayagam et al., 2008).

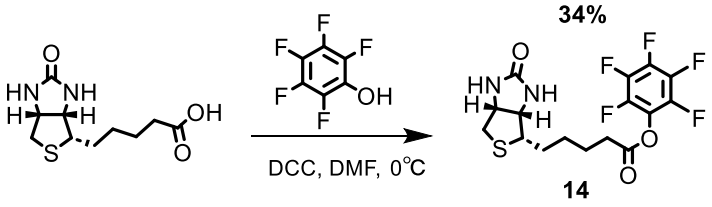

Figure 3.2.3.5: d-Biotin was converted to an activated PFP-ester (14). The weakly acidic d-biotin was reacted with DCC to form an O-acylisourea which hydrolyses to yield the activated ester (**14**) in the form of PFP-biotin.

The electronegativity of the fluorine atoms, along with the delocalisation of electrons across the aromatic ring, attracts electron density away from the carbonyl rendering it more susceptible to

nucleophilic attack by amines (Das and Theato, 2016). Despite activation, the yields for this esterification reaction were consistently poor. It was found that the solubility of d-biotin in DMF was poor at lower temperatures, however, dissolution was achieved by heating to 70 °C before cooling. Despite heating, the hot filtration used during purification of the product decreased yields. However, when removing the hot filtration the yield increased (Table 3.2.3.5). The product was eventually synthesised in a large enough quantity to take the PFP-biotin ester (**14**) forward.

Table 3.2.3.5: Summary of the attempts to activate d-biotin.

Attempt	Yield (%)	Heating	Hot Filtration
1	9.3	N	Y
2	26	Y	Y
3	23	Y	Y
4	34	Y	N

3.2.3.6. Step 5: Biotinylation of 1,11-diazido -3,6,9-trioxaundecane

The coupling of linker (**13)** to the affinity handle (**14**) proceeded with no issues, due to the ester being activated no coupling agent was required (Figure 3.2.3.6). Here the diisopropylethylamine (DIPEA) acts as a non-nucleophilic base and the product was obtained in modest yields (Table 3.2.3.6).

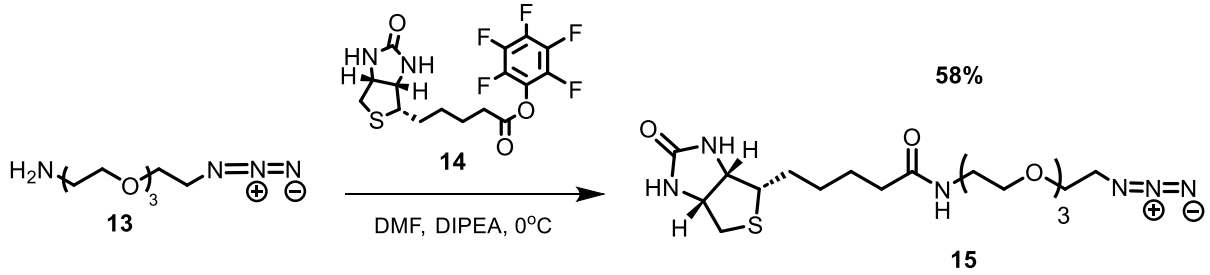

Figure 3.2.3.6: Linker (13) was biotinylated with a PFP-biotin ester (14). Formation of biotinylated azide (**15)** when coupling amine (**13**) and PFP-biotin (**14**) in the presence of a non-nucleophilic base (DIPEA).

Table 3.2.3.6: Comparison of biotinylation reaction attempts

Attempt	Time (Days)	Yield (%)
1	5	58
2	1	51
3	1	43

An alternative method was also trialled in an attempt to bypass the low yields (Table 3.2.3.6), obtained when sequentially activating d-biotin with PFP. This alternative reaction used PFP-trifluoracetic acid (PFP-TFA) ensuring PFP-biotin remains in solution before the addition of amine (**13)**, meaning the low yielding purification could be avoided (Figure 3.2.3.6.1)(Chambers et al., 2013). Using the PFP-TFA method yielded the d-biotin-linker (**15**) as a white solid in low yield (27%), in addition, the synthesis was

complicated by the formation of a waxy insoluble solid and therefore was not expected to be suitable for future use without optimisation.

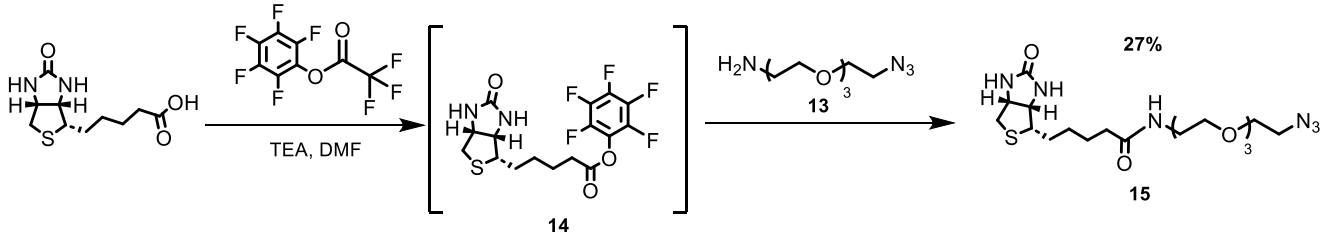

Figure 3.2.3.6.1: Planned *in situ* formation of PFP-biotin before addition of linker (13) to form azide (15). An *in situ* method of synthesising azide **15** was trialled as an alternative method could potentially shorten the synthesis while also by-passing the poor yields associated with isolating PFP-biotin (**14**).

3.2.3.7. Step 6: Reaction of 1-azido-3,6,9-trioxaundecan-11-amidobiotin

The synthesis of linker (**15)** allows for two possibilities, reduction to amine (**16)** or the formation of a 1,2,3-triazole (**20)** *via* click chemistry (Figure 3.2.3.7).

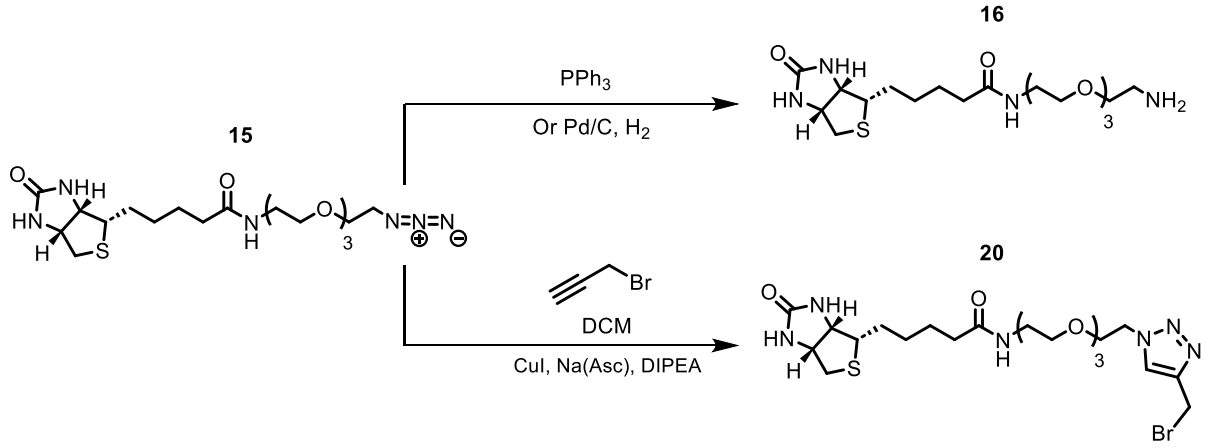

Figure 3.2.3.7: Azide (15) can be reduced to amine 16 or undergo a cycloaddition with propargyl bromide to from triazole (20). Summary of two potential routes. **Top:** Reduction to the amine 16 via Staudinger reduction or hydrogenation. **Bottom:** Click reaction to form alkyl bromide (**20**), would shorten the route and allow for S-alkylation with p(s)pGpp earlier in the synthetic sequence..

Due to the absence of chromophores in both the starting material and product, a selective TLC stain was employed consisting of 4-di-methylaminocinnamaldehyde and sulfuric acid in ethanol (Groningsson and Jansson, 1979). This allows the formation of an intensely red/pink coloured Schiff base with the N-1 uriedo position of d-biotin allowing for diagnostic TLCs (Figure 3.2.3.7.1).

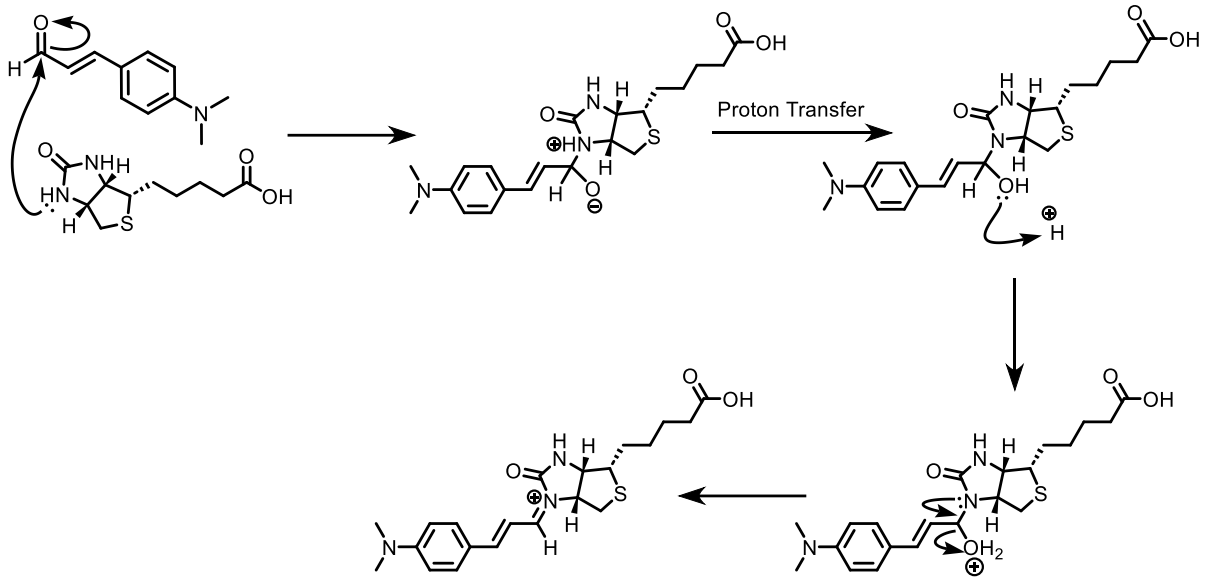

Figure 3.2.3.7.1: Cinnamaldehyde forms intensely coloured Schiff bases with d-biotin in acidic conditions. Mechanism showing the formation of a Schiff base *via* reductive amination using 1% (w/v) 4-di-methylaminocinnamaldehyde and 1% (v/v) sulfuric acid in ethanol (Groningsson and Jansson, 1979).

With a TLC method available for reaction monitoring a Staudinger reduction (Figure 3.2.3.7.2a) was used as seen when preparing amine (**13**) (section 3.2.3.4). Despite this method being used previously with great success, the solvent was swapped to DCM as biotin has poor solubility in diethyl ether. The reaction was unsuccessful when using DCM as the solvent, which could be attributed to the hydrochloride salt of the product being soluble in DCM. To circumvent this solubility issue, the ammonium acetate salt was also generated by treating with 1 M acetic acid. After silica column purification, the major fraction was analysed *via* infrared spectroscopy. The diagnostic azide peak (2000-2000 cm^{-1}) present in the starting material was observed, indicating the reaction was unsuccessful (Gai et al., 2011)). An alternative literature method was trialled using THF/H_2O, which produced the desired amine (**16**) in a low yield (36%) (Figure 3.2.3.7.2bi) (Yang et al., 2011). The click reaction (Figure 3.2.3.7) was then trialled with a method directly from the literature with no success (Counsell et al., 2021).

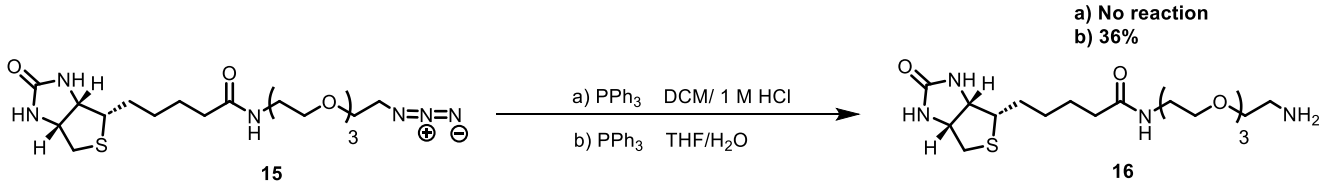

Figure 3.2.3.7.2: Staudinger reduction of azide (15) to amine (16) in two different solvent systems. i) Biphasic mixture of DCM and 1 M hydrochloric acid. **ii)** Miscible solvent mixture of tetrahydrofuran (THF) and H_2O.

3.2.3.8. Step 7: Bromoacetylation of biotin-PEG_3-amine (**16**) to yield a functionalised linker (**17**)

With two components of the capture compound in place, (affinity handle and PEG linker), the ppGpp structural analog p(s)pGpp)) needed to be attached. In order to do this, one end of the linker was furnished with a reactive cap, in the form of a bromoacetyl group donated by bromoacetic anhydride (Figure 3.2.3.8.). The soft nucleophilic character of the sulphur atom in a thiophosphate allows for the stabilisation of negative charges during the transition state with the bromoacetyl group, favouring it over a reaction with the oxyanionic charges of a phosphate ester, where the charge density is higher and more energy is required to reach the transition state.

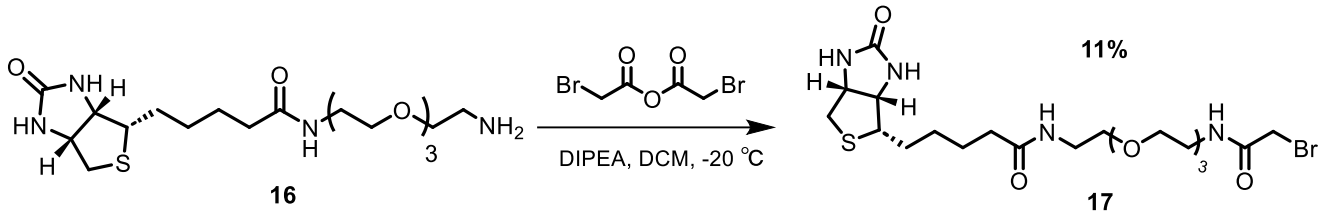

Figure 3.2.3.8: Amine (16) was furnished with a reactive bromoacetyl group: Amine (**16**) undergoes an S_N2 reaction with bromoacetic anhydride to form bromoacetic acid and functionalised linker (**17**).

Bromoacetylation reactions required several purifications by silica column chromatography (0→ 100% MeOH in DCM) to remove several biotin containing impurities. The desired bromoacetylated-linker-handle system (**17**) was eventually synthesised in a very low yield (11%) with analysis by ^{1}H NMR identifying animpurity that had not been detected by TLC and UV-based detection inchromatographic analyses. Further investigations by mass spectrometry indicated this impurity did not contain any bromine atoms and, as a result, was unlikely to form side products in the final coupling reaction to from capture compound (**19**).

3.2.3.9. Step 8: Enzymatic synthesis of p(s)pGpp with the *Bacillus subtilis* phosphotransferase YjbM

The attachment of ppGpp to the functionalised linker (**17**) was expected to be difficult as it would require high purity or high chemo-selectivity to ensure any structurally similar nucleotides within the reaction mixture were not forming potential side products. Phosphate-diesters are also susceptible to nuclease activityTherefore high chemo-selectivity was chosen as a way of circumventing enzymatic degradation and side product formation. The *B. subtilis* phosphotransferase YjbM was used because this enzyme forms (p)ppGpp from GTP/GDP and ATP, however, when replacing the GTP/GDP substrate with GDPβS, a structural analog that furnishes a sulphur atom on the β-phosphate in place of an oxygen, p(s)pGpp is formed. This increases the nucleophilicity and as a result the reactivity ensuring chemo-selectivity (Figure 3.2.3.9).

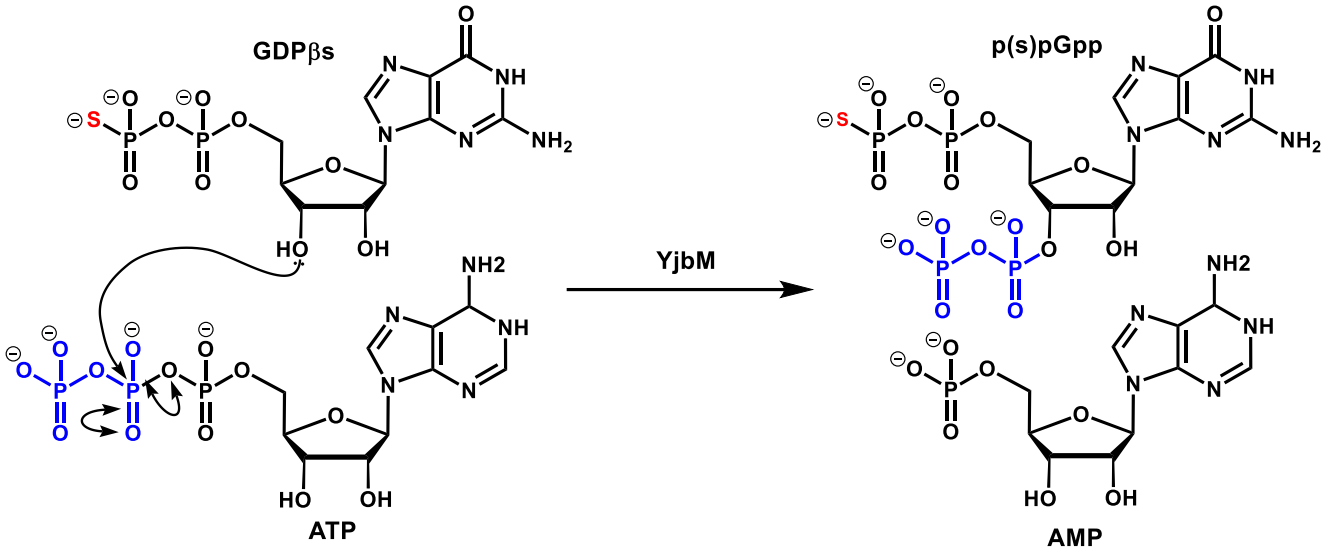

Figure 3.2.3.9: The *B. subtilis* enzyme YjbM is exploited to synthesise the ppGpp structural analog p(s)pGpp. Mechanism of the formation of p(s)pGpp catalysed by the *B. subtilis* phosphotransferase YjbM. In an S_N2 manner the 3'-oxygen of GDPβS attacks the 5'-β-phosphate of ATP to attach a bis-phosphate forming p(s)pGpp and AMP as a side product.

This reaction was monitored by PEI cellulose TLC using 1 M KH_2PO_4 as the mobile phase. Here compounds are separated based on their charge, with the higher charges having greater retention times. The use of a selective stain, that converts sulphur containing compounds orange was also employed, allowing the formation of p(s)pGpp to be visualised (Figure 3.2.3.9.1) (Bäumler and Rippstein, 1961).

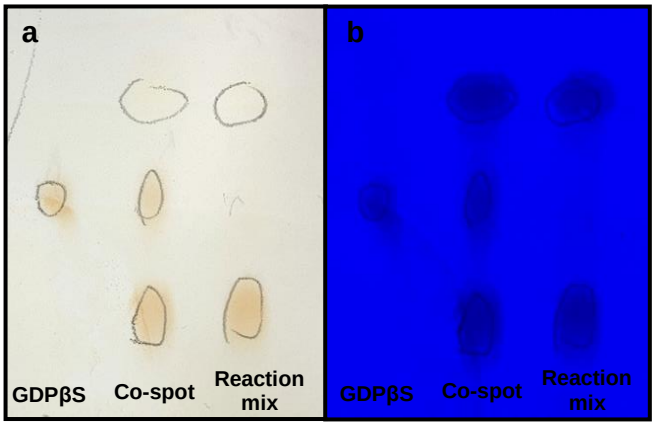

Figure 3.2.3.9.1: The YjbM phosphotransferase reaction can be visualised by PEI cellulose TLC and a sulphur stain. a) Cellulose TLC illustrating the ability of the sulphur selective stain to highlight the phosphorothioate in p(s)pGpp. **b)** The same TLC under (UV 280) nm showing the presence of guanosine and adenosine nucleotides which absorb in this range.

Once GDPβS had been completely converted, the desired p(s)pGpp was freeze dried and dissolved in water to form a 5 mM solution and purified by ion pairing reverse phase high performance liquid

chromatography (RP-HPLC). Reverse phase chromatography functions inversely to normal silica chromatography, it consists of using a non-polar stationary phase such as graphite or C18 and polar solvent mixes, with the fastest moving compounds being the most polar (Huang et al., 2013). Ion pairing reagents are typically used when trying to separate partly charged organic analytes as they can increase differences in retention times between structurally similar molecules, with TEA and TFA often being used. However, the lab group previously had great success with TEAB so this was used. Initially RP-chromatography was trialled with AMP and GDPβS standards as these would be present in the reaction mixture, allowing for the p(s)pGpp peak to be identified (Figure 3.2.3.9.2).

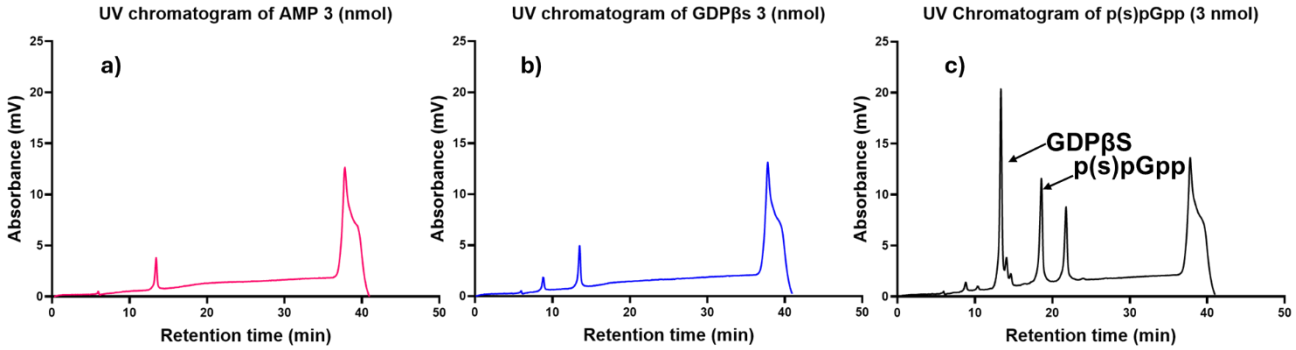

Figure 3.2.3.9.2: RP-HPLC separates p(s)pGpp from other nucleotides. UV chromatograms of **a)** AMP (3 nmol). **b)** GDPβS (3 nmol), **c)** crude p(s)pGpp. Traces obtained using a GEMINI® 5 µm C18 110 Å LC column (250 × 4.6 mm), 3 → 50% B, 38 min, Mobile phase A (Triethylammonium bicarbonate (TEAB) 100 mM, acetonitrile (MeCN) 0.5% v/v)) and Mobile phase B (TEAB 100 mM, MeCN 50% v/v).

The initial gradient was gradually shortened to assess whether separation between structurally similar nucleotides and the product p(s)pGpp peak was maintained (Figure 3.2.3.9.3). As a result the purification times were able to be reduced from 38 min to 27 min while maintaining resolution this allowed for purifications to be performed quickly without risk of co-elution.

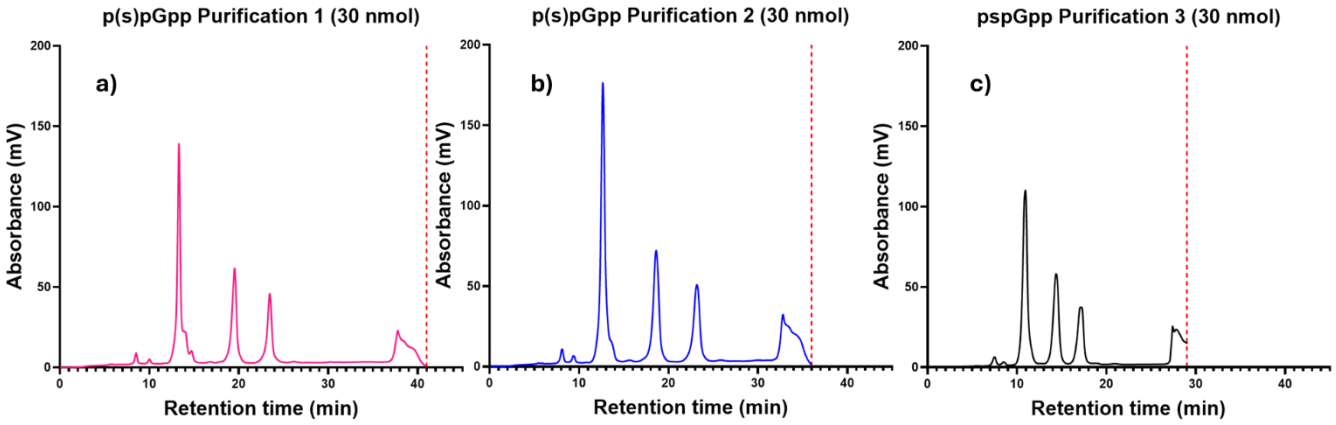

Figure 3.2.3.9.3: RP purifications can be shortened while maintaining resolution. 30 nmol injections of crude p(s)pGpp on a GEMINI® 5 µm C18 110 Å LC column (250 × 10 mm), 3 → 50% B, Mobile phase A (TEAB 100 mM, MeCN 0.5% v/v) and Mobile phase B (TEAB 100 mM, MeCN 50% v/v). **a)** Gradient over 38 mins. **b)** Gradient over 33 min. **c)** Gradient over 27 min.

The amount loaded was progressively increased to ensure that separation between the three peaks was maintained, at around 500 nmol the detector became saturated, so this scale was used to purify the remaining crude p(s)pGpp collecting the middle peak (~13 min) (Figure 3.2.3.9.4a). The rest of the crude p(s)pGpp was purified at this scale before re-injecting a small amount of the collected fraction to confirm homogeneity (Figure 3.2.3.9.4b).

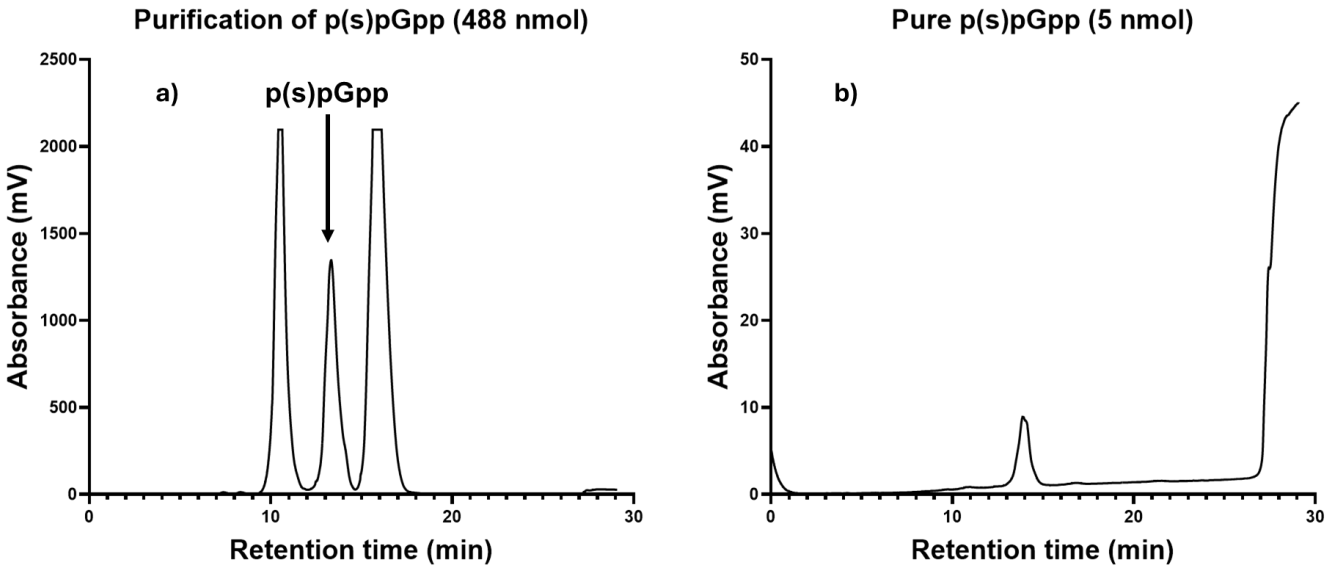

Figure 3.2.3.9.4: p(s)pGpp is separated from GDPβS and structurally similar nucleotides using RP-HPLC. a) p(s)pGpp purification at a 500 nmol scale. **b)** Purified p(s)pGpp was reinjected to assess purity at a 5 nmol scale. Traces obtained using a GEMINI® 5 µm C18 110 Å LC column (250 x 10 mm), 3 → 50% B, 27 min, Mobile phase A (TEAB 100 mM, MeCN 0.5% v/v) and Mobile phase B (TEAB 100 mM, MeCN 50% v/v).

The product was determined to be present by electrospray ionisation (ESI) mass spectrometry (MS). However, the ^{31}P NMR spectrum, suggested several structurally similar nucleotides were co-eluting or the presence of a diastereomer due to the chiral β-phosphate (Figure 3.2.3.9.5a).

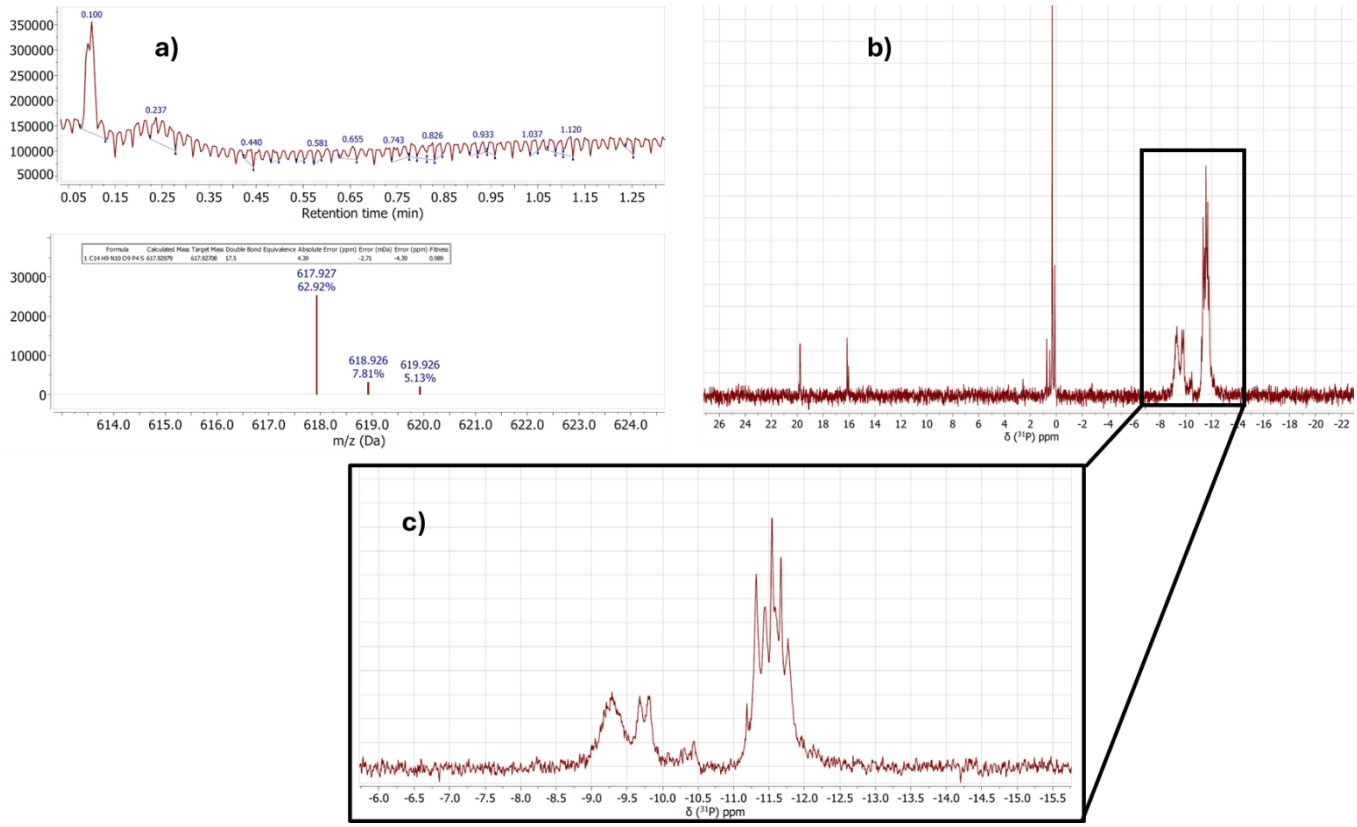

Figure 3.2.9.3.5: The ppGpp structural analog p(s)pGpp was purified by RP-HPLC. a) The desired p(s)pGpp peak was identified by direct infusion ESI-MS (617.92708 m/z). **b)** ^{31}P NMR of p(s)pGpp showing the presence of other nucleotides and diastereomeric peaks of thiophosphates ~16-20 ppm, indicating the product needs further purification.

The RP-HPLC method of purification was not suitable for large scale purification of the highly charged nucleotide due to potential co-elution and pH changes when considering TEAB as an ion-pair reagent. As a result anion exchange chromatography was trialled because this had previously been implemented in the synthesis of capture compounds to purify nucleotides with great success (Wang et al., 2019a, Haas et al., 2022). The method separates compounds based on their charge state.The packing material typically retains compounds with an opposing charge, in this instance a Nucleopac PA-100 4 mm × 250 mm column was used. The stationary phase consists of non-polymeric beads functionalised with quaternary ammonium groups making them positively charged, while the mobile phase consists of two concentrations of NH_4HCO_3 (A = 50 mM and B = 500 mM). By gradually increasing mobile phase B the salt concentration increases, this disrupts ionic interactions between the negatively charged molecules and positively charged packing material. Therefore, as p(s)pGpp carries a -6 charge in basic conditions it may be separable from GMP, GDPβS, ADP, ATP e.t.c as a higher concentration of salt is required to break these interactions. To assess the ability of anion exchange chromatography to separate similar nucleotides, varying concentrations of ATP, GMP, GDP, GDPβS, GTP and ppGpp were injected. As expected, the nucleotides possessing the most negative charge had the longer retention times (Figure 3.2.9.3.6).

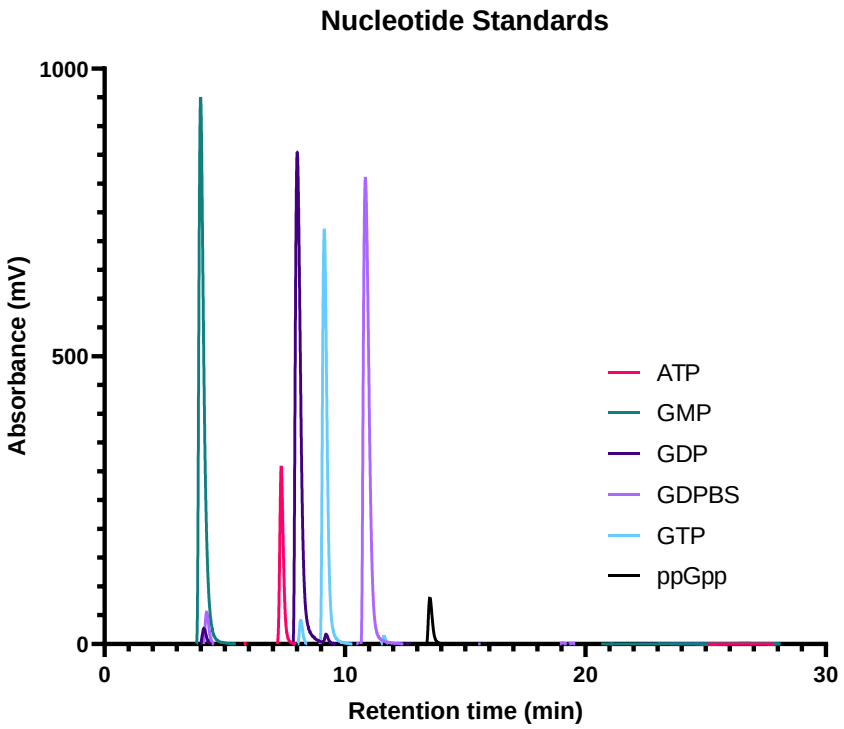

Figure 3.2.9.3.6: Anion exchange chromatography separates structurally similar nucleotides by their charge state. Nucleotide standards ATP, GMP, GDP, GDPβS, GTP and ppGpp were injected onto a Nucleopac PA-100, 4 mm × 250 mm column and ran with NH_4HCO_3 (A = 50 mM and B = 500mM), 9-91% B, over 21 min. Resolution between charge state differences of ±1 were maintained.

Once resolution between charge states was confirmed the crude p(s)pGpp was injected in gradually larger amounts, starting at around 20 nmol and increasing to around 80 nmol (Figure 3.2.9.3.7a). Despite increasing the amounts of p(s)pGpp resolution was maintained. As a result the remaining compound was purified at this scale along with previously prepared crude p(s)pGpp, this resulted in 1.15 µmol of purified p(s)pGpp confirmed by ESI-MS before reinjecting a sample to assess purity (Figure 3.2.9.3.7c) and submitting for analysis by high resolution mass spectrometry (Figure 3.2.9.3.7d). Overall, favouring the anion exchange methodology allowed us to avoid using TEAB as an ion-pair reagent. When used over prolonged periods of time, TEAB often decomposes into TEA, water and carbonic acid which further degrades to CO_2. Upon soft effervescence due to CO_2 escaping solution the pH increases which results in shifted retention times and unsatisfactory fraction collection. Additionally, the resolution of the peaks was significantly improved under the ammonium bicarbonate conditions employed in the anion exchange methodology.

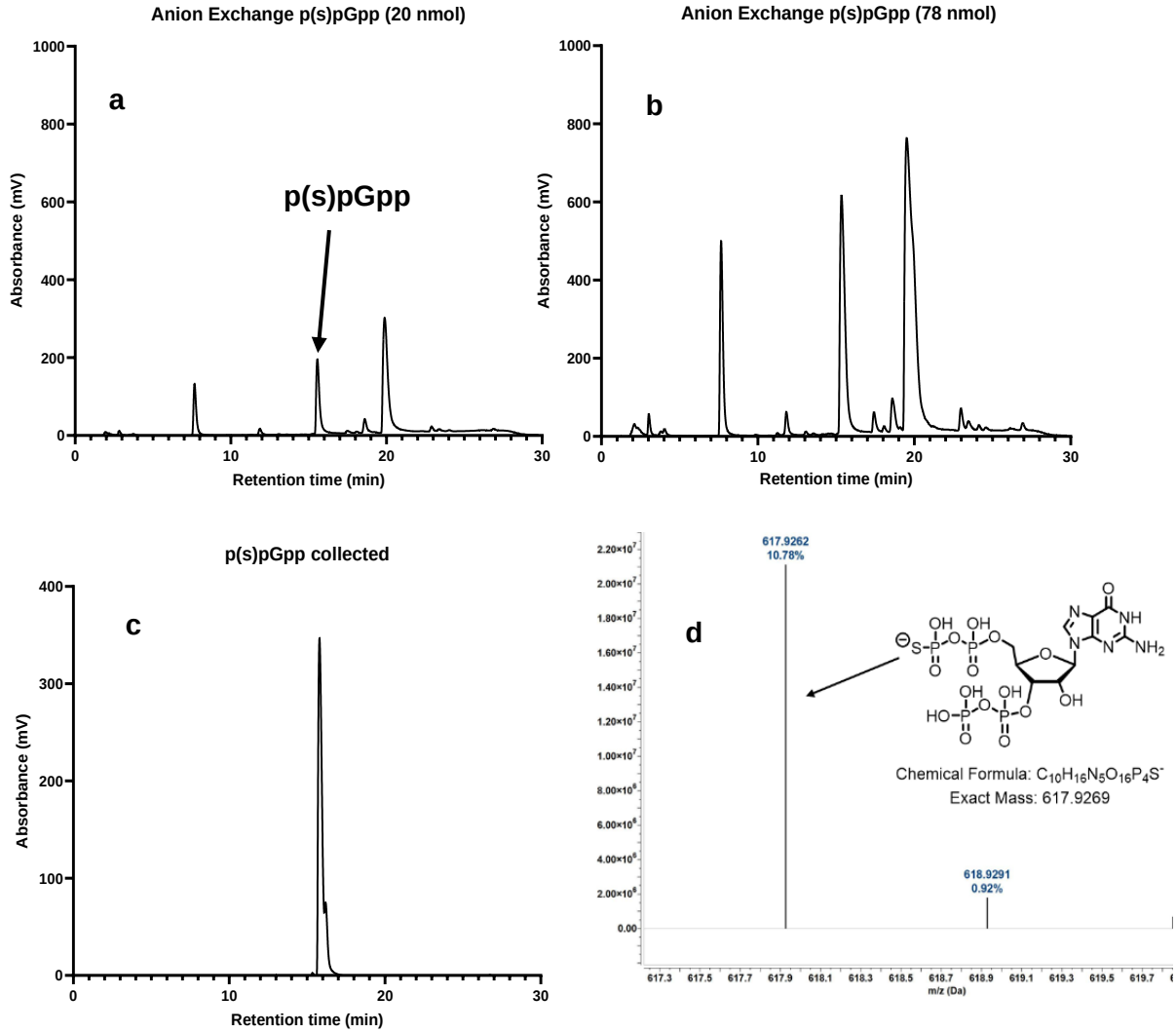

Figure 3.2.9.3.7:p(s)pGpp was obtained by anion exchange chromatography. a) Crude p(s)pGpp (20 nmol) injection. **b)** Crude p(s)pGpp (78 nmol) injection. **c)** Almost pure p(s)pGpp was collected due to the presence of a shoulder. **d)** ESI-MS of p(s)pGpp showing the [M-H] adduct at 617.9262 m/z. Traces obtained using a Nucleopac PA-100, 4 mm × 250 mm column and ran with NH_4HCO_3 (A = 50 mM and B = 500 mM), 9-91% B, over 21 mins. Resolution between charge state differences of ±1 were maintained.

3.2.3.10. Step 9: Alkylation of p (s)pGpp using the functionalised linker (**17)**

The final step in the synthesis of capture compound (**19**) was to utilise the nucleophilic phosphorothioate of p(s)pGpp and couple the nucleotide to functionalised linker (**17)** *via* S_N2 chemistry (Figure 3.2.3.10).

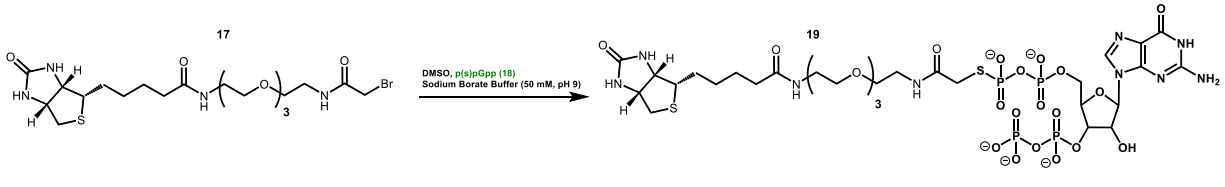

Figure 3.2.3.10: Alkylation of p(s)pGpp using linker (17) to form the desired capture compound (19). The final step in the synthetic route to the desired non-covalent capture compound (**19**), showing the coupling of functionalised linker (**17**) to p(s)pGpp (**18**) in sodium borate buffer (pH 9, 50 mM).

p(s)pGpp (1 eqv) was dissolved in ddH_2O and sodium borate buffer (pH 9, 50 mM) before functionalised linker (**17**) in DMSO was added in excess (4 eqv). Despite previous issues with RP-HPLC it was used to monitor the reaction across several timepoints. As it was assumed that the retention time of the desired compound would differ significantly to the starting material due to the decrease in charge state and hydrophobicity associated with the addition of linker (**17**)**.** After 4 h a new peak was observable as the assumed product formed, with the largest difference occurring between 0 and 8 h, showing clear formation of two new peaks (Figure 3.2.3.10.1).

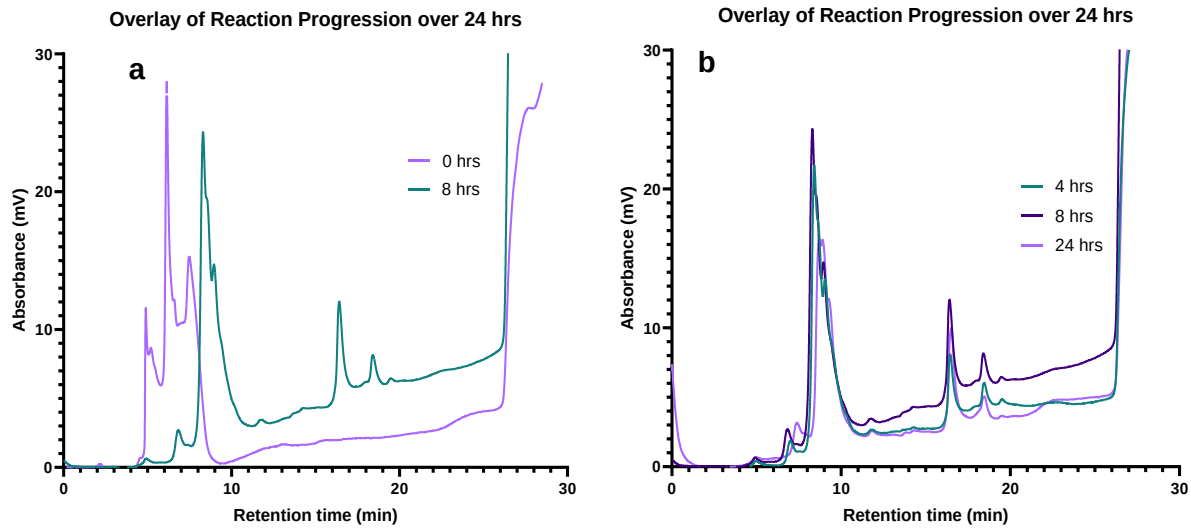

Figure 3.2.3.10.1: Formation of the assumed capture compound (19) was observed by RP-HPLC. a) UV chromatograms showing the formation of two new peaks (16 min and 18 min), one of which contains product. **b**) UV chromatograms of three timepoints: 4 h; 8 h and 24 h, overlayed to show the gradual increase in size of the product peak. Traces obtained using a GEMINI® 5 µm C18 110 Å LC column (250 × 10 mm) 3 → 50 %B, 27 min.

Any side products formed may be be in low concentrations and as a result their respective peaks may also be smaller than the desired compound peak. This was a safe assumption as the only chromophores capable of absorbing at 260 nm would be in the form of nucleotides. As a result, the peak observed at ~16 min was assumed to be the product and collected after optimisation of the purification scale (Figure 3.2.3.10.2a). Despite this, the peak at ~18 min was also collected before re-injecting the former (~16 min) to obtain a cleaner UV trace (Figure 3.2.3.10.2b). Analysis by ESI-MS confirmed the synthesis of the desired capture compound (**19**) in the first peak (~16 min) once the charge states were deconvoluted (Figure 3.2.3.10.2di). Overall, the desired compound was obtained on a 290 nmol scale (15%).

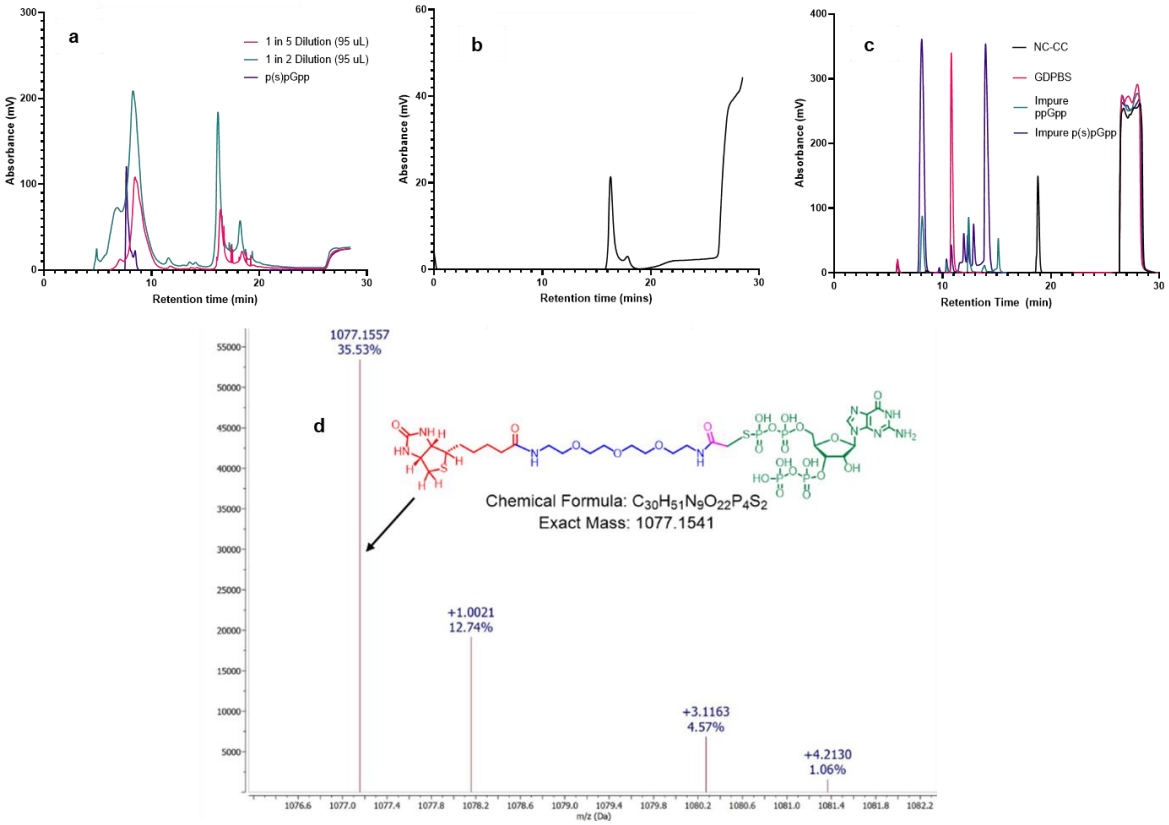

Figure 3.2.3.10.2: RP-HPLC and mass spectrometry show formation of capture compound 19. a) Overlay of the increasing injection volumes to maximise efficiency of purification with p(s)pGpp used as a standard. **b)** Pure non-covalent capture compound collected and reinjected for proof of increased purity (5 nmol). **c)** Overlay of impure nucleotides p(s)pGpp, ppGpp and GDPβS along with capture compound **19** traces. Mobile phase A (HFIP 50 mM, MeCN 0.5% v/v) and Mobile phase B (HFIP 50 mM, MeCN 50% v/v), 27 min. **d)** ESI-MS of the capture compound 1077.1557 m/z identified by deconvoluting the charge states. All traces obtained using a GEMINI® 5 µm C18 110 Å LC column (250 × 10 mm) 3 → 18 %B, 27 min

3.3. Discussion

The aim of this chapter was to synthesise, purify and characterise a non-covalent protein capture compound 19, using cheap readily available starting materials and accessible chemistry. With compound 19 in hand, we planned to identify novel ppGpp interactors across different pathways allowing us to determine their role in the staphylococcal stringent response. Details for the capture experiments are listed in chapter 4.

The initial route (Scheme 1) was our preferred strategy as it included the incorporation of a chromophore that would allow for reaction monitoring by UV. We hoped visualisation by UV would allow for differentiation from any non-UV active side products and improve the purification strategies. However, too many challenges arose with this synthesis, including product degradation/low yields and difficulties in separatiion from TEG. In order to combat these problems, a different protecting group for primary alcohols could have been implemented in place of DMT. Silyl ethers (SiR_3), such as: trimethylsilyl (TMS), *t*-butyldimethylsilyl (TBS) and triisopropysilyl (TIPS) are inert under most conditions and commonly used when dealing with primary alcohols (Bols and Pedersen, 2017, Dong et al., 2019). Silyl ethers tolerate most reaction conditions that would affect alcohols while also being easily cleaved in the presence of an acid like TFA or fluoride ions typically produced by tetra-n-butylammonium fluoride (TBAF). The cleavage of these protecting groups would not have affected the latter stages of the synthesis as the xylene core would be relatively stable under removal conditions. This methodology could afford a new pathway to a non-covalent capture compound, without changing the overall plan of the synthetic route, just the reagents used.

As a result of the difficulties associated with purification and yield in Scheme 1 an alternative synthetic startegy (Scheme 2) was trialled. The route detailed in Scheme 2 was successful in providing the desired capture compound (**19**), however, it was obtained on a microgram scale. This was enough for the required purpose, however, the overall yield for the synthetic route was low, at 0.1%. There are numerous steps that could be taken to significantly improve the overall yield of this route by increasing the yields of individual steps. The steps earlier in the synthesis, such as tosylation, azide substitution and selective Staudinger reduction, provided moderately high yields and good purity.

In the latter stages of the synthesis, formation of PFP-biotin (Figure 3.2.3.5) displayed poor to moderate yields at 34-39% when comparing to the 70-90% yielded by others in the literature (Vallinayagam et al., 2008, Zhou et al., 2017). The main difference between (Vallinayagam et al., 2008) and (Zhou et al., 2017) is the coupling agent used, both employ carbodiimides in the form of DCC and N- (3-Dimethylaminopropyl)-N′-ethylcarbodiimide (EDC) respectively. Despite both coupling agents activating the carboxyl groups for direct reactions with primary amines, DCC is more sterically hindered than EDC and as a result this may have affected the reaction (ThermoFisher, 2024). The activation of d-biotin by PFP could also have been avoided altogether by trialling uronium salts such as 1-[Bis

(dimethylamino)methylene]-1*H*-1,2,3-triazolo[4,5-*b*]pyridinium 3-oxid hexafluorophosphate (HATU) or 2-(6-Chloro-1-H-benzotriazole-1-yl)-1,1,3,3-tetramethylaminium hexafluorophosphate (HCTU). In these reactions the carboxyl group is deprotonated by a non-nucleophilic organic base like DIPEA, this carboxylate then attacks the to form an unstable *O*-acyl (tetramethyl)isouronium (OAt) salt. The OAt salt attacks the isouranium salt to form an active OAt ester and upon addition of an amine it is quickly acylated to afford the desired amide(Carpino et al., 2000, Carpino, 1993). Hur *et al* describe a method for activating biotin with HATU and obtaining high yields(Hur et al., 2010). Therefore, it would be worth trialling EDC in place of DCC and HATU or HCTU to improve yield in the future.

The formation of linker (**15**) **(**Figure 3.2.3.6) gave moderate yields of 43-58%, which when compared to the literature was significantly lower than the 94% reported (Zhou et al., 2017). Although these yields were acceptable, they could have been greatly improved by optimising the gradient used during purification by silica column chromatography. The solvent system of DCM:MeOH is widely used and was suitable for this purification, however, it is an incredibly polar solvent mixture which frequently causes co-elution of compounds. To prevent co-elution, a shallower gradient could have been employed or more isocratic holds inserted to maximise separation between compounds with similar polarity (Schellinger and Carr, 2006). The lowest yields in this synthesis came when performing the Staudinger reduction of linker (**15**) to form amine (**16**) (Figure 3.2.3.7.2). This reaction was particularly difficult to replicate, with many of the attempts resulting in failure to isolate the product or with poor yields <15%. The method used was a mixture of a reaction cited in the literature and the successful Staudinger reaction used earlier in the synthetic route (*Step 3*). Upon completion, the reaction mixture was concentrated under reduced pressure removing the THF/H_2O solvent system. The remaining residue was suspended in HCl (1M) to form the hydrochloride salt, allowing the insoluble triphenylphosphine to be removed by filtration before treating the filtrate with KOH to reform the amine and extracting with DCM. The low yields with this step could be associated with product solubility issues in certain solvents causing the product to be lost during washes/extraction, the numerous columns required to remove the triphenylphosphine oxide side product could also contribute to the low yield. Low yields could have been avoided by following the literature method directly. In the literature procedure the purification solely consists of washing with diethyl ether and DCM (Yang et al., 2011). Hydrogenation reactions may have provided an alternative method for azide reductions where Staudinger reductions are used (Figure 3.2.3.4). Typically, catalytic hydrogenations are performed under pressure to reduce the activation energy required (Molés Pérez, 1981). However, when using a metal catalyst such as palladium the activation energy is significantly lowered, not only this but the surface area of the catalyst is often maximised by adsorbing onto an inert carbon support, drastically increasing the rate of reaction (Rylander, 1979, Mao et al., 2021). As no ligands are involved in this reaction, it is uncommon for side reactions to occur. Reactions are often quantitative with purification consisting of catalyst removal by celite filtration often being sufficient, this methodology had been previously implemented to afford the desired amine linker (**16**) (Hur et al., 2010).

Modifying the route to incorporate click chemistry would also be an interesting option to explore. Click chemistry is essentially an azide-alkyne [3+2] cycloaddition catalysed by copper (I) (Figure 3.2.3.3.1). The presence of the copper activates the slow reactive alkyne group, increasing the rate of reaction by ~10^8 fold, while also templating the reaction to favour the formation of a regiospecific 1,4, disubstituted triazole (Kolb et al., 2001, Fantoni et al., 2021, Rostovtsev et al., 2002). Despite attempting a click reaction with azide (**15**) using the literature methodology, the product was not formed (Counsell et al., 2021). However, optimising this procedure could potentially shorten the synthetic route, allowing alkylation of p(s)pGpp upon purification, while also incorporating a chromophore to allow for reaction monitoring by UV (280 nm). The triazole moiety in the final capture compound would also be incredibly stable, being able to withstand a range of pHs and reactive functionalities, exhibiting its practicality in a biological setting (Sletten and Bertozzi, 2011).

The bromoacetylation of amine (**16**) to form the functionalised linker (**18**) when following the literature method of (Yang et al., 2016) provided low yield and purity while also requiring purification by column chromatography (Figure 3.2.3.8). In a similar manner to forming linker (**15**)**,** the gradient used for this purification could have been made shallower to avoid a larger difference in retention times, this would have allowed for separation between the structurally similar side product detected in ^{1}H NMR.

After trialling the purification of p(s)pGpp by ion pairing RP-HPLC, anion exchange chromatography was implemented with great success. However, upon the synthesis of capture compound (**19**), we returned to RP-HPLC using TEAB as an ion pair reagent. The main downfall of TEAB is the presence of the bicarbonate anion that in solution can become protonated forming carbonic acid. Carbonic acid is unstable and can undergo decarboxylation to form H_2O and carbon dioxide (CO_2) gas. As this CO_2 (g) diffuses into the surrounding air, the pH of the solution rises which can drastically affect retention times making it difficult to consistently predict what time a compound will elute from the column. In addition to fluctuating pH, bicarbonate anions have high conductivity and are likely to be more ionised than the sample which can result in a lower MS signal (Sharma et al., 2012). Although this purification method provided the desired capture compound, an attempt to optimise this procedure was made using hexafluoro-isopropanol (HFIP). As a mobile phase modifier HFIP, unlike TEAB, maintains a consistent pH due to its high stability, while also preventing the suppression of peaks in mass spectrometry and is now commonly used for separating oligonucleotides (Basiri et al., 2017). Introduing HFIP to the mobile phase was extremely effective and showed the ability of the buffer to separate the desired capture compound from multiple structurally similar nucleotides (Figure 3.2.3.10.2).

When exploring synthetic methods for the production of a capture compound, it was noted that (Haas et al., 2022) directly attached a pentynyl functionalised linker to the β-5'-phosphate of ppGpp with phosphoramidite chemistry. Phosphoramidites are amido-phosphite-diesters that are highly reactive towards nucleophiles, typically they are furnished with an N,N-diisopropyl group that is displaced upon attack, and were first introduced in the 1970s (Beaucage and Caruthers, 1981, Letsinger et al., 1975). To form this pentynyl-ppGpp analog, guanosine was chemoselectively bis-diphosphorylated at both the 3' and 5' position using phosphoryl chloride, $NaHCO_3$ and RNase T_2. To the newly 3'-,5'-phosphorylated guanosine apentynyl-fluorenylmethyloxycarbonyl-N,N-diisopropyl phosphoramidite was introduced. This phosphoramidite was then oxidised with MCPBA and dissolved in methanol to form a 2'-3' cyclophosphate. This cyclophosphate was regioselectivity hydrolysed using ribonuclease T_2 to give the pGpp-clickable product in 61% yield (Haas et al., 2022, Haas et al., 2019). With the alkyne moiety attached, an additional chemoselective phosphorylation at the 3'-position yielded the ppGpp-linker-azide (57%) before a click reaction with commercially available amino-PEG_3-azide linkers yielded the ppGpp-linker product along with a range of other nucleotide analogs in 57-84% yields (Scheme 3). This methodology highlights the efficiency of click reactions when synthesising modified nucleotides, as the linker can be formed directly on the nucleotide before attachment to the affinity handle instead of the opposite.

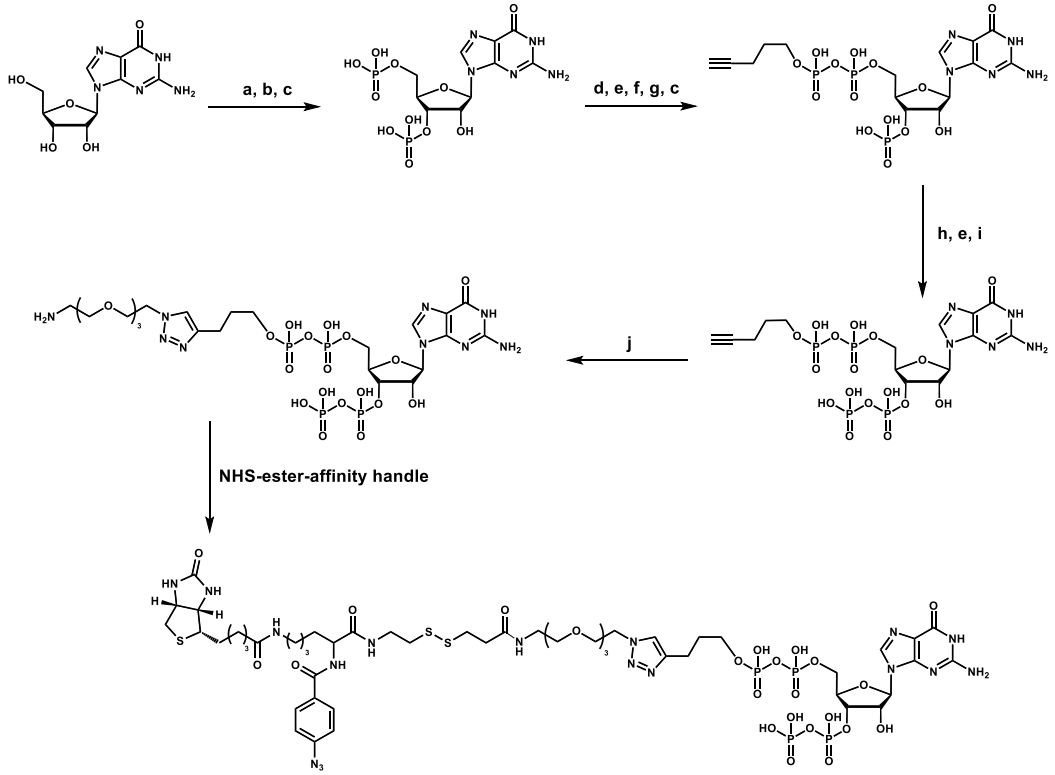

Scheme 3: Synthetic route towards a ppGpp photoaffinity capture compound used by *Haas et al.*: a) $P_2Cl_4O_3$ (11 equiv), 0 °C, 3 h. **b)** $NaHCO_3$ (1 M), 0 °C. **c)** RNase T_2, pH 7.5, 37 °C, 12 h. **d)** (FmO)(pentynylO)P-N*i*Pr_2 (2.2 equiv), ETT (5.0 equiv), DMF, rt, 15 min. **e)** *m*CPBA (3.0 equiv), −20 °C, 15 min. **f)** MeOH, 37 °C, 4 h. **g)** piperidine/DMF (1/4 v/v), rt, 30 min. **h)** $(FmO)_2$P-N*i*Pr_2 (3.0 equiv), ETT (5.0 equiv), DMF, rt, 15 min. **i)** DBU, rt, 30 min. **j)** Amino-PEG_3-azide (1.5 equiv), Na-ascorbate (1.8 equiv), $CuSO_4 \cdot 5\,H_2O$ (0.35 equiv), TEAA-buffer (pH 7, 200 mM), rt, 3 h.

The original ppGpp-protein capture compound paper written by (Wang et al., 2019a) used a similar methodology to the one employed in this chapter with p(s)pGpp being produced by GDPβS, ATP and YjbM(Steinchen et al., 2015a). However, the modified nucleotide was purified using monoQ column chromatography where a salt gradient was used to gradually elute the compounds. Using solid phase Fmoc-peptide synthesis, a peptide chain was used in place of a PEG-linker, which was biotinylated before bromoacetylating the N-terminus with bromoacetic anhydride. This functionalised bromoacetyl linker was cleaved from the solid phase support and purified by RP-HPLC before reacting directly with p(s)pGpp to afford the desired capture compounds (Scheme 4). The simplicity of solid phase-peptide synthesis provides high yields despite the introduction of additional synthetic steps when comparing to using a commercially available linker such as PEG. Not only this but solid phase-peptidesynthesis presents the option of furnishing certain side chains with any functionalities required. However, the optimisation of the designed route (Scheme 2) would allow for an economically viable and efficient synthesis of a ppGpp-capture compound.

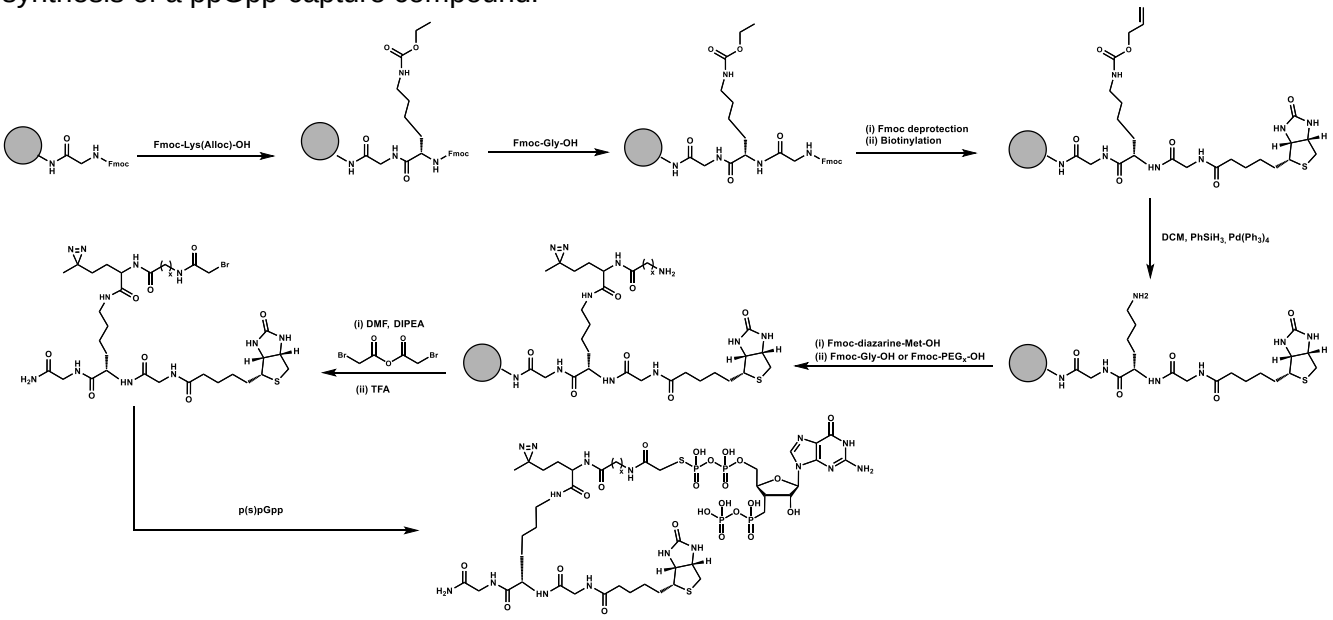

Scheme 4: Synthetic route used by *Wang et al* to reach a ppGpp photoaffinity capture compound. The route uses traditional solid phase peptide synthesis, and biotinylation before deprotection of the Lys(Alloc) region to yield a biotinylated amine linker attached to the solid support. The lysine portion of the linker is further elongated with diazirine furnished methionine and glycine before being bromoacetylated, cleaved from the support with TFA and coupled with p(s)pGpp to give the product.

Throughout this chapter we have described the purification of a novel ppGpp-protein capture compound (**19**) on a small scale, using a combination of methods from the literature and novel ideas. Key areas of the synthetic route have been identified for optimisation such as: amide coupling agents in place of activating d-biotin with PFP; substituting the late stage Staudinger reduction with a catalytic hydrogenation; RP-HPLC purification of the bromoacetyl linker (**18**); and anion exchange purification (monoQ) of the final capture compound (**19**). In the following chapters, the binding selectivity of this novel compound is explored, prior to description of its use with lysates of the pathogen MRSA where a multitude of ppGpp binding partners implicated in the stringent response signalling network were identified.

Chapter 4

Isolation of novel ppGpp protein-interactors

4.1. Introduction

It is well known that the conformational flexibility of (p)ppGpp allows it to adopt both enclosed and elongated forms, with this flexibility being responsible for its ability to bind to numerous proteins across a wide range of cellular processes (Steinchen and Bange, 2016). It is because of the conformational flexibility , that mapping the (p)ppGpp signalling network is so difficult to achieve. Several attempts to further elucidate (p)ppGpp binding partners have been made with varying degrees of success. Several methodologies such as DRaCALA, and the newly introduced capture compound procedures have all been trialled, primarily in *E. coli*(Zhang et al., 2018, Wang et al., 2019a, Haas et al., 2022, Corrigan et al., 2016). The four interacting GTPases RsgA, RbgA, Era and HflX were isolated using the methodology DRaCALA in *S. aureus* by Corrigan *et al* (Corrigan et al., 2016). Zhang *et al* were then able to isolate around 12 novel interaction partners using this methodology, along with the aforementioned GTPases, adding further validity to this approach. However, their K_d values were determined solely by densitometry, and characterisation by biophysical methods was absent (Zhang et al., 2018).

Capture compound approaches followed DRaCALA and were incredibly successful with ~50 putative targets being identified by Wang *et al* when utilising a chemo-enzymatic method to generate ppGpp analogs before furnishing with a UV activated cross linker. The interaction of ppGpp with, PurF, which is responsible for converting phosphoribosyl pyrophosphate (PRPP) to ribosylamine-5-phosphate and as such is important for purine nucleotide synthesis, was later characterised (Wang et al., 2019a). Haas *et al* also used capture compounds and mass spectrometry, identifying ~185 putative targets along with ApaH, the first non-nudix hydrolase that can hydrolyse pppGpp to pGpp (Haas et al., 2022). Capture compound approaches combined with mass spectrometry techniques appear to offer high throughput strategies for simultaneously identifying multiple protein interactors . Despite both previously designed capture compounds from Wang et al and Haas et al operating using covalent cross linkers, the sample preparation methodologies utilised in each study were vastly different, with Wang *et al* employing a SILAC approach and Haas *et al* choosing to design several chemical probes with various linker attachment sites.

It is clear that despite the capability of capture compounds to identify ppGpp interacting proteins, more probing of the ppGpp interactome is required in order to enable a more complete understanding of this complex signalling network. The synthesis and purification of our capture compound was completed as described in Chapter 3. In this chapter, we describe the assessment of our capture compound's selectivity using immuno-blotting techniques and the isolation of novel ppGpp interactors using the capture compound in pull-down assays with subsequent mass spectrometry inspired by the above methodologies. This work was performed to identify key *S. aureus* ppGpp interactors, before binding characterisation could be performed, furthering our understanding of how the response is mediated under different stress conditions in this organism.

4.2. Results

4.2.1. Capture compound displays selectivity towards known ppGpp-binding partners

In order to assess selectivity of the capture compound, its interactions with known ppGpp binders and a negative control were necessary. These were accomplished by interrogations of the ribosomal GTPases RsgA, RbgA, HflX and Era that had previously been purified in our lab by using pET28b:RA-GTPase plasmids (Corrigan et al., 2016). These plasmids encode the desired proteins linked to N-terminal hexa-histidine tags under T7 promoter control. The plasmids were introduced into the *E. coli* strain BL21 DE3, which contains the DE3 prophage responsible for producing the T7 polymerase when induced by IPTG, allowing for expression. The incorporation of the 6xHis-Tag allowed for purification by IMAC chromatography using a column packed with nickel-NTA-agarose resin. The integrities of the previously purified proteins that had been stored at -80 °C were re-assessed by running aliquots on a 12% SDS-PAGE followed by Coomassie staining (Figure 4.2.1). The proteins exhibited high purity indicating no degradation, with the expected molecular weights of 36.1 kDa (RsgA), 35.7 kDa (RbgA), 49.4 kDa (HflX) and 36.5 kDa (Era).

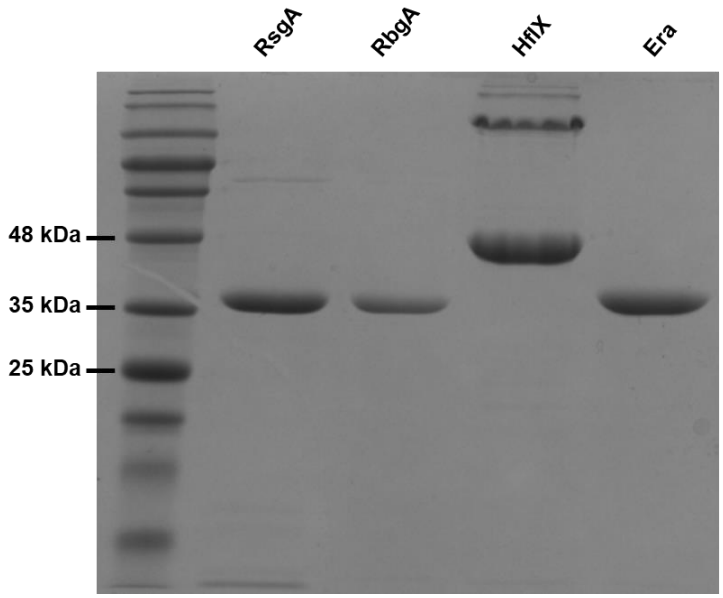

Figure 4.2.1: SDS-PAGE of the Ribosomal GTPases. Ribosomal GTPases: RsgA, RbgA, HflX and Era were normalised to concentrations of 10 µM before loading alongside pre-stained blue protein standard. 12% SDS-PAGE were electrophoresised at 200 V, for 45 min and stained using Coomassie Brilliant Blue stain as described in the materials and methods section 2.4.2.1

The next step was to adsorb the GTPases alongside controls onto polyvinyldifluoride (PVDF) membranes, to which proteins adhere through hydrophobic and dipole interactions (Xiang et al., 2021, Weiss, 2012, Tarlton and Knight, 1996). Non-specific binding to the proteins (10 µM) was blocked by incubating the membrane in BSA (5% w/v) solution. The blot was then incubated with 10 nM capture compound, followed by Streptavidin-HRP conjugate. The Streptavidin moiety was expected to bind readily to the biotin affinity handle and the HRP would then catalyse peroxide oxidation of luminol introduced when coating the membrane with ECL reagent. The luminescence produced was expected

to be easily detected using an Imager. As expected, the MBP negative control exhibited no luminescence due to a lack of binding to the capture compound, the biotin "positive" control did not produce a signal due to its inability to adhere to the PVDF membrane, while all four GTPases bound to the ppGpp capture compound (Figure 4.2.1.1).

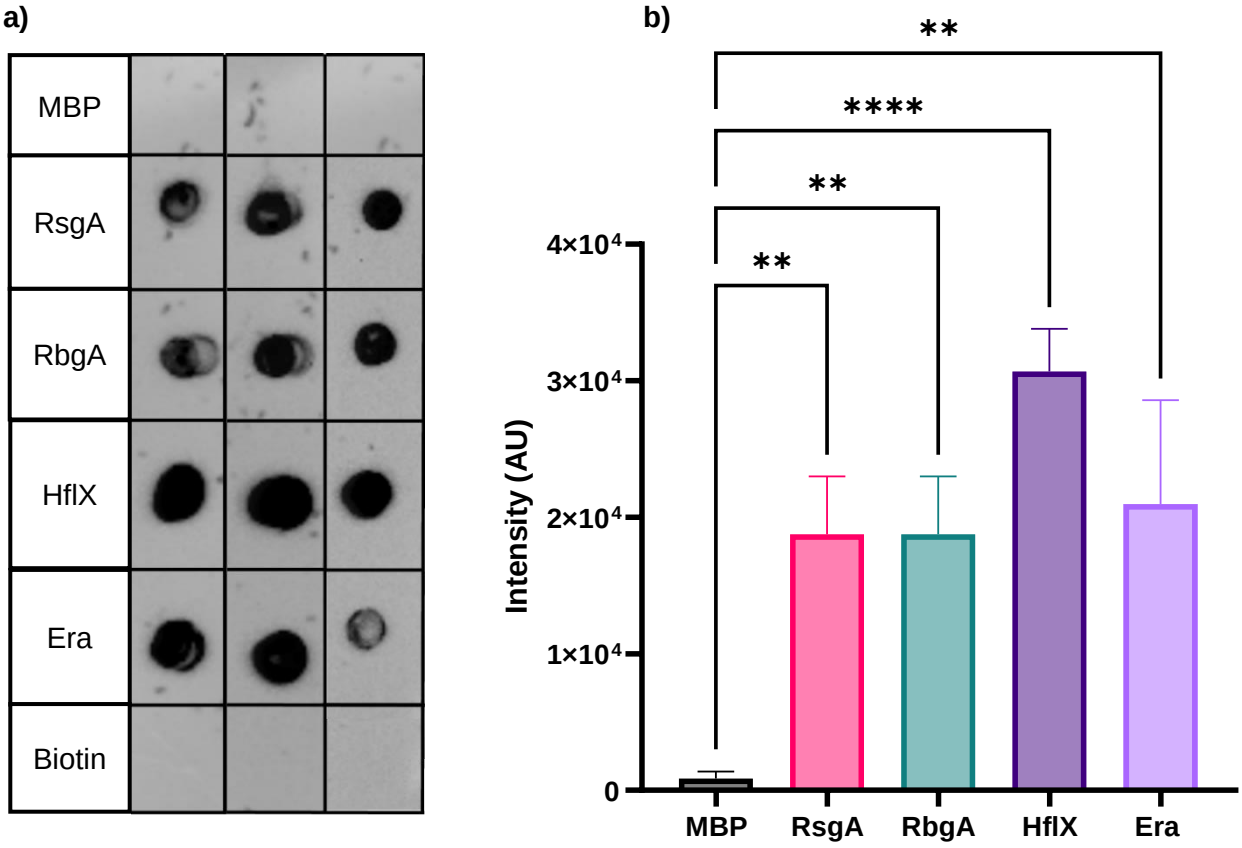

Figure 4.2.1.1: Capture compound exhibits selectivity to the ppGpp binding ribosomal GTPases. a) PVDF membrane imaged shortly after exposure to ECL reagent and hydrogen peroxide. The dark spots are the result of protein-capture compound complex bound to streptavidin-HRP oxidising luminol, which is indicative of protein binding. Note the absence of spots in the MBP negative control and the biotin positive control. Due to its charge, biotin was incapable of binding to the membrane on its own and so there is no signal while MBP does not display binding. **b)** Relative intensities were plotted with statistical significance of each protein of interest being compared to MBP by one-way ANOVA. The relative intensities were calculated using imageJ densitometry. The experiments were performed in triplicate and p values are represented as follows: **, $p < 0.01$; ***, $p < 0.001$

4.2.2. Development of a pulldown procedure

4.2.2.1. Lysate preparation

Selectivity of the capture compound was established in section 4.2.1, so the development of an appropriate pull-down methodology was explored. In order to efficiently isolate ppGpp-binding proteins, a cell lysate in high enough concentration was essential. Examination of the literature that used capture compounds revealed common procedures based on Laventie *et al*. These procedures were adapted to prepare cytoplasmic and membrane fractions of *S. aureus* and experimental details are outlined in the

methods section 2.4.3.1. We found several crucial steps such as passing the cytoplasmic fractions over a desalting column to remove free nucleotides and solubilising the membrane fraction using DDM. The concentration of the cytoplasmic and membrane fractions were then determined by a colorimetric BioRad protein assay using BSA as a calibration standard . The literature had reported values of around 10 mg/mL for use in pulldown assays, however, our values were consistently lower at ~1 mg/mL, perhaps due to differences in density across cultures as the doubling rate of *E. coli* (20 min) is larger than that of *S. aureus* (90 min).

4.2.2.2. Trial pulldowns using lysates from cells expressing the histidine-tagged GTPase Era

Once the method for generating lysates of sufficient concentration was established, the next step was to demonstrate a proof of concept, namely that the capture compound was capable of isolating ppGpp binding proteins from lysates before it was used in a tandem pulldown and mass spectrometry experiment (Figure 4.2.2.2).

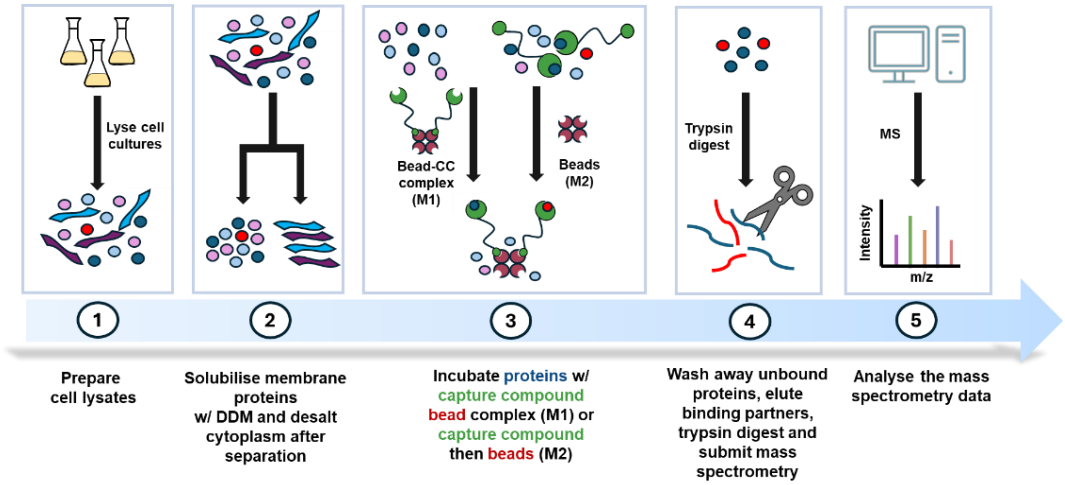

Figure 4.2.2.2: Workflow of the capture compound pulldown and mass spectrometry analysis. **1.** Lysate generation was performed as described in section 2.4.3.1 using overnight cultures of the desired strain in TSB supplemented with spectinomycin when required. **2.** Cytoplasmic proteins and membrane proteins were separated by ultracentrifugation. **3.** Protein "capture" was performed using either M1 – Proteins were incubated with a pre-made magnetic streptavidin bead-capture compound complex; M2- Proteins were incubated with the capture compound allowing binding before incubation with streptavidin beads. **4.** The isolated proteins were eluted from the beads and capture compound by heating and subjected to trypsin digestion before submission to mass spectrometry. **5.** Mass spectra of fragmentation patterns were analysed to identify the protein and its abundance.

To demonstrate capture in a complex mixture we took advantage of two bacterial strains; a deletion mutant USA300 Δ*era* pCN55iTET, which does not possess the GTPase Era, and USA300 Δ*era* pCN55iTET-*era*-His, which is complemented with the His-tagged GTPase (Wood et al., 2019). The presence of an anhydrotetracycline (atet) inducible promoter allows for expression of His-tagged Era upon addition during exponential phase. The presence of the poly-histidine tag allows for protein detection using Western immunoblotting.

Using a procedure from (Laventie et al., 2017) and coupling buffer recipes for magnetic streptavidin beads provided by Invitrogen, a pulldown methodology was attempted with the following adaptations: The Invitrogen bead coupling buffer consisted of NaCl (1M), Tris (10 mM) and EDTA (1mM). EDTA is typically used to reduce the risk of protein degradation by metalloproteinases in a sample as it chelates to co-factors such as Mg^{2+} and Ca^{2+}. However, it was removed from the coupling buffer as metal ions such as Mg^{2+} and Mn^{2+} have been identified as important co-factors for ppGpp binding by mediating its conformation (Steinchen and Bange, 2016). The capture compound functions in a non-covalent manner and the high salt concentrations (1 M) in the suggested coupling buffer would disrupt specific interactions leading to poor capture efficiency. As a result they were lowered to 230 mM and the lysate concentration was reduced to 3 mg/mL from 10 mg/mL. The binding capacity of streptavidin beads was calculated using information provided by the Invitrogen product manual, to guarantee that capture compound was always in excess, ensuring saturation of the bead surface (Equation 4.2.2.2).

Equation 4.2.2.2: $Binding\ capacity\ (Beads) = 200\ pmol\ of\ biotin\ peptide/mg\ of\ bead$
$Beads\ (40\ \mu L) = Beads\ (0.4\ mg) \therefore Binding\ capacity = 80\ pmol$
$Capture\ compound\ (2\ nmol) = 25x\ Excess$

Initially, the capture compound was incubated with streptavidin beads for 30 min at room temperature before incubating with the lysate for an additional 30 mins (Figure 4.2.2.2.1) in line with the M1 method (Figure 4.2.2.2.). A negative control, termed “bead control” was introduced, this control contained streptavidin beads but did not contain capture compound. The control was treated in an identical manner before mixing with lysates. Samples were then washed and any captured proteins were eluted from the beads by boiling (95 °C) in elution buffer containing SDS (5% w/v). The pulldown eluents were expected to contain the ppGpp-binding protein Era-His, where the presence of this diagnostic protein would allow us to determine the success of the M1 work-flow. In order to detect Era-His ; the eluents and samples of the lysates prior to the pulldown were analysed by SDS-PAGE and subsequent Western immunoblotting as described in materials and methods section 2.4.2.10. It was clear to see that before the pulldown procedure, Era-His was readily identifiable in the lysate as it would be one of only a few luminescent bands (4.2.2.2.1a, Lane 1). As expected the Δ*era* lysate exhibited a lack of the His-tagged protein. However, the protein signal was also absent in the pulldown eluent of the strain capable of producing His-Era indicating the capture compound bead complex was not capable of isolating Era-His during the pulldown (Figure 4.2.2.2.1a, Lane 2-3). We also introduced an experiment which involved spiking wildtype lysates of JE2 with 100 ng of His-tagged-GTPases RsgA and HflX (Figure 5b). The addition of these proteins occurred just prior to performing the pulldown. The JE2 lysate exhibited no binding which was expected due to the lack of His-tags while the visible band at ~32 kDa in the eluent was attributed to RsgA and showed the capture compound was capable of isolating ppGpp binders from a complex mixture of proteins (Figure 4.2.2.2.1b, lane 2).

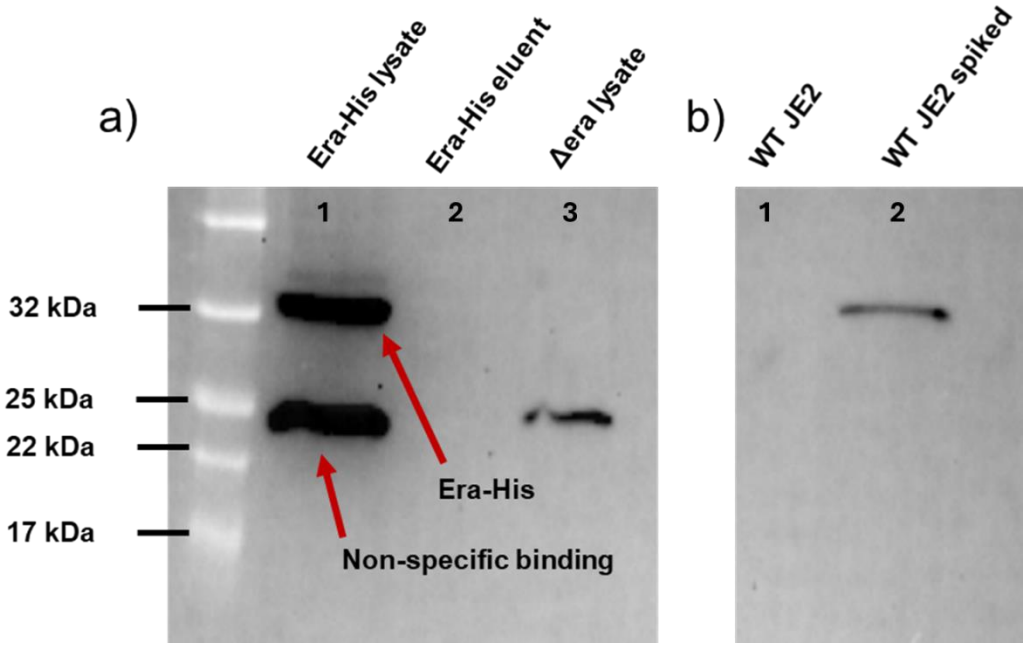

Figure 4.2.2.2.1: Western blot of lysates prior to the pulldown and pulldown eluents. Cell lysates and pulldown eluents were resolved on a 12% SDS-PAGE 200 V, 400 mA, 45 mins before transferring to a PVDF membrane activated by methanol. The membrane was then blocked with 5% milk solution and human IgG to prevent binding of proteinA before adding the HRP-conjugated α-His-antibody, washing with TBST and activating with ECL reagent and hydrogen peroxide **a)** Lane 1 – Lysate from JE2Δera PCN55iTET Era-His, with a band present at 32 kDa representative of Era-His and a non specific binder at ~24 kDa. Lane 2 – Pulldown eluent of the Era-His lysate, the absence of bands is attributable to the capture compound failing to isolate the His-tagged GTPase. Lane 3 – Lysate from LACΔera PCN55iTET which acted as the negative control. **b)** Lane 1 – Lysate from the wildtype JE2 control. Lane 2 – Pulldown eluent from the WT JE2 lysate spiked with 100 ng of RsgA-His and HflX-His, the band present at 32 kDa is attributable to RsgA-His which was successfully isolated by the capture compound.

Upon reviewing the literature, it was established that capture compounds are often incubated for longer periods of time with the lysates before introduction of the beads (Laventie et al., 2017, Haas et al., 2022). The rationale behind lysate incubation prior to the introduction of the beads is a bead coated with multiple capture compounds is significantly more sterically hindered than a free molecule of capture compound, increasing the difficulty of protein capture. The free capture compound method (M2) was trialled alongside the initial methodology (M1) with longer incubation times, so that comparisons could be directly drawn between the two. As before SDS-PAGE anlayses of the lysates and pulldown eluents were performed and this time, bands were first visualised using silver stain(Figure 4.2.2.2.2ab). Silver staining is considerably more sensitive than Coomassie staining with a lower detection limit of 0.1 ng

protein allowing for the detection of proteins in the pulldown eluent that was not previously possible(Kumar, 2018, Switzer et al., 1979).

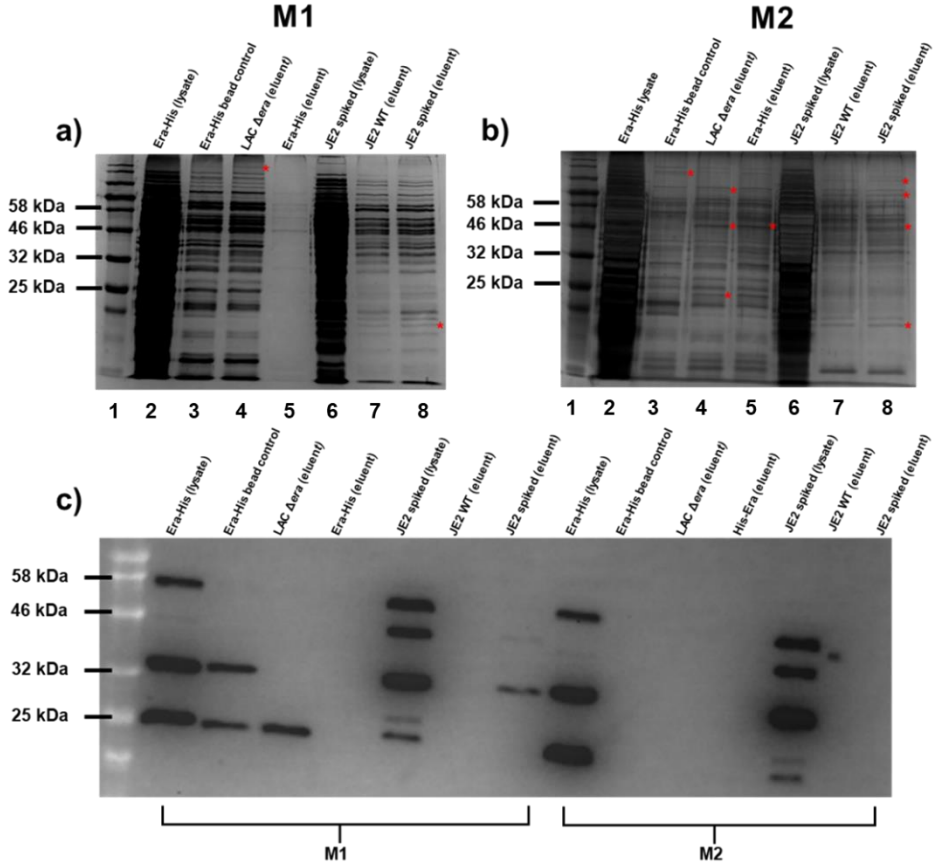

Figure 4.2.2.2.2: Silver staining provides insight into the ability of the capture compound to capture specific proteins when compared to the bead control. a) Silver stain of lysates and pulldown eluent using M1 showed little difference in protein isolation except two bands in the spiked WT eluent (lane 8) and LAC Δ*era* eluent (lane 4) when comparing to the bead control (lane 3). **b)** Silver stains of lysate and eluent using M2 with differences in protein isolation in comparison to the bead control (lane 3) highlighted in red. **c)** Western blot comparing the detection of his-tagged GTPases Era, HflX and RsgA across lysate and pulldown eluents using "capture" methodologies M1 and M2. Western blots were performed in triplicate.

The greatest differences in silver stain intensities were seen with the M2 protocol, multiple bands were present in the pulldown experiments but not the bead control suggesting enrichment by the capture compound (Figure 4.2.2.2.2ab). In opposition to the literature, M1 seemed to show the best results by Western immunoblot. The blot included the bead control along with Era-His lysate (lane 1) and spiked lysate (lane 6) as additional controls. The isolation of RsgA-His and HflX-His from the spiked lysate pulldown (lane 8) again showed the capability of the capture compound to selectively enrich ppGpp binding proteins despite M2 displaying zero isolation of the proteins of interest (Figure 4.2.2.2.2c).The capture compound was designed to isolate proteins that would otherwise be present in lower abundance in the bead control, therefore in tandem with the lysate preparation, procedure M2 was chosen for the pulldown experiments in stationary phase wildtype bacteria as it showed the greatest difference across bead control and capture experiments.

4.2.3. Pulldown experiments

The isolation of novel ppGpp interactors using capture compound methodologies has been performed using both *E. coli* and *S.* Typhimurium; with capture compounds of different structures and using both soluble and membrane fractions (Haas et al., 2022, Wang et al., 2019a). However, these studies have solely investigated stationary phase bacteria. While ppGpp levels are higher in stationary phase at around 700 μM, the alarmones are also present at basal levels in exponential phase cells (approximately 50 μM) (Hauryliuk and Atkinson, 2017). Therefore, it stands to reason that there could be a specific subset of proteins that are upregulated/more likely to interact with (p)ppGpp across both growth phases (Büke et al., 2022, Ferullo and Lovett, 2008). In addition , the effects stress may impose on the proteome and therefore the (p)ppGpp interactome has also not been investigated. Hence for our pulldown experiments, we obtained lysates from stationary and exponential phase cultures, along with lysates from strains that had been subjected to nutrient starvation. Here we chose to induce amino acid starvation by exposing exponential phase cells to the antibiotic mupirocin for 10 mins. In addition, we also isolated proteins from bacteria that had been internalised by macrophages, to ascertain if specific protein sets that interact with (p)ppGpp are upregulated in these environments.

Lysates were prepared as for stationary phase cells, except the membrane and cytoplasmic fractions were recombined after desalting and solubilisation, in order to avoid the concentrations of the membrane fractions being too low for individual use in the pulldowns. Each type of lysate was subjected to the same pulldown procedure as previously described in M2 of section 4.2.2 with four replicates and a bead control allowing for comparisons across data sets.

4.2.4. Mass spectrometry and statistical analysis

The mass spectrometry experiments were performed as described in section 2.4.3.3 and the data were uploaded to Perseus software. Protein species were identified using the SAUSA_300 genome during the proteomics experiment and their relative abundances were reported by Label Free Quantification (LFQ), which is calculated by integrating under the Gaussian of the detected peptide ion peak (Mehta et al., 2020, Noor et al., 2019). The datasets were filtered to remove any repeats arising from reversed amino acid sequences and potential contaminations. The LFQ data were then Log(2) transformed to follow a normal distribution ensuring highly abundant and less abundant proteins are on the same scale. The datasets were then filtered for valid values, ensuring that a protein must be identified at least twice across three replicates, ultimately reducing the matrix size. The data were then normalised by subtracting the median LFQ value: due to the data being log2 transformed, subtraction between two logs is the same as dividing two non logs. Any not a number (NaN) values from these normalised data that arise due to the log of 0 being undefined, were then imputed using a normal distribution. Comparisons between the bead controls and capture experiments were drawn using students two sample t-test with a false discovery rate (FDR) of 0.05. With the FDRs of these datacompleted, the matrices were ordered by q-value: q-values are an analog of p-values and are defined as “the minimum false discovery rate at which an observed score is deemed significant” -essentially the q-value reports the proportion of significant features that are “false positives” (Storey and Tibshirani, 2003, Storey, 2003). Volcano plots were generated using -log (p) values and the differences between the sample groups of bead control and capture experiment (Figure 4.2.4).

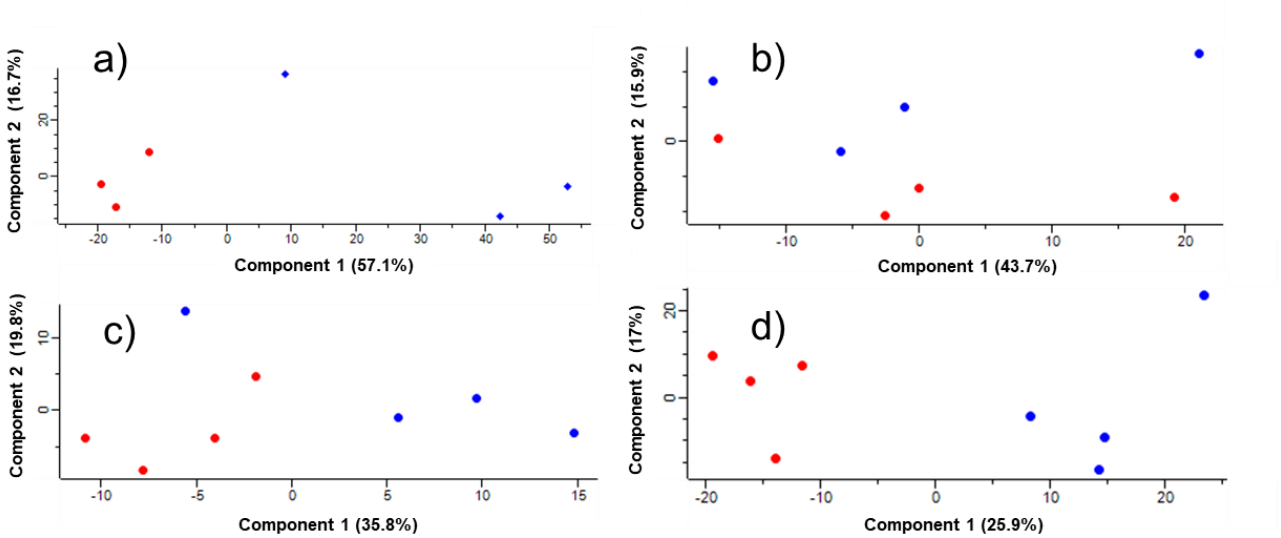

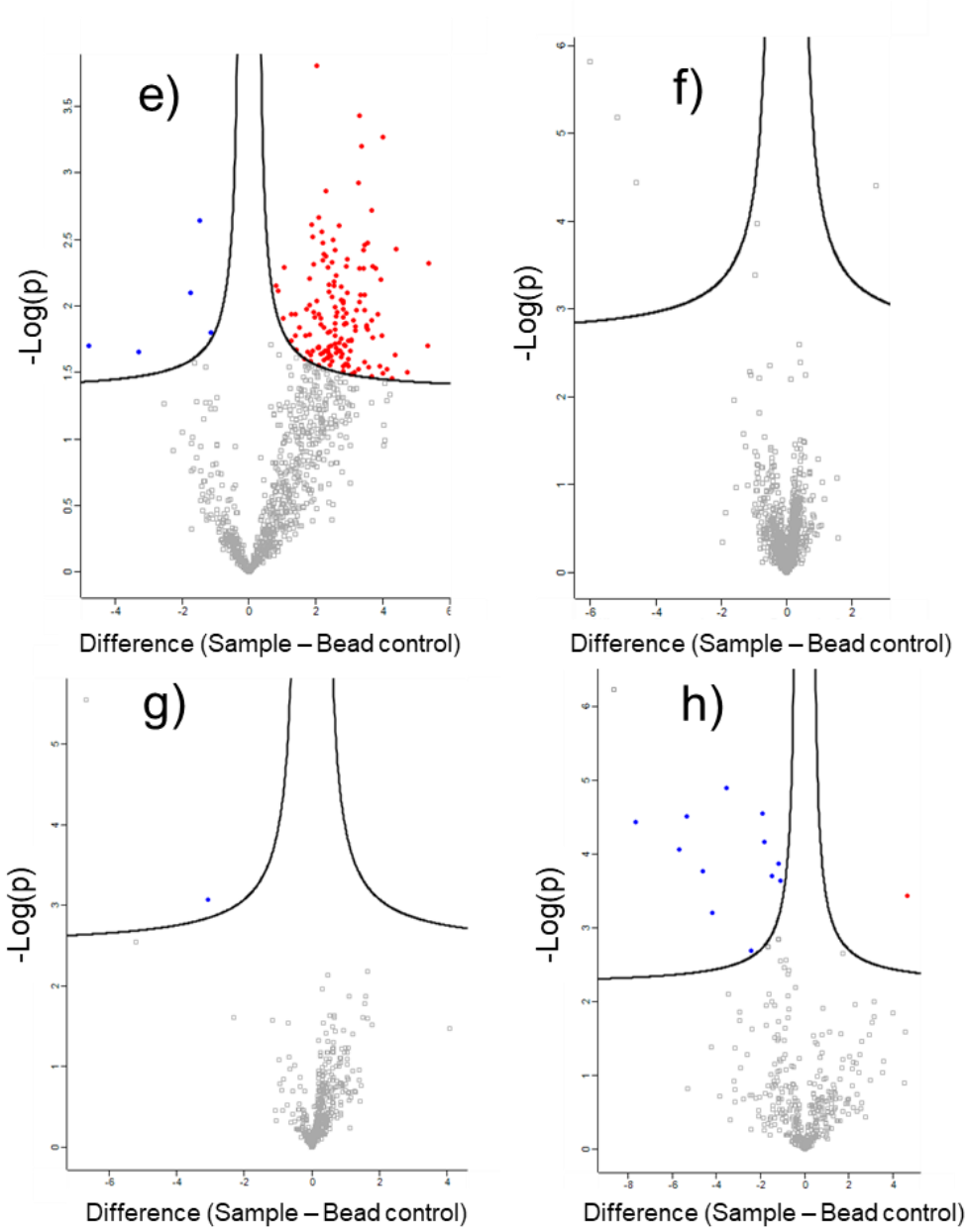

Figure 4.2.4a-d: Principal component analysis (PCA) of replicates across each capture experiment. Plots display the similarity across replicates of each pulldown experiment. The closer the grouping the greater the similarity. Bead control (blue), capture experiments (red). **a)** stationary phase, **b)** exponential phase, **c)** mupirocin stress, **d)** macrophage stress. **e-h: Volcano plots displaying the significant differences between proteins isolated by the capture compound.** The y-axis is plotted as -LogP for ease of viewing as higher probabilities are higher up the graph, while the transformation of probabilities simplifies the numbers as they are often orders of magnitude apart, the difference between capture experiment and control is represented Log2 (x-y) (x-axis)**.** Proteins displayed past the right contour were significantly enriched by the capture compound to some capacity (red), compared toproteins that were more present in the bead control (blue). Any proteins that are present on either side of the contours that are not highlighted exceeded the q-value threshold of 0.05 and were not investigated. **e)** stationary phase, **f)** exponential phase, **g)** mupirocin induced stress, **h)** internalisation by macrophage stress.

The proteomics data includes an incredibly vast array of measured variables, not all of which are helpful in deciphering patterns. In order to assess consistency across replicates principal component analysis (PCA) was performed. PCA essentially reduces the large number of variables into a smaller more manageable set of variables by linear combination. The new variables conserve the majority of information from the uncompressed variables, ultimately simplifying the data at the expense of accuracy. PCA plots indicated similarity across the capture experiments for each condition. This was expected as the capture compound should be capable of isolating similar proteins across different replicates, with the exception of exponential phase which exhibited a greater degree of variance (Figure 4.2.4b). However, the streptavidin-conjugated dynabead controls showed more variation across their replicates, this was also expected as there was nothing capable of isolating specific proteins. The beads however, are slightly "sticky" due to streptavidin's hydrophobic domains meaning some proteins adhere and are isolated more than once (Schwidop et al., 1990). Following PCA analysis, volcano plots were graphed, which contain truncation lines. Iff there is a small difference it is more likely that this is due to an error with a small sample size so the curved contours attempt to reflect this by having a more stringent p value cut off. The matrices were then ordered by q-value: q-values are an analog of p-values and are defined as "the minimum false discovery rate at which an observed score is deemed significant" - essentially the q-value reports the proportion of significant features that are "false leads" (Storey and Tibshirani, 2003, Storey, 2003). Each data point on the volcano plot represents a protein and those present beyond the top right contours were deemed significantly enriched by the capture compound.

With significant proteins being determined, we examined each data set. Stationary phase experiments (Figure 4.2.4e) displayed the greatest number of significant proteins with 162 being enriched. Whilst exponential phase showed the presence of a protein past the right contour, the q-value was determined as 0 making it unreliable (Figure 4.2.4f). The mupirocin experiment showed no significantly enriched proteins. When considering the culture was exposed to stress during mid-exponential phase, the similarity to the exponential phase is not surprising. The macrophage-based experiments led to the enrichment of just one protein (Figure 4.2.4f), identified as ribosomal protein RpmA (L27), which is implicated in growth (Maguire et al., 2001). While data using the exponential phase and stressed lysates revealed little, the large collection of significantly enriched proteins present in the stationary phase data was of great interest. These were investigated further as stationary phase is when (p)ppGpp levels should be at their highest in the absence of stress (~700 μM in contrast to 50 μM in exponential phase).

4.2.5. Bioinformatic characterisation of (p)ppGpp binding proteins isolated from stationary phase lysates

Proteins from the mass spectrometry data were reported by gene locus and accession number (Table 1, Appendix). We first compared their identities against hit-lists from previous capture compound studies that used *E. coli* and *S.* Typhimurium lysates. We found that 20 of the 162 proteins had been previously identified, including PurF the key ppGpp-binder identified in the initial ppGpp-capture compound study,

validating the method used for the identification of ppGpp binding proteins (Figure 4.2.5) (Wang et al., 2019a, Haas et al., 2022).

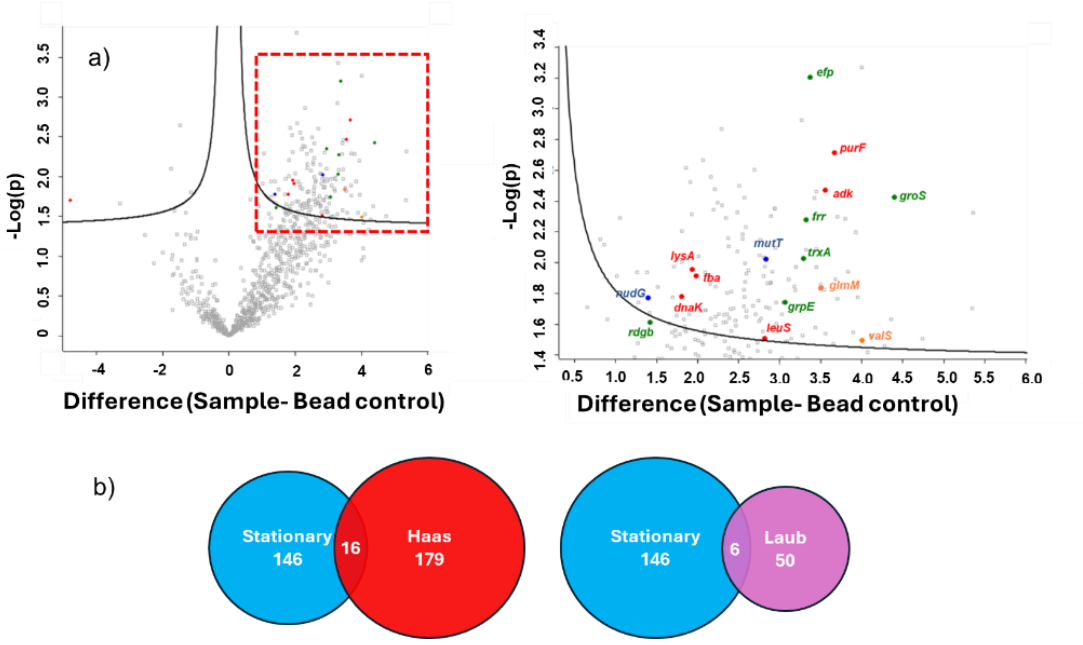

Figure 4.2.5: Volcano plot demonstrating the capture compound's ability to significantly enrich proteins from lysate and comparison to previously captured targets. a) Stationary phase pulldown analysis showing 162 significantly enriched proteins. Significance threshold was set to an FDR of 0.05 using a students two sample t-test. Previously identified proteins by capture compound and DRaCALA methodologies have been colour coded. Red:(Wang et al., 2019a), Blue: (Zhang et al., 2018, Haas et al., 2022), Green: (Haas et al., 2022, Wang et al., 2019a), Orange: Two or more studies. **b)** Venn diagrams demonstrating overlap of our captured proteins with previous capture compound studies. Blue: our stationary phase hits; red: (Haas et al., 2022); pink: (Wang et al., 2019a).

With a list of potential ppGpp interactors now established, the next step was to determine the respective pathways and roles of these 162 proteins. First, the list was subjected to analysis using the Kyoto encyclopaedia of genes and genomes (KEGG). KEGG utilises several different interaction classifications: pathways; brite; and modules -with pathways and brite being of most use to us. Overall KEGG can be defined as an ontology database that visually represents functional hierarchies of biologics, including molecules/proteins and cells, that allows for systematic analysis of gene functions and involvements of proteins in their respective pathways (Kanehisa and Goto, 2000). Using KEGG, 138 of the 162 proteins were successfully mapped to 20 different biological functions across the cell including: enzymes; peptidases; chaperones; transcription factors and ribosome biogenesis (Figure 4.2.5.1a). KEGG mapper also allows the mapping of groups of proteins onto metabolic maps. Using KEGG mapper for our 162 proteins we highlighted numerous metabolic processes that could be regulated by (p)ppGpp in the cell (Figure 4.2.5.1b).

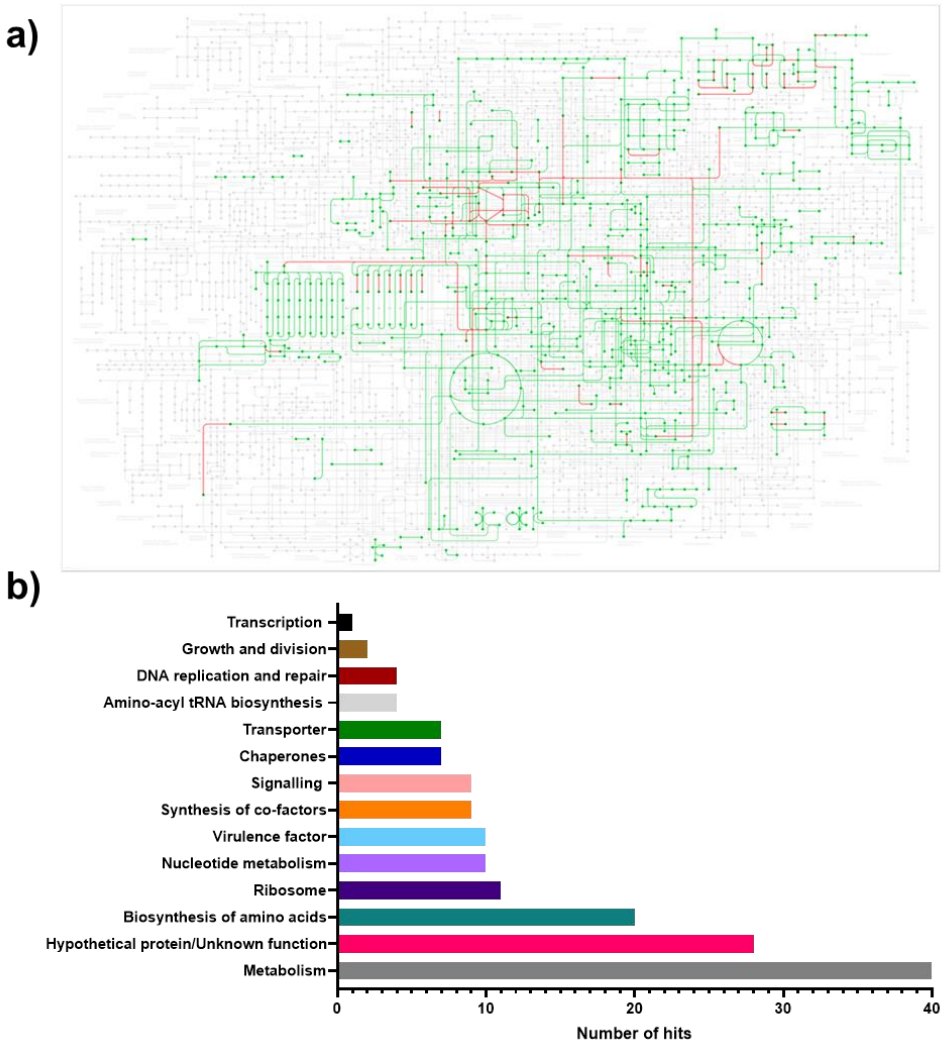

Figure 4.2.5.1: **KEGG mapping reveals protein hits that span numerous cellular processes. a)** KEGG pathway mapping of the potential hits and their respective pathways within the cell, showing the extensive range of functionality ppGpp posseses. Green: pathways involving enriched proteins. Red: pathways involving proteins more present in the bead control. **b)** Summary of the proteins mapped to cellular processes by KEGG.

Although 162 of these proteins were deemed significantly enriched by the capture compound and others considered significantly absent by statistical analysis, binding of the enriched proteins to ppGpp must be confirmed by biophysical methods and their interactions thoroughly characterised. Around half of all the proteins identified were allocated as enzymes involved in metabolic pathways, however, there was an extensive range of cellular processes identified during KEGG mapping, all of which had the potential to reveal novel binding partners. Hence, in the next chapter we describe the use of a high throughput differential radial capillary action of ligand assay (DRaCALA) using a previously constructed open reading frame (ORFeome) protein expression library containing expression vectors for the majority of proteins in *S. aureus* COL, to further investigate these potential ppGpp interactors.

4.3. Discussion

In this chapter we aimed to optimise a pulldown procedure for the isolation of ppGpp binding proteins. We implemented two procedures M1 and M2 before deciding on M1 and using lysates from strains grown to various growth phases and stress conditions, with the hope of particular subsets of proteins being upregulated, potentially allowing us to identify novel ppGpp interactors in previously unexplored processes. These pulldown-enriched proteins were then submitted for tandem mass spectrometry and statistical analysis of the proteomics data obtained was performed using a stringent FDR cut off. We then began the process of identifying the proteins by gene locus, while drawing comparisons to previous ppGpp capture compound studies. This led us to the discovery that 12.3% of our significantly enriched proteins had previously been captured adding validity to our protein-capture approach. With the protein identities established, we then began categorising the proteins by their cellular functions, providing us with an insight into what processes were being targeted by ppGpp, with the majority being involved in metabolism. This list of proteins and their respective functions is to be investigated further in the next chapter in order to characterise and confirm any potential interactions with ppGpp.

When performing pulldown procedures there were several considerations to be taken into account, some of which could be improved. Firstly, high lysate concentrations increase the likelihood of the capture compound enriching proteins of a lower abundance throughout the sample. Therefore, using lysate concentrations of 3 mg/mL compared to the 10 mg/mL used by Laventie *et al* may have led to isolation of a smaller range of proteins. To counteract this, both membrane and cytoplasmic fractions were re-combined and passed through a 3 kDa MWCO spin column, after solubilising with DDM and desalting. However, the presence of the detergent DDM when passing the lysates through the concentrator could lead to an unknown increase in detergent concentration, meaning DDM micelle (70 kDa) concentrations increase and aggregation can occur, potentially resulting in protein degradation (Strop and Brunger, 2005). The increased concentration of DDM had the capacity to unexpectedly alter our results *via* misidentification of protein fragments, however, the problem was rectified in the latter pulldowns with exponential phase and stress conditions by adding DDM after passing through a concentrator.

KEGG mapping revealed that the majority of proteins were involved in metabolism (Figure 4.2.5.1b). This was not surprising as previous studies have revealed (p)ppGpp binding partners in both the de novo and salvage purine synthesis pathways across multiple species such as *S. aureus, B. subtilis and E. coli*. These include the aforementioned PurF, the GMP kinase Gmk, the GMP synthase GuaA, the IMP dehydrogenase GuaB and the hypoxanthine phosphoribosyltransferase HprT (Wang et al., 2019, Hochstadt-Ozer and Cashel, 1972, Kriel et al., 2012, Anderson et al., 2019, Liu et al., 2015). Numerous uncharacterised proteins were enriched, alongside ~30 proteins involved in amino acid biosynthesis and ribosomal processes. This finding is also unsurprising as it is known that the previously characterised ribosomal GTPases are (p)ppGpp interaction partners, and that the CodY transcription

factor plays a role in mediating amino acid biosynthesis through fluctuating (p)ppGpp and GTP levels (Geiger et al., 2010, Geiger et al., 2012). There were, however, some more interesting processes identified such as previously uncharacterised pathways involved in nucleotide metabolism and even virulence factors. (p)ppGpp has been shown to be important for pathogenicity in *S. aureus*, with a synthetase-off, hydrolase-on mutant of Rel showing decreased virulence in a kidney infection mouse model, while deletion of codY restored virulence (Geiger et al., 2010). High level vancomycin resistance was also seen in a clinical isolate of MRSA, along with increased expression of the toxic phenol soluble modulins, increased lysis of neutrophils, increased intracellular survival and adherence to endothelial cells in vitro (Li et al., 2020). Despite (p)ppGpp's apparent links with virulence, a definitive ppGpp-protein binder, directly involved with these processes remains undiscovered.

The lack of overlap between our results and Haas et al and Wang et al could be explained by several reasons. Haas et al used an extensive range of ppGpp capture compounds in order to probe the structure activity relationship with the binders, while we only used one capture compound. Secondly, the lack of a covalent cross-linker may have led to the loss of some binding proteins during the washing steps of our pulldowns. Finally, neither of these capture compound studies were investigating *S. aureus*. It is likely that expression of certain proteins differs across species making it difficult to capture the same proteins in significant abundances. Even when comparing significantly enriched proteins between Haas *et al* and Wang *et al*, only 10 proteins were common between the two. When comparing overlapping proteins with our study, we managed to isolate the key binder of the Wang et al study – PurF, as well as elongation factor-Ts, elongation factor-P and the heat shock proteins GroS, GrpE from Haas et al. The remaining proteins shared between the studies were all involved in some sort of metabolism (Table 2-4, Appendix).

Despite the two possible pulldown methodologies (M1 and M2) differing only slightly, there was a large impact on the proteins that were isolated by the capture compound across these two procedures as seen in the silver stains and western blots (Figure 4.2.2.2.2). M1 involved coating streptavidin beads with the capture compound before incubating with the treated lysates, while M2 involved free capture compound interacting with proteins by its p(s)pGpp moiety before the addition of streptavidin magnetic dynabeads, which would capture the compound by its biotin-affinity handle. M2 was chosen in preference to the initial methodology as it lacked the steric hindrance associated with a bead-compound complex. As a result, capture was improved and analysis by silver stain showed a greater difference in protein banding patterns when comparing to the bead control. Coomassie staining was not suitable for analysis due to the low concentration of the pulldown eluents and, as a result, silver staining was implemented due to its increased sensitivity, allowing detection as low as 0.1 ng protein per band. However, silver staining has drawbacks, mainly the formation of silver mirrors during the development step and an intense background if the process is not terminated quickly enough, this is most visible in the lanes containing lysate (Figure 4.2.2.2.2ab, Lane 2 and 6). Cytoplasmic fractions contain many free

nucleotides such as ppGpp, may interfere in the assay by blocking binding sites of the capture compound in a direct or allosteric manner. Nucleotides were removed using a PD10 column. Membrane proteins are often incorporated into lipid bi-layers and possess poor solubility as a result addition of a surfactant such as DDM aids solubility.

With proteins now isolated by pulldown experiments there were two options for proteomic analysis: shotgun proteomics also referred to as bottom-up proteomics - where proteins undergo proteolysis to yield peptides which are further fragmented; or top-down proteomics – where intact proteins are ionised and later fragmented (Yates, 2015). We utilised shotgun proteomics due to its ability to identify proteins from complex mixtures, while also avoiding some of the limitations associated with top-down methods such protein ionisation and fragmentation in the gas phase (Zhang et al., 2013). Before proteomic analysis can take place, the samples must be efficiently cleaned and prepared for mass spectrometric analysis. There are several methods that can be used when preparing samples for proteomics, which range from gel based, to solution or filter based. The samples we submitted where prepared by S-trap proteomics previously described in section 2.4.3.3, this method is an improvement on most current methods due to shorter centrifugation times and a greater ability for generating detectable peptide sequences which improves output (Haile Mariam et al., 2018, Ludwig et al., 2018).

When analysing proteomics data, the software generates theoretical peptide fragments based on the *S. aureus* proteome provided, which are then scored against the experimentally observed fragments, searching for a match so that the protein responsible is determined. However, when performing experiments such as the pulldown using lysates of bacteria isolated from infected macrophages, there is the possibility of carry over proteins belonging to white blood cells present in the sample that cannot be linked to the provided proteome. Therefore, the algorithm will attempt to match the *in silico* generated fragments to all of the available fragments regardless of their origin. As a result the false discovery rate increases, making it more difficult to identify significant hits. During the normalisation process, we utilised the median average, to identify our 162 proteins from stationary phase lysates. However during trypsin digestion a standard is sometimes added in known concentration that can then be used to normalise all of the LFQ data allowing for more accurate estimates of abundance. This is something that could be trialled in future experiments.

The only experiment to yield a significantly enriched protein besides stationary phase was the macrophage pulldown with the aforementioned ribosomal protein RpmA. Highly conserved in most bacterial species, RpmA has been shown to play a key role in tRNA substrate stabilisation through cross linking with the 3' end of A and P site tRNAs, with deletion mutants in *E. coli* leading to a lack of tRNA cross linking and growth defects (Maguire et al., 2001, Wower et al., 1998). In *S. aureus* and *B. subtilis*, RpmA has an extended N-terminal domain that protrudes directly into the peptidyl transferase centre interfering with tRNA stabilisation by occluding key residues, however, it is readily cleaved by

another protein Prp with both being essential for survival (Wall et al., 2015, Spilman et al., 2012). It is currently unclear what the role of this N-terminal extension is and why the bacteria do not simply express the shortened version of the protein present in most other bacteria such as *E. coli*. However, it is postulated that the peptide released upon cleavage may act as a regulatory switch or environmental sensor involved in regulating ribosome assembly, with overexpression of the peptide leading to a small decrease in growth rate (Wall et al., 2015). A ppGpp binding protein that limits cell growth during stress is not unusual and has been seen in the form of the aforementioned translational GTPases in section 4.1. However, RelA is known to complex to the 50S ribosomal subunit during stress while also binding (p)ppGpp, therefore RpmA may have been enriched as a result of it complexing to Rel (Richter et al., 1975, Ramagopal and Davis, 1974).

The lack of significantly enriched proteins across 3 of 4 experiment types could be explained by low protein abundance. In macrophage experiments, bacteria are exposed to donor macrophages and internalised within 6 hours, after this time period extra-cellular bacteria are washed away and internalised bacteria are eventually “rescued” by selectively lysing the macrophages with saponin. Ultimately the pellets we used for lysis contain mainly cellular debris from the macrophages and internalised bacteria, of which there is a significantly lower number when comparing to other pulldown experiments. Although the lysates from exponential and mupirocin experiments were passed through a spin concentrator, some ppGpp binders would be at undetectable levels. This is due to ppGpp halting growth, meaning some proteins-binders would be expressed less during exponential phase, with the exception of translation factors. Despite efforts to minimise loss of proteins at low abundance, the use of lower lysate concentrations (3 mg/mL), as expected, led to some protein-binders being lost during the pulldown procedure and sample preparation (Feist and Hummon, 2015).

Although Laub *et al* had great success in the original ppGpp capture compound paper using a SILAC approach described in section 4.1. SILAC systems can be difficult to design as they requires a high degree of isotopically labelled atom incorporation with low labelling success shifting the ratio in favour of unlabelled protein making identification difficult (Zhang and Neubert, 2009, Zhang et al., 2014, Elias et al., 2005). Some methods have been described which attempt to resolve this by measuring isotopic label incorporation for individual protein, however this is not very cost effective and also time consuming (Spellman et al., 2008). In order to be able to effectively generate a ratio of heavy/light atoms SILAC also requires proteins to be isolated in two independent analyses (Zhang et al., 2014). In contrast to this, with an effective experimental design SILAC can be simple to implement and identification of protein interactors can be simple due to the known difference in heavy/light peptides (Zhang and Neubert, 2009). It is also possible to use samples directly after lysis so that minimal variables are affected by sample preparation. Furthermore, around 50 putative ppGpp targets were identified using this methodology, however, we simply did not have the resources to generate isotopically labelled media or time to generate an effective media for SILAC (Wang et al., 2019a). The most recent capture

compound by Haas *et al* did not use a SILAC approach but made use of a covalent capture-compound and included a competition control during their pulldown procedures (Haas et al., 2022). This control included a 1000-fold excess of (p)ppGpp in comparison to the bead control and capture experiments in order to outcompete their covalent capture compound and reduce the number of false positives. This inspired us to include our own competition control with 100-fold excess of ppGpp alongside the bead and capture experiments, however, the differences in proteomics results between the competition and capture experiment were negligible, perhaps due to a lower concentration of competitive nucleotides and so were not included in this analysis.

Overall, we were able to demonstrate the ability of our non-covalent capture compound to selectively isolate known ppGpp binders through interactions with the translational GTPases, before developing our own pulldown procedure based on previous methodologies and the use of shotgun proteomics to circumvent the use of SILAC. The key difference to previous approaches such as Laventie *et al* , Haas *et al* and Wang *et al* was our wash method, which contained a significantly lower concentration of salt to prevent the disruption of specific interactions. Several growth and stress conditions were then investigated using this procedure with varying degrees of success, with the unstressed stationary phase experiment being the most successful, isolating 162 proteins for further investigation by binding characterisation methods which we explore in the following chapter.

Chapter 5:

Characterisation of novel-ppGpp interacting proteins

5.1. Introduction

There are a variety of techniques that can be used to investigate protein binding interactions with small ligands. These techniques include isothermal calorimetry, microscale thermophoresis (MST), NMR assays and differential radial capillary action of ligand assay (DRaCALA) (Roelofs et al., 2011, Duff et al., 2011, Shortridge et al., 2008). DRaCALA operates on the ability of nitrocellulose to immbolise proteins at the point of application while free ligands annulate outwards from the application point due to the bulk movement of the solvent by capillary action (Fig 1.6.1).

This technique has been used to great success and is incredibly useful for high throughput screening of potential protein interactors, as it does not require protein purification, with whole cell lysates being sufficient as long as the protein is over expressed to a sufficient level. When used in a 96-well plate format, it allows for large scale screening of protein over-expression libraries, but it can also be used with purified recombinant protein for a more accurate determination of binding affinities(Orr and Lee, 2017). DRaCALA has revealed numerous novel interaction partners across several species, such as *Bacillus anthracis*, *E. coli,* and more relevant to us, *S. aureus* by Corrigan *et al*, identifying the tight binding translational GTPases: RsgA (K_d = 2.2 μM); RbgA (K_d = 2.9 μM); HflX (K_d = 3.4 μM); Era (K_d = 4.2 μM)(Corrigan et al., 2016, Bennison et al., 2021, Zhang et al., 2018).

In this chapter, we describe the use of a high throughput DRaCALA methodology previously implemented by Corrigan *et al* to identify ppGpp binding targets from a hit list established by the pulldown tandem mass spectrometry experiments performed in Chapter 4. We then used several biophysical and chemical techniques such as NMR and *in vitro* reaction assays to confirm binding, along with an MST trial to determine a binding affinity for our putative targets.

5.2. Results

5.2.1. Protein over-expression using a pre-established ORFeome library

The 162 significant hits identified in the stationary phase dataset needed to be filtered prior to focusing on a small number of potential interactors to further characterise. In order to reduce the size of the hit list we followed one criterion, namely, that the proteins should be involved in processes previously implicated in the stringent response or be important for staphylococcal growth or virulence - this led to us shortlisting ~60 proteins of interest. To screen for binding to all 60 proteins, we made use of a previously constructed ORFeome protein over-expression library that was available in the lab. This library contains 2,343 open reading frames (ORFs), which cover 85.5% of the genes, of S. *aureus* strain COL in plasmids fused to an N-terminal 6x-His-tag in an *E. coli* expression strain. The His-tags allow for later purification if required. The *E. coli* strain, T7IQ, encodes the T7-RNAP within the *lac* operon on the chromosome and two plasmids: LacIQ encoding the *lacI* repressor, which prevents transcription of a portion of the *lac* operon, and pVL791 encoding the protein of interest under T7 RNAP promoter control (Figure 5.2.1). Once in early exponential phase, the introduction of IPTG inhibits the function of LacI, which subsequently allows for the expression of the T7-RNAP that is capable of inducing protein production of the desired protein.

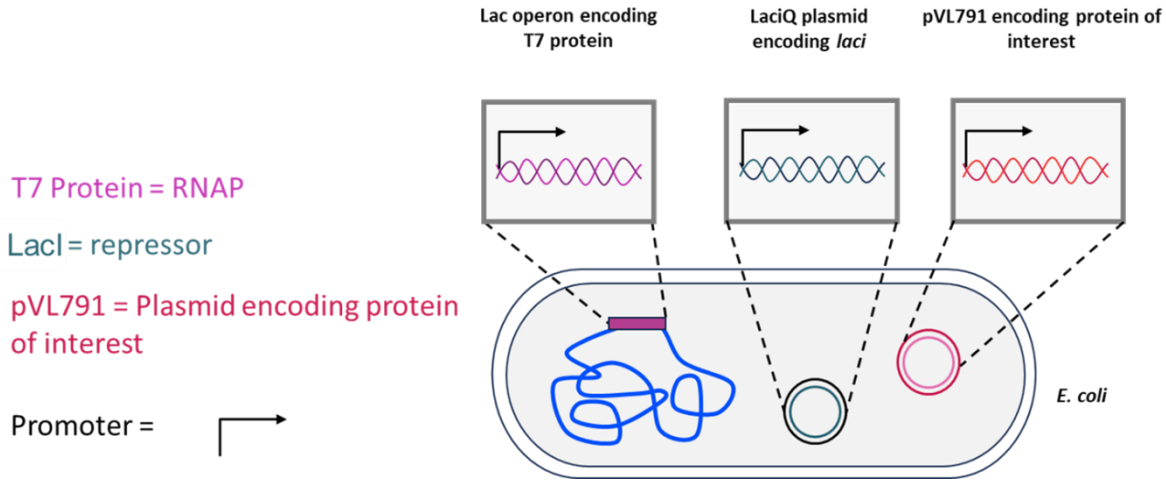

Figure 5.2.1: T7IQ allows for the expression of the desired His-tagged proteins in the presence of IPTG. The pVL791 plasmid encodes the his-tagged protein under tight IPTG-inducible control of the T7 promoter which allows for protein expression to be induced when desired.

Our 60 chosen strains from the library were grown in 96 well deep plates and expression of the protein-His fusions were induced. Cultures were pelleted and lysed, before being analysed by SDS-PAGE to confirm the expression of the desired proteins (Figure 5.2.1.1). The majority of the proteins (39/60, 65%) were expressed to a visible level, along with a positive control in the form of the known ppGpp-binder RsgA. Several cultures did not grow on the first induction attempt, possibly due to toxic expression or poor inoculation. Irrespective of the expression success rate, all 60 of the whole-cell lysates were screened using DRaCALA with [α-^{32}P]-ppGpp.

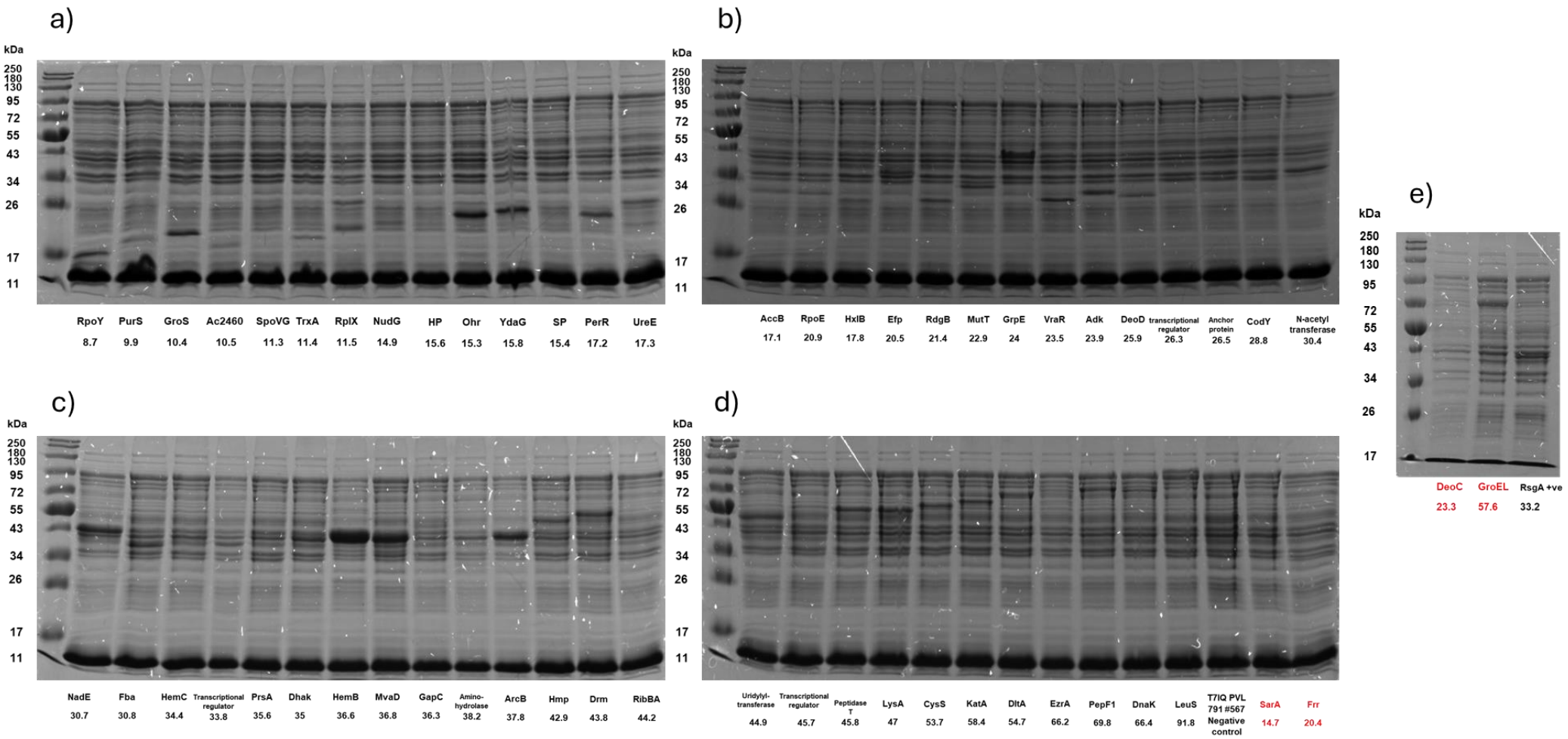

Figure 5.2.1.1: SDS-PAGE to assess protein expression from the ORFeome library. a-d) Proteins in increasing size order (listed below name in kDa) with exception of proteins in red which did not grow successfully the first time. Cultures were grown to an OD_{600} of 0.3-0.5 at 37 °C before the addition of IPTG (1 mM) to induce protein expression and incubated (30 °C, O/N). Cells were lysed in the presence of PMSF (1 mM), DNase (2 mg/mL), lysozyme (50 mg/mL) and subjected to 3x freeze thaw cycles (-80 °C, 20 mins). Lysates were then run on 12% SDS-PAGE (400 mA, 200 V, 45 mins) and stained with Coomassie.

5.2.2. Synthesis of [α-^{32}P]-ppGpp using the bifunctional ppGpp synthetase Rel_{Seq}

To begin the screening process with DRaCALA, the synthesis of our ligand [α-^{32}P]-ppGpp was required. Making use of an RSH-homolog from the bacterium *Streptococcus equisimilis* termed Rel_{seq}, it was possible to catalyse the formation of ^{32}P-pppGpp by addition of a pyro-phosphate from ATP to the 3'-position of α-^{32}P-GTP *via* S_N2 chemistry (Figure 5.2.2a).

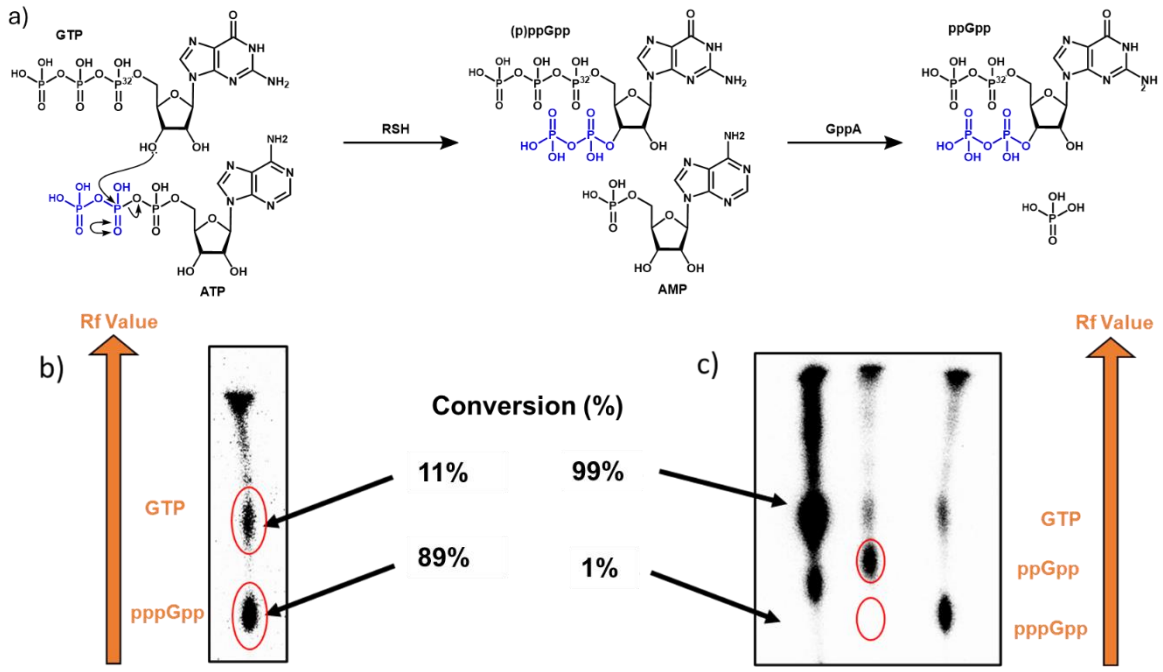

Figure 5.2.2: Rel_{seq} catalysed formation of pppGpp and subsequent cleavage by GppA to ppGpp is monitored by TLC. a) The 3'-hydroxy group of GTP attacks the 5'-β-phosphate of ATP to yield AMP and [α-^{32}P]-pppGpp. The [α-^{32}P]-pppGpp is then cleaved by guanosine pentaphosphate 5′-phosphohydrolase A (GppA) to give inorganic phosphate and the desired radiolabelled [α-^{32}P]-ppGpp. **b)** TLC of Rel_{seq} reaction mixture showing the formation of [α-^{32}P]-pppGpp (bottom) from [α-^{32}P]-GTP. **c)** TLC showing the formation of the desired [α-^{32}P]-ppGpp nucleotide (Lane 2) from [α-^{32}P]-pppGpp (Lane 3) in almost 100% yield catalysed by GppA. TLCs were run on PEI cellulose TLC with a mobile phase of 1.5 M KH_2PO_4 (pH 3.6). Images were obtained by exposure to an IP-plate and visualised using a Typhoon FLA7000 Phosphoimager. Conversions were determined using pixel densitometry.

This reaction proceeded as expected, forming the pre-cursor nucleotide [α-^{32}P]-pppGpp in good yield with 89% conversion as seen by TLC (Figure 5.2.2b). The higher negative charge of [α-^{32}P]-pppGpp leads to a greater retention factor on a TLC, allowing for it to be easily distinguished from the [α-^{32}P]-GTP starting material. The desired [α-^{32}P]-ppGpp was then formed by cleavage using the guanosine pentaphosphate 5′-phosphohydrolase A (GppA) to give the product in nearly 100% yield as seen by the complete absence of pppGpp on TLC (Figure 5.2.2c). GppA is heavily involved in the metabolism of pppGpp to ppGpp and was first identified with *gpp* mutants in *E. coli* having increased pppGpp accumulation and reduced ppGpp accumulation in their lysates (Somerville and Ahmed, 1979, Hara and Sy, 1983). It also exhibits high specificity for pppGpp even in the presence of other nucleotides in

5-fold excess, making it suitable for the production of [α-^{32}P]-ppGpp that was used in our DRaCALA experiments (Somerville and Ahmed, 1979).

5.2.3. High throughput radio-labelled DRaCALA with whole cell lysates

The [α-^{32}P]-ppGpp, was mixed with whole-cell lysates of the expression strains grown using the ORFeome library and dotted onto nitrocellulose membranes to perform DRaCALA (Figure 5.2.3a). From the spots produced the fraction of ppGpp bound (Fb) to each protein was then calculated by determining the area and intensity of each spot by pixel densitometry (Equation 5.2.3) (Roelofs et al., 2011).

Equation 5.2.3:

$$Fb = \frac{(Intensity_{Inner} - Intensity_{Background})}{Intensity_{Total}}$$

$$Intensity_{Background} = Area_{inner} \times \frac{(Intensity_{Total} - Intensity_{Inner})}{(Area_{Total} - Area_{inner})}$$

$$\therefore Fb = \frac{(Intensity_{Inner} - \left[Area_{inner} \times \frac{(Intensity_{Total} - Intensity_{Inner})}{(Area_{Total} - Area_{inner})}\right]}{Intensity_{Total}}$$

A positive (pVL791-*rsgA*) and a negative control (empty vector) were also included in each assay (Figure 5.2.3a). It stands to reason that the positive control RsgA (+ve) displayed the greatest intensity signal and the negative control T7IQ pVL791 displayed almost no binding to ^{32}P-ppGpp. Whole cell lysates contain every protein in the cell at the time of lysis, hence the slight background level of ppGpp binding in almost all of the expression lysates, with the exception of 6 strains that were absent from the analysis due to failed growth (Figure 5.2.3a, red cross). When analysing each spot, it was important to ensure the measurement areas were larger than the actual dot to account for the “edge effect”, where evaporation during annulation leads to areas of higher concentration and greater intensity (Roelofs et al., 2011). The data from across the replicates were analysed and any spots deemed to be deformed were removed from the analysis, before averaging and organising by percentage binding with respect to the RsgA positive control (Figure 5.2.3b).

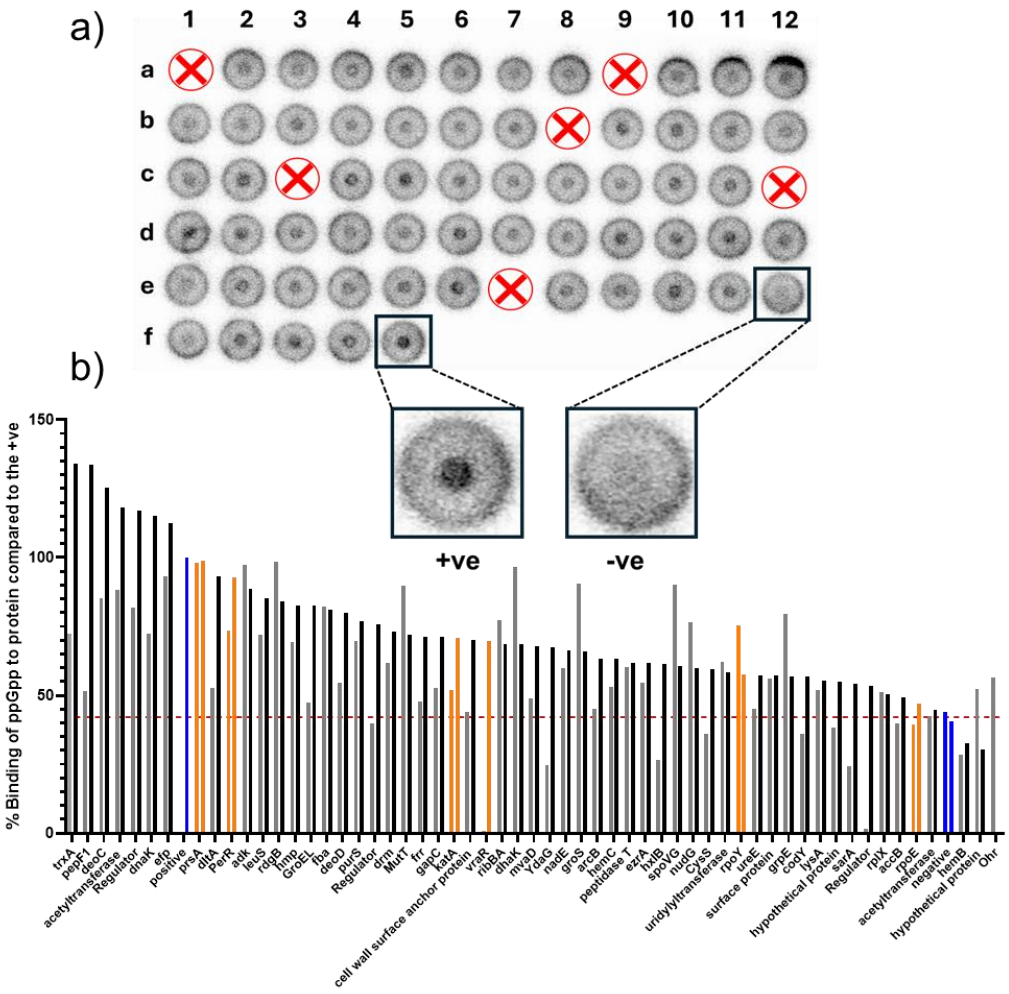

Figure 5.2.3: Whole cell lysate high throughput DRaCALA with [α-^{32}P]-ppGpp. a) DRaCALA of 60/162 proteins using whole cell lysates and [α-^{32}P]-ppGpp (1.6 nM). The outer dot circle is due to free ligand annulating outwards while the inner circle is due to proteins binding to the radiolabelled ppGpp. **b)** The DRaCALA spots were subject to pixel densitometry so that the fraction of ppGpp bound could be calculated, these values were then transformed into percentage binding with respect to the positive control (RsgA). Two technical replicates (grey = technical 1, black = technical 2). Proteins chosen to be investigated = orange. Positive and negative controls = blue. Threshold of the negative control = red hashed line.

5.2.4. Rationale for choosing group 1 proteins for further characterisation

From the above analysis, six proteins were chosen to be investigated further; PrsA; PerR; KatA; VraR; RpoY and RpoE. PrsA was chosen as it had the highest similarity between replicates and showed strong binding compared to the positive control RsgA. It is a chaperone implicated in cell wall stress, and antimicrobial tolerance. Upregulation of PrsA expression occurs upon cell wall stress that is detected by the vancomycin resistance associated regulatory two-component system (VraRS). The protein also mediates oxacillin resistance, with deletion altering resistance levels in three different MRSA strain backgrounds. PrsA also plays a role in host immune evasion with a recent study demonstrating the immunoglobulin-binding protein A requires PrsA for secretion and stabilisation in *S. aureus* (Lin et al., 2024).

PerR also displayed good binding with respect to the positive control and is an enzyme implicated in staphylococcal virulence. Previous studies have found PerR controls transcription of genes involved in producing oxidative stress proteins, such as alkylhydroperoxide, bacteriofierritin, thioredoxin B and KatA, and studies in the Corrigan lab link the stringent response to survival in the presence of reactive oxygen species (Choudhury et al., 2023). PerR may mediate expression of these genes by acting as a peroxide sensor, with additional peroxide leading to induction of the majority of the *perR* regulon except for itself and the ferric uptake regulator *fur* (Horsburgh et al., 2001). KatA, as the sole catalase in *S. aureus*, is important for survival in a murine skin abscess infection model, while it does not affect pathogenicity. PerR however is required for virulence with significantly smaller lesions forming in the inactivated *perR* gene strain (Horsburgh et al., 2001). This is important as when internalised by a macrophage, the primary stress the bacteria experiences will be exposure to reactive oxygen species. PerR has also been identified as a transcriptional regulator of the pore forming leukocidin LukAB, as during infection of human polymorphonuclear neutrophils, upregulation of PerR leads to increased cytotoxicity (Savin et al., 2024). This phenotype is also present with exposure to neat H_2O_2, suggesting PerR detects reactive oxygen species produced by host immune cells and upregulates production of LukAB as a result, heavily implicating it in virulence (Savin et al., 2024).

KatA was chosen for further characterisation as it is intrinsically linked with PerR. KatA is responsible for detoxifying H_2O_2 levels of up to 100 mM, while this may not be experienced upon internalisation by macrophages or intracellularly, with H_2O_2 levels being ~2 μM to 1-100 nM respectively (Sies and Jones, 2020, Imlay, 2019, Lyublinskaya and Antunes, 2019). *S. aureus* is a coloniser of the nares, with peroxide levels reaching millimolar levels in this environment. This is, in part, due to competing bacteria such as *Streptococcus pneumoniae*, which use their lactate and pyruvate oxidases to produce millimolar levels of H_2O_2 (Lisher John et al., 2017, Liu et al., 2015a). With this in mind, Cosgrove *et al* saw a significant decrease in nasal colonisation of cotton rats when comparing inactive *katA* mutants to wildtype (Cosgrove et al., 2007b, Horsburgh et al., 2001). KatA has also been implicated in lowering external peroxide levels and as a result of this, levels of reactive oxygen species such as HOCl also decrease due to myeloperoxidases having less substrate. It is also induced upon macrophage internalisation and deemed essential for survival in this instance (Das et al., 2008).

As mentioned previously when discussing PrsA, the VraRS-two component system is involved in relaying information about cell wall stress. Cell wall-targeting antibiotics are known to induce expression of the (p)ppGpp synthetases RelP and RelQ (Gratani and Wolz), linking cell wall stress and the stringent response. Therefore it seemed sensible to investigate one of its constituents proteins, VraR. Antibacterials that target cell wall peptidoglycan synthesis such as β-lactams and vancomycin trigger the activation of this two-component system, which then co-ordinates expression of a multitude of genes involved in exposure to cell wall inhibitors including those involved in the biosynthesis of peptidoglycan, heavily implicating it in antimicrobial tolerance (Kuroda et al., 2000, Fan et al., 2007).

The final two proteins chosen to be investigated were the RNAP subunit RpoE (δ) and the small accessory subunit RpoY (ε), despite the former barely clearing the threshold of the negative control (Weiss et al., 2014, Weiss and Shaw, 2015). As mentioned in Chapter 1, ppGpp is reported to not bind directly to RNAP in the Firmicutes as it does in *E. coli*. However, when these ppGpp interaction studies were performed, they utilised core RNAP from *Bacillus subtilis*, which lacked these accessory subunits (Krasny and Gourse 2004). The possibility therefore remains that (p)ppGpp could interact with the RNAP from the Firmicutes, but only with distinct regions of the polymerase.

5.2.5. IMAC purification of potential group 1 ppGpp interactors

When purifying a recombinant protein, it is possible that it may co-purify with the ligand (p)ppGpp, which may mask observable binding to our ^{32}P-ppGpp. In order to avoid a loss of signal when performing DRaCALA, the expression vectors were introduced into a (p)ppGpp^0 *E. coli* strain - MG1655 Δ*relA* Δ*spoT* pTARA. This strain contains the pTARA plasmid with the T7 polymerase under the control of an arabinose-inducible promoter, allowing for expression of our genes from the T7 promoter in pVL791. It also has a deletion of the two *E. coli* (p)ppGpp synthetases RelA and SpoT. The expression between the original T7IQ strains with IPTG inducible promoters and the new MG1655 Δ*relA* Δ*spoT* strains were then compared by SDS-PAGE alongside controls (Figure 5.2.5).

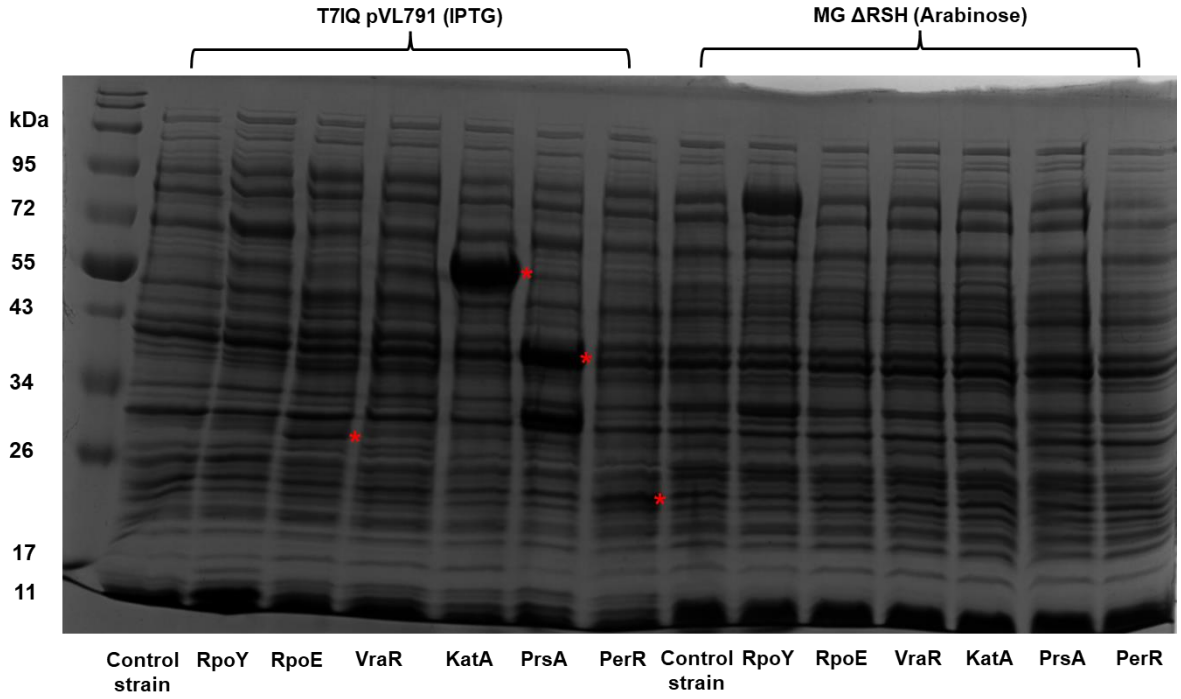

Figure 5.2.5: Protein expression of T7IQ strains compared to MG1655 ΔRSH strains. Small scale protein inductions of the IPTG (1 mM) inducible T7IQ expression strains compared to the arabinose (10 mM) inducible MG ΔRSH expression strains showing the efficiency of the former. Induction conditions of 30 °C for 1 hr were adhered to for all strains and lysates were normalised to an OD_{600} of 1 before running a 12% SDS-PAGE (400 mA, 200 V, 45 mins) and staining with Coomassie.

By comparing the two expression systems it was established that T7IQ would be more efficient in terms of protein production. With the correct expression system established, a small-scale induction was performed to ensure that the desired proteins were present in each lysate (Figure 5.2.5.1a), before purifying *via* IMAC chromatography – previously described in section 2.4.2.4 A typical IMAC chromatogram allows for visualisation of the lysate being loaded onto the column along with elution of the desired His-tagged protein from the nickel column. As the concentration of imidazole increases the protein can be seen to elute with its concentration gradually increasing (Figure 5.2.5.1b).

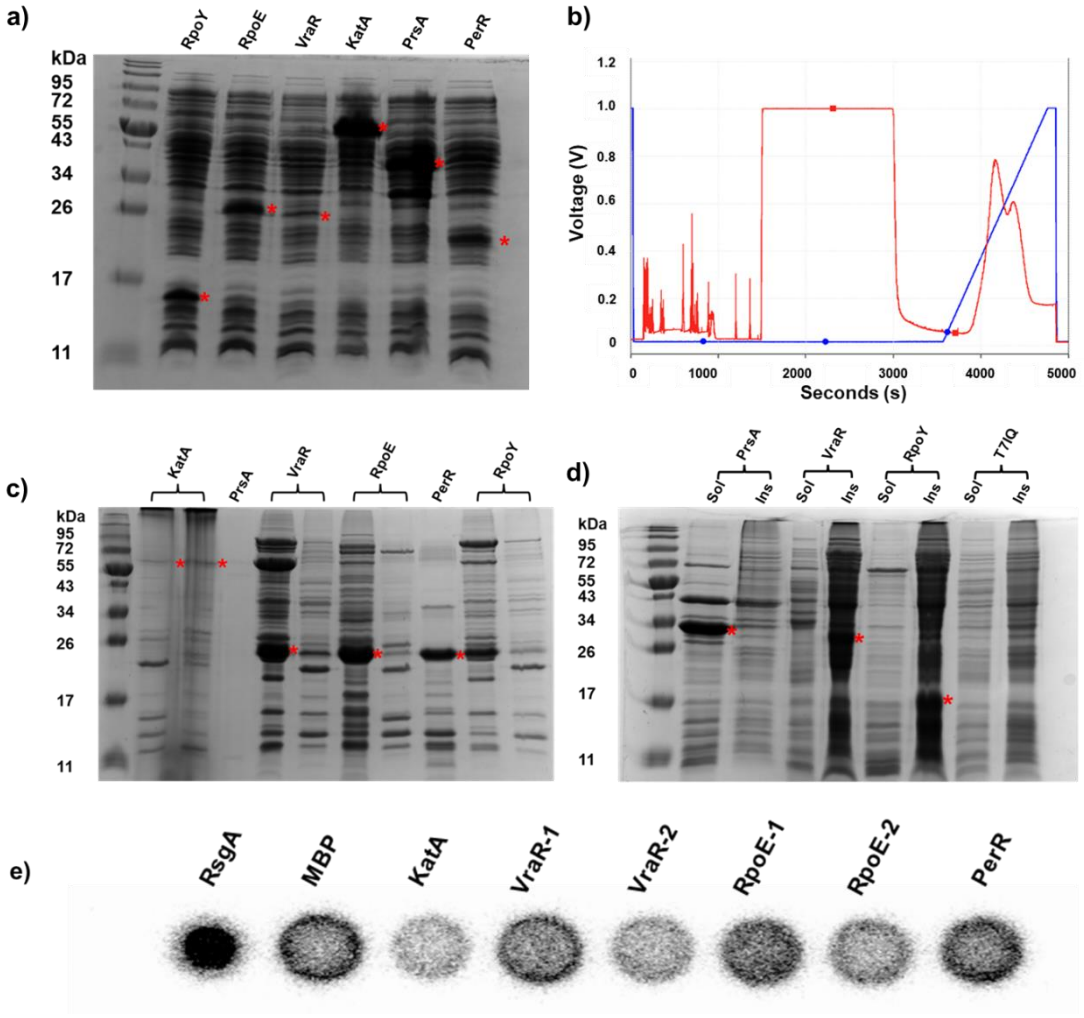

Figure 5.2.5.1: Proteins were expressed and purified by IMAC chromatography to allow for DRaCALA with recombinant protein. a) Small scale protein expression. **b)** A typical IMAC purification trace (PerR). UV trace = red. Concentration of imidazole = blue. **c)** Protein purity assessment with relevant fractions. **d)** Solubility test of PrsA, VraR, RpoY alongside control strain with their soluble and insoluble fractions. Relevant bands marked with a red asterisk. **e)** DRaCALA with recombinant protein and [α-^{32}P]-ppGpp, showing binding to the positive control RsgA.

The appropriate fractions were then pooled, followed by dialysis to remove imidazole, as not only can this cause solubility and activity issues with prolonged exposure, due to its amphoteric nature when preparing samples for SDS-PAGE, the boiling step can cause acid-labile bonds to hydrolyse (Bornhorst and Falke, 2000, Hamilton et al., 2003). Pooled fractions were then passed through a protein

concentrator (3 kDa) and their concentrations determined by a BioRad assay before analysing by 15% SDS-PAGE (Figure 5.2.5.1c). Despite expression being visible in the original lysates, some fractions contained little to no protein, as in the cases of KatA and PrsA. One explanation for this was that some of the protein was being lost in the insoluble fraction. In order to assess this, solubility was investigated by collecting the pellet after lysis and running it on SDS-PAGE alongside the respective lysate, revealing that both VraR and RpoY were trapped in the insoluble fraction (Figure 5.2.5.1d). Despite this, proteins that were successfully purified were subject to DRaCALA with adjusted concentrations to 10 μM, unfortunately no binding to ^{32}P-ppGpp was observable (Figure 5.2.5.1e).

5.2.6. Rationale for choosing group 2 proteins for further characterisation

No binding of ^{32}P-ppGpp was observed to the 4 purified proteins tested above. Therefore, we decided to select 7 random other proteins from our list of 60 for further investigation: Ac2460, Adk, MvaD, LysA UreE, HxlB and Ohr. We repeated the DRaCALA assay using whole cell lysates from protein over-expression strains (Figure 5.2.6). Overall these proteins displayed lower binding with respect to the positive control than the initial six, however we decided to characterise them further.

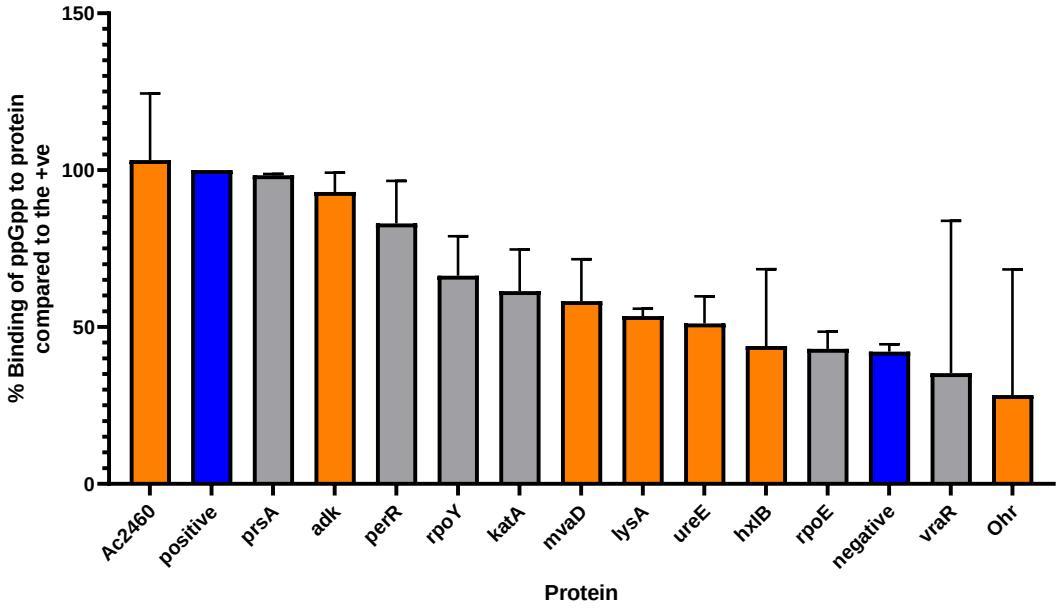

Figure 5.2.6: Comparison of percentage binding with respect to RsgA between both groups of proteins. The number of hits close to the threshold of the negative control for group 2 was closer than group 1. However, their identification in a previous genome wide DRaCALA screen along with their involvement in stress processes and metabolism highlighted them as interesting proteins. Group 1 is coloured grey. Group 2 is highlighted in orange with both negative (MBP) and positive (RsgA) controls highlighted in blue.

Acetyltransferase 2460 was chosen as it displayed a very strong signal in relation to the positive control RsgA. It is a hypothetical protein in terms of structure, predicted to function as an acetyltransferase. Other acetyltransferases, such as YfiQ in *E. coli*, have been found to acetylate the cAMP-CRP regulon in a ppGpp-dependent manner. The cAMP-CRP regulon controls transcription of energy related genes such as the *lac* operon(Ro et al., 2021). CRP is readily acetylated by acetyl-phosphate and its ability to

bind to DNA is influenced by its acetylation state. When considering ppGpp controls acetyl phosphate levels, this makes it an attractive target (Davis et al., 2018, Fernández-Coll and Cashel, 2018)

MvaD is involved in the essential mevalonate (MVA) pathway and is responsible for decarboxylating and dehydrating phosphorylated MVA phosphate to isopentenyl pyrophosphate (IPP) and its isomer dimethylallyl pyrophosphate (DMAPP) (Reichert et al., 2018, Bloch et al., 1959). These two molecules are precursors to isoprenoids, incredibly important molecules involved in aerobic respiration, cell wall synthesis, membrane stabilisation, protein translation and even gene transcription (Holstein and Hohl, 2004). One study utilising transcriptomics by Balibar *et al*, suggests that that *S. aureus* is capable of monitoring isoprenoid precursors and redistributing energy spent on certain pathways to ensure growth and survival. Strains with inactive proteins from earlier steps in the MVA pathway such as MvaA and MvaS could be rescued by the addition of MVA while, genes under expressing the *mvaK1-mvaD-mvaK2* operon were not able to be rescued by this addition, implying MvaD it is essential for a normal growth rate (Balibar et al., 2009).

LysA is involved in amino acid biosynthesis and catalyses the decarboxylation of the acetyl diaminopimelate to L-lysine and is responsible for the synthesis of the peptidoglycan cell-wall (Wiltshire and Foster, 2001).

Urease is a metalloenzyme that is integral in dealing with stress induced by acidic environments as it hydrolyses urea into carbon dioxide and ammonia, where the latter is then readily protonated, reducing the concentration of H^+ ions, raising the pH as a result (Cotter and Hill, 2003, Mobley et al., 1995). 90% of S*. aureus* strains possess urease, which is encoded by the gene cluster *ureABCEFGD*, with the main subunits being *ureA, ureB* and *ureC* while *ureE, ureF, ureG* and *ureD* encode accessory proteins (Murchan et al., 2004). These genes have been found to have increased transcription in biofilm growth, with *ureE* most likely acting as a building block for metallo-centre assembly (Resch et al., 2005).

HxlB is involved in the glycolysis pathway where it acts as a 6-phospho 3-hexuloisomerase converting between fructose 6-phosphate and d-arabino-hex-3-ulose-6-phosphate. With its role, HxlB is involved in gluconeogenesis and was found to be upregulated in planktonic cells when compared to biofilm cells in S*. epidermidis* (Martínez-García et al., 2021).

Ohr aids bacteria in dealing with oxidative stress and is involved in the previously mentioned PerR regulon. In a study with a *msaABCR S. aureus* deletion mutant, the *ohr* transcript was downregulated with increased susceptibility to organic peroxide stress (Pandey et al., 2019). An inducible expression plasmid of *ohr* was then transformed into this deletion mutant, with overexpression causing increased resistance when compared to wildtype (Pandey et al., 2019). Another study has shown it is important for increased survival inside macrophages (Saikolappan et al., 2015).

The adenylate kinase Adk is responsible for catalysing the transfer of a terminal phosphate group between ATP and AMP in a reversible manner, it is therefore heavily involved in the purine synthesis pathway. (p)ppGpp is synthesised form ATP and GTP/GDP meaning Adk plays a key role in both mediating ppGpp levels by limiting an essential substrate and cellular energy levels (Dzeja and Terzic, 2009).

5.2.7. IMAC purification of potential group 2 ppGpp interactors

Inducible strains of this new list of protein interactors were grown using the ORFeome library and the level of expression assessed (Figure 5.2.7a). All the strains were sufficiently expressing the desired proteins, with the exception of Adk, which was not included in this gel. They were then purified using IMAC chromatography as seen in the example purification of Adk (Figure 5.2.7b). The appropriate fractions were combined, and the proteins concentrated in a spin concentrator (3 kDa) where they are retained in the reservoir before measuring the concentration by BCA assay. The protein purity was then assessed by SDS-PAGE. The protein concentrations were : Ohr (570 µM), Ac2460 (477µM), Adk (257 µM), MvaD (223 µM), HxlB (89 µM), and LysA (26 µM), UreE (31 µM),h was mostly impure (Figure 5.2.7c). Proteins were then utilised in a DRaCALA experiment, where diluted samples (10 µM) were spotted alongside concentrated samples for each protein in triplicate. Again, the only protein to display binding was the positive control RsgA (Figure 5.2.7d).

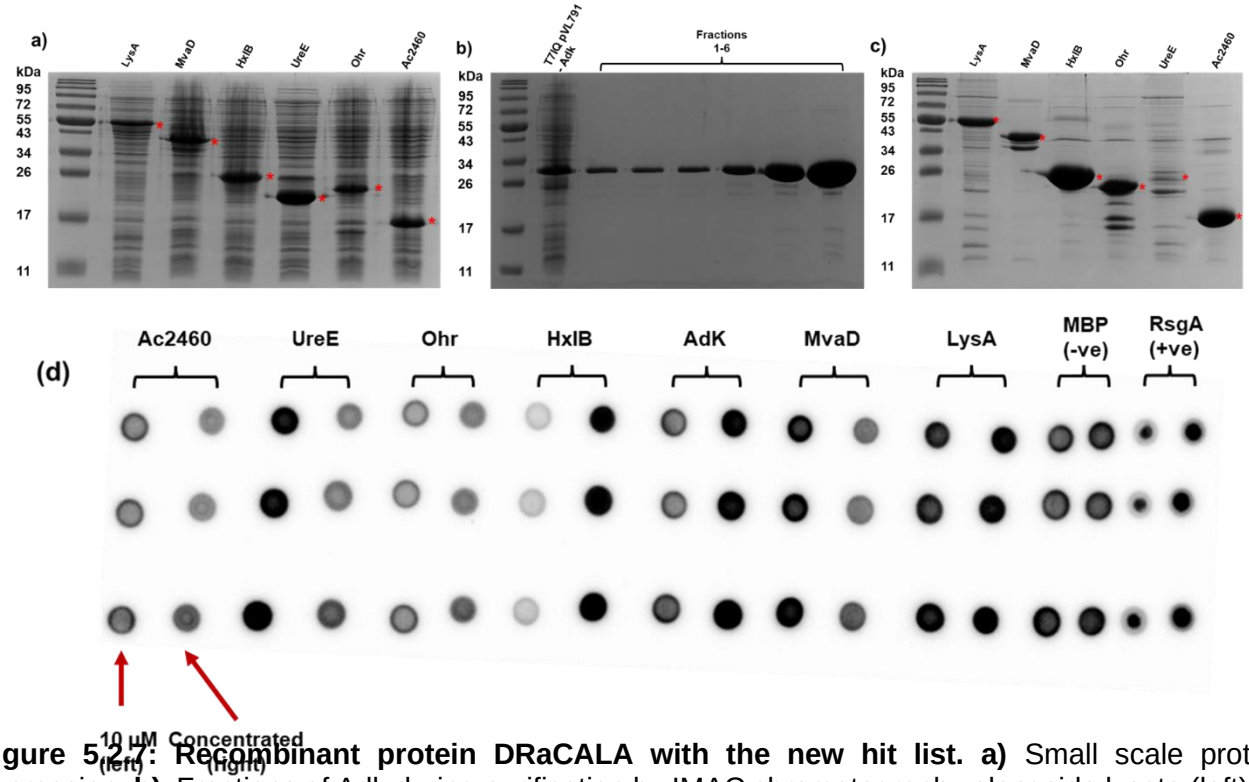

Figure 5.2.7: Recombinant protein DRaCALA with the new hit list. a) Small scale protein expression. **b)** Fractions of Adk during purification by IMAC chromatography alongside lysate (left). **c)** Protein purity after purification. **d)** DRaCALA was performed with diluted proteins (10 µM) to minimise interactions with impurities and concentrated samples in case the proteins were too dilute. Only the positive control RsgA displayed binding. Performed in technical triplicate.

All of the purified proteins appeared to be promising ppGpp-interacting candidates by whole cell lysate DRaCALAs when comparing to a known binder (Figure 5.2.3), and the incorporation of magnesium into the buffer to act as a co-factor had been accounted for. Upon reviewing the study performed by Wang *et al*, it was noted that a lot of their identified hits had high μM K_d values, much weaker than other binders previously characterised in our lab, such as the GTPases (Table 5.2.7).

Table 5.2.7: Summary of known ppGpp binding partners and their K_d values

*Red = Identified by Wang *et al*

Protein	Function	K_d (μM)
Gsk	Inosine guanosine kinase	0.4 ± 0.07
PurF	Glutamine amidophosphoribosyltransferase	1.6
SpeC	Ornithine decarboxylase	1.6 ± 0.05
RsgA	Ribosomal GTPase	2.2 ± 0.2
GdhA	Glutamate dehydrogenase	2.8 ± 0.04
Rbga	Ribosomal GTPase	2.9 ± 0.4
Gpt	Xanthine-guanine phosphoribosyltransferase	3.2 ± 0.05
HflX	Ribosomal GTPase	3.4 ± 0.4
Era	Ribosomal GTPase	4.2 ± 0.6
Hpt	Hypoxanthine phosphoribosyltransferase	32 ± 4
Upp	Uracil phosphoribosyltransferase	47 ± 3
GpmA	Phosphoglycerate mutase	52 ± 3
PurA	Adenylsuccinoate synthetase	61 ± 4
Cmk	Cytidylate kinase	79 ± 1
FolC	Dihydrofolate synthase	130 ± 3
Icd	Isocitrate dehydrogenase	132 ± 5
Gnd	6-phosphogluconate dehydrogenase	175 ± 3
Pgk	phosphoglycerate kinase	493 ± 30
Mpl	UDP-MurNAc0L-Ala-γ-D-Glu-meso-DAP ligase	752 ± 46

It is known that there is a large concentration range of (p)ppGpp in the cell, going from 50 μM in exponential phase to 1-2 mM during stress, and as highlighted by Steinchen *et al*, different cellular targets bind (p)ppGpp with vastly different affinities. This interaction modality, presumably, leads to an inhibition hierarchy, with different cellular processes inhibited at different stress levels. This inhibition hierarchy made us reassess the application of the DRaCALA method for the identification of low K_d interacting proteins. It is likely that we are missing binding to our tested proteins when performing

DRaCALA, as there is simply not enough ^{32}P-ppGpp (ca 20 nM) to saturate the binding site of weaker interactors. This left us searching for a new way of confirming ppGpp binding targets with several available methods.

5.2.8. ^{31}P NMR can be used to detect ppGpp binding proteins.

Before determining K_ds for every protein purified to date, which would be very labour intensive, we filtered out any definite non-binding proteins using NMR. No phosphates would be present in the proteins, while ppGpp has a distinct NMR trace due to its characteristic four phosphates. Therefore, if ppGpp were mixed with a potential binder a change in chemical shift could arise due to the shielding of the nuclei being altered or a change in intensity could occur due to binding. Firstly, this proof of concept was established using the known ppGpp binding protein Era, which binds with a K_d of 4.2 μM and a negative control in the form of MBP (Figure 5.2.8).

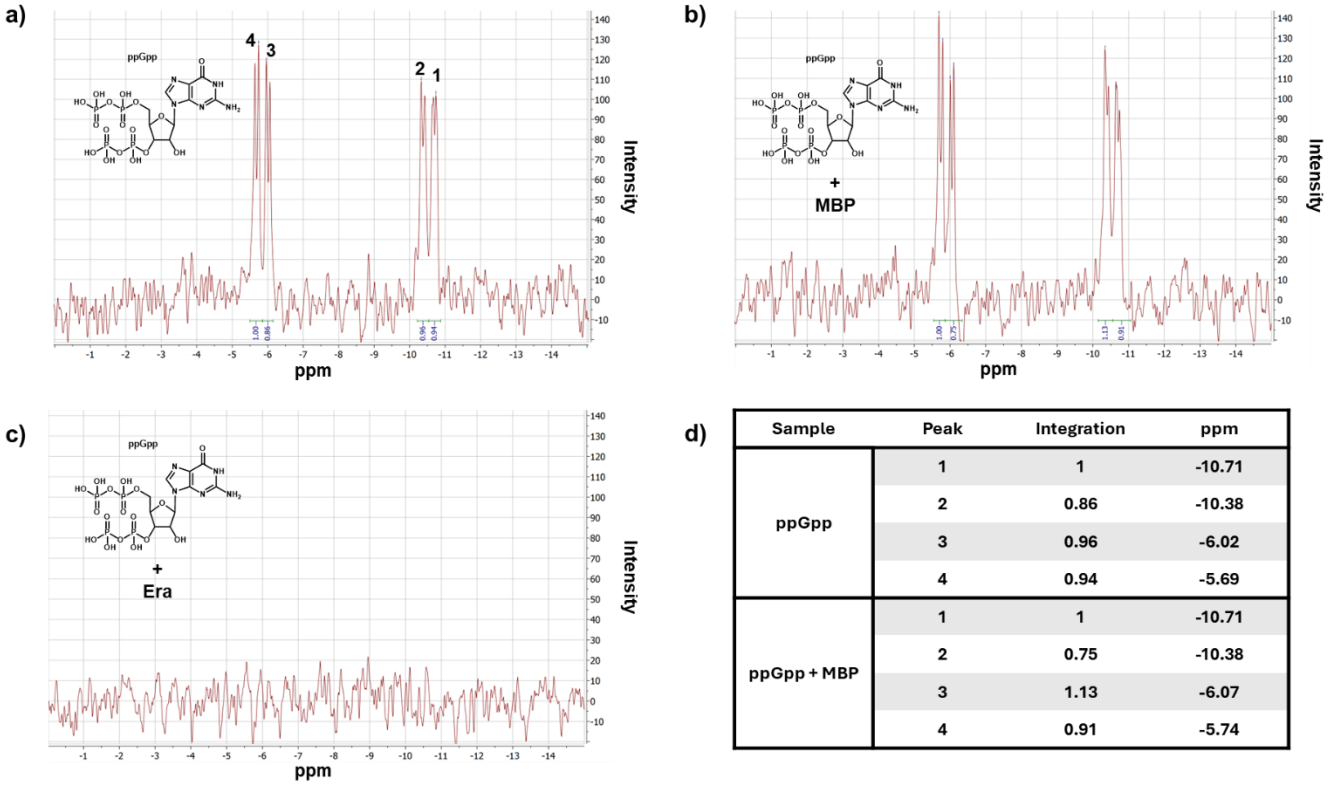

Sample	Peak	Integration	ppm
ppGpp	1	1	-10.71
	2	0.86	-10.38
	3	0.96	-6.02
	4	0.94	-5.69
ppGpp + MBP	1	1	-10.71
	2	0.75	-10.38
	3	1.13	-6.07
	4	0.91	-5.74

Figure 5.2.8: The signals produced by the phosphates of ppGpp in ^{31}P NMR are abolished by the GTPase Era. a) ^{31}P NMR trace of ppGpp with peaks numbered (167 μM). **b)** ^{31}P NMR trace of ppGpp in the presence of a non-binding protein MBP (45 μM) showing no difference (ppGpp:MBP, 4:1). **c)** ^{31}P NMR trace of ppGpp in the presence of the known binding protein Era (86 μM) showing the absence of peaks (ppGpp:Era, 2:1). **d)** Table showing the chemical shift (ppm) and integration values of each peak across a-b and how they are almost identical due to a lack of binding.

The presence of the ppGpp binding protein Era completely abolishes the signals produced by the phosphates of ppGpp. This can be explained by the tumbling rate of molecules in solution. Small molecules such as ppGpp tumble rapidly and as a result the decay of the NMR signal occurs much slower, whereas large molecules have a slower tumbling rate this results in a rapid signal decay, making

it difficult to distinguish signal from noise. Therefore, when ppGpp binds to Era in solution it will form a larger complex, with a larger tumbling time and signal is lost. As such, signal loss is a direct confirmation of binding and we can therefore conclude that Era is binding to ppGpp. In contrast, MBP did not shift the ppGpp signal at all, with virtually no difference in integration value or chemical shift.

Therefore, this methodology was used to aid in filtering our hit list by first investigating the binding of proteins of high purity - HxlB, Adk, Ac2460, Ohr, and MvaD. The remaining proteins were put aside to be further purified by size exclusion chromatography. $MgCl_2$ (10 mM) was included in the buffer to ensure that if these proteins were weak binders the necessary co-factor was present to facilitate binding, however, this changed the appearance of peaks 1-2 for ppGpp, perhaps due to chelation (Figure 5.2.8.1a).

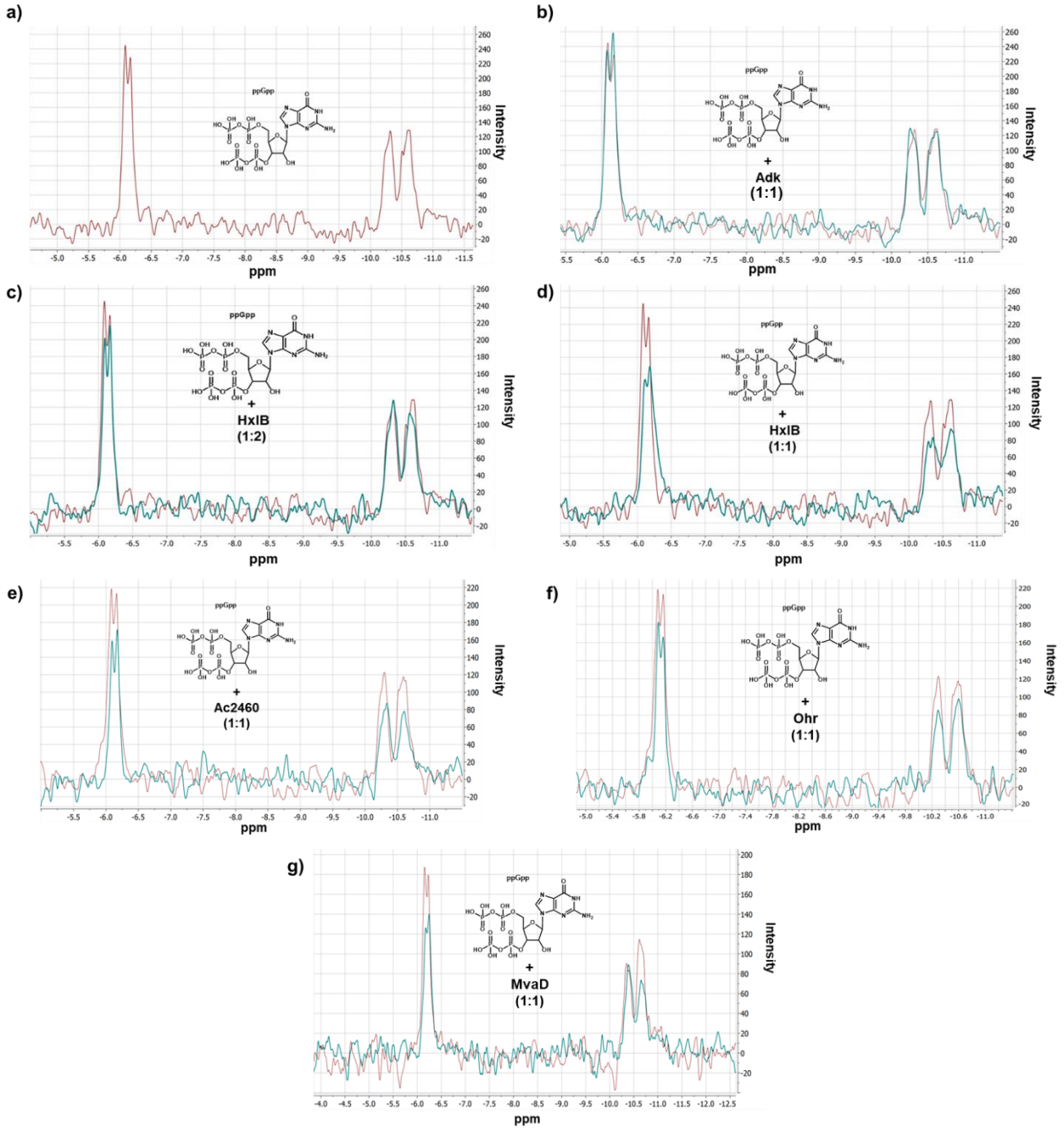

Figure 5.2.8.1: ^{31}P NMR allows for the identification of four putative ppGpp binding proteins. a) A P^{31} NMR trace of ppGpp for calibration in the presence of magnesium with the merging of two peaks ~-6 ppm **b)** ppGpp mixed in a 1:1 ratio with Adk. No change in peak integration or chemical shift occurred. **c-d)** ppGpp mixed with HxlB in a 1:1 and 2:1 ratio respectively. There was a progressive decrease in integration of both sets of peaks at ~-6ppm and ~-10.5 ppm when the concentration of HxlB was increased. **e-f)** In the presence of Ac2460, Ohr and MvaD there was a reduction in signal of ppGpp, suggesting binding towards the proteins. Concentration of ppGpp (167 μM) and magnesium (10 mM). For more details see section 2.4.4.4 of materials and methods.

Using this ^{31}P NMR technique, four of these five proteins were highlighted as potential binders, with visible differences being established between the ppGpp standards and ppGpp mixed with the proteins of interest (Figure 5.2.8.1b-g). Adk did not present a noticeable difference - a higher concentration of protein may have produced a change in signal. HxlB was initially used in a protein:ppGpp (1:2) ratio and a slight decrease in signal was observed (Figure 5.2.8.1c). The concentration was later altered to an equal ratio where the signal decreased further (Figure 5.2.8.1d), supporting the notion of HxlB being a ppGpp-binder. Ac2460, Ohr and MvaD all decreased the signal of their respective standard when in a 1:1 ratio, hinting towards a degree of ppGpp binding. It was noted, however, that most of these proteins must bind with a lower affinity than Era, in line with the lack of obvious binding observed when using DRaCALA.

In order to characterise this binding, we would need to determine a K_d value. Characteristion is possible using NMR techniques in a titration series, however, there were several reasons this method was not suitable: The amount of protein required, the length of each run lasting four hours alongside spectrometer time being precious. All in all this did not fit with the number of protein interactions we were aiming to elucidate. We also were not aiming to characterise binding at the molecular level, as it was not appropriate at this point in the project. However, once appropriate hits were identified it would be interesting to revisit this technique and perform a titration to characterise the exact interactions occurring in binding i.e. which protein residues are involved in binding.

5.2.9. Investigating ppGpp binding to HxlB using microscale thermophoresis

In order to reduce the amount of sample used, we proceeded with microscale thermophoresis (MST) as the method for determining a K_d value. This technique has several advantages over other commonly used approaches such as isothermal calorimetry or thermashift assays, namely the reduced amount of protein required.

Thermophoresis can be described as the movement of particles in the presence of a temperature gradient. During MST, fluorescently labelled protein is mixed with ligand in a capillary before using an IR-laser to induce a microscopic temperature gradient, emanating outwards from the centre (Figure 5.2.9). This gradient causes fluorescently labelled proteins present on the higher temperature side of the gradient (at the centre) to experience more collisions with higher energy molecules, thus they move down the temperature gradient towards the outer edges until a steady state distribution is reached (Wang et al., 2012b). Outwards movement is determined by measuring the homogenous fluorescence distribution inside the capillary before heating and after. However, temperature related intensity changes also occur, where the intensity of the fluorophore is altered by temperature gradient; conformational changes or proximity of ligands (Baaske et al., 2010). When the fluorescently labelled protein is bound to a ligand it travels through the solution slower, so there is a smaller decrease in relative fluorescence. Protein ligand binding is determined by a sigmoidal binding curve obtained by serially diluting the binding substrate and plotting the fluorescence against the ligand concentration. The dissociation constant (K_d) can then be calculated by applying the law of mass action, which states that reaction rate between proteins and ligand is proportional to the product of the concentration of the reactants (Guldberg and Waage, 1964).

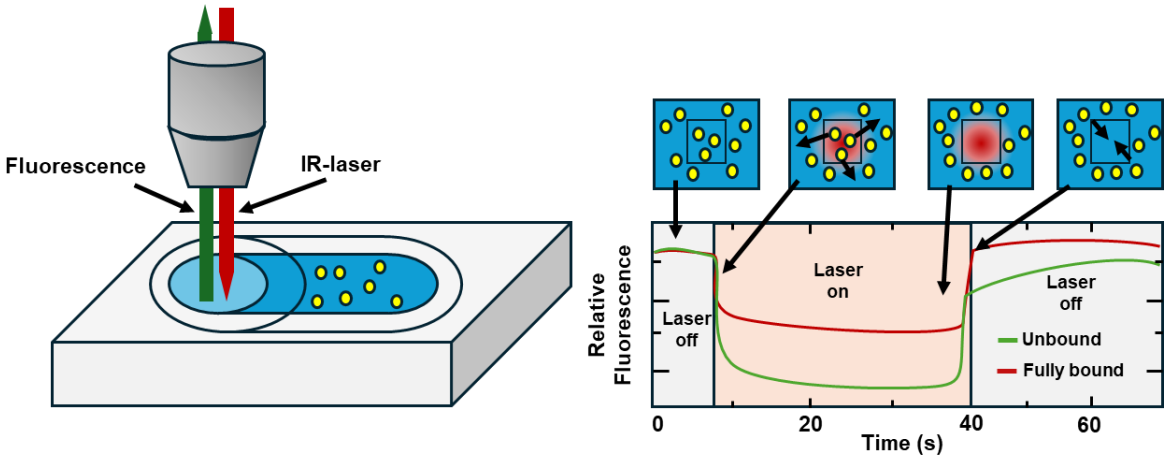

Figure 5.2.9: Schematic of microscale thermophoresis (MST) including an example trace. MST relies on the induction of a temperature gradient by an infrared. This gradient originates at the centre of the capillary that contains a mixture of fluorescently tagged target (protein) and ligand. Causing the fluorescently tagged molecules to travel down this gradient, and such, a decrease in relative fluorescence at the centre of the capillary. The gradient soon dissipates eventually returning molecules to a homogenous distribution upon cooling. Fluorescently tagged molecules bound to ligands (red) will travel away from this hotspot slower than unbound molecules (green), causing a smaller decrease in fluorescence. Upon repeating with serial dilutions of the ligand with the binding affinity of the ligand eventually being determined.

HxlB provided the largest change in signal when assessing binding by NMR spectroscopy and so it was chosen to be further investigated by MST. The incorporation of a fluorescent tag was required, as the synthesis of a plasmid capable of expressing the desired His-HxlB protein with an added fluorescent tag like green fluorescent protein (GFP) was not time efficient and the GFP fluorophore could have affected binding. We made use of the monolith His-tag labelling kit RED-Tris-NTA 2nd generation dye, which exhibits high affinity binding to 6xHis-tags. Before we could probe the binding of ppGpp to HxlB, we needed to assess the binding of the monolith dye to the His-tag of HxlB (Figure 5.2.9.1).

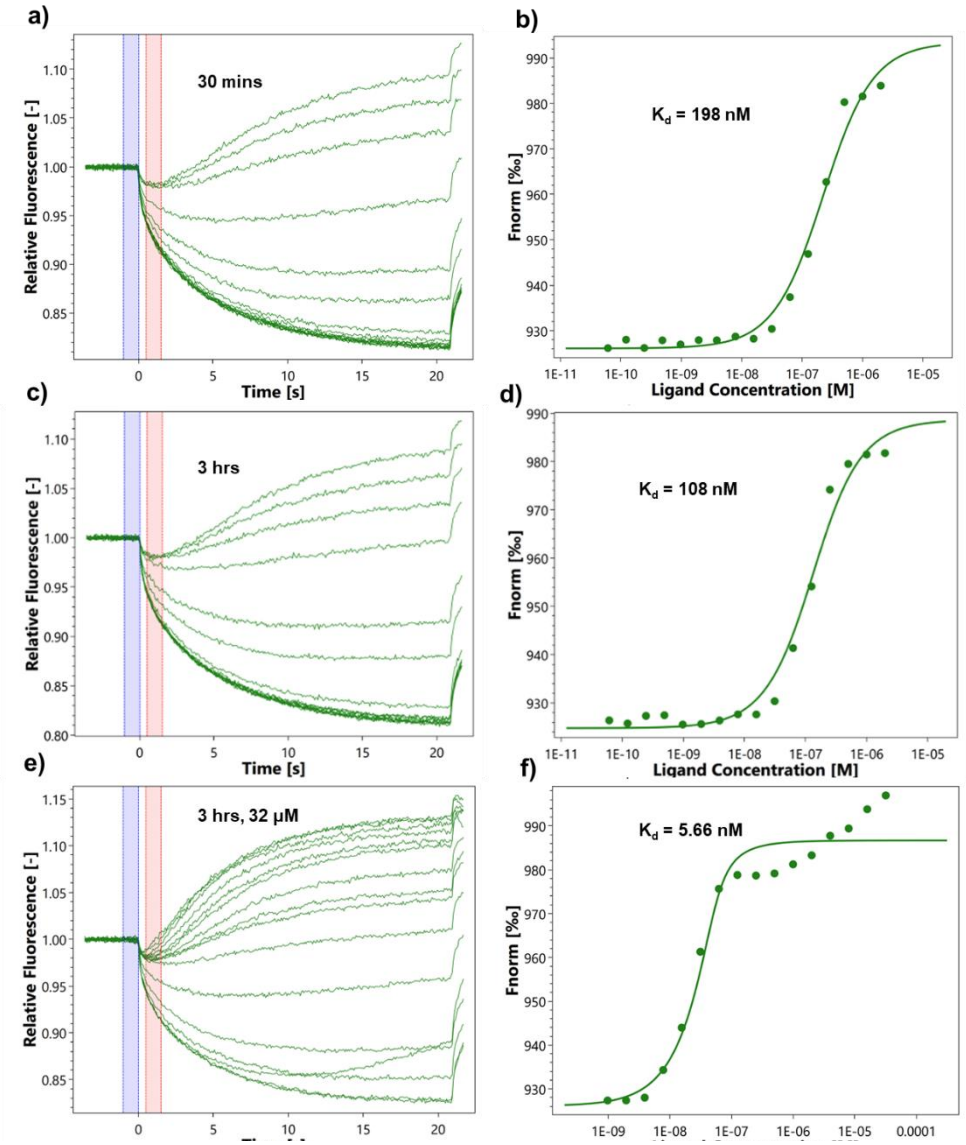

Figure 5.2.9.1: MST traces alongside binding curves between HxlB and monolith-red his-tag dye. The monolith dye has high affinity for 6xHis-tags allowing for the fluorescence change occurring during MST to be determined for HxlB. **a-b)** After a 30 minute incubation the calculated K_d (198 nM) for the binding of HxlB to the dye was too low for use in determining the binding affinity of HxlB to ppGpp. **c-d**) A longer incubation time was used which almost halved the K_d (108 nM). **e-f)** In order to further decrease the K_d the starting concentration of the protein was increased to avoid null points at the bottom of the sigmoidal curve allowing for a more accurate K_d to be determined (5.66 nM). Fluorescence wavelengths $\lambda_{Excitation}$ = 650 nm, $\lambda_{Emission}$ = 670 nm. Experiments performed in technical triplicate.

The procedure was performed as described in section 2.4.5.3 by mixing HxlB with the dye and incubating the protein for 30 mins. However the K_d obtained was too weak, ifor use with the dye (Figure 5.2.9.1a-b). In order to improve the K_d , the incubation time was increased to 3 hrs, which dramatically increased the K_d value towards an acceptable range (Figure 5.2.9.1c-d). Despite the improvement in K_d, the sigmoidal curve did not display saturation along with a lot of null points ranging from 1^{-10} M to 1^{-8} M. A more accurate value was soon determined by increasing the concentration of protein present in the first tube of the dilution series from 2 µM to 32 µM, with the intention of leaving around three points at the lower plateau, allowing us to establish the correct method for use with ppGpp (Figure 5.2.9.1e-f).

Following the optimisation of dye attachment, the dye (100 nM) was adhered to the protein (200 nM) and spun to remove aggregates leaving a 50 nM solution. The dye-protein complex was mixed with serial dilutions of ppGpp starting at 1 µM (Figure 5.2.9.2a-b). There was a complete absence of binding using these concentrations. In an attempt to remedy this absence, the concentration of HxlB to dye was adjusted to 32 µM, ensuring that HxlB was nearly saturated, however, this adjustment did not improve the degree of binding (Figure 5.2.9.2c-d).

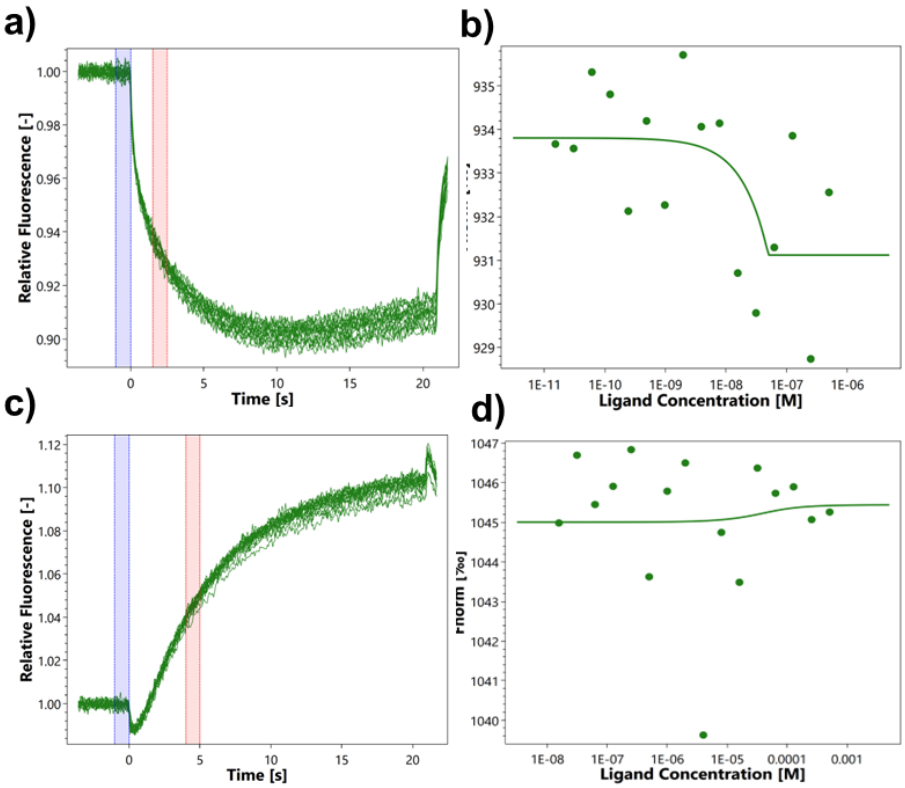

Figure 5.2.9.2: MST traces and binding curves of the interaction between HxlB and ppGpp. a-b) The initial concentrations of HxlB (50 nM) and ppGpp (1 µM) showed no observable interaction. **c-d)** To remedy this, the concentration of HxlB was increased to 32 µM in an attempt to maximise binding to the dye. The increased HxlB concentration made little change, this was attributed to a lack of Mg^{2+} ions in the buffer which were present in the ^{31}P NMR binding experiments.

The conclusion from the MST experiment was that HxlB may be a weak ppGpp binder and as a result it likely requires Mg^{2+} as a cofactor, as Mg^{2+} was present when binding was observed by ^{31}P NMR. However, Mg^{2+} was not able to be readily induced into the buffer system used in these experiments (PBS-T) due to solubility issues causing precipitates. To avoid solubility issues , proteins were dialysed into a HEPES buffer system containing Mg^{2+} and NP-40 as a replacement detergent for TWEEN-20 (Khavrutskii et al., 2013). The new buffer system provided poor dye-labelling efficiency even when increasing concentration of the dye to 50 nM, the K_d stayed at too high of a level. Regardless, binding of HxlB to ppGpp was investigated, which unsurprisingly did not produce a sigmoidal curve, indicating that the buffer system needed optimisation. Optimisation would be time consuming, and dye-reagent was limited, and so was not continued. The dissociation constant of HxlB was later determined by another member of the laboratory by isothermal calorimetry (ITC) and yielded a K_d of 25.3 μM.

5.2.10. *In vitro* assessment of HxlB activity in the presence of ppGpp

Fructose-6-phosphate (F6P) is a glycolytic pathway intermediate that is readily phosphorylated to fructose 1,6-biphosphate (Figure 5.2.10a), which undergoes a series of chemical transformations to eventually produce pyruvate, feeding into the tricarboxylic acid (TCA) cycle. F6P is also linked to the non-oxidative pentose phosphate pathway where it is isomerised by HxlB in order to produce d-arabino-hex-3-ulose-6-phosphate, which is later transformed into more useful pentose precursors for nucleotide synthesis (Figure 5.2.10.1). In order to investigate the effect ppGpp has on the enzymatic activity of HxlB and its metabolites, we utilised an assay from Merck that is capable of linking F6P levels to fluorescence. Using the provided F6P stock, a standard curve was plotted using F6P sample concentrations of 0.1 - 0.6 nmol alongside a blank and fluorescence intensity ($\lambda_{excitation}$ = 535/ $\lambda_{emission}$ = 587 nm). The rationale behind this was to utilise the linear regression of the plot to determine the slope. F6P was then incubated with HxlB in a 1:10 ratio, with assay buffer as a negative control. HxlB was also incubated with ppGpp and F6P, to determine if ppGpp can inhibit the enzymatic reaction (Figure 5.2.10b). After 10 mins the relative fluorescence intensity was recorded and converted to nmol of fructose by using the previously made standard curve and rearranging y = mx+c to solve for x using the linear portion of the curve. If HxlB was inhibited by ppGpp, the concentration of F6P should be a similar level to the no-HxlB negative control. This was the case, however there was not a significant difference by one way ANOVA comparison between the sample containing HxlB and the ppGpp sample or negative control, indicating that the assay needs to be optimised.

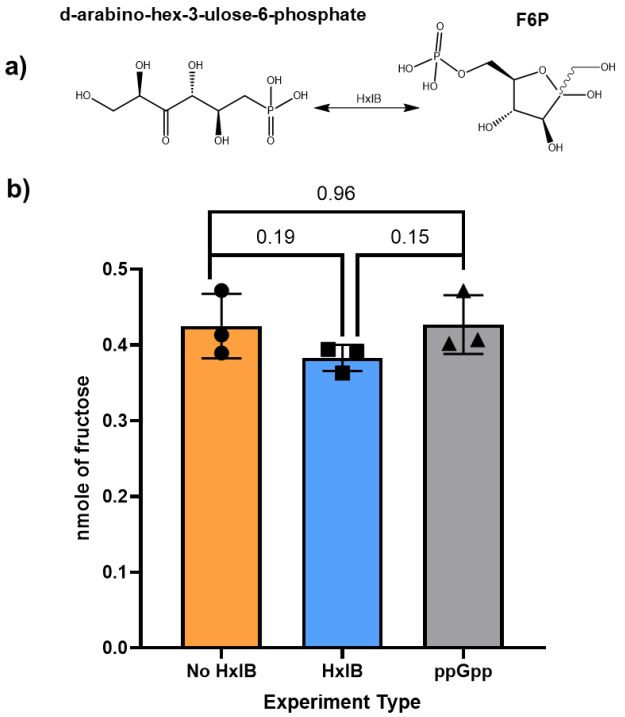

Figure 5.2.10: HxlB catalyses the isomerisation of fructose 6-phosphate to d-arabino-hex-3-ulose-6-phosphate but is not significantly inhibited by ppGpp. a) Reaction scheme of the isomerisation catalysed by HxlB. **b)** Summary of the fructose-6-phosphate assay with a slight difference in nmol of fructose between HxlB and HxlB in the presence of ppGpp. Difference was not significant by way of an unpaired parametric t-test with a p-value threshold of 0.05.

5.3. Discussion

In this chapter, we attempted to characterise the binding of ppGpp to a number of potential interacting proteins. Firstly we used DRaCALA with whole cell lysates that contained over expressed proteins of interest as DRaCALA had been greatly successful in previous interaction studies such as Corrigan *et al* and Zhang *et al*. The DRaCALA methodology successfully indicated several proteins were capable of binding to ppGpp, prompting us to select candidates for purification. Purification originally began with group of six proteins RpoY, RpoE, PerR, VraR, PrsA and KatA which were purified and used in a recombinant protein DRaCALA experiment which yielded no successful binders. However, there were several proteins that were not successfully purified using the IMAC methodology meaning they were absent from ppGpp interaction experiments. To effectively purify some of these proteins (PrsA, VraR, RpoE and RpoY) we decided to introduce an MBP-tag with the aim of improving solubility, while fusing an MBP-tag to PrsA could provide a different avenue for purification with the potential of using amylose resin (Riggs, 2000). The attachment of an MBP-tag was only successful for RpoY, forming RpoY-MBP with a linker that was susceptible to cleavage by thrombin after purification. This cleavage was successful. There was a large difference in size between free MBP and the desired MBP-free RpoY meaning size exclusion would have been suitable for isolating RpoY, however, this was not performed due to time pressures. VraR and RpoE were later purified using nickel resin chromatography and gravity filtration followed by passage over a PD-10 desalting column to remove imidazole before concentrating. PrsA was cleaned up slightly using a MonoQ column, which is an anion exchange column that uses a salt gradient to elute the protein of interest, before effectively purifying using nickel-NTA resin and phosphate buffered imidazole. These proteins were of sufficient purity to assess binding to ppGpp but this was not performed due to time constraints.

Due to the lack of success in the group 1 proteins we decided to investigate a second set of proteins termed group 2 comprising, HxlB, Adk, LysA, UreE, MvaD, Ohr. Purification of these proteins by IMAC allowed for recombinant DRaCALA, which again led to no proteins displaying a significant signal, this was attributed to the low amount [α-^{32}P]-ppGpp (1.6 nM) not being sufficient for the detection of weak binding proteins.

While DRaCALA was not sensitive enough to determine binding for our proteins, ^{31}P NMR helped to filter our hit list and was essential for identifying four putative ppGpp binding proteins (HxlB, Ohr, MvaD and Ac2460). Upon grouping these four proteins alongside our other purified proteins: VraR, PrsA, RpoY and RpoE, we thought it would be interesting to investigate their binding further using *silico* methods to identify likely ppGpp binding sites along with key residues. With this information, mutant proteins could be expressed that alter residues deemed important for binding. These variant proteins could then be used to compare the difference in ppGpp interactions compared to wildtype protein, allowing for the identification of key interacting residues. These *in silico* techniques are currently

underway for HxlB using a predicted protein structure as there are currently no crystal structures available.

With P^{31} NMR identifying potential binders, MST seemed a promising technique that allowed for the use of small quantities of protein, however, there are teething issues associated with this technique. The inclusion of Mg^{2+} seems essential for aiding binding of ppGpp to weak protein binders, which is not possible in the PBS-T buffer suggested for use by Monolith, while the dye had poor affinity to HxlB in the alternative buffer system we trialled. Wienken *et al* states that "the affinity of biomolecules are highly dependent on the surrounding matrix" meaning that there can be decreases in affinity caused by interactions with the buffer system due to viscosity or ionic strength of other components (Wienken et al., 2010). Meaning the buffer system required optimisation, along with other details of the method, for example increasing MST power, or laser intensity to increase the signal, however, these changes can also increase noise and at high intensities dissociation of the dye from the 6xHis-tag occurs (Wienken et al., 2010). To circumvent issues associated with MST when attempting to characterise other proteins of interest, the temperature or media used for protein expression could be optimised to improve the yield of protein. A higher yield of protein allow for more definitive methods such as isothermal calorimetry to be used, as ITC was successful for determining a K_d for ppGpp to HxlB. It would also be worth choosing and assessing some other proteins from the initial significant protein list in the same manner.

S. aureus is capable of surviving acidic conditions and readily colonises the host's skin (pH ~4.7) but is killed rapidly at pH 2 (Lambers et al., 2006). Adaptations that allow survival in these acidic environments are typically caused by the induction of *sodA via* the *sigB* pathway. As *sodA* mutants exhibit acid sensitivity, implying acid stress eventually leads to oxidative stress (Clements and Foster, 1999, Cotter and Hill, 2003). Therefore, it is imperative that *S. aureus* has systems in place that allow it to survive in acidic environments high in reactive oxygen species such as the ones encountered when internalised by neutrophils. The fact that PerR, KatA and Ohr were all pulled down by the capture compound suggests that the likelihood of ppGpp binding to proteins involved in the oxidative stress response is high. This is corroborated by the observation that Ohr displayed some binding by slightly reducing the ppGpp signals *via* NMR.

The current F6P assay displayed a slight difference when comparing HxlB and its function to HxlB in the presence of ppGpp, however the difference was not significant, potentially due to the assay buffer, temperature, incubation time or even the ratio of protein to nucleotide. The inhibition of HxlB by ppGpp may prevent the formation of intermediates in the pentose phosphate pathway such as ribulose-6-phosphate potentially limiting purine nucleotide synthesis and GTP synthesis as a result. In order to gain a more complete understanding of how ppGpp affects glycolysisoptimisation of the F6P assay alongside metabolomics examining the abundance of certain glycolytic metabolites is currently

underway. The identification of HxlB as a ppGpp binding protein is a great success for this capture compound approach as there has not previously been an enzyme identified in the glycolysis pathway that has been suggested to have a role in the stringent response. By reanalysing our 162 hits, we subsequently noticed that 19 of these, including HxlB, are involved in key metabolic pathways, including glycolysis, the pentose phosphate pathway and purine metabolism (Figure 5.3). These data provide exciting new insights into the possible role (p)ppGpp has in regulating central metabolism, which we aim to confirm with our metabolomic assays in the near future.

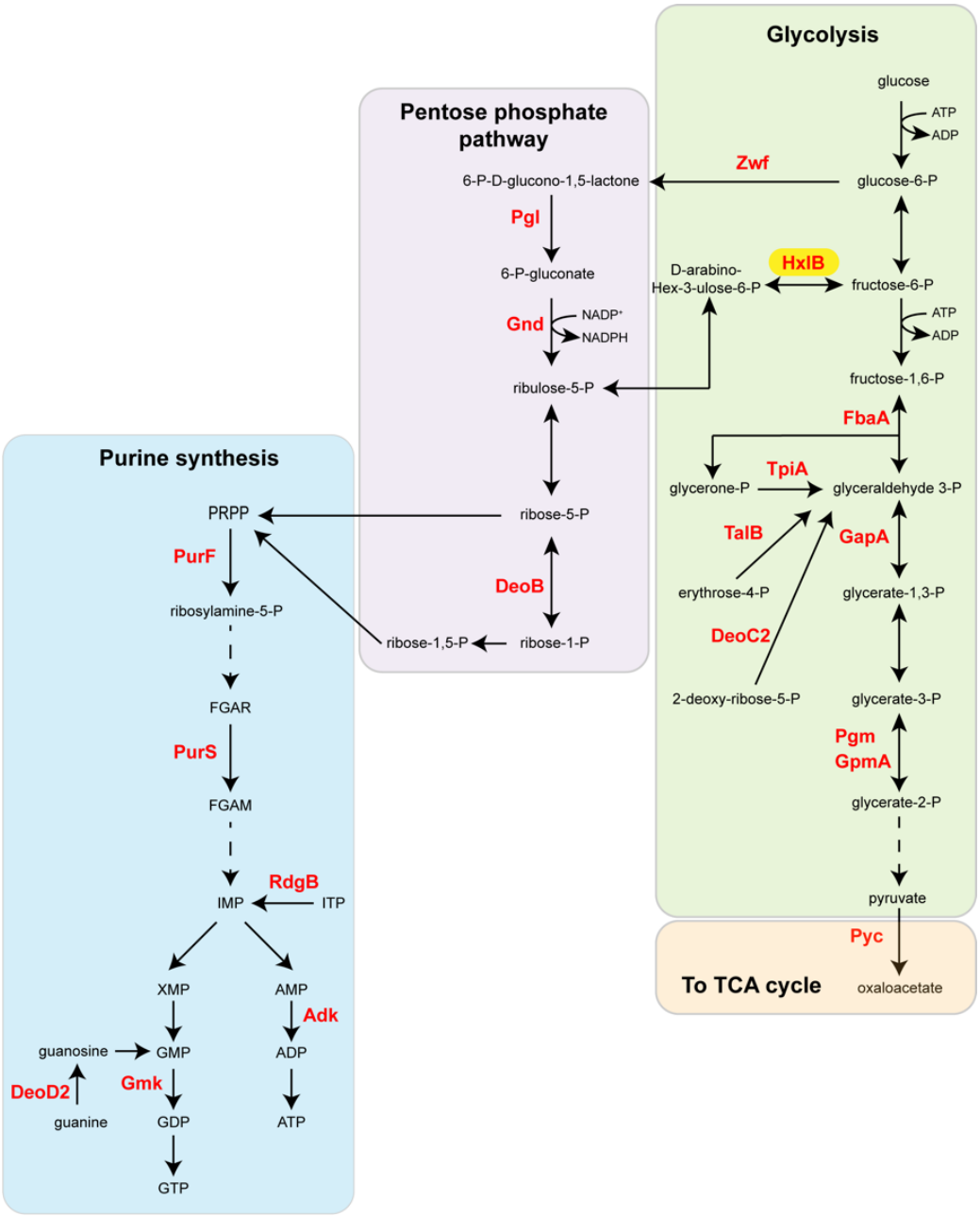

Figure 5.3: A summary of a trifecta central carbon metabolism pathways; glycolysis, pentose phosphate pathway and purine nucleotide synthesis.Proteins deemed statistically significant by the pull-down assay, are highlighted in red, indicating that a large number of ppGpp binding proteins are likely involved in metabolism. The main protein of interest in this study - HxlB is highlighted in yellow. While other proteins of note such as PurF previously identified by Wang *et al* and GpmA in both the former and Haas *et al*.

Overall, this chapter described the identification of a novel-ppGpp binding partner HxlB. This protein is involved in glycolysis, a pathway that has not previously been associated with the stringent response. The identification of this protein along with several other putative targets involved in various processes linked to stress, confirms that our capture compound methodology described over the past three chapters is efficient for the isolation of previously unrecognised ppGpp-interactors.

Chapter 6

Development of a ppGpp quantification assay using an enzyme linked immunosorbent assay (ELISA) and the fluorescent chemo-sensor PyDPA

6.1. Introduction

Bacteria are consistently exposed to stressors from their external environment including nutrient starvation/reactive oxygen species and antibiotics. As a result of this bacteria are capable of fine tuning certain cellular processes to provide more favourable survival conditions through the use of (p)ppGpp. Levels of (p)ppGpp are strictly regulated at around 10-100 μM to allow for optimal growth and homeostasis while basal levels are more difficult to determine with some estimates at 10-90 pmol/OD (Zborníková et al., 2019, Varik et al., 2017, Steinchen et al., 2020). It has previously been shown that wild-type and (p)ppGpp^0 strains of *Actinobacillus pleuropneumoniae* have different transcription profiles, with basal levels of (p)ppGpp regulating the transcription of genes involved in *de novo* synthesis of purine nucleotides (Li et al., 2020). In (p)ppGpp^0 *B. subtilis*, GTP levels are elevated, this leads to the dysregulation of the GTP-dependent transcriptional repressor CodY. When levels of GTP are high, CodY is activated and prevents the transcription of genes involved in the biosynthesis of branched chain amino acids (Steinchen et al., 2020, Kriel et al., 2012, Kriel et al., 2014, Molle et al., 2003). In a similar manner, (p)ppGpp^0 *S. aureus* also suffer detrimental effects demonstrated by its inability to survive in minimal media. This is most likely explained by the shared GTP-binding motif present in CodY between both strains (Pohl et al., 2009, Petranovic et al., 2004). Therefore, despite low concentrations, basal levels of (p)ppGpp are important for cell survival and stress tolerance (Salzer and Wolz, 2023). This is further exemplified by (p)ppGpp null strains of *E. coli* that are incapable of growing in minimal media due to their amino acid auxotrophic phenotype (Potrykus et al., 2011, Salzer and Wolz, 2023).

Under serious stress, (p)ppGpp levels are capable of exceeding 1 mM within seconds of the stressor being detected, this large concentration range allows for the mediation of multiple cellular processes including: transcription, translation, ribosome biogenesis DNA damage and carbon metabolism, allowing the stringent response to prioritise processes required for survival instead of acting as an all or nothing switch (Steinchen et al., 2020, Irving et al., 2020).

Gaining an insight into the intricacies of the SR under certain (p)ppGpp concentrations is therefore a critical point into understanding this stress response further. While several methodologies exist for probing (p)ppGpp levels they are often costly, laborious, and require a specialist skillset. As such, a simple, inexpensive and safe methodology for the quantification of (p)ppGpp remains elusive. In this chapter we describe the use of a highly versatile and sensitive enzyme-linked immunosorbent assay (ELISA) technique, as well as a fluorescent chemo-sensor-based approach to detect (p)ppGpp levels in cell lysates.

6.2. Results

6.2.1. Enzyme linked immunosorbent assay (ELISA)

Since their development in 1972 enzyme linked immunosorbent assays (ELISAs) have been implemented to quantify substrate levels in solution(Engvall and Perlmann, 1972). There are several variants of these assays: direct, indirect, sandwich and competition, however, they all function under the same premise: the biomolecule of interest (antigen) is coated to an immobilised surface and a "reporter" antibody is added (enzyme-antibody conjugate). Upon incubating the new complex with the enzyme specific substrate, a measurable read out occurs in the form of fluorescence or a shift in absorbance range allowing for quantification (Alhajj et al., 2024).

As a result, ELISA methodologies have been used to measure levels of various nucleotides such as c-di-AMP that are plagued by the same quantification issues associated with (p)ppGpp. With the identification and purification of the novel pneumococcal c-di-AMP binding protein CabP and the commercial production of biotin labelled c-di-AMP, a competitive ELISA methodology was developed (Underwood et al., 2014, Bai et al., 2013, Bai et al., 2014). The assay functions as described above in a 96-well plate, with the key change being incubation of the antigen (CabP) with both c-di-AMP and biotin-c-di-AMP. Streptavidin-HRP (horse radish peroxidase) is then added, followed by the addition of a reactive substrate to provide a measurable signal. This high throughput methodology is competitive, with an inverse relationship between signal intensity and the amount of c-di-AMP present in lysates as it outcompetes the biotinylated nucleotide analog. With a sensitivity range as low as ~10 nM this procedure is suitable for analysis of cell lysates (Underwood et al., 2014).

6.2.2. Development of an ELISA for quantification of ppGpp

Using the same principles described above, we set out to develop our own competitive ELISA (Figure 6.2.2). Here, the previously described biotin-ppGpp capture compound (**19**) would function in a manner analogous to biotin-c-di-AMP and would compete with native ppGpp for binding to a purified recombinant protein. If bound, the biotin-ppGpp could be detecting using streptavidin-HRP along with 3,3′,5,5′-Tetramethylbenzidine (TMB) acting as the measurable chromogenic substrate. TMB is readily oxidised by HRP with the addition of one electron, shifting its absorbance to the blue range ($\lambda_{Absorbance}$ = 288 nm → $\lambda_{Absorbance}$ = 370 nm). The addition of a further electron by oxidising with sulphuric acid leads to a yellow coloured di-cation that absorbs at $\lambda_{Absorbance}$ = 450 nm, a distinct enough absorption to be measured (Zhang et al., 2020, Josephy, 1985).

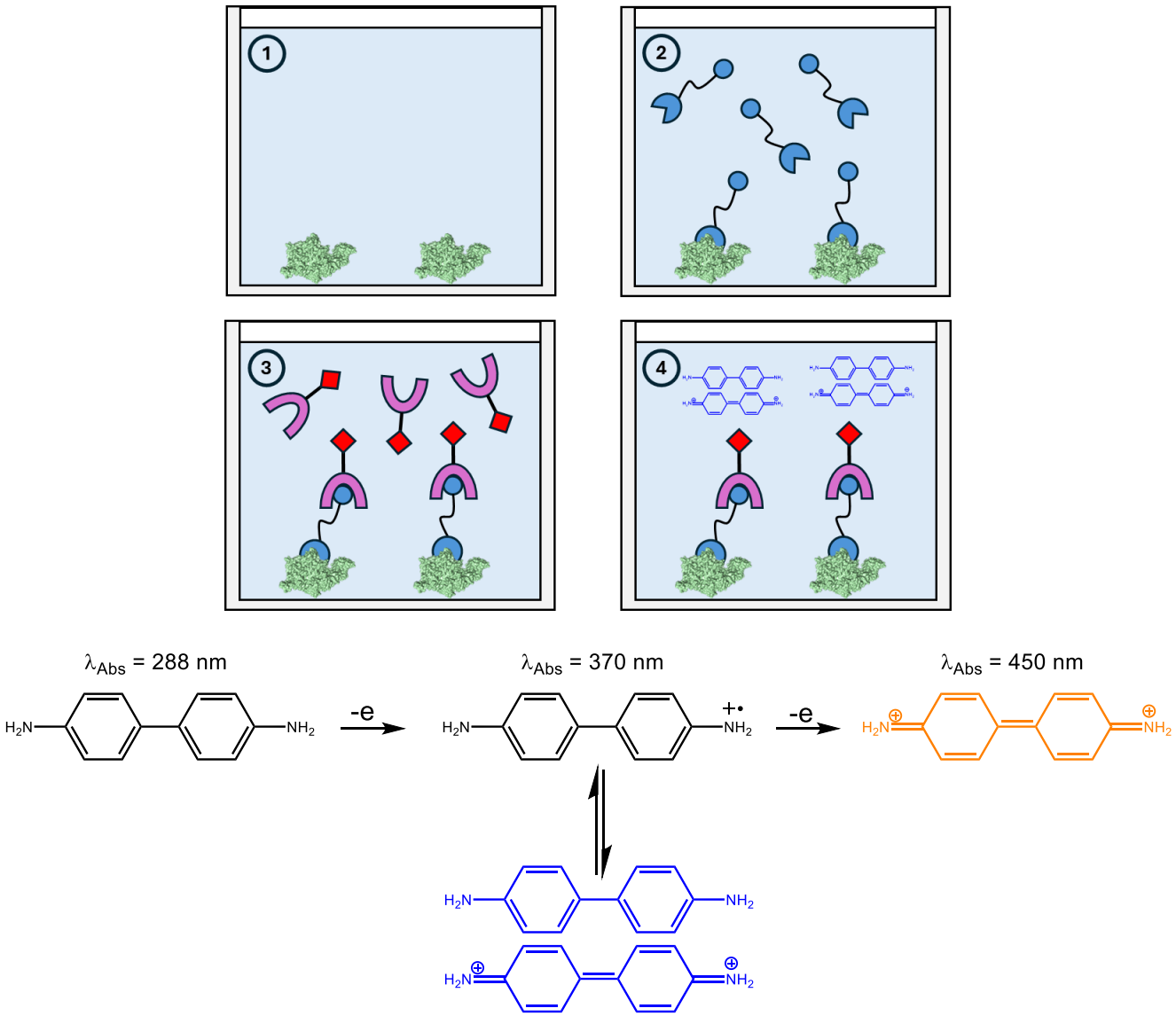

Figure 6.2.2: Summary of the designed ELISA: 1. The wells are coated with the binding protein and BSA is used to block any on-specific binding sites **2.** The protein is incubated with the capture compound allowing for binding (biotin-ppGpp) **3.** After washing away unbound capture compound addition of Streptavidin-HRP leads to the formation of the biotin-streptavidin-complex **4.** Upon its addition, TMB is readily oxidised by streptavidin-HRP through the addition of one electron, forming its blue charge transfer complex ($\lambda_{Absorbance}$ = 370 nm). Further oxidation occurs through the addition of sulphuric acid when the assay is complete, forms a yellow di-cation ($\lambda_{Absorbance}$ = 450 nm) that is used for measurements.

When exploring proteins to coat the well of the 96 well plates, the GTPase HflX was chosen as it has a low micromolar binding affinity with a K_d of 3.4 ± 0.4 µM for ppGpp (Bennison et al., 2021). A dose response curve was firstly established using serial dilutions of capture compound to gauge the binding of the capture compound to HflX in comparison to a bovine serum albumin (BSA) control (Figure 6.2.2.1a). Here, we observed increased binding of biotin-ppGpp to HflX as the ligand concentration increased, while no binding to BSA occurred. However, the results which displayed a large amount of variability. The sensitivity limit was deemed to be around 50 nM, which in principle is suitable for detection, however, the amount of capture compound required (25 pmol) per run was not feasible when

considering the amount we had available (290 nmol), so a concentration just above the sensitivity limit was chosen (64 nM). Equal concentrations of nucleotides were then used in competition assays to determine whether the binding could be blocked firstly by unlabelled ppGpp, and secondly by structurally similar nucleotides. However, no significant differences in binding occurred when tested by one-way ANOVA compared to no competition (Figure 6.2.2.1b).

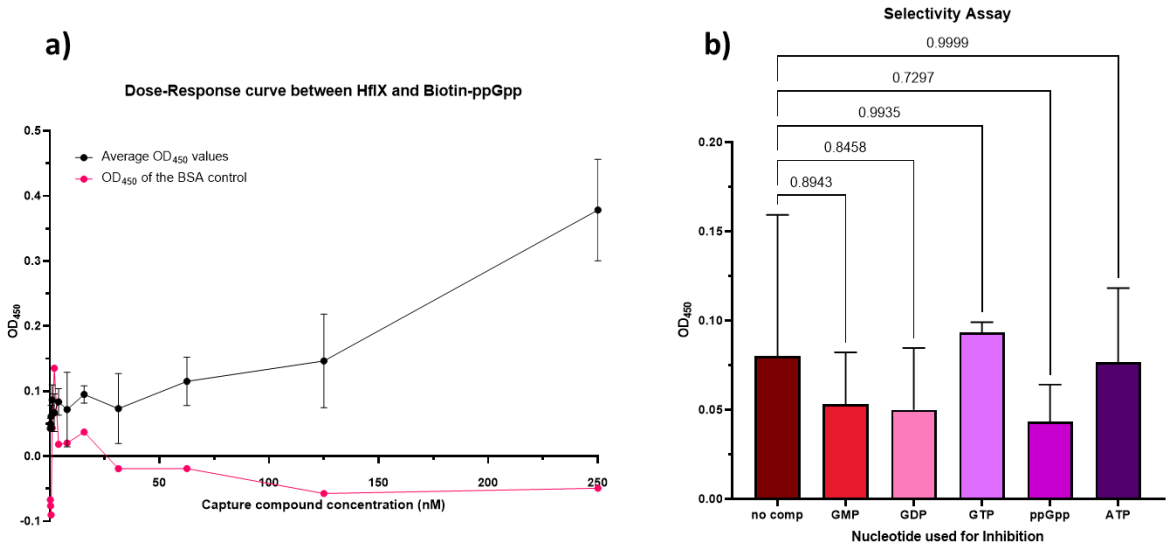

Figure 6.2.2.1: Assessment of sensitivity and selectivity of the capture compound.3a: Dose response curve plotted using serial dilutions of 250 nM capture compound with a consistent amount of HflX (10 ug/mL) coating each well. **3b:** Selectivity assay performed with capture compound (250 nM) by itself and in competition with structurally similar nucleotides: GMP, GDP, GTP, ppGpp, ATP all in a 100 fold excess (25 µM). One-way ANOVA performed by multiple pairwise comparison with respect to the no competition control showed no significant difference.

With low sensitivity meaning that large amounts of capture compound would need to be used, and with ppGpp not able to compete at these concentrations, this method was deemed not suitable for quantification of ppGpp in cell lysates. Therefore, a far more selective and sensitive methodology was explored.

6.2.3. Fluorescent chemo-sensors allow specific analyte recognition

Compounds that are comprised of a binding site and fluorophore that interact upon exposure to analytes are referred to as fluorescent chemo-sensors (Czarnik, 1994, Wu et al., 2017). Analytes can range from proteins, cations and anions to radical species, with the fluorescent chemo-sensors operating through several photophysical mechanisms, including: chelation induced enhanced fluorescence that relies on an organic photon receptor with a high excited state energy transferring energy to populate the excited state of a nearby metal centre, which fluoresces upon de-excitation (Wu et al., 2017); intermolecular charge transfer in which electron delocalisation or charge interactions in π-π stacking systems alter optoelectronic properties (Jagtap et al., 2012, Lu et al., 2022); or photoinduced electron transfer that functions on the basis of a weakly electronically coupled receptor and fluorophore ensuring their

individual properties are maintained. The molecule is designed so that upon excitation the receptor has enough energy to transfer an electron to the fluorophore. When this occurs the excited state energy is larger than the sum of the oxidation and reduction potentials of both components. Upon binding of the analyte/substrate to the receptor the oxidation potential increases ensuring photoinduced electron transfer fails and fluorescence remains (Daly et al., 2015, Wu et al., 2017). Aggregation induced emission (AEI) is another emission mechanism that can be explained by preventing energy release through the restriction of movement. A hydrophobic molecule that is able to rotate freely and vibrate can be forced to aggregate by increasing the amount of water present in solution. This leads to the restriction of bond movements by steric hinderance and as a result a pathway for de-excitation to occur is removed, forcing the excitons to decay in a radiative manner (Kwok et al., 2015).

There is a plethora of structural options available when designing fluorescent chemo-sensors, however, previous research has reported great success when utilising the bis-Zn-dipicolylamine (DPA) moiety. This receptor has shown great selectivity towards pyrophosphate binding groups making it inherently useful for nucleotide detection (Lee et al., 2003, Lee et al., 2004). X-ray structures show the mode of action of DPA relies on oxygen atoms from inorganic phosphates binding to the di-nuclear zinc complex by connecting the two metal ions forming either penta-coordinated or hexa-coordinated Zn^{2+} ions in a 1:2 ratio (Lee et al., 2003, Kim et al., 2009).

A method for quantifying ppGpp arose from research investigating ppGpp quantification in the form of the fluorescent chemo-sensor PyDPA consisting of a pyrene (Py) moiety connected to DPA (Figure 6.2.3). PyDPA was first synthesised in 2005 and its synthetic route optimised in 2019 (Rhee et al., 2008, Cho et al., 2005, Conti et al., 2019). PyDPA displays a high sensitivity and selectivity towards ppGpp over other aqueous anions over a broad pH range and functions by intermolecular charge transfer when π-π stacking occurs between the pyrene moieties providing a distinctive excimer emission ($\lambda_{Emission}$ = 470 nm) (Cho et al., 2005).

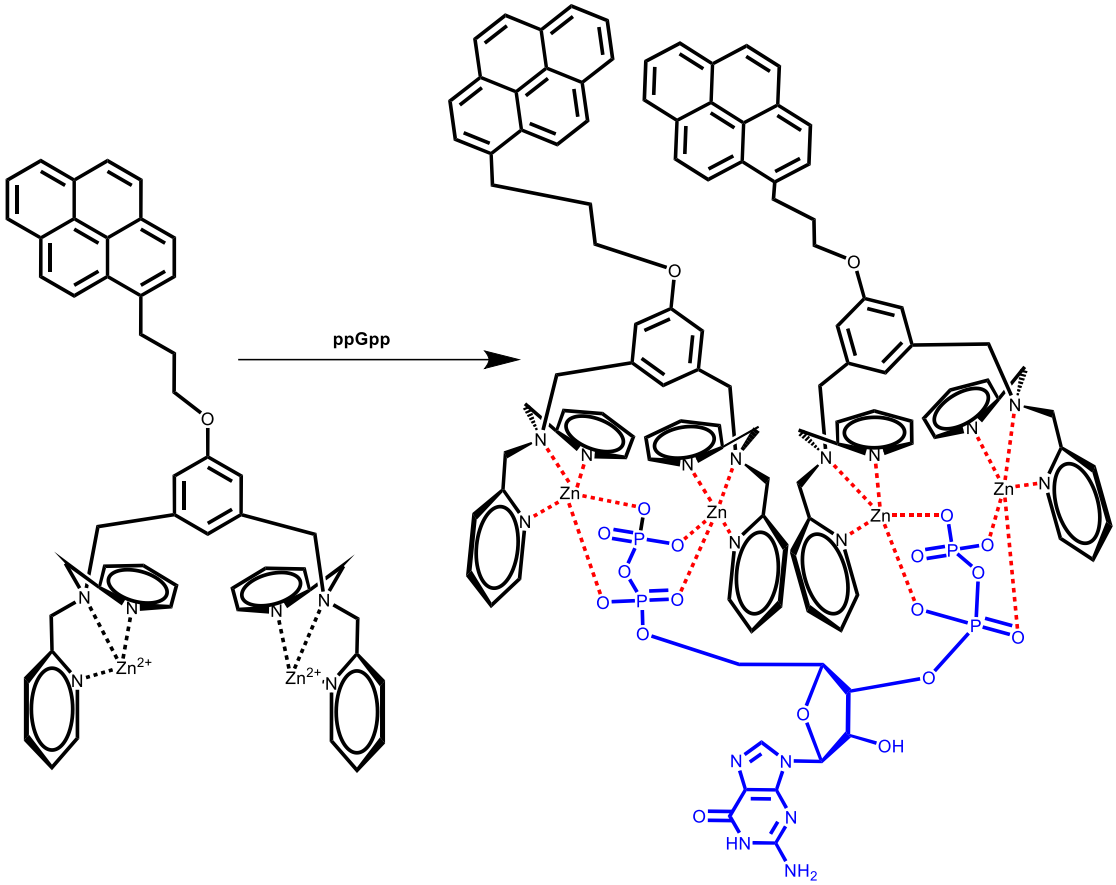

Figure 6.2.3: ppGpp chelates the Zn^{2+} ions present in PyDPA providing a 2:1 stoichiometry. The distinct excimer emission ($\lambda_{Emission}$ = 470 nm) caused by π-π stacking of the pyrene moieties only occurs in the presence of ppGpp.

Both the selectivity and sensitivity of DPA compounds have already been established, so we set out to synthesise PyDPA for use in measuring ppGpp concentrations in both wildtype MRSA under stress conditions, as well as synthetase deletion mutants that are available in the lab. Providing insight into the synthetases responsible for ppGpp production under a given stress such as nutrient starvation or reactive oxygen species.

6.2.4. Synthesis of the fluorescent chemo-sensor PyDPA

The synthesis of PyDPA was previously reported in a linear fashion over six steps with a poor overall yield of 9% (Rhee et al., 2008). A new route designed to synthesise the compound was published in 2019. Despite the incorporation of 2 additional steps, this convergent route significantly improved the overall yield up to 67% (Conti et al., 2019). As a result, this method was used as the backbone for the synthesis of our own PyDPA.

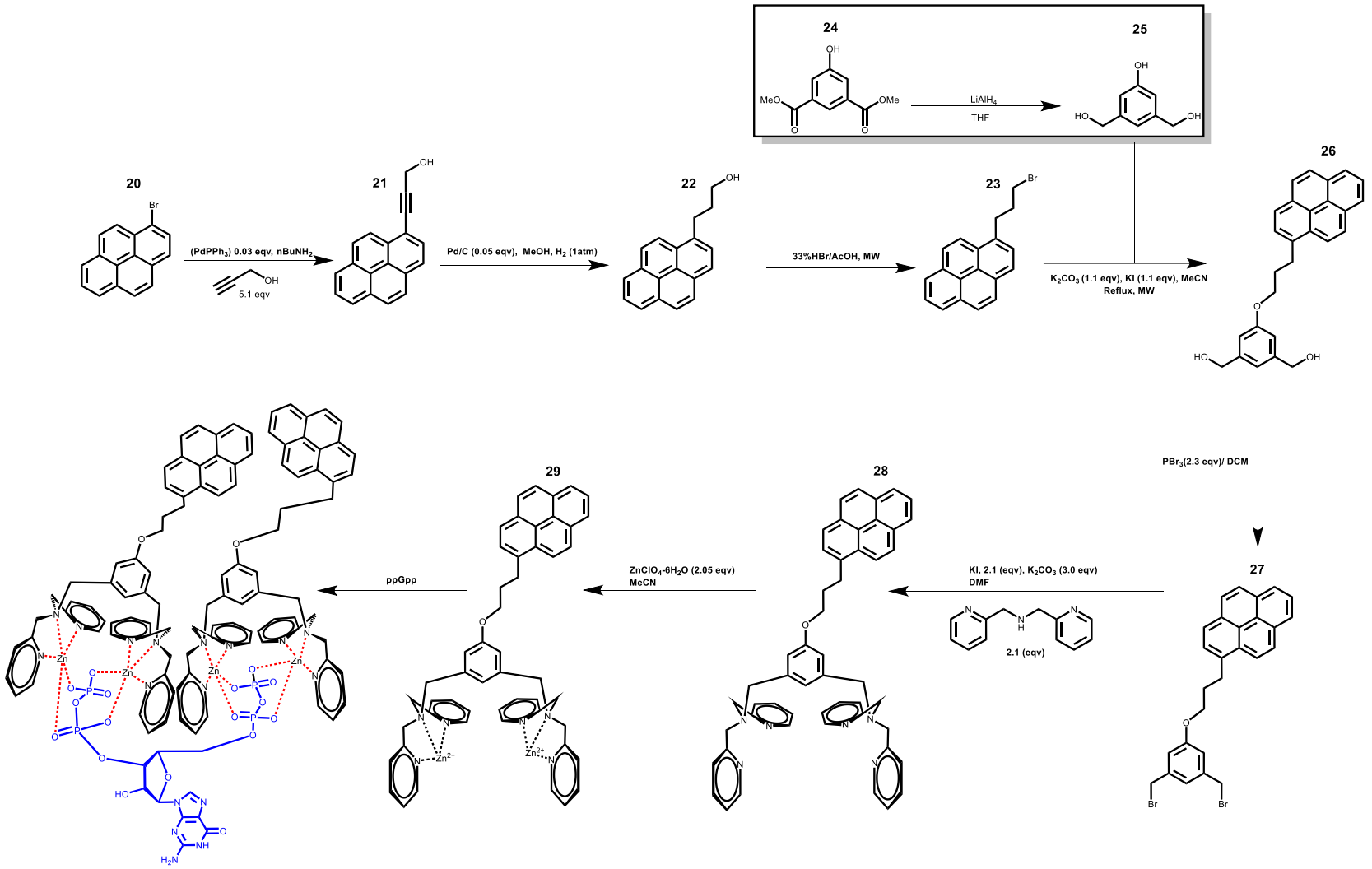

Scheme 5: Synthetic route implemented to reach the chemo-sensor PyDPA in eight steps. This convergent synthesis significantly improved the overall yield of PyDPA by changing the order of the coupling and bromination steps, while also utilising intricate coupling chemistry along with previously unused microwave conditions (Conti et al., 2019, Steinchen et al., 2020). Compounds are numbered in the order in which they appear.

6.2.4.1. Copper free Sonogashira-Hagihara cross coupling between an aryl halide **(20)** and propargyl alcohol

The basis of PyDPA is the pyrene moiety responsible for producing the fluorescence when π-π stacking occurs. Pyrene is a hydrophobic relatively unreactive structure, however the incorporation of a halide opens up the possibility of palladium cross-coupling chemistry (Devendar et al., 2018). The Sonogashira-Hagihara coupling is a method of forming carbon-carbon bonds between aryl/vinyl halides (sp^2 hybridised) and terminal alkynes (sp-hybridised) under mild conditions using palladium (0) and a copper (I) co-catalyst in the presence of an amine (Mohajer et al., 2021, Sonogashira, 2002, Sonogashira et al., 1975). Sonogahsira reactions tolerate a wide range of ligands under various conditions, thus they are used in the synthesis of natural products, pharmaceuticals and complex heterocycles. The use of copper-free Sonogoshiras has also been investigated with good success under both organic solvent and aqueous conditions, with the former methodology being used in the synthesis of PyDPA (Figure 6.2.4.1) (Vo and Elofsson, 2017).

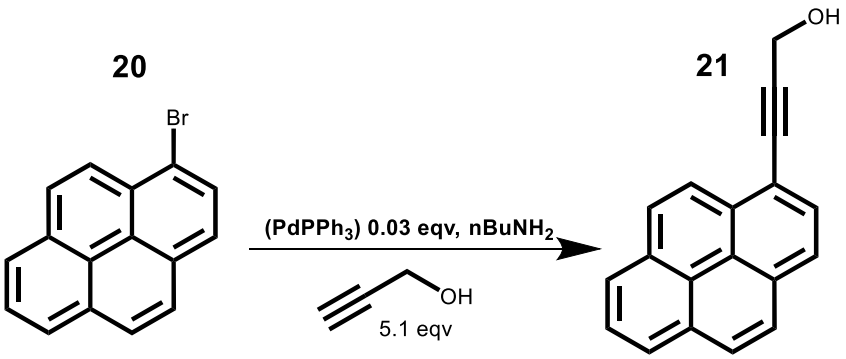

Figure 6.2.4.1: Copper free Sonogoshira coupling of 1-bromo-pyrene with propargyl alcohol. Tetrakis palladium triphenylphosphine was used as the catalyst along with n-butylamine and the terminal alkyne in large excess to ensure reaction progression.

The reaction is designed to be simple with separation of the desired product by silica chromatography being the only purification step due to the larger difference in polarity between propargyl alcohol and the product (21). Two attempts were made on both a small scale (1 g) and large scale (3 g) with different purification systems being trialled. The small-scale attempt followed the literature using Hexane:EtOAc (92:8 →40:60), while the latter attempt used shallower stepwise gradient elution which gave excellent separation (Conti et al., 2019). Both reactions attempts were successful in generating pure product as a yellow waxy solid with modest yields of 66% and 54%, respectively.

6.2.4.2. Reduction of an aryl-hydroxyalkyne **(21)** to an alcohol **(22)** by palladium catalysed hydrogenation

Reduction of alkynes to alkanes is limited to only a few reagents due to the strength of the reducing agent required. Hydrogenations using palladium or platinum are often used, alternatively nickel alloyed with aluminium can be employed as reduction catalysts in the form of Raney-nickel (Liu et al., 2024). We chose the Pd-catalysed hydrogenation procedure (Figure 6.2.4.2) as it is often associated with quantitative yields and high purity, while also avoiding the flammability risks as Raney-nickel hydrogenation catalysts.

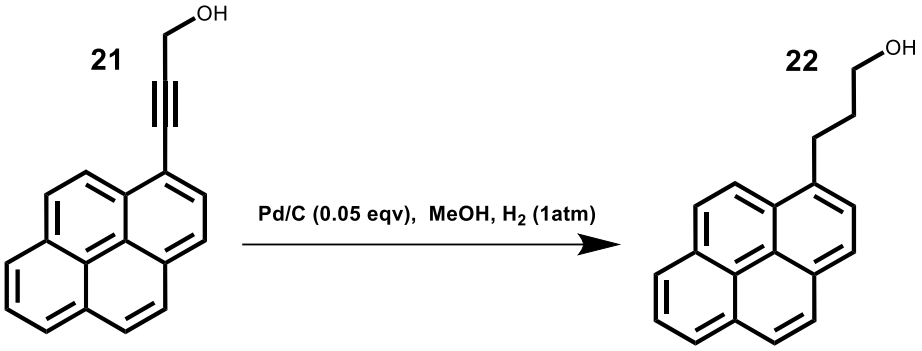

Figure 6.2.4.2: Hydrogenation of aryl-alkyne (21) to alcohol (22). Palladium adsorbed on carbon was used as the catalyst for this reaction to yield alcohol(**22**). The dispersal of the palladium increases surface area and reaction rate as a result.

Hydrogenation of 21 was repeated on two different scales (500 mg and 1500 mg). Upon completion the purification involved filtering off the solid catalyst using celite to provide the product (**22**) as a yellow powder in high purity and almost quantitative yields in the second attempt, 93% and 99.8% respectively, allowing continuation of the synthesis.

6.2.4.3. Bromination of a primary alcohol **(22)** to an alkyl-halide **(23)**

Activating the α-carbon by substituting alcohols with alkyl halides is common practice as it allows for new functionalities to be explored, this is typically performed by substituting an alcohol group with a chlorine, bromine or iodine atom. The previous syntheses of PyDPA activate this position with bromine, for which there are several methodologies available: Phosphorus tribromide (PBr_3) is a widely used method for bromination and is even used in the latter stages of this synthesis. In this instance the primary alcohol is activated by the phosphorus and displaces a bromide anion. The now electrophilic α-carbon undergoes S_N2 substitution with the bromide ion displacing the phospho-ester (PBr_2OH) as a good leaving group (Romero et al., 2015). Other options include hydrobromic acid (HBr) and hydrogen peroxide (H_2O_2) in ether or the use of carbon tetrabromide (CBr_4) and PPh_3 (Schmucker et al., 2013, Shin et al., 2020). Conti *et al* use 33% HBr in acetic acid under microwave radiation to ensure universal heating and no temperature gradients in solution. The alcohol is activated as it is protonated by acetic acid, allowing for the bromide ion to displace the $^+OH_2$ cation (Figure 6.2.4.3).

Figure 6.2.4.3: Bromination of alcohol (22) to form alkyl bromide (23). Relatively harsh conditions using 33% HBr and AcOH produce the brominated product as the sole product.

As in the previous hydrogenation reaction, the synthesis was performed on both a small (450 mg) and large scale (1500 mg) with no purification required after a basic work-up with 50% $NaHCO_3$. The product was obtained as a viscous brown oil in modest to good yields of 67% and 88%, respectively. With the synthesis of the aromatic building block (**23**) being complete, the synthesis of the second building block (**25**) was now required.

6.2.4.4. Reduction of dimethyl 5-hydroxyisophthalate **(24)** to 3,5,-dihydroxymethyl phenol **(25)**

Reductions of carbonyl compounds typically require mild to strong reducing agents, for example sodium borohydride is commonly used to reduce aldehydes and ketones to alcohols by acting as a source of hydride ions (Imamoto, 1991). However, when reducing acids, and esters to alcohols significantly stronger reducing agents are required. Lithium borohydride is the logical next step as its solubility in ethers allow reactions that are not possible with $NaBH_4$ to take place, while also being milder than extreme reducing agents such as $LiAlH_4$ (Nystrom et al., 1949). However, upon inspection of the literature it was not capable of reducing the required phthalate (**24**) Figure 6.2.4.4) unless bound to wang-resin (Dahan and Portnoy, 2003). In an attempt to avoid using $LiAlH_4$, several procedures (Figure 6.2.4.4) were trialled which utilised the aforementioned milder reducing agents.

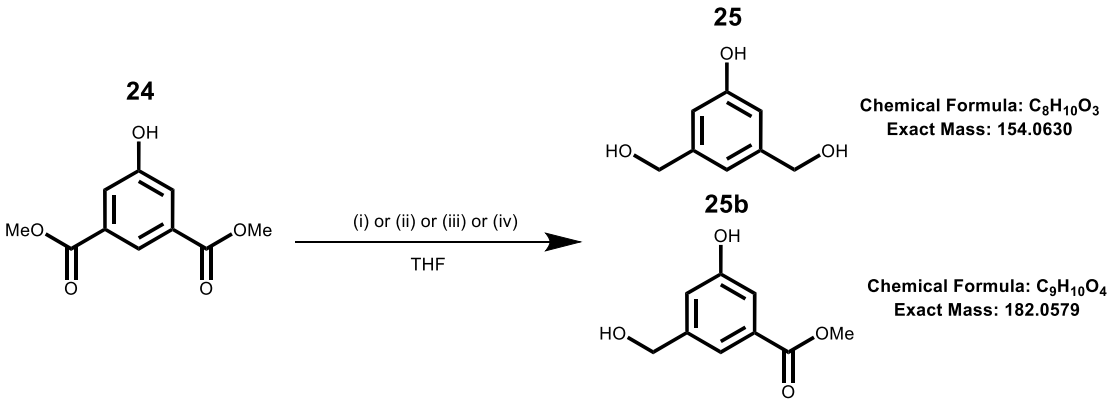

Figure 6.2.4.4: Reduction of phthalate (24) to triol (25) *via* several methodologies: (i) $NaBH_4$, $CaCl_2$, THF, unsuccessful (ii) $LiBH_4$, THF, reflux, formed side product (iii) $LiAlH_4$, THF, reflux, low yield 17% (iv) $LiAlH_4$, H_2SO_4, THF, high yield 74%.

The first attempted synthesis (Figure 6.2.4.4i) made use of calcium borohydride ($Ca(BH_4)_2$)) a stronger reducing agent than the usually employed $NaBH_4$. $NaBH_4$ was used in the presence of calcium chloride ($CaCl_2$) to generate the $Ca(BH_4)_2$ *in situ* and generate NaCl as a by product which precipitated out of the ethanol solution due to poor solubility (Pinho and Macedo, 2005, Matsui et al., 1956). However, this procedure did notreduce any of the starting material after 24 h, evidenced by lack or product formation on TLC.

An excess of $LiBH_4$ was then trialled in THF to encourage reaction progression, with heating under vigorous reflux (Figure 6.2.4.4ii). Despite the relatively harsh conditions and a reaction time of 48 hrs the desired triol **25** was not formed with reduction of only one ester occurring, evidenced by the [M-H] adduct observed in mass spectrometry m/z 181.050.

With the options of alternative reducing agents exhausted, the conditions for (ii) were repeated but with $LiAlH_4$ in place of $LiBH_4$ (Figure 6.2.4.4iii) as per the literature (Rhee et al., 2008). These incredibly harsh conditions led to the formation of the product and upon reaction completion, water was added to both quench any unreacted $LiAlH_4$ and protonate the resultant RO^- ions. This formed a white precipitate of aluminium hydroxide ($Al(OH)_3$) and lithium hydroxide (LiOH), the biphasic mixture was then passed through $MgSO_4$ to both dry the solution and filter the insoluble $Al(OH)_3$. The dry organic phase was then concentrated under reduced pressure and the crude product was purified by silica chromatography (DCM:MeOH,1:0→0:1) to provide the product as a colourless oil in poor yield (16%).

To improve the yield of this reaction, a key change was made in (iv) that involved swapping the water quench with 10% H_2SO_4, this would be much more violent due to the increased acidity, however, it would ensure protonation so that any product in its alkoxide form was not lost in the aqueous layer (Ronde et al., 2009). The solvent and aqueous layer were evaporated and the residue redissolving in a small amount d of water. The pH of the solution was assessed using universal indicator paper to confirm acidic conditions. The aqueous layer was then extracted with ethyl acetate and the organics dried ($MgSO_4$), before removing the solvent and purifying by silica chromatography to remove any mono-reduced side products, giving the pure product as a colourless oil with a significantly improved yield of 74%.

6.2.4.5 Microwave assisted Williamson ether synthesis of an alkyl-bromide **(23)** with a triol **(25)**

With the generation of both building blocks of PyDPA, they were linked together using a Williamson ether synthesis (Figure 6.2.4.5) (Conti et al., 2019). As described in chapter 3 the alcohol was deprotonated, then alkylated forming an ether and a halide salt.

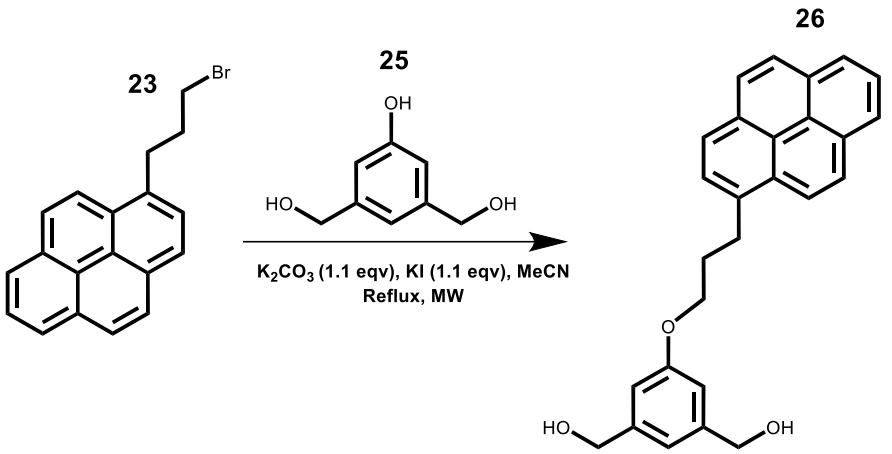

Figure 6.2.4.5: Reaction of alkyl bromide (23) and triol (25) under microwave conditions. Microwave conditions and the use of K_2CO_3 promote selectivity of the phenolic oxygen of (**25)** ensuring no side products are formed with the primary alcohols.

In this reaction a Finkelstein like halide exchange occurs between the alkyl-bromide (KBr) and potassium iodide (KI) forming KBr and an alkyl-iodide. This alkyl-iodide is more reactive due to the smaller difference in electronegativity between the iodine atom and the α-carbon, the iodine atom is more readily displaced by an ion carrying a full negative charge i.e. an alkoxide. In this reaction the alkoxide is formed using potassium carbonate as the base for a regioselective deprotonation as the pK_a of its conjugate acid is 10.25, making it suitable for the deprotonation of phenols (pK_a ~10) not primary alcohols (pK_a ~16). The microwave conditions allow for universal heating, while also aligning the dipoles of the triol and pyrenes delocalised aromatic systems to favour the phenolic oxygen in a regioselective manner. Using a microwave reactor, the reactions were heated to reflux under an inert atmosphere. Monitoring by TLC was difficult with the formation of numerous spots and streaking. To counteract this streaking, 1% TEA was added to the mobile phase allowing for better separation between impurities. Product identification was possible due to polarity difference with the starting materials and the pyrene moiety absorbing at long-wave ultraviolet ($\lambda_{Absorbance}$ = 355 nm). After redissolving the crude material in EtOAc and performing an aqueous work-up, purification by flash column chromatography would typically be performed. However, when loading the column the crude product was insoluble in EtOAc, possibly due to a change in crystal structure. After numerous solubility tests the crude material was found to dissolve in dioxane. A column was then performed using a non-polar mobile phase (Hexane:EtOAc, 90:10) to regain the product now solubilised at the cost of co-elution with impurities. Flash column chromatography (DCM:MeOH:TEA, 95:4:1) was then performed on the impure but solubilised product using an incredibly shallow gradient, providing excellent separation, with the pure product being isolated as a colourless oil in poor yield (13%).

6.2.4.6. Bromination of a diol **(26)** with phosphorus tribromide

The next step in the synthesis of PyDPA was to activate the benzyl positions of diol (**26**) by bromination so that they can later be substituted with dipicolylamine. A bromination was previously performed in this synthesis boasting yields ~70% (Section 6.2.4.3), so it would seem sensible to repeat this procedure, however, due to the presence of the strong acid (HBr) and stability of the phenol group it is possible that an elimination of the ether group could take place reforming the starting materials of the previous step (Whitehead et al., 1951) (Figure 6.2.4.6).

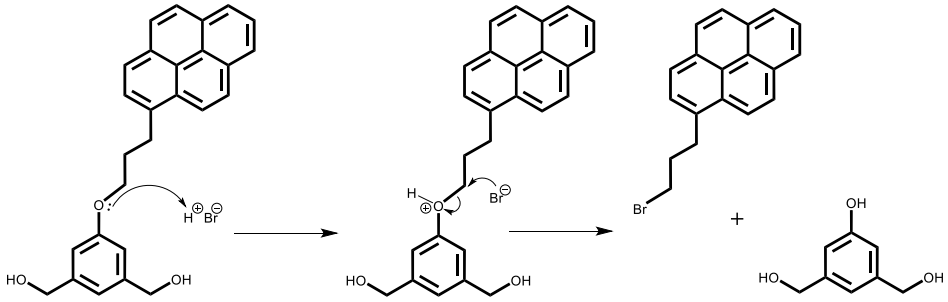

Figure 6.2.4.6: Mechanism of ether elimination in the presence of a strong acid. Strong acids such as: HBr and HI are capable of cleaving ether bonds by promoting the formation of a stable leaving group through protonation.

To avoid this potential elimination, the literature favoured PBr_3 was used (Figure 6.2.4.6.1). The potential of forming impurities in this reaction was minimal with the mono-substituted side product being the only real concern.

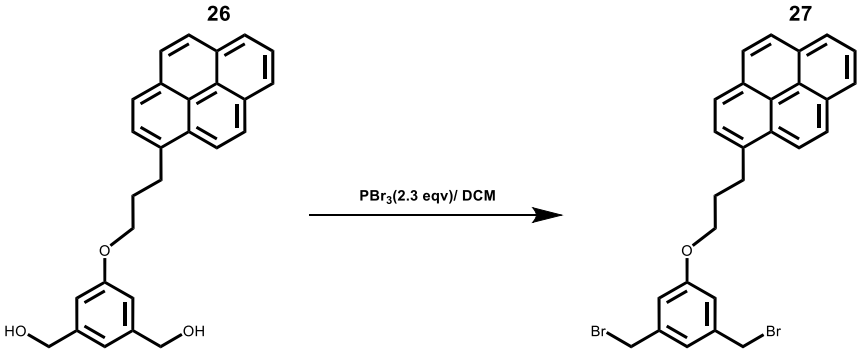

Figure 6.2.4.6.1: Activation of benzylic carbons using PBr3 yields a di-bromo ether. Substitution of the primary alcohols with bromine activates **27** allowing for further substitutions in the next step.

Despite using excess PBr_3 to ensure di-substitution, progression was slow. This could be attributed to the large reaction volume (50 mL) guided by the original literature. To increase the reaction rate, another 2 equivalents of PBr_3 were added. The compounds UV absorption decreased from the level it was exhibiting in previous steps, however, due to the hydrophobicity and associated low polarity it was easily identified on a silica TLC. After 24 hrs, methanol was added to quench any unreacted PBr_3 and the mixture was washed with saturated brine before drying ($MgSO_4$). The crude compound was then dry

loaded with celite and purified by flash column chromatography (hexane:DCM, 1:2) providing pure product as a white solid in high yield (64%).

6.2.4.7. Dipicolylamine furnishes the benzylic positions of alkyl di-bromide **(27)**

In order to introduce sensitivity towards ppGpp the compound must be furnished with dipicolylamine, this allows subsequent chelation to zinc, a key interaction required for ppGpp binding (Figure 6.2.4.7).

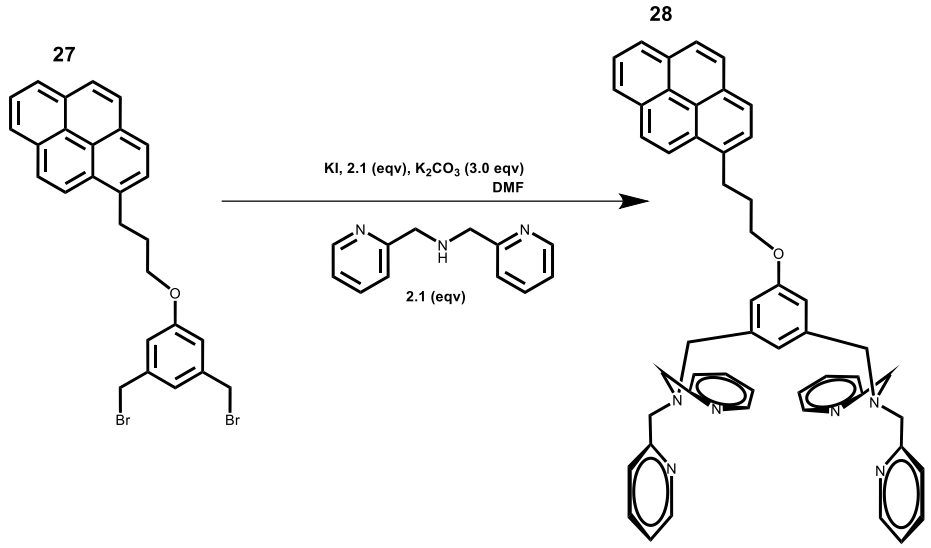

Figure 6.2.4.7: Attachment of the phosphate sensitive dipicolylamine (DPA) moiety by nucleophilic substitution. Formation of the more reactive alkyl-iodides, allows for an immediate reaction with DPA.

This bromide displacement reaction functions in the same manner as the microwave assisted Williamson ether synthesis (section 6.2.4.5) with the exception of microwave radiation, which is not required, and K_2CO_3, which now deprotonates the quaternary amine cation (Conti et al., 2019, Rhee et al., 2008). Conti *et al* also substituted MeCN for another polar aprotic solvent DMF, this is commonly used for S_N2 reactions due to its ability to solvate and stabilise the cation (Sherwood et al., 2024). After 24 hrs the reaction was complete, DMF was removed and the remaining material partitioned into water and EtOAc before drying (Na_2SO_4). Due to the introduction of the incredibly polar DPA groups, the compound did not move on silica without a highly polar mobile phase, so flash chromatography (DCM:MeOH:TEA, 90:9:1 → 60:39:1) with a very shallow multi-step gradient was employed to isolate pure unchelated PyDPA as a slightly yellow oil in moderate yield (61%).

6.2.4.8. Chelation of unchelated PyDPA **(28)** to zinc ions forms the functional fluorescent chemo-sensor PyDPA

The formation of functional PyDPA occurs through the chelation of two zinc atoms to the DPA units attached to the benzylic carbons (Figure 6.2.4.8). This step involved dissolving **28** in MeCN and adding a slight excess of zinc perchlorate hexahydrate before leaving to stir for 6 hours (Rhee et al., 2008, Conti et al., 2019).

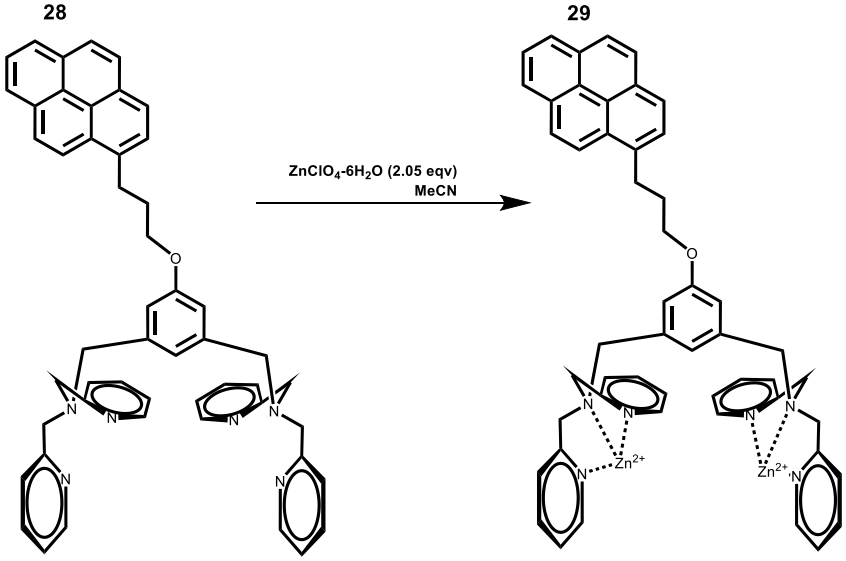

Figure 6.2.4.8: Chelation of Zinc activates PyDPA to ppGpp binding. The chelation of Zn^{2+} ions allows for ppGpp binding and subsequent pyrenyl interactions

After the allocated time the MeCN was removed under reduced pressure and the residue dried on a high-vacuum line to provide pure functional PyDPA in quantitative yield (218 mg, 0.184 mmol, 100%).

6.2.5. PyDPA offers a range of sensitivity while maintaining ppGpp selectivity

Once the synthesis of PyDPA was completed, it was dissolved in DMSO and used to measure fluorescence ($\lambda_{Excited}$ = 355nm, $\lambda_{Measured}$= 485 nm) with a range of ppGpp concentrations. Starting from 1 mM, a serial dilution of ppGpp was made to 0.48 nM while keeping a constant concentration of PyDPA (20 µM). The assay was successful in determining a sensitivity range with the relative fluorescence signal peaking at 7.81 µM (Figure 6.2.5). This can be explained by the stoichiometry required for fluorescence to take place: when ppGpp complexes two units of PyDPA, π-π stacking of the pyrenyl moieties occurs, producing a significant shift in the ratio of its excimer emission intensity compared to monomer emission intensity allowing detection (Rhee et al., 2008, Lee et al., 2004). However, when this ratio is not achieved, fluorescence is not possible. As a result, PyDPA should always be in excess of ppGpp to gain precise readings.

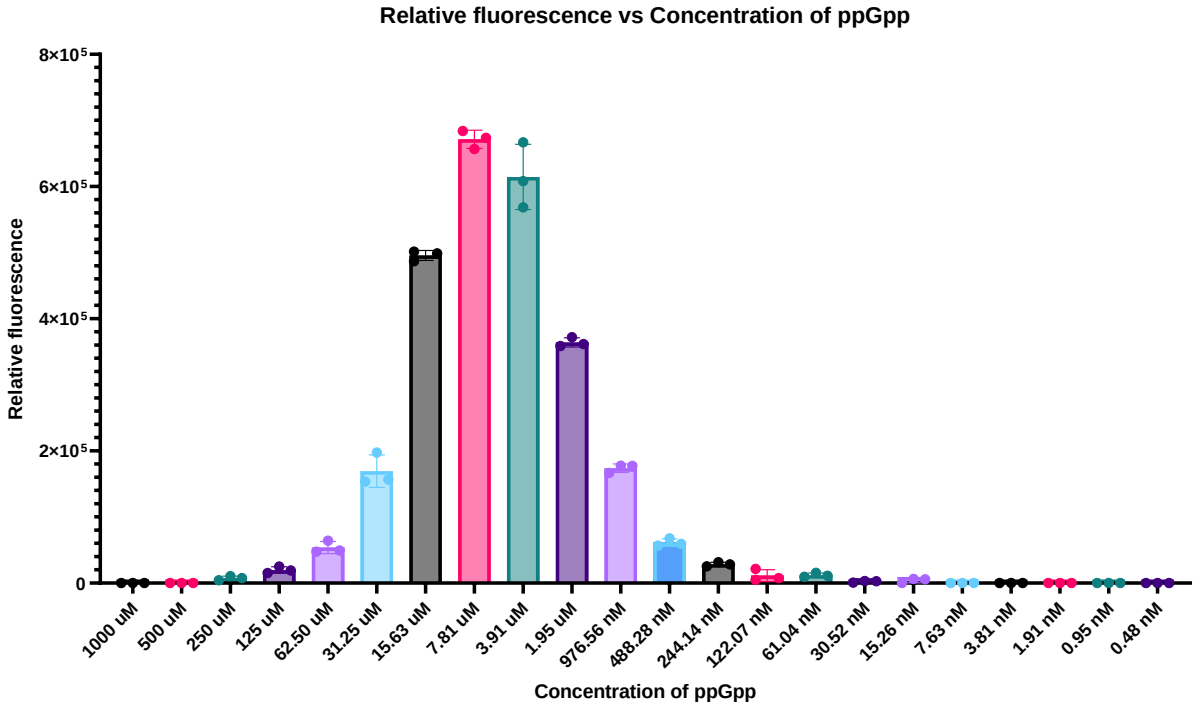

Figure 6.2.5: Assessment of the fluorescence response of PyDPA as a function of ppGpp concentration. The sensitivity range of PyDPA is ~100 µM. For accurate readings titrations with PyDPA should be performed to ensure the chemo-sensor is in excess.

With a defined sensitivity range of PyDPA established, its specificity towards ppGpp was assessed using a selectivity assay with structurally similar nucleotides (Figure 6.2.5.1).

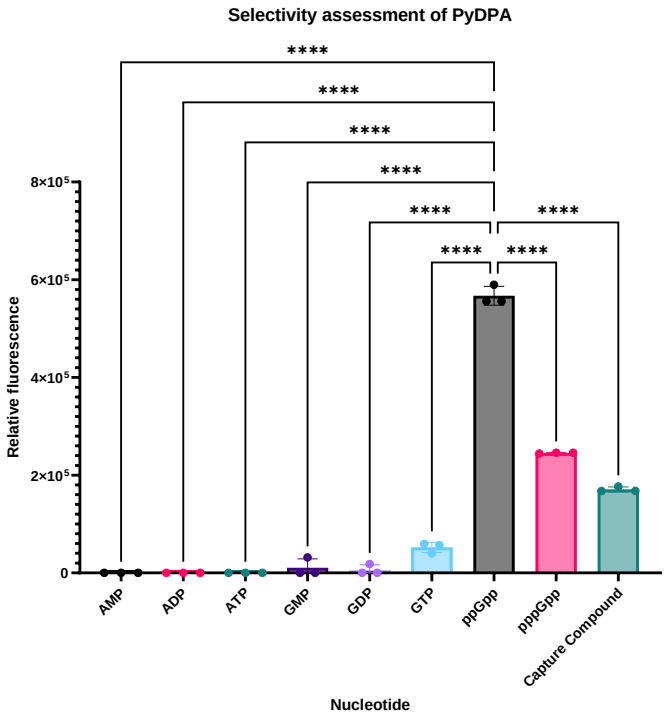

Figure 6.2.5.1: PyDPA fluoresces in the presence of (p)ppGpp in a selective manner. Relative fluorescence of various nucleotides (7 μM) mixed with PyDPA (20 μM). There is a statistically significant difference in relative fluoresences values when comparing structurally similar nucleotides to ppGpp by one-way ANOVA.

To assess selectivity, nucleotide (14 μM) and PyDPA (40 μM) stocks were prepared according to the literature before mixing thoroughly in a 1:1 ratio and measuring fluorescence ($\lambda_{Excited}$ = 355nm, $\lambda_{Measured}$= 485 nm) (Conti et al., 2019). It is clear that binding to PyDPA relies on the presence of both 3'- and 5'-phosphates, with nucleotides possessing one set of bis-phosphates such as ADP and GDP producing no signal (Figure 6.2.5.1). The penta-phosphate pppGpp did produce signal, albeit significantly weaker than its tetra-phosphate signalling partner. The capture compound was also included in this assay to gauge the effect of a linker attached to the phosphates, which was significant and to be expected. Overall, the data here confirm the synthesis of the selective fluorescent chemo-sensor PyDPA for use in future biological experiments.

6.3. Discussion

With the aim of generating a method for quantifying ppGpp, the development of a selective ELISA was attempted to no avail (Section 6.2.2.), however, it was completed by synthesis of the chemo-sensor PyDPA. This compound could now be used to determine ppGpp levels in both wildtype MRSA and deletion mutants of the (p)ppGpp synthetases to help establish what synthetase is responsible for dealing with a given stress. In work that I plan to complete post thesis submission, alongside growth curves, I will use the chemo-sensor to monitor ppGpp production and identify the concentration at which growth is inhibited by half in strains that will then be subjected to metabolomics, complementing the work in chapter 5.

Currently, there are no ELISA methods for determining ppGpp concentrations but great success with c-di-AMP had been reported, so the development of an ELISA method was attempted first (Underwood et al., 2014). As previously mentioned, there are variations of ELISA methodologies such as direct, indirect, and sandwich, all of which have their advantages/disadvantages. Direct ELISAs use one antibody and as a result are quicker due to the decreased number of steps, however, there are a limited number of primary conjugated antibodies available. Indirect ELISAs utilise primary antibodies, which have numerous epitopes and secondary antibodies that can bind to these epitopes enhancing the signal. The use of two different antibodies allows for the measurement of signals by different methods such as colorimetric or chemiluminescence at the expense of introducing an extra labelling step, while also introducing the potential for cross-reactivity giving a false signal. Our attempt at an ELISA is an example of a sandwich-ELISA, as the protein HflX was coated to the cell before the addition of the capture compound (antigen) and subsequent addition of streptavidin-HRP and TMB. Sandwich ELISAs are highly specific as two antibodies are used for capture and detection of the antigen. Despite this, our methodology lacked sensitivity in comparison to the ci-di-AMP ELISA which required only 1.5 nM of biotin-ci-di-AMP for a signal and carried large variation across numerous replicates. This was originally attributed to the ether chain of the capture compound not being long enough and interfering with binding. However, this could not have been the case as the capture compound had previously been used in a dot-blot where it displayed binding to HflX. An alternative method that could be developed would not directly measure ppGpp levels in a sample but would measure the levels of GTP, which is a key component in the synthesis of (p)ppGpp. This could be done using commercially available biotin-GTP and another protein that displays GTP binding, such as HprT, in place of HflX as this displays GTPase activity (Kriel et al., 2012, Polkinghorne et al., 2008, Anderson et al., 2019). However, this method would be indirect and possibly tricky to set up.

With regards to PyDPA, the synthesis has already been optimised with almost no places for improvements to be made (Conti et al., 2019). The overall yield for this synthesis was low at 1.7% over eight steps, however, this could be attributed to the poor yield associated with the microwave assisted Williamson ether synthesis (section 6.2.4.5). In this reaction, the microwave reactor failed meaning

stirring did not occur, with many of the reaction components being insoluble in the solvent. Sedimentation of the salts and poor mixing occurred as a result, potentially hindering reaction progression. Besides the inability to repeat the reaction due time constraints, alternative brominating agents in the form of a α,α-Dibromo-β-dicarbonyl compounds could be explored for the latter stage bromination. Such alternatives involve a modified Appel reaction where triphenyl phosphine is kept constant but the toxic/corrosive PBr_3 is replaced by α,α-dibromoacetoacetate (Appel, 1975, Cui et al., 2014). Producing the desired alkyl/benzyl bromide in almost quantitative yield with ethyl acetoacetate as a safe by-product (Appel, 1975, Cui et al., 2014). In place of $LiAlH_4$ another reducing agent such as di-isobutyl aluminium (DIBAL) could have been trialled for the reduction of phthalate (**24**) if there were no solubility issues (Galatsis, 2001). Typically, DIBAL reductions are performed at -78 °C (dry ice and acetone bath) to decrease the reaction rate and favour the formation of a stable hemiacetal co-ordinated to aluminium that cannot undergo a second reduction due to the absence of a π-bond. Upon mild acidic work up, this intermediate collapses to yield an aldehyde and aluminium ether. However, by running the reaction at room temperature and keeping the DIBAL in slight excess it is possible to form the desired alcohol, this would avoid the use of $LiAlH_4$ and allow the use of a slightly milder reducing agent (Mascitti, 2012).

Upon synthesis we were able to demonstrate the selectivity of PyDPA and the concentration range in which it functions using a buffer system. Its use in *S. aureus* cell lysates will provide an insight into (p)ppGpp levels, however, it is unable to differentiate between ppGpp and pppGpp (Figure 6.2.5.1). It may also display affinity towards other analytes such as cAMP albeit by a different fluorescence mechanism, while structural analogs of the compound display affinity to NADP (Oh and Hong, 2013, Rhee et al., 2010). In order to assess the likelihood of these analytes interfering, it would be imperative to run a competition assay with PyDPA in the presence of these phosphates with negative and positive controls.

Despite the need to perform a competition assay with NADP and cAMP, the simplicity of using PyDPA cannot be overstated. It is simply mixed with sample in excess before measuring fluorescence of the excimer ($\lambda_{Excimer}$= 475 nm) and can be performed in a 96 well plate for high-throughput experiments while also possessing excellent sensitivity that depends on the molar ratio with the target nucleotide. The ability to implement PyDPA in a high throughput system will be incredibly useful when contrasting levels of ppGpp between mutants to determine the importance of a given synthetase under stress or when examining what stressors induce ppGpp synthesis.

As stated previously, other methods for quantifying ppGpp do exist but they are all associated with their own drawbacks. Radiolabelling in both assay and TLC form, involves working with a radioactive isotope increasing risk towards the user's health. Distinguishing ppGpp between inorganic phosphates and ppApp is also difficult regardless of whether one dimensional or two-dimensional chromatography is

used (Gallant et al., 1972, HAMAGISHI et al., 1980). A modern high throughput radiolabelling procedure in *E. coli* has been developed. This uses microtiter plates and TLC to provide almost real time insight into ppGpp levels but still faces the same issues mentioned above (Fernández-Coll and Cashel, 2019). The method is also not very applicable to many other bacterial species as it uses MOPS media and does not tolerate other media very well. Due to amino acid auxotrophy, *S. aureus* cannot grow on MOPS meaning that another method is required for ppGpp quantification in our target bacterium (Mashburn et al., 2005, Fernández-Coll and Cashel, 2019).

HPLC methods have drastically improved with the incorporation of mass spectrometry instruments and their resolution however, they lack the opportunity for high throughput and operation often requires specialist training, while the expense of the equipment also limits its use. Nanoclusters provide an interesting on/off fluorescence measurement of ppGpp levels and are promising with the potential of tuning for emission purposes, simplicity of preparation and compatibility within a biological system (Xu and Suslick, 2010). The production of europium quantum dots allows for rapid indication of ppGpp levels and with a detection range of 23 μM, this is low enough to determine both basal and adaptational ppGpp levels (Rong et al., 2020, Varik et al., 2017). The synthesis of the quantum dots is complete within 2-3 days and with the presence of a UV lamp, ppGpp levels can be recorded with a mobile phone allowing for rapid quantification upon synthesis. However, they are not selective, often displaying binding towards GTP, GDP and GMP, limiting their use.

Another method that can be used to provide insight into ppGpp levels involves the gene fusion of stress relevant promoters such as *rpoS* with GFP for real time monitoring of stress levels (Funabashi et al., 2002). However these methods do not provide information on ppGpp levels directly, just the physical status of the cell and whether interactors of ppGpp are activated or inhibited (Nemecek et al., 2006, Funabashi et al., 2002, Fernández-Coll and Cashel, 2019). For a direct measure of an analyte a fluorescent biosensor would be needed, which was beyond the scope of this work.

The methods described above all offer unique insights into the stress levels of bacteria whether through real time fluorescence or densitometry of radiolabelled TLCs to quantify ppGpp. However, each method requires a lot of attention, expensive equipment or specialist training making them difficult to access and utilise for most laboratories. PyDPA is not exempt from this with its synthesis requiring traditional laborious chemical methodologies but even when prepared in low yields, only a small amount would be required per run making it incredibly useful for a long period of time if stored correctly. PyDPA will be used to quantify ppGpp levels during different phases of growth for both wildtype JE2 and deletion mutants in both stressed and unstressed conditions, allowing for the relationship between synthetases and specific stressors to be deciphered. These growth curves may also allow us to determine a (p)ppGpp concentration at which the growth rate is halved, providing an excellent basis for assessing a change in HxlB metabolites such as F6P to further elucidate the elaborate signalling network.

Chapter 7: Discussion

7.1. Final discussion

The SR is an almost ubiquitous response in prokaryotes to external stresses such as nutrient starvation, antibiotic exposure or reactive oxygen species. The response affects multiple facets of normal cellular processes such as transcription, ribosomal assembly, translation and virulence (Geiger et al., 2012, Majerczyk et al., 2008, Pohl et al., 2009, Corrigan et al., 2016, Srivatsan and Wang, 2008). However, many of the mechanisms of action with regard to the SR remain undetermined due to the large array of targets (p)ppGpp acts upon (appendix tables 5-7). The conformational flexibility of the phosphate moieties and their ability to adopt enclosed or elongated conformations, allows us to rationalise the plethora of binding partners available to these alarmones (figure 1.5.1.) (Steinchen and Bange, 2016). Additionally, the mechanisms of interference across the transcriptome also differ across bacterial species, for example in *E. coli* the direct binding of (p)ppGpp to two distinct binding sites on the RNAP-DksA complex leads to an alteration of the transcriptional profile of ~750 genes including *rrn* (Geiger et al., 2010, Potrykus and Cashel, 2008, Kästle et al., 2015, Handke et al., 2008). In *S. aureus* despite the end result being the same, the effect of (p)ppGpp is indirect as it does not bind to the RNAP. Instead it modulates the concentration of other nucleotide pools such as GTP. Reductions in GTP levels allow for the derepression of the CodY regulon, enabling the transcription of 143 genes involved in virulence and amino acid biosynthesis (figure 1.5.3b) (Majerczyk et al., 2008, Handke et al., 2008). Due to these regulatory mechanisms, the SR is ultimately linked to an increase in survival by rapid transition to a slow growth phenotype leading to a decrease in metabolic activities. As these “dormant cells” have not undergone any genetic mutations, they promote antibiotic tolerance, implicating the SR in persister cell formation and repeat infections as a result (Hobby et al., 1942, Wood et al., 2013, Amato et al., 2013, Korch et al., 2003). The importance of antibiotic resistance and tolerant *S. aureus* strains cannot be overstated, as they result in extensive pressures on the community and healthcare systems, as evidenced in 2003 when up to 400,000 inpatients in the US had *S. aureus*-related infections. The inpatients alone resulted in an economic burden of around $14.5 billion and an additional $12.5 billion for those requiring surgical intervention (Noskin et al., 2007). The prevalence of MRSA in health care was also noted to have risen in 2008 due to newly discovered virulence factors that contributed to necrotising, frequently lethal, pneumonia along with a variety of other potentially fatal infections in otherwise healthy individuals, making MRSA responsible for more deaths than HIV infection in that year (Noskin et al., 2007, Boucher and Corey, 2008, Rasigade and Vandenesch, 2014).

For these reasons it is important that the intricate (p)ppGpp signalling network of the SR is further characterised through the probing of (p)ppGpp interactions with potential binders. In this study we synthesised a ppGpp capture compound capable of isolating novel (p)ppGpp effectors from MRSA lysates in order to assist the mapping of this complicated stress response.

The initial capture compound design was influenced in part by the primary capture compound paper for (p)ppGpp by Wang *et al* who utilised a cocktail of capture compounds consisting of a biotin affinity

handle, a variable length peptide linker attached to either the 3'- and 5'- phosphates, a diazirine cross-linker and a thiolated ppGpp mimic termed p(s)pGpp. Our compound consisted of three key pieces - a biotin affinity handle and a variable length linker in the form of polyethylene glycol attached to p(s)pGpp (Chapter 3, scheme 1). The 5'-β-phosphate of ppGpp was chosen as the attachment point for the linker as not many nucleotides have a bis-phosphate attached to the 3'-position, which we believed could also be involved in the ability of (p)ppGpp to bind to so many targets. The guanine base was dismissed as an attachment point, as when viewing (p)ppGpp in complex with different effectors the guanine base seems to direct binding through aromatic interactions meaning structural hinderance may have interfered with binding (Steinchen et al., 2015a). Shortly after the synthesis of our capture compound, Haas *et al* released a study where they synthesised a small library of (p)ppGpp capture compounds with structural variations including the linker attachment point at the guanine base and 3'- and 5'- β-phosphates (Figure 1.6.2.2). Based on the number of significant hits they obtained for each compound, it was found that linker attachment to the 5'-β-phosphate yielded the highest number of potential interacting proteins, vindicating our decision.

In contrast to Haas *et al* and Wang *et al*, our capture compound was designed to function in a non-covalent manner relying purely on specific interactions to potential interactors instead of using a photo-activated cross-linker. This was used to investigate the SR in *S. aureus*. Organic synthesis of the compound began by generating the linker and affinity handle first and although several synthetic routes were initially proposed, the route we eventually settled on consisted of simple substitution and coupling chemistry (Chapter 3, scheme 1). However, the yields were unsatisfactory in key steps such as the late-stage Staudinger synthesis (36%) and bromoacetylation (11%), significantly impacting the amount of material available for input into the final coupling reaction with the enzymatically generated p(s)pGpp. Although there was enough material available for our needs, the synthesis could be improved by employing different reactions such as hydrogenations in place of the Staudinger reactions or click reactions to bypass both the Staudinger and bromoactylation steps in one pot, while also introducing a chromophore for reaction monitoring during chromatography. Optimising the HPLC purification conditions of p(s)pGpp and the capture compound by modifying the gradients and using newer equipment would also dramatically increase the yield. The simplicity of being able to replace the TEG in our capture compound with other PEG variants in the first step, also allows for (p)ppGpp interactions to be probed further. While the development of a pppGpp capture compound could have been explored this would have been difficult as it was previously discovered by another member of the laboratory that GDPβs was not tolerated as a substrate by the long-RSH Rel. Although the SAS RelP and RelQ were more versatile in their substrate acceptance they preferentially synthesise ppGpp, as a result this direction was not pursued. Therefore, despite its drawbacks in yield, a backbone synthetic route leading to a novel non-covalent (p)ppGpp capture compound was established.

With our capture compound displaying binding to the (p)ppGpp target GTPases; RsgA, RbgA, HflX and Era identified by Corrigan *et al*, we set about developing a pulldown methodology (Figure 4.2.2.1). This methodology drew inspiration from previous studies such as Laventie *et al* for identifying c-di-GMP binding proteins, and ultimately led to a streamlined approach for using the compound to assess (p)ppGpp binding in lysates from different growth phases and stress conditions. Wang *et al* also implemented a SILAC methodology using a lysine and arginine auxotrophic strain of *E. coli* AT713 (figure 1.6.2.1). While this approach would have provided further insight into the signalling network, due to both a lack of resources and the lack of *S. aureus* auxotrophic behaviour, we were not able to generate our own SILAC minimal media and implement this in an *S. aureus* background. Nevertheless, upon obtaining the results from our pulldown methodology we had isolated around 160 potential (p)ppGpp binding targets in stationary phase MRSA lysates, including 20 proteins previously identified using capture compound approaches (appendix table 1-4) (Haas et al., Wang et al., 2019a). Using KEGG mapping we were able to determine these proteins were involved in multiple cellular processes including: RNAP assembly; TCS involved in cell wall stress; adaptation to ROS; and carbon metabolism. The lack of targets identified in the remaining pulldown experiments with: exponential phase lysates; mupirocin stressed lysates and lysates obtained post macrophage internalisation could be explained by (p)ppGpp levels being naturally higher in stationary phase than exponential phase. As the cell does not require inhibition of processes involved in growth during proliferation and as supply essentially meets demand there are fewer (p)ppGpp targets available for binding during this growth phase. The pulldowns using bacteria internalised by macrophages had a significantly lower number of *S. aureus* cells available for lysis, while the protein concentration determined before the pulldown was likely not accurate due to the remnants of macrophage proteins. The significance values were also heavily altered due to the lack of a proteome attributed to the primary human macrophages, to avoid this a standardised cell line could be used.

A lower number of significant hits from these additional pulldown experiments led to us focusing our efforts on the stationary phase dataset. After expression of the proteins of interest using the ORFeome library, we assessed binding to ppGpp using DRaCALA with whole cell lysates to narrow down our search radius. DRaCALA had previously been used to a high degree of success by Zhang *et al* (appendix table 5) and Corrigan *et al* identifying the ribosomal GTPases. However, upon purification of promising hits we utilised, the DRaCALA technique with recombinant protein and discovered it was not useful for the identification of weak binders with high micromolar binding affinities. Two separate groups of proteins were investigated in this manner and every protein we tested except the positive control of RsgA did not provide a positive result. To avoid working our way through the remaining ~140 proteins, we sought out a new method for sensing ppGpp binding and settled on ^{31}P NMR. This was incredibly successful and allowed for the detection of a reduction in the phosphate signals across four potential ppGpp binding proteins from our Group 2 potential binders (figure 5.2.2.2). In the future, it would be worth expressing more protein and investigating these interactions further to determine exactly which

phosphates were involved in binding. In addition to confirming binding interactions of proteins in group 2, purifying some of the proteins from Group 1 to assess their binding by NMR methods before later determining a K_d using ITC would be beneficial and limit the protein required for initial testing with 40-100 µM being sufficient in our NMR studies. Although MST was a promising technique to trial due to its low protein concentration requirement, it was ultimately unsuccessful for determining a K_d due to poor binding of the dye to the 6xHis-tag. Optimisation of the buffer conditions may improve this but until then, the use of ITC will be sufficient as demonstrated by another member of the lab when determining a K_d for HxlB (25.3µM).

The role of (p)ppGpp binding proteins in central metabolism and nucleotide synthesis has already been demonstrated by PurF, Gmk and HprT. So the identification of the isomerase HxlB as an interaction partner is interesting as its main product, D-arabino-hex-3-ulose 6-phosphate, is a linking product between glycolysis and the pentose phosphate pathway. This product is readily transformed into ribulose-5-phosphate, the precursor to R5P and ultimately PRPP, directly affecting the synthesis of purine nucleotides to ensure GTP pools stay depleted under stress. Our fructose 6-phosphate assays aimed to investigate whether (p)ppGpp acts as an inhibitor of HxlB (figure 5.2.4.1). While these assay noted a trend towards inhibition, significance was not reached. Therefore, optimisation of the F6P assay by modifying temperature or protein-ligand ratios may help us better characterise the interaction between HxlB and (p)ppGpp. The binding between HxlB and (p)ppGppremains important, as if (p)ppGpp acts as an inhibitor of HxlB preventing purine nucleotide synthesis through a lack of d-arabino-hex-3-ulose 6-phosphate, then it stands to reason that F6P concentrations will increase. As a result, the concentration of each intermediate following F6P will increase ultimately leading to an increase in pyruvate concentration. Pyruvate is a key player in gluconeogenesis and the production of amino acids, potentially implicating HxlB in the starvation response (figure 5.3). When considering HxlB was identified in stationary phase where bacteria are enduring nutrient poor conditions, this is exciting.

In order to further investigate the role of HxlB in the stringent response we are working in collaboration with the University of Nebraska Medical Centre where we will make use of their state-of- the-art metabolomics facilities to quantify glycolytic metabolites along with other metabolites linked to HxlB. Metabolomics will be done in both true nutrient starved conditions and stationary phase in order to determine the effect HxlB has on maintaining the SR through its interaction with (p)ppGpp.

The synthesis of the selective fluorescent chemo-sensor PyDPA also addresses a separate aim of the project, which was to be able to selectively and accurately quantify (p)ppGpp levels (figure 6.2.5.1 and 6.2.5.2). Having access to this complex allows us to probe (p)ppGpp levels under various stress conditions and across various synthetase mutants furthering our understanding of which synthetases are responsible for (p)ppGpp production under a given stress.

Overall, in this study we aimed to design a synthetic route for a non-covalent capture compound capable of isolating novel ppGpp interaction partners in *S. aureus*. This was completed, providing us with some insight into the stringent response signalling network and its effect on various processes. Although characterisation of some proteins still remains, they are heavily involved in important cellular processes such as the foldase PrsA being involved in β-lactam resistance by influencing PBP2a levels(Jousselin et al., 2015). Other proteins involved in metabolism such as the positive binders MvaD and Ac2460 identified by ^{31}P NMR are also worth characterising. It is widely known that the SR has an effect on virulence, so proteins involved in dealing with the host immune system and antibiotic resistance such as PerR, Ohr, KatA and VraR respectively are all interesting targets that should have their binding to (p)ppGpp validated. The staphylococcal RNAP subunits RpoE and RpoY pose an interesting prospect, as if their binding to (p)ppGpp can be confirmed this may suggest an entirely new regulatory mechanism for transcription across Bacillota with the formation of the RNAP complex being inhibited by allosteric binding instead of (p)ppGpp binding directly to the RNAP. The role of (p)ppGpp in purine nucleotide synthesis has previously been shown by Wang *et al*, with PurF being directly inhibited by the alarmones. Therefore, the identification of the 3-hexulose-6-phosphate HxlB as a binder of (p)ppGpp suggests an interesting mechanism for modulating carbon metabolism. The number of putative hits we have identified, along with the definitive hit HxlB, underlines the potential capture compounds have for the mapping of cellular signalling networks when compared to other approaches such as DRaCALA. However, capture compound approaches for other signalling nucleotides such as GTP or NADPH may be significantly messier due to the increased number of binding partners and shared binding modes, necessitating a greater number of controls and more stringent criteria for determining significant hits.

In conclusion, the role of HxlB in the SR is currently being investigated further in a collaboration with the University of Nebraska Medical Centre, where we will use metabolomics to quantify glycolytic metabolites in the absence and induction of the SR. All in all, we believe this work can hopefully be used to aid in the mapping and understanding of the (p)ppGpp signalling network, which may eventually lead to the potential development of novel therapeutics.

Supplementary information

2-[2-[2-[2- (4-methylphenyl)sulfonyloxyethoxy]ethoxy]ethoxy]ethyl 4-methylbenzenesulfonate (11)

^{1}H NMR analysis

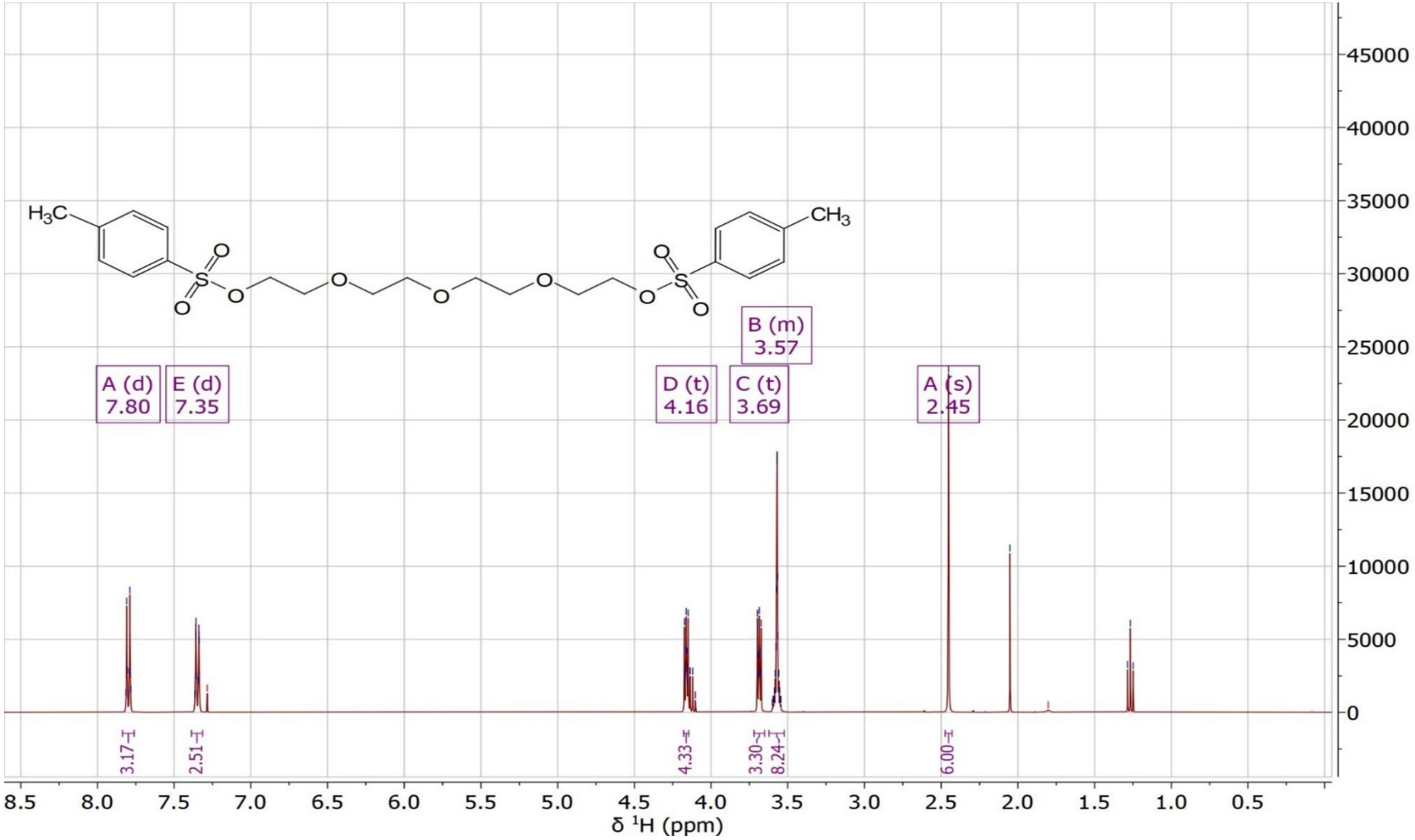

HRMS (ESI+)

User Spectra

Fragmentor Voltage	Collision Energy	Ionization Mode
125	0	ESI

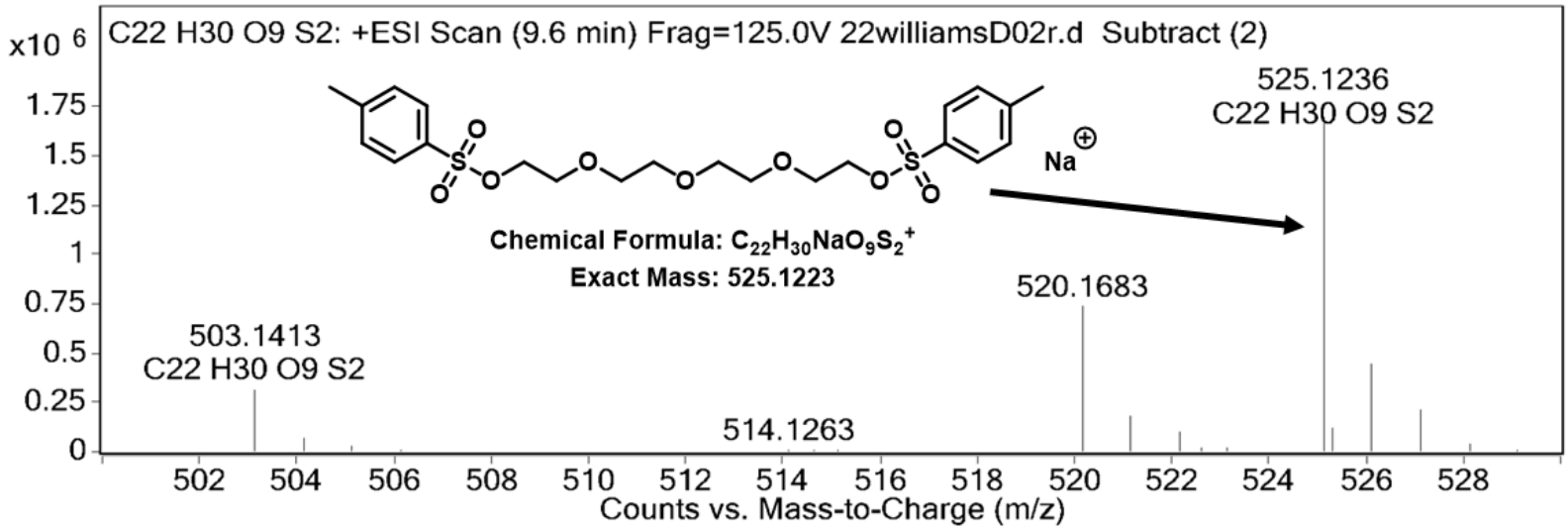

Peak List

m/z	z	Abund	Formula	Ion	PPM Difference	Calculated m/z
503.1413	1	315905.63	C22 H30 O9 S2	(M+H)+	-1.75	503.1404
520.1683	1	735516.5				
525.1236	1	1693847.75	C22 H30 O9 S2	(M+Na)+	-2.38	525.1223
526.1268	1	445971.88	C22 H30 O9 S2	(M+Na)+	-2.36	526.1255

1,11-diazido -3,6,9-trioxaundecane (12)

^{1}H NMR analysis

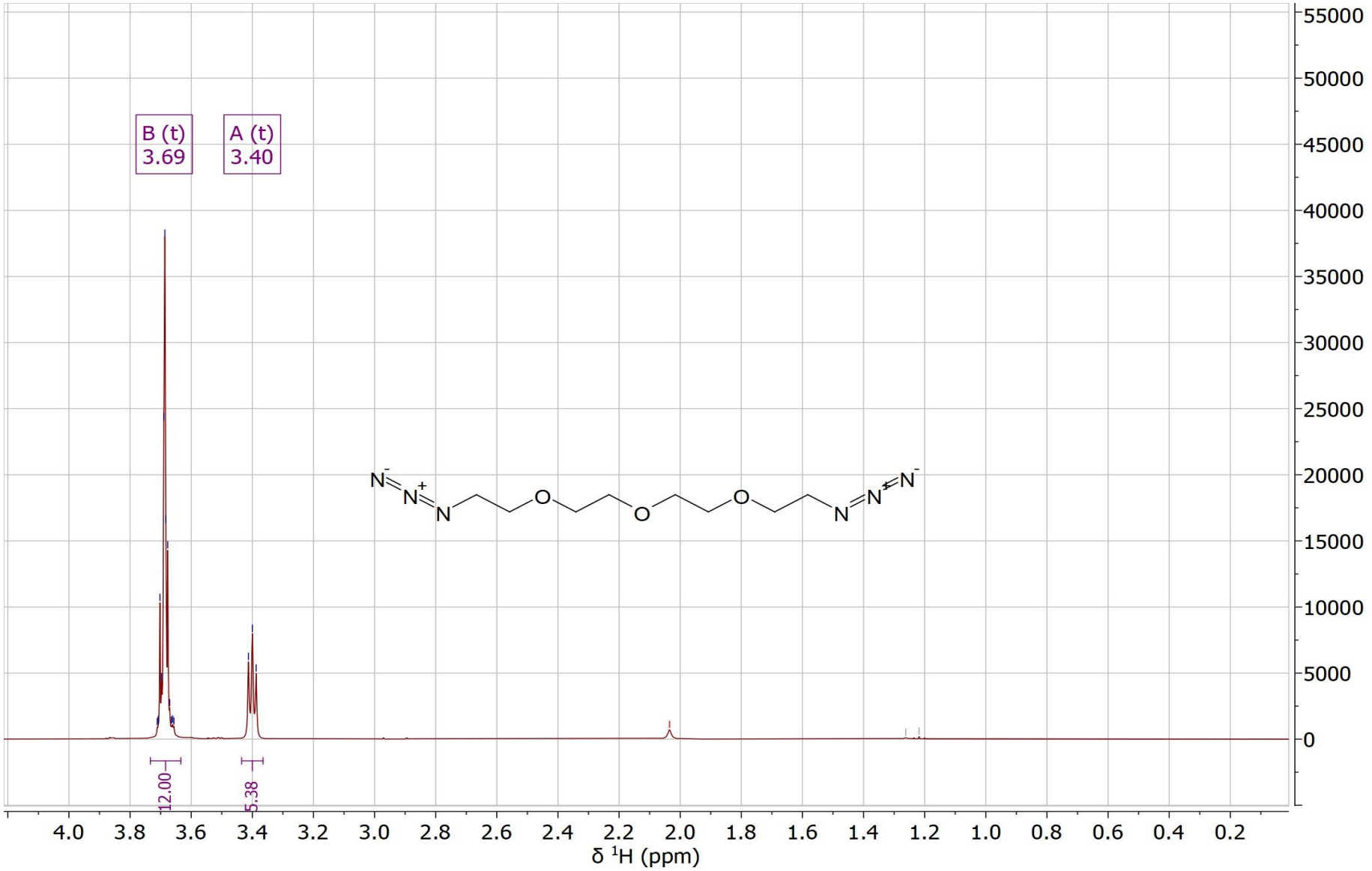

HRMS (ESI+)

User Spectra

Fragmentor Voltage	Collision Energy	Ionization Mode
125	0	ESI

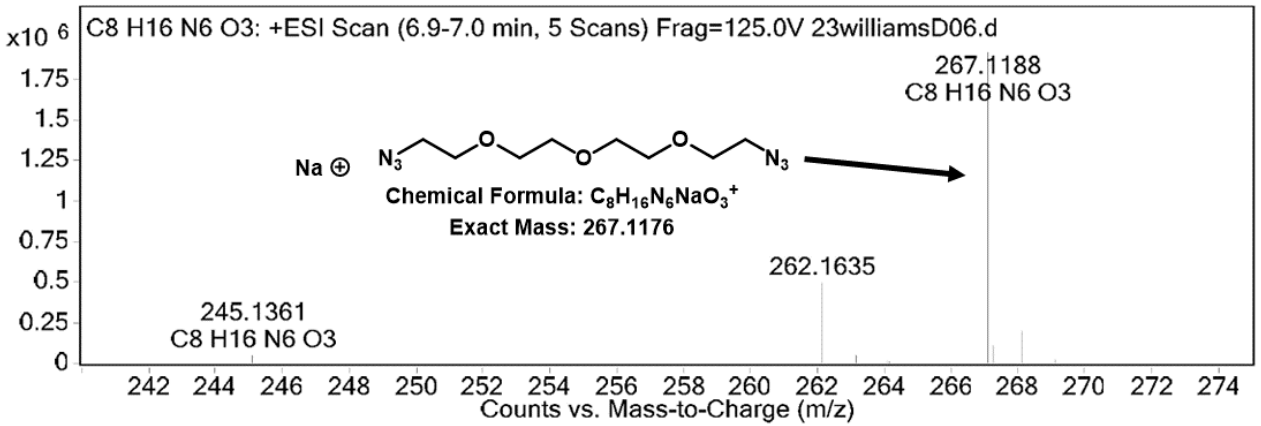

Peak List

m/z	z	Abund	Formula	Ion	PPM Difference	Calculated m/z
61.0083		73621.29				
64.0164		125908.75				
81.5215		130313.77				
142.0455		43119.82				
217.1302		194676.88				
245.1361		48714.23	C8 H16 N6 O3	(M+H)+	-1.83	245.1357
262.1635	1	496939.84				
263.1649	1	49225.35				
267.1188	1	1914453.25	C8 H16 N6 O3	(M+Na)+	-4.34	267.1176
267.2473		112429.33				
268.121	1	200229.34	C8 H16 N6 O3	(M+Na)+	-4.45	268.1198
283.0919		61542.38				

Infrared Spectrum

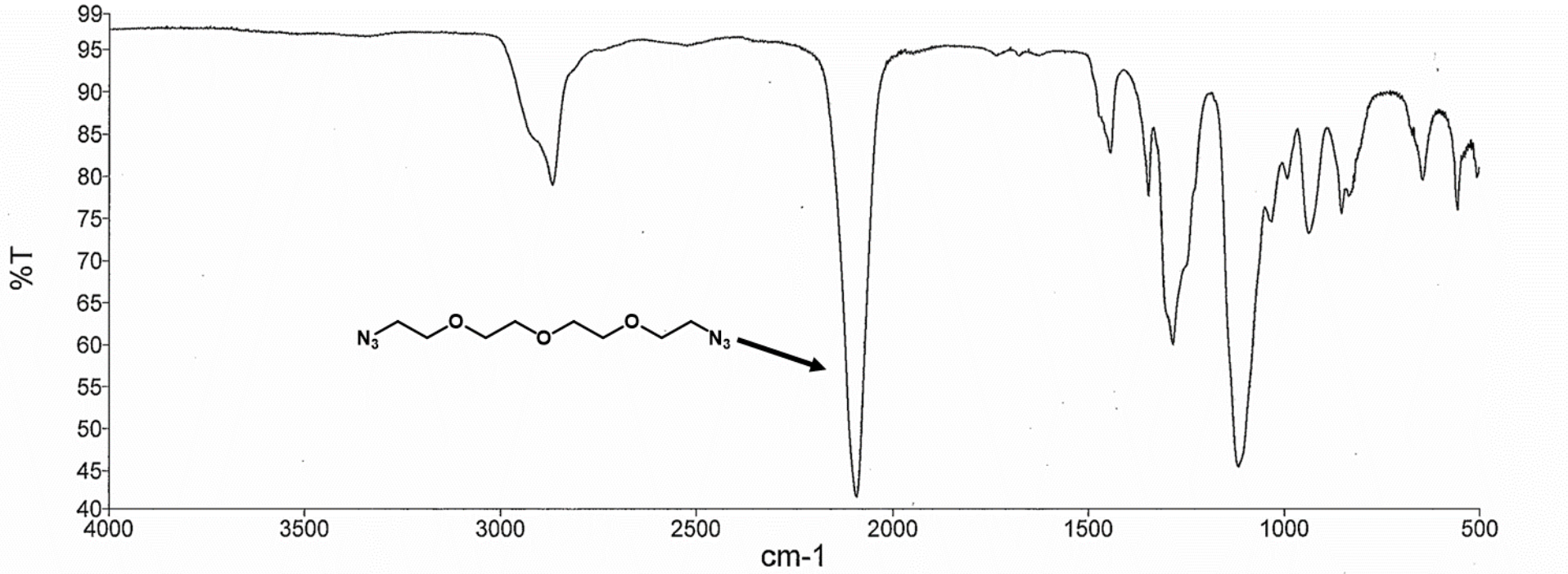

Sample Name	Description	Quality Checks	Pathlength (mm)
MG10	Sample 004 by ftir Date Wednesday, July 21 2021	The Quality Checks do not report any warnings for the sample.	1

1-azido-3,6,9-trioxaundecan-11-amine hydrochloride (13)

^{1}H NMR analysis

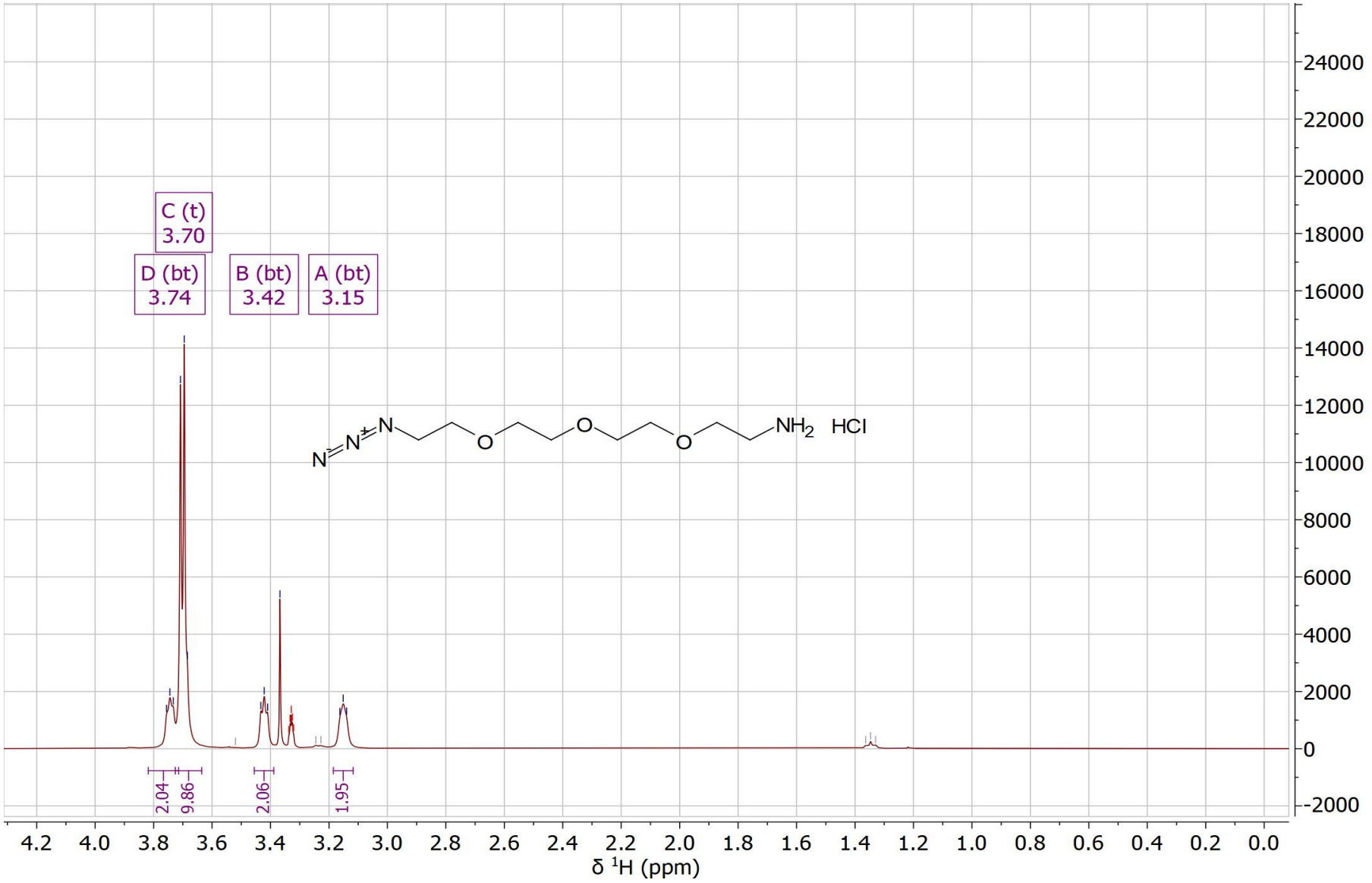

HRMS (ESI+)

User Spectra

Fragmentor Voltage	Collision Energy	Ionization Mode
125	0	ESI

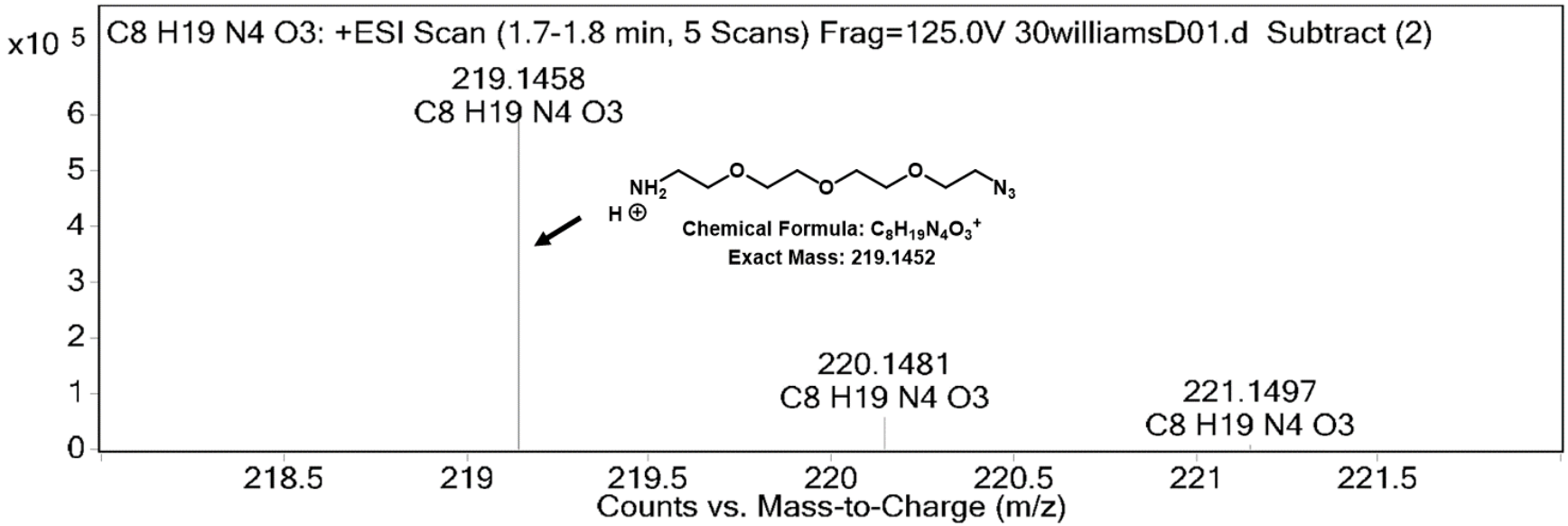

Peak List

m/z	z	Abund	Formula	Ion	PPM Difference	Calculated m/z
219.1458	1	596456.38	C8 H19 N4 O3	M+	-3.03	219.1452

Pentafluorophenyl 5-[(3aS,4S,6aR)-2-oxohexahydro-1H-thieno[3,4-d]imidazol-4-yl]pentanoate (14)

^{1}H NMR analysis

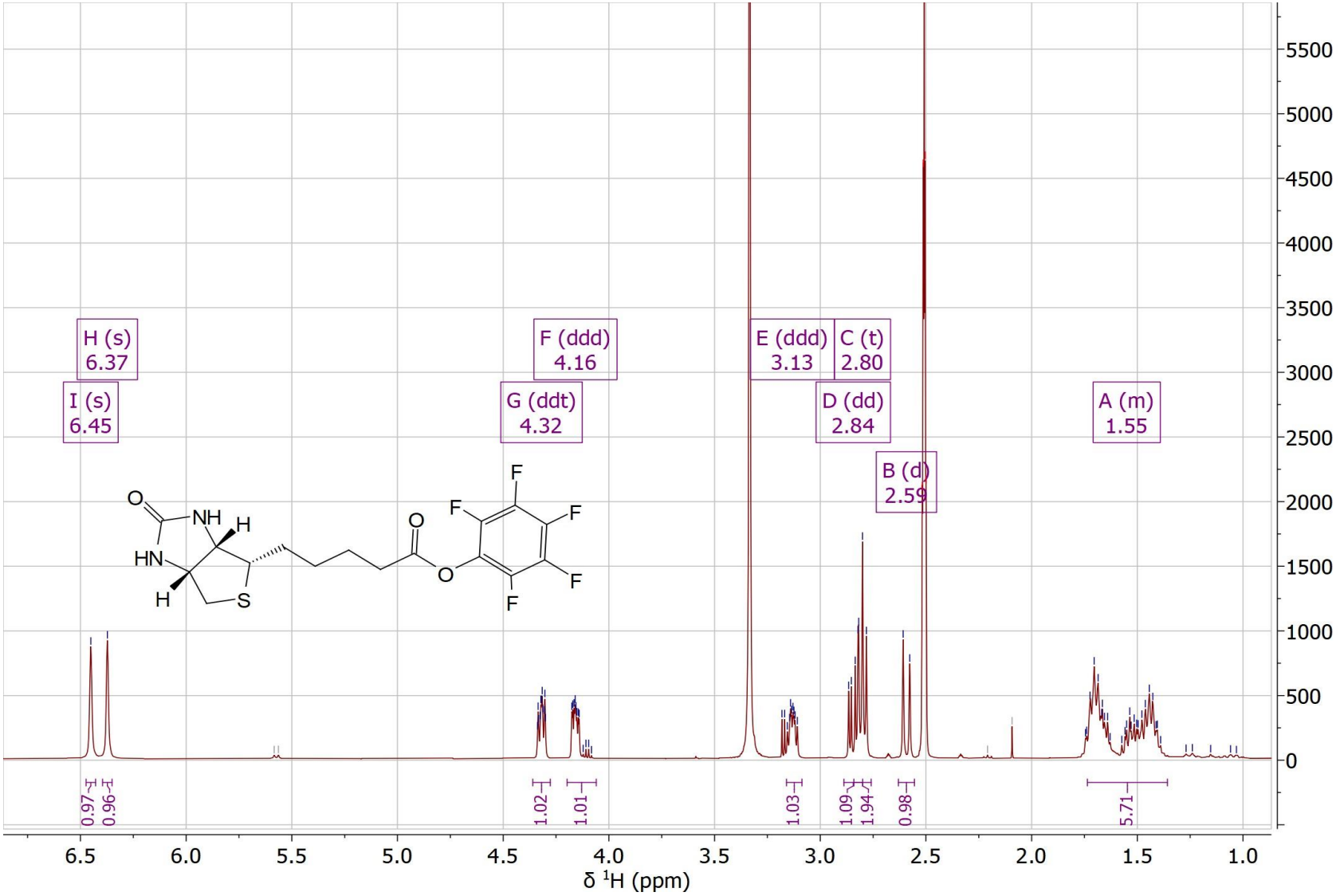

^{19}F NMR analysis

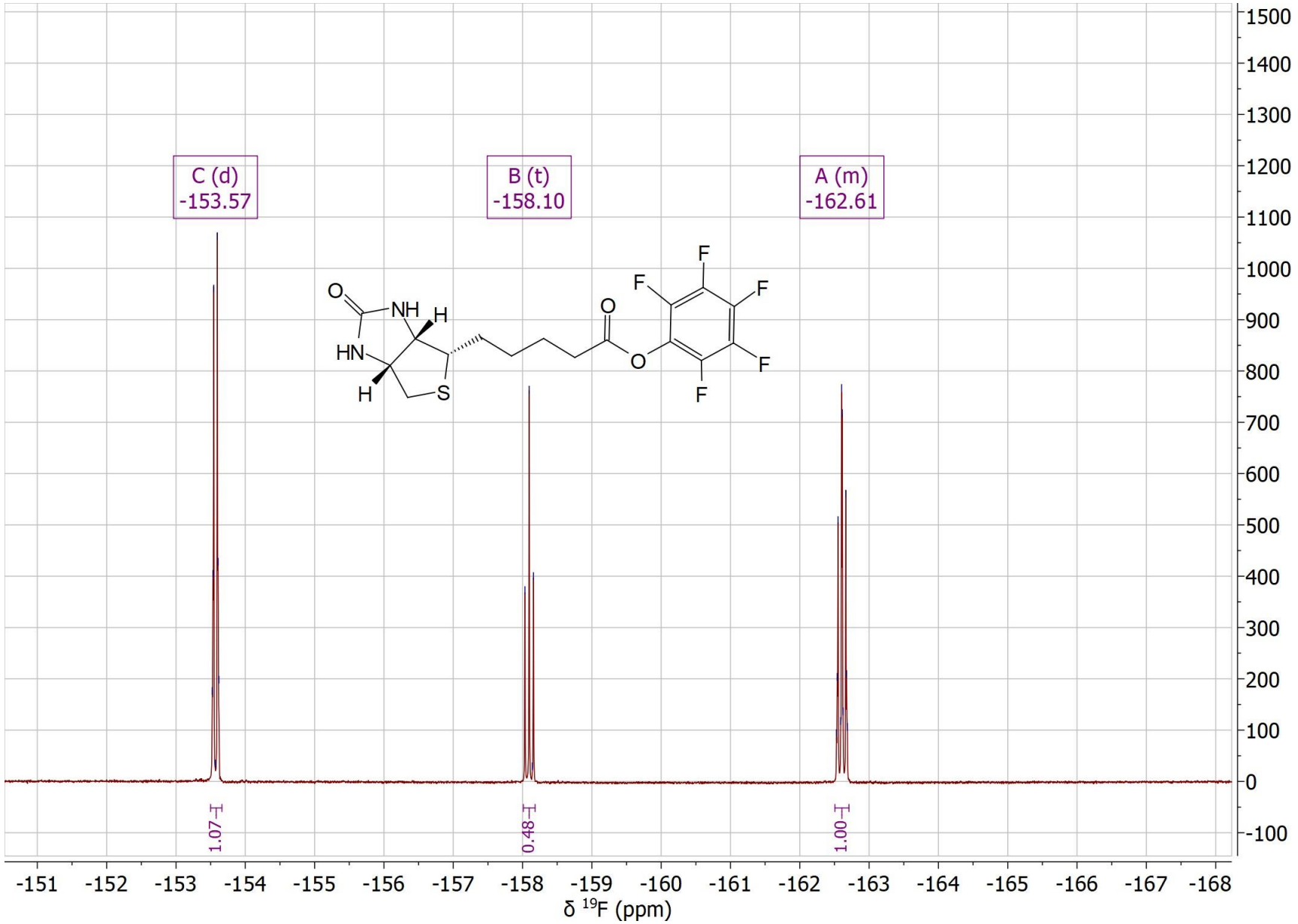

HRMS (ESI+)

User Spectra

Fragmentor Voltage	Collision Energy	Ionization Mode
125	0	ESI

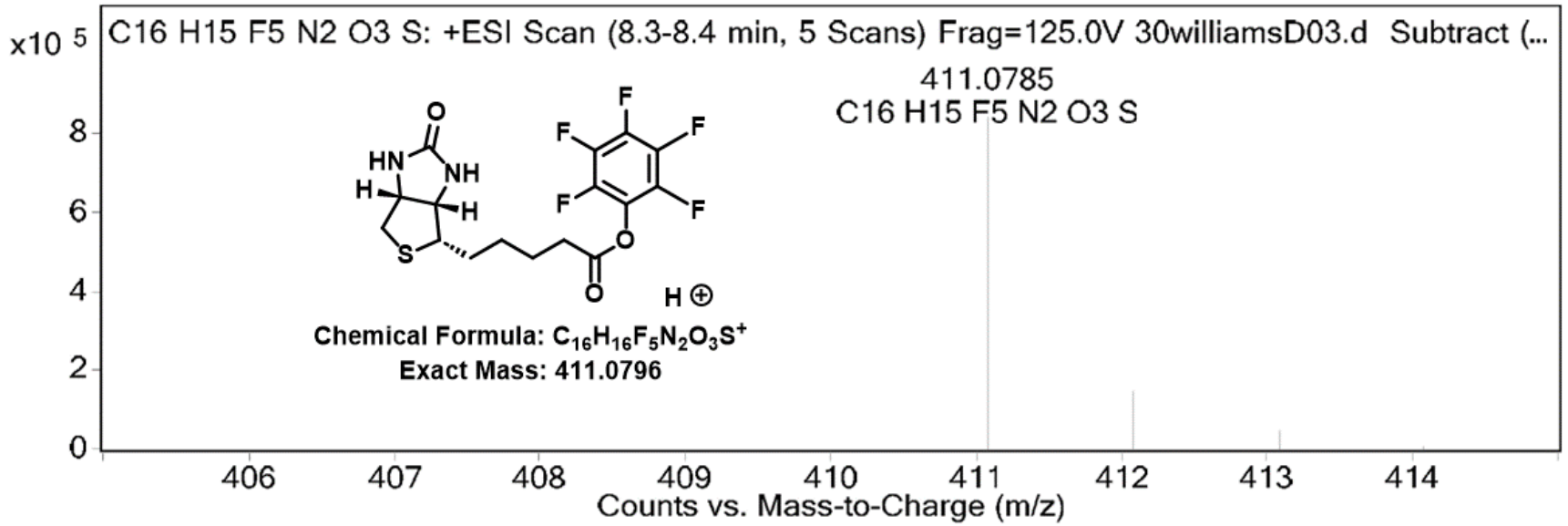

Peak List

m/z	z	Abund	Formula	Ion	PPM Difference	Calculated m/z
411.0785	1	841442.25	C16 H15 F5 N2 O3 S	(M+H)+	2.72	411.0796

N-[2-[2-[2- (2-Azidoethoxy)ethoxy]ethoxy]ethyl]hexahydro-2-oxo- (3aS,4S,6aR)- 1H-thieno[3,4-d]imidazole-4-pentanamide (15)

^{1}H NMR analysis

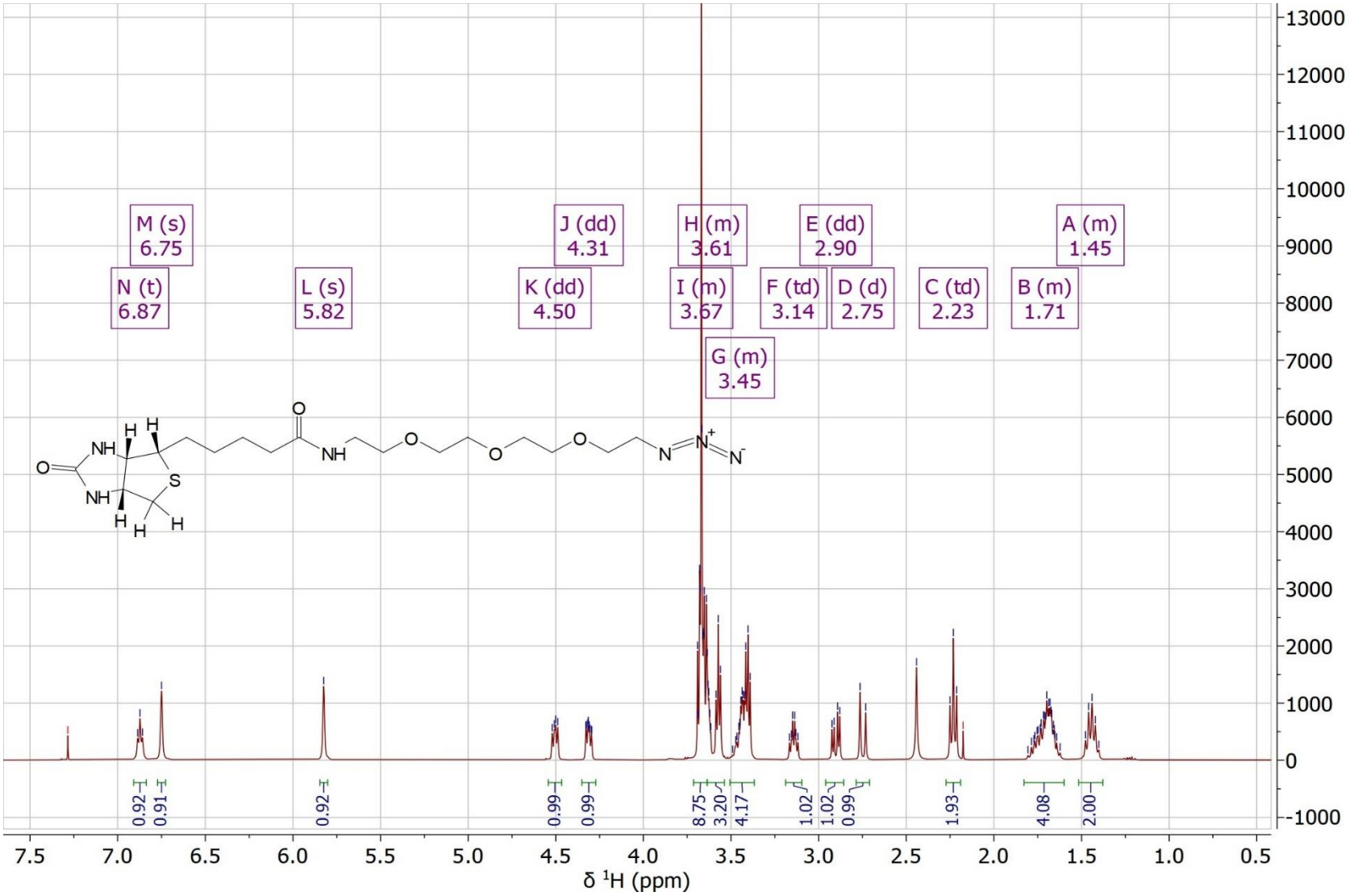

HRMS (ESI+)

User Spectra

Fragmentor Voltage	Collision Energy	Ionization Mode
125	0	ESI

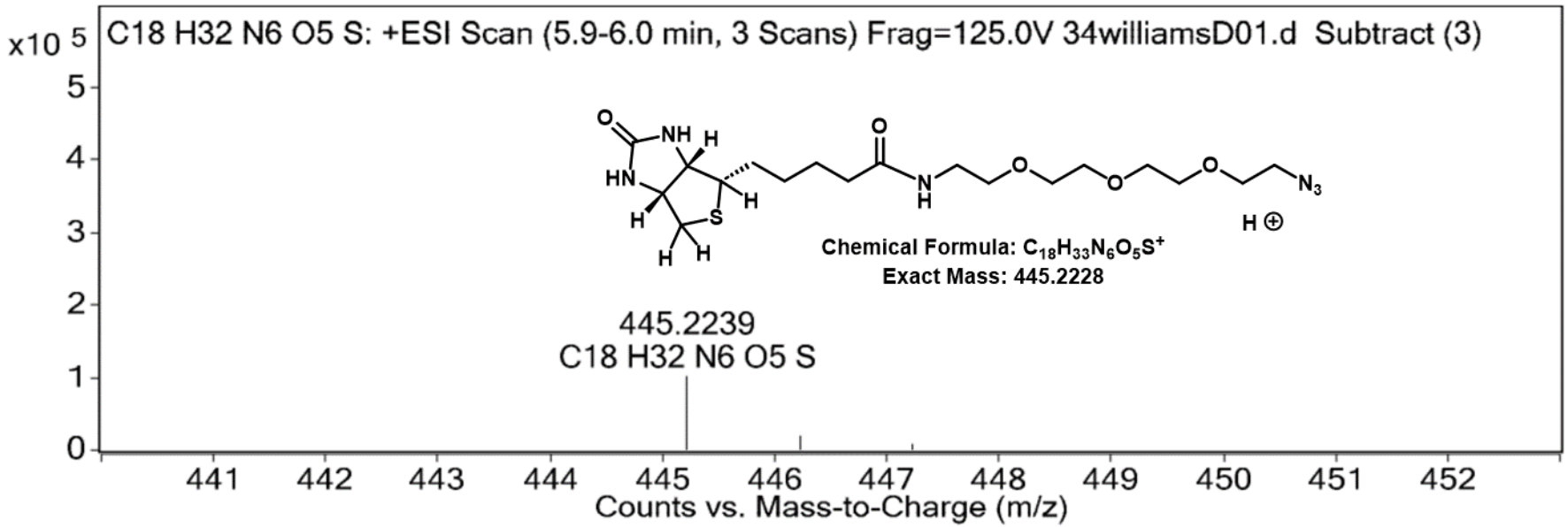

Peak List

m/z	z	Abund	Formula	Ion	PPM Difference	Calculated m/z
445.2239	1	100605.47	C18 H32 N6 O5 S	(M+H)+	-2.62	445.2228
467.2068	1	532062.5	C18 H32 N6 O5 S	(M+Na)+	-4.51	467.2047
468.2083	1	108938.72	C18 H32 N6 O5 S	(M+Na)+	-1.92	468.2074

1H-Thieno[3,4-d]imidazole-4-pentanamide, N-[2-[2-[2-(2-aminoethoxy)ethoxy]ethoxy]ethyl]hexahydro-2-oxo-,(3aS,4S,6aR) (16)

^{1}H NMR analysis

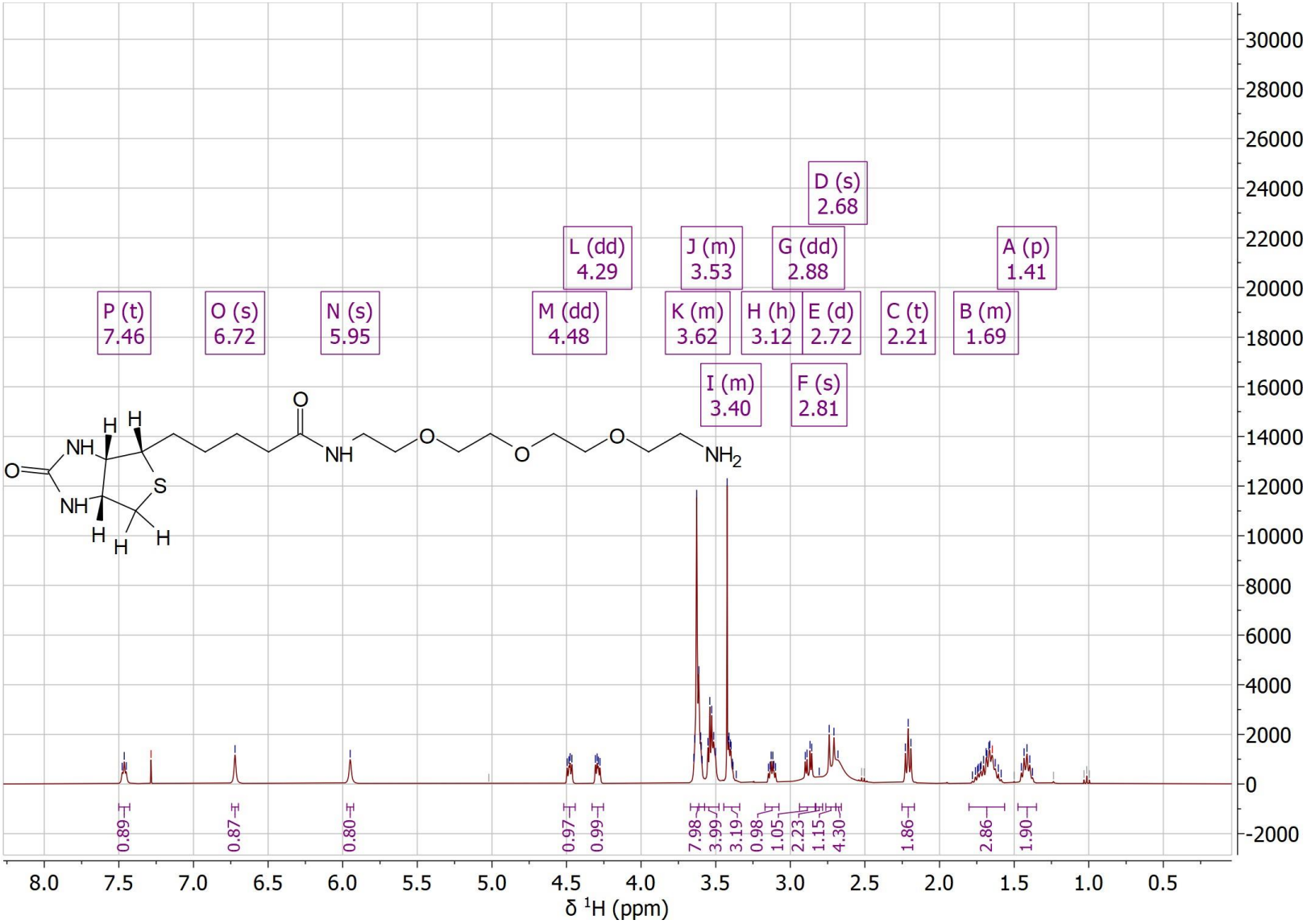

HRMS (ESI+)

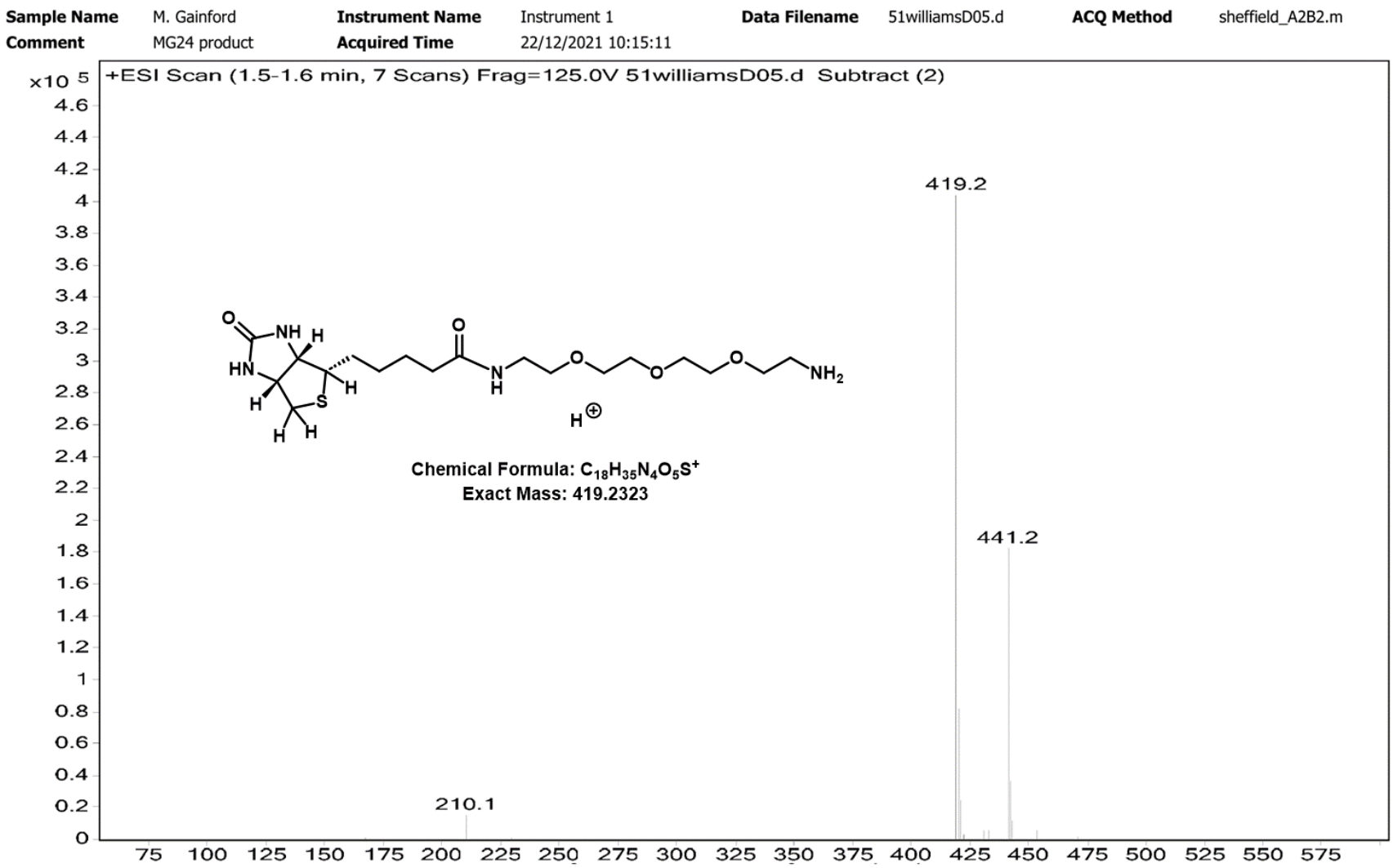
Sample Name M. Gainford
Instrument Name Instrument 1
Data Filename 51williamsD05.d
ACQ Method sheffield_A2B2.m
Comment MG24 product
Acquired Time 22/12/2021 10:15:11
+ESI Scan (1.5-1.6 min, 7 Scans) Frag=125.0V 51williamsD05.d Subtract (2)
x10 5
419.2
441.2
210.1
Chemical Formula: C18H35N4O5S+
Exact Mass: 419.2323

H-Thieno[3,4-d]imidazole-4-pentanamide, N-(14-bromo-13-oxo-3,6,9-trioxa-12-azatetradec-1-yl)hexahydro-2-oxo-,(3aS,4S,6aR) (17)

^{1}H NMR analysis

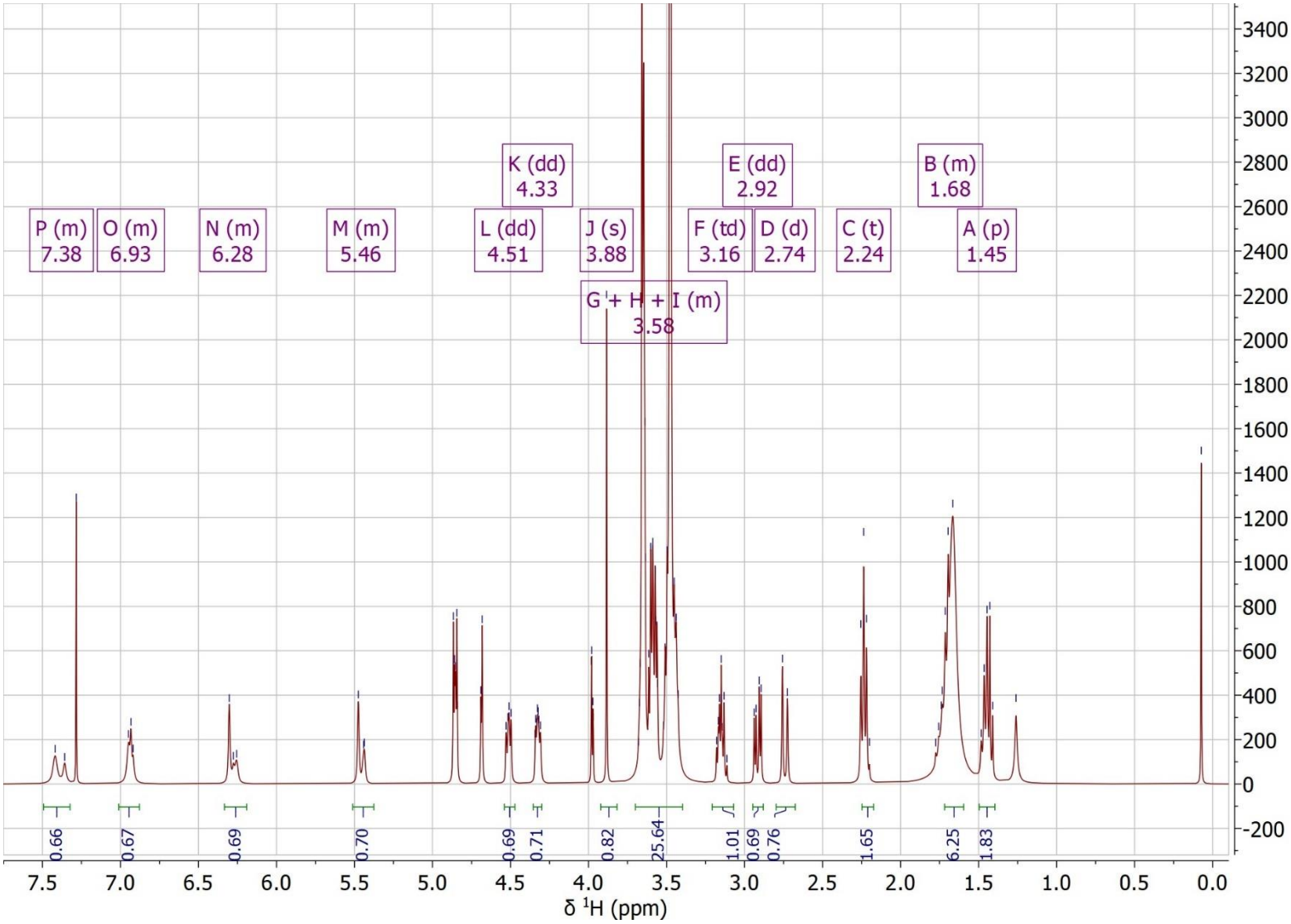

LCMS (ESI+)

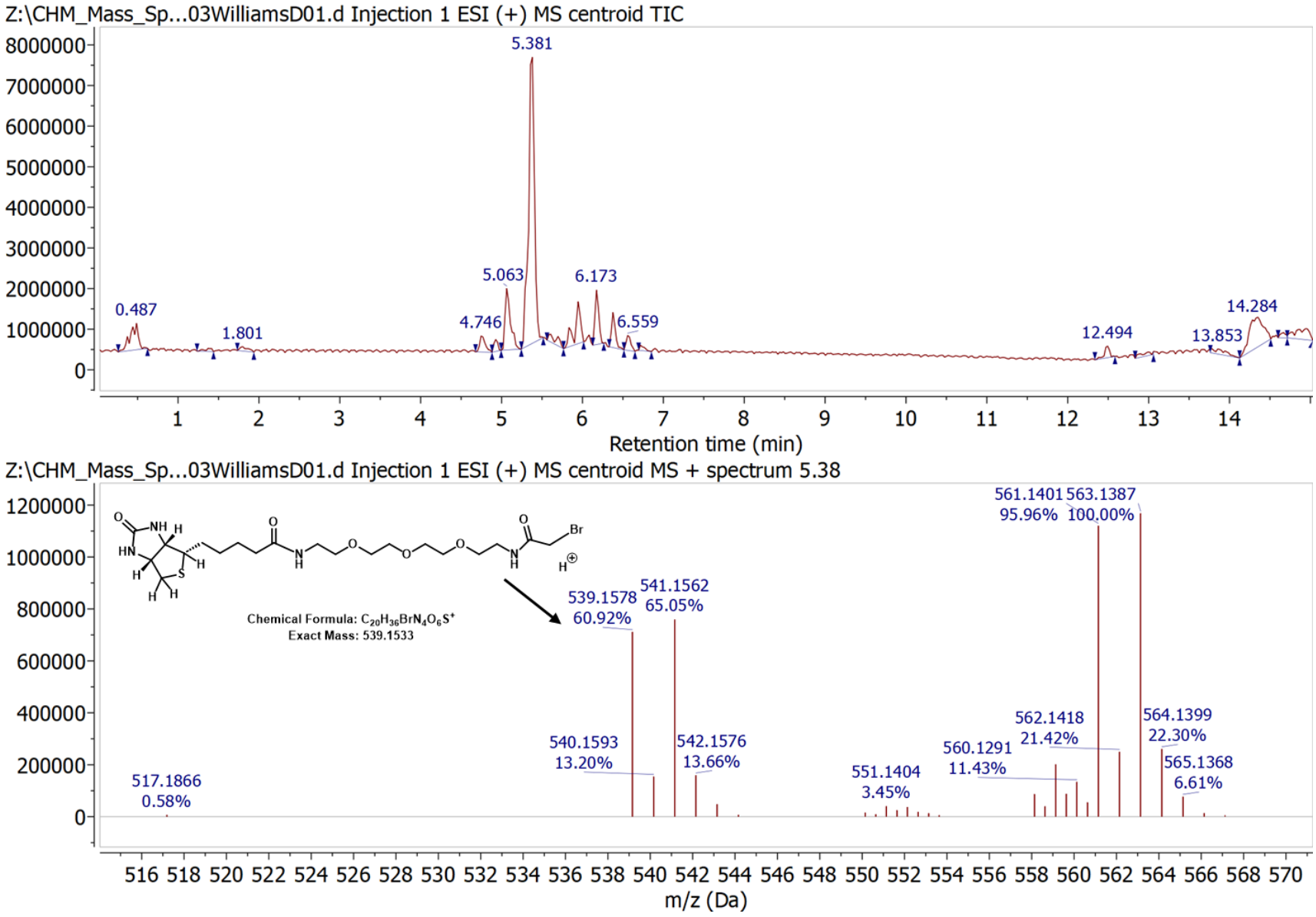
Z:\CHM_Mass_Sp...03WilliamsD01.d Injection 1 ESI (+) MS centroid TIC
5.381
5.063
6.173
0.487
1.801
4.746
6.559
12.494
13.853
14.284
Retention time (min)
Z:\CHM_Mass_Sp...03WilliamsD01.d Injection 1 ESI (+) MS centroid MS + spectrum 5.38
Chemical Formula: C20H36BrN4O6S+
Exact Mass: 539.1533
561.1401 95.96%
563.1387 100.00%
539.1578 60.92%
541.1562 65.05%
540.1593 13.20%
542.1576 13.66%
562.1418 21.42%
564.1399 22.30%
560.1291 11.43%
565.1368 6.61%
551.1404 3.45%
517.1866 0.58%
m/z (Da)

([(2R,3S,4R,5R)-5-(2-amino-6-oxo-1H-purin-9-yl)-4-hydroxy-2-[[hydroxy(phosphonooxy)phosphoryl]oxymethyl]oxolan-3-yl] phosphono thiophosphate) p(s)pGpp (18)

^{31}P NMR analysis

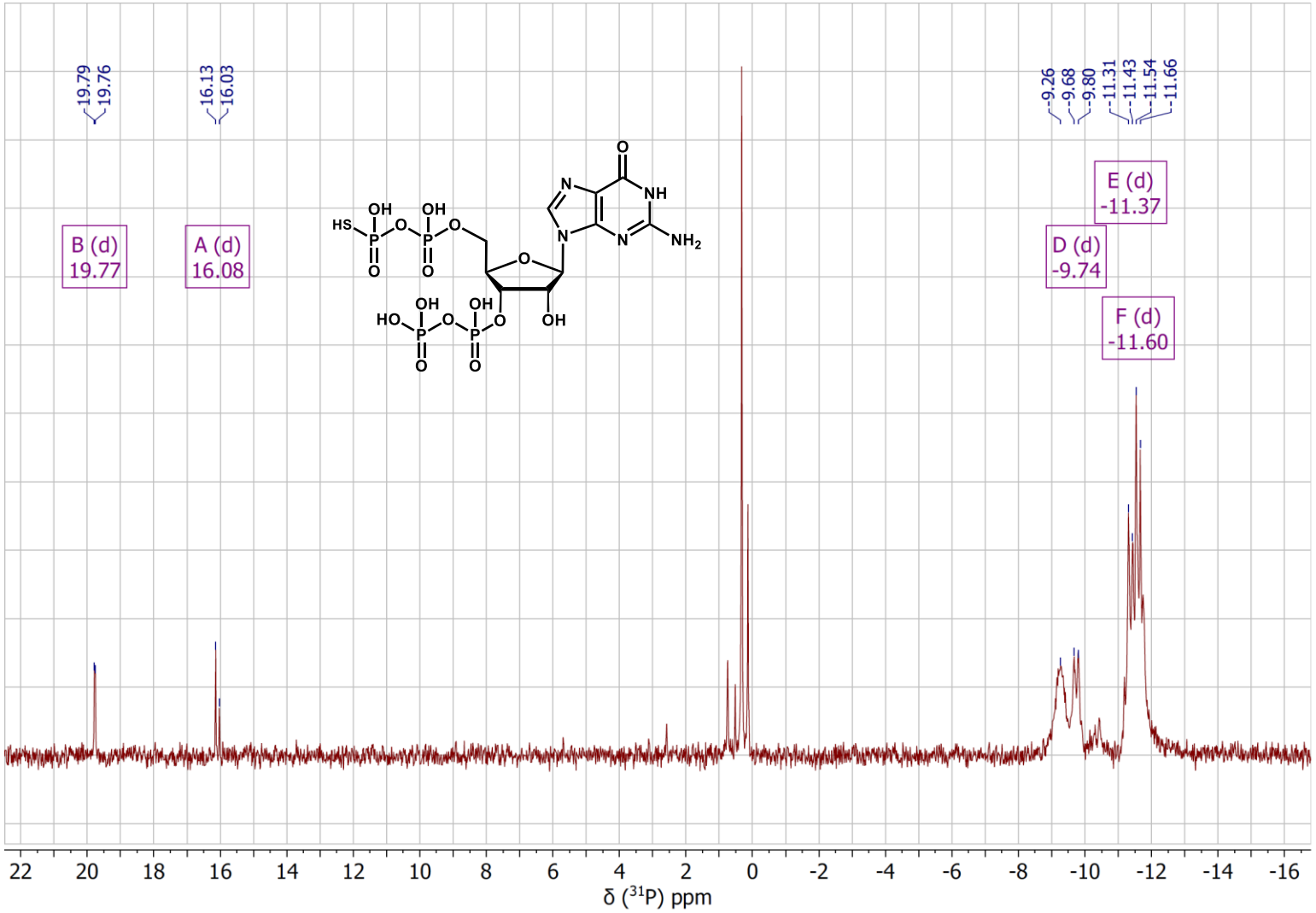

HRMS (ESI-)

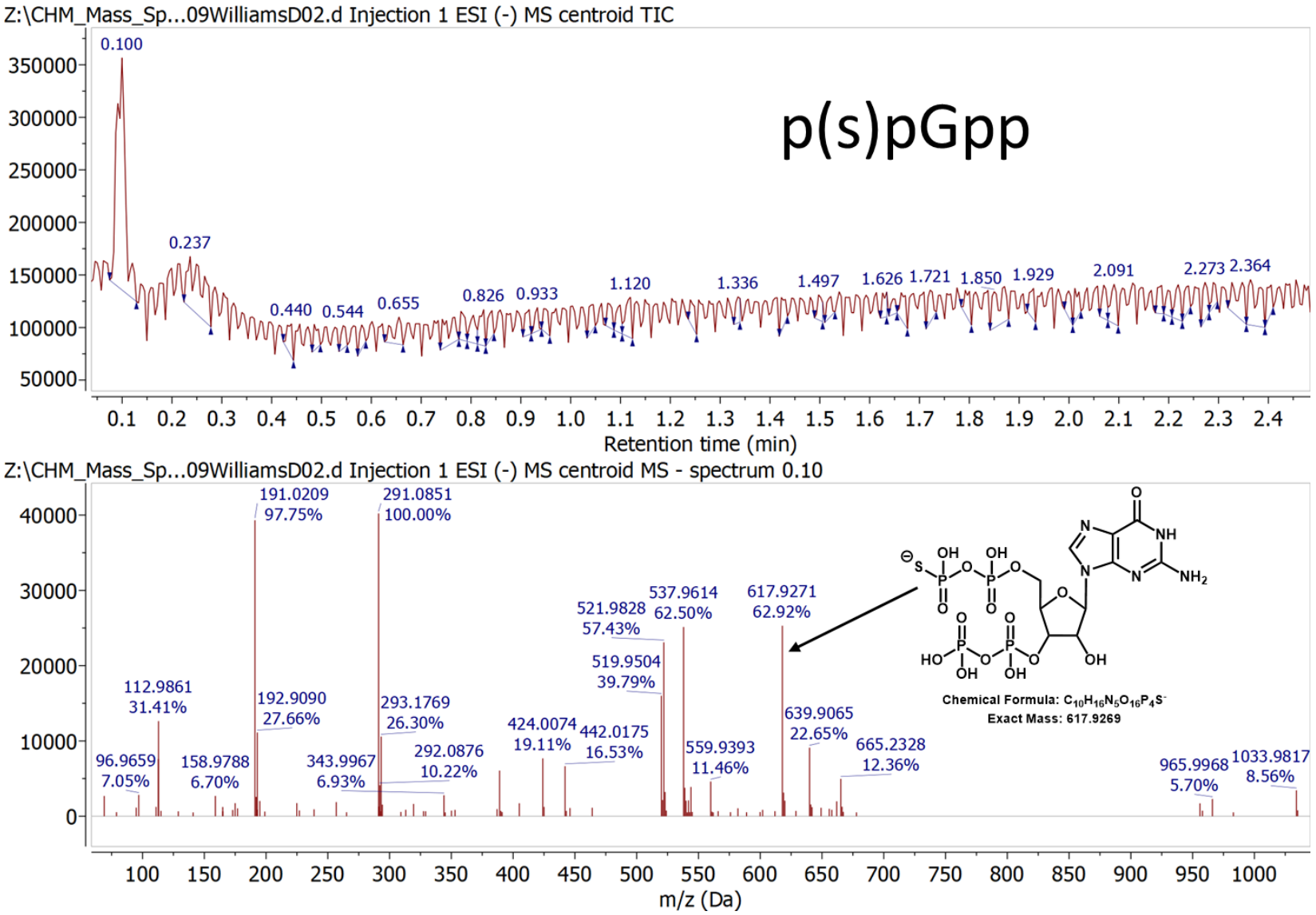
Z:\CHM_Mass_Sp...09WilliamsD02.d Injection 1 ESI (-) MS centroid TIC
p(s)pGpp
Retention time (min)
Z:\CHM_Mass_Sp...09WilliamsD02.d Injection 1 ESI (-) MS centroid MS - spectrum 0.10
m/z (Da)
191.0209 97.75%
291.0851 100.00%
537.9614 62.50%
617.9271 62.92%
521.9828 57.43%
519.9504 39.79%
112.9861 31.41%
192.9090 27.66%
293.1769 26.30%
424.0074 19.11%
442.0175 16.53%
639.9065 22.65%
559.9393 11.46%
665.2328 12.36%
96.9659 7.05%
158.9788 6.70%
343.9967 6.93%
292.0876 10.22%
965.9968 5.70%
1033.9817 8.56%
Chemical Formula: C10H16N5O16P4S-
Exact Mass: 617.9269

Guanosine 3'-diphosphate-5'-phosphoryl-phosphorylthio-11-amido-3,6,9-trioxaundecan-1-biotin (Capture compound 19)

HPLC trace in HFIP buffer

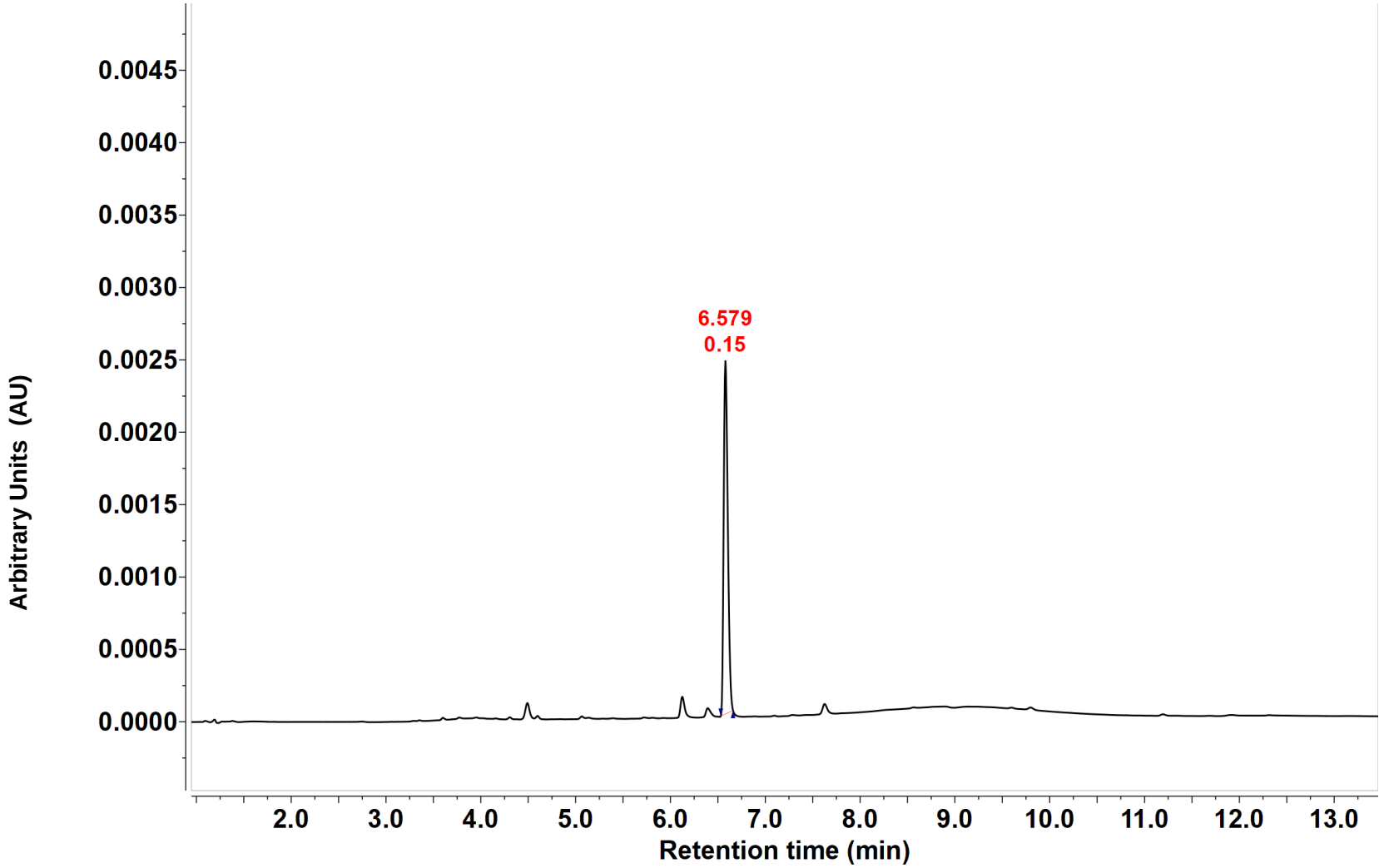

HRMS (ESI-)

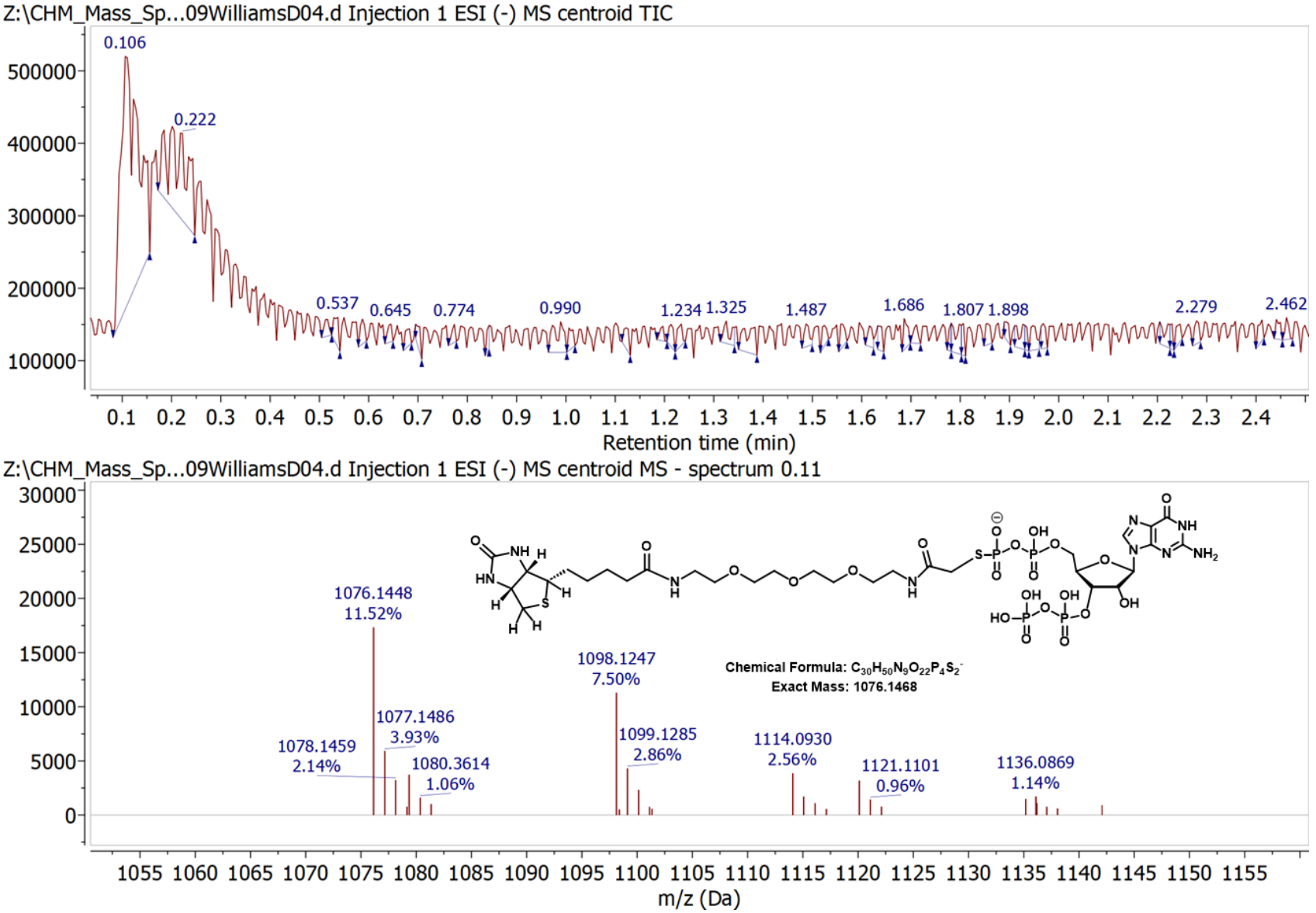
Z:\CHM_Mass_Sp...09WilliamsD04.d Injection 1 ESI (-) MS centroid TIC
0.106
0.222
0.537
0.645
0.774
0.990
1.234
1.325
1.487
1.686
1.807
1.898
2.279
2.462
Retention time (min)
Z:\CHM_Mass_Sp...09WilliamsD04.d Injection 1 ESI (-) MS centroid MS - spectrum 0.11
1076.1448
11.52%
1077.1486
3.93%
1078.1459
2.14%
1080.3614
1.06%
1098.1247
7.50%
1099.1285
2.86%
1114.0930
2.56%
1121.1101
0.96%
1136.0869
1.14%
Chemical Formula: C30H50N9O22P4S2-
Exact Mass: 1076.1468
m/z (Da)

3-Pyren-1-yl-prop-2-yn-1-ol (21)

^{1}H NMR analysis

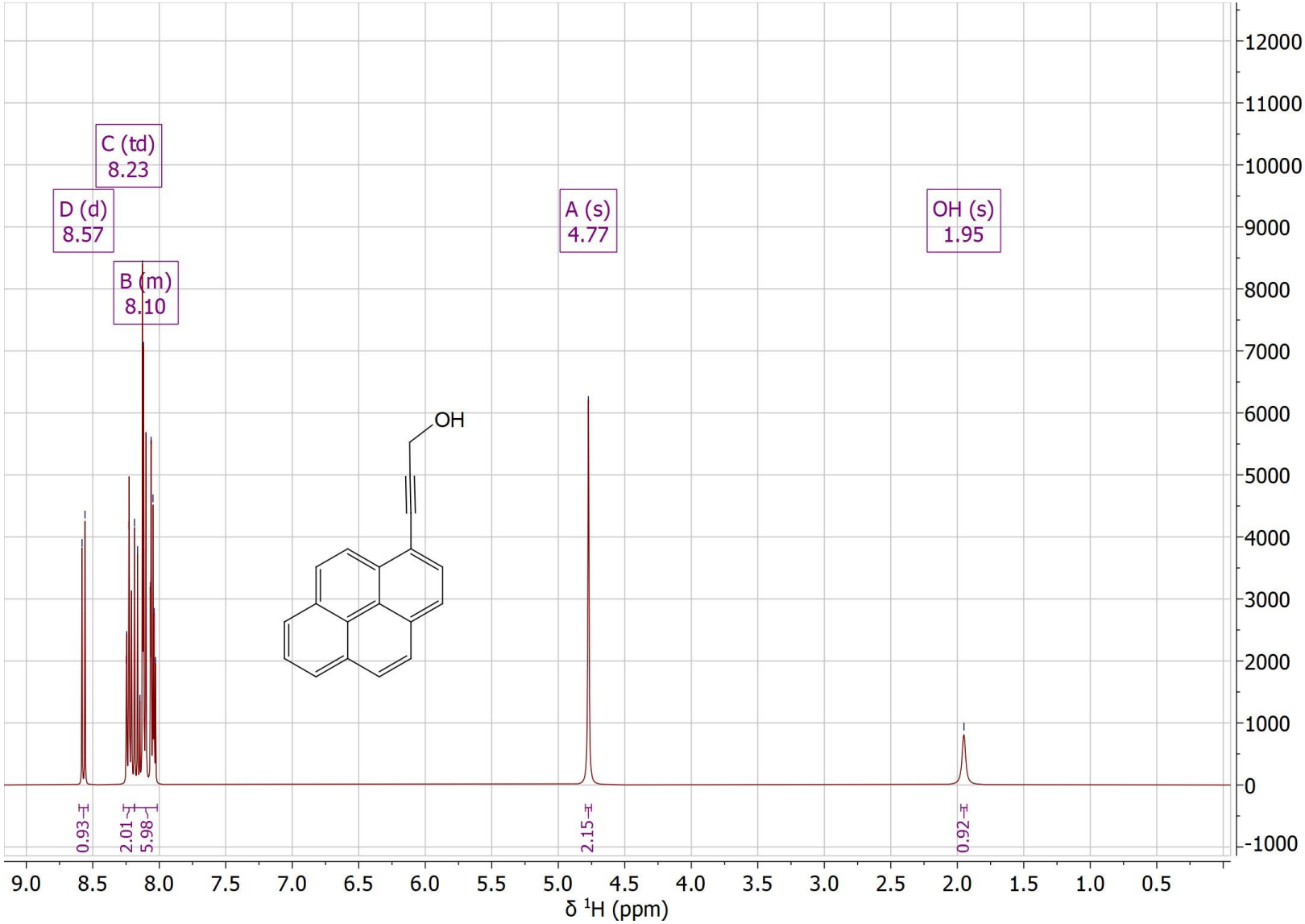

3- (pyren-1-yl)propan-1-ol (22)

^{1}H NMR analysis

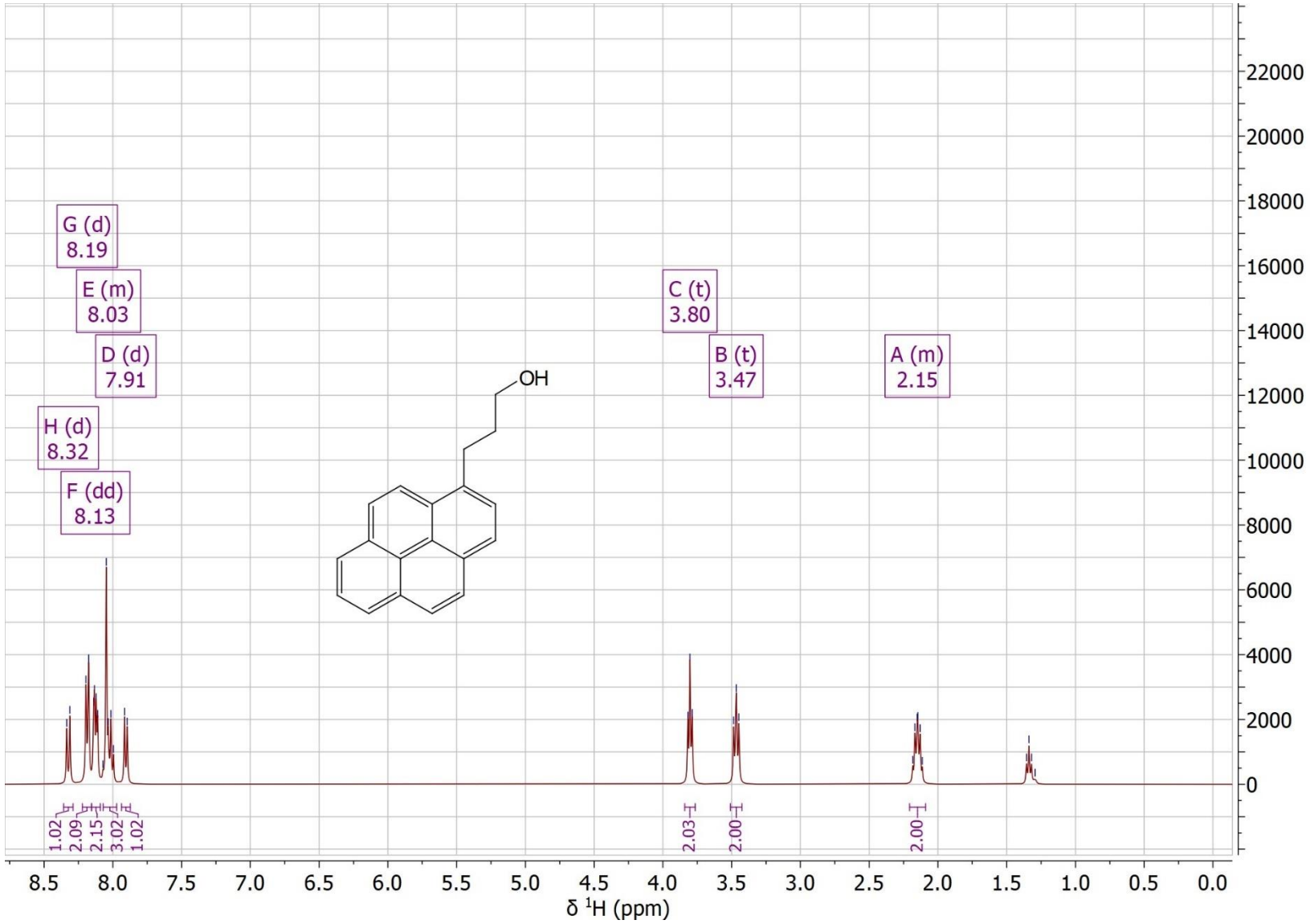

1- (3-bromopropyl)pyrene (23)

^{1}H NMR analysis

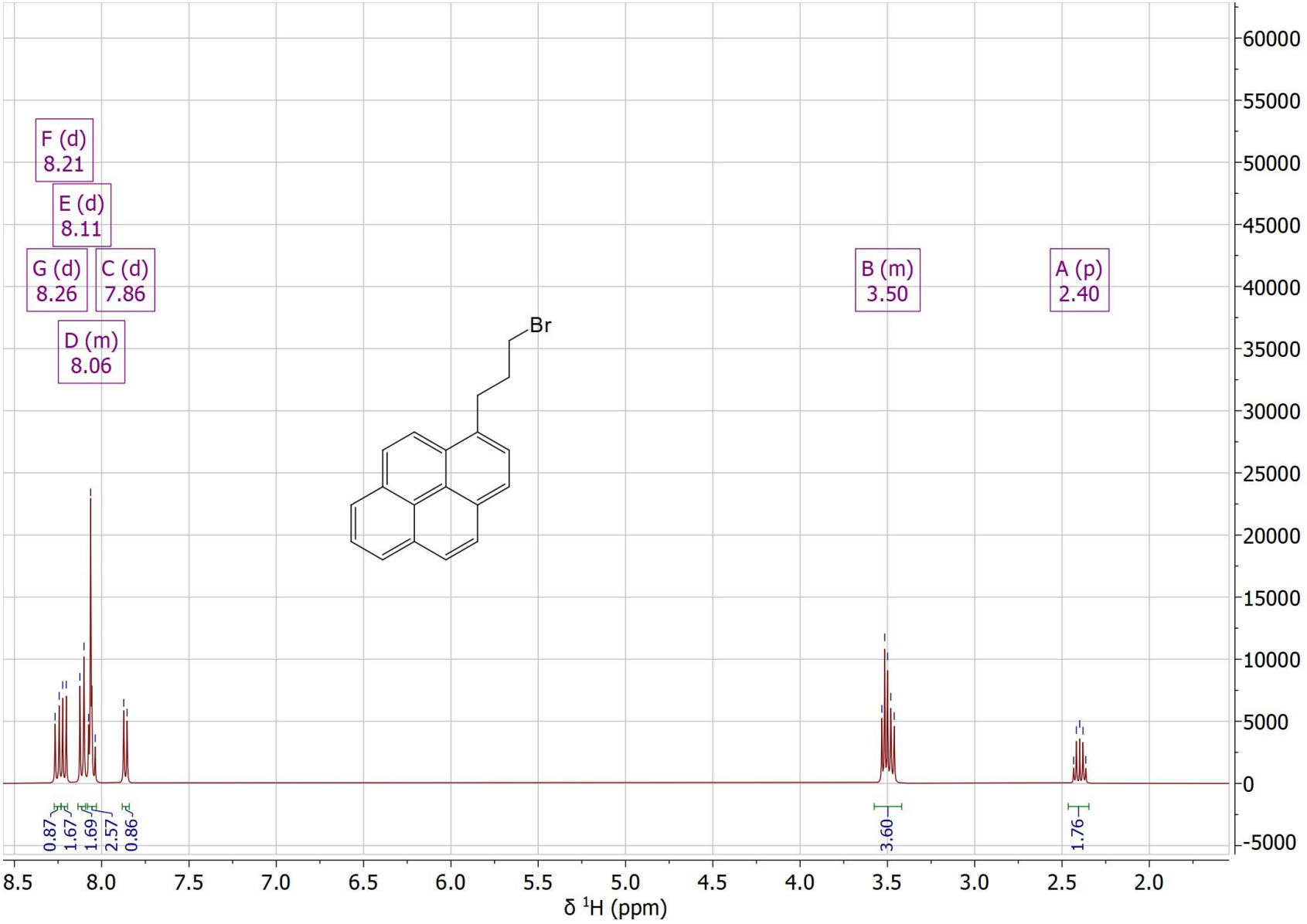

3,5-Bis-(hydroxymethyl)phenol (25)

^{1}H NMR analysis

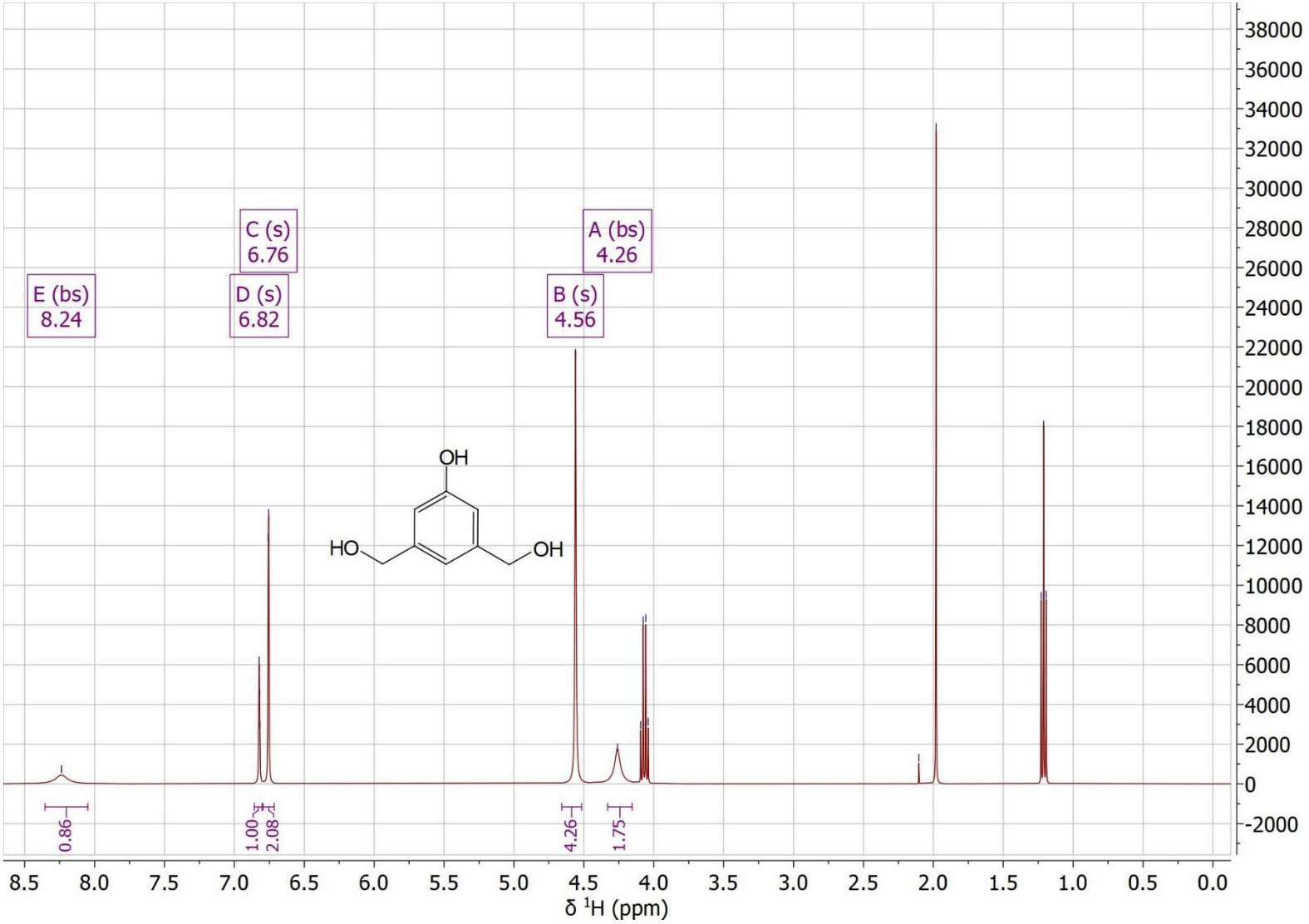

(5-[3-(pyren-1-yl)propoxy]-1,3-phenylene)dimethanol (26)

^{1}H NMR analysis

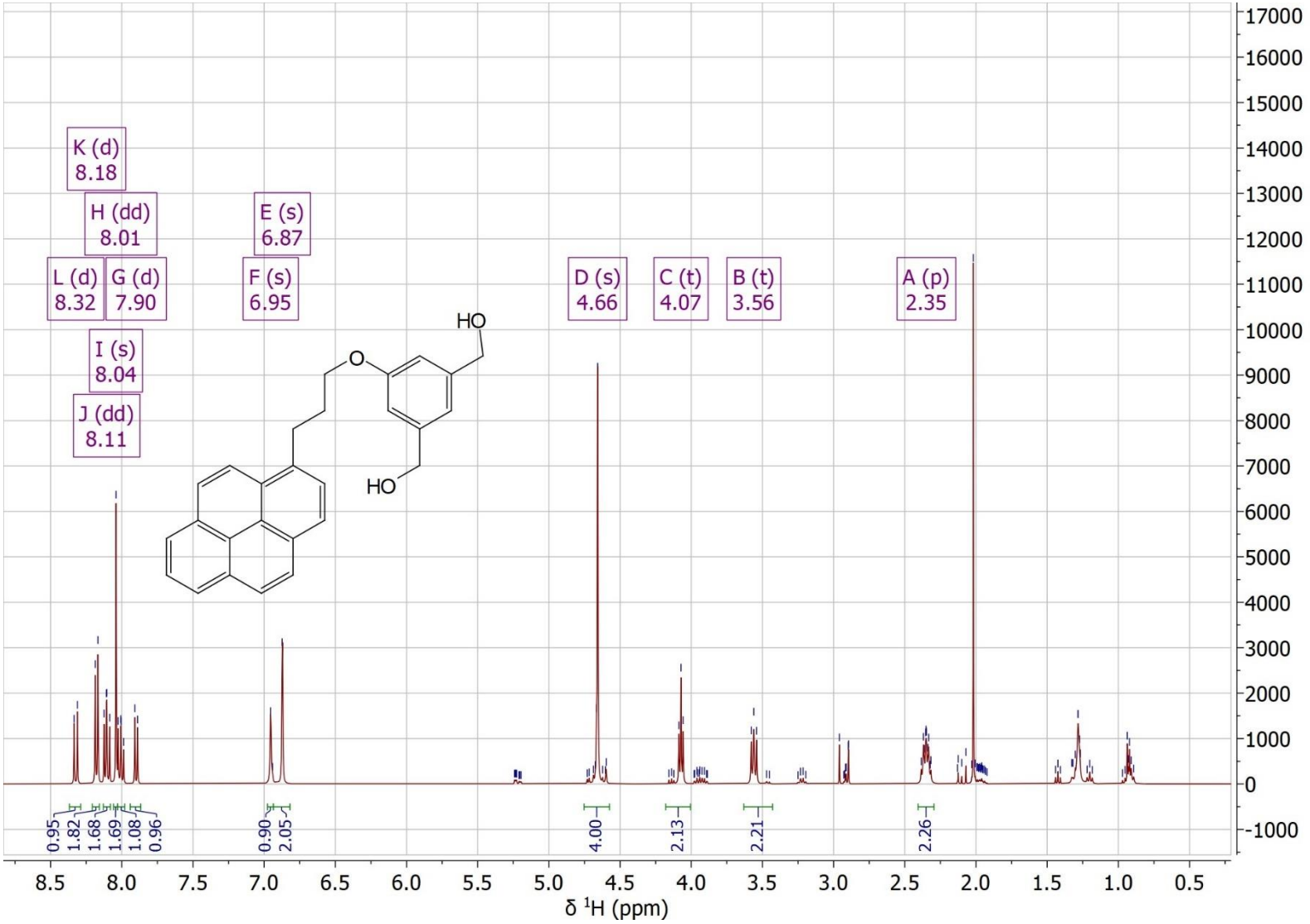

(5-[3-(pyren-1-yl)propoxy]-1,3-phenylene)dibromide (27)

^{1}H NMR analysis

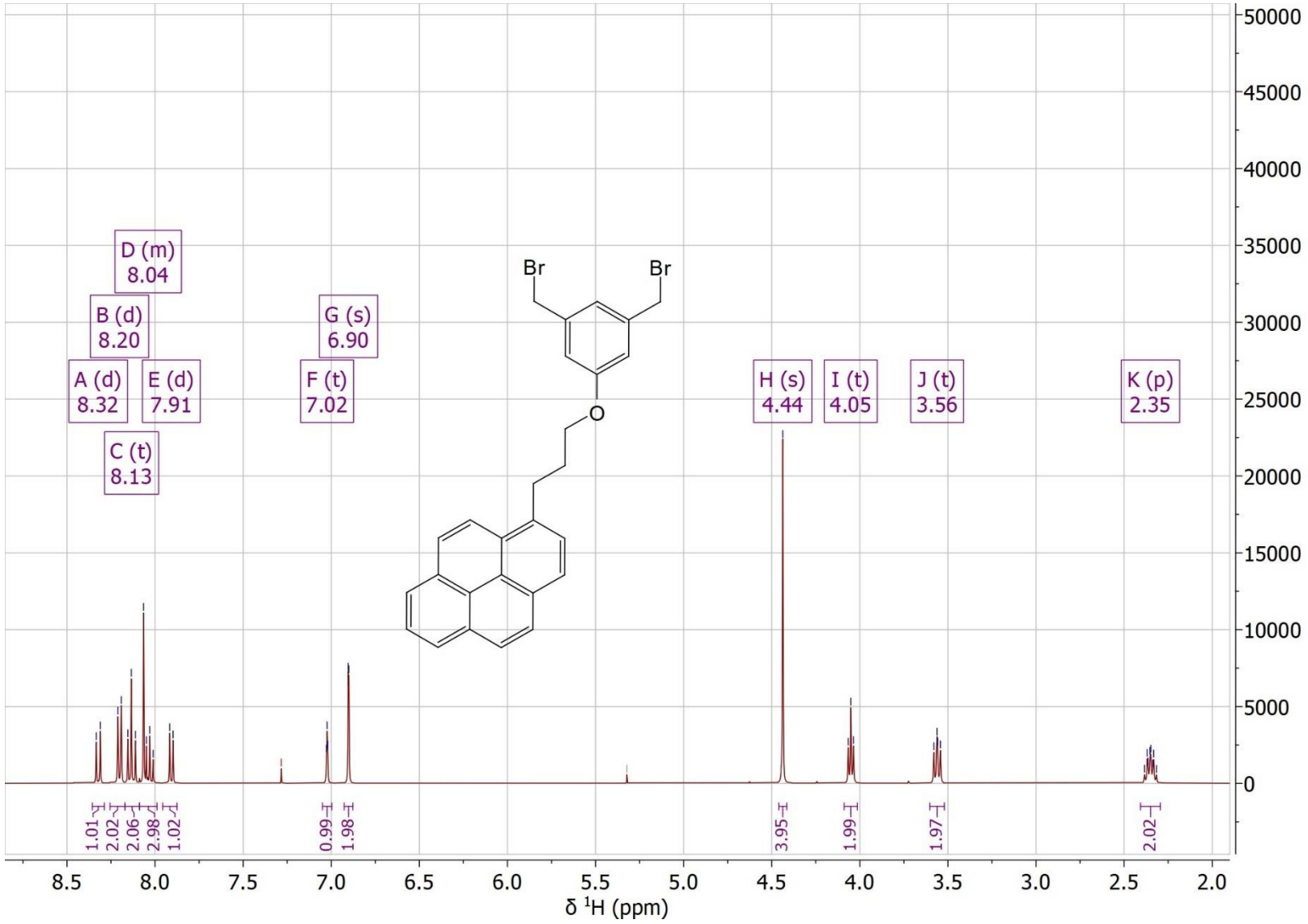

5-[3-(1-Pyrenyl)propoxy]-*N*^{1},*N*^{1},*N*^{3},*N*^{3}-tetrakis(2-pyridinylmethyl)-1,3-benzenedimethanamine (28)

^{1}H NMR analysis

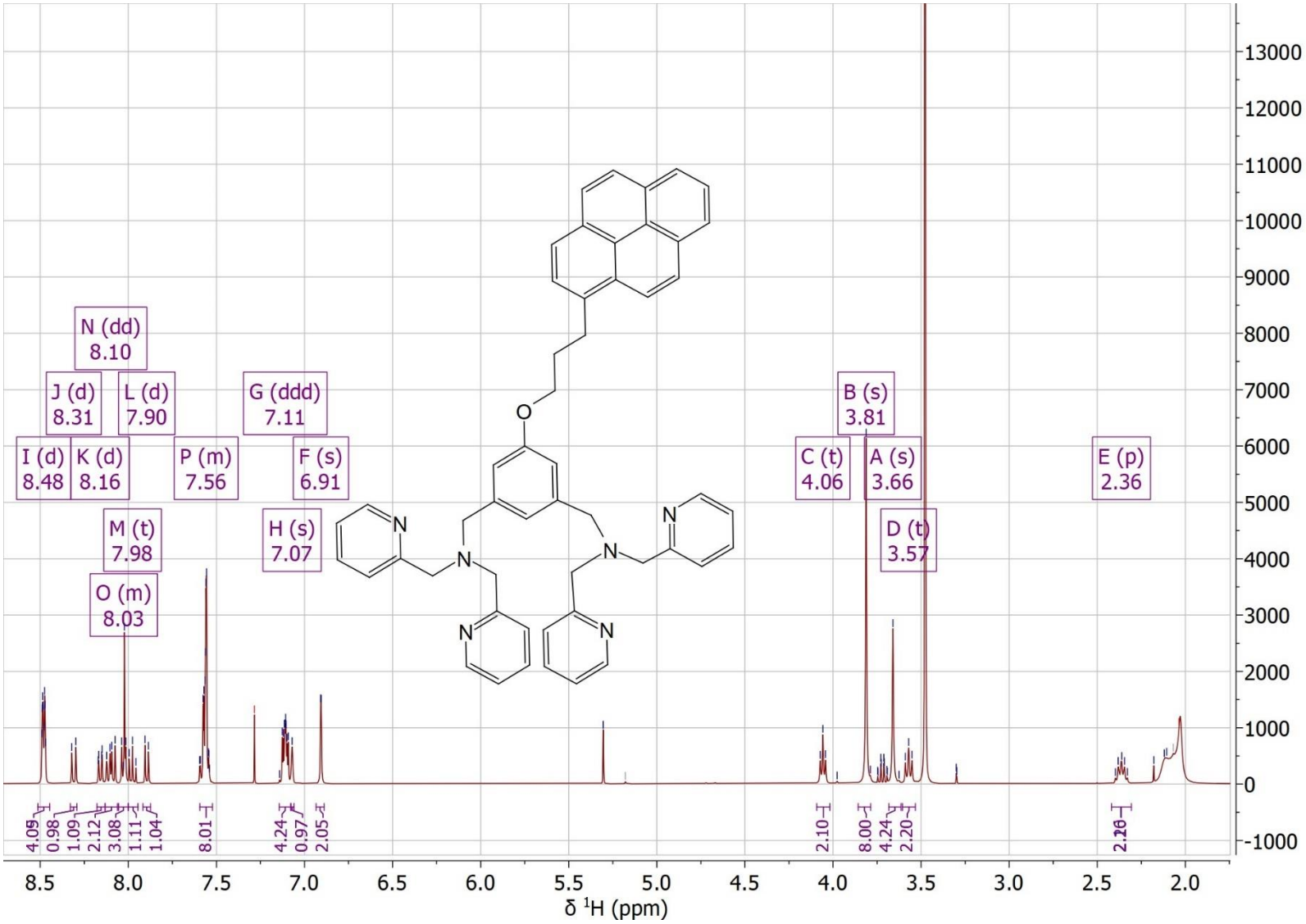

PyDPA (29)

^{1}H NMR analysis

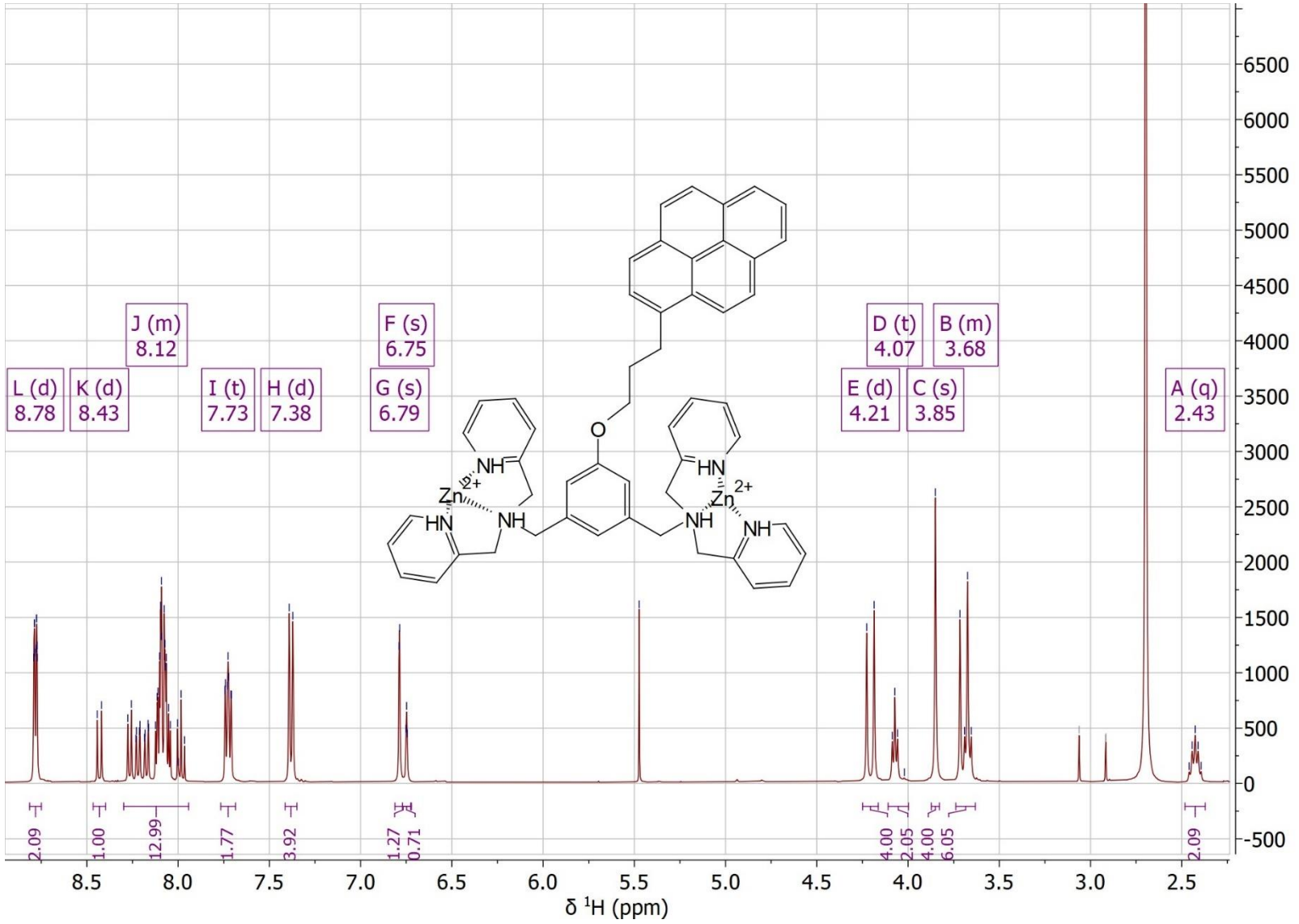

Bibliography

ALEGRIA, T. G. P., MEIRELES, D. A., CUSSIOL, J. R. R., HUGO, M., TRUJILLO, M., DE OLIVEIRA, M. A., MIYAMOTO, S., QUEIROZ, R. F., VALADARES, N. F., GARRATT, R. C., RADI, R., DI MASCIO, P., AUGUSTO, O. & NETTO, L. E. S. 2017. Ohr plays a central role in bacterial responses against fatty acid hydroperoxides and peroxynitrite. *Proceedings of the National Academy of Sciences,* 114**,** E132-E141.

ALHAJJ, M., ZUBAIR, M. & FARHANA, A. 2024. Enzyme Linked Immunosorbent Assay. *StatPearls*. Treasure Island (FL): StatPearls Publishing

Copyright © 2024, StatPearls Publishing LLC.

AMATO, S. M., ORMAN, M. A. & BRYNILDSEN, M. P. 2013. Metabolic control of persister formation in Escherichia coli. *Molecular cell,* 50**,** 475-487.

ANDERSON, B. W., LIU, K., WOLAK, C., DUBIEL, K., SHE, F., SATYSHUR, K. A., KECK, J. L. & WANG, J. D. 2019. Evolution of (p)ppGpp-HPRT regulation through diversification of an allosteric oligomeric interaction. *Elife,* 8.

ANDERSON, B. W., SCHUMACHER, M. A., YANG, J., TURDIEV, A., TURDIEV, H., SCHROEDER, J. W., HE, Q., LEE, V. T., BRENNAN, R. G. & WANG, J. D. 2022. The nucleotide messenger (p)ppGpp is an anti-inducer of the purine synthesis transcription regulator PurR in Bacillus. *Nucleic Acids Res,* 50**,** 847-866.

ANDERSON, K. L., ROUX, C. M., OLSON, M. W., LUONG, T. T., LEE, C. Y., OLSON, R. & DUNMAN, P. M. 2010. Characterizing the effects of inorganic acid and alkaline shock on the Staphylococcus aureus transcriptome and messenger RNA turnover. *FEMS Immunol Med Microbiol,* 60**,** 208-50.

APPEL, R. 1975. Tertiary Phosphane/Tetrachloromethane, a Versatile Reagent for Chlorination, Dehydration, and P□N Linkage. *Angewandte Chemie International Edition in English,* 14**,** 801-811.

ARAVIND, L. & KOONIN, E. V. 1998. The HD domain defines a new superfamily of metal-dependent phosphohydrolases. *Trends in biochemical sciences,* 23**,** 469-472.

ARENZ, S., BOCK, L. V., GRAF, M., INNIS, C. A., BECKMANN, R., GRUBMÜLLER, H., VAIANA, A. C. & WILSON, D. N. 2016. A combined cryo-EM and molecular dynamics approach reveals the mechanism of ErmBL-mediated translation arrest. *Nature Communications,* 7**,** 12026.

ARORA, S., GORDON, J. & HOOK, M. 2021. Collagen Binding Proteins of Gram-Positive Pathogens. *Front Microbiol,* 12**,** 628798.

ATKINSON, G. C., TENSON, T. & HAURYLIUK, V. 2011. The RelA/SpoT homolog (RSH) superfamily: distribution and functional evolution of ppGpp synthetases and hydrolases across the tree of life. *PLoS One,* 6**,** e23479.

AU - FERNÁNDEZ-COLL, L. & AU - CASHEL, M. 2019. Using Microtiter Dish Radiolabeling for Multiple In Vivo Measurements Of Escherichia coli (p)ppGpp Followed by Thin Layer Chromatography. *Journal of Visualized Experiments***,** e59595.

BAASKE, P., WIENKEN, C. J., REINECK, P., DUHR, S. & BRAUN, D. 2010. Optical Thermophoresis for Quantifying the Buffer Dependence of Aptamer Binding. *Angewandte Chemie International Edition,* 49**,** 2238-2241.

BABA, T., BAE, T., SCHNEEWIND, O., TAKEUCHI, F. & HIRAMATSU, K. 2008. Genome Sequence of *Staphylococcus aureus* Strain Newman and Comparative Analysis of Staphylococcal Genomes: Polymorphism and Evolution of Two Major Pathogenicity Islands. *Journal of Bacteriology,* 190**,** 300-310.

BABA, T., TAKEUCHI, F., KURODA, M., YUZAWA, H., AOKI, K.-I., OGUCHI, A., NAGAI, Y., IWAMA, N., ASANO, K., NAIMI, T., KURODA, H., CUI, L., YAMAMOTO, K. & HIRAMATSU, K. 2002. Genome and virulence determinants of high virulence community-acquired MRSA. *The Lancet,* 359**,** 1819-1827.

BAI, Y., YANG, J., EISELE, L. E., UNDERWOOD, A. J., KOESTLER, B. J., WATERS, C. M., METZGER, D. W. & BAI, G. 2013. Two DHH subfamily 1 proteins in Streptococcus pneumoniae possess cyclic di-AMP phosphodiesterase activity and affect bacterial growth and virulence. *J Bacteriol,* 195**,** 5123-32.

BAI, Y., YANG, J., ZARRELLA, T. M., ZHANG, Y., METZGER, D. W. & BAI, G. 2014. Cyclic di-AMP impairs potassium uptake mediated by a cyclic di-AMP binding protein in Streptococcus pneumoniae. *J Bacteriol,* 196**,** 614-23.

BAKER, M. D. & ACHARYA, K. R. 2004. Superantigens: structure-function relationships. *Int J Med Microbiol,* 293**,** 529-37.

BALIBAR, C. J., SHEN, X. & TAO, J. 2009. The mevalonate pathway of Staphylococcus aureus. *J Bacteriol,* 191**,** 851-61.

BASIRI, B., VAN HATTUM, H., VAN DONGEN, W. D., MURPH, M. M. & BARTLETT, M. G. 2017. The Role of Fluorinated Alcohols as Mobile Phase Modifiers for LC-MS Analysis of Oligonucleotides. *J Am Soc Mass Spectrom,* 28**,** 190-199.

BATTESTI, A. & BOUVERET, E. 2006. Acyl carrier protein/SpoT interaction, the switch linking SpoT-dependent stress response to fatty acid metabolism. *Mol Microbiol,* 62**,** 1048-63.

BATTESTI, A. & BOUVERET, E. 2009. Bacteria possessing two RelA/SpoT-like proteins have evolved a specific stringent response involving the acyl carrier protein-SpoT interaction. *Journal of bacteriology,* 191**,** 616-624.

BEAUCAGE, S. L. & CARUTHERS, M. H. 1981. Deoxynucleoside phosphoramidites—A new class of key intermediates for deoxypolynucleotide synthesis. *Tetrahedron Letters,* 22**,** 1859-1862.

BECKER, K., HEILMANN, C. & PETERS, G. 2014. Coagulase-negative staphylococci. *Clin Microbiol Rev,* 27**,** 870-926.

BELITSKY, B. R. & SONENSHEIN, A. L. 2011. CodY-Mediated Regulation of Guanosine Uptake in *Bacillus subtilis*. *Bacteriology,* 193**,** 6276-6287.

BELJANTSEVA, J., KUDRIN, P., JIMMY, S., EHN, M., POHL, R., VARIK, V., TOZAWA, Y., SHINGLER, V., TENSON, T., REJMAN, D. & HAURYLIUK, V. 2017. Molecular mutagenesis of ppGpp: turning a RelA activator into an inhibitor. *Scientific Reports,* 7**,** 41839.

BELOUSOFF, M. J., EYAL, Z., RADJAINIA, M., AHMED, T., BAMERT, R. S., MATZOV, D., BASHAN, A., ZIMMERMAN, E., MISHRA, S., CAMERON, D., ELMLUND, H., PELEG, A. Y., BHUSHAN, S., LITHGOW, T. & YONATH, A. 2017. PDB: 5T7V -Structural Basis for Linezolid Binding Site Rearrangement in the *Staphylococcus aureus* Ribosome. *mBio,* 8**,** e00395-17.

BENNISON, IRVING & CORRIGAN 2019. The Impact of the Stringent Response on TRAFAC GTPases and Prokaryotic Ribosome Assembly. *Cells,* 8**,** 1313.

BENNISON, D. J., NAKAMOTO, J. A., CRAGGS, T. D., MILÓN, P., RAFFERTY, J. B. & CORRIGAN, R. M. 2021. The Stringent Response Inhibits 70S Ribosome Formation in Staphylococcus aureus by Impeding GTPase-Ribosome Interactions. *mBio,* 12**,** e0267921.

BERGER-BÄCHI, B. & ROHRER, S. 2002. Factors influencing methicillin resistance in staphylococci. *Arch Microbiol,* 178**,** 165-71.

BIOLOGY, B. S. F. C. 2020. *Ribosomes* [Online]. https://bscb.org/learning-resources/. Available: https://bscb.org/learning-resources/softcell-e-learning/ribosome/ [Accessed 02/12/2020 2020].

BITTNER, A. N., KRIEL, A. & WANG, J. D. 2014. Lowering GTP level increases survival of amino acid starvation but slows growth rate for Bacillus subtilis cells lacking (p) ppGpp. *Journal of bacteriology,* 196**,** 2067-2076.

BLEUL, L., FRANCOIS, P. & WOLZ, C. 2022. Two-Component Systems of S. aureus: Signaling and Sensing Mechanisms. *Genes,* 13**,** 34.

BLOCH, K., CHAYKIN, S., PHILLIPS, A. H. & DE WAARD, A. 1959. Mevalonic Acid Pyrophosphate and Isopentenylpyrophosphate. *Journal of Biological Chemistry,* 234**,** 2595-2604.

BOARETTI, M., CANEPARI, P., LLEÒ, M. D. M. & SATTA, G. 1993. The activity of daptomycin on Enterococcus faecium protoplasts: indirect evidence supporting a novel mode of action on lipoteichoic acid synthesis. *Journal of Antimicrobial Chemotherapy,* 31**,** 227-235.

BOLES, B. R., THOENDEL, M., ROTH, A. J. & HORSWILL, A. R. 2010. Identification of Genes Involved in Polysaccharide-Independent Staphylococcus aureus Biofilm Formation. *PLOS ONE,* 5**,** e10146.

BOLS, M. & PEDERSEN, C. M. 2017. Silyl-protective groups influencing the reactivity and selectivity in glycosylations. *Beilstein J Org Chem,* 13**,** 93-105.

BORNHORST, J. A. & FALKE, J. J. 2000. Purification of proteins using polyhistidine affinity tags. *Methods Enzymol,* 326**,** 245-54.

BOUCHER, H. W. & COREY, G. R. 2008. Epidemiology of Methicillin-Resistant *Staphylococcus aureus*. *Clinical Infectious Diseases,* 46**,** S344-S349.

BOUTTE, C. C. & CROSSON, S. 2011. The complex logic of stringent response regulation in Caulobacter crescentus: starvation signalling in an oligotrophic environment. *Molecular microbiology,* 80**,** 695-714.

BOYLE-VAVRA, S., LI, X., ALAM, M. T., READ, T. D., SIETH, J., CYWES-BENTLEY, C., DOBBINS, G., DAVID, M. Z., KUMAR, N., EELLS, S. J., MILLER, L. G., BOXRUD, D. J., CHAMBERS, H. F., LYNFIELD, R., LEE, J. C. & DAUM, R. S. 2015. USA300 and USA500 clonal lineages of Staphylococcus aureus do not produce a capsular polysaccharide due to conserved mutations in the cap5 locus. *mBio,* 6.

BRADFORD, M. M. 1976. A rapid and sensitive method for the quantitation of microgram quantities of protein utilizing the principle of protein-dye binding. *Anal Biochem,* 72**,** 248-54.

BROWN, A., FERNÁNDEZ, I. S., GORDIYENKO, Y. & RAMAKRISHNAN, V. 2016. Ribosome-dependent activation of stringent control. *Nature,* 534**,** 277-280.

BUGLINO, J., SHEN, V., HAKIMIAN, P. & LIMA, C. D. 2002. Structural and Biochemical Analysis of the Obg GTP Binding Protein. *Structure,* 10**,** 1581-1592.

BUTLAND, G., PEREGRÍN-ALVAREZ, J. M., LI, J., YANG, W., YANG, X., CANADIEN, V., STAROSTINE, A., RICHARDS, D., BEATTIE, B. & KROGAN, N. 2005. Interaction network containing conserved and essential protein complexes in Escherichia coli. *Nature,* 433**,** 531-537.

BÄUMLER, J. & RIPPSTEIN, S. 1961. Dünnschichtchromatographischer Nachweis von Insektiziden. *Helvetica Chimica Acta,* 44**,** 1162-1164.

BÜKE, F., GRILLI, J., COSENTINO LAGOMARSINO, M., BOKINSKY, G. & TANS, S. J. 2022. ppGpp is a bacterial cell size regulator. *Curr Biol,* 32**,** 870-877.e5.

CAMARGO, I. L., NEOH, H. M., CUI, L. & HIRAMATSU, K. 2008. Serial daptomycin selection generates daptomycin-nonsusceptible Staphylococcus aureus strains with a heterogeneous vancomycin-intermediate phenotype. *Antimicrob Agents Chemother,* 52**,** 4289-99.

CAO, M., KOBEL, P. A., MORSHEDI, M. M., WU, M. F. W., PADDON, C. & HELMANN, J. D. 2002. Defining the Bacillus subtilis σW regulon: a comparative analysis of promoter consensus search, run-off transcription/macroarray analysis (ROMA), and transcriptional profiling approaches. *Journal of molecular biology,* 316**,** 443-457.

CAO, Z., BASSANI, D. M. & BIBAL, B. 2018. Photoreduction of Thioether Gold(III) Complexes: Mechanistic Insight and Homogeneous Catalysis. *Chemistry – A European Journal,* 24**,** 18779-18787.

CAPPARELLI, R., PARLATO, M., BORRIELLO, G., SALVATORE, P. & IANNELLI, D. 2007. Experimental phage therapy against Staphylococcus aureus in mice. *Antimicrob Agents Chemother,* 51**,** 2765-73.

CARPINO, L. A. 1993. 1-Hydroxy-7-azabenzotriazole. An efficient peptide coupling additive. *Journal of the American Chemical Society,* 115**,** 4397-4398.

CARPINO, L. A., IMAZUMI, H., FOXMAN, B. M., VELA, M. J., HENKLEIN, P., EL-FAHAM, A., KLOSE, J. & BIENERT, M. 2000. Comparison of the Effects of 5- and 6-HOAt on Model Peptide Coupling Reactions Relative to the Cases for the 4- and 7-Isomers. *Organic Letters,* 2**,** 2253-2256.

CARRILERO, L., URWIN, L., WARD, E., CHOUDHURY, N. R., MONK, I. R., TURNER, C. E., STINEAR, T. P. & CORRIGAN, R. M. 2023. Stringent Response-Mediated Control of GTP Homeostasis Is Required for Long-Term Viability of Staphylococcus aureus. *Microbiol Spectr,* 11**,** e0044723.

CASHEL, M. 1975. Regulation of bacterial ppGpp and pppGpp. *Annu Rev Microbiol,* 29**,** 301-18.

CASHEL, M. 1996. The stringent response. *Escherichia coli and Salmonella Cellular and*. *Molecular Biology*.

CASHEL, M. & GALLANT, J. 1969. Two Compounds implicated in the Function of the RC Gene of *Escherichia coli*. *Nature,* 221**,** 838-841.

CHAMBERS, H. F. & DELEO, F. R. 2009. Waves of resistance: *Staphylococcus aureus* in the antibiotic era. *Nature Reviews Microbiology,* 7**,** 629-641.

CHAMBERS, J. M., LINDQVIST, L. M., WEBB, A., HUANG, D. C., SAVAGE, G. P. & RIZZACASA, M. A. 2013. Synthesis of biotinylated episilvestrol: highly selective targeting of the translation factors eIF4AI/II. *Org Lett,* 15**,** 1406-9.

CHATTERJI, D., FUJITA, N. & ISHIHAMA, A. 1998. The mediator for stringent control, ppGpp, binds to the β-subunit of Escherichia coli RNA polymerase. *Genes to Cells,* 3**,** 279-287.

CHEN, B. B., LIU, M. L., ZHAN, L., LI, C. M. & HUANG, C. Z. 2018. Terbium(III) Modified Fluorescent Carbon Dots for Highly Selective and Sensitive Ratiometry of Stringent. *Analytical Chemistry,* 90**,** 4003-4009.

CHEN, E., SHAFFER, M. G., BILODEAU, R. E., WEST, R. E., 3RD, OBERLY, P. J., NOLIN, T. D. & CULYBA, M. J. 2023. Clinical rel mutations in Staphylococcus aureus prime pathogen expansion under nutrient stress. *mSphere,* 8**,** e0024923.

CHEN, S. S., SPERLING, E., SILVERMAN, J. M., DAVIS, J. H. & WILLIAMSON, J. R. 2012. Measuring the dynamics of *E. coli* ribosome biogenesis using pulse-labeling and quantitative mass spectrometry. *Molecular BioSystems,* 8**,** 3325.

CHO, H. K., LEE, D. H. & HONG, J.-I. 2005. A fluorescent pyrophosphate sensor via excimer formation in water. *Chemical Communications***,** 1690-1692.

CHOUDHURY, N. R., URWIN, L., SALAMAGA, B., PRINCE, L. R., RENSHAW, S. A. & CORRIGAN, R. M. 2023. Determining the importance of the stringent response for methicillin-resistant Staphylococcus aureus virulence using a zebrafish model of infection. *bioRxiv***,** 2023.07.12.548523.

CLAUDITZ, A., RESCH, A., WIELAND, K. P., PESCHEL, A. & GÖTZ, F. 2006. Staphyloxanthin plays a role in the fitness of Staphylococcus aureus and its ability to cope with oxidative stress. *Infect Immun,* 74**,** 4950-3.

CLEGG, J., SOLDAINI, E., MCLOUGHLIN, R. M., RITTENHOUSE, S., BAGNOLI, F. & PHOGAT, S. 2021. Staphylococcus aureus Vaccine Research and Development: The Past, Present and Future, Including Novel Therapeutic Strategies. *Front Immunol,* 12**,** 705360.

CLEMENTS, M. O. & FOSTER, S. J. 1999. Stress resistance in Staphylococcus aureus. *Trends Microbiol,* 7**,** 458-62.

COATHAM, M. L., BRANDON, H. E., FISCHER, J. J., SCHÜMMER, T. & WIEDEN, H.-J. 2016. The conserved GTPase HflX is a ribosome splitting factor that binds to the E-site of the bacterial ribosome. *Nucleic Acids Research***,** gkv1524.

CONTI, G., MINNECI, M. & SATTIN, S. 2019. Optimised Synthesis of the Bacterial Magic Spot (p)ppGpp Chemosensor PyDPA. *ChemBioChem,* 20**,** 1717-1721.

CORRIGAN, R. M., BELLOWS, L. E., WOOD, A. & GRÜNDLING, A. 2016. ppGpp negatively impacts ribosome assembly affecting growth and antimicrobial tolerance in Gram-positive bacteria. *Proceedings of the National Academy of Sciences,* 113**,** E1710-E1719.

CORRIGAN, R. M., BOWMAN, L., WILLIS, A. R., KAEVER, V. & GRÜNDLING, A. 2015. Cross-talk between two nucleotide-signaling pathways in Staphylococcus aureus. *Journal of Biological Chemistry,* 290**,** 5826-5839.

CORRIGAN, R. M., MIAJLOVIC, H. & FOSTER, T. J. 2009. Surface proteins that promote adherence of Staphylococcus aureusto human desquamated nasal epithelial cells. *BMC Microbiology,* 9**,** 22.

COSGROVE, K., COUTTS, G., JONSSON, I.-M., TARKOWSKI, A., KOKAI-KUN, J. F., MOND, J. J. & FOSTER, S. J. 2007a. Catalase (KatA) and alkyl hydroperoxide reductase (AhpC) have compensatory roles in peroxide stress resistance and are required for survival, persistence, and nasal colonization in Staphylococcus aureus. *Journal of bacteriology,* 189**,** 1025-1035.

COSGROVE, K., COUTTS, G., JONSSON, I.-M., TARKOWSKI, A., KOKAI-KUN JOHN, F., MOND JAMES, J. & FOSTER SIMON, J. 2007b. Catalase (KatA) and Alkyl Hydroperoxide Reductase (AhpC) Have Compensatory Roles in Peroxide Stress Resistance and Are Required for Survival, Persistence, and Nasal Colonization in Staphylococcus aureus. *Journal of Bacteriology,* 189**,** 1025-1035.

COTTER, P. D. & HILL, C. 2003. Surviving the acid test: responses of gram-positive bacteria to low pH. *Microbiol Mol Biol Rev,* 67**,** 429-53, table of contents.

COUNSELL, A. J., YU, M., SHI, M., JONES, A. T., BATTEN, J. M., TURNER, P., TODD, M. H. & RUTLEDGE, P. J. 2021. Copper(ii) complexes of N-propargyl cyclam ligands reveal a range of coordination modes and colours, and unexpected reactivity. *Dalton Transactions,* 50**,** 3931-3942.

COURVALIN, P. 2006. Vancomycin Resistance in Gram-Positive Cocci. *Clinical Infectious Diseases,* 42**,** S25-S34.

CROSSE, A. M., GREENWAY, D. L. & ENGLAND, R. R. 2000. Accumulation of ppGpp and ppGp in Staphylococcus aureus 8325-4 following nutrient starvation. *Lett Appl Microbiol,* 31**,** 332-7.

CRUZ, A. R., BOER, M. A. D., STRASSER, J., ZWARTHOFF, S. A., BEURSKENS, F. J., DE HAAS, C. J. C., AERTS, P. C., WANG, G., DE JONG, R. N., BAGNOLI, F., VAN STRIJP, J. A. G., VAN KESSEL, K. P. M., SCHUURMAN, J., PREINER, J., HECK, A. J. R. & ROOIJAKKERS, S. H. M. 2021. Staphylococcal protein A inhibits complement activation by interfering with IgG hexamer formation. *Proc Natl Acad Sci U S A,* 118.

CUI, X.-M., GUAN, Y.-H., LI, N., LV, H., FU, L.-A., GUO, K. & FAN, X. 2014. A mild and efficient method for bromination of alcohols using α,α-dibromo-β-dicarbonyl compounds as halogen sources. *Tetrahedron Letters,* 55**,** 90-93.

CZARNIK, A. W. 1994. Chemical Communication in Water Using Fluorescent Chemosensors. *Accounts of Chemical Research,* 27**,** 302-308.

DAHAN, A. & PORTNOY, M. 2003. Synthesis of Poly(aryl benzyl ether) Dendrimers on Solid Support. *Macromolecules,* 36**,** 1034-1038.

DAI, Y., CHANG, W., ZHAO, C., PENG, J., XU, L., LU, H., ZHOU, S. & MA, X. 2017. VraR Binding to the Promoter Region of agr Inhibits Its Function in Vancomycin-Intermediate Staphylococcus aureus (VISA) and Heterogeneous VISA. *Antimicrobial Agents and Chemotherapy,* 61**,** 10.1128/aac.02740-16.

DALEBROUX, Z. D. & SWANSON, M. S. 2012. ppGpp: magic beyond RNA polymerase. *Nat Rev Microbiol,* 10**,** 203-12.

DALY, B., LING, J. & DE SILVA, A. P. 2015. Current developments in fluorescent PET (photoinduced electron transfer) sensors and switches. *Chemical Society Reviews,* 44**,** 4203-4211.

DAS, A. & THEATO, P. 2016. Activated Ester Containing Polymers: Opportunities and Challenges for the Design of Functional Macromolecules. *Chemical Reviews,* 116**,** 1434-1495.

DAS, D., SAHA, S. S. & BISHAYI, B. 2008. Intracellular survival of Staphylococcus aureus: correlating production of catalase and superoxide dismutase with levels of inflammatory cytokines. *Inflamm Res,* 57**,** 340-9.

DAVIS, J. H., TAN, Y. Z., CARRAGHER, B., POTTER, C. S., LYUMKIS, D. & WILLIAMSON, J. R. 2016. Modular Assembly of the Bacterial Large Ribosomal Subunit. *Cell,* 167**,** 1610-1622.e15.

DAVIS, R., ÉCIJA-CONESA, A., GALLEGO-JARA, J., DE DIEGO, T., FILIPPOVA, E. V., KUFFEL, G., ANDERSON, W. F., GIBSON, B. W., SCHILLING, B., CANOVAS, M. & WOLFE, A. J. 2018. An acetylatable lysine controls CRP function in E. coli. *Mol Microbiol,* 107**,** 116-131.

DE JONG, N. W. M., RAMYAR, K. X., GUERRA, F. E., NIJLAND, R., FEVRE, C., VOYICH, J. M., MCCARTHY, A. J., GARCIA, B. L., VAN KESSEL, K. P. M., VAN STRIJP, J. A. G., GEISBRECHT, B. V. & HAAS, P.-J. A. 2017. Immune evasion by a staphylococcal inhibitor of myeloperoxidase. *Proceedings of the National Academy of Sciences,* 114**,** 9439-9444.

DEBACKER, A. J., SHARMA, V. K., MEDA KRISHNAMURTHY, P., O'REILLY, D., GREENHILL, R. & WATTS, J. K. 2019. Next-Generation Peptide Nucleic Acid Chimeras Exhibit High Affinity and Potent Gene Silencing. *Biochemistry,* 58**,** 582-589.

DENG, J., ERDJUMENT-BROMAGE, H. & NEUBERT, T. A. 2019. Quantitative Comparison of Proteomes Using SILAC. *Curr Protoc Protein Sci,* 95**,** e74.

DEURENBERG, R. H. & STOBBERINGH, E. E. 2008. The evolution of Staphylococcus aureus. *Infection, Genetics and Evolution,* 8**,** 747-763.

DEVENDAR, P., QU, R.-Y., KANG, W.-M., HE, B. & YANG, G.-F. 2018. Palladium-Catalyzed Cross-Coupling Reactions: A Powerful Tool for the Synthesis of Agrochemicals. *Journal of Agricultural and Food Chemistry,* 66**,** 8914-8934.

DING, C. C., ROSE, J., SUN, T., WU, J., CHEN, P. H., LIN, C. C., YANG, W. H., CHEN, K. Y., LEE, H., XU, E., TIAN, S., AKINWUNTAN, J., ZHAO, J., GUAN, Z., ZHOU, P. & CHI, J. T. 2020. MESH1 is a cytosolic NADPH phosphatase that regulates ferroptosis. *Nat Metab,* 2**,** 270-277.

DONG, R., LIU, R., GAFFNEY, P. R. J., SCHAEPERTOENS, M., MARCHETTI, P., WILLIAMS, C. M., CHEN, R. & LIVINGSTON, A. G. 2019. Sequence-defined multifunctional polyethers via liquid-phase synthesis with molecular sieving. *Nature Chemistry,* 11**,** 136-145.

DUFF, M. R., JR., GRUBBS, J. & HOWELL, E. E. 2011. Isothermal titration calorimetry for measuring macromolecule-ligand affinity. *J Vis Exp*.

DZEJA, P. & TERZIC, A. 2009. Adenylate kinase and AMP signaling networks: metabolic monitoring, signal communication and body energy sensing. *Int J Mol Sci,* 10**,** 1729-1772.

D'ALÉO, A., MOORE, E. G., XU, J., DAUMANN, L. J. & RAYMOND, K. N. 2015. Optimization of the Sensitization Process and Stability of Octadentate Eu(III) 1,2-HOPO Complexes. *Inorganic Chemistry,* 54**,** 6807-6820.

ELIAS, J. E., HAAS, W., FAHERTY, B. K. & GYGI, S. P. 2005. Comparative evaluation of mass spectrometry platforms used in large-scale proteomics investigations. *Nat Methods,* 2**,** 667-75.

ENGVALL, E. & PERLMANN, P. 1972. Enzyme-Linked Immunosorbent Assay, Elisa: III. Quantitation of Specific Antibodies by Enzyme-Labeled Anti-Immunoglobulin in Antigen-Coated Tubes1. *The Journal of Immunology,* 109**,** 129-135.

ERNST, C. M. & PESCHEL, A. 2019. MprF-mediated daptomycin resistance. *International Journal of Medical Microbiology,* 309**,** 359-363.

ERNST, C. M., STAUBITZ, P., MISHRA, N. N., YANG, S. J., HORNIG, G., KALBACHER, H., BAYER, A. S., KRAUS, D. & PESCHEL, A. 2009. The bacterial defensin resistance protein MprF consists of separable domains for lipid lysinylation and antimicrobial peptide repulsion. *PLoS Pathog,* 5**,** e1000660.

FAN, X., LIU, Y., SMITH, D., KONERMANN, L., SIU, K. W. M. & GOLEMI-KOTRA, D. 2007. Diversity of Penicillin-binding Proteins. *Journal of Biological Chemistry,* 282**,** 35143-35152.

FANG, F. C. 2011. Antimicrobial actions of reactive oxygen species. *mBio,* 2.

FANTONI, N. Z., EL-SAGHEER, A. H. & BROWN, T. 2021. A Hitchhiker's Guide to Click-Chemistry with Nucleic Acids. *Chemical Reviews,* 121**,** 7122-7154.

FEIST, P. & HUMMON, A. B. 2015. Proteomic challenges: sample preparation techniques for microgram-quantity protein analysis from biological samples. *Int J Mol Sci,* 16**,** 3537-63.

FERNÁNDEZ-COLL, L. & CASHEL, M. 2018. Contributions of SpoT Hydrolase, SpoT Synthetase, and RelA Synthetase to Carbon Source Diauxic Growth Transitions in Escherichia coli. *Front Microbiol,* 9**,** 1802.

FERNÁNDEZ-COLL, L. & CASHEL, M. 2019. Using Microtiter Dish Radiolabeling for Multiple In Vivo Measurements Of Escherichia coli (p)ppGpp Followed by Thin Layer Chromatography. *JoVE***,** e59595.

FERULLO, D. J. & LOVETT, S. T. 2008. The Stringent Response and Cell Cycle Arrest in Escherichia coli. *PLOS Genetics,* 4**,** e1000300.

FISCHER, M., ZIMMERMAN, T. P. & SHORT, S. A. 1982. A rapid method for the determination of guanosine 5'-diphosphate-3'-diphosphate and guanosine 5'-triphosphate-3'-diphosphate by high-performance liquid chromatography. *Analytical Biochemistry,* 121**,** 135-139.

FISHER, J. F. & MOBASHERY, S. 2020. Constructing and deconstructing the bacterial cell wall. *Protein Sci,* 29**,** 629-646.

FLEISCHER, B. & SCHREZENMEIER, H. 1988. T cell stimulation by staphylococcal enterotoxins. Clonally variable response and requirement for major histocompatibility complex class II molecules on accessory or target cells. *J Exp Med,* 167**,** 1697-707.

FOSTER, T. 1996. *Staphylococcus,* University of Texas Medical Branch at Galveston.

FOSTER, T. J., GEOGHEGAN, J. A., GANESH, V. K. & HÖÖK, M. 2014. Adhesion, invasion and evasion: the many functions of the surface proteins of Staphylococcus aureus. *Nat Rev Microbiol,* 12**,** 49-62.

FOSTER, T. J. & HÖÖK, M. 1998. Surface protein adhesins of Staphylococcus aureus. *Trends Microbiol,* 6**,** 484-8.

FOWLER, T., WANN, E. R., JOH, D., JOHANSSON, S., FOSTER, T. J. & HÖÖK, M. 2000. Cellular invasion by Staphylococcus aureus involves a fibronectin bridge between the bacterial fibronectin-binding MSCRAMMs and host cell β1 integrins. *European journal of cell biology,* 79**,** 672-679.

FRANCIS, T. 1960. On the doctrine of original antigenic sin. *Proceedings of the American Philosophical Society,* 104**,** 572-578.

FUNABASHI, H., MIE, M., YANAGIDA, Y., KOBATAKE, E. & AIZAWA, M. 2002. Fluorescent monitoring of cellular physiological status depending on the accumulation of ppGpp. *Biotechnology Letters,* 24**,** 269-273.

FURUKAWA, H., TSAY, J., JACKOWSKI, S., TAKAMURA, Y. & ROCK, C. 1993. Thiolactomycin resistance in Escherichia coli is associated with the multidrug resistance efflux pump encoded by emrAB. *Journal of bacteriology,* 175**,** 3723-3729.

FUSZ, S., SRIVATSAN, S. G., ACKERMANN, D. & FAMULOK, M. 2008. Photocleavable Initiator Nucleotide Substrates for an Aldolase Ribozyme. *The Journal of Organic Chemistry,* 73**,** 5069-5077.

GALATSIS, P. 2001. Diisobutylaluminum Hydride. *Encyclopedia of Reagents for Organic Synthesis*.

GALLANT, J., MARGASON, G. & FINCH, B. 1972. On the turnover of ppGpp in Escherichia coli. *J Biol Chem,* 247**,** 6055-8.

GAO, W., CHUA, K., DAVIES, J. K., NEWTON, H. J., SEEMANN, T., HARRISON, P. F., HOLMES, N. E., RHEE, H.-W., HONG, J.-I., HARTLAND, E. L., STINEAR, T. P. & HOWDEN, B. P. 2010. Two Novel Point Mutations in Clinical *Staphylococcus aureus* Reduce Linezolid Susceptibility and Switch on the Stringent Response to Promote Persistent Infection. *PLoS Pathogens,* 6**,** e1000944.

GARST, A. D., EDWARDS, A. L. & BATEY, R. T. 2011. Riboswitches: structures and mechanisms. *Cold Spring Harb Perspect Biol,* 3.

GAUDARD, P., SAOUR, M., MORQUIN, D., DAVID, H., ELIET, J., VILLIET, M., DAURES, J. P. & COLSON, P. 2019. Acute kidney injury during daptomycin versus vancomycin treatment in cardiovascular critically ill patients: a propensity score matched analysis. *BMC Infect Dis,* 19**,** 438.

GEIGER, T., FRANCOIS, P., LIEBEKE, M., FRAUNHOLZ, M., GOERKE, C., KRISMER, B., SCHRENZEL, J., LALK, M. & WOLZ, C. 2012. The Stringent Response of *Staphylococcus aureus* and Its Impact on Survival after Phagocytosis through the Induction of Intracellular PSMs Expression. *PLoS Pathogens,* 8**,** e1003016.

GEIGER, T., GOERKE, C., FRITZ, M., SCHÄFER, T., OHLSEN, K., LIEBEKE, M., LALK, M. & WOLZ, C. 2010. Role of the (p)ppGpp Synthase RSH, a RelA/SpoT Homolog, in Stringent Response and Virulence of *Staphylococcus aureus*. *Infection and Immunity,* 78**,** 1873-1883.

GEIGER, T., KASTLE, B., GRATANI, F. L., GOERKE, C. & WOLZ, C. 2014. Two Small (p)ppGpp Synthases in *Staphylococcus aureus* Mediate Tolerance against Cell Envelope Stress Conditions. *Journal of Bacteriology,* 196**,** 894-902.

GENESTIER, A.-L., MICHALLET, M.-C., PRÉVOST, G., BELLOT, G., CHALABREYSSE, L., PEYROL, S., THIVOLET, F., ETIENNE, J., LINA, G. & VALLETTE, F. M. 2005. Staphylococcus aureus Panton-Valentine leukocidin directly targets mitochondria and induces Bax-independent apoptosis of human neutrophils. *The Journal of clinical investigation,* 115**,** 3117-3127.

GHERARDI, G., DI BONAVENTURA, G. & SAVINI, V. 2018. Chapter 1 - Staphylococcal Taxonomy. *In:* SAVINI, V. (ed.) *Pet-To-Man Travelling Staphylococci*. Academic Press.

GILLET, Y., ISSARTEL, B., VANHEMS, P., FOURNET, J. C., LINA, G., BES, M., VANDENESCH, F., PIÉMONT, Y., BROUSSE, N., FLORET, D. & ETIENNE, J. 2002. Association between Staphylococcus aureus strains carrying gene for Panton-Valentine leukocidin and highly lethal necrotising pneumonia in young immunocompetent patients. *Lancet,* 359**,** 753-9.

GORWITZ, R. J., KRUSZON-MORAN, D., MCALLISTER, S. K., MCQUILLAN, G., MCDOUGAL, L. K., FOSHEIM, G. E., JENSEN, B. J., KILLGORE, G., TENOVER, F. C. & KUEHNERT, M. J. 2008. Changes in the prevalence of nasal colonization with Staphylococcus aureus in the United States, 2001-2004. *J Infect Dis,* 197**,** 1226-34.

GRATANI, F. L., HORVATEK, P., GEIGER, T., BORISOVA, M., MAYER, C., GRIN, I., WAGNER, S., STEINCHEN, W., BANGE, G., VELIC, A., MAČEK, B. & WOLZ, C. 2018. Regulation of the opposing (p)ppGpp synthetase and hydrolase activities in a bifunctional RelA/SpoT homologue from *Staphylococcus aureus*. *PLOS Genetics,* 14**,** e1007514.

GREEN, N. M. 1963a. AVIDIN. 1. THE USE OF (14-C)BIOTIN FOR KINETIC STUDIES AND FOR ASSAY. *Biochem J,* 89**,** 585-91.

GREEN, N. M. 1963b. AVIDIN. 4. STABILITY AT EXTREMES OF PH AND DISSOCIATION INTO SUB-UNITS BY GUANIDINE HYDROCHLORIDE. *Biochem J,* 89**,** 609-20.

GREENWAY, D. L. & ENGLAND, R. R. 1999. The intrinsic resistance of Escherichia coli to various antimicrobial agents requires ppGpp and sigma s. *Lett Appl Microbiol,* 29**,** 323-6.

GRONINGSSON, K. & JANSSON, L. 1979. TLC Determination of Biotin in a Lyophilized Multivitamin Preparation. *Journal of Pharmaceutical Sciences,* 68**,** 364-366.

GROSZ, M., KOLTER, J., PAPROTKA, K., WINKLER, A. C., SCHÄFER, D., CHATTERJEE, S. S., GEIGER, T., WOLZ, C., OHLSEN, K., OTTO, M., RUDEL, T., SINHA, B. & FRAUNHOLZ, M. 2014. Cytoplasmic replication of Staphylococcus aureus upon phagosomal escape triggered by phenol-soluble modulin α. *Cell Microbiol,* 16**,** 451-65.

GU, H., RAPAKOUSIOU, A., CASTEL, P., GUIDOLIN, N., PINAUD, N., RUIZ, J. & ASTRUC, D. 2014. Living Ring-Opening Metathesis–Polymerization Synthesis and Redox-Sensing Properties of Norbornene Polymers and Copolymers Containing Ferrocenyl and Tetraethylene Glycol Groups. *Organometallics,* 33**,** 4323-4335.

GULDBERG, C. M. & WAAGE, P. 1964. *Studier over affiniteten*, NTH-Trykk.

GÖRKE, B. & STÜLKE, J. 2008. Carbon catabolite repression in bacteria: many ways to make the most out of nutrients. *Nature Reviews Microbiology,* 6**,** 613-624.

HAAS, T. M., EBENSPERGER, P., EISENBEIS, V. B., NOPPER, C., DÜRR, T., JORK, N., STECK, N., JESSEN-TREFZER, C. & JESSEN, H. J. 2019. Magic spot nucleotides: tunable target-specific chemoenzymatic synthesis. *Chemical Communications,* 55**,** 5339-5342.

HAAS, T. M., LAVENTIE, B.-J., LAGIES, S., HARTER, C., PRUCKER, I., RITZ, D., SALEEM-BATCHA, R., QIU, D., HÜTTEL, W., ANDEXER, J., KAMMERER, B., JENAL, U. & JESSEN, H. J. Photoaffinity Capture Compounds to Profile the Magic Spot Nucleotide Interactomes**. *Angewandte Chemie,* n/a**,** e202201731.

HAAS, T. M., LAVENTIE, B.-J., LAGIES, S., HARTER, C., PRUCKER, I., RITZ, D., SALEEM-BATCHA, R., QIU, D., HÜTTEL, W., ANDEXER, J., KAMMERER, B., JENAL, U. & JESSEN, H. J. 2022. Photoaffinity Capture Compounds to Profile the Magic Spot Nucleotide Interactomes**. *Angewandte Chemie International Edition,* 61**,** e202201731.

HAMAGISHI, Y., OKI, T., TONE, H. & INUI, T. 1980. A Radioimmunoassay for Guanosine-5'-Diphosphate-3'-Diphosphate and Adenosine-5'-Triphosphate-3'-Diphosphate. *The Journal of Biochemistry,* 88**,** 1785-1892.

HAMAGISHI, Y., YOSHIMOTO, A. & OKI, T. 1981. Determination of guanosine tetraphosphate (ppGpp) and adenosine pentaphosphate (pppApp) in various microorganisms by radioimmunoassay. *Archives of Microbiology,* 130**,** 134-137.

HAMILTON, S., ODILI, J., PACIFICO, M. D., WILSON, G. D. & KUPSCH, J. M. 2003. Effect of imidazole on the solubility of a his-tagged antibody fragment. *Hybrid Hybridomics,* 22**,** 347-55.

HAMMER, N. D. & SKAAR, E. P. 2011. Molecular mechanisms of Staphylococcus aureus iron acquisition. *Annu Rev Microbiol,* 65**,** 129-47.

HAMMER, N. D. & SKAAR, E. P. 2013. Powerful genetic resource for the study of methicillin-resistant Staphylococcus aureus. *mBio,* 4.

HANDKE, L. D., SHIVERS, R. P. & SONENSHEIN, A. L. 2008. Interaction of Bacillus subtilis CodY with GTP. Am Soc Microbiol.

HARA, A. & SY, J. 1983. Guanosine 5'-triphosphate, 3'-diphosphate 5'-phosphohydrolase. Purification and substrate specificity. *J Biol Chem,* 258**,** 1678-83.

HASELTINE, W. A. & BLOCK, R. 1973. Synthesis of guanosine tetra- and pentaphosphate requires the presence of a codon-specific, uncharged transfer ribonucleic acid in the acceptor site of ribosomes. *Proc Natl Acad Sci U S A,* 70**,** 1564-8.

HASHEMIZADEH, Z., HADI, N., MOHEBI, S., KALANTAR-NEYESTANAKI, D. & BAZARGANI, A. 2019. Characterization of SCCmec, spa types and Multi Drug Resistant of methicillin-resistant Staphylococcus aureus isolates among inpatients and outpatients in a referral hospital in Shiraz, Iran. *BMC Res Notes,* 12**,** 614.

HAURYLIUK, V. & ATKINSON, G. C. 2017. Small Alarmone Synthetases as novel bacterial RNA-binding proteins. *RNA Biology,* 14**,** 1695-1699.

HAURYLIUK, V., ATKINSON, G. C., MURAKAMI, K. S., TENSON, T. & GERDES, K. 2015. Recent functional insights into the role of (p)ppGpp in bacterial physiology. *Nat Rev Microbiol,* 13**,** 298-309.

HEATH, R. J., JACKOWSKI, S. & ROCK, C. O. 1994. Guanosine tetraphosphate inhibition of fatty acid and phospholipid synthesis in Escherichia coli is relieved by overexpression of glycerol-3-phosphate acyltransferase (plsB). *Journal of Biological Chemistry,* 269**,** 26584-26590.

HEATH, R. J. & ROCK, C. O. 1995. Regulation of Malonyl-CoA Metabolism by Acyl-Acyl Carrier Protein and β-Ketoacyl-Acyl Carrier Protein Synthases in Escherichia coli (∗). *Journal of Biological Chemistry,* 270**,** 15531-15538.

HEIDARY, M., KHOSRAVI, A. D., KHOSHNOOD, S., NASIRI, M. J., SOLEIMANI, S. & GOUDARZI, M. 2017. Daptomycin. *Journal of Antimicrobial Chemotherapy,* 73**,** 1-11.

HELENA-BUENO, K., RYBAK, M. Y., EKEMEZIE, C. L., SULLIVAN, R., BROWN, C. R., DINGWALL, C., BASLÉ, A., SCHNEIDER, C., CONNOLLY, J. P. R., BLAZA, J. N., CSÖRGŐ, B., MOYNIHAN, P. J., GAGNON, M. G., HILL, C. H. & MELNIKOV, S. V. 2024. A new family of bacterial ribosome hibernation factors. *Nature,* 626**,** 1125-1132.

HIMENO, H. 2004. A novel GTPase activated by the small subunit of ribosome. *Nucleic Acids Research,* 32**,** 5303-5309.

HIRSCHHAUSEN, N., SCHLESIER, T., SCHMIDT, M. A., GÖTZ, F., PETERS, G. & HEILMANN, C. 2010. A novel staphylococcal internalization mechanism involves the major autolysin Atl and heat shock cognate protein Hsc70 as host cell receptor. *Cellular microbiology,* 12**,** 1746-1764.

HOBBY, G. L., MEYER, K. & CHAFFEE, E. 1942. Observations on the Mechanism of Action of Penicillin. *Proceedings of the Society for Experimental Biology and Medicine,* 50**,** 281-285.

HOLLAND, L. M., O'DONNELL, S. A. T., RYJENKOV, D. A., GOMELSKY, L., SLATER, S. R., FEY, P. D., GOMELSKY, M. & O'GARA, J. P. 2008. A staphylococcal GGDEF domain protein regulates biofilm formation independently of cyclic dimeric GMP. *Journal of bacteriology,* 190**,** 5178-5189.

HOLSTEIN, S. A. & HOHL, R. J. 2004. Isoprenoids: Remarkable diversity of form and function. *Lipids,* 39**,** 293-309.

HORSBURGH, M. J., CLEMENTS, M. O., CROSSLEY, H., INGHAM, E. & FOSTER, S. J. 2001. PerR controls oxidative stress resistance and iron storage proteins and is required for virulence in Staphylococcus aureus. *Infect Immun,* 69**,** 3744-54.

HOWDEN, B. P., SMITH, D. J., MANSELL, A., JOHNSON, P. D., WARD, P. B., STINEAR, T. P. & DAVIES, J. K. 2008. Different bacterial gene expression patterns and attenuated host immune responses are associated with the evolution of low-level vancomycin resistance during persistent methicillin-resistant Staphylococcus aureus bacteraemia. *BMC Microbiol,* 8**,** 39.

HUANG, Z., JAYASEELAN, S., HEBERT, J., SEO, H. & NIU, L. 2013. Single-nucleotide resolution of RNAs up to 59 nucleotides by high-performance liquid chromatography. *Anal Biochem,* 435**,** 35-43.

HUR, W., SUN, Z., JIANG, T., MASON, D. E., PETERS, E. C., ZHANG, D. D., LUESCH, H., SCHULTZ, P. G. & GRAY, N. S. 2010. A Small-Molecule Inducer of the Antioxidant Response Element. *Chemistry & Biology,* 17**,** 537-547.

IHARA, Y., OHTA, H. & MASUDA, S. 2015. A highly sensitive quantification method for the accumulation of alarmone ppGpp in Arabidopsis thaliana using UPLC-ESI-qMS/MS. *Journal of Plant Research,* 128**,** 511-518.

IMAIZUMI, A., KOJIMA, H. & MATSUI, K. 2006. The effect of intracellular ppGpp levels on glutamate and lysine overproduction in Escherichia coli. *Journal of biotechnology,* 125**,** 328-337.

IMAMOTO, T. 1991. 4.1 - Reduction of Saturated Alkyl Halides to Alkanes. *In:* TROST, B. M. & FLEMING, I. (eds.) *Comprehensive Organic Synthesis.* Oxford: Pergamon.

IMLAY, J. A. 2003. Pathways of oxidative damage. *Annu Rev Microbiol,* 57**,** 395-418.

IMLAY, J. A. 2019. Where in the world do bacteria experience oxidative stress? *Environmental Microbiology,* 21**,** 521-530.

IRVING, S. E., CHOUDHURY, N. R. & CORRIGAN, R. M. 2020. The stringent response and physiological roles of (pp)pGpp in bacteria. *Nature Reviews Microbiology*.

IRVING, S. E., CHOUDHURY, N. R. & CORRIGAN, R. M. 2021. The stringent response and physiological roles of (pp)pGpp in bacteria. *Nat Rev Microbiol,* 19**,** 256-271.

IRVING, S. E. & CORRIGAN, R. M. 2018. Triggering the stringent response: signals responsible for activating (p)ppGpp synthesis in bacteria. *Microbiology,* 164**,** 268-276.

ITO, T., KATAYAMA, Y. & HIRAMATSU, K. 1999. Cloning and nucleotide sequence determination of the entire mec DNA of pre-methicillin-resistant Staphylococcus aureus N315. *Antimicrob Agents Chemother,* 43**,** 1449-58.

ITO, T., KUWAHARA-ARAI, K., KATAYAMA, Y., UEHARA, Y., HAN, X., KONDO, Y. & HIRAMATSU, K. 2014. Staphylococcal Cassette Chromosome mec (SCCmec) Analysis of MRSA. *In:* JI, Y. (ed.) *Methicillin-Resistant Staphylococcus Aureus (MRSA) Protocols*. Totowa, NJ: Humana Press.

JAGTAP, S. P., MUKHOPADHYAY, S., COROPCEANU, V., BRIZIUS, G. L., BRÉDAS, J. L. & COLLARD, D. M. 2012. Closely stacked oligo(phenylene ethynylene)s: effect of π-stacking on the electronic properties of conjugated chromophores. *J Am Chem Soc,* 134**,** 7176-85.

JAHANTIGH, H. R., FAEZI, S., HABIBI, M., MAHDAVI, M., STUFANO, A., LOVREGLIO, P. & AHMADI, K. 2022. The Candidate Antigens to Achieving an Effective Vaccine against Staphylococcus aureus. *Vaccines,* 10**,** 199.

JAIN, N., DHIMOLE, N., KHAN, A. R., DE, D., TOMAR, S. K., SAJISH, M., DUTTA, D., PARRACK, P. & PRAKASH, B. 2009. *E. coli* HflX interacts with 50S ribosomal subunits in presence of nucleotides. *Biochem Biophys Res Commun,* 379**,** 201-5.

JENAL, U., REINDERS, A. & LORI, C. 2017. Cyclic di-GMP: second messenger extraordinaire. *Nature Reviews Microbiology,* 15**,** 271-284.

JEVONS, M. P. 1961. "Celbenin" - resistant Staphylococci. *British Medical Journal,* 1**,** 124-125.

JI, C. J., KIM, J. H., WON, Y. B., LEE, Y. E., CHOI, T. W., JU, S. Y., YOUN, H., HELMANN, J. D. & LEE, J. W. 2015. Staphylococcus aureus PerR Is a Hypersensitive Hydrogen Peroxide Sensor using Iron-mediated Histidine Oxidation. *J Biol Chem,* 290**,** 20374-86.

JIMMY, S., SAHA, C. K., KURATA, T., STAVROPOULOS, C., OLIVEIRA, S. R. A., KOH, A., CEPAUSKAS, A., TAKADA, H., REJMAN, D., TENSON, T., STRAHL, H., GARCIA-PINO, A., HAURYLIUK, V. & ATKINSON, G. C. 2020. A widespread toxin-antitoxin system exploiting growth control via alarmone signaling. *Proc Natl Acad Sci U S A,* 117**,** 10500-10510.

JOMAA, A., STEWART, G., MARTÍN-BENITO, J., ZIELKE, R., CAMPBELL, T. L., MADDOCK, J. R., BROWN, E. D. & ORTEGA, J. 2011. Understanding ribosome assembly: the structure of in vivo assembled immature 30S subunits revealed by cryo-electron microscopy. *Rna,* 17**,** 697-709.

JORDAN, S., HUTCHINGS, M. I. & MASCHER, T. 2008. Cell envelope stress response in Gram-positive bacteria. *FEMS Microbiol Rev,* 32**,** 107-46.

JORES, L. & WAGNER, R. 2003. Essential Steps in the ppGpp-dependent Regulation of Bacterial Ribosomal RNA Promoters Can Be Explained by Substrate Competition. *Journal of Biological Chemistry,* 278**,** 16834-16843.

JOSEPHY, P. D. 1985. Oxidative activation of benzidine and its derivatives by peroxidases. *Environmental Health Perspectives,* 64**,** 171-178.

JOSSE, J., LAURENT, F. & DIOT, A. 2017. Staphylococcal Adhesion and Host Cell Invasion: Fibronectin-Binding and Other Mechanisms. *Front Microbiol,* 8**,** 2433.

JOUSSELIN, A., MANZANO, C., BIETTE, A., REED, P., PINHO, M. G., ROSATO, A. E., KELLEY, W. L. & RENZONI, A. 2015. The Staphylococcus aureus Chaperone PrsA Is a New Auxiliary Factor of Oxacillin Resistance Affecting Penicillin-Binding Protein 2A. *Antimicrob Agents Chemother,* 60**,** 1656-66.

JULIAN, K., KOSOWSKA-SHICK, K., WHITENER, C., ROOS, M., LABISCHINSKI, H., RUBIO, A., PARENT, L., EDNIE, L., KOETH, L., BOGDANOVICH, T. & APPELBAUM, P. C. 2007. Characterization of a daptomycin-nonsusceptible vancomycin-intermediate Staphylococcus aureus strain in a patient with endocarditis. *Antimicrob Agents Chemother,* 51**,** 3445-8.

JUNG, D., ROZEK, A., OKON, M. & HANCOCK, R. E. W. 2004. Structural Transitions as Determinants of the Action of the Calcium-Dependent Antibiotic Daptomycin. *Chemistry & Biology,* 11**,** 949-957.

KAISER, J. C., KING, A. N., GRIGG, J. C., SHELDON, J. R., EDGELL, D. R., MURPHY, M. E. P., BRINSMADE, S. R. & HEINRICHS, D. E. 2018. Repression of branched-chain amino acid synthesis in Staphylococcus aureus is mediated by isoleucine via CodY, and by a leucine-rich attenuator peptide. *PLoS Genet,* 14**,** e1007159.

KANEHISA, M. & GOTO, S. 2000. KEGG: kyoto encyclopedia of genes and genomes. *Nucleic Acids Res,* 28**,** 27-30.

KARAOLIS, D. K., RASHID, M. H., CHYTHANYA, R., LUO, W., HYODO, M. & HAYAKAWA, Y. 2005. c-di-GMP (3'-5'-cyclic diguanylic acid) inhibits Staphylococcus aureus cell-cell interactions and biofilm formation. *Antimicrob Agents Chemother,* 49**,** 1029-38.

KATAYAMA, Y., ITO, T. & HIRAMATSU, K. 2000. A new class of genetic element, staphylococcus cassette chromosome mec, encodes methicillin resistance in Staphylococcus aureus. *Antimicrob Agents Chemother,* 44**,** 1549-55.

KAZMIERCZAK, M. J., WIEDMANN, M. & BOOR, K. J. 2005. Alternative sigma factors and their roles in bacterial virulence. *Microbiol Mol Biol Rev,* 69**,** 527-43.

KHAVRUTSKII, L., YEH, J., TIMOFEEVA, O., TARASOV, S. G., PRITT, S., STEFANISKO, K. & TARASOVA, N. 2013. Protein purification-free method of binding affinity determination by microscale thermophoresis. *J Vis Exp*.

KIELKOPF, C. L., BAUER, W. & URBATSCH, I. L. 2020. Bradford Assay for Determining Protein Concentration. *Cold Spring Harb Protoc,* 2020**,** 102269.

KIHIRA, K., SHIMIZU, Y., SHOMURA, Y., SHIBATA, N., KITAMURA, M., NAKAGAWA, A., UEDA, T., OCHI, K. & HIGUCHI, Y. 2012. Crystal structure analysis of the translation factor RF3 (release factor 3). *FEBS Letters,* 586**,** 3705-3709.

KIM, S. K., LEE, D. H., HONG, J.-I. & YOON, J. 2009. Chemosensors for Pyrophosphate. *Accounts of Chemical Research,* 42**,** 23-31.

KIRBY, W. M. 1944. EXTRACTION OF A HIGHLY POTENT PENICILLIN INACTIVATOR FROM PENICILLIN RESISTANT STAPHYLOCOCCI. *Science,* 99**,** 452-3.

KOLB, H. C., FINN, M. G. & SHARPLESS, K. B. 2001. Click Chemistry: Diverse Chemical Function from a Few Good Reactions. *Angew Chem Int Ed Engl,* 40**,** 2004-2021.

KORCH, S. B., HENDERSON, T. A. & HILL, T. M. 2003. Characterization of the hipA7 allele of Escherichia coli and evidence that high persistence is governed by (p) ppGpp synthesis. *Molecular microbiology,* 50**,** 1199-1213.

KOURTIS, A. P., HATFIELD, K., BAGGS, J., MU, Y., SEE, I., EPSON, E., NADLE, J., KAINER, M. A., DUMYATI, G., PETIT, S., RAY, S. M., HAM, D., CAPERS, C., EWING, H., COFFIN, N., MCDONALD, L. C., JERNIGAN, J. & CARDO, D. 2019. Vital Signs: Epidemiology and Recent Trends in Methicillin-Resistant and in Methicillin-Susceptible *Staphylococcus aureus* Bloodstream Infections — United States. *MMWR. Morbidity and Mortality Weekly Report,* 68**,** 214-219.

KRAEMER, J., SANDERLIN, A. & LAUB, M. 2019. The stringent response inhibits DNA replication initiation in E. coli by modulating supercoiling of oriC. mBio 10: e01330-19.

KRETSCHMER, D., BREITMEYER, R., GEKELER, C., LEBTIG, M., SCHLATTERER, K., NEGA, M., STAHL, M., STAPELS, D., ROOIJAKKERS, S. & PESCHEL, A. 2021. Staphylococcus aureus Depends on Eap Proteins for Preventing Degradation of Its Phenol-Soluble Modulin Toxins by Neutrophil Serine Proteases. *Front Immunol,* 12**,** 701093.

KRETSCHMER, D., GLESKE, A. K., RAUTENBERG, M., WANG, R., KÖBERLE, M., BOHN, E., SCHÖNEBERG, T., RABIET, M. J., BOULAY, F., KLEBANOFF, S. J., VAN KESSEL, K. A., VAN STRIJP, J. A., OTTO, M. & PESCHEL, A. 2010. Human formyl peptide receptor 2 senses highly pathogenic Staphylococcus aureus. *Cell Host Microbe,* 7**,** 463-73.

KRIEL, A., ALYCIA, SOK, LIU, K., ASHLEY, WINNIE, RENDON, S., CHEN, R., BENJAMIN & JUE 2012. Direct Regulation of GTP Homeostasis by (p)ppGpp: A Critical Component of Viability and Stress Resistance. *Molecular Cell,* 48**,** 231-241.

KRIEL, A., BRINSMADE, S. R., TSE, J. L., TEHRANCHI, A. K., BITTNER, A. N., SONENSHEIN, A. L. & WANG, J. D. 2014. GTP Dysregulation in Bacillus subtilis Cells Lacking (p)ppGpp Results in Phenotypic Amino Acid Auxotrophy and Failure To Adapt to Nutrient Downshift and Regulate Biosynthesis Genes. *Journal of Bacteriology,* 196**,** 189-201.

KRÜGER, L., HERZBERG, C., WICKE, D., BÄHRE, H., HEIDEMANN, J. L., DICKMANNS, A., SCHMITT, K., FICNER, R. & STÜLKE, J. 2021. A meet-up of two second messengers: the c-di-AMP receptor DarB controls (p)ppGpp synthesis in Bacillus subtilis. *Nature Communications,* 12**,** 1210.

KUMAR, G. 2018. Principle and Method of Silver Staining of Proteins Separated by Sodium Dodecyl Sulfate–Polyacrylamide Gel Electrophoresis. *In:* KURIEN, B. T. & SCOFIELD, R. H. (eds.) *Protein Gel Detection and Imaging: Methods and Protocols*. New York, NY: Springer New York.

KUMAR, V., CHEN, Y., ERO, R., AHMED, T., TAN, J., LI, Z., WONG, A. S. W., BHUSHAN, S. & GAO, Y.-G. 2015. Structure of BipA in GTP form bound to the ratcheted ribosome. *Proceedings of the National Academy of Sciences,* 112**,** 10944-10949.

KURODA, M., KUWAHARA-ARAI, K. & HIRAMATSU, K. 2000. Identification of the Up- and Down-Regulated Genes in Vancomycin-Resistant Staphylococcus aureus Strains Mu3 and Mu50 by cDNA Differential Hybridization Method. *Biochemical and Biophysical Research Communications,* 269**,** 485-490.

KUSHWAHA, G. S., PATRA, A. & BHAVESH, N. S. 2020. Structural Analysis of (p)ppGpp Reveals Its Versatile Binding Pattern for Diverse Types of Target Proteins. *Frontiers in microbiology,* 11**,** 575041-575041.

KWOK, R. T. K., LEUNG, C. W. T., LAM, J. W. Y. & TANG, B. Z. 2015. Biosensing by luminogens with aggregation-induced emission characteristics. *Chemical Society Reviews,* 44**,** 4228-4238.

KÄSTLE, B., GEIGER, T., GRATANI, F. L., REISINGER, R., GOERKE, C., BORISOVA, M., MAYER, C. & WOLZ, C. 2015. rRNA regulation during growth and under stringent conditions in taphylococcus aureus. *Environmental Microbiology,* 17**,** 4394-4405.

KÖSTER, H., LITTLE, D. P., LUAN, P., MULLER, R., SIDDIQI, S. M., MARAPPAN, S. & YIP, P. 2007. Capture compound mass spectrometry: a technology for the investigation of small molecule protein interactions. *Assay Drug Dev Technol,* 5**,** 381-90.

LACEY, K. A., GEOGHEGAN, J. A. & MCLOUGHLIN, R. M. 2016. The Role of Staphylococcus aureus Virulence Factors in Skin Infection and Their Potential as Vaccine Antigens. *Pathogens,* 5.

LAM, J. C. & STOKES, W. 2023. The Golden Grapes of Wrath - Staphylococcus aureus Bacteremia: A Clinical Review. *American Journal of Medicine,* 136**,** 19-26.

LAMBERS, H., PIESSENS, S., BLOEM, A., PRONK, H. & FINKEL, P. 2006. Natural skin surface pH is on average below 5, which is beneficial for its resident flora. *Int J Cosmet Sci,* 28**,** 359-70.

LANDGRAF, J. R., WU, J. & CALVO, J. M. 1996. Effects of nutrition and growth rate on Lrp levels in Escherichia coli. *Journal of bacteriology,* 178**,** 6930-6936.

LAVENTIE, B. J., GLATTER, T. & JENAL, U. 2017. Pull-Down with a c-di-GMP-Specific Capture Compound Coupled to Mass Spectrometry as a Powerful Tool to Identify Novel Effector Proteins. *Methods Mol Biol,* 1657**,** 361-376.

LAZAR, J. T. & TABOR, J. J. 2021. Bacterial two-component systems as sensors for synthetic biology applications. *Current Opinion in Systems Biology,* 28**,** 100398.

LEE, D. H., IM, J. H., SON, S. U., CHUNG, Y. K. & HONG, J.-I. 2003. An Azophenol-based Chromogenic Pyrophosphate Sensor in Water. *Journal of the American Chemical Society,* 125**,** 7752-7753.

LEE, D. H., KIM, S. Y. & HONG, J.-I. 2004. A Fluorescent Pyrophosphate Sensor with High Selectivity over ATP in Water. *Angewandte Chemie International Edition,* 43**,** 4777-4780.

LEGAULT, L., JEANTET, C. & GROS, F. 1972. Inhibition of in vitro protein synthesis by ppGpp. *FEBS Lett,* 27**,** 71-75.

LEMOS, J. A., LIN, V. K., NASCIMENTO, M. M., ABRANCHES, J. & BURNE, R. A. 2007. Three gene products govern (p) ppGpp production by Streptococcus mutans. *Molecular microbiology,* 65**,** 1568-1581.

LETSINGER, R. L., FINNAN, J. L., HEAVNER, G. A. & LUNSFORD, W. B. 1975. Nucleotide chemistry. XX. Phosphite coupling procedure for generating internucleotide links. *Journal of the American Chemical Society,* 97**,** 3278-3279.

LI, G., ZHAO, Q., LUAN, T., HU, Y., ZHANG, Y., LI, T., WANG, C., XIE, F., ZHANG, W., LANGFORD, P. R. & LIU, S. 2020. Basal-Level Effects of (p)ppGpp in the Absence of Branched-Chain Amino Acids in Actinobacillus pleuropneumoniae. *Journal of Bacteriology,* 202**,** 10.1128/jb.00640-19.

LI, M., DU, X., VILLARUZ, A. E., DIEP, B. A., WANG, D., SONG, Y., TIAN, Y., HU, J., YU, F. & LU, Y. 2012. MRSA epidemic linked to a quickly spreading colonization and virulence determinant. *Nature medicine,* 18**,** 816-819.

LIN, M.-H., LIU, C.-C., LU, C.-W. & SHU, J.-C. 2024. Staphylococcus aureus foldase PrsA contributes to the folding and secretion of protein A. *BMC Microbiology,* 24**,** 108.

LINA, G., PIÉMONT, Y., GODAIL-GAMOT, F., BES, M., PETER, M. O., GAUDUCHON, V., VANDENESCH, F. & ETIENNE, J. 1999. Involvement of Panton-Valentine leukocidin-producing Staphylococcus aureus in primary skin infections and pneumonia. *Clin Infect Dis,* 29**,** 1128-32.

LINK, H., FUHRER, T., GEROSA, L., ZAMBONI, N. & SAUER, U. 2015. Real-time metabolome profiling of the metabolic switch between starvation and growth. *Nature Methods,* 12**,** 1091-1097.

LISHER JOHN, P., TSUI HO-CHING, T., RAMOS-MONTAÑEZ, S., HENTCHEL KRISTY, L., MARTIN JULIA, E., TRINIDAD JONATHAN, C., WINKLER MALCOLM, E. & GIEDROC DAVID, P. 2017. Biological and

Chemical Adaptation to Endogenous Hydrogen Peroxide Production in Streptococcus pneumoniae D39. *mSphere,* 2**,** 10.1128/msphere.00291-16.

LIU, C.-H., XU, M., LUO, Q., WANG, Z., TAN, W., ZHAO, X. & JIA, X. 2024. Inexpensive and mild hydrogenation condition: Raney Ni-catalyzed reduction of alkenes and alkynes using Et3SiH at ambient temperature. *Tetrahedron,* 160**,** 134040.

LIU, C. M., PRICE, L. B., HUNGATE, B. A., ABRAHAM, A. G., LARSEN, L. A., CHRISTENSEN, K., STEGGER, M., SKOV, R. & ANDERSEN, P. S. 2015a. Staphylococcus aureus and the ecology of the nasal microbiome. *Science Advances,* 1**,** e1400216.

LIU, G. Y., ESSEX, A., BUCHANAN, J. T., DATTA, V., HOFFMAN, H. M., BASTIAN, J. F., FIERER, J. & NIZET, V. 2005. Staphylococcus aureus golden pigment impairs neutrophil killing and promotes virulence through its antioxidant activity. *J Exp Med,* 202**,** 209-15.

LIU, K., ANGELA, PISITHKUL, T., KATHY, KENNETH, AMADOR-NOGUEZ, D., JAMES & JUE 2015b. Molecular Mechanism and Evolution of Guanylate Kinase Regulation by (p)ppGpp. *Molecular Cell.,* 57**,** 735-749.

LOVELAND, A. B., BAH, E., MADIREDDY, R., ZHANG, Y., BRILOT, A. F., GRIGORIEFF, N. & KOROSTELEV, A. A. 2016. Ribosome•RelA structures reveal the mechanism of stringent response activation. *eLife,* 5**,** e17029.

LOWY, F. D. 1998. *Staphylococcus aureus* Infections. *New England Journal of Medicine,* 339**,** 520-532.

LU, C., LI, N., JIN, Y., SUN, Y. & WANG, J. 2022. Physical Mechanisms of Intermolecular Interactions and Cross-Space Charge Transfer in Two-Photon BDBT-TCNB Co-Crystals. *Nanomaterials (Basel),* 12.

LUONG, T., SALABARRIA, A. C. & ROACH, D. R. 2020. Phage Therapy in the Resistance Era: Where Do We Stand and Where Are We Going? *Clin Ther,* 42**,** 1659-1680.

LYUBLINSKAYA, O. & ANTUNES, F. 2019. Measuring intracellular concentration of hydrogen peroxide with the use of genetically encoded H(2)O(2) biosensor HyPer. *Redox Biol,* 24**,** 101200.

LÖFFLER, B., HUSSAIN, M., GRUNDMEIER, M., BRÜCK, M., HOLZINGER, D., VARGA, G., ROTH, J., KAHL, B. C., PROCTOR, R. A. & PETERS, G. 2010. Staphylococcus aureus panton-valentine leukocidin is a very potent cytotoxic factor for human neutrophils. *PLoS Pathog,* 6**,** e1000715.

MACIAG, M., KOCHANOWSKA, M., LYZEŃ, R., WEGRZYN, G. & SZALEWSKA-PAŁASZ, A. 2010. ppGpp inhibits the activity of Escherichia coli DnaG primase. *Plasmid,* 63**,** 61-7.

MAGNUSSON, L. U., GUMMESSON, B., JOKSIMOVIĆ, P., FAREWELL, A. & NYSTRÖM, T. 2007. Identical, independent, and opposing roles of ppGpp and DksA in Escherichia coli. *J Bacteriol,* 189**,** 5193-202.

MAGUIRE, B. A., MANUILOV, A. V. & ZIMMERMANN, R. A. 2001. Differential effects of replacing Escherichia coli ribosomal protein L27 with its homologue from Aquifex aeolicus. *J Bacteriol,* 183**,** 6565-72.

MAJERCZYK, C. D., SADYKOV, M. R., LUONG, T. T., LEE, C., SOMERVILLE, G. A. & SONENSHEIN, A. L. 2008. Staphylococcus aureus CodY negatively regulates virulence gene expression. *J Bacteriol,* 190**,** 2257-65.

MALACHOWA, N. & DELEO, F. R. 2010. Mobile genetic elements of *Staphylococcus aureus*. *Cellular and Molecular Life Sciences,* 67**,** 3057-3071.

MANAV, M. C., BELJANTSEVA, J., BOJER, M. S., TENSON, T., INGMER, H., HAURYLIUK, V. & BRODERSEN, D. E. 2018. Structural basis for (p)ppGpp synthesis by the Staphylococcus aureus small alarmone synthetase RelP. *Journal of Biological Chemistry,* 293**,** 3254-3264.

MANDELLI, A. P., MAGRI, G., TORTOLI, M., TORRICELLI, S., LAERA, D., BAGNOLI, F., FINCO, O., BENSI, G., BRAZZOLI, M. & CHIAROT, E. 2024. Vaccination with staphylococcal protein A protects mice against systemic complications of skin infection recurrences. *Front Immunol,* 15**,** 1355764.

MAO, Z., GU, H. & LIN, X. 2021. Recent Advances of Pd/C-Catalyzed Reactions. *Catalysts,* 11**,** 1078.

MARTINEK, K., SEMENOV, A. N. & BEREZIN, I. V. 1981. Enzymatic synthesis in biphasic aqueous-organic systems. I. Chemical equilibrium shift. *Biochim Biophys Acta,* 658**,** 76-89.

MARTÍNEZ-GARCÍA, S., PERALTA, H., BETANZOS-CABRERA, G., CHAVEZ-GALAN, L., RODRÍGUEZ-MARTÍNEZ, S., CANCINO-DIAZ, M. E. & CANCINO-DIAZ, J. C. 2021. Proteomic comparison of biofilm vs. planktonic Staphylococcus epidermidis cells suggests key metabolic differences between these conditions. *Research in Microbiology,* 172**,** 103796.

MASCITTI, V. 2012. *4- (5-CYANO-PYRAZOL-1-YL) -PIPERIDINE DERIVATIVES AS GPR 119 MODULATORS*. USA patent application.
MASHBURN, L. M., JETT, A. M., AKINS, D. R. & WHITELEY, M. 2005. Staphylococcus aureus serves as an iron source for Pseudomonas aeruginosa during in vivo coculture. *J Bacteriol,* 187**,** 554-66.
MATSUI, M., MIYANO, M. & TOMITA, K. 1956. Calcium Borohydride Reduction of β-Ketoesters. *Bulletin of the Agricultural Chemical Society of Japan,* 20**,** 139-140.
MCADOW, M., MISSIAKAS, D. M. & SCHNEEWIND, O. 2012. Staphylococcus aureus secretes coagulase and von Willebrand factor binding protein to modify the coagulation cascade and establish host infections. *J Innate Immun,* 4**,** 141-8.
MCCALLUM, N., MEIER, P. S., HEUSSER, R. & BERGER-BÄCHI, B. 2011. Mutational analyses of open reading frames within the vraSR operon and their roles in the cell wall stress response of Staphylococcus aureus. *Antimicrob Agents Chemother,* 55**,** 1391-402.
MCDONOUGH, K. A. & RODRIGUEZ, A. 2011. The myriad roles of cyclic AMP in microbial pathogens: from signal to sword. *Nat Rev Microbiol,* 10**,** 27-38.
MCGUINNESS, W. A., MALACHOWA, N. & DELEO, F. R. 2017. Vancomycin Resistance in Staphylococcus aureus *Yale J Biol Med,* 90**,** 269-281.
MECHOLD, U., MURPHY, H., BROWN, L. & CASHEL, M. 2002. Intramolecular regulation of the opposing (p) ppGpp catalytic activities of Rel Seq, the Rel/Spo enzyme from Streptococcus equisimilis. *Journal of bacteriology,* 184**,** 2878-2888.
MECHOLD, U., POTRYKUS, K., MURPHY, H., MURAKAMI, K. S. & CASHEL, M. 2013. Differential regulation by ppGpp versus pppGpp in Escherichia coli. *Nucleic Acids Res,* 41**,** 6175-89.
MEHTA, S., EASTERLY, C. W., SAJULGA, R., MILLIKIN, R. J., ARGENTINI, A., EGUINOA, I., MARTENS, L., SHORTREED, M. R., SMITH, L. M., MCGOWAN, T., KUMAR, P., JOHNSON, J. E., GRIFFIN, T. J. & JAGTAP, P. D. 2020. Precursor Intensity-Based Label-Free Quantification Software Tools for Proteomic and Multi-Omic Analysis within the Galaxy Platform. *Proteomes,* 8.
MERLIE, J. P. & PIZER, L. I. 1973. Regulation of phospholipid synthesis in Escherichia coli by guanosine tetraphosphate. *Journal of bacteriology,* 116**,** 355-366.
MILLER, L. G., EELLS, S. J., DAVID, M. Z., ORTIZ, N., TAYLOR, A. R., KUMAR, N., CRUZ, D., BOYLE-VAVRA, S. & DAUM, R. S. 2015. Staphylococcus aureus skin infection recurrences among household members: an examination of host, behavioral, and pathogen-level predictors. *Clin Infect Dis,* 60**,** 753-63.
MILLER, L. G., TAN, J., EELLS, S. J., BENITEZ, E. & RADNER, A. B. 2012. Prospective investigation of nasal mupirocin, hexachlorophene body wash, and systemic antibiotics for prevention of recurrent community-associated methicillin-resistant Staphylococcus aureus infections. *Antimicrob Agents Chemother,* 56**,** 1084-6.
MILON, P., TISCHENKO, E., TOMSIC, J., CASERTA, E., FOLKERS, G., LA TEANA, A., RODNINA, M. V., PON, C. L., BOELENS, R. & GUALERZI, C. O. 2006. The nucleotide-binding site of bacterial translation initiation factor 2 (IF2) as a metabolic sensor. *Proceedings of the National Academy of Sciences,* 103**,** 13962-13967.
MIRONOV, A. S., GUSAROV, I., RAFIKOV, R., LOPEZ, L. E., SHATALIN, K., KRENEVA, R. A., PERUMOV, D. A. & NUDLER, E. 2002. Sensing small molecules by nascent RNA: a mechanism to control transcription in bacteria. *cell,* 111**,** 747-756.
MOBLEY, H. L., ISLAND, M. D. & HAUSINGER, R. P. 1995. Molecular biology of microbial ureases. *Microbiol Rev,* 59**,** 451-80.
MOHAJER, F., HERAVI, M. M., ZADSIRJAN, V. & POORMOHAMMAD, N. 2021. Copper-free Sonogashira cross-coupling reactions: an overview. *RSC Adv,* 11**,** 6885-6925.
MOHAMED, N., TEETERS, M. A., PATTI, J. M., HÖÖK, M. & ROSS, J. M. 1999. Inhibition of Staphylococcus aureus adherence to collagen under dynamic conditions. *Infect Immun,* 67**,** 589-94.
MOIOLA, M., MEMEO, M. G. & QUADRELLI, P. 2019. Stapled Peptides—A Useful Improvement for Peptide-Based Drugs. *Molecules,* 24**,** 3654.
MOLLE, V., NAKAURA, Y., SHIVERS, R. P., YAMAGUCHI, H., LOSICK, R., FUJITA, Y. & SONENSHEIN, A. L. 2003. Additional Targets of the Bacillus subtilis Global Regulator CodY Identified by

Chromatin Immunoprecipitation and Genome-Wide Transcript Analysis. *Journal of Bacteriology,* 185**,** 1911-1922.

MOLÉS PÉREZ, L. 1981. *Chemical Kinetics - James H. Espenson*.

MURCHAN, S., AUCKEN, H. M., O'NEILL G, L., GANNER, M. & COOKSON, B. D. 2004. Emergence, spread, and characterization of phage variants of epidemic methicillin-resistant Staphylococcus aureus 16 in England and Wales. *J Clin Microbiol,* 42**,** 5154-60.

MURRAY, C. J. L., IKUTA, K. S., SHARARA, F., SWETSCHINSKI, L., ROBLES AGUILAR, G., GRAY, A., HAN, C., BISIGNANO, C., RAO, P., WOOL, E., JOHNSON, S. C., BROWNE, A. J., CHIPETA, M. G., FELL, F., HACKETT, S., HAINES-WOODHOUSE, G., KASHEF HAMADANI, B. H., KUMARAN, E. A. P., MCMANIGAL, B., ... & NAGHAVI, M. 2022. Global burden of bacterial antimicrobial resistance in 2019: a systematic analysis. *The Lancet,* 399**,** 629-655.

MUSOLINO, S., PEI, Z., BI, L., DILABIO, G. & WULFF, J. 2021. Structure-function relationships in aryl diazirines reveal optimal design features to maximize C-H insertion †. *Chemical Science,* 12.

MWANGI, M. M., WU, S. W., ZHOU, Y., SIERADZKI, K., DE LENCASTRE, H., RICHARDSON, P., BRUCE, D., RUBIN, E., MYERS, E., SIGGIA, E. D. & TOMASZ, A. 2007. Tracking the in vivo evolution of multidrug resistance in Staphylococcus aureus by whole-genome sequencing. *Proc Natl Acad Sci U S A,* 104**,** 9451-6.

ML:YNARCZYK, A., ML:YNARCZYK, G. & JELJASZEWICZ, J. 1998. The Genome of *Staphylococcus aureus*: A Review. *Zentralblatt für Bakteriologie,* 287**,** 277-314.

NANAMIYA, H., KASAI, K., NOZAWA, A., YUN, C. S., NARISAWA, T., MURAKAMI, K., NATORI, Y., KAWAMURA, F. & TOZAWA, Y. 2008. Identification and functional analysis of novel (p) ppGpp synthetase genes in Bacillus subtilis. *Molecular microbiology,* 67**,** 291-304.

NAVARRO LLORENS, J. M., TORMO, A. & MARTÍNEZ-GARCÍA, E. 2010. Stationary phase in gram-negative bacteria. *FEMS microbiology reviews,* 34**,** 476-495.

NEMECEK, S., MARISCH, K., JURIC, R. & BAYER, K. 2006. Design of transcriptional fusions of stress sensitive promoters and GFP to monitor the overburden of E.coli hosts during recombinant protein production. *Microbial Cell Factories,* 5**,** S24.

NEUBAUER, J. L., IMMORMINO, R.M., DOLLINS, D.E., ENDO-STREETER, S.T., PEMBLE IV, C.W., YORK, J.D. 2012. The NatA Acetyltransferase Complex Bound To ppGpp.

NOOR, Z., ADHIKARI, S., RANGANATHAN, S. & MOHAMEDALI, A. 2019. Quantification of Proteins From Proteomic Analysis. *In:* RANGANATHAN, S., GRIBSKOV, M., NAKAI, K. & SCHÖNBACH, C. (eds.) *Encyclopedia of Bioinformatics and Computational Biology.* Oxford: Academic Press.

NOSKIN, G. A., RUBIN, R. J., SCHENTAG, J. J., KLUYTMANS, J., HEDBLOM, E. C., JACOBSON, C., SMULDERS, M., GEMMEN, E. & BHARMAL, M. 2007. National Trends in *Staphylococcus aureus* Infection Rates: Impact on Economic Burden and Mortality over a 6-Year Period (1998-2003). *Clinical Infectious Diseases,* 45**,** 1132-1140.

NYSTROM, R. F., CHAIKIN, S. W. & BROWN, W. G. 1949. Lithium Borohydride as a Reducing Agent. *Journal of the American Chemical Society,* 71**,** 3245-3246.

O'BRIEN, E. C. & MCLOUGHLIN, R. M. 2019. Considering the 'Alternatives' for Next-Generation Anti-Staphylococcus aureus Vaccine Development. *Trends Mol Med,* 25**,** 171-184.

O'ROURKE, E. J., CHEVALIER, C., PINTO, A. V., THIBERGE, J. M., IELPI, L., LABIGNE, A. & RADICELLA, J. P. 2003. Pathogen DNA as target for host-generated oxidative stress: role for repair of bacterial DNA damage in Helicobacter pylori colonization. *Proc Natl Acad Sci U S A,* 100**,** 2789-94.

OGSTON, A. 1984. “On Abscesses”. *Reviews of Infectious Diseases,* 6**,** 122-128.

OH, J. & HONG, J.-I. 2013. Discrimination of Redox-Responsible Biomolecules by a Single Molecular Sensor. *Organic Letters,* 15**,** 1210-1213.

OKOTH, R. & BASU, A. 2013. End-labeled amino terminated monotelechelic glycopolymers generated by ROMP and Cu(I)-catalyzed azide-alkyne cycloaddition. *Beilstein J Org Chem,* 9**,** 608-12.

ONG, S. E., BLAGOEV, B., KRATCHMAROVA, I., KRISTENSEN, D. B., STEEN, H., PANDEY, A. & MANN, M. 2002. Stable isotope labeling by amino acids in cell culture, SILAC, as a simple and accurate approach to expression proteomics. *Mol Cell Proteomics,* 1**,** 376-86.

ORR, M. W. & LEE, V. T. 2017. Differential Radial Capillary Action of Ligand Assay (DRaCALA) for High-Throughput Detection of Protein-Metabolite Interactions in Bacteria. *Methods Mol Biol,* 1535**,** 25-41.

OURSEL, D., LOUTELIER-BOURHIS, C., ORANGE, N., CHEVALIER, S., NORRIS, V. & LANGE, C. M. 2007. Identification and relative quantification of fatty acids in Escherichia coli membranes by gas chromatography/mass spectrometry. *Rapid Communications in Mass Spectrometry,* 21**,** 3229-3233.

PALMQVIST, N., FOSTER, T., TARKOWSKI, A. & JOSEFSSON, E. 2002. Protein A is a virulence factor in Staphylococcus aureus arthritis and septic death. *Microb Pathog,* 33**,** 239-49.

PANDEY, S., SAHUKHAL, G. S. & ELASRI, M. O. 2019. The msaABCR Operon Regulates the Response to Oxidative Stress in Staphylococcus aureus. *J Bacteriol,* 201.

PAPAYANNOPOULOS, V. 2018. Neutrophil extracellular traps in immunity and disease. *Nature Reviews Immunology,* 18**,** 134-147.

PAPP-WALLACE, K. M., ENDIMIANI, A., TARACILA, M. A. & BONOMO, R. A. 2011. Carbapenems: past, present, and future. *Antimicrob Agents Chemother,* 55**,** 4943-60.

PARSHIN, A., SHIVER, A. L., LEE, J., OZEROVA, M., SCHNEIDMAN-DUHOVNY, D., GROSS, C. A. & BORUKHOV, S. 2015. DksA regulates RNA polymerase in *Escherichia coli* through a network of interactions in the secondary channel that includes Sequence Insertion 1. *Proceedings of the National Academy of Sciences,* 112**,** E6862-E6871.

PASZTOR, L., ZIEBANDT, A. K., NEGA, M., SCHLAG, M., HAASE, S., FRANZ-WACHTEL, M., MADLUNG, J., NORDHEIM, A., HEINRICHS, D. E. & GÖTZ, F. 2010. Staphylococcal major autolysin (Atl) is involved in excretion of cytoplasmic proteins. *J Biol Chem,* 285**,** 36794-803.

PATEL, A. H., NOWLAN, P., WEAVERS, E. D. & FOSTER, T. 1987. Virulence of protein A-deficient and alpha-toxin-deficient mutants of Staphylococcus aureus isolated by allele replacement. *Infect Immun,* 55**,** 3103-10.

PATHANIA, A., ANBA-MONDOLONI, J., GOMINET, M., HALPERN, D., DAIROU, J., DUPONT, L., LAMBERET, G., TRIEU-CUOT, P., GLOUX, K. & GRUSS, A. 2021. (p)ppGpp/GTP and Malonyl-CoA Modulate Staphylococcus aureus Adaptation to FASII Antibiotics and Provide a Basis for Synergistic Bi-Therapy. *mBio,* 12.

PATTI, J. M., BREMELL, T., KRAJEWSKA-PIETRASIK, D., ABDELNOUR, A., TARKOWSKI, A., RYDÉN, C. & HÖÖK, M. 1994. The Staphylococcus aureus collagen adhesin is a virulence determinant in experimental septic arthritis. *Infect Immun,* 62**,** 152-61.

PAUL, B. J., BARKER, M. M., ROSS, W., SCHNEIDER, D. A., WEBB, C., FOSTER, J. W. & GOURSE, R. L. 2004. DksA: a critical component of the transcription initiation machinery that potentiates the regulation of rRNA promoters by ppGpp and the initiating NTP. *Cell,* 118**,** 311-22.

PAUL, B. J., BERKMEN, M. B. & GOURSE, R. L. 2005. DksA potentiates direct activation of amino acid promoters by ppGpp. *Proc Natl Acad Sci U S A,* 102**,** 7823-8.

PAUSCH, P., ABDELSHAHID, M., STEINCHEN, W., SCHÄFER, H., GRATANI, F. L., FREIBERT, S.-A., WOLZ, C., TURGAY, K., WILSON, D. N. & BANGE, G. 2020. PDB: 6YXA - Structural Basis for Regulation of the Opposing (p)ppGpp Synthetase and Hydrolase within the Stringent Response Orchestrator Rel. *Cell Reports,* 32**,** 108157.

PAUSCH, P., STEINCHEN, W., WIELAND, M., KLAUS, T., FREIBERT, S.-A., ALTEGOER, F., WILSON, D. N. & BANGE, G. 2018. Structural basis for (p)ppGpp-mediated inhibition of the GTPase RbgA. *Journal of Biological Chemistry,* 293**,** 19699-19709.

PERIASAMY, S., CHATTERJEE, S. S., CHEUNG, G. Y. & OTTO, M. 2012. Phenol-soluble modulins in staphylococci: What are they originally for? *Commun Integr Biol,* 5**,** 275-7.

PETRANOVIC, D., GUÉDON, E., SPERANDIO, B., DELORME, C., EHRLICH, D. & RENAULT, P. 2004. Intracellular effectors regulating the activity of the Lactococcus lactis CodY pleiotropic transcription regulator. *Mol Microbiol,* 53**,** 613-21.

PINHO, S. P. & MACEDO, E. A. 2005. Solubility of NaCl, NaBr, and KCl in Water, Methanol, Ethanol, and Their Mixed Solvents. *Journal of Chemical & Engineering Data,* 50**,** 29-32.

PLUMET, L., AHMAD-MANSOUR, N., DUNYACH-REMY, C., KISSA, K., SOTTO, A., LAVIGNE, J. P., COSTECHAREYRE, D. & MOLLE, V. 2022. Bacteriophage Therapy for Staphylococcus Aureus

Infections: A Review of Animal Models, Treatments, and Clinical Trials. *Front Cell Infect Microbiol,* 12**,** 907314.

POHL, K., FRANCOIS, P., STENZ, L., SCHLINK, F., GEIGER, T., HERBERT, S., GOERKE, C., SCHRENZEL, J. & WOLZ, C. 2009. CodY in Staphylococcus aureus: a Regulatory Link between Metabolism and Virulence Gene Expression. *Journal of Bacteriology,* 191**,** 2953-2963.

POLAKIS, S. E., GUCHHAIT, R. B. & LANE, M. D. 1973. Stringent control of fatty acid synthesis in Escherichia coli: possible regulation of acetyl coenzyme A carboxylase by ppGpp. *Journal of Biological Chemistry,* 248**,** 7957-7966.

POLKINGHORNE, A., ZIEGLER, U., GONZÁLEZ-HERNÁNDEZ, Y., POSPISCHIL, A., TIMMS, P. & VAUGHAN, L. 2008. Chlamydophila pneumoniae HflX belongs to an uncharacterized family of conserved GTPases and associates with the Escherichia coli 50S large ribosomal subunit. *Microbiology,* 154**,** 3537-3546.

POTRYKUS, K. & CASHEL, M. 2008. (p) ppGpp: still magical? *Annu. Rev. Microbiol.,* 62**,** 35-51.

POTRYKUS, K., MURPHY, H., PHILIPPE, N. & CASHEL, M. 2011. ppGpp is the major source of growth rate control in *E. coli*. *Environmental Microbiology,* 13**,** 563-575.

PRATICÒ, D. 2001. In vivo measurement of the redox state. *Lipids,* 36 Suppl**,** S45-7.

PRIETO, J., AGUILAR, L., GIMÉNEZ, M. J., TORO, D., GÓMEZ-LUS, M. L., DAL-RÉ, R. & BALCABAO, I. P. 1998. In vitro activities of co-amoxiclav at concentrations achieved in human serum against the resistant subpopulation of heteroresistant Staphylococcus aureus: a controlled study with vancomycin. *Antimicrob Agents Chemother,* 42**,** 1574-7.

PROCTOR, R. A. 2012. Is there a future for a Staphylococcus aureus vaccine? *Vaccine,* 30**,** 2921-7.

PULSCHEN, A. A., SASTRE, D. E., MACHINANDIARENA, F., CROTTA ASIS, A., ALBANESI, D., DE MENDOZA, D. & GUEIROS-FILHO, F. J. 2017. The stringent response plays a key role in acillus subtilis survival of fatty acid starvation. *Molecular Microbiology,* 103**,** 698-712.

RADA, B. 2019. Neutrophil Extracellular Traps. *Methods Mol Biol,* 1982**,** 517-528.

RAMAGOPAL, S. & DAVIS, B. D. 1974. Localization of the Stringent Protein of Escherichia coli on the 50S Ribosomal Subunit. *Proceedings of the National Academy of Sciences,* 71**,** 820-824.

RAO, F., SEE, R. Y., ZHANG, D., TOH, D. C., JI, Q. & LIANG, Z. X. 2010. YybT is a signaling protein that contains a cyclic dinucleotide phosphodiesterase domain and a GGDEF domain with ATPase activity. *J Biol Chem,* 285**,** 473-82.

RAO, N., CANNELLA, B., CROSSETT, L. S., YATES, A. J., JR. & MCGOUGH, R., 3RD 2008. A preoperative decolonization protocol for staphylococcus aureus prevents orthopaedic infections. *Clin Orthop Relat Res,* 466**,** 1343-8.

RASIGADE, J.-P. & VANDENESCH, F. 2014. *Staphylococcus aureus*: A pathogen with still unresolved issues. *Infection, Genetics and Evolution,* 21**,** 510-514.

RAYNER, C. & MUNCKHOF, W. J. 2005. Antibiotics currently used in the treatment of infections caused by Staphylococcus aureus. *Intern Med J,* 35 Suppl 2**,** S3-16.

REICHERT, S., EBNER, P., BONETTI, E.-J., LUQMAN, A., NEGA, M., SCHRENZEL, J., SPRÖER, C., BUNK, B., OVERMANN, J., SASS, P., FRANÇOIS, P. & GÖTZ, F. 2018. Genetic Adaptation of a Mevalonate Pathway Deficient Mutant in Staphylococcus aureus. *Frontiers in Microbiology,* 9.

REISS, C. W., XIONG, Y. & STROBEL, S. A. 2017. Structural basis for ligand binding to the guanidine-I riboswitch. *Structure,* 25**,** 195-202.

RESCH, A., ROSENSTEIN, R., NERZ, C. & GÖTZ, F. 2005. Differential gene expression profiling of Staphylococcus aureus cultivated under biofilm and planktonic conditions. *Appl Environ Microbiol,* 71**,** 2663-76.

RHEE, H.-W., KIM, K.-S., HAN, P.-L. & HONG, J.-I. 2010. Label-free fluorescent real-time monitoring of adenylyl cyclase. *Bioorganic & Medicinal Chemistry Letters,* 20**,** 1145-1147.

RHEE, H. W., LEE, C. R., CHO, S. H., SONG, M. R., CASHEL, M., CHOY, H. E., SEOK, Y. J. & HONG, J. I. 2008. Selective fluorescent chemosensor for the bacterial alarmone (p)ppGpp. *J Am Chem Soc,* 130**,** 784-5.

RICHTER, D., NOWAK, P. & KLEINERT, U. 1975. Escherichia coli stringent factor binds to ribosomes at a site different from that of elongation factor Tu or G. *Biochemistry,* 14**,** 4414-4420.

RIES, O., LÖFFLER, P. M. G., RABE, A., MALAVAN, J. J. & VOGEL, S. 2017. Efficient liposome fusion mediated by lipid–nucleic acid conjugates. *Organic & Biomolecular Chemistry,* 15**,** 8936-8945.

RIGGS, P. 2000. Expression and purification of recombinant proteins by fusion to maltose-binding protein. *Molecular Biotechnology,* 15**,** 51-63.

RISSEEUW, M. D. P., DE CLERCQ, D. J. H., LIEVENS, S., HILLAERT, U., SINNAEVE, D., VAN DEN BROECK, F., MARTINS, J. C., TAVERNIER, J. & VAN CALENBERGH, S. 2013. A "Clickable" MTX Reagent as a Practical Tool for Profiling Small-Molecule–Intracellular Target Interactions via MASPIT. *ChemMedChem,* 8**,** 521-526.

RO, C., CASHEL, M. & FERNÁNDEZ-COLL, L. 2021. The secondary messenger ppGpp interferes with cAMP-CRP regulon by promoting CRP acetylation in Escherichia coli. *PLoS One,* 16**,** e0259067.

ROELOFS, K. G., WANG, J., SINTIM, H. O. & LEE, V. T. 2011. Differential radial capillary action of ligand assay for high-throughput detection of protein-metabolite interactions. *Proceedings of the National Academy of Sciences,* 108**,** 15528-15533.

ROGHANIAN, M., SEMSEY, S., LØBNER-OLESEN, A. & JALALVAND, F. 2019. (p) ppGpp-mediated stress response induced by defects in outer membrane biogenesis and ATP production promotes survival in Escherichia coli. *Scientific Reports,* 9**,** 2934.

ROJAS, A.-M., EHRENBERG, M., ANDERSSON, S. G. E. & KURLAND, C. G. 1984a. ppGpp inhibition of elongation factors Tu, G and Ts during polypeptide synthesis. *Molecular and General Genetics MGG,* 197**,** 36-45.

ROJAS, A.-M., EHRENBERG, M. N., ANDERSSON, S. G. E. & KURLAND, C. G. 1984b. ppGpp inhibition of elongation factors Tu, G and Ts during polypeptide synthesis. *Molecular Genetics and Genomics,* 197**,** 36-45.

ROMERO, M. A., GONZÁLEZ-DELGADO, J. A. & ARTEAGA, J. F. 2015. Synthesis of Stilbene Derivatives: A Comparative Study of their Antioxidant Activities. *Natural Product Communications,* 10**,** 1934578X1501000731.

RONDE, N. J., TOTEV, D., MÜLLER, C., LUTZ, M., SPEK, A. L. & VOGT, D. 2009. Molecular-Weight-Enlarged Multiple-Pincer Ligands: Synthesis and Application in Palladium-Catalyzed Allylic Substitution Reactions. *ChemSusChem,* 2**,** 558-574.

RONG, M., YE, J., CHEN, B., WEN, Y., DENG, X. & LIU, Z.-Q. 2020. Ratiometric fluorescence detection of stringent ppGpp using Eu-MoS2 QDs test paper. *Sensors and Actuators B: Chemical,* 309**,** 127807.

ROSENBACH, F. J. 1884. *Mikro-organismen bei den Wund-Infections-Krankheiten des Menschen*.

ROSS, W., SANCHEZ-VAZQUEZ, P., ALBERT, LEE, J.-H., HECTOR & RICHARD 2016a. ppGpp Binding to a Site at the RNAP-DksA Interface Accounts for Its Dramatic Effects on Transcription Initiation during the Stringent Response. *Molecular Cell,* 62**,** 811-823.

ROSS, W., SANCHEZ-VAZQUEZ, P., CHEN, A. Y., LEE, J. H., BURGOS, H. L. & GOURSE, R. L. 2016b. ppGpp Binding to a Site at the RNAP-DksA Interface Accounts for Its Dramatic Effects on Transcription Initiation during the Stringent Response. *Mol Cell,* 62**,** 811-823.

ROSS, W., VRENTAS, C. E., SANCHEZ-VAZQUEZ, P., GAAL, T. & GOURSE, R. L. 2013. The magic spot: a ppGpp binding site on E. coli RNA polymerase responsible for regulation of transcription initiation. *Mol Cell,* 50**,** 420-9.

ROSTOVTSEV, V. V., GREEN, L. G., FOKIN, V. V. & SHARPLESS, K. B. 2002. A Stepwise Huisgen Cycloaddition Process: Copper(I)-Catalyzed Regioselective "Ligation" of Azides and Terminal Alkynes. *Angewandte Chemie International Edition,* 41**,** 2596-2599.

ROUNTREE, P. M. & FREEMAN, B. M. 1955. Infections caused by a particular phage type of Staphylococcus aureus. *Med J Aust,* 42**,** 157-61.

RUTHERFORD, S. T. & BASSLER, B. L. 2012. Bacterial quorum sensing: its role in virulence and possibilities for its control. *Cold Spring Harb Perspect Med,* 2.

RUWE, M., RÜCKERT, C., KALINOWSKI, J. & PERSICKE, M. 2018. Functional Characterization of a Small Alarmone Hydrolase in Corynebacterium glutamicum. *Frontiers in Microbiology,* 9.

RYLANDER, P. 1979. Chapter 1 - Hydrogenation Catalysts, Reactors, and Reaction Conditions. *In:* RYLANDER, P. (ed.) *The Catalytic Hydrogenation in Organic Syntheses*. Academic Press.

SAID, H. M. 2009. Cell and molecular aspects of human intestinal biotin absorption. *J Nutr,* 139**,** 158-62.

SAIKOLAPPAN, S., DAS, K. & DHANDAYUTHAPANI, S. 2015. Inactivation of the organic hydroperoxide stress resistance regulator OhrR enhances resistance to oxidative stress and isoniazid in Mycobacterium smegmatis. *J Bacteriol,* 197**,** 51-62.

SAJISH, M., TIWARI, D., RANANAWARE, D., NANDICOORI, V. K. & PRAKASH, B. 2007. A Charge Reversal Differentiates (p)ppGpp Synthesis by Monofunctional and Bifunctional Rel Proteins. *Journal of Biological Chemistry,* 282**,** 34977-34983.

SAKR, A., BRÉGEON, F., MÈGE, J.-L., ROLAIN, J.-M. & BLIN, O. 2018. *Staphylococcus aureus* Nasal Colonization: An Update on Mechanisms, Epidemiology, Risk Factors, and Subsequent Infections. *Frontiers in Microbiology,* 9.

SALZER, A. & WOLZ, C. 2023. Role of (p)ppGpp in antibiotic resistance, tolerance, persistence and survival in Firmicutes. *microLife,* 4.

SAMARRAI, W., LIU, D. X., WHITE, A.-M., STUDAMIRE, B., EDELSTEIN, J., SRIVASTAVA, A., WIDOM, R. L. & RUDNER, R. 2011. Differential responses of Bacillus subtilis rRNA promoters to nutritional stress. *Journal of bacteriology,* 193**,** 723-733.

SANCHEZ-VAZQUEZ, P., DEWEY, C. N., KITTEN, N., ROSS, W. & GOURSE, R. L. 2019. Genome-wide effects on Escherichia coli transcription from ppGpp binding to its two sites on RNA polymerase. *Proceedings of the National Academy of Sciences,* 116**,** 8310-8319.

SAVIN, A., ANDERSON EXENE, E., DYZENHAUS, S., PODKOWIK, M., SHOPSIN, B., PIRONTI, A. & TORRES VICTOR, J. 2024. Staphylococcus aureus senses human neutrophils via PerR to coordinate the expression of the toxin LukAB. *Infection and Immunity,* 92**,** e00526-23.

SAYED, A., MATSUYAMA, S.-I. & INOUYE, M. 1999. Era, an Essential Escherichia coli Small G-Protein, Binds to the 30S Ribosomal Subunit. *Biochemical and Biophysical Research Communications,* 264**,** 51-54.

SCHELLINGER, A. P. & CARR, P. W. 2006. Isocratic and gradient elution chromatography: a comparison in terms of speed, retention reproducibility and quantitation. *J Chromatogr A,* 1109**,** 253-66.

SCHMUCKER, W., KLUMPP, S., HENNRICH, F., KAPPES, M. & WAGENKNECHT, H.-A. 2013. A simple pyrene “click”-type modification of DNA affects solubilisation and photoluminescence of single-walled carbon nanotubes. *RSC Advances,* 3**,** 6331-6333.

SCHREIBER, G., RON, E. Z. & GLASER, G. 1995. ppGpp-mediated regulation of DNA replication and cell division in Escherichia coli. *Current microbiology,* 30**,** 27-32.

SCHRÖDER, T., GARTNER, M., GRAB, T. & BRÄSE, S. 2007. A new azide staining reagent based on "click chemistry". *Org Biomol Chem,* 5**,** 2767-9.

SCHWIDOP, W. D., KLOSSEK, P., MÜLLER, R. & CLAUS, R. 1990. Procedure for the purification of streptavidin by hydrophobic interaction chromatography. *J Chromatogr,* 520**,** 325-31.

SCIENTIFIC, T. 2024. Avidin-Biotin Interaction. Available: https://www.thermofisher.com/uk/en/home/life-science/protein-biology/protein-biology-learning-center/protein-biology-resource-library/pierce-protein-methods/avidin-biotin-interaction.html.

SEVERIN, A., WU, S. W., TABEI, K. & TOMASZ, A. 2005. High-Level β-Lactam Resistance and Cell Wall Synthesis Catalyzed by the mecA Homologue of *Staphylococcus sciuri* Introduced into *Staphylococcus aureus*. *Journal of Bacteriology,* 187**,** 6651-6658.

SHARMA, M. R., BARAT, C., WILSON, D. N., BOOTH, T. M., KAWAZOE, M., HORI-TAKEMOTO, C., SHIROUZU, M., YOKOYAMA, S., FUCINI, P. & AGRAWAL, R. K. 2005. Interaction of Era with the 30S ribosomal subunit implications for 30S subunit assembly. *Molecular cell,* 18**,** 319-329.

SHARMA, V. K., GLICK, J. & VOUROS, P. 2012. Reversed-phase ion-pair liquid chromatography electrospray ionization tandem mass spectrometry for separation, sequencing and mapping of sites of base modification of isomeric oligonucleotide adducts using monolithic column. *J Chromatogr A,* 1245**,** 65-74.

SHERLOCK, M. E., SUDARSAN, N. & BREAKER, R. R. 2018. Riboswitches for the alarmone ppGpp expand the collection of RNA-based signaling systems. *Proceedings of the National Academy of Sciences,* 115**,** 6052-6057.

SHERWOOD, J., ALBERICIO, F. & DE LA TORRE, B. G. 2024. N,N-Dimethyl Formamide European Restriction Demands Solvent Substitution in Research and Development. *ChemSusChem,* 17**,** e202301639.

SHIN, Y., QAYYUM, M. Z., PUPOV, D., ESYUNINA, D., KULBACHINSKIY, A. & MURAKAMI, K. S. 2021. Structural basis of ribosomal RNA transcription regulation. *Nature Communications,* 12**,** 528.

SHIN, Y., VRANIC, S., JUST-BARINGO, X., GALI, S. M., KISBY, T., CHEN, Y., GKOUTZIDOU, A., PRESTAT, E., BELJONNE, D., LARROSA, I., KOSTARELOS, K. & CASIRAGHI, C. 2020. Stable, concentrated, biocompatible, and defect-free graphene dispersions with positive charge. *Nanoscale,* 12**,** 12383-12394.

SHINEFIELD, H., BLACK, S., FATTOM, A., HORWITH, G., RASGON, S., ORDONEZ, J., YEOH, H., LAW, D., ROBBINS, J. B. & SCHNEERSON, R. 2002. Use of a Staphylococcus aureus conjugate vaccine in patients receiving hemodialysis. *New England Journal of Medicine,* 346**,** 491-496.

SHLAES, D. M., SAHM, D., OPIELA, C. & SPELLBERG, B. 2013. The FDA reboot of antibiotic development. *Antimicrob Agents Chemother,* 57**,** 4605-7.

SHORTRIDGE, M. D., HAGE, D. S., HARBISON, G. S. & POWERS, R. 2008. Estimating protein-ligand binding affinity using high-throughput screening by NMR. *J Comb Chem,* 10**,** 948-58.

SHYP, V., TANKOV, S., ERMAKOV, A., KUDRIN, P., ENGLISH, B. P., EHRENBERG, M., TENSON, T., ELF, J. & HAURYLIUK, V. 2012. Positive allosteric feedback regulation of the stringent response enzyme RelA by its product. *EMBO reports,* 13**,** 835-839.

SIES, H. & JONES, D. P. 2020. Reactive oxygen species (ROS) as pleiotropic physiological signalling agents. *Nature Reviews Molecular Cell Biology,* 21**,** 363-383.

SILVERMAN JARED, A., PERLMUTTER NANCY, G. & SHAPIRO HOWARD, M. 2003. Correlation of Daptomycin Bactericidal Activity and Membrane Depolarization in Staphylococcus aureus. *Antimicrobial Agents and Chemotherapy,* 47**,** 2538-2544.

SINHA, A. K. & WINTHER, K. S. 2021. The RelA hydrolase domain acts as a molecular switch for (p)ppGpp synthesis. *Commun Biol,* 4**,** 434.

SINHA, A. K., WINTHER, K. S., ROGHANIAN, M. & GERDES, K. 2019. Fatty acid starvation activates RelA by depleting lysine precursor pyruvate. *Molecular Microbiology,* 112**,** 1339-1349.

SINHA, B., FRANCOIS, P. P., NUSSE, O., FOTI, M., HARTFORD, O. M., VAUDAUX, P., FOSTER, T. J., LEW, D. P., HERRMANN, M. & KRAUSE, K. H. 1999. Fibronectin-binding protein acts as Staphylococcus aureus invasin via fibronectin bridging to integrin alpha(5)beta(1). *Cellular Microbiology,* 1**,** 101-117.

SLETTEN, E. M. & BERTOZZI, C. R. 2011. From Mechanism to Mouse: A Tale of Two Bioorthogonal Reactions. *Accounts of Chemical Research,* 44**,** 666-676.

SOMERVILLE, C. R. & AHMED, A. 1979. Mutants of Escherichia coli defective in the degradation of guanosine 5'-triphosphate, 3'-diphosphate (pppGpp). *Molecular and General Genetics MGG,* 169**,** 315-323.

SONG, H., DHARMASENA, M. N., WANG, C., SHAW, G. X., CHERRY, S., TROPEA, J. E., JIN, D. J. & JI, X. 2020. Structure and activity of PPX/GppA homologs from Escherichia coli and Helicobacter pylori. *Febs j,* 287**,** 1865-1885.

SONG, S. & WOOD, T. K. 2020. ppGpp ribosome dimerization model for bacterial persister formation and resuscitation. *Biochemical and Biophysical Research Communications,* 523**,** 281-286.

SONOGASHIRA, K. 2002. Development of Pd–Cu catalyzed cross-coupling of terminal acetylenes with sp2-carbon halides. *Journal of Organometallic Chemistry,* 653**,** 46-49.

SONOGASHIRA, K., TOHDA, Y. & HAGIHARA, N. 1975. A convenient synthesis of acetylenes: catalytic substitutions of acetylenic hydrogen with bromoalkenes, iodoarenes and bromopyridines. *Tetrahedron Letters,* 16**,** 4467-4470.

SPAAN, A. N., VAN STRIJP, J. A. G. & TORRES, V. J. 2017. Leukocidins: staphylococcal bi-component pore-forming toxins find their receptors. *Nat Rev Microbiol,* 15**,** 435-447.

SPELLMAN, D. S., DEINHARDT, K., DARIE, C. C., CHAO, M. V. & NEUBERT, T. A. 2008. Stable Isotopic Labeling by Amino Acids in Cultured Primary Neurons: Application to Brain-derived Neurotrophic Factor-dependent Phosphotyrosine-associated Signaling. *Molecular & Cellular Proteomics,* 7**,** 1067-1076.

SPILMAN, M. S., DAMLE, P. K., DEARBORN, A. D., RODENBURG, C. M., CHANG, J. R., WALL, E. A., CHRISTIE, G. E. & DOKLAND, T. 2012. Assembly of bacteriophage 80α capsids in a Staphylococcus aureus expression system. *Virology,* 434**,** 242-50.

SRIVATSAN, A. & WANG, J. D. 2008. Control of bacterial transcription, translation and replication by (p) ppGpp. *Current opinion in microbiology,* 11**,** 100-105.
STAPELS, D. A., GEISBRECHT, B. V. & ROOIJAKKERS, S. H. 2015. Neutrophil serine proteases in antibacterial defense. *Curr Opin Microbiol,* 23**,** 42-8.
STAPELS, D. A., RAMYAR, K. X., BISCHOFF, M., VON KÖCKRITZ-BLICKWEDE, M., MILDER, F. J., RUYKEN, M., EISENBEIS, J., MCWHORTER, W. J., HERRMANN, M., VAN KESSEL, K. P., GEISBRECHT, B. V. & ROOIJAKKERS, S. H. 2014. Staphylococcus aureus secretes a unique class of neutrophil serine protease inhibitors. *Proc Natl Acad Sci U S A,* 111**,** 13187-92.
STAUDINGER, H. & MEYER, J. 1919. Über neue organische Phosphorverbindungen III. Phosphinmethylenderivate und Phosphinimine. *Helvetica Chimica Acta,* 2**,** 635-646.
STEFANOVIC, B., HELLERBRAND, C., HOLCIK, M., BRIENDL, M., ALIEBHABER, S. & BRENNER, D. A. 1997. Posttranscriptional regulation of collagen alpha1(I) mRNA in hepatic stellate cells. *Mol Cell Biol,* 17**,** 5201-9.
STEIN JR, J. & BLOCH, K. 1976. Inhibition of E. coliβ-hydroxydecanoyl thioester dehydrase by ppGpp. *Biochemical and biophysical research communications,* 73**,** 881-884.
STEINCHEN, W. & BANGE, G. 2016. The magic dance of the alarmones (p)ppGpp. *Molecular Microbiology,* 101**,** 531-544.
STEINCHEN, W., SCHUHMACHER, J. S., ALTEGOER, F., FAGE, C. D., SRINIVASAN, V., LINNE, U., MARAHIEL, M. A. & BANGE, G. 2015a. Catalytic mechanism and allosteric regulation of an oligomeric (p)ppGpp synthetase by an alarmone. *Proc Natl Acad Sci U S A,* 112**,** 13348-53.
STEINCHEN, W., SCHUHMACHER, J. S., ALTEGOER, F., FAGE, C. D., SRINIVASAN, V., LINNE, U., MARAHIEL, M. A. & BANGE, G. 2015b. PDB: 5DEC - Catalytic mechanism and allosteric regulation of an oligomeric (p)ppGpp synthetase by an alarmone. *Proceedings of the National Academy of Sciences,* 112**,** 13348-13353.
STEINCHEN, W., VOGT, M. S., ALTEGOER, F., GIAMMARINARO, P. I., HORVATEK, P., WOLZ, C. & BANGE, G. 2018. PDB: 6FGJ - Structural and mechanistic divergence of the small (p)ppGpp synthetases RelP and RelQ. *Scientific Reports,* 8.
STEINCHEN, W., ZEGARRA, V. & BANGE, G. 2020. (p)ppGpp: Magic Modulators of Bacterial Physiology and Metabolism. *Frontiers in Microbiology,* 11.
STENT, G. S. & BRENNER, S. 1961. A genetic locus for the regulation of ribonucleic acid synthesis. *Proc Natl Acad Sci U S A,* 47**,** 2005-14.
STOREY, J. D. 2003. The positive false discovery rate: a Bayesian interpretation and the q-value. *The Annals of Statistics,* 31**,** 2013-2035, 23.
STOREY, J. D. & TIBSHIRANI, R. 2003. Statistical significance for genomewide studies. *Proceedings of the National Academy of Sciences,* 100**,** 9440-9445.
STROP, P. & BRUNGER, A. T. 2005. Refractive index-based determination of detergent concentration and its application to the study of membrane proteins. *Protein Sci,* 14**,** 2207-11.
SUN, D., LEE, G., LEE, J. H., KIM, H.-Y., RHEE, H.-W., PARK, S.-Y., KIM, K.-J., KIM, Y., KIM, B. Y., HONG, J.-I., PARK, C., CHOY, H. E., KIM, J. H., JEON, Y. H. & CHUNG, J. 2010. A metazoan ortholog of SpoT hydrolyzes ppGpp and functions in starvation responses. *Nature Structural & Molecular Biology,* 17**,** 1188-1194.
SUTHERLAND, C. & MURAKAMI, K. S. 2018. An Introduction to the Structure and Function of the Catalytic Core Enzyme of Escherichia coli RNA Polymerase. *EcoSal Plus,* 8.
SWINEHART, D. F. 1962. The Beer-Lambert Law. *Journal of Chemical Education,* 39**,** 333.
SWITZER, R. C., MERRIL, C. R. & SHIFRIN, S. 1979. A highly sensitive silver stain for detecting proteins and peptides in polyacrylamide gels. *Analytical Biochemistry,* 98**,** 231-237.
SY, J. & LIPMANN, F. 1973. Identification of the Synthesis of Guanosine Tetraphosphate (MS I) as Insertion of a Pyrophosphoryl Group into the 3'-Position in Guanosine 5'-Diphosphate. *Proceedings of the National Academy of Sciences,* 70**,** 306-309.
TAGAMI, T., YAMBE, Y., TANAKA, T., TANAKA, T., OGO, A., YOSHIZUMI, H., KAISE, K., HIGASHI, K., TANABE, M., SHIMAZU, S., USUI, T., SHIMATSU, A. & NARUSE, M. 2012. Short-term effects of β-adrenergic antagonists and methimazole in new-onset thyrotoxicosis caused by Graves' disease. *Intern Med,* 51**,** 2285-90.

TAKADA, H., ROGHANIAN, M., MURINA, V., DZHYGYR, I., MURAYAMA, R., AKANUMA, G., ATKINSON, G. C., GARCIA-PINO, A. & HAURYLIUK, V. 2020. The C-terminal RRM/ACT domain is crucial for fine-tuning the activation of 'long'RelA-SpoT homolog enzymes by ribosomal complexes. *Frontiers in microbiology,* 11**,** 277.

TAMMAN, H., ERNITS, K., ROGHANIAN, M., AINELO, A., JULIUS, C., PERRIER, A., TALAVERA, A., AINELO, H., DUGAUQUIER, R., ZEDEK, S., THUREAU, A., PÉREZ, J., LIMA-MENDEZ, G., HALLEZ, R., ATKINSON, G. C., HAURYLIUK, V. & GARCIA-PINO, A. 2023. Structure of SpoT reveals evolutionary tuning of catalysis via conformational constraint. *Nat Chem Biol,* 19**,** 334-345.

TAMMAN, H., VAN NEROM, K., TAKADA, H., VANDENBERK, N., SCHOLL, D., POLIKANOV, Y., HOFKENS, J., TALAVERA, A., HAURYLIUK, V., HENDRIX, J. & GARCIA-PINO, A. 2020. A nucleotide-switch mechanism mediates opposing catalytic activities of Rel enzymes. *Nature Chemical Biology,* 16**,** 834-840.

TANI, T. H., KHODURSKY, A., BLUMENTHAL, R. M., BROWN, P. O. & MATTHEWS, R. G. 2002. Adaptation to famine: a family of stationary-phase genes revealed by microarray analysis. *Proceedings of the National Academy of Sciences,* 99**,** 13471-13476.

TARLTON, J. F. & KNIGHT, P. J. 1996. Clarification of immunoblots on polyvinylidene difluoride (PVDF) membranes for transmission densitometry. *Journal of Immunological Methods,* 191**,** 65-69.

THELWALL, S., NSONWU, O., ROONEY, G. & HOPE, R. 2019. Public Health England - Annual epidemiological commentary: Gram-negative bacteraemia, MRSA bacteraemia, MSSA bacteraemia and *C. difficile* infections, up to and including financial year April 2017 to March 2018. Available: https://assets.publishing.service.gov.uk/government/uploads/system/uploads/attachment_data/file/843870/Annual_epidemiological_commentary_April_2018-March_2019.pdf [Accessed 19/11/2020].

THERMOFISHER. 2024. *Carbodiimide Crosslinker Chemistry* [Online]. ThermoFisher Scientific. Available: https://www.thermofisher.com/uk/en/home/life-science/protein-biology/protein-biology-learning-center/protein-biology-resource-library/pierce-protein-methods/carbodiimide-crosslinker-chemistry.html [Accessed 24/04/2024 2024].

THITIANANPAKORN, K., AIBA, Y., TAN, X.-E., WATANABE, S., KIGA, K., SATO'O, Y., BOONSIRI, T., LI, F.-Y., SASAHARA, T., TAKI, Y., AZAM, A. H., ZHANG, Y. & CUI, L. 2020. Association of mprF mutations with cross-resistance to daptomycin and vancomycin in methicillin-resistant Staphylococcus aureus (MRSA). *Scientific Reports,* 10**,** 16107.

TIPPER, D. J. & STROMINGER, J. L. 1965. Mechanism of action of penicillins: a proposal based on their structural similarity to acyl-D-alanyl-D-alanine. *Proc Natl Acad Sci U S A,* 54**,** 1133-41.

TIWARI, S., JAMAL, S. B., HASSAN, S. S., CARVALHO, P., ALMEIDA, S., BARH, D., GHOSH, P., SILVA, A., CASTRO, T. L. P. & AZEVEDO, V. 2017. Two-Component Signal Transduction Systems of Pathogenic Bacteria As Targets for Antimicrobial Therapy: An Overview. *Front Microbiol,* 8**,** 1878.

TOJO, S., KUMAMOTO, K., HIROOKA, K. & FUJITA, Y. 2010. Heavy involvement of stringent transcription control depending on the adenine or guanine species of the transcription initiation site in glucose and pyruvate metabolism in Bacillus subtilis. *Journal of bacteriology,* 192**,** 1573-1585.

TOLTZIS, P. 2023. 116 - Coagulase-Negative Staphylococci and Micrococcaceae. *In:* LONG, S. S. (ed.) *Principles and Practice of Pediatric Infectious Diseases (Sixth Edition)*. Philadelphia: Elsevier.

TOMASZ, A. 1979. The mechanism of the irreversible antimicrobial effects of penicillins: how the beta-lactam antibiotics kill and lyse bacteria. *Annu Rev Microbiol,* 33**,** 113-37.

TONG, S. Y. C., DAVIS, J. S., EICHENBERGER, E., HOLLAND, T. L. & FOWLER, V. G. 2015. *Staphylococcus aureus* Infections: Epidemiology, Pathophysiology, Clinical Manifestations, and Management. *Clinical Microbiology Reviews,* 28**,** 603-661.

TOUATI, D. 2000. Iron and Oxidative Stress in Bacteria. *Archives of Biochemistry and Biophysics,* 373**,** 1-6.

TOULOKHONOV, II, SHULGINA, I. & HERNANDEZ, V. J. 2001. Binding of the transcription effector ppGpp to Escherichia coli RNA polymerase is allosteric, modular, and occurs near the N terminus of the beta'-subunit. *J Biol Chem,* 276**,** 1220-5.

TRACEY A. TAYLOR, C. G. U. 2020. *Staphylococcus aureus*. StatPearls Publishing.

TROTTER, C. L., MCVERNON, J., RAMSAY, M. E., WHITNEY, C. G., MULHOLLAND, E. K., GOLDBLATT, D., HOMBACH, J. & KIENY, M. P. 2008. Optimising the use of conjugate vaccines to prevent disease caused by Haemophilus influenzae type b, Neisseria meningitidis and Streptococcus pneumoniae. *Vaccine,* 26**,** 4434-45.

TSUBAKISHITA, S., KUWAHARA-ARAI, K., SASAKI, T. & HIRAMATSU, K. 2010. Origin and molecular evolution of the determinant of methicillin resistance in staphylococci. *Antimicrob Agents Chemother,* 54**,** 4352-9.

TUFFS, S. W., GONCHEVA, M. I., XU, S. X., CRAIG, H. C., KASPER, K. J., CHOI, J., FLANNAGAN, R. S., KERFOOT, S. M., HEINRICHS, D. E. & MCCORMICK, J. K. 2022. Superantigens promote Staphylococcus aureus bloodstream infection by eliciting pathogenic interferon-gamma production. *Proceedings of the National Academy of Sciences,* 119**,** e2115987119.

TURNER, N. A., SHARMA-KUINKEL, B. K., MASKARINEC, S. A., EICHENBERGER, E. M., SHAH, P. P., CARUGATI, M., HOLLAND, T. L. & FOWLER, V. G., JR. 2019. Methicillin-resistant *Staphylococcus aureus*: an overview of basic and clinical research. *Nature Reviews Microbiology,* 17**,** 203-218.

UEHARA, Y. 2022. Current Status of Staphylococcal Cassette Chromosome mec (SCCmec). *Antibiotics (Basel),* 11.

UICKER, W. C., SCHAEFER, L. & BRITTON, R. A. 2006. The essential GTPase RbgA (YlqF) is required for 50S ribosome assembly in Bacillus subtilis. *Mol Microbiol,* 59**,** 528-40.

UNDERWOOD, A. J., ZHANG, Y., METZGER, D. W. & BAI, G. 2014. Detection of cyclic di-AMP using a competitive ELISA with a unique pneumococcal cyclic di-AMP binding protein. *J Microbiol Methods,* 107**,** 58-62.

UTTLEY, A. H., COLLINS, C. H., NAIDOO, J. & GEORGE, R. C. 1988. Vancomycin-resistant enterococci. *Lancet,* 1**,** 57-8.

VADIA, S., TSE, J. L., LUCENA, R., YANG, Z., KELLOGG, D. R., WANG, J. D. & LEVIN, P. A. 2017. Fatty Acid Availability Sets Cell Envelope Capacity and Dictates Microbial Cell Size. *Curr Biol,* 27**,** 1757-1767.e5.

VALLINAYAGAM, R., WEBER, J. & NEIER, R. 2008. Novel Bioconjugates of Aminolevulinic Acid with Vitamins. *Organic Letters,* 10**,** 4453-4455.

VAN HAL, S. J., PATERSON, D. L. & GOSBELL, I. B. 2011. Emergence of daptomycin resistance following vancomycin-unresponsive Staphylococcus aureus bacteraemia in a daptomycin-naïve patient--a review of the literature. *Eur J Clin Microbiol Infect Dis,* 30**,** 603-10.

VARIK, V., OLIVEIRA, S. R. A., HAURYLIUK, V. & TENSON, T. 2017. HPLC-based quantification of bacterial housekeeping nucleotides and alarmone messengers ppGpp and pppGpp. *Scientific Reports,* 7**,** 11022.

VESTERGAARD, M., FREES, D. & INGMER, H. 2019. Antibiotic Resistance and the MRSA Problem. *Microbiology Spectrum,* 7**,** 10.1128/microbiolspec.gpp3-0057-2018.

VIDLUND, J., GELALCHA, B. D., GILLESPIE, B. E., AGGA, G. E., SCHNEIDER, L., SWANSON, S. M., FRADY, K. D. & KERRO DEGO, O. 2024. Efficacy of novel staphylococcal surface associated protein vaccines against Staphylococcus aureus and non-aureus staphylococcal mastitis in dairy cows. *Vaccine,* 42**,** 1247-1258.

VINELLA, D., ALBRECHT, C., CASHEL, M. & D'ARI, R. 2005. Iron limitation induces SpoT-dependent accumulation of ppGpp in Escherichia coli. *Molecular microbiology,* 56**,** 958-970.

VINOGRADOVA, D. S., ZEGARRA, V., MAKSIMOVA, E., NAKAMOTO, J. A., KASATSKY, P., PALESKAVA, A., KONEVEGA, A. L. & MILÓN, P. 2020. How the initiating ribosome copes with ppGpp to translate mRNAs. *PLOS Biology,* 18**,** e3000593.

VO, D. D. & ELOFSSON, M. 2017. Synthesis of 4-Formyl-2-arylbenzofuran Derivatives by PdCl(C3H5)dppb-Catalyzed Tandem Sonogashira Coupling-Cyclization under Microwave Irradiation - Application to the Synthesis of Viniferifuran Analogues. *ChemistrySelect,* 2**,** 6245-6248.

VOS, T., LIM, S. S., ABBAFATI, C., ABBAS, K. M., ABBASI, M., ABBASIFARD, M., ABBASI-KANGEVARI, M., ABBASTABAR, H., ABD-ALLAH, F., ABDELALIM, A., ABDOLLAHI, M., ABDOLLAHPOUR, I., ABOLHASSANI, H., ABOYANS, V., ABRAMS, E. M., ABREU, L. G., ABRIGO, M. R. M., ABU-RADDAD, L. J., ABUSHOUK, A. I., … & MURRAY, C. J. L. 2020. Global burden of 369 diseases and injuries in 204

countries and territories, 1990–2019: a systematic analysis for the Global Burden of Disease Study 2019. *The Lancet,* 396**,** 1204-1222.

VRIELING, M., TUFFS, S. W., YEBRA, G., VAN SMOORENBURG, M. Y., ALVES, J., PICKERING, A. C., PARK, J. Y., PARK, N., HEINRICHS, D. E., BENEDICTUS, L., CONNELLEY, T., SEO, K. S., MCCORMICK, J. K. & FITZGERALD, J. R. 2020. Population Analysis of Staphylococcus aureus Reveals a Cryptic, Highly Prevalent Superantigen SElW That Contributes to the Pathogenesis of Bacteremia. *mBio,* 11.

WACKER, M., WANG, L., KOWARIK, M., DOWD, M., LIPOWSKY, G., FARIDMOAYER, A., SHIELDS, K., PARK, S., ALAIMO, C., KELLEY, K. A., BRAUN, M., QUEBATTE, J., GAMBILLARA, V., CARRANZA, P., STEFFEN, M. & LEE, J. C. 2014. Prevention of Staphylococcus aureus infections by glycoprotein vaccines synthesized in Escherichia coli. *J Infect Dis,* 209**,** 1551-61.

WALL, E. A., CAUFIELD, J. H., LYONS, C. E., MANNING, K. A., DOKLAND, T. & CHRISTIE, G. E. 2015. Specific N-terminal cleavage of ribosomal protein L27 in Staphylococcus aureus and related bacteria. *Mol Microbiol,* 95**,** 258-69.

WANG, B., DAI, P., DING, D., DEL ROSARIO, A., GRANT, R. A., PENTELUTE, B. L. & LAUB, M. T. 2019a. Affinity-based capture and identification of protein effectors of the growth regulator ppGpp. *Nature Chemical Biology,* 15**,** 141-150.

WANG, B., GRANT, R. A. & LAUB, M. T. 2020. ppGpp Coordinates Nucleotide and Amino-Acid Synthesis in E. coli During Starvation. *Mol Cell,* 80**,** 29-42.e10.

WANG, J., LIU, Y., WAN, D., FANG, X., LI, T., GUO, Y., CHANG, D., SU, L., WANG, Y., ZHAO, J. & LIU, C. 2012a. Whole-genome sequence of Staphylococcus aureus strain LCT-SA112. *J Bacteriol,* 194**,** 4124.

WANG, J. D., SANDERS, G. M. & GROSSMAN, A. D. 2007a. Nutritional control of elongation of DNA replication by (p) ppGpp. *Cell,* 128**,** 865-875.

WANG, J. J., ZHENG, R. T., GAO, J. W. & CHEN, G. 2012b. Heat conduction mechanisms in nanofluids and suspensions. *Nano Today,* 7**,** 124-136.

WANG, R., BRAUGHTON, K. R., KRETSCHMER, D., BACH, T.-H. L., QUECK, S. Y., LI, M., KENNEDY, A. D., DORWARD, D. W., KLEBANOFF, S. J., PESCHEL, A., DELEO, F. R. & OTTO, M. 2007b. Identification of novel cytolytic peptides as key virulence determinants for community-associated MRSA. *Nature Medicine,* 13**,** 1510-1514.

WANG, X., SHEN, Y., HUANG, W. & ZHOU, Y. 2019b. Characterisation of community-acquired Staphylococcus aureus causing skin and soft tissue infections in a children's hospital in Shanghai, China. *Epidemiol Infect,* 147**,** e323.

WASSENBERG, M. W. M., DE WIT, G. A. & BONTEN, M. J. M. 2011. Cost-Effectiveness of Preoperative Screening and Eradication of Staphylococcus aureus Carriage. *PLOS ONE,* 6**,** e14815.

WEBER, H., POLEN, T., HEUVELING, J., WENDISCH, V. F. & HENGGE, R. 2005. Genome-wide analysis of the general stress response network in Escherichia coli: σS-dependent genes, promoters, and sigma factor selectivity. *Journal of bacteriology,* 187**,** 1591-1603.

WEISS, A., IBARRA, J. A., PAOLETTI, J., CARROLL, R. K. & SHAW, L. N. 2014. The δ subunit of RNA polymerase guides promoter selectivity and virulence in Staphylococcus aureus. *Infect Immun,* 82**,** 1424-35.

WEISS, A. & SHAW, L. N. 2015. Small things considered: the small accessory subunits of RNA polymerase in Gram-positive bacteria. *FEMS Microbiol Rev,* 39**,** 541-54.

WEISS, A. J. 2012. Overview of membranes and membrane plates used in research and diagnostic ELISPOT assays. *Methods Mol Biol,* 792**,** 243-56.

WEIß, E., SCHLATTERER, K., BECK, C., PESCHEL, A. & KRETSCHMER, D. 2020. Formyl-Peptide Receptor Activation Enhances Phagocytosis of Community-Acquired Methicillin-Resistant Staphylococcus aureus. *J Infect Dis,* 221**,** 668-678.

WERTHEIM, H. F., VOS, M. C., OTT, A., VAN BELKUM, A., VOSS, A., KLUYTMANS, J. A., VAN KEULEN, P. H., VANDENBROUCKE-GRAULS, C. M., MEESTER, M. H. & VERBRUGH, H. A. 2004. Risk and outcome of nosocomial Staphylococcus aureus bacteraemia in nasal carriers versus non-carriers. *Lancet,* 364**,** 703-5.

WHITEHEAD, E. V., DEAN, R. A. & FIDLER, F. A. 1951. The Preparation and Physical Properties of Sulfur Compounds Related to Petroleum. II. Cyclic Sulfides1. *Journal of the American Chemical Society,* 73**,** 3632-3635.

WIENKEN, C. J., BAASKE, P., ROTHBAUER, U., BRAUN, D. & DUHR, S. 2010. Protein-binding assays in biological liquids using microscale thermophoresis. *Nature Communications,* 1**,** 100.

WILKE, G. A. & BUBECK WARDENBURG, J. 2010. Role of a disintegrin and metalloprotease 10 in Staphylococcus aureus alpha-hemolysin-mediated cellular injury. *Proc Natl Acad Sci U S A,* 107**,** 13473-8.

WILSON, G. J., SEO, K. S., CARTWRIGHT, R. A., CONNELLEY, T., CHUANG-SMITH, O. N., MERRIMAN, J. A., GUINANE, C. M., PARK, J. Y., BOHACH, G. A. & SCHLIEVERT, P. M. 2011. A novel core genome-encoded superantigen contributes to lethality of community-associated MRSA necrotizing pneumonia. *PLoS pathogens,* 7**,** e1002271.

WILTSHIRE, M. D. & FOSTER, S. J. 2001. Identification and analysis of Staphylococcus aureus components expressed by a model system of growth in serum. *Infect Immun,* 69**,** 5198-202.

WINTERBOURN, C. C., HAMPTON, M. B., LIVESEY, J. H. & KETTLE, A. J. 2006. Modeling the reactions of superoxide and myeloperoxidase in the neutrophil phagosome: implications for microbial killing. *J Biol Chem,* 281**,** 39860-9.

WOLZ, C., GEIGER, T. & GOERKE, C. 2010. The synthesis and function of the alarmone (p) ppGpp in firmicutes. *International Journal of Medical Microbiology,* 300**,** 142-147.

WOOD, A., IRVING, S. E., BENNISON, D. J. & CORRIGAN, R. M. 2019. The (p)ppGpp-binding GTPase Era promotes rRNA processing and cold adaptation in *Staphylococcus aureus*. *PLOS Genetics,* 15**,** e1008346.

WOOD, T. K., KNABEL, S. J. & KWAN, B. W. 2013. Bacterial persister cell formation and dormancy. *Appl Environ Microbiol,* 79**,** 7116-21.

WOWER, I. K., WOWER, J. & ZIMMERMANN, R. A. 1998. Ribosomal protein L27 participates in both 50 S subunit assembly and the peptidyl transferase reaction. *J Biol Chem,* 273**,** 19847-52.

WU, D., SEDGWICK, A. C., GUNNLAUGSSON, T., AKKAYA, E. U., YOON, J. & JAMES, T. D. 2017. Fluorescent chemosensors: the past, present and future. *Chemical Society Reviews,* 46**,** 7105-7123.

XIANG, Y., ZHENG, Y., LIU, S., LIU, G., LI, Z. & DONG, W. 2021. Comparison of the sensitivity of Western blotting between PVDF and NC membranes. *Sci Rep,* 11**,** 12022.

XIAO, H., KALMAN, M., IKEHARA, K., ZEMEL, S., GLASER, G. & CASHEL, M. 1991. Residual guanosine 3 ‘, 5 ‘-bispyrophosphate synthetic activity of relA null mutants can be eliminated by spoT null mutations. *Journal of Biological Chemistry,* 266**,** 5980-5990.

XU, H. & SUSLICK, K. S. 2010. Water-Soluble Fluorescent Silver Nanoclusters. *Advanced Materials,* 22**,** 1078-1082.

XU, Y., RIVAS, J. M., BROWN, E. L., LIANG, X. & HÖÖK, M. 2004. Virulence potential of the staphylococcal adhesin CNA in experimental arthritis is determined by its affinity for collagen. *J Infect Dis,* 189**,** 2323-33.

YAMAGUCHI, T., ONO, D. & SATO, A. 2020. Staphylococcal Cassette Chromosome mec (SCCmec) Analysis of MRSA. *In:* JI, Y. (ed.) *Methicillin-Resistant Staphylococcus Aureus (MRSA) Protocols: Cutting-Edge Technologies and Advancements*. New York, NY: Springer US.

YANG, J., ANDERSON, B. W., TURDIEV, A., TURDIEV, H., STEVENSON, D. M., AMADOR-NOGUEZ, D., LEE, V. T. & WANG, J. D. 2020a. The nucleotide pGpp acts as a third alarmone in Bacillus, with functions distinct from those of (p) ppGpp. *Nat Commun,* 11**,** 5388.

YANG, J., ANDERSON, B. W., TURDIEV, A., TURDIEV, H., STEVENSON, D. M., AMADOR-NOGUEZ, D., LEE, V. T. & WANG, J. D. 2020b. The nucleotide pGpp acts as a third alarmone in Bacillus, with functions distinct from those of (p)ppGpp. *Nature Communications,* 11**,** 5388.

YANG, P.-Y., LIU, K., ZHANG, C., CHEN, G. Y. J., SHEN, Y., NGAI, M. H., LEAR, M. J. & YAO, S. Q. 2011. Chemical Modification and Organelle-Specific Localization of Orlistat-Like Natural-Product-Based Probes. *Chemistry – An Asian Journal,* 6**,** 2762-2775.

YANG, P.-Y., ZOU, H., CHAO, E., SHERWOOD, L., NUNEZ, V., KEENEY, M., GHARTEY-TAGOE, E., DING, Z., QUIRINO, H., LUO, X., WELZEL, G., CHEN, G., SINGH, P., WOODS, A. K., SCHULTZ, P. G. & SHEN, W. 2016. Engineering a long-acting, potent GLP-1 analog for microstructure-based transdermal delivery. *Proceedings of the National Academy of Sciences,* 113**,** 4140.

YANG, S.-J., KREISWIRTH, B. N., SAKOULAS, G., YEAMAN, M. R., XIONG, Y. Q., SAWA, A. & BAYER, A. S. 2009. Enhanced Expression of dltABCD Is Associated with the Development of Daptomycin

Nonsusceptibility in a Clinical Endocarditis Isolate of Staphylococcus aureus. *The Journal of Infectious Diseases,* 200**,** 1916-1920.

YANG, Y. H., JIANG, Y. L., ZHANG, J., WANG, L., BAI, X. H., ZHANG, S. J., REN, Y. M., LI, N., ZHANG, Y. H., ZHANG, Z., GONG, Q., MEI, Y., XUE, T., ZHANG, J. R., CHEN, Y. & ZHOU, C. Z. 2014. Structural insights into SraP-mediated Staphylococcus aureus adhesion to host cells. *PLoS Pathog,* 10**,** e1004169.

YASUKAWA, N., KANIE, T., KUWATA, M., MONGUCHI, Y., SAJIKI, H. & SAWAMA, Y. 2017. Palladium on Carbon-Catalyzed Benzylic Methoxylation for Synthesis of Mixed Acetals and Orthoesters. *Chemistry – A European Journal,* 23**,** 10974-10977.

YIN, S., DAUM, R. S. & BOYLE-VAVRA, S. 2006. VraSR two-component regulatory system and its role in induction of pbp2 and vraSR expression by cell wall antimicrobials in Staphylococcus aureus. *Antimicrob Agents Chemother,* 50**,** 336-43.

ZARRELLA, T. M. & BAI, G. 2020. The Many Roles of the Bacterial Second Messenger Cyclic di-AMP in Adapting to Stress Cues. *J Bacteriol,* 203.

ZBORNÍKOVÁ, E., KNEJZLÍK, Z., HAURYLIUK, V., KRÁSNÝ, L. & REJMAN, D. 2019. Analysis of nucleotide pools in bacteria using HPLC-MS in HILIC mode. *Talanta,* 205**,** 120161.

ZHANG, G., DEINHARDT, K. & NEUBERT, T. A. 2014. Stable isotope labeling by amino acids in cultured primary neurons. *Methods Mol Biol,* 1188**,** 57-64.

ZHANG, G. & NEUBERT, T. A. 2009. Use of stable isotope labeling by amino acids in cell culture (SILAC) for phosphotyrosine protein identification and quantitation. *Methods Mol Biol,* 527**,** 79-92, xi.

ZHANG, P., WANG, Y., CHANG, Y., XIONG, Z. H. & HUANG, C. Z. 2013. Highly selective detection of bacterial alarmone ppGpp with an off-on fluorescent probe of copper-mediated silver nanoclusters. *Biosens Bioelectron,* 49**,** 433-7.

ZHANG, X., YANG, Q., LANG, Y., JIANG, X. & WU, P. 2020. Rationale of 3,3',5,5'-Tetramethylbenzidine as the Chromogenic Substrate in Colorimetric Analysis. *Analytical Chemistry,* 92**,** 12400-12406.

ZHANG, Y., MANDAVA, C. S., CAO, W., LI, X., ZHANG, D., LI, N., ZHANG, Y., ZHANG, X., QIN, Y. & MI, K. 2015. HflX is a ribosome-splitting factor rescuing stalled ribosomes under stress conditions. *Nature structural & molecular biology,* 22**,** 906-913.

ZHANG, Y., ZBORNÍKOVÁ, E., REJMAN, D. & GERDES, K. 2018. Novel (p)ppGpp Binding and Metabolizing Proteins of *Escherichia coli*. *mBio,* 9**,** e02188-17.

ZHANG, Y.-M., MARRAKCHI, H., WHITE, S. W. & ROCK, C. O. 2003. The application of computational methods to explore the diversity and structure of bacterial fatty acid synthase. *Journal of lipid research,* 44**,** 1-10.

ZHANG, Y. E., BÆRENTSEN, R. L., FUHRER, T., SAUER, U., GERDES, K. & BRODERSEN, D. E. 2019. (p)ppGpp Regulates a Bacterial Nucleosidase by an Allosteric Two-Domain Switch. *Molecular Cell,* 74**,** 1239-1249.e4.

ZHOU, C., ABDEL-RAHMAN, M. A., LI, W., LIU, K. & ZHANG, A. 2017. Thermoresponsive dendronized copolymers for protein recognitions based on biotin–avidin interaction. *Chinese Chemical Letters,* 28**,** 832-838.

ZHU, M. & DAI, X. 2019. Growth suppression by altered (p)ppGpp levels results from non-optimal resource allocation in *Escherichia coli*. *Nucleic Acids Research,* 47**,** 4684-4693.

ZHU, M. & DAI, X. 2023. Stringent response ensures the timely adaptation of bacterial growth to nutrient downshift. *Nature Communications,* 14**,** 467.

ZINSER, E. R. & KOLTER, R. 2000. Prolonged stationary-phase incubation selects for lrp mutations in Escherichia coli K-12. *Journal of Bacteriology,* 182**,** 4361-4365.

ZUO, Y., WANG, Y. & STEITZ, T. A. 2013. The mechanism of E. coli RNA polymerase regulation by ppGpp is suggested by the structure of their complex. *Mol Cell,* 50**,** 430-6.